

ETH Diss. No.: 17882

# Hierarchically Structured Conjugated Polymers via Supramolecular Self-Assembly

A dissertation submitted to

**ETH Zurich**

for the degree of  
**Doctor of Sciences**

Presented by

**Eike Jahnke**

Dipl. Chem., Freie Universität Berlin

born: July 9, 1979

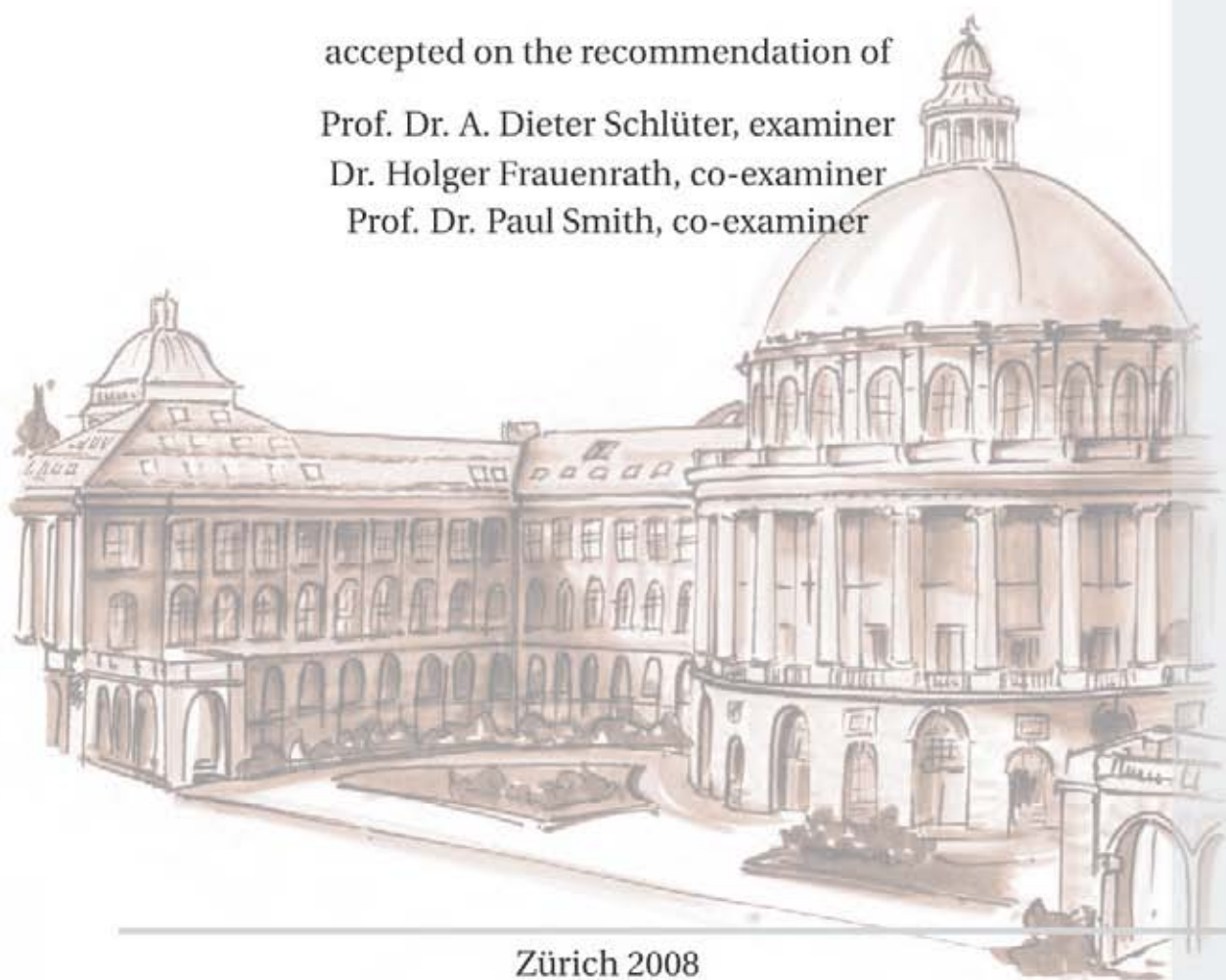
citizen of Germany

accepted on the recommendation of

Prof. Dr. A. Dieter Schlüter, examiner

Dr. Holger Frauenrath, co-examiner

Prof. Dr. Paul Smith, co-examiner



Zürich 2008



---

## Danksagung

Diese Dissertation wäre ohne die Hilfe einer Vielzahl von Personen nicht oder nur qualitativ eingeschränkt zustande gekommen, und es ist mir eine Pflicht und Freude mich an dieser Stelle bei allen Helfern zu bedanken.

An erster Stelle möchte ich meinem direkten Betreuer, Dr. Holger Frauenrath, für die unschätzbare wertvolle wissenschaftliche Anleitung danken. Die zahllosen wissenschaftlichen aber auch persönlichen Diskussionen haben mir immer weitergeholfen und damit entscheidend zum Erfolg und zur Qualität dieser Arbeit beigetragen.

Meinem Doktorvater, Prof. Dieter Schlüter, gilt es für alle nur erdenklichen Ressourcen zu danken, auf die ich während meiner gesamten Arbeit zurückgreifen konnte.

Allen meinen Laborkollegen, Xu Rui, Jialong Yuan, Tobias Hoheisel, Jan Gebers und Sonja Neuhaus möchte ich für die großartige Unterstützung im Labor danken. Die (Arbeits)atmosphäre war immer hervorragend und ermöglichte jeder Zeit eine reibungslose Zusammenarbeit und fruchtbare Diskussionen. Ebenso gilt es die überragenden Masterarbeiten von Anne-Sophie Millerioux, Jan Weiß und Sonja Neuhaus zu betonen, die sich mit einzelnen Aspekten unserer Forschung auf beeindruckende Weise auseinandergesetzt haben und erheblich zum Umfang meiner eigenen Arbeit beigetragen haben. Dies gilt in ähnlicher Weise für die Forschungsstudenten, Tobias Hoheisel, Anne-Sophie Millerioux, Petra Fesser, Matthias Grabowski und Damien Rolland, die während meiner Betreuung Fortschritte ermöglicht haben, die ich allein in dieser Zeit nie hätte schaffen können.

Der gesamten Arbeitsgruppe gilt natürlich ebenso Dank, da jeder in seiner Weise zum Erfolg meiner Arbeit beigetragen hat. Ich möchte aber trotzdem Alexander Ossenbach herausstellen, der mir wissenschaftlich aber vor allem auch persönlich immer freundschaftlich zur Seite stand. Dr. Jeroen van Heijst möchte ich für die etlichen Korrekturen danken, die er an unseren Manuskriptentwürfen vorgenommen hat und Ding Yi für die theoretische Begleitung unseres Projekts.

Bei der Betreuung der Studenten in den Praktika haben Peter Walde und Lera Tomasic in Ihren Funktionen unsere Arbeit als Assistenten stets unterstützt und geholfen, die Betreuung in einem zeitlich überschaubaren Rahmen zu halten.

In Bezug auf an der ETH Zürich zur Verfügung stehenden Ressourcen, möchte ich mich besonders bei Dr. Heinz Rüegger bedanken, der mich in allen Fragen der NMR Spektroskopie angeleitet hat; Peter Walde danke ich für die Nutzung spektroskopischer Ausrüstung einschließlich der nötigen Einweisungen; Martin Colussi, der mir die Geheimnisse der GPC erläutert hat; Dr. Kirill Feldman und allen anderen Mitarbeitern der Arbeitsgruppe Smith für ihre freundliche Unterstützung bei Messungen jeglicher Art und für die Zurverfügungstellung eines Labors, das wir als Dunkelkammer "mißbrauchten"; Marie-Pierre Collin, die mich in die IR Spektroskopie in flüssiger Phase eingeführt hat; Jan Kovacovic, der unsere Hochdruckreaktionen betreut hat; den Doktoren Volker Gramlich und

---

Bernd Schweizer für die Aufklärung von leider viel zu wenigen Kristallstrukturen; dem Team von Dr. Amrein in der Massenspektrometrie, besonders Louis Bertschi und Oliver Scheidegger, die sich intensiv mit unseren Proben auseinandergesetzt haben; dem Team der Elementaranalyse, die selbst unzureichend beschriftete Proben immer anstandslos gemessen haben; und schließlich dem netten “Schalter-Team”, das uns stets freundlich mit allem Nötigen versorgt hat.

Diese Arbeit wäre in dieser Form aber auch nicht ohne die Hilfe von ausserhalb des Departements für Materialien zustande gekommen, da sehr viele Ergebnisse in Kooperationen erhalten wurden.

Hier ist zuerst die hervorragende Arbeit der Gruppe um Prof. Jürgen P. Rabe von der Humboldt Universität zu Berlin im Bereich der SFM zu nennen, die uns einen genauen Einblick in unser System ermöglicht hat. Im besonderen die “magischen” Hände von Dr. Nikolai Severin sind hier herauszustellen, der immer die schärfsten Bilder erzeugt hat und auch durch seine Anleitung von Paul Kreuzkamp und Sonja Neuhaus enorm zum Erfolg dieser Arbeit beigetragen hat.

Unsere Versuche, TEM als Bildgebungsverfahren zu nutzen, wurden von Dr. Ishikawa (ETH), Dr. Ingo Lieberwirth (MPI für Polymerforschung, Mainz, Deutschland) und Dr. Jürgen Hartmann (MPI für Kolloid und Grenzflächenforschung, Golm, Deutschland) tatkräftig unterstützt. Alle Beteiligten haben geduldigst unsere Proben vermessen und auch den letzten Kontrast herausgeholt.

Die Arbeiten zur Festkörper-NMR, die mein Projekt über zweieinhalb Jahre begleiteten waren nur in Kooperation mit der Expertengruppe um Prof. Beat Meier (ETH) möglich. Die drei Mitarbeiter Alexandre Arnold, Jacco van Beek und Rene Verel haben einen erheblichen Anteil an der erfolgreichen Aufklärung der Selbstorganisation unseres Systems geleistet.

Die freundliche Einladung von Prof. Bäuerle (Universität Ulm, Deutschland) hat es mir ermöglicht, CD Spektroskopie an unseren Polymeren zu erlernen, durchzuführen und zu verstehen. Hierbei halfen auch Frau Dr. Mena Osteritz und Dr. Günther Götz (Ulm) die mich tatkräftig unterstützten, sowie die Gruppe um Prof. Glockshuber (ETH), die mir ein CD-Spektrometer in unserer unmittelbaren Umgebung zur Verfügung stellten.

All die wissenschaftlichen Leistungen und Erkenntnisse, die in dieser Arbeit erbracht und erlangt wurden wären nicht möglich gewesen ohne die uneingeschränkte Unterstützung, die ich von meiner Familie erfahren habe. Ich möchte mich zuerst bei meiner lieben Schwester Carmen Marschner bedanken, die durch ihre Illustrationen diese Arbeit auch optisch sehr ansehnlich gemacht hat, und mir half meine eigene künstlerische Talentfreiheit zu überspielen. Natürlich gilt auch meinen Eltern und Schwiegereltern der größtmögliche Dank, da sie mich immer uneingeschränkt unterstützt haben und mir diesen Lebensweg erst ermöglichten.

Zu guter Letzt möchte ich meiner Frau Doreen danken, deren Liebe und Zuneigung mir immer eine große Unterstützung sind. Doreen und unsere geliebte Tochter Leni bieten mir immer ein glückliches, sorgenfreies aber auch erfrischend wissenschaftsfreies zu Hause, was das Fundament nicht nur dieser Arbeit darstellt.

---

## List of Publications

Parts of this Ph. D. thesis have been published in scientific journals or books, were presented in talks as well as on posters at several occasions by the author of this thesis.

### Publications (peer-reviewed)

- [1] “Topochemical Polymerization in Supramolecular Polymers of Oligopeptide Functionalized Diacetylenes”, E. Jahnke, I. Lieberwirth, N. Severin, J. P. Rabe, H. Frauenrath, *Angew. Chem. Int. Ed.* **2006**, *45*, 5383-5386.
- [2] “Functional, Hierarchically Structured Poly(diacetylene)s via Supramolecular Self-Assembly”, E. Jahnke, N. Severin, J. P. Rabe, H. Frauenrath, *Macromol. Biosci.* **2007**, *7*, 136-143.
- [3] “Strategies Toward Hierarchically Structured Optoelectronically Active Polymers”, E. Jahnke, H. Frauenrath, in *Tomorrow's Chemistry Today – Concepts in Nanoscience, Organic Materials, and Environmental Chemistry*, B. Pignataro (ed.), Wiley-VCH, Weinheim, Deutschland, **2007**.
- [4] “Molecular Level Control over Hierarchical Structure Formation and Polymerization of Oligopeptide-Polymer Conjugate Based Macromonomers”, E. Jahnke, N. Severin, J. P. Rabe, H. Frauenrath, *Adv. Mater.* **2008**, *20*, 409-414. [Highlighted in *Nachr. Chem.* **2008**, *56*, 404.]
- [5] “Chiroptical Properties of Multiple-Helical, Oligopeptide-Substituted Poly(diacetylene)s in Solution”, J. Weiß, E. Jahnke, H. Frauenrath, *Macromol. Rapid Commun.* **2008**, *29*, 330-339.
- [6] “A General Concept for The Preparation of Hierarchically Structured Conjugated Polymers”, H. Frauenrath, E. Jahnke, *Chem. Eur. J.* **2008**, *14*, 2942-2955.
- [7] “Consecutive Conformational Transitions and Deaggregation of Multiple-Helical Poly(diacetylene)s”, J. Weiß, E. Jahnke, N. Severin, J. P. Rabe, H. Frauenrath, *Nano Letters* **2008**, *8*, 1660-1666.
- [8] “Synthesis of Diacetylene-Containing Peptide Building Blocks and Amphiphiles, their Self-Assembly and Topochemical Polymerization in Organic Solvents”, E. Jahnke, J. Weiß, S. Neuhaus, T. Hoheisel, H. Frauenrath, *Chem. Eur. J.* **2009**, *14*, 388-404.

### Publications (others)

- [9] “Topochemical Polymerization in Supramolecular Polymers of Oligopeptide Substituted Diacetylenes”, H. Frauenrath, E. Jahnke, A.-S. Millerioux, I. Lieberwirth, N. Severin, J. P. Rabe, *Polym. Prepr.* **2006**, *47*, 457-458.

- 
- [10] “Toward Functional, Hierarchically Structured, Optoelectronic Materials”, H. Frauenrath, E. Jahnke, A.-S. Millerieux, I. Lieberwirth, N. Severin, J. P. Rabe, *Polym. Prepr.* **2006**, *47*, 459-460.

## Talks

- [1] “Making Macromolecules Know How to Behave: Creation of Polymer Materials for Optoelectronics”, 4.11.2005, 12<sup>th</sup> Meeting of the Materials Alumni of ETH Zurich, Zurich Switzerland.
- [2] “Carbon-Rich Nanostructured Materials from Defined Precursors – Self-Organization of Peptide Functionalized Diacetylenes”, 6.2.2006, Meeting of the Fellows of the “Fonds der chemischen Industrie”, Heidelberg, Germany
- [3] “Hierarchically Structured Conjugated Polymers via Supramolecular Self-Assembly”, 7.7.2007, Prof. Moore Group Seminar, Department of Chemistry, University of Illinois, Urbana-Champaign, IL, USA.
- [4] “Hierarchically Structured Conjugated Polymers via Supramolecular Self-Assembly”, 12.7.2007, Prof. Gellman Group Seminar, Department of Chemistry, University of Wisconsin, Madison, WI, USA.
- [5] “Hierarchically Structured Conjugated Polymers via Supramolecular Self-Assembly”, 5.4.2008, Prof. Tykwinski Group Seminar, Department of Chemistry, University of Alberta, Edmonton, AB, Canada.

## Poster Contributions

- [1] “Toward Carbon-Rich Nanostructured Materials via Self-Assembly of Oligopeptide Functionalized Diacetylenes”, 15.8.2005, International Symposium on Novel Aromatic Compounds (ISNA-11), St. John's, NFL, Canada.
- [2] “1D Topochemical Polymerization in Self-Assembled Ribbons of Diacetylenes with  $\beta$ -Sheet Forming Oligopeptide Residues”, 18.11.2005, Annual Meeting of the Polymer Group Switzerland (PGS), Neuchâtel, Switzerland. (1<sup>st</sup> Poster price)
- [3] “Toward Functional Polymers for Optoelectronic Applications at the Interface with the Biosciences”, 29.6.2006, 1<sup>st</sup> Materials Research Center Graduate Symposium at ETH, Zurich, Zurich, Switzerland.
- [4] “Hierarchically Structured, Optoelectronic Materials from Diacetylene Functionalized Oligopeptides”, 9.7.2006, ORCHEM, Bad Nauheim, Germany. (3<sup>rd</sup> Poster price)

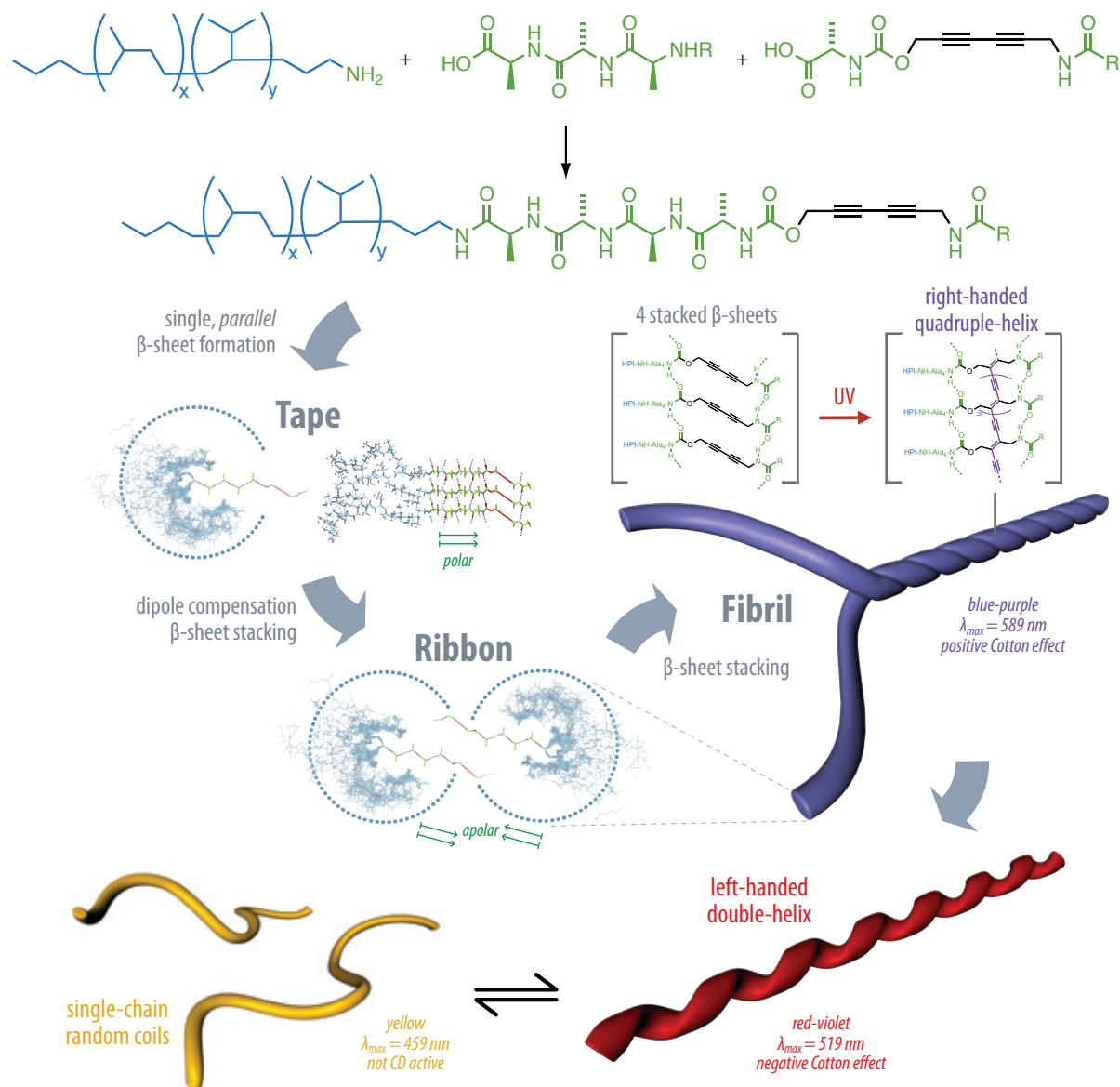
- 
- [5] "Toward Functional Polymers for Optoelectronic Applications at the Interface with the Biosciences", 7.8.2006, BASF Symposium on Bioinspired Materials for the Chemical Industry, Strasbourg, France.
- [6] "Toward Hierarchically Structured Materials for Optoelectronic Applications at the Interface with the Biosciences", 30.8.2006, European Chemistry Congress, Budapest, Hungary.
- [7] "Topochemical Polymerizations in Supramolecular Polymers of Oligopeptide Substituted Diacetylenes", 10.9.2006, ACS Meeting, San Francisco, CA, USA.
- [8] "Topochemical Polymerizations in Supramolecular Polymers of Oligopeptide Substituted Diacetylenes", 4.10.2006, Polydays 2006, Berlin, Germany.
- [9] "Toward Functional, Hierarchically Structured, Optoelectronic Materials via Self-Assembly", 13.10.2006, Fall Meeting of the Swiss Chemical Society (SCS), Zurich, Switzerland.
- [10] "Topochemical Polymerizations in Supramolecular Polymers of Oligopeptide Substituted Diacetylenes", 13.10.2006, Fall Meeting of the Swiss Chemical Society (SCS), Zurich, Switzerland.
- [11] "A Model for the Hierarchical Self-Organization of Diacetylene Functionalized Oligopeptide Polymer Conjugates", 12.9.2007, Fall Meeting of the Swiss Chemical Society (SCS), Lausanne, Switzerland.
- [12] "Molecular Level Control over Hierarchical Structure Formation and Polymerizability of Oligopeptide Substituted Diacetylenes", 15.10.2007, ESF Meeting on Stimuli Responsive Polymer Materials (STIPOMAT), Les Diablerets, Switzerland.
- [13] "Hierarchically Structured Poly(diacetylene)s via Supramolecular Self-Assembly", 28.2.2008, Makromolekulares Kolloquium, 28.2.-1.3.2008, Freiburg, Germany.
- [14] "Hierarchically Structured Conjugated Oligomers and Polymers", 8.5.2008, ETH Micro and Nano Science Platform Industry Day 2008, Zurich, Switzerland.





## Summary

In the present thesis, the synthesis, controlled hierarchical self-assembly, and polymerization of novel macromonomers based on diacetylene-functionalized oligopeptide-polymer conjugates was investigated as a pathway toward hierarchically structured  $\pi$ -conjugated polymers.



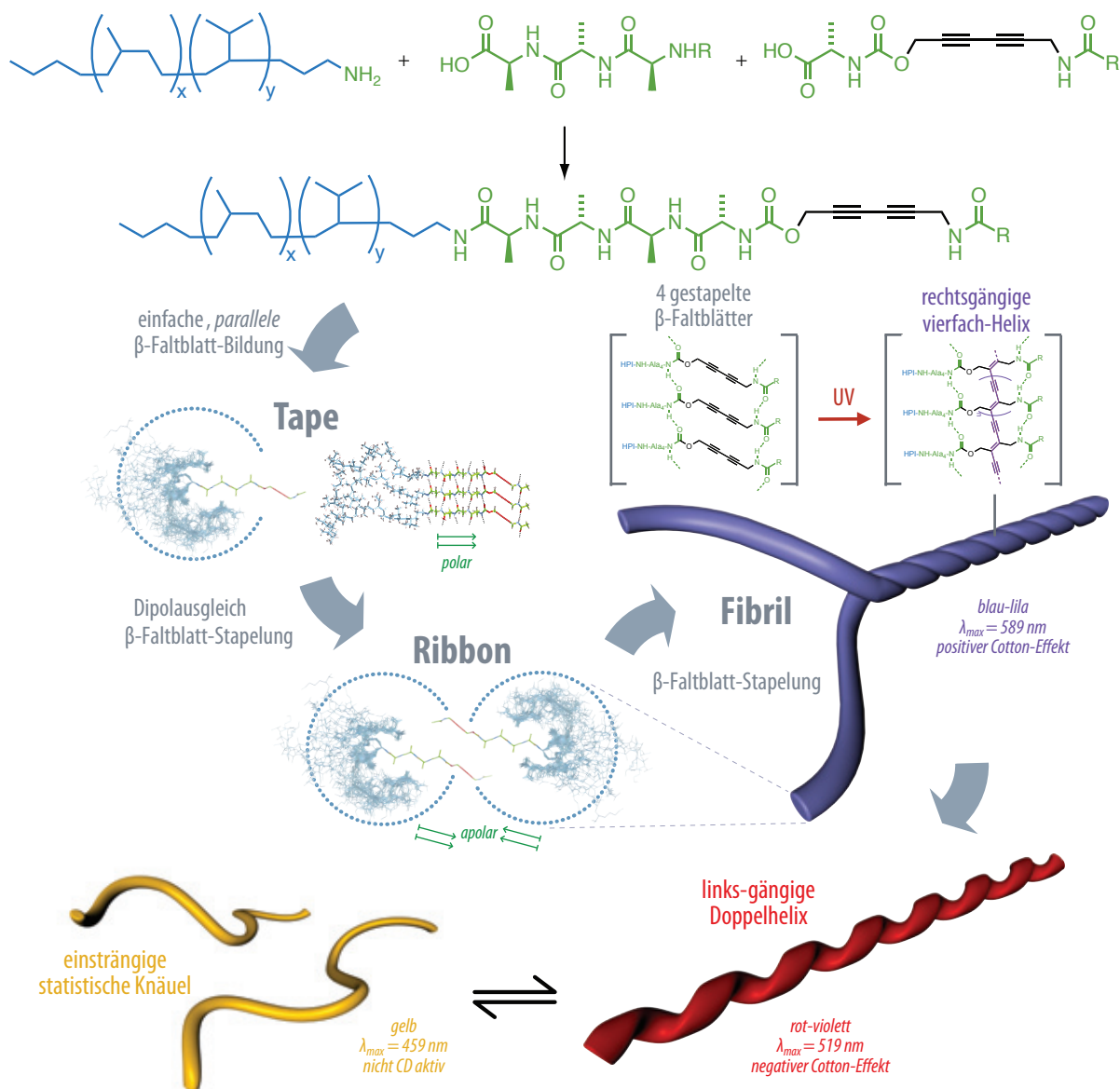
For this purpose, a modular synthetic strategy for the preparation of the oligopeptide-polymer conjugates used as the macromonomers was developed and implemented that allowed for the rapid synthesis of a large variety of differently functionalized derivatives. IR-spectroscopic investigations in organic solution as well as solid state NMR experiments unambiguously confirmed that some of the macromonomers formed  $\beta$ -sheet secondary structures. Furthermore, the chosen oligopeptide-polymer conjugates gave rise to different higher structures such as single-stranded

---

tapes, double-stranded helical ribbons, or quadruple-stranded helix bundles, as was evidenced by transmission electron microscopy (TEM) and scanning force microscopy (SFM) imaging techniques. This superstructure formation was rationalized to result from a simple set of parameters such as the non-equidistant placement, the exact distribution, and the total number of N-H $\cdots$ O=C hydrogen-bonding sites in the macromonomers. The precise control of the secondary and higher structure formation allowed for the design of macromonomers suitable for a topochemical diacetylene polymerization within the self-assembled aggregates. Thus, the supramolecular polymers were converted into conjugated polymers under retention of their hierarchical structures. Accordingly, highly functionalized, soluble poly(diacetylene)s were obtained that had a predictable single-stranded, double-helical, or quadruple-helical quaternary structure which were characterized by spectroscopic as well as imaging techniques. Furthermore, the poly(diacetylene)s exhibited a two-step solvatochromism upon the addition of hydrogen-bond breaking cosolvents. The color transitions were accompanied by two defined, successive conformational transitions, as was evidenced by CD spectroscopy. In conclusion, the  $\pi$ -conjugated synthetic polymers obtained with the chosen strategy exhibited both quaternary structures and dynamic folding properties similar to typical biopolymers.

## Zusammenfassung

Im Rahmen der vorliegenden Arbeit wurden die Synthese, die kontrollierte hierarchische Selbstorganisation sowie die Polymerisation von neuartigen Makromonomeren auf Oligopeptid-Polymer-Basis im Hinblick auf die Darstellung von hierarchisch strukturierten  $\pi$ -konjugierten Polymeren untersucht.



Zur Darstellung der Oligopeptid-Polymer-Konjugate, die als Makromonomere eingesetzt wurden, ist eine modulare Synthesestrategie erarbeitet worden. Dies ermöglichte die rasche Synthese einer Vielzahl unterschiedlich funktionalisierter Derivate. Mit Hilfe von IR-spektroskopischen Untersuchungen in organischer Lösung sowie mittels Festkörper-NMR-Spektroskopie konnte zweifelsfrei nachgewiesen werden, dass die Makromonomere  $\beta$ -Faltblatt-artige Sekundärstrukturen bilden. Darüber hinaus konnte mit Hilfe von Transmissionselektronenmikroskopie (TEM) sowie

---

Rasterkraftmikroskopie (*scanning force microscopy*, SFM) gezeigt werden, dass auch höhere Strukturen wie einzelne  $\beta$ -Faltblatt-*Tapes*, zweifach-helikale *Ribbons* oder vierfach-helikale *Fibrils* aus den Makromonomeren gebildet wurden. Diese hierarchische Strukturbildung wurde durch eine begrenzte Anzahl von Parametern im molekularen Aufbau der Makromonomere kontrolliert, wie etwa der Anzahl von N-H $\cdots$ O=C Wasserstoffbrücken und ihrer Anordnung mit ungleichen Abständen. Die so kontrollierbare Bildung höherer Strukturen ermöglichte eine topochemische Polymerisation der Diacetylene innerhalb der erhaltenen Aggregate. Dies hatte zur Folge, dass die vormals supramolekularen Polymere in  $\pi$ -konjugierte Polymere unter Erhalt der hierarchischen Strukturen überführt werden konnten. Die erzeugten Poly(diacetylen)e waren demnach hoch funktionalisierte, lösliche Polymere mit vorhersagbaren einfach-helikalen, doppel-helikalen sowie vierfach-helikalen Quartärstrukturen. Letztere konnten mittels Bildgebungsverfahren und durch CD-Spektroskopie nachgewiesen werden. Die Zugabe von Wasserstoffbrücken-brechenden Lösungsmitteln zu den Polymerlösungen löste definierte zweiseitige Farbwechsel aus, mit denen zwei aufeinander folgende, wohldefinierte Konformationsänderungen einhergingen, wie mittels CD-Spektroskopie gezeigt werden konnte. Folglich wiesen die erhaltenen synthetischen  $\pi$ -konjugierten Polymere sowohl Quartärstrukturen als auch ein dynamisches Faltungsverhalten auf, wie es sonst nur von Biopolymeren bekannt war.

---

## List of Abbreviations

Ac	acetyl
anal.	analysis
b	broad signal (NMR)
Boc <sub>2</sub> O	di- <i>tert.</i> -butyl dicarbonate
calcd	calculated
CD	circular dichroism
CIDS	circular intensity differential scattering
CP	cross polarization (NMR)
d	doublet (NMR)
$\delta$	chemical shift (NMR)
DEAD	diethyl azodicarboxylate
DOQSY	double quantum single quantum correlation spectroscopy (NMR)
DCE	1,2-dichloroethane
DCM	dichloromethane
DIEA	diisopropylethylamine
DIPA	diisopropylamine
DMF	<i>N,N</i> -dimethylformamide
DMSO	dimethylsulfoxide
$\epsilon$	extinction coefficient (UV)
EDCI	1-ethyl-3-(3-dimethyl-aminopropyl)carbodiimide hydrochloride
EI	electron impact ionization
eq.	equivalents
ESI	electrospray ionization
FCC	flash column chromatography
Fmoc	<i>N</i> -(9-fluorenylmethyloxycarbonyl)
GPC	gel permeation chromatography
<sup>1</sup> H NMR	proton nuclear magnetic resonance
<sup>13</sup> C NMR	carbon 13 nuclear magnetic resonance
HFIP	hexafluoroisopropanol
HMDS	hexamethyldisilazane
HOBt	1-hydroxybenzotriazole
HPLC	high performance liquid chromatography
HRMS	high resolution mass spectrometry
HV	high vacuum
IR	infra red
<i>J</i>	<i>J</i> coupling constant (NMR)

---

LHMDS	lithium hexamethyldisilazid
m	multiplet (NMR)
M	molar
$[M]^+$	molecular ion (MS)
MALDI	matrix assisted laser desorption ionization (MS)
MALDI-TOF	matrix assisted laser desorption ionization time of flight (MS)
MAS	magic angle spinning
$\bar{M}_n$	number average molecular weight
m.p.	melting point
MS	mass spectrometry
m/z	mass to charge ration (MS)
NIS	<i>N</i> -iodo-succinimide
NMR	nuclear magnetic resonance
NOESY	Nuclear Overhauser Enhancement Spectroscopy (NMR)
OPV	oligo(phenylene vinylene)s
OT	oligo(thiophene)s
Pd/C	palladium on charcoal
PDI	polydispersity index
PEO	poly(ethylene oxide)
$\bar{P}_n$	average degree of polymerization
ppm	parts per million (NMR)
PyBOP	(benzotriazol-1-yloxy)tripyrrolidinophosphonium hexafluorophosphate
REDOR	rotational echo double resonance (NMR)
$R_f$	retention or retardation factor (thin layer chromatography)
s	singlet (NMR)
SAED	selected area electron diffraction
SFM	scanning force microscopy
t	triplet (NMR)
TBAF	tetrabutylammonium fluoride
TEA	triethylamine
TEM	transmission electron microscopy
TFA	trifluoroacetic acid
THF	tetrahydrofuran
TLC	thin layer chromatography
TMEDA	tetramethylethylenediamine
TMS	trimethylsilyl
UV	ultraviolet

# Table of Contents

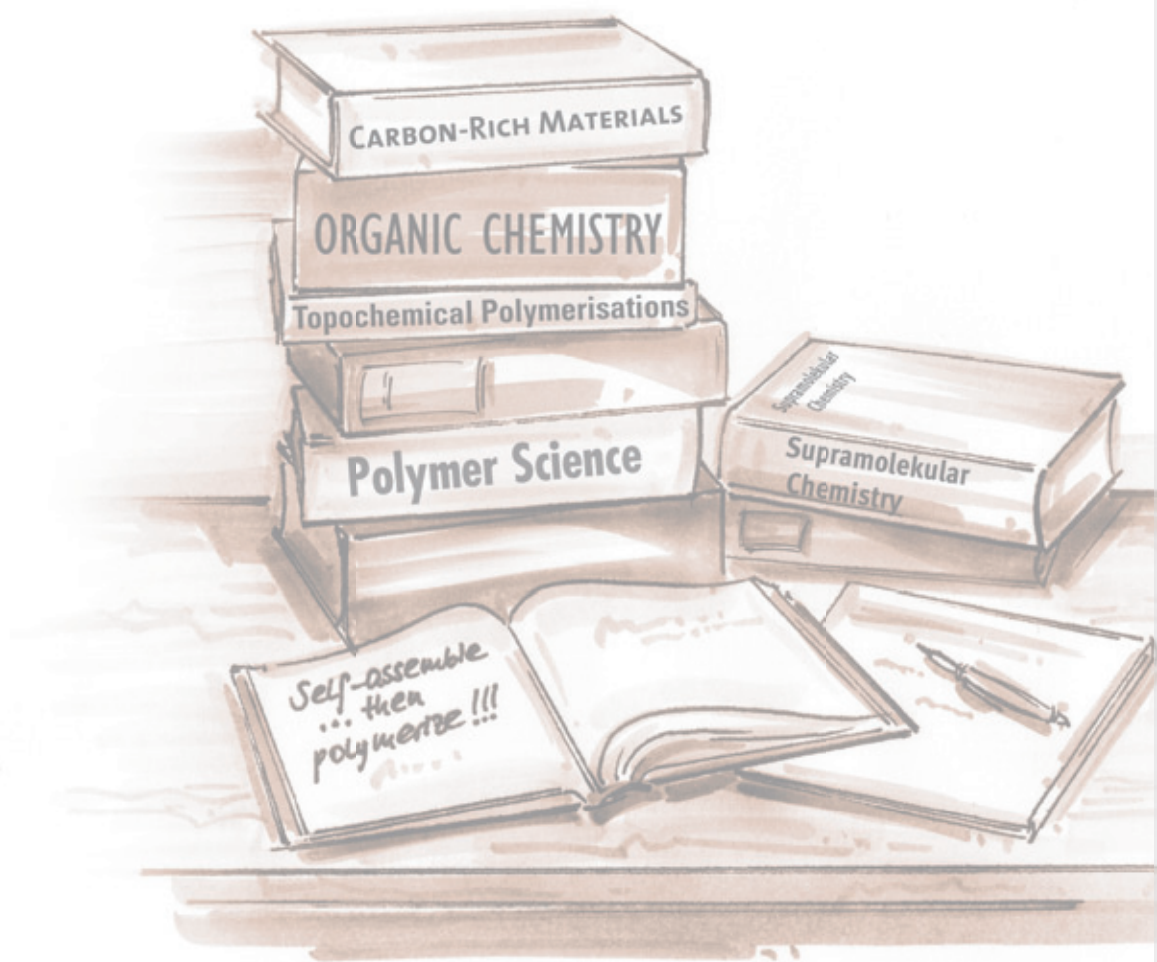
<b>1</b>	<b>Introduction</b>	<b>3</b>
1.1	A Novel Approach Toward Hierarchically Structured Conjugated Polymers . . . . .	3
1.1.1	Motivation . . . . .	3
1.1.2	Supramolecular Approaches Towards Optoelectronic Materials . . . . .	5
1.1.3	Polymer Science and Hierarchically Structured Materials . . . . .	7
1.1.4	“Self-Assemble, then Polymerize” – A Complementary Approach . . . . .	11
1.2	Hierarchical Structures From Oligo- and Polypeptides . . . . .	13
1.2.1	Self-Assembly of Amyloid Proteins . . . . .	13
1.2.2	Self-Assembly of Synthetic Oligopeptides and Peptidomimetics . . . . .	17
1.2.3	Self-Assembly of Oligopeptide-Polymer Conjugates . . . . .	21
1.2.4	Implications for the Molecular Design . . . . .	25
1.3	Synthesis and Properties of Poly(diacetylene)s . . . . .	27
1.3.1	The Topochemical Polymerization of Diacetylenes . . . . .	27
1.3.2	Topochemical Polymerizations in Hydrogen-Bonded Systems . . . . .	28
1.3.3	Chromism of Poly(diacetylenes) . . . . .	34
1.3.4	Toward Hierarchically Structured Poly(diacetylene)s . . . . .	41
<b>2</b>	<b>Outline</b>	<b>45</b>
<b>3</b>	<b>Results and Discussion</b>	<b>49</b>
3.1	Synthesis . . . . .	49
3.1.1	Molecular Design and Synthetic Strategy . . . . .	49
3.1.2	Oligopeptide Building Blocks . . . . .	50
3.1.3	Oligopeptide-Polymer Conjugate Building Blocks . . . . .	52
3.1.4	Characterization of the Oligopeptide-Polymer Conjugates . . . . .	56
3.1.5	Diacetylene Building Blocks . . . . .	58
3.1.6	Preparation of the Macromonomers . . . . .	70
3.1.7	Variation of the Macromonomers . . . . .	80

---

3.1.8	Preparation of Model Compounds . . . . .	84
3.1.9	Conclusions . . . . .	86
3.2	Secondary and Higher Structure Formation . . . . .	87
3.2.1	IR Spectroscopic Investigations . . . . .	87
3.2.2	Solid State NMR Investigations . . . . .	98
3.2.3	Electron and X-ray Diffraction . . . . .	108
3.2.4	Gelation Experiments . . . . .	110
3.2.5	Imaging of Higher Structures by Transmission Electron Microscopy . . . . .	112
3.2.6	Imaging of Higher Structures by Scanning Force Microscopy . . . . .	115
3.2.7	Further Investigations Concerning the Higher Structure Formation . . . . .	126
3.3	Model for the Self-Assembly of Macromonomers <b>92-103</b> . . . . .	127
3.4	UV Induced Topochemical Polymerization . . . . .	131
3.4.1	Polymerization of the Macromonomers <b>92-103</b> . . . . .	131
3.4.2	Polymerization of the Model Compounds . . . . .	140
3.4.3	Characterization of the Poly(diacetylene)s . . . . .	142
3.5	Chiroptical Properties of the Poly(diacetylene)s . . . . .	146
3.5.1	Evidence for Helical Poly(diacetylene)s in Solution . . . . .	146
3.5.2	Comparison of Supramolecular Aggregates versus Covalent Polymers . . . . .	149
3.6	Solvatochromism and Conformational Transitions . . . . .	152
3.7	Synthesis of Higher Oligo(ethynylene)s . . . . .	162
<b>4</b>	<b>Conclusions and Outlook</b>	<b>171</b>
<b>5</b>	<b>Experimental Part</b>	<b>175</b>
5.1	Instrumentation . . . . .	175
5.2	Chromatography . . . . .	176
5.3	General Procedures . . . . .	177
5.4	Syntheses . . . . .	178
<b>6</b>	<b>References</b>	<b>231</b>
<b>7</b>	<b>Spectra Appendix</b>	<b>241</b>
<b>8</b>	<b>Curriculum Vitae</b>	<b>333</b>



# Introduction





# 1 Introduction

## 1.1 A Novel Approach Toward Hierarchically Structured Conjugated Polymers

### 1.1.1 Motivation

Nature defines the “state of the art” in terms of constructing materials and will still do so in the future. Biomaterials such as silk, collagen, or wood exhibit extraordinary properties, which can be regarded as even more remarkable since they are produced under mild, physiological conditions. The superior properties of biopolymers mainly originate from their structural order on different length scales. In proteins, for example, the amino acid sequence (primary structure) predetermines different chain segments to attain well-defined conformations like, for instance,  $\alpha$ -helices or  $\beta$ -sheets (secondary structure). These are then folded into a specific spatial arrangement (tertiary structure) that determines the overall topographic shape of the macromolecules in solution. Finally, several of these folded macromolecules may serve as subunits that self-assemble into the active protein complex or structure protein (quaternary structure).

Biological systems often achieve this kind of hierarchical structure formation utilizing a combined “bottom-up” and “top-down” approach. Thus, the information to adopt a certain higher structure is programmed on the molecular level. At the same time, the macromolecules are carefully guided to find the desired structure among the manifold of energetically similar possibilities, for instance, by using template molecules (e. g., chaperone proteins) or by means of sophisticated processing procedures (e. g., the spinning of a spider silk thread).

Accordingly, the preparation of hierarchically structured synthetic polymers has been recognized as an important field of research,<sup>1-6</sup> not only to mimic natural materials but also to provide means to interact with the latter. The recent advances on the field of optoelectronic devices aimed at applications in the life sciences, e. g., the development of new generations of biomedical devices, require the development of optoelectronically active synthetic materials that offer a diverse chemical functionality and a degree of hierarchical structural order similar to biomaterials. However, while polymer

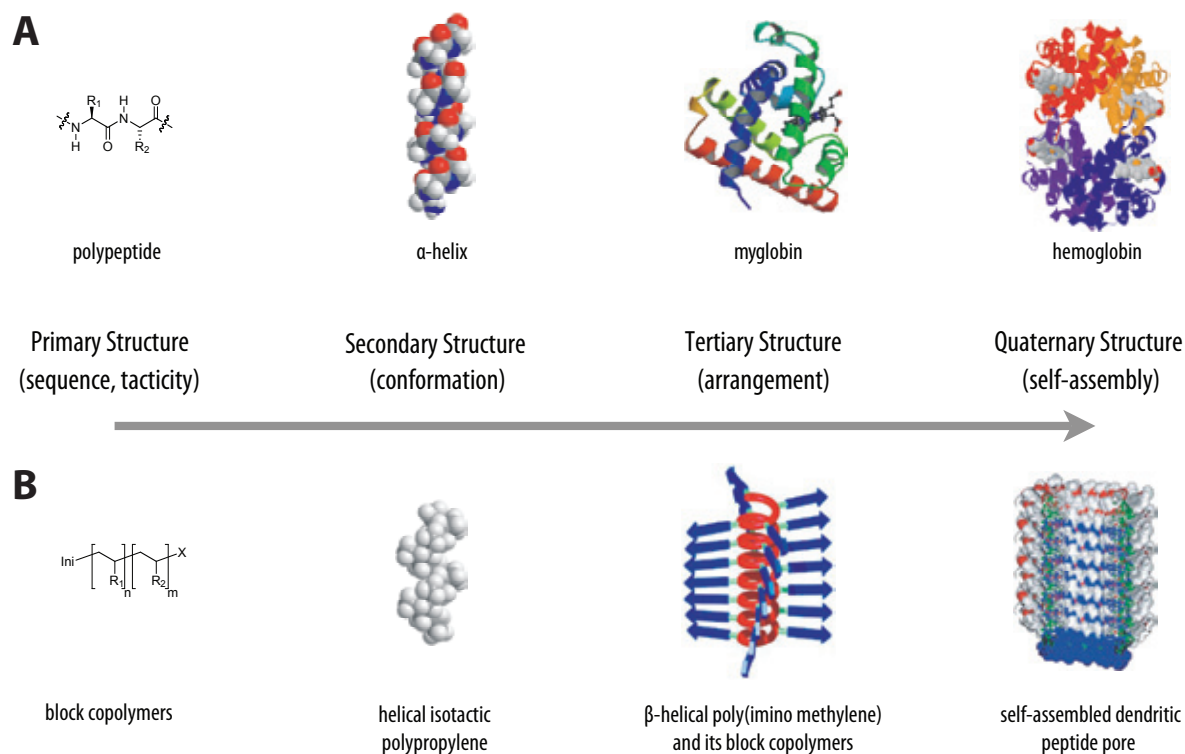


**Figure 1:** A) Natural polymers like polypeptides derive their extraordinary properties from a controlled hierarchical structure formation reaching from a perfect primary to a well-defined quaternary structure. B) Polymer scientists can hardly compete with their structural perfection although some major achievements were made in recent years. Image reproduced from [1].

chemists have been striving to understand the basic principles of hierarchical structure formation in biopolymers over the past three decades and huge progress has been made on the field of synthetic polymer chemistry in general, the tools at hand to exert a control of polymer structure comparable to biological systems are still limited in scope (Figure 1).<sup>4</sup> The most successful attempts to prepare hierarchically structured polymer materials were based on combined strategies which made use of the achievements of several research areas such as modern organic and polymer chemistry,<sup>5</sup> as well as materials science and supramolecular chemistry.<sup>6</sup>

Thus, the supramolecular self-assembly of monodisperse,  $\pi$ -conjugated oligomers has been extensively studied as a means for the creation of hierarchically structured, optoelectronically active materials.<sup>7</sup> This “supramolecular approach” attempts to alleviate the shortcomings of common materials’ processing procedures such as chemical vapor deposition by providing a pathway toward highly ordered, nanostructured arrays of  $\pi$ -conjugated oligomers from solution (*vide infra*).

The most successful contributions from the field of polymer science aiming at preparing hierarchically structured polymers have resulted from a transfer of the “foldamer” concept<sup>8–10</sup> to the world of high molecular weight polymer materials. These polymers comprise interactions between “sticky sites” in the side chains of non-adjacent repeating units which serve to induce the formation

of stable folded conformations due to cooperative intrachain supramolecular interactions and, thus, mimic the folding mechanism observed in biopolymers (*vide infra*).

Based on the opinion that the preparation of hierarchically structured optoelectronically active materials will impossibly be achieved by approaching the problem from a distinct research area, this thesis aims at the development of a holistic approach that makes use of the advantages of modern organic chemistry, polymer science as well as supramolecular chemistry. The introduction aims to provide the background information from different fields, such as the “supramolecular” as well as the “foldamer” approach, and the supramolecular self-assembly of short oligopeptides, their polymer conjugates as well as amyloid proteins, which inspired the molecular design of the macromonomers investigated in this thesis. Thereafter, a rationale for choosing poly(diacetylene) as the  $\pi$ -conjugated backbone will be given that led to the successful preparation of well-defined, soluble  $\pi$ -conjugated polymers with predictable multi-stranded, multiple-helical quaternary structures exhibiting a rich folding behavior that finds analogies only in the realm of biopolymers.

### 1.1.2 Supramolecular Approaches Towards Optoelectronic Materials

Supramolecular chemistry, defined as the “chemistry beyond molecules” by Jean-Marie Lehn,<sup>11,12</sup> has enriched the chemical toolbox tremendously. The supramolecular self-assembly of monodisperse oligo(phenylene vinylene)s (OPV), for instance, led to the formation of interesting  $\pi$ -conjugated organic materials for the fabrication of organic electronic devices.<sup>7</sup> Usually, such  $\pi$ -conjugated oligomers were processed by chemical vapor deposition,<sup>13</sup> giving rise to highly ordered domains and, consequently, superior optoelectronic properties due to their well-defined chemical structure. These methods are, however, inferior to solution processing when it comes to larger devices in terms of costs.<sup>14</sup> With the self-organization of OPV in solution, a pathway toward highly ordered, nanostructured arrays of  $\pi$ -conjugated oligomers could be provided that makes use of the more convenient solution-processing techniques.<sup>6</sup> In a particularly interesting recent example reported by Meijer *et al.*, OPV equipped with nucleobases were co-assembled with complementary oligonucleotides leading to the formation of right-handed helical fibrillar aggregates, as could be proved by scanning force microscopy (SFM) imaging and circular dichroism (CD) spectroscopy (Figure 2A).<sup>15</sup> The mutual dependence of the complementary hydrogen-bonding partners became clear when the concentration of one component was changed or a non-complementary oligonucleotide was used. Another approach towards a helical assembly of OPV utilized a foldamer based on the ureidophthalimide motif to which chirally substituted OPV were attached as the side chains and organized into six blades helically twisted around the foldamer backbone (Figure 2B).<sup>16</sup> The secondary structure formation of the polymers due to the self-assembly of the side chains was dependent first on the molecular weight

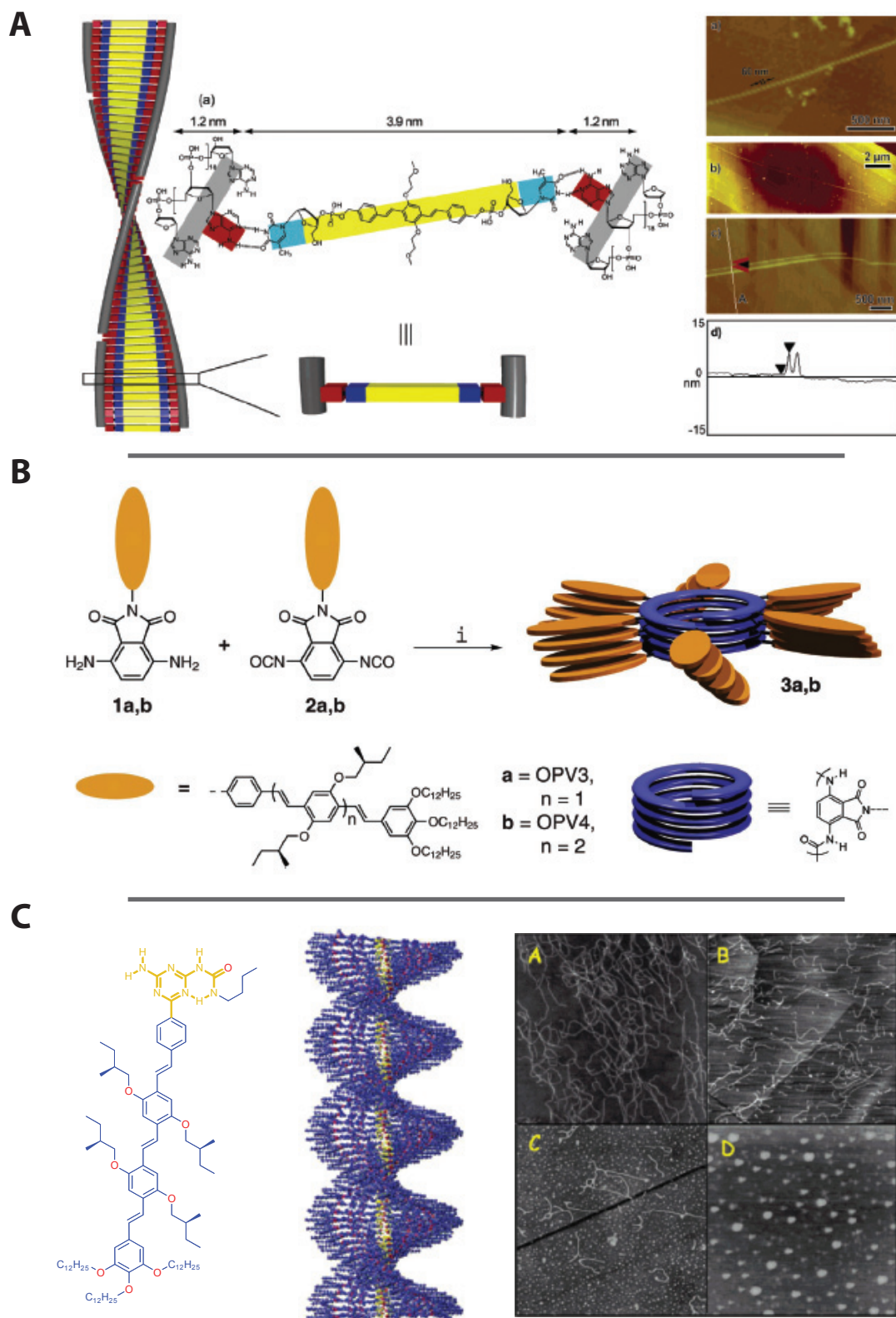


**Figure 2:** A) Structural model and SFM images of nucleobase-equipped OPV co-assembled with oligonucleotides. B) Phthalimido-based OPV foldamer attaining a six-folded helix. C) Model and SFM images of supramolecular aggregates of an oligo(phenylene vinylene) carrying a head group capable of hydrogen-bonding. Images reproduced from [15], [16] and [17].

(i. e., a minimum number of repeat units was necessary to allow for the formation of at least one full helix turn) and, secondly, on the solvents that were used, as evidenced by CD spectroscopic investigations. Likewise, chiral OPV with terminal ureido-*s*-triazine units were observed to form dimers via quadruple hydrogen-bonding which further organized into helical columnar structures by  $\pi$ - $\pi$  stacking (Figure 2C).<sup>17,18</sup> This hierarchical structure formation in solution was, again, solvent-dependent and it was, thus, possible to transfer the helical structures to surfaces under the right conditions, i. e., choice of solvent, concentration as well as temperature. Similarly interesting materials were obtained from molecules comprising a perylene bisimide dye hydrogen-bonded to two OPV units, which can be regarded as donor-acceptor-donor dye arrays, were shown to exhibit photoinduced electron transfer capabilities, and gave rise to fibrillar features suitable for the manufacturing of semi-conducting devices.<sup>19,20</sup>

Another class of  $\pi$ -conjugated oligomers that have been extensively studied in recent years concerning their self-assembly are the oligo(thiophene)s (OT). The latter are interesting organic semiconductors if well-ordered phases can be achieved.<sup>21</sup> Thus, OT with chiral oligo(ethylene oxide) side chains were investigated and found to give rise to chiral superstructures in polar organic solvents such as *n*-butanol.<sup>22-26</sup> The formation of right-handed helical aggregates was driven mainly by  $\pi$ - $\pi$  stacking interactions that were broken at elevated temperatures. The processing, i. e., the fabrication of monolayers, could be achieved from solution. In order to enhance the self-assembly of a series of quater-, quinque-, and sexithiophenes, Shinkai *et al.* attached two cholesteryl amides to both ends of the OT and, in this way, obtained efficient organogelators.<sup>27</sup> The gels were stabilized by networks of fibrillar features, as could be shown by transmission electron microscopy (TEM). An interesting thermochromism was observed that was attributed to a change in conjugation length upon aggregation during the sol-gel transition. OT have also been incorporated into block copolymers with poly(ethylene oxide)<sup>28-32</sup> or poly(styrene),<sup>33-35</sup> giving rise to ordered nanoscopic domains when processed from selective solvents. These phenomena were proved by UV-vis as well as fluorescence spectroscopic investigations that clearly indicated an aggregation of the OTs by  $\pi$ - $\pi$  stacking interactions.

### 1.1.3 Polymer Science and Hierarchically Structured Materials

The examples given above highlight the power of a combined approach of, in this case, supramolecular self-assembly and organic chemistry leading to well organized, hierarchically structured, optoelectronically active materials from monodisperse  $\pi$ -conjugated oligomers. An interesting alternative to these systems are  $\pi$ -conjugated polymers because they would offer the advantage of being solution-processible, e. g., by ink-jet printing methodologies.<sup>36</sup> The relatively low degree of inter-

nal order and purification issues such as the complete removal of transition metal catalysts that are typically applied during the preparation of the conjugated polymers, often lead to inferior electronic properties, e. g., in terms of charge carrier mobility.<sup>37</sup> The first aspect may be solved if hierarchically structured conjugated polymers were available, making investigations toward such structures an attractive research goal.

On the field of conventional (i. e., non-conjugated) polymer synthesis, the goal of hierarchical structure formation has been achieved most successfully when the concept of “foldamers” was transferred to the world of high molecular weight polymer materials.<sup>8–10</sup> The introduction of helicity to polymer backbones such as poly(olefin)s or poly(methacrylate)s, is also observed whenever the tacticity of the polymers is well-controlled and, at the same time, sterically demanding side chains are attached to every repeat unit which hinder the free rotation around the backbone bonds.<sup>38</sup> However, the higher structure formation in foldamers has a completely different origin. Here, the side chains contain “sticky sites”, and interactions between the latter in non-adjacent repeating units induce the formation of stable folded conformations due to cooperative intrachain supramolecular interactions. Thus, the folding mechanism mimics related processes in biopolymers such as proteins.

Nolte and Cornelissen *et al.* provided a particular beautiful example, reporting on the preparation of oligopeptide substituted poly(isocyanide)s (Figure 3A).<sup>39,40</sup> These polymers attained a stable tertiary structure, i. e., a  $4_1$ -helical backbone stabilized by oligopeptide side chains that were aligned in four “blades” of helically twisted  $\beta$ -sheet arrays, as could be evidenced by NOESY NMR and other techniques. Depending on the length and configuration of the oligopeptide residues, the isocyanide monomers were shown to preorganize efficiently in solution, such that the formation of extremely high molecular weight polymers occurred upon the addition of a strong acid such as trifluoroacetic acid (TFA) whereas, typically, a nickel catalyst was needed for the polymerization.<sup>41,42</sup> Furthermore, the preparation of block copolymers containing charged poly(isocyanide) and poly(styrene) segments was reported by the same authors. These were found to form so called “superamphiphiles” that spontaneously self-assembled into a large variety of interesting superstructures like superhelices, vesicles and micellar rods in aqueous solution depending on the pH (Figure 3B).<sup>43</sup> Not less interesting was an investigation of block copolymers of poly(isocyanide)s with poly( $\gamma$ -benzyl-L-glutamate) segments.<sup>44</sup> It could be shown that the polypeptide polymer segment attained an  $\alpha$ -helical conformation while the second block was also helical due to the parallel  $\beta$ -sheet formation of the oligopeptide side chains. This accumulation of controlled secondary structure formation was completely unprecedented in the realm of synthetic polymer architectures.

The above examples highlight the achievements of modern polymer chemistry in terms of a controlled higher structure formation. However, the particular synthetic requirements in the prepara-



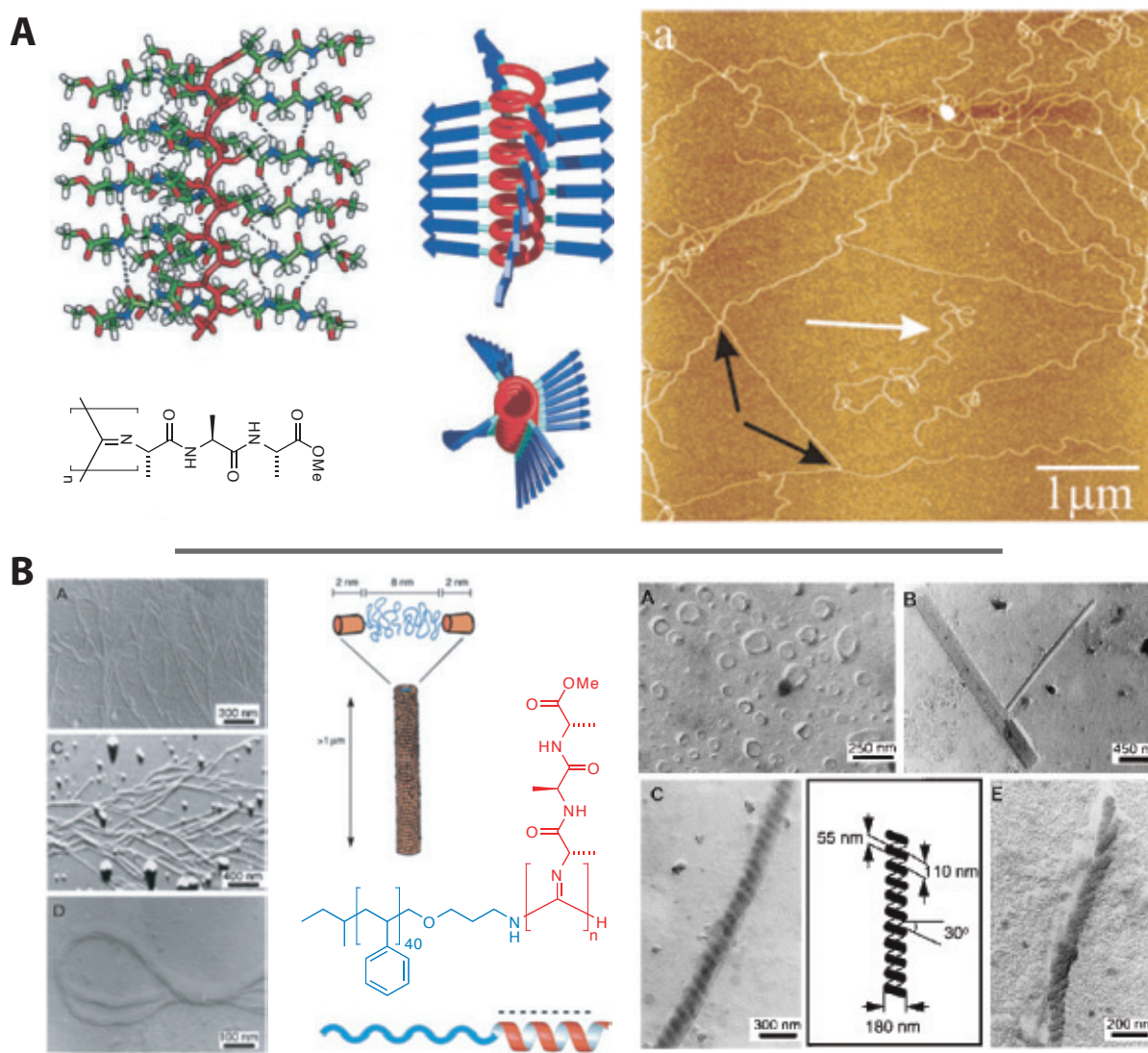


**Figure 3:** A) Structural model of a poly(isocyno dipeptide) foldamer, and an SFM image of the polymers obtained with acid initiators. B) "Superamphiphile" aggregates from poly(styrene)-poly(isocyanide) block copolymers PS<sub>40</sub>-b-PIAA<sub>20</sub> (left) and PS<sub>40</sub>-b-PIAA<sub>10</sub> (right). Images reproduced from [39], [40] and [41].

tion of *conjugated* polymers have severely limited the number of similarly hierarchically structured materials so far.

Pu *et al.* reported different types of conjugated polymers with fixed main chain chirality containing binaphthyl units in their backbone which exhibited very interesting optoelectronic activity (Figure 4). Thus, they were able to construct a light emitting diode using one of their oligothiophene based polymers, while an oligo(phenylene ethynylene) derived material was used as an enantioselective fluorescent sensor. Furthermore, an enhanced nonlinear optical response of the polymers could be achieved by exchanging the hexyloxy chains at the binaphthyl units with nitro- as well as alkylamino groups to generate a "push-pull" effect.<sup>45–51</sup>

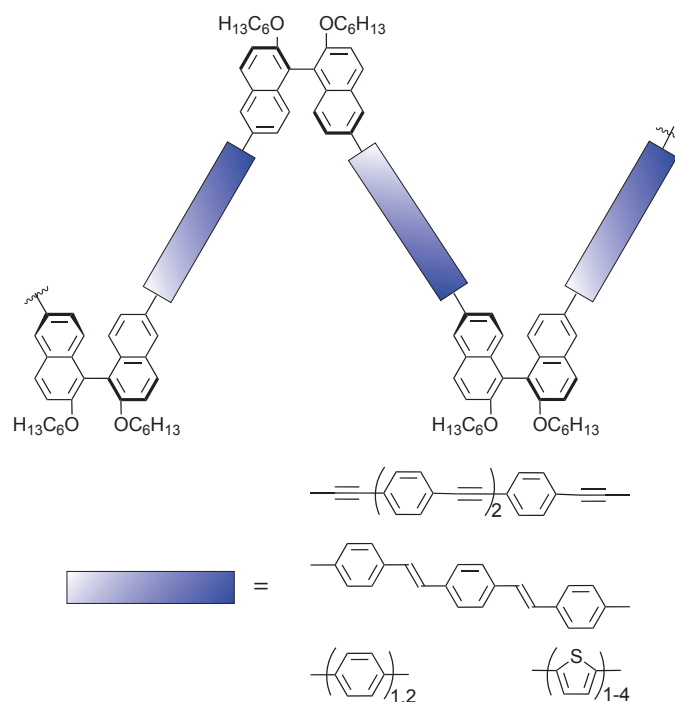


**Figure 4:** Different binaphthyl based helical conjugated polymers containing various  $\pi$ -conjugated spacers such as oligophenylenes, oligothiophenes, oligo(phenylene vinylene)s or oligo(phenylene ethylene)s were reported by Pu *et al.*<sup>45</sup>

Meijer *et al.* did not only investigate superstructures formed by oligothiophenes (*vide supra*) but were also interested in the polymeric materials.<sup>52–56</sup> They found that chirally substituted poly(thiophene)s formed non-aggregated helical superstructures in (aqueous) solution, as could be evidenced by the characteristic UV and CD spectra. Especially the water-soluble derivatives were proposed as biosensing materials.<sup>56</sup>

Another class of highly interesting conjugated polymers are the poly(phenyl acetylene)s that have been described by Okamoto and coworkers.<sup>38,57,58</sup> They reported on *per se* non-chiral, carboxylic acid functionalized poly(phenyl acetylene)s that attained an excess helicity upon supramolecular interactions with chiral additives such as amino acids or amino alcohols. Furthermore, their helix sense could be switched by using the enantiomeric forms of the additives.

The most extensive investigations in the field of  $\pi$ -conjugated foldamers has been carried out by Masuda and coworkers who studied various types of poly(acetylene) derivatives. Thus, they investigated the polymerization of *N*-propargyl amides which they found to proceed with high *cis*-stereoselectivity.<sup>59–63</sup> The rigidity of the obtained polymers increased upon the incorporation of homochiral side chains, and the chiral polymers exhibited a large optical rotation with opposite sign as compared to the monomers, as well as a strong CD effect for the main-chain chromophore. The authors attributed these observations to the presence of stable folded conformations due to cooper-

ative intramolecular hydrogen-bonding. They also investigated related functionalized polymers and typically observed a complex temperature, solvent, and pH dependent helicity.<sup>64,65</sup>

Masuda *et al.* also reported on the related polymerization of chiral and achiral alkyl poly(propargyl carbamate)s,<sup>66</sup> G2 lysine dendron functionalized phenyl acetylenes,<sup>67</sup> and P-chiral *N*-propargyl phosphonamides.<sup>68,69</sup> Furthermore, an attempt toward a photoswitchable poly(acetylene) was undertaken using glutamic propargyl amide that was equipped with azobenzene side chains. However, the UV irradiation needed for the switching only led to a decrease in helicity, as judged from the CD spectra, which did not recover upon the reisomerization of the diazo group.<sup>70,71</sup>

More recently, Tang *et al.* performed similar investigations on L-valine-substituted phenyl acetylenes<sup>72-74</sup> which they obtained by a rhodium-catalyzed reaction. The products attained helical conformations in solution that could be influenced by the choice of solvent or the addition of a base to a polymer with free carboxylic acid side chain residues. Helical poly(phenyl acetylene)s could also be prepared by introducing three (a)chiral alkyloxy chains in positions 3, 4 and 5 of the phenyl ring.<sup>75</sup> These “G1 dendrons”, as they were referred to by the authors Percec and Meijer *et al.*, induced a dynamic (homochiral) helicity, as was judged from temperature dependent CD measurements as well as X-ray analyses on oriented films that allowed to distinguish different helix diameters indicating different helical packings.

#### 1.1.4 “Self-Assemble, then Polymerize” – A Complementary Approach

The preceding examples of hierarchically structured synthetic polymers all share one crucial characteristic in that they have been prepared using the same general approach which can be described as “polymerize, then fold into a hierarchical structure”. In other words, the “foldamer approach” firstly depends on a well-defined polymerization procedure, while the folding into higher structures occurs only afterwards. However, it is worth noting that the control over the polymer primary structure which can be achieved even with modern polymerization methods is inherently poor, for instance, in terms of regioselectivity and stereospecificity of monomer incorporation. Starting from such preconditions, an efficient and defect-free folding into a well-defined final conformation is hard to achieve. For example, a low degree of tacticity would lead to stereochemical defects irreversibly incorporated into the polymer, prompting the subsequent folding to fail or produce defective structures.

Alternatively, a complementary strategy can be envisioned in which the sequence of events is reversed (Figure 5). Such a strategy may be paraphrased as “self-assemble into a hierarchical structure, then polymerize” and would require the preparation of appropriately functionalized macromonomers which are supposed to first self-assemble into uniform supramolecular polymers<sup>76</sup>

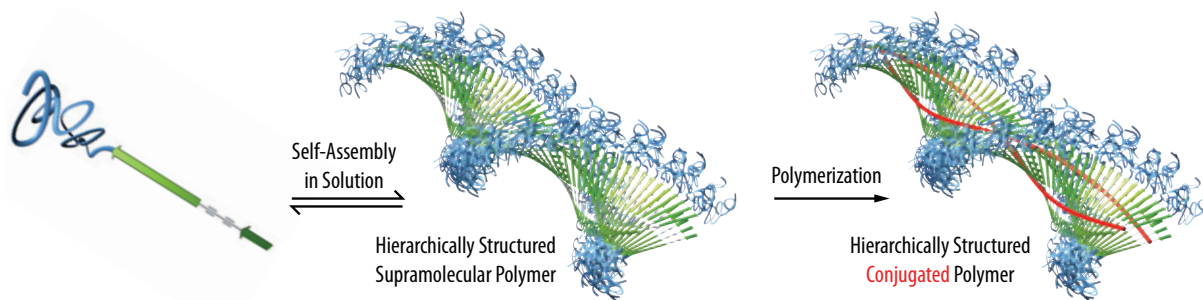


**Figure 5:** Conceptual sketch of the sequence of events in the proposed “self-assemble into a hierarchical structure, then polymerize” methodology. First, the macromonomers equipped with an appropriate supramolecular synthon form hierarchically structured supramolecular polymers by self-assembly in solution and, secondly, these structures are converted into  $\pi$ -conjugated polymers under retention of the previously attained structure.

with a defined, finite number of strands in solution. A propensity to the formation of hierarchical structures should already be present at this stage of the process, whereas an ill-defined assembly into micellar or one-dimensional vesicular aggregates should be suppressed or completely excluded. In the final step, the supramolecular polymers would then be converted into functional, possibly multi-stranded,  $\pi$ -conjugated polymers under retention or, at least, controlled conversion of their previously assembled hierarchical structure.

Such a complementary general strategy would, hence, combine several advantageous concepts like the supramolecular preorganization of monomers prior to polymerization<sup>42,77</sup> and covalent capture as a versatile concept for the fixation of supramolecular materials.<sup>78</sup> The former characteristic displays a crucial advantage over the “foldamer approach” since the self-assembly process is dynamic in nature and, thus, allows for a “self-healing” of the formed structures such that defects can be corrected. Furthermore, the overall hierarchical structure formation may be influenced by external stimuli such as solvent quality, temperature or the presence of other reagents *prior* to the covalent fixation. The transformation into covalently linked polymers, on the other hand, will inevitably be accompanied by geometric changes in the architecture of the structures that must not endanger the integrity of the self-assembled hierarchical structures. For the realization of this concept, some prerequisites will have to be fulfilled:

- Most importantly, a reliable supramolecular synthon<sup>79</sup> is needed that fosters the formation of uniform supramolecular polymers with a defined, finite number of polymer strands.
- These supramolecular polymers must show a predictable or, at least, rationally explicable propensity to form higher-order structures in solution.
- The repeating units of the supramolecular polymers and their polymerizable functions need to be arranged in a well-defined manner such that individual strands of the supramolecular polymers are unambiguously converted into single covalent polymer backbones.

- The applied polymerization methodology must be performed under conditions compatible with the self-assembly process and *vice versa*.
- The formation of the covalent polymer backbone should proceed under retention or, at least, controlled conversion of the previously self-assembled hierarchical structures; this requires, in particular, the structural constraints and consequences of the covalent capture process to be commensurate with the placement of the polymerizable functions in the self-assembled aggregates.

Resulting from an evaluation of the above requirements and an assessment of our research goal, i. e., the preparation of hierarchically structured polymers with  $\pi$ -conjugated backbones, we have chosen macromonomers based on  $\beta$ -sheet-forming oligopeptide-polymer conjugates as the supramolecular synthon and the UV-induced topochemical diacetylene polymerization<sup>80,81</sup> as the methodology for the covalent capture. This polymerization technique appeared to be highly appropriate because it is atom-efficient, initiator- and catalyst-free and it, furthermore, proceeds with high stereo- and regiospecificity way in the sense of a *trans*-stereospecific 1,4-polyaddition.<sup>80,81</sup> Additionally, the obtained poly(diacetylene)s are interesting  $\pi$ -conjugated, photoconductive polymers that are known to, e. g., undergo color transitions upon external stimuli (*vide infra*). The polymerization is possible whenever diacetylenes are placed at an appropriate distance and packing angle. As will be shown in the following sections,  $\beta$ -sheet-forming oligopeptide-polymer conjugates are reliable supramolecular synthons that were shown to form uniform nanoscopic aggregates. The latter often exhibit the propensity to form hierarchical structures in solution which can be well-rationalized in some cases.<sup>82-84</sup> Furthermore, the packing distance between adjacent  $\beta$ -strands within a single  $\beta$ -sheet is very close to the ideal geometric requirements of the topochemical diacetylene polymerization which made both systems appear mutually compatible in the sense of the general requirements formulated above.

## 1.2 Hierarchical Structures From Oligo- and Polypeptides

### 1.2.1 Self-Assembly of Amyloid Proteins

Since we chose  $\beta$ -sheet forming oligopeptide segments as the supramolecular synthon in our strategy towards hierarchically structured polymers, which are one of nature's most commonly applied motifs for self-organizing molecules into defined materials, a closer look at their appearance in biological systems seems to be a suitable starting point. One well-investigated class of nanostructures that are formed by the self-assembly of  $\beta$ -sheet-forming oligopeptide strands are the fibrous protein

deposits referred to as “amyloids”. They have received increasing attention in recent years because they are assumed to be associated with several severe diseases such as Alzheimer’s, Parkinson’s, and Huntington’s disease, as well as various prion diseases and type II diabetes.<sup>85–88</sup> Their exact role in context with these diseases<sup>85,87</sup> as well as the actual formation mechanism(s)<sup>88</sup> are still a matter of debate, and different, sometimes conflicting structural models have been proposed for specific examples. There is, in fact, no evidence that all examples of amyloid fibrils need to be formed via the same mechanism or that they rely on exactly the same structural elements. By contrast, there are examples of different structure models, and different oligopeptide fragments from the same protein (or even one and the same oligopeptide under different conditions) may self-organize into different types of aggregates.<sup>86</sup> Nevertheless, the formation of amyloid fibrils appears to follow a generic pattern in the sense that (*i*) they are formed from a range of structurally non-related precursor proteins, (*ii*) their internal structure is rich in  $\beta$ -sheet structures, and (*iii*) their nanoscopic morphology is very similar. Thus, typical amyloid fibrils are helically twisted filaments of several micrometers in length and a width on the order of 10 nm. They exhibit a cross- $\beta$ -sheet signature in X-ray diffractograms with a 4.7 Å meridional reflection and a broader equatorial one at a spacing of typically 6–12 Å, which means that their spine structures most likely contain a finite number of stacked (“laminated”) parallel or antiparallel  $\beta$ -sheets aligned in the direction of the fibril axis.<sup>89,90</sup>

In a number of important examples,<sup>91–98</sup> such as protofilaments from the full length amyloid protein A $\beta$  associated with Alzheimer’s disease,<sup>91–93</sup> the yeast prion proteins Sup35p<sup>94</sup> and Ure2p,<sup>95,96</sup> or human amylin associated with type II diabetes,<sup>97</sup> the presence of stacked parallel, in-register (not laterally displaced)  $\beta$ -sheets, has recently been conclusively established. In these specific examples, the terminal region of the precursor protein is folded into serpentine structures of  $\beta$ -strands which then aggregate into parallel, in-register  $\beta$ -sheet structures such that the stacked  $\beta$ -sheets have an alternating  $\beta$ -strand directionality (Figure 6A-C).

A somewhat different model has been proposed for fibrils from insulin<sup>98</sup> where the three disulfide bonds place constraints on the molecular structure of the fibrils. Here, the two oligopeptide chains of the insulin molecule are assumed to rearrange their conformation and stack in a way that they form a pair of parallel  $\beta$ -sheets with opposite  $\beta$ -strand directionality which then further self-assemble into a variety of entwined fibrils (Figure 6D-F). In other cases, parallel  $\beta$ -helix spine structures have been proposed,<sup>99–101</sup> and it appears that, until to date, antiparallel  $\beta$ -sheets have only been demonstrated in amyloid-like fibrils from relatively short oligopeptides composed of 15 residues or less.<sup>86</sup> Interestingly, the somewhat surprising prevalence of parallel  $\beta$ -sheet structures has recently been correlated with the presence of specific amino acid sequences.<sup>102,103</sup> For example, the oligopeptide GlyAsnAsnGlnGlnAsnTyr **1** in the  $\beta$ -sheet forming domain of the yeast prion protein Sup35p

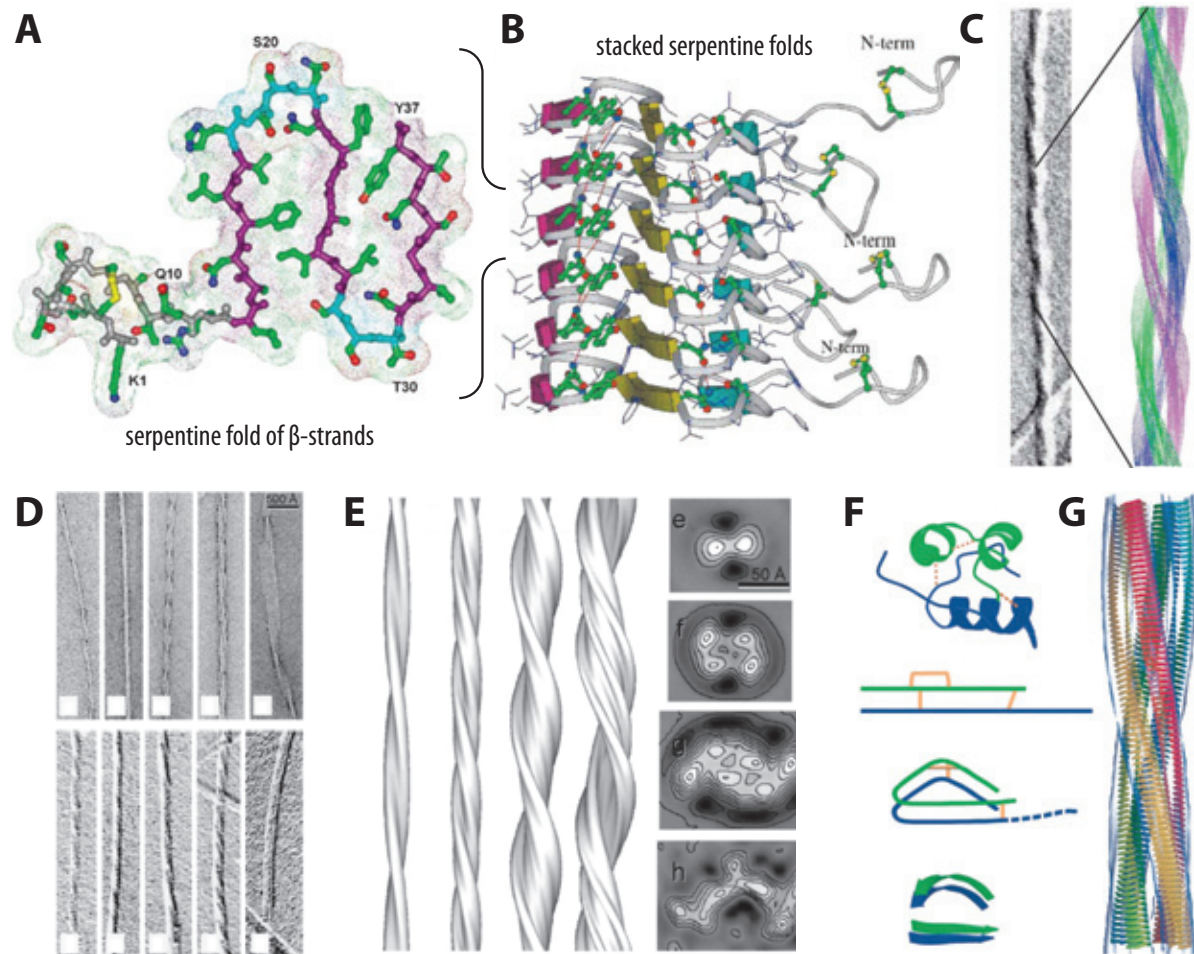


**Figure 6:** Representative examples of TEM images and proposed structural models for amyloid fibrils from *A-C*) human amylin and *D-F*) insulin; *A*) proposed serpentine fold with three  $\beta$ -strands from human amylin; *B*) protofilament model showing a stack of these serpentine folds; *C*) electron micrograph of a human amylin fibril (shadowed) and a model consisting of three entwined protofilaments; *D*) a variety of negatively stained (top) and shadowed (bottom) left-handed helical filaments from insulin; *E*) surface representation of 3D maps and contoured density cross-sections of these insulin filaments; *F*) the native conformation of the two insulin chains (green, blue) can be rearranged into two pairs of parallel  $\beta$ -strands which stack to form the protofilaments; *G*) a model of three entwined protofilaments overlaid with a TEM density map (transparent gray surface). Images reproduced from [98] and [99].

has been shown to form tight pairs of parallel, in-register  $\beta$ -sheets with opposite strand directionality.<sup>102</sup> The dimerization proceeds under complete exclusion of solvent molecules and is based on both the self-complementary topology of the resulting  $\beta$ -sheet surfaces and the presence of the Asn and Gln side chain amide groups as, likewise, self-complementary hydrogen-bond donors and acceptors (Figure 7). These are arranged in such a way that an efficient interstrand, intrasheet hydrogen-bonding can only be realized in case of a parallel, in-register  $\beta$ -strand orientation within the  $\beta$ -sheets. This structural motif has been termed a “dry steric zipper”, and a whole range of related structures have recently been described and associated with amyloid fibril formation.<sup>103</sup>

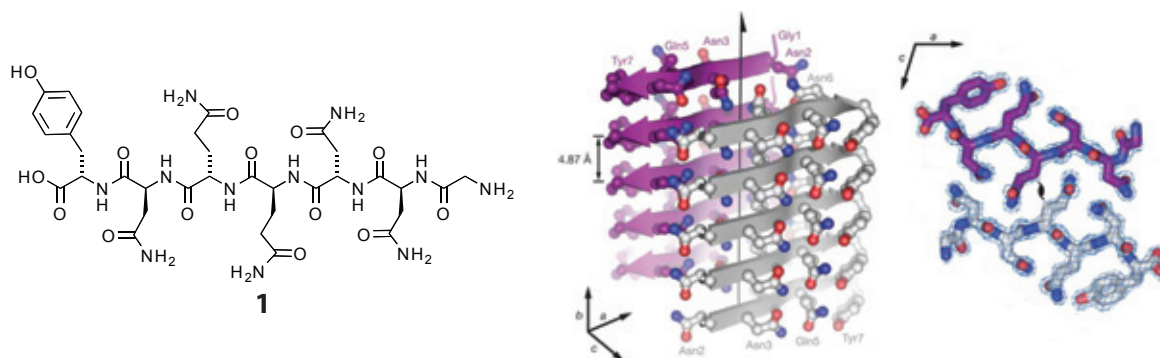


**Figure 7:** Crystal structure of the dry steric zipper motif observed in fibrils of the oligopeptide **1** from the spine structure of the yeast prion protein Sup35p; a pair of parallel  $\beta$ -sheets (gray, purple) forms under exclusion of solvent due to self-complementary topology (compare cross-section on the right) and hydrogen-bonding sites in the side chain amides. Images reproduced from [103].

Looking at the process of amyloid fibril formation with the eyes of a polymer chemist and leaving aside both the diversity and complexity of biological structures for a moment, an analogy to rod-coil block copolymers comes to mind. It looks like the prerequisite for the formation of well-defined, high aspect ratio filaments relies on some sort of “phase segregation” between, on one side, the  $\beta$ -strands as relatively short, monodisperse, and preorganized crystallizable segments and, on the other side, the connecting turns and loops as well as the remainder of the proteins, all of which create a “soft shell” around the filaments. In the case of Ure2p, for example, the protein retains its native activity even after fibrillization. It has been proposed that the protofilament spines are just formed from a small segment and that the major part of the protein remains in its native conformation, “dangling at the edges” of the filaments. It may seem trivial to state that the crystallization of the former is the driving force for fibrillization for which reason it may not come as a surprise that proteins with relatively disordered terminal domains constitute an important family of amyloidogenic proteins. However, a less obvious conclusion is that the soft shell around the crystalline core also plays a crucial role in that it helps to provide sufficient solubility to allow for a fast aggregation into well-defined, high aspect-ratio, one-dimensional aggregates and prevents the premature precipitation of large polycrystalline assemblies. Of course, the obtained fibrils are, ultimately, completely insoluble. This and the fact that comparably large oligopeptide segments have to be appropriately folded as the first step of self-assembly probably render amyloid based systems themselves too complex to be utilized as supramolecular scaffolds in synthetic chemistry. However, it would be a sufficient simplification if short, linear oligopeptides were utilized to form  $\beta$ -sheets, and synthetic polymer segments were employed in order to take over the role of the globular domains attached to the fibrils’ core. These may even enhance phase segregation and provide improved solubility in a larger range of protic or aprotic solvents.



### 1.2.2 Self-Assembly of Synthetic Oligopeptides and Peptidomimetics

The interest in the formation of amyloid fibers has inspired the preparation of short peptidomimetics aimed at mimicking and understanding the corresponding self-assembly processes. For instance, Kelly *et al.* investigated the peptidomimetic molecule **2** comprising of two (Val-Thr)<sub>2</sub> tetrapeptides equipped with ionogenic *N,N*-dimethyl-ethylenediamine residues that were connected to a dibenzofuran moiety to enforce an interdigitated antiparallel  $\beta$ -sheet arrangement of the oligopeptides.<sup>104</sup> Depending on different parameters such as concentration, pH, ionic strength and incubation time, these building blocks gave rise to various fibrillar aggregates (Figure 8) by the formation of intermolecular  $\beta$ -sheets, as evidenced by imaging and spectroscopic techniques.

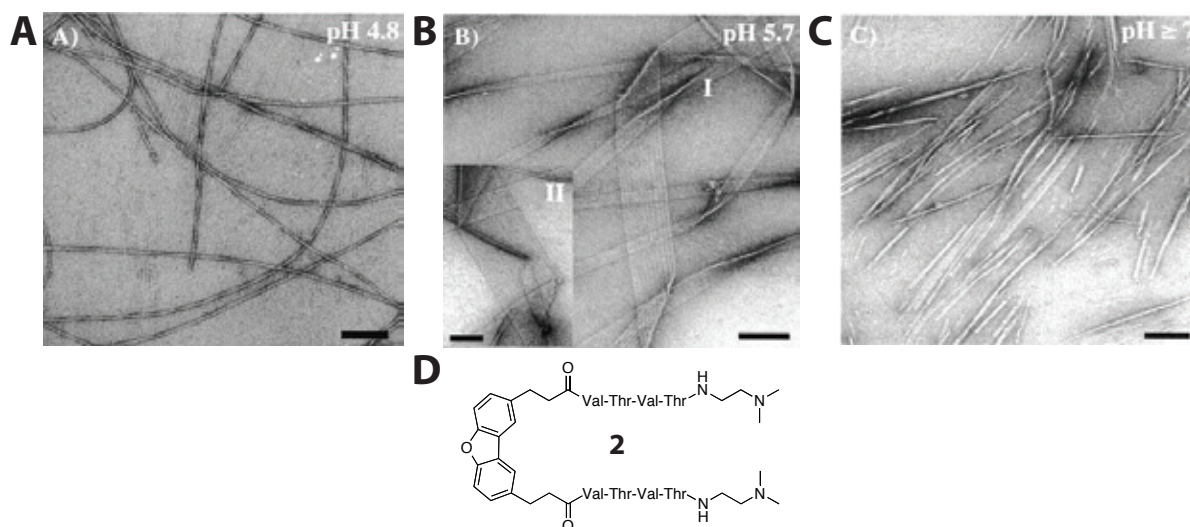


**Figure 8:** A variety of quaternary structures was found for the self-assembly of **2** depending on the pH and the incubation time. A) pH = 4.8, 2 weeks incubation time; B) pH = 5.7, 3 months incubation time; C) pH = 7.0, 2 weeks incubation time. The scale bars represent 100 nm. Images reproduced from [104].

A similarly reliable formation of fibrillar features from  $\beta$ -sheet-forming oligopeptides has recently been used even in the context of a materials science application. Thus, the N-terminal and middle region of the amyloidogenic yeast protein Sup35p already mentioned above has been prepared, self-assembled into fibers and used as a scaffold to deposit gold particles.<sup>105</sup> It was possible to produce metal fibers with diameters of several hundred nanometers which could be positioned between two electrodes and were shown to exhibit an ohmic conductivity behavior indicative of a continuous metal deposition.

A very important contribution to the understanding of the self-organization of short, linear oligopeptides into  $\beta$ -sheets and higher structures has been provided by Boden and coworkers who thoroughly investigated the hierarchical self-organization of different oligopeptides.<sup>82–84,106,107</sup> Starting

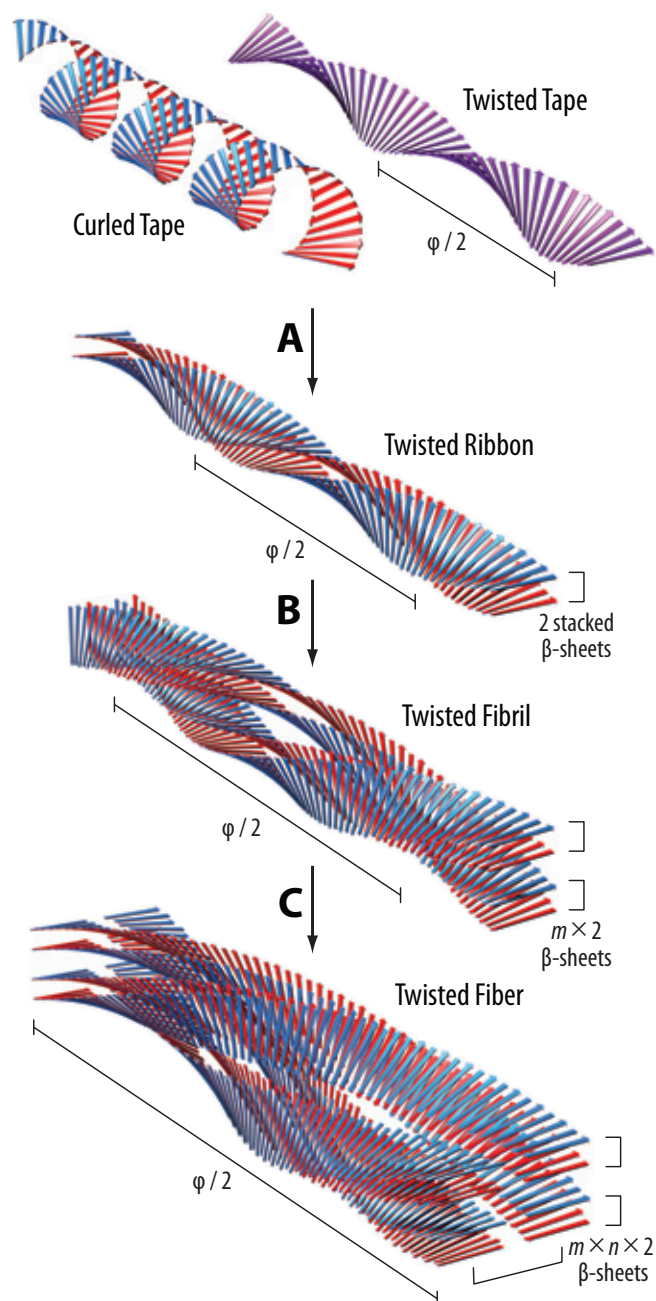


**Figure 9:** Schematic summary of Boden's model for the step-wise hierarchical selforganization of oligopeptides in protic media; *A*) depending on the amino acid sequence, oligopeptides will aggregate into single  $\beta$ -sheet tapes with different helical superstructures; *B*) amphiphilic tapes will dimerize into ribbons via  $\beta$ -sheet stacking, hiding the more solvophobic surfaces; *C*) ribbons may further stack into fibrils which can further aggregate into fibers via edge-to-edge attraction.

from the 24-residue peptide K24,<sup>84,106</sup> which had been prepared in analogy to the  $\beta$ -sheet forming transmembrane domain of a protein, data from wide-angle X-ray diffraction, IR- as well as CD spectroscopy revealed that in solutions of methanol or 2-chloroethanol K24 self-assembled predominantly via the formation of antiparallel  $\beta$ -sheet structures, leading to a macroscopic gelation of the solvents already at low peptide concentrations. TEM measurements proved the existence of one-

dimensional tape-like objects exhibiting a width of 6.6 to 8.1 nm which was in very good agreement with the extended length of one molecule. Rheological investigations of the obtained organogels revealed that the tapes had a monomolecular thickness and that the lower limit of the persistence length was around 13 nm, indicative of a moderately stiff polymer. These investigations led to the *de novo* design of the 11-residue oligopeptides DN1,<sup>84,106</sup> P<sub>11</sub>-1 and P<sub>11</sub>-2<sup>82,83,107</sup> that acted as gela-tors in very polar (aqueous) solvents. These oligopeptides were designed to aggregate strictly via the formation of antiparallel  $\beta$ -sheets. However, the amino acid sequence was chosen such that P<sub>11</sub>-1 had a comparably lower amphiphilic character, i. e., P<sub>11</sub>-2 featured an alternating sequence of hydrophilic and hydrophobic amino acids, leading to strongly amphiphilic  $\beta$ -sheet surfaces. TEM investigations on both systems revealed distinct differences in the mode of self-assembly, leading to different nanoscopic structures. P<sub>11</sub>-1 formed left-handed helically curled tapes with a pitch of approximately 30 nm, whereas the amphiphilic nature of P<sub>11</sub>-2 induced the formation of ribbons (double tapes) by a face-to-face association of the hydrophobic sides of the molecules in the aqueous environment (Figure 9). These ribbons had a “twisted” as opposed to a “curled” helical fine structure and were found to form tetrameric twisted fibrils upon prolonged storage in solution. These fibrils further assembled into fibers that could be described as dimeric fibrils or octameric ribbons.

Based on these experimental findings, Boden, Fishwick *et al.* developed a remarkably intuitive generalized model (Figure 9) that explained the observed hierarchical structure formation.<sup>82</sup> As a first step, the  $\beta$ -strands attain a chiral rod conformation, exhibiting a right-handed helical twist that found its origin in the L-chirality of the natural amino acids. This enabled the self-assembly of the oligopeptides into single antiparallel  $\beta$ -sheet tapes with different left-handed helical superstructures, depending on the nature of the tapes' surfaces. For instance, the tapes formed by P<sub>11</sub>-1 tended to “curl” into tubular left-handed helices in order to hide the comparably more hydrophobic surface inside. Alternatively, the formation of ribbons (double tapes) via a stacking of  $\beta$ -sheets as observed for P<sub>11</sub>-2 led to structures exposing only hydrophilic surfaces to the environment. These ribbons underwent further  $\beta$ -sheet stacking via their more hydrophilic surfaces to yield fibrils; and the latter may, finally, form fibers via an edge-to-edge attraction.

The most important implication of this model is that distinct types of supramolecular interactions with significantly different energies are associated with each level of self-organization.<sup>82</sup> The self-assembly into single  $\beta$ -sheet tapes occurs due to N–H $\cdots$ O=C hydrogen-bonding. By contrast, both the  $\beta$ -sheet stacking of tapes into ribbons via the more hydrophobic  $\beta$ -sheet surfaces as well as the subsequent stacking of ribbons into fibrils via the more hydrophilic surfaces will depend on the chemical nature and the topology of the involved surfaces and may be mediated by diverse kinds of interactions, e. g., hydrogen-bonding, electrostatic, van der Waals, or repulsive steric interactions.

However, the initial ribbon formation process is expected to be significantly supported by the hydrophobic effect in aqueous media and will, typically, be substantially more favorable than the formation of fibrils. Finally, fiber formation will strongly depend on the exact chemical nature of the  $\beta$ -sheets' edges and, again, be significantly less favorable than the other processes. In conclusion, the distinct levels of self-organization are associated with what may be regarded as an orthogonal set of interactions, all of which may be addressed individually by changing the molecular structure or the chemical environment.

Secondly, it is the inherent helical twisting of  $\beta$ -sheet-based fibrillar aggregates on all levels of self-organization which is the main factor responsible for the formation of uniform one-dimensional aggregates with a defined and finite number of laminated  $\beta$ -sheet tapes.<sup>82</sup> The observed helical pitch  $\psi$  of the final aggregate is a mere compromise in order to maintain the N-H $\cdots$ O=C hydrogen-bond connectivity between all amino acid residues in all  $\beta$ -strands of all incorporated  $\beta$ -sheet tapes. Thus, increasing the number of laminated tapes must lead to an unwinding of the helical twist until it completely disappears in a whole layer of infinitely stacked  $\beta$ -sheets. Likewise, increasing the length of the constituent oligopeptide  $\beta$ -strands will result in a decreased  $\beta$ -sheet twisting. Assuming that there is an optimal degree of twisting for individual  $\beta$ -strands of a given length and chemical structure, the unwinding process must be associated with an elastic energy penalty which counteracts and, at a certain point, compensates the enthalpy gain associated with  $\beta$ -sheet stacking, prohibiting an "unlimited"  $\beta$ -sheet lamination.

In summary, it is the interplay of the significantly different aggregation enthalpies on the distinct levels of self-organization combined with the energetic penalty associated with readjusting the helix geometry upon aggregation that controls the formation of well-defined aggregates with a finite number of laminated tapes and, consequently, a finite diameter. The result is a uniform thermodynamic equilibrium structure with a defined, finite number of laminated  $\beta$ -sheets that can be fine-tuned by a judicious choice of the oligopeptide's molecular structure.

The presented model provides elegant explanations for most aspects of the observed oligopeptide self-organization. However, it can not be considered as universal since it completely ignores the formation of parallel  $\beta$ -sheets and the accompanied implications concerning residual dipole moments. The authors limited the scope of their description to an antiparallel arrangement of the oligopeptides since their systems were specifically aimed at this motif. Of course, the assumed antiparallel  $\beta$ -sheet formation implicitly excluded any residual dipole moment component in the  $\beta$ -sheet plane perpendicular to the tapes' axes. Conversely, the assumption of amphiphilic  $\beta$ -sheets implicitly included the presence of dipole moment components perpendicular to the  $\beta$ -sheet plane. Nevertheless, one has to be aware that, for example, the formation of  $\beta$ -sheets with parallel  $\beta$ -strand orientation should re-

sult in a non-zero dipole moment component in the  $\beta$ -sheet plane perpendicular to the tape axis.<sup>108</sup> Likewise, the presence of an odd number of N-H $\cdots$ O=C backbone hydrogen-bonding sites should result in a residual dipole moment component in tape direction.<sup>109</sup> While the latter can straightforwardly be compensated on the ribbon level, it would constitute a non-negligible additional energetic contribution to ribbon formation even in the case of non-amphiphilic  $\beta$ -sheet tapes.

### 1.2.3 Self-Assembly of Oligopeptide-Polymer Conjugates

The above examples serve to highlight that pure oligopeptides are versatile supramolecular scaffolds. Accordingly, also hybrid structures of oligo- as well as polypeptides with synthetic polymers received an increasing attention in terms of materials applications<sup>110,111</sup> and in context with an improved understanding of the origin of neurodegenerative diseases.<sup>85</sup> The attachment of synthetic polymer chains significantly enlarged the scope of the peptides, in particular with respect to the accessible chemical environments, e. g., due to the tunable solubility.<sup>112</sup>

The first thorough investigations on oligopeptide polymer conjugates was performed by Mutter, Toniolo *et al.*<sup>113-117</sup> The authors investigated the self-organization of homologous series of oligo-(L-valine) (1–8 residues) and oligo-(L-alanine) (1–8 and 10 residues) derivatives that were covalently connected to poly(ethylene oxide) (PEO) with an average molecular weight  $\overline{M}_n = 10,000$ . Mostly CD spectroscopic data<sup>113-115</sup> as well as IR studies<sup>116,117</sup> proved that the oligopeptide attained different higher structures such as random coil,  $\alpha$ -helical or  $\beta$ -sheet conformations in aqueous or ethanol solutions, depending primarily on the incorporated number of amino acids, i. e., a minimum of five N-H $\cdots$ O=C hydrogen-bonds was found to be needed for a stable intramolecular  $\beta$ -sheet aggregation. The mode of self-assembly was further influenced by the concentration, solvent, pH or the ionic strength. In the case of the observed  $\beta$ -sheet formation, the presence of tapes could be assumed. However, the limited imaging techniques available at that time did not allow for a direct proof of such higher structures.

The same motif, i. e., an oligopeptide attached to the water soluble PEO, was used twenty years later by Lynn *et al.* who attached the  $\beta$ -sheet forming fragment A $\beta_{10-35}$  of the  $\beta$ -amyloid protein associated with Alzheimer's disease to the corresponding polymer.<sup>118-121</sup> This example is interesting in so far as it allows to directly compare the pure amyloidogenic oligopeptides (*vide supra*) with the related polymer conjugates. Thus, a reversible, pH-dependent aggregation into parallel  $\beta$ -sheet structures was observed which led to the formation of nanoscopic helical fibrillar features similar to the ones obtained from the pure oligopeptide and other amyloidogenic oligopeptides. The obtained superstructures exhibited a diameter of roughly 9 nm, a large superhelical pitch of 110 nm, and were found to consist of six laminated  $\beta$ -sheets. Interestingly, these oligopeptide-PEO conjugates did not

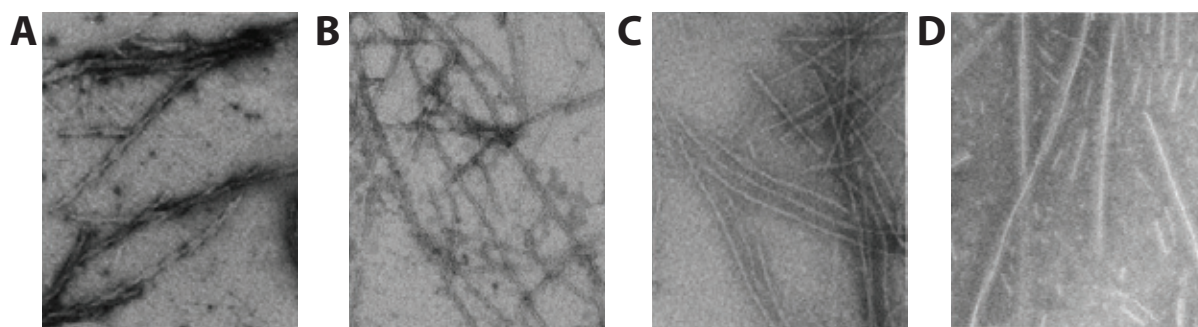


**Figure 10:** Mixtures of the pure oligopeptide  $A\beta$  and its corresponding PEO conjugates comprising A) 0%; B) 33%; C) 50%; D) 100% (w/w) of the conjugates showed an decreasing tendency to form lateral aggregates. Images reproduced from [119].

show any further tendency to form larger aggregates which is fundamentally different to the behavior of the pure oligopeptides and, consequently, no insoluble material was formed (Figure 10). The work presented by Klok, Hamley *et al.* dealing with block copolymers of a monodisperse, amphiphilic oligopeptide and PEO showed a similar behavior.<sup>122</sup> The oligopeptide-polymer conjugates exhibited a hierarchical self-organization that was interpreted in terms of the model presented by Boden *et al.* (*vide supra*). Thus, the oligopeptides first formed helical tapes driven by the formation of antiparallel  $\beta$ -sheets, as evidenced by IR spectroscopy which then further aggregated into defined fibrils. The latter were found to be more stable towards changes of the pH as compared to the pure parent oligopeptide.

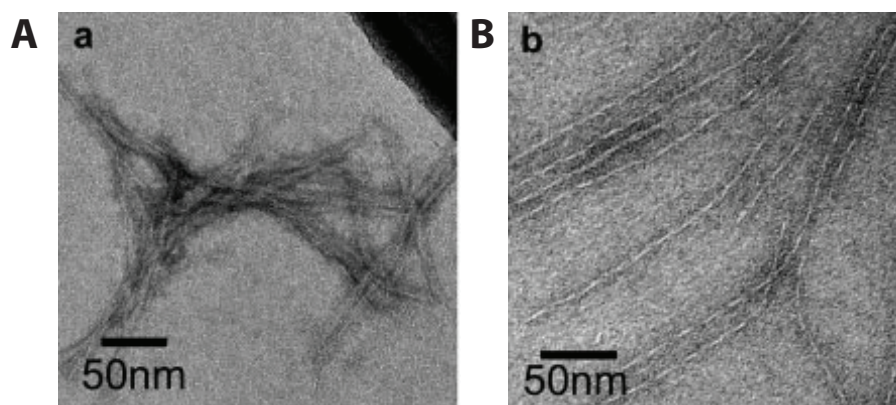


**Figure 11:** A) TEM investigations on aggregates formed by an oligopeptide having 11 residues showed pronounced entanglements of the fibers, while; B) the attachment of a PEO chain to the same oligopeptide led to much better defined structures. Images reproduced from [126].

Inspired by the L-alanine- as well as glycine-rich  $\beta$ -sheet domains of spider silk that are responsible for the remarkable mechanical properties of this biomaterial,<sup>123</sup> Sogah *et al.* equipped the tetrapeptide  $(\text{Gly-Ala})_2$  with PEO chains.<sup>124</sup> These oligopeptide-polymer conjugates led to a material

that was stabilized by  $\beta$ -sheet formation and exhibited properties similar to native silk from *Bombyx mori* the silk worm. In a later study, the same group introduced a tetra-L-alanine segment into their system which gave rise to a substantial improvement of the materials' mechanical properties, most likely due to a better  $\beta$ -sheet formation.<sup>125</sup> Messersmith *et al.* presented a similar approach by using an 11-residue oligopeptide that itself had been found to form nanoscopic fibers in earlier studies (Figure 11A).<sup>126</sup> Thus, oligo- or poly(ethylene glycol) segments were attached to this oligopeptide as well as to a shorter version (7 residues) of the latter. Contrary to the pure oligopeptides, the obtained conjugates did not tend to entangle, form larger bundles, or aggregate laterally. As was shown by IR spectroscopic investigations, the driving force for the aggregation was  $\beta$ -sheet formation. The investigation of the higher structure formation by TEM revealed the presence of well-defined fibrillar features exhibiting a helical pitch of approximately 20 nm (Figure 11B) while the pure oligopeptide formed broader less defined aggregates.

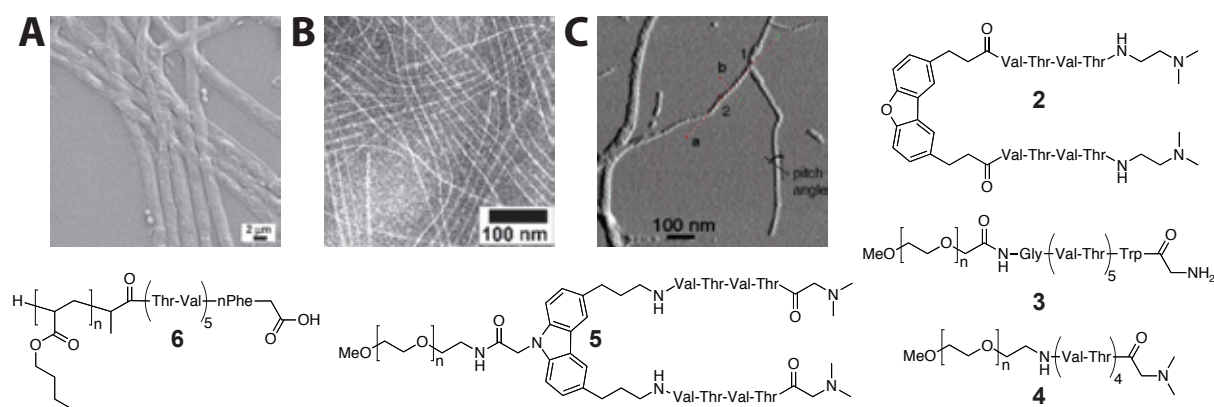


**Figure 12:** A) A scanning electron micrograph of the microfibers obtained from **3** proved their narrowly disperse diameters; B) a negatively stained TEM image of the nanoscopic filaments observed in the case of **5** showed no signs of lateral aggregation; C) the helical fine structure of the nanoscopic filaments formed by the self-assembly of **6** could be proved by SFM imaging. Images reproduced from [127], [129], and [130].

Substantial contributions to the field of oligopeptide-polymer conjugates were made by the group of Börner and coworkers.<sup>127–129</sup> For instance, they investigated the self-organization of PEO-NH-Gly(ValThr)<sub>5</sub>TrpGly-NH<sub>2</sub> **3** the amino acid sequence of which was designed for an antiparallel  $\beta$ -sheet assembly.<sup>127</sup> The resulting  $\beta$ -sheet tapes exhibited strongly amphiphilic surfaces and were found to form extremely long microfibers instead of nanoscopic aggregates. However, their dimensions were surprisingly uniform, i. e., the observed diameters were found in the narrow range of 2.0 ( $\pm$  0.5)  $\mu\text{m}$  while the height of the fibers was measured to be 50 ( $\pm$  5) nm (Figure 12A). The authors assumed that a large number of laminated  $\beta$ -sheets were aligned parallel to the fiber axis while, at the same time, a stacking of  $\beta$ -sheets occurred perpendicular to the long diameter of the microfibers. It was possible

to reduce the size of the obtained filaments to the nanoscopic level by either using a shorter oligopeptide segment or changing to an organic solvent which reduced the influence of the  $\beta$ -sheet surfaces' amphiphilicity. While the shorter linear PEO-NH-(ValThr)<sub>4</sub>C(O)CH<sub>2</sub>NMe<sub>2</sub> **4** did not show any tendency toward fibrillization at all, polymer conjugates **5** that were architecturally closely related to the peptidomimetics **2** used by Kelly *et al.*<sup>104</sup> gave rise to defined nanoscopic aggregates.<sup>130</sup> Thus, the conjugates **5** were found to produce uniform ribbons exhibiting a height of 1.4 ( $\pm$  0.1) nm and a lateral spacing of closely packed ribbons of 13.6 ( $\pm$  1) nm (Figure 12B). No tendency toward the formation of higher aggregates such as bundles could be observed in these cases, as opposed to filaments from the pure peptidomimetic molecules **5**. Similarly, the poly(butyl acrylate) substituted derivative pBuA-C(O)NH-(Val-Thr)<sub>5</sub>-nPheGlyOH **6** (nPhe = 4-nitrophenylalanine) self-assembled into left-handed helically twisted nanoscopic filaments with a height of 2.9 ( $\pm$  0.5) nm, a helix pitch of 37.4 ( $\pm$  3) nm, and lengths of up to 2.3  $\mu$ m (Figure 12C).<sup>129</sup>

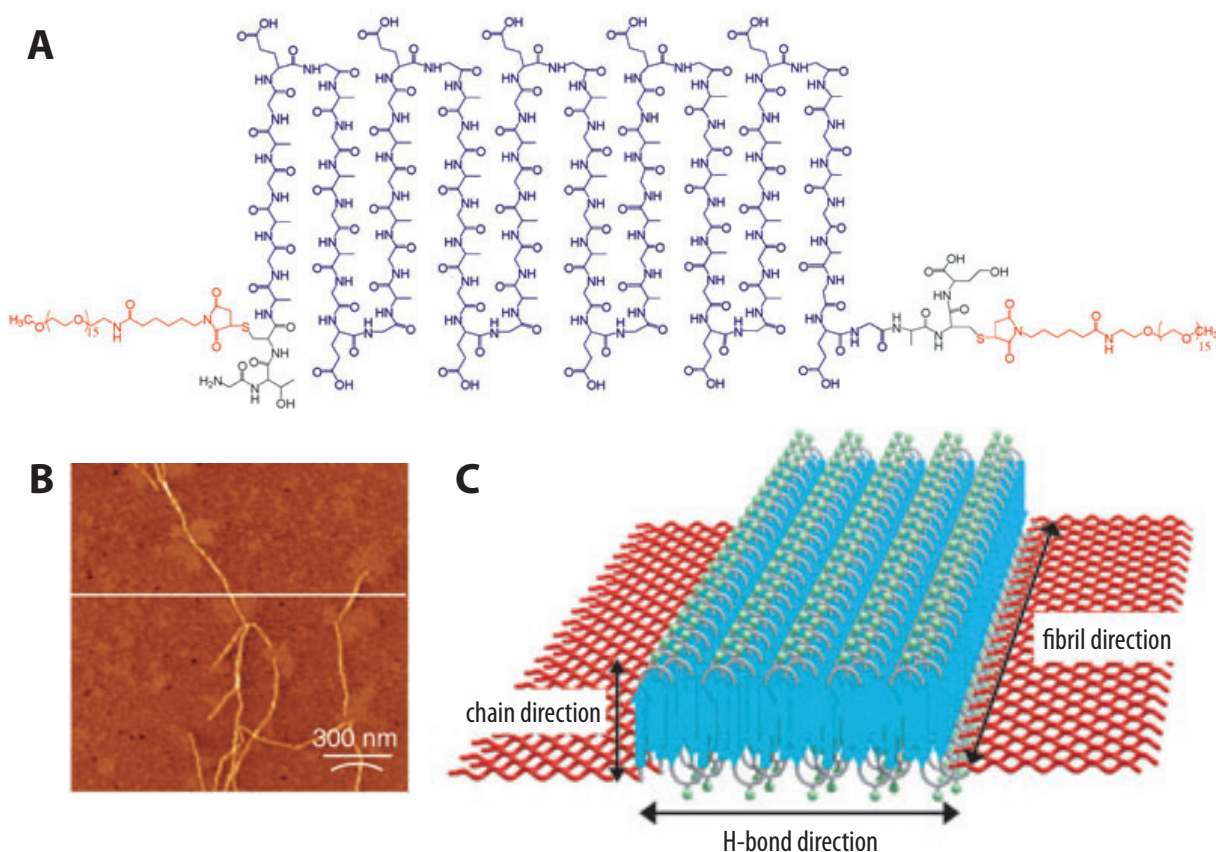


**Figure 13:** A) Schematic representation of the PEO-oligopeptide-conjugates prepared by van Hest *et al.* indicating the intramolecular  $\beta$ -sheet arrangement; B) SEM image of fibrils formed by ([Ala-Gly]<sub>3</sub>-Glu-Gly)<sub>10</sub> recorded on a mica surface; C) schematic illustration of the  $\beta$ -sheet fibrils. Image reproduced from [131].

Another interesting, although entirely different approach towards nanostructures obtained from oligopeptide-polymer conjugates has been presented by van Hest *et al.*<sup>131</sup> They prepared mono-



disperse polypeptides of the type  $([\text{Ala} - \text{Gly}]_3 - \text{Glu} - \text{Gly})_n$  with  $n = 10, 20$  by protein engineering and connected PEO chains to both ends. The  $(\text{Ala} - \text{Gly})_3$  sequences formed an antiparallel, intramolecular  $\beta$ -sheet while the  $\text{Glu} - \text{Gly}$  sequences served as turns. Due to a lateral stacking of these  $\beta$ -sheets, fibrillar features were formed that could be imaged by SFM (Figure 13).

Summarizing the above investigations on the self-assembly of oligopeptides and oligopeptide-polymer conjugates, several conclusions can be drawn. In aprotic organic solvents, the formation of stable single  $\beta$ -sheet tapes can be achieved with shorter oligopeptide segments because the  $\text{N-H}\cdots\text{O}=\text{C}$  hydrogen-bonding is stronger in the absence of competition from the solvent. The single  $\beta$ -sheet tapes formed by such shorter oligopeptides favor a stronger helical twisting and, therefore, disfavor higher aggregation via  $\beta$ -sheet stacking. Furthermore, the mutual attraction of  $\beta$ -sheets is noticeably reduced in apolar solvents as compared to protic media due to the absence of the hydrophobic effect leading to systems with a lower number of laminated  $\beta$ -sheets. Also an alternating sequence of hydrophilic and hydrophobic amino acids which leads to amphiphilic tape surfaces will suppress higher aggregation because of a selectively favored dimerization of tapes into ribbons. This effect should occur irrespective of the environment, i. e., either the hydrophilic or hydrophobic surfaces will aggregate, depending on the solvent quality.

Furthermore, the decoration of the  $\beta$ -sheet tape edges with polymer segments introduces an element of phase segregation unknown in the realm of pure oligopeptides which strongly favors the formation of filaments with a lower number of laminated sheets and prevents bundle formation. Aggregation via  $\beta$ -sheet stacking would lead to a successive restriction of the space available to the polymer segments which would require a chain extension. The latter would, however, only be thermodynamically favorable if the associated entropic penalty was overcompensated by an enthalpic contribution, e. g., from a crystallization of the polymer segments. Hence, while the general considerations concerning the self-assembly of oligopeptides remain valid, the attachment of amorphous polymer segments to the tape edges plays a role similar to the “soft shell” of amyloid proteins or, for instance, electrostatic repulsion in the case of pure oligopeptides, although the thermodynamic origin of the effect is different, i. e., entropic in nature.

### 1.2.4 Implications for the Molecular Design

For the envisaged topochemical diacetylene polymerization using self-assembled oligopeptide fibrils as supramolecular scaffolds, the polymerizable diacetylene moieties must be placed in-register at the  $\beta$ -strand identity period of around  $4.8\text{\AA}$ . An antiparallel  $\beta$ -strand arrangement would, hence, be detrimental, and a viable strategy to achieve parallel  $\beta$ -sheet formation is needed. Considering

the prevalence of  $\beta$ -sheet-rich proteins with parallel  $\beta$ -sheet structures in nature, it may seem a little disappointing that more or less all investigations on synthetic oligopeptides and their polymer conjugates either quietly assumed, experimentally observed, or deliberately targeted predominantly antiparallel  $\beta$ -sheet formation. With the exception of Lynn's and Meredith's investigations on PEO conjugates of amyloidogenic oligopeptides which exhibited the same parallel  $\beta$ -sheet structure as the unmodified amyloid proteins, there is virtually no example of a synthetic oligopeptide or its polymer conjugate which was specifically designed for parallel  $\beta$ -sheet formation. The only exception is the work by Mori *et al.* who prepared *N*-acetylated, L-thyrosine- and L-threonine-based dipeptides which were equipped with diacetylene functions in their side chains.<sup>132,133</sup> These reportedly attained a parallel orientation, allowing for a partial polymerization of the diacetylenes. In this context, it is important to acknowledge that, for simple oligopeptides, an antiparallel  $\beta$ -strand orientation should usually be preferred because of the favorable compensation of the molecular dipoles and the more optimal hydrogen-bond geometries. Furthermore, it can straightforwardly be enforced by including additional complementary interaction sites in the side chains or at the  $\beta$ -strand termini, as it had been done in the above examples by Boden, Kelly, or Börner.<sup>82–84,104,106,107,127–129</sup>

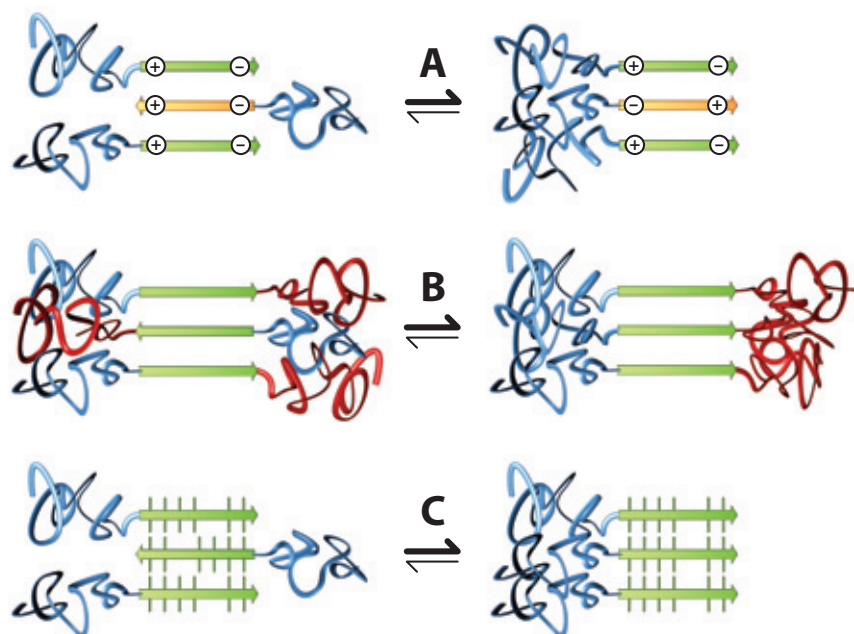


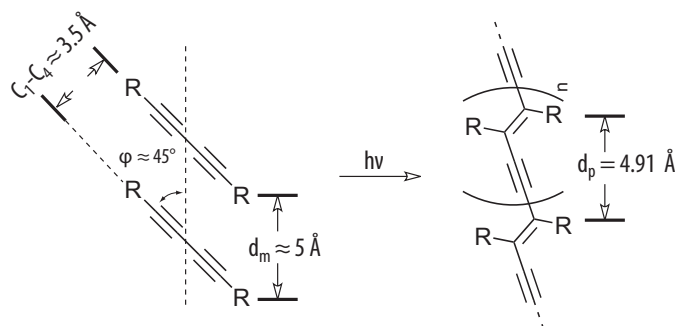
**Figure 14:** Possible strategies to enforce a parallel  $\beta$ -strand orientation; A) the inclusion of complementary interaction sites requires the preparation of two different, mutually complementary molecules; B) oligopeptides equipped with two different, immiscible polymer segments may favor a parallel orientation due to phase segregation; C) likewise, the non-equidistant placement of  $N-H \cdots O=C$  backbone hydrogen-bonding sites or additional side chain interaction sites may induce a parallel  $\beta$ -strand alignment.

While no similarly straightforward method to enforce parallel  $\beta$ -sheet formation has previously been described, the simple inclusion of appropriately placed complementary interaction sites (e. g., pairs of acid/base, hydrogen-bond donor/acceptor, or cationogenic/anionogenic functionalities) should be expected to give rise to a parallel  $\beta$ -strand alignment only if two different, mutually complementary types of molecules are employed and co-assembled (Figure 14A). An alternative strategy may be the attachment of two different, non-miscible polymer segments to the oligopeptide termini, which would favor a parallel aggregation due to phase segregation. Finally, a desymmetrization of the interactions responsible for  $\beta$ -sheet formation such as, for instance, a non-equidistant placement of the N–H $\cdots$ O=C backbone hydrogen-bonding sites by including a non-peptidic spacer, can be envisaged to induce parallel  $\beta$ -sheet formation because, only in this way, the maximum number of hydrogen-bonds can be achieved. It is interesting to note that this last strategy appears to be closely related to one “approach” toward parallel  $\beta$ -sheets utilized in biology. The described “dry steric zipper” motif (Section 1.2.1) frequently observed in amyloid fibrils incorporates additional, self-complementary side chain N–H $\cdots$ O=C type hydrogen-bonding sites placed in a way that the stabilizing interstrand, intrasheet hydrogen-bonding can only be realized in a parallel  $\beta$ -sheet structure (Figure 7). The recently demonstrated generic nature and abundance of this motif in fibrous proteins makes this last strategy seem most promising for its utilization in the preparation of self-assembled scaffolds for the topochemical diacetylene polymerization.

## 1.3 Synthesis and Properties of Poly(diacetylene)s

### 1.3.1 The Topochemical Polymerization of Diacetylenes

By definition, a topochemical reaction is possible only in the crystalline state since the reacting species do not change their places (greek: *topos* = place).<sup>81</sup> Ideally, the centers of gravity of the reactants do not move while certain rearrangements of the reactive sites of the molecules are still allowed, leaving the symmetry of the parent crystal intact. One very famous example of such a reaction is the topochemical polymerization of diacetylene derivatives that was developed by Wegner *et al.*<sup>80,134–136</sup> They found that certain crystals of molecules comprising the diacetylene unit rapidly attained a deep red or purple color upon UV irradiation while solutions of the same derivatives did not show a comparable reactivity. The investigation of the process revealed that the obtained poly(diacetylene)s (PDAs) were examples of crystalline polymers having a fully  $\pi$ -conjugated backbone featuring alternating double and triple bonds in consecutive conjugation.<sup>137</sup> Obviously, the crystal lattice of the monomers controlled the reaction which took place only if the *sp*-hybridized carbons of the diacetylene functions were aligned in a certain geometry in the parent crystals (Scheme 1).<sup>138–140</sup>



**Scheme 1:** The geometric prerequisites for a successful topochemical polymerization of diacetylenes are a parallel arrangement of the  $sp$ -hybridized carbon chains at a distance of roughly  $5 \text{ \AA}$  as well as an inclination angle of approximately  $45^\circ$ , i. e., the geometry of the polymer in its *all-trans* configuration is nearly preformed.

In detail, the diacetylenes have to be aligned in a ladder-like arrangement, exhibiting a repeating distance  $d_m$  of approximately  $5 \text{ \AA}$ . At the same time, the inclination angle  $\phi$  between the packing direction of the molecules and the diacetylene axes has to attain a value near  $45^\circ$ . The rationale behind these criteria is, first, the fact that carbons  $C_1$  and  $C_4$  of adjacent molecules have to get into Van-der-Waals distance and, secondly, the geometry of the formed polymer, featuring an identity period  $d_p = 4.91 \text{ \AA}$  in its *all-trans* configuration, must be already preformed. Thus, the activation energy of this 1,4-polyaddition reaction is small since the crystal structure of the monomer can remain intact and no lattice energy is lost during the transformation.

### 1.3.2 Topochemical Polymerizations in Hydrogen-Bonded Systems

Since the topochemical diacetylene polymerization is possible whenever these criteria are fulfilled, it is not restricted to 3D single-crystals and has been performed in various other types of ordered phases as well. In the following section, a brief discussion of examples will be given that will focus on hydrogen-bonded systems.

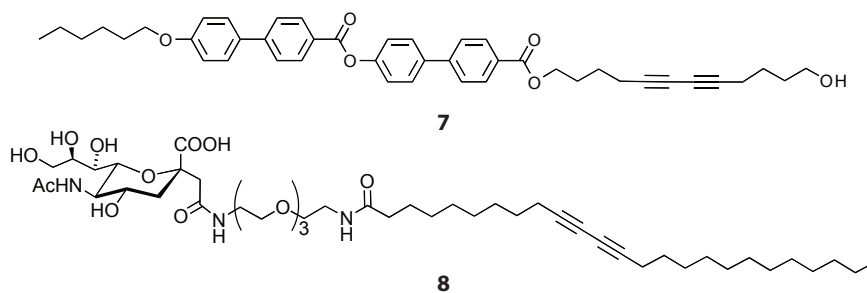


**Figure 15:** Diacetylene derivative **7** formed bilayers that yielded highly photo stable poly(diacetylene)s after UV irradiation, whereas **8** was co-assembled with the long-alkyl chain diynoic acid to form polymerizable bilayers.

After Wegner had described the topochemical polymerization in the crystalline state, the same group also investigated the process in ordered multilayers of the cadmium salt of tricoso-10,12-diyonic acid that had been prepared by the Langmuir-Blodgett technique.<sup>141</sup> A head-to-head and tail-to-tail orientation of the long alkyl chain acids could be proved by X-ray analyses, and the polymerization was found to be possible by irradiating the sample with UV light having a wavelength of 254 nm. Similar diacetylene-containing carboxylic acids were polymerized in monolayers at the air-water interface by Ringsdorf and coworkers<sup>142</sup> who followed the polymerization by measuring the surface pressure which dropped instantaneously upon UV irradiation, indicating a successful conversion. Highly ordered two-dimensional bilayers of the bis-(biphenyl) ester-functionalized, rigid molecule **7** (Figure 15) containing two biphenyl moieties could also be polymerized.<sup>143</sup> The corresponding polymers were found to be very photostable during a prolonged treatment with strong laser irradiation which was needed for determining the third order non-linear activities of the obtained film.

Similarly, polymerized bilayers have been used in the preparation of materials aimed at applications in the field of biosensing,<sup>144</sup> based on the poly(diacetylene) backbones' well-known solvato-, thermo- and mechanochromism (Section 1.3.3). Thus, the amphiphile **8** carrying a sialic acid group was mixed with the unfunctionalized long-alkyl chain diynoic acid. The system self-assembled to form bilayers that could be polymerized and were then decorated with the sialic acid residues. The latter interacted with receptors on the surface of the influenza virus which could be detected by the accompanied color change of the poly(diacetylene) bilayer.

While hydrogen-bonding played already a role in some of the previous cases, it was definitely the main driving force for the alignment of the diacetylenes in a very recently published study by Stupp *et al.* who equipped peptide-amphiphiles with a correspondingly functionalized end group.<sup>145</sup> Thus, they attached 10,12-pentacosadiynoic acid to a linear hexa- (**9**) as well as to a branched heptapeptide (**10**). These structures were found to form gels stabilized by  $\beta$ -sheet-nanofibers (Figure 16) in aqueous solution when treated with ammonium hydroxide vapor. Upon UV irradiation, the gels as well as solutions that had not been treated with the base turned dark purple or blue. Obviously, the oligopeptides were aligned already to a certain extent in solution. A UV-vis analysis revealed a global absorption maximum around 550 nm for the linear as well as the branched derivative which additionally featured a second absorption at 630 nm which was attributed to another backbone conformation (Section 1.3.3).

Kim *et al.* investigated a similar system by attaching dipeptides to 10,12-pentacosadiynoic acid, namely L-Ala-L-Ala (**11**) and D-Ala-D-Ala (**12**).<sup>146</sup> After cooling an EtOH/water mixture containing these derivatives from 60 °C to room temperature, microscopic ribbon-shaped precipitates were ob-

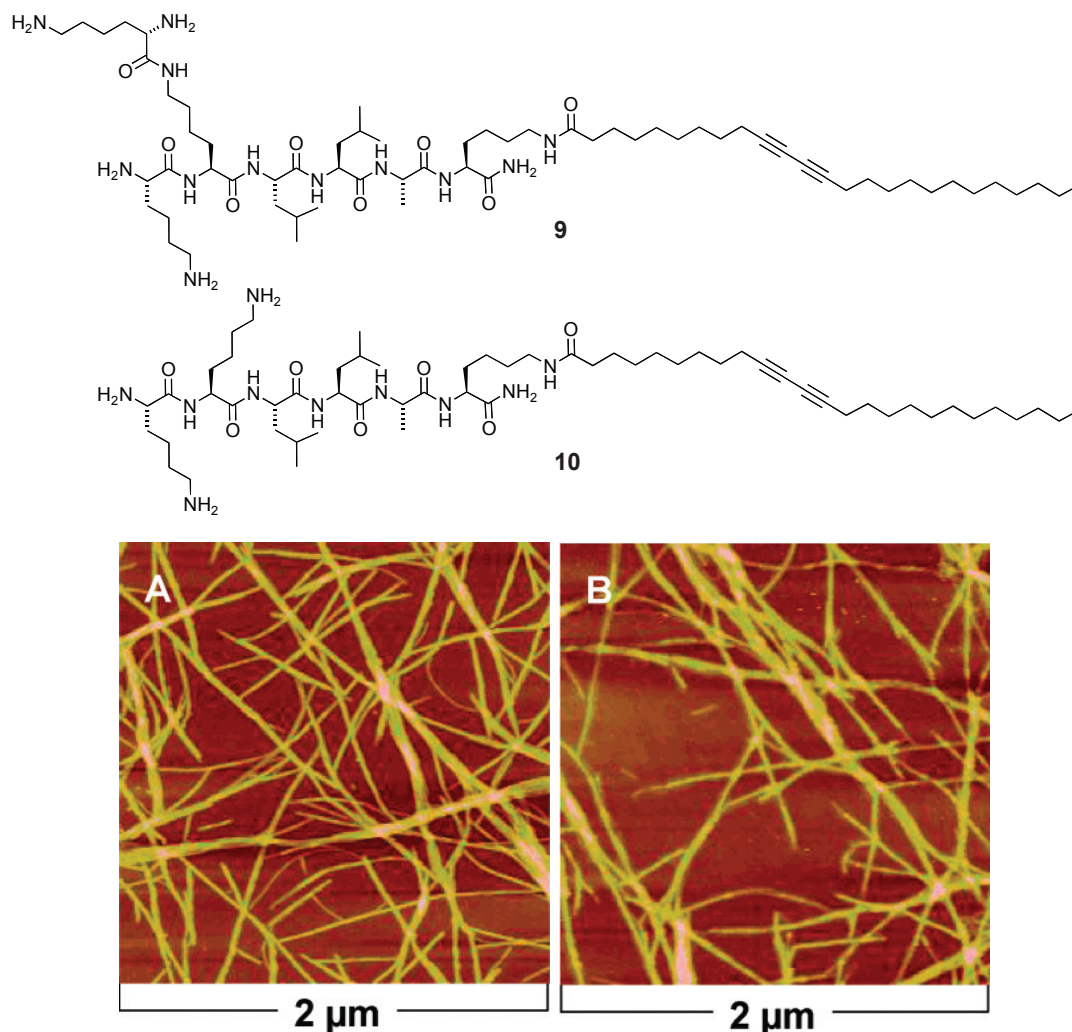


**Figure 16:** A) Fibers formed by diacetylene-functionalized peptide-amphiphiles before irradiation were virtually equal to B) the polymerized objects. The width of the nanoscopic aggregates was stated to be on the order of 5 nm. Images reproduced from [145].

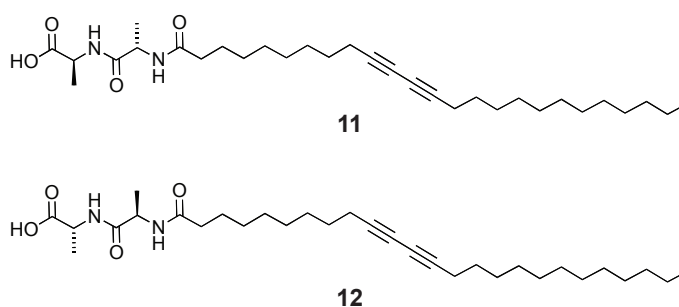


**Figure 17:** Dipeptide-functionalized amphiphiles prepared by Kim *et al.*

served by scanning electron microscopy. Addition of the glycopeptide-antibiotic vancomycin, which selectively binds to terminal D-Ala-D-Ala residues, caused the precipitation of spherical particles instead of ribbons, whereas the precipitates of the L-Ala-L-Ala-phospholipid remained unchanged. Ac-Lys(Ac)-D-Ala-D-Ala, a vancomycin-specific ligand, induced regeneration of the ribbon-shaped

structures, demonstrating the reversibility of the morphologies. The UV-polymerization was found to be possible within both kinds of structures and stabilized the morphologies, as could be evidenced by fluorescence microscopy.

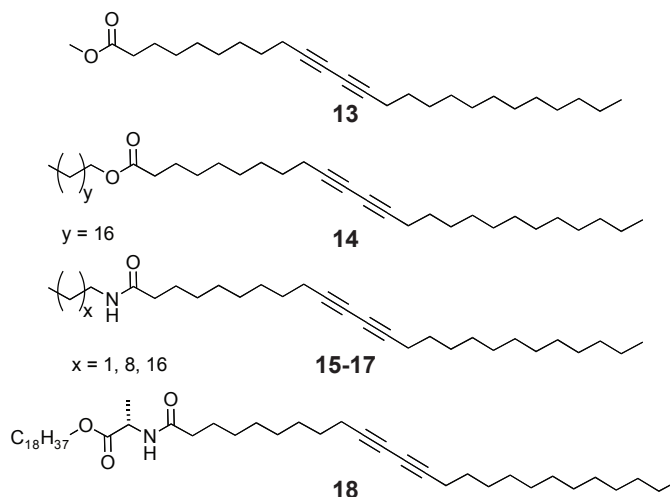


**Figure 18:** Diacetylene-functionalized low molecular weight organogelators prepared by Weiss *et al.*

A detailed investigation on the poly(diacetylene) formation within the gel-state was performed by Weiss *et al.*<sup>147</sup> The very popular 10,12-pentacosadiynoic acid was transformed into a series of low molecular weight organogelators (**13-18**) by a peptide coupling or esterification with another correspondingly functionalized long or short alkyl chain (Figure 18). The gelating efficiency increased with increasing alkyl chain length, presumably due to greater London dispersion forces. Moreover, a comparison between ester and amide derivatives confirmed the role of strong intermolecular hydrogen-bonding for the aggregation which resulted in an overall better polymerizability upon UV irradiation.

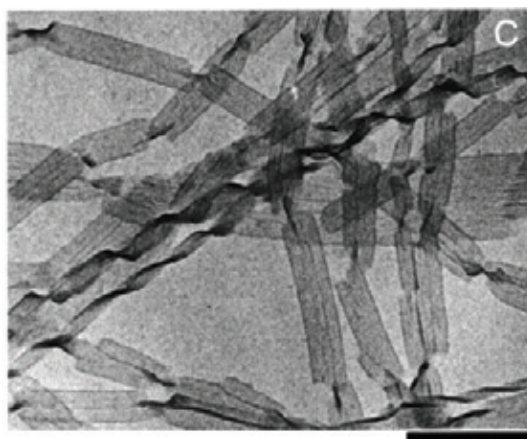


**Figure 19:** Microstructures obtained from a glutamine-functionalized long alkyl chain derivative after polymerization. Image reproduced from [148].

Stevens *et al.* used the same diynoic acid in a study of the photopolymerization of amino acid functionalized derivatives.<sup>148</sup> The different amino acids were connected via an amide bond, and all derivatives could be topochemically polymerized yielding blue aqueous solutions. Both hydrogen-bonding interactions and molecular chirality determined the growth of microstructures into twisted features (Figure 19).

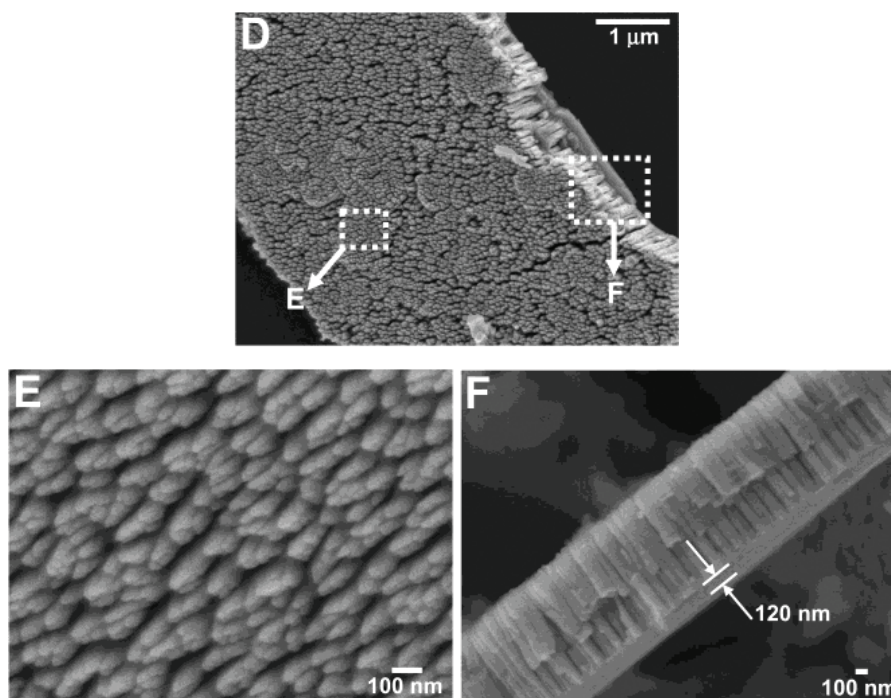


**Figure 20:** Scanning electron micrographs of the “nanotube carpets” formed by diacetylene-containing lipids on a glass slide. Images reproduced from [149].

Diacetylene lipids with quaternary ammonium salts as their end group were found to self-assemble into monodisperse nanotubes exhibiting a wall thickness of 27 nm, an internal diameter of 35 nm, and an average length of approximately 1 μm.<sup>149</sup> TEM as well as SAXS investigations revealed that the tube wall comprised five lipid bilayers with a spacing of 57.8 Å. After casting solutions containing these nanotubes onto glass surfaces, a polymerization by UV irradiation was possible, as indicated by a color transition from colorless to blue. Interestingly, an alignment of these nanotubes into carpet-like structures (Figure 20) could be observed by dropping chloroform onto samples dried on a glass slide. The mechanism of the formation was stated to be unclear.

Sugar-functionalized diacetylenes were prepared and found to gel organic solvents or water due to the formation of fibrillar structures, which could be polymerized upon UV-irradiation, as well.<sup>150</sup> The derivatives reported by Masuda and coworkers (19, 20) contained sugar residues on both sides of the diacetylene and self-assembled into nanofibers driven by intermolecular hydrogen-bonding



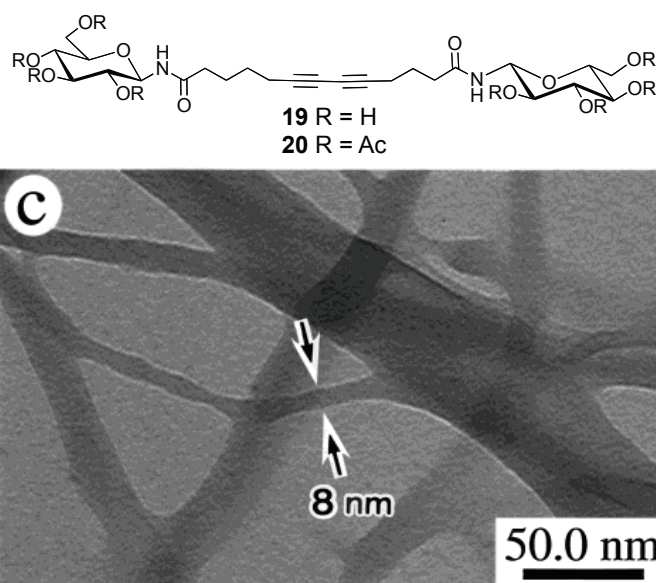


**Figure 21:** Polymerized nanofibers formed by the acetylated, sugar-functionalized diacetylene **20**. Image reproduced from [150].

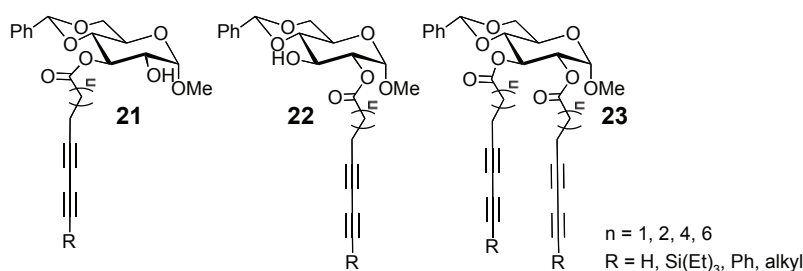


**Figure 22:** Carbohydrate-based diacetylenes reported by Wang *et al.*

(Figure 21).<sup>150</sup> Both **19** and **20** formed such morphologies which stayed intact during the polymerization. The features formed by the derivatives exhibiting free hydroxy functions on the sugar were much larger and more rigid, presumably due to enhanced interlayer interactions by hydrogen-bonding. In the other example reported by Wang *et al.*, diacetylene-containing glycolipids with one or two diacetylene-lipids per sugar unit were prepared (Figure 22).<sup>151</sup> Short chain glycolipids and derivatives with a free hydroxyl group formed gels in aqueous solution, whereas very long chain diacetylene lipids gelled ethanol or hexane. Consequently, the chain length as well as the position of the diyne were proposed to affect the self-assembling properties significantly.

Additionally, open-chain sugar derivatives, i. e., aldonamides carrying 1,3-nonadiynyl units were investigated by Fuhrhop and O'Brien.<sup>152,153</sup> The efficiency of the polymerization of the gels formed by gluconamide derivatives in water was heavily dependent on the length of the methylene spacer that bridged the diacetylene unit and the amide functionality.<sup>152</sup> Only one derivative exhibiting a single methylene group could be polymerized by UV-irradiation. However, the tubular structures that

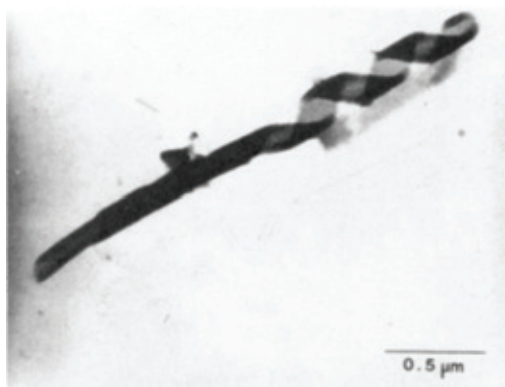


**Figure 23:** TEM image of a polymerized assembly of aldonamide-functionalized diacetylenes. Image reproduced from reference [153].

had been observed prior to the polymerization were destroyed as proved by electron microscopy. The aldonamide derivatives reported by O'Brien were readily polymerized, yielding interesting microstructures (Figure 23).

### 1.3.3 Chromism of Poly(diacetylenes)

It has long been known that poly(diacetylene)s show interesting color transitions upon a diversity of external stimuli such as heat, mechanical stress, pH variations, or binding events to side-chains attached to the polymer backbone. Although the research in this area has been ongoing for 30 years and several research groups were involved, the underlying mechanism is still not completely understood on the molecular level and is, therefore, still a matter of debate. The first systematic investigations of the phenomenon were carried out by Chance and Patel *et al.* who studied an early class of soluble, urethane-based poly(diacetylene)s (Figure 24).<sup>154–157</sup>

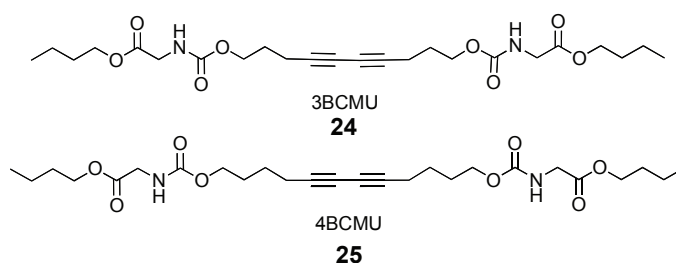


**Figure 24:** Soluble, urethane-based diacetylene derivatives that have been heavily investigated in the literature.

This class of poly(diacetylene)s was equipped with carboxyl methyl urethane (CMU) side chains that were connected via a spacer consisting of  $n$  methylene groups and terminated by a butyl (B) terminus and were, thus, named  $n$ BCMU. The most prominent derivatives were equipped with three or

four methylene groups and were referred to as 3BCMU (**24**) and 4BCMU (**25**). The polymerization of the parent diacetylenes was carried out by  $\gamma$ -irradiation, and the resulting soluble polymers P3BCMU (**P24**) as well as P4BCMU (**P25**) were purified by extracting residual monomer. When taken up in  $\text{CHCl}_3$ , the poly(diacetylene) solutions attained an intense yellow color which changed reversibly to dark blue when hexane was added. A precipitation of dark blue material occurred when the hexane content was further increased. Such a precipitation did not occur, however, when the blue solutions aged or were subjected to ultracentrifugation. Since the color transitions in these “true” solutions of the polymers were concentration-independent, the involved processes were assigned as a single-chain phenomenon.<sup>154</sup> The corresponding UV spectra showed a shift from the yellow form with an absorption maximum at 470 nm to another one, exhibiting two absorption maxima at 570 and 620 nm. This process coincided with changes in the IR spectra that could be interpreted in terms of the formation of hydrogen-bonds in the side chains. Furthermore, the solid state UV spectra of **P24** were comparable to the ones in the blue solutions.<sup>157</sup> Accordingly, the authors attributed the color transitions with conformational changes within the side chains. Thus, the ester and urethane groups were well-solvated in the yellow  $\text{CHCl}_3$  solutions, causing a non-planar polymer backbone. The subsequent addition of the non-solvent hexane led to the formation of hydrogen-bonds which was accompanied by a planarization of the  $\pi$ -conjugated backbone. The effective conjugation length, i. e., the  $\pi$ -conjugated polymer segments in which an electron delocalization over several  $\pi$ -bonds is possible, was stated to have increased from about seven repeat units in the yellow form to approximately thirty in the blue state. These values were obtained by using a model that had been developed for polyenes<sup>158</sup> and may, therefore, have given rise to improper results. Also the assumed statistical bond rotations that determine the effective conjugation length may not be in good agreement to the restrictions of such rotations found in  $\pi$ -conjugated systems.

In a later study,<sup>159</sup> Chance *et al.* reported very similar results on a simplified urethane-based system in which the butyl esters had been replaced by simple phenyl groups (**26**, **27**). In these cases, the polymers were barely soluble in DMF, and  $\text{CHCl}_3$  or MeOH acted as the non-solvents. The color transitions from yellow to blue were found to be analogous to the previous case (Figure 25).

In an effort to corroborate the proposed theory of side-chain-induced variations of the effective conjugation length, the same authors investigated **P24** with Raman spectroscopy.<sup>160</sup> They reported a shift to lower frequencies during the transition from yellow to blue which was interpreted in terms of an increased effective conjugation length. The rationale is that the vibrational energies of the carbon-carbon double as well as triple bonds are expected to vary with the conjugation length. In more detail, an increased delocalization of electrons within the backbone should weaken the C=C and C $\equiv$ C bonds causing a decrease in the Raman active vibrational frequencies.

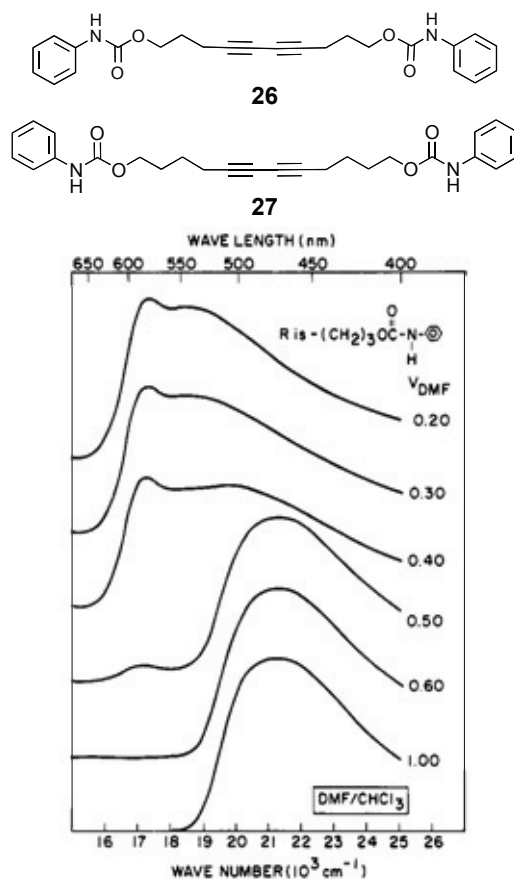


**Figure 25:** UV-vis spectra of a poly(diacetylene) formed from **26**. The spectra change from the yellow form in pure DMF to a blue form upon the addition of CHCl<sub>3</sub>. Image reproduced from [159].

The single-chain model was further supported by the work of the group of Heeger who investigated **P25** by quasielastic light scattering techniques.<sup>161</sup> They determined the hydrodynamic radius  $R_H$  of the polymer in a CHCl<sub>3</sub>/hexane mixture. With an increasing proportion of hexane, the hydrodynamic radius increased abruptly, which led the authors conclude that the initial coil-like structure was transformed into a rigid rod. The presence of aggregates was excluded by light scattering experiments of the red solutions but the significance of these results remained questionable because the red form was investigated in solutions that were three orders of magnitude lower concentrated than the yellow solutions they used as a reference. Likewise, the explanation for the coil structure of the yellow form, which was attributed to a butatriene-like  $\pi$ -system that allowed rotations around the single bonds, was not very convincing. Consequently, Heeger *et al.* investigated the system further and observed thermochromism in toluene solutions of **P25**.<sup>162</sup> Thus, hot solutions attained a yellow color which, however, changed to red upon lowering the temperature from 72 to below 55 °C. The UV-vis spectra revealed that the corresponding bathochromic shift that was accompanied by an isosbestic point (Figure 26) and, thus, led to the conclusion that a single rod-coil transition was responsible for the phenomenon.

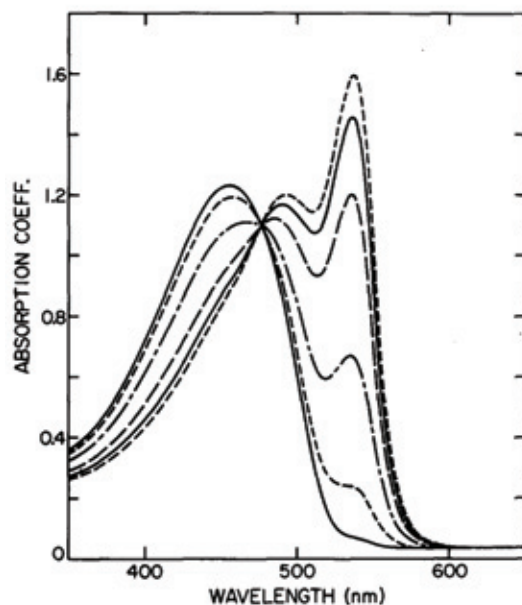


**Figure 26:** A series of UV-vis spectra measured at different temperatures from 72 °C (solid line) to 56 °C (dashed line) in toluene solution showed a bathochromic shift from 450 (yellow form) to 530 nm (red form) accompanied by an isobestic point. Image reproduced from [162].

In the light of the new results, the authors revised their previously proposed butatriene hypothesis. Based on calculations and molecular models, an *all-cis*-configuration of the double bonds in the polymer backbone was proposed that was stated to be flexible enough to form coils. Consequently, the low-temperature red phase was assigned to the *all-trans* configuration.<sup>162,163</sup>

An opposing theory about the color transitions observed in poly(diacetylene) solutions was published by Wegner *et al.* who proposed a worm-like chain model (Figure 27) for the yellow state and aggregation phenomena of individual polymer chains leading to microgels or semicrystalline colloids which then caused the changed absorption behavior in the red or blue state.<sup>164</sup>

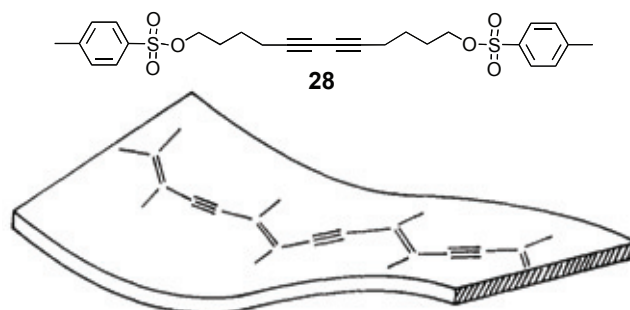


**Figure 27:** top) Structure of the tosylated monomer used by Wegner *et al.* bottom) Sketch of the worm-like chain of the poly(diacetylene)s in the yellow state. Image reproduced from [164].

The basis for their theory were investigations on “PTS-12” (**P28**), a poly(diacetylene) obtained from the tosylated monomer **28**, and **P24** which were studied by UV-vis, resonance Raman, and  $^{13}\text{C}$  NMR-spectroscopy. Crystals of **P28** were red-purple while orange or yellow colors were observed when the material was dissolved in DCE or DMF. The corresponding UV-vis spectra exhibited absorption maxima at 505, 535 as well as 570 nm for the solid state while the solutions only exhibited one featureless absorption at 470 nm. Upon the addition of polar solvents such as nitrobenzene, small bathochromic shifts were observed. Light scattering experiments performed at equal and, therefore, comparable concentrations of **P24** in  $\text{CHCl}_3$  showed a dramatic increase in light scattering intensity for the blue state compared to the yellow solution. This was interpreted in terms of an aggregation of the polymers. A rough estimation of the aggregate size hinted at about 150 chains in the case of the blue form which could, hence, not be regarded as a “true” solution anymore.

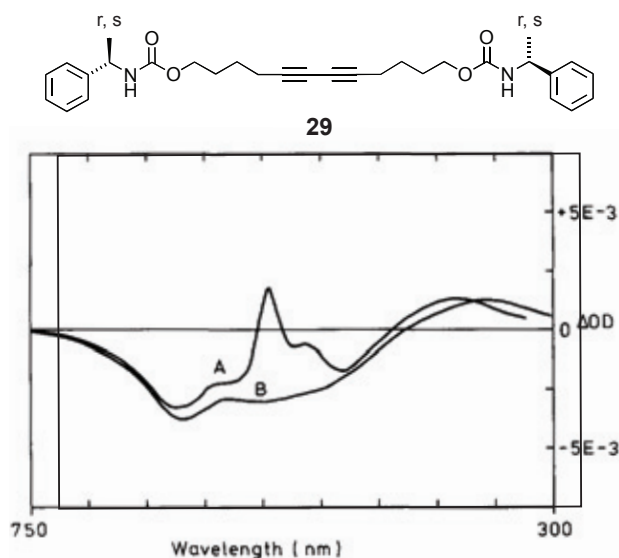


**Figure 28:** *top*) Chiral monomers used by Ando *et al.* *bottom*) CD spectra of the  $\text{CHCl}_3$ /hexane mixture (A) as well as the pure yellow  $\text{CHCl}_3$  solution before filtration showed distorted CD spectra due to a CIDS effect. Image reproduced from [165].

The worm-like chain model was supported by Ando and coworkers who equipped BCMU derivatives (**29**) with chiral end groups and investigated their system with CD spectroscopy.<sup>165</sup> After dissolving the polymers in  $\text{CHCl}_3$ , the expected yellow solutions were obtained. However, the CD spectra suffered from a pronounced circular intensity differential scattering (CIDS) effect that occurs when aggregates with sizes on the order of the wavelength of the incident light are present.<sup>166</sup> Thus, the solutions were filtered and neither a CIDS effect nor real circular dichroism was detectable in the range from 340–720 nm which was interpreted in terms of a random conformation of the polymer chains in the yellow solution. Upon the addition of hexane, the expected color change was induced,

accompanied by the recurrence of an intense CD signal without CIDS effect indicative of a helical conformation of the polymers in the red state. Moreover, films of two enantiomeric derivatives cast from  $\text{CHCl}_3$  onto glass slides led to either a positive or a negative Cotton effect. Because the signals had a bisignate character indicative of an exciton coupling, the formation of aggregates of polymer backbones allowing for a spectroscopic interaction was proposed.

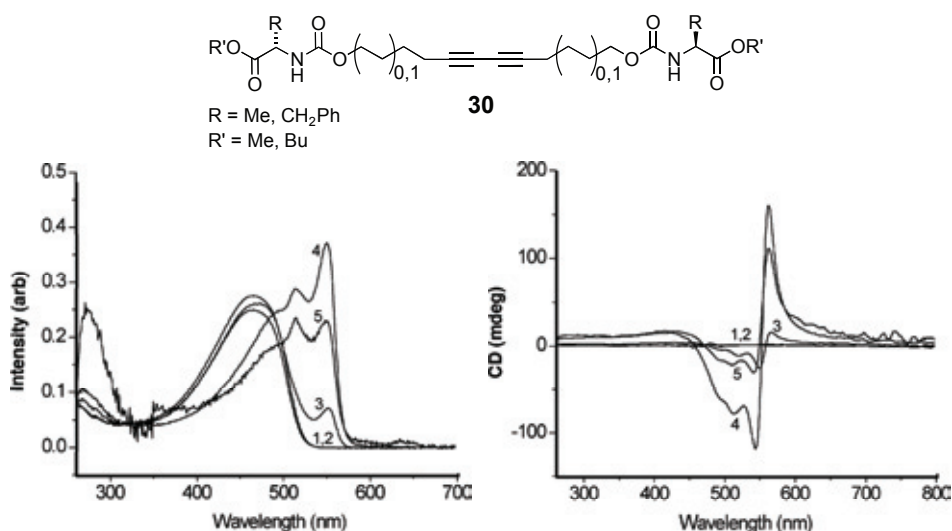


**Figure 29:** *top*) Chiral monomers investigated by Hanks *et al.* *bottom left*) UV-vis spectra in mixtures of  $\text{CHCl}_3$  and hexane at ratios of (1) 1:0, (2) 2:1, (3) 1:1, (4) 1:2 and (5) 1:10; *bottom right*) CD spectra of the same solutions. Images reproduced from [167].

Recently, Hanks *et al.* investigated new poly(diacetylene)s obtained from monomers **30** that were related to **P24**. The authors did not observe any CIDS effects when measuring CD spectra of polymers featuring chiral side chains.<sup>167</sup> Thus, they interpreted their observed solvatochromism in terms of a single-chain phenomenon although the polymer backbone gave rise to a clear bisignate Cotton effect (Figure 29) in the red form and a precipitation after the addition of too much non-solvent was observed. This may, hence, be better interpreted as an aggregation of polymer chains already in the red form instead of conformational changes of well-dissolved, individual chains.

An interesting thermo- as well as solvatochromism of urea-based poly(diacetylene)s (**P31-33**) in organogels has been reported recently by Moreau *et al.*<sup>168</sup> When the polymerized gels were drop-cast on quartz plates and heated, a color change from blue to red occurred via an intermediate purple state. During the blue-to-purple transition which was also followed by IR spectroscopy, no significant changes in hydrogen-bonding pattern was observed. The subsequent purple-to-red transition was found to be reversible, which led the authors to propose the following model for the thermochromism. The original blue form that was formed upon irradiation represented a kinetically

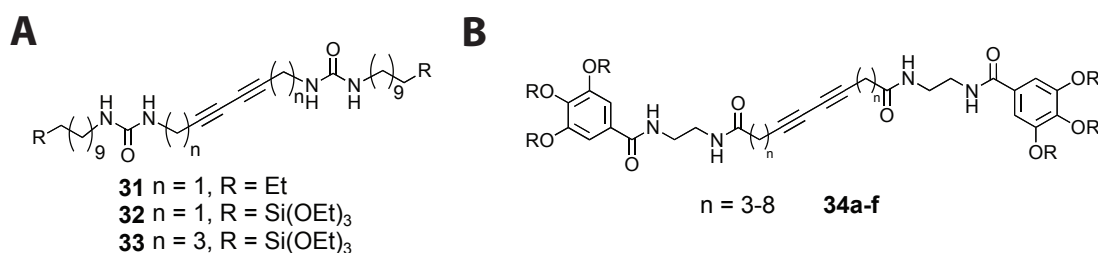


**Figure 30:** A) Urea-based diacetylene monomers prepared by Moreau *et al.* and; B) the organogelators investigated by Fujita *et al.*

trapped, strained form of the polymer which was released upon heating the sample to 40 °C, accompanied by the color transition to purple. Further heating to higher temperatures induced thermal motions in the side chains and, therefore, torsions in the backbone, giving rise to a change to a red color. Thus, the authors considered a single-chain model. One has to state though, that all presented UV spectra probably showed mixtures of several poly(diacetylene) species and, consequently, the interpretations of the authors should be considered with care.

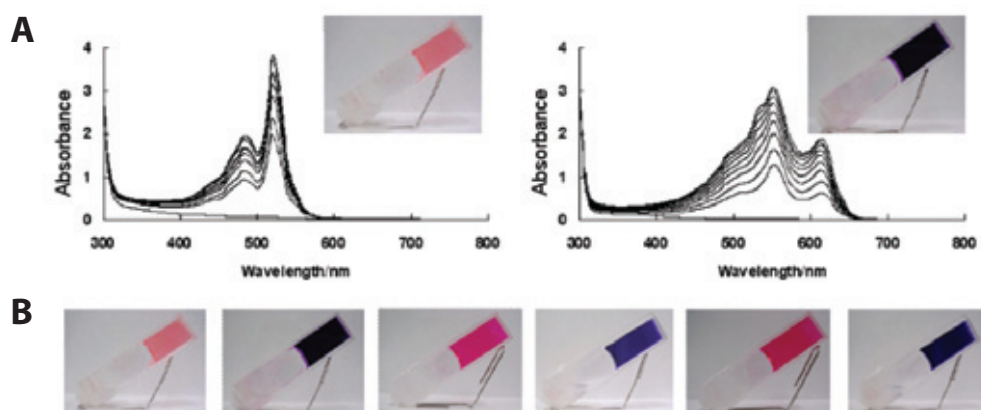


**Figure 31:** A) UV spectra of irradiated gels formed by **34a-f** exhibiting an odd or even number of methylene groups show distinctly different absorption maxima; B) Alternating red and blue gels were obtained from compounds **34a-f**. Images reproduced from [169].

Most recently, Fujita *et al.* investigated amide based organo-gelators (**34**) exhibiting a variable number of methylene groups between the polymer backbone and the amide function.<sup>169</sup> They observed a clear odd-even effect, i. e., the irradiation of derivatives having an odd number of methylene groups in the spacer yielded red gels while the others attained a blue color upon irradiation (Figure 31). Molecular models showed that derivatives having an odd number of methylene groups in the spacer supposedly led to a “more strained” conformation of the polymer backbones and, thus, to a shorter effective conjugation length as compared to molecules with an even number of methylene groups. Possible aggregation phenomena were, unfortunately, neither investigated nor discussed.



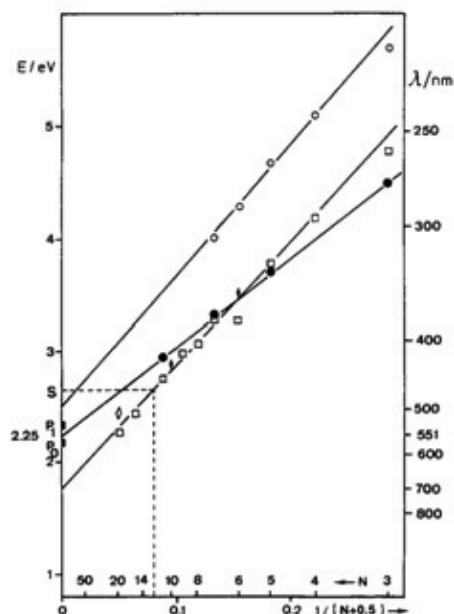


**Figure 32:** Plot of measured model compounds by Giesa *et al.* (•) into the plot of calculated optical transition energies  $E$  of several polyenes (□), polyynes (○) and polyenyynes (◆) against the number of conjugated multiple bonds  $N$  published by Wegner. Image reproduced from [170].

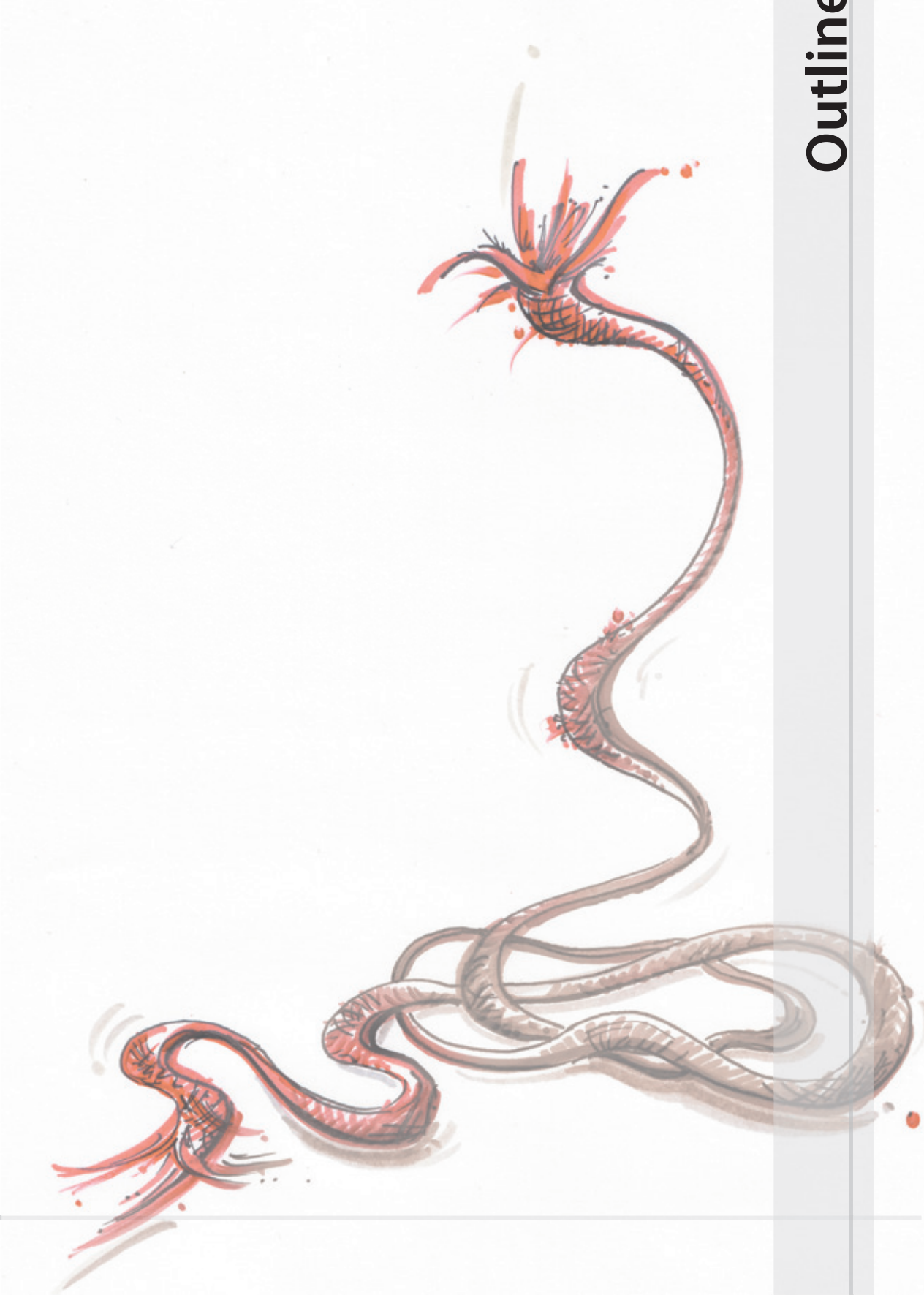
Aiming at a clarification of the origin of the color transitions found for poly(diacetylene)s on a molecular level, Giesa and coworkers prepared monodisperse unsubstituted, alternating *trans*-enyne oligomers that served as model compounds for the poly(diacetylene) backbone.<sup>170</sup> The obtained UV-vis absorption maxima of the different compounds were plotted against the number of conjugated multiple bonds in analogy to a graph previously published by Wegner.<sup>164</sup> The authors found a good linear relation between the transition energies and the reciprocal number of  $\pi$ -conjugated double bonds, although the slope differed from the plots obtained before (Figure 32). They concluded that the often assumed comparability of poly(ene)s and poly(diacetylene)s is not generally applicable. Furthermore, they were able to extrapolate the maximum absorption wavelength for an infinitely large effective conjugation length to be 551 nm. Thus, this value can be regarded as the ultimate limit of absorption energy for a single infinite polymer segment. All observed absorptions beyond that wavelength can, consequently, *not* be attributed to an increased effective conjugation *alone*. The authors came to the final conclusion that a single chain phenomenon as proposed by Chance, Heeger *et al.* can be considered as partially invalidated and that contributions from an aggregation of polymer chains as proposed by Wegner *et al.* will always be superimposed.

### 1.3.4 Toward Hierarchically Structured Poly(diacetylene)s

The above examples from a variety of research areas serve to show that a combination of the topochemical diacetylene polymerization as a means of covalent capture and the supramolecular self-

---

assembly of oligopeptide-polymer conjugates may be a perfect match. The self-assembly of the oligopeptide-polymer conjugates may give rise to well-defined hierarchical structures based on the formation of  $\beta$ -sheets. The internal structure of these  $\beta$ -sheets, at the same time, establishes an intra-strand distance between adjacent oligopeptides just appropriate for the topochemical polymerization. The latter, on the other hand, is an initiator-free, highly selective polymerization furnishing  $\pi$ -conjugated polymers, which would, supposedly, only marginally interfere with the self-assembly. Based on the combination of these two concepts, the novel “self-assemble, then polymerize” approach is to be developed in the present thesis.



# Outline



## 2 Outline

A new concept aimed at the preparation of hierarchically structured poly(diacetylene)s that can be paraphrased as “*self-assemble, then polymerize*” is going to be developed in the present thesis. The strategy is based on a combination of the supramolecular self-assembly of  $\beta$ -sheet-forming oligopeptide-polymer conjugates and the topochemical diacetylene polymerization which furnishes well-defined  $\pi$ -conjugated polymers. For this purpose, the following specific goals will have to be achieved:

- A modular synthetic approach for the preparation of an oligopeptide-polymer conjugate equipped with a suitable polymer segment, a short oligopeptide sequence aiming at the formation of parallel  $\beta$ -sheets, a diacetylene functionality, and a functional end group will be elaborated.
- The secondary structure formation of the obtained macromonomers in organic solution is going to be investigated predominantly by solution phase IR spectroscopy, whereas the higher structure formation will be studied mainly by scanning force microscopy (SFM).
- In case of a successful self-assembly, the different macromonomers will be subjected to UV-irradiation in organic solution in order to initiate the topochemical diacetylene polymerization which will be followed by UV-vis spectroscopy.
- The potential formation of hierarchically structured poly(diacetylene)s will be elucidated by means of CD spectroscopy and with imaging techniques such as SFM.
- If the topochemical reaction of the diacetylene macromonomers is successful, the scope of the concept may be extended toward oligo(ethynylene)s as molecular precursors for multiple-stranded  $\pi$ -conjugated polymers (“graphite ribbons”).





## Results & Discussion





## 3 Results and Discussion

### 3.1 Synthesis

#### 3.1.1 Molecular Design and Synthetic Strategy

Based on the above described findings concerning the supramolecular self-organization of oligopeptides and their polymer conjugates (Section 1.2) as well as the topochemical diacetylene polymerization using self-assembled scaffolds (1.3.2), we have chosen the following molecular design for our own investigations (Figure 33).

- A short oligo(L-alanine) segment is envisioned to induce self-assembly in solution via the formation of  $\beta$ -sheets.
- A hydrophobic, flexible polymer segment is needed to provide good solubility in organic solvents and prevent the formation of higher aggregates or even insoluble material resulting from a stacking of the  $\beta$ -sheets.
- The diacetylene is to be incorporated directly into the  $\beta$ -sheet array connected via a short flexible linker.
- An end group serves to introduce additional hydrogen-bonding sites and/or chemical functionality.

We have chosen an oligo-L-alanine sequence since such structures have a high propensity to form  $\beta$ -sheet type secondary structures. Aiming at a self-assembly in organic media, a short sequence of four L-alanines was considered adequate given the observed successful  $\beta$ -sheet formation of PEO-functionalized oligopeptides reported by Mutter *et al.* which started at the pentapeptide level already even in aqueous solution.<sup>171</sup> We chose hydrogenated poly(isoprene) as the polymer segment because of the ease of its preparation and end functionalization as well as its inherent non-uniformity in chain length and constitution. The latter reduces the glass-transition temperature of the material which serves to prevent a crystallization of the side-chains and, hence, a global ordering of the macromonomers in solution. The diacetylene moiety was envisioned to be connected directly into

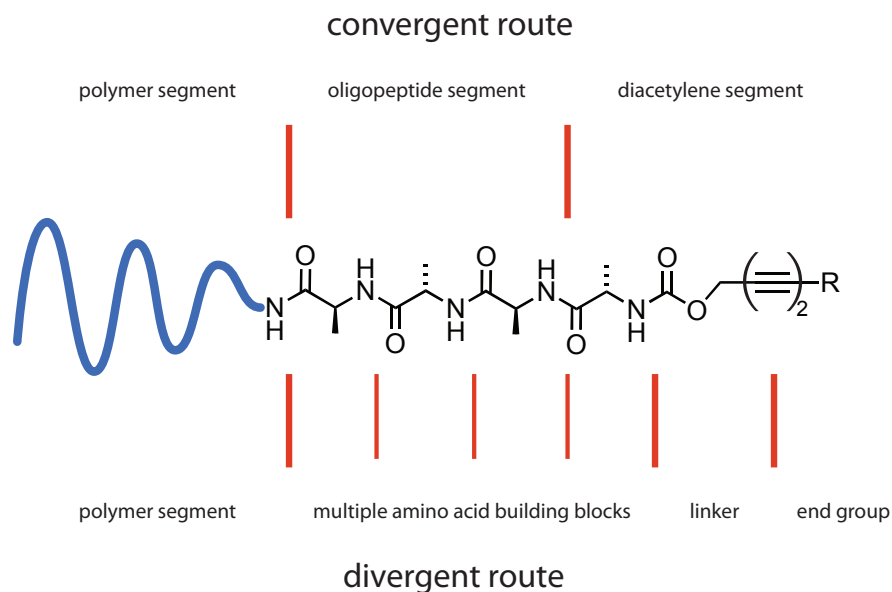


**Figure 33:** Generally, two different synthetic pathways were considered possible. *top:* The *convergent* synthesis makes use of only two coupling reactions, i. e., the attachment of the oligopeptide to the polymer followed by the connection of a prefabricated diacetylene building block. *bottom:* In the *divergent* pathway, all building blocks are connected sequentially.

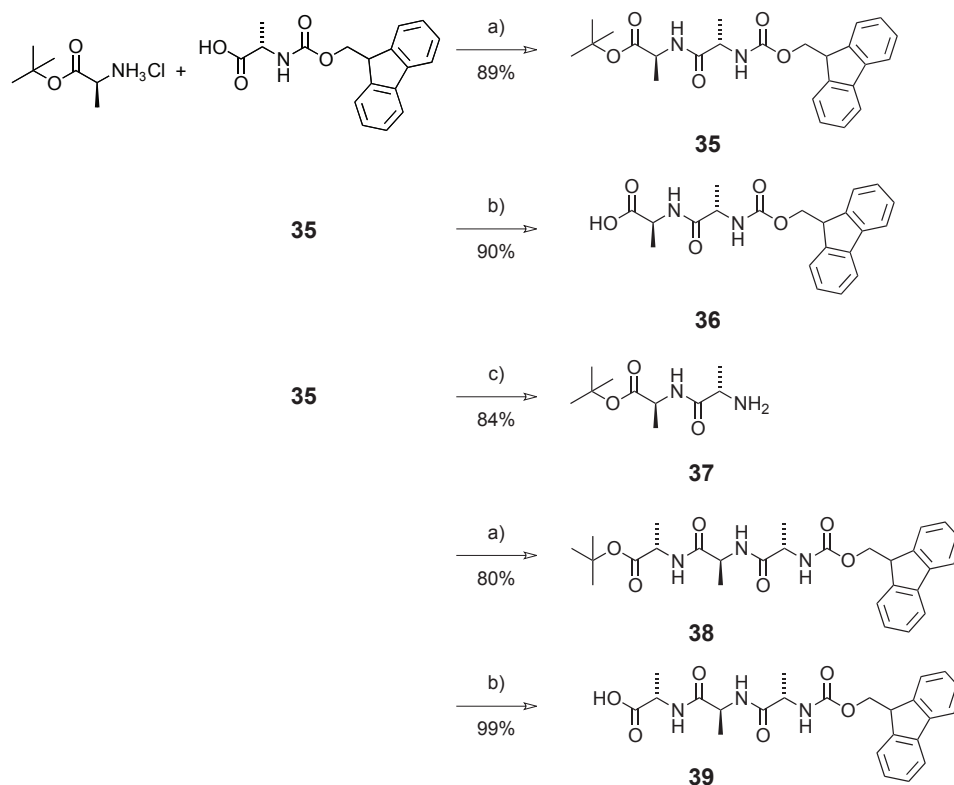
the oligopeptide only separated by a short flexible linker that allowed for the adjustment of the required inclination angle before the polymerization and to accommodate minor changes of the geometry during this process. Finally, an end group was incorporated to control the parallel  $\beta$ -sheet formation as outlined in Section 1.2.4 as well as to potentially introduce additional chemical functionality.

The preparation of the macromonomers can be carried out by a completely sequential, i. e., *divergent* synthesis (Figure 33 bottom). Such a strategy would, however, include many reactions diminishing the overall yield. A completely *convergent* synthesis may be disadvantageous as well due to conceivable solubility issues of the pure oligopeptide building blocks that would potentially be needed. Thus, a compromise (Figure 33 top) is considered as the best synthetic strategy in which parts of the oligopeptide sequence are connected to the solubility-conveying polymer segment first, while a prefabricated diacetylene building block carrying the end group as well as the linker are attached in the final step.

### 3.1.2 Oligopeptide Building Blocks

The oligo(L-alanine) building blocks were prepared by standard solution phase peptide coupling procedures which made use of *N*-(9-fluorenylmethyloxycarbonyl) (Fmoc) and *tert*-butyl esters as an orthogonal pair of protecting groups for the amine and carboxylic acid functionality respec-

tively. (Benzotriazol-1-yloxy)tripyrrolidinophosphonium hexafluorophosphate (PyBOP) or a combination of 1-hydroxybenzotriazole (HOBt) and 1-ethyl-3-(3-dimethyl-aminopropyl)carbodiimide hydrochloride (EDCI) were used as peptide coupling promoters (Scheme 2). Thus, *N*-(9-fluorenylmethyloxycarbonyl)-*L*-alanine was coupled to *L*-alanine *tert*-butyl ester hydrochloride in a PyBOP-promoted peptide coupling reaction to yield *N*-(9-fluorenylmethyloxycarbonyl)-*L*-alanyl-*L*-alanine *tert*-butyl ester **35** in 89% on a 10 g scale after purification by column chromatography. In order to cleave the *tert*-butyl ester, the compound was treated with trifluoroacetic acid (TFA) in DCM. A report<sup>172</sup> claiming that the addition of triethylsilane would be advantageous in these kinds of TFA promoted *tert*-butyl ester deprotections could not be verified and was, hence, not applied. After removal of the solvents in high vacuum (HV) and a recrystallization from DCM, **36** was obtained in 90% yield.



**Scheme 2:** Synthesis of di-, and trimeric alanine building blocks. *Reagents and Conditions:* a) PyBOP, DIEA, DCM/DMF, r.t.; b) trifluoroacetic acid, DCM; c) piperidine, chloroform.

The preparation of tripeptide building blocks required the removal of one of the orthogonal protecting groups. It was found to be advantageous to cleave the base-labile Fmoc group of **35** and subsequently attach an other Fmoc-protected *L*-alanine because the involved building blocks were significantly less expensive. For this purpose, **35** was treated with piperidine in  $\text{CHCl}_3$  according to a standard protocol in solution phase peptide chemistry. Typically, the reaction mixture was

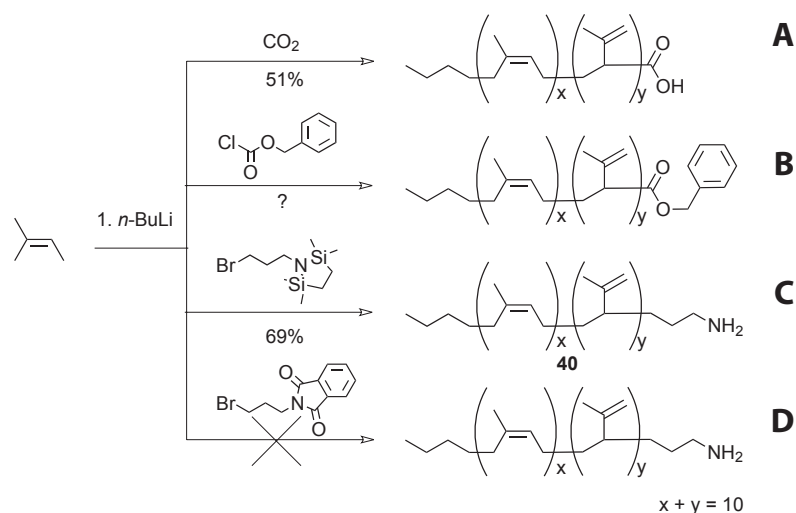
stirred over night, the solvents were removed *in vacuo*, and a purification by column chromatography gave rise to pure **37** in a yield of 84%. In contrast to reports in the literature,<sup>173</sup> the use of 4-(aminomethyl)piperidine as the base did not lead to a complete precipitation of the vinylidene fluorene-adduct formed as a side product, making a subsequent chromatographic step still necessary. Therefore, we continued to use the much cheaper piperidine in all following steps. Subsequently, **37** was coupled to *N*-(9-fluorenylmethyloxycarbonyl)-L-alanine using, again, PyBOP as the promoter. The alanine-trimer **38** was obtained by recrystallization from DCM in 80% yield. The *tert*-butyl ester was then cleaved by TFA to obtain the desired building block **39** in 99% yield.

This set of oligopeptide building blocks enabled a flexible synthetic strategy for the subsequent preparation of the oligopeptide-polymer conjugate.

### 3.1.3 Oligopeptide-Polymer Conjugate Building Blocks

The polymer of choice was poly(isoprene) since it is rather easily accessible via a living anionic polymerization protocol. Thus, the average degree of polymerization  $\bar{P}_n$  can be adjusted by the monomer/initiator ratio, the molecular weight distribution is expected to be narrow, and the introduction of an end group can be controlled. Poly(isoprene) is also non-uniform with regard to the constitution of its repeat units due to the competing 1,2- and 1,4-addition reactions during the polymerization. As a consequence, the obtained hydrophobic polymer is absolutely unable to crystallize, giving rise to a good solubility and favorable effects during the self-assembly of the system. Preferable functional end groups for the subsequent connection to an oligopeptide segment are carboxylic acid or amine functions. Preliminary investigations<sup>174</sup> had shown that a carboxylic acid end group can be introduced by quenching the living chain ends with dry ice (Scheme 3A). Although that procedure worked acceptably well, the contamination of the system with water due to the condensation of moisture onto the cold dry ice could not be completely avoided. As a consequence, a rather large amount of unfunctionalized material was obtained. To circumvent this issue, benzyl chloroformate was used as the quencher to introduce the carboxylic acid in the form of its benzyl ester (Scheme 3B). Because the obtained mass spectra of the product were hard to interpret, we were not able to exclude that a double or even threefold addition of chain ends to the carbonyl group had occurred and we, therefore, abandoned this methodology. These setbacks were overcome by the introduction of an amine functionality that additionally allowed for the connection of the oligopeptide from the N-terminus which is the standard procedure in the solid phase synthesis of oligopeptides. The required building blocks are generally cheaper, and the chemistry involved has been extensively documented in the literature. Thus, the polymerization reaction was quenched with 1-(3-bromopropyl)-2,2,5,5-tetramethyl-1-aza-2,5-disilacyclopentane (Scheme 3C). The silyl protecting group was subsequently

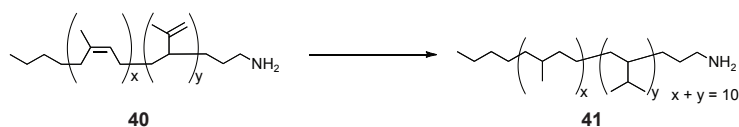
removed *in situ* by the addition of aqueous HCl. Attempts to replace this rather expensive reagent by *N*-(3-bromopropyl)phthalimide (Scheme 3D) failed, most likely due to side reactions of the living anionic chain ends with the imide functionality. This was indicated by an intensification of the reaction color to orange after the quencher had been added to the reaction, although a quick decoloration caused by the deactivation of the living chain ends had been anticipated.



**Scheme 3:** Synthesis of differently end-functionalized polymer coil segments. The introduction of a carboxylic acid is possible by quenching the reaction with dry ice. However, an amine functionality is better from a synthetic as well as a strategic perspective and can be achieved by the use of 1-(3-bromopropyl)-2,2,5,5-tetramethyl-1-aza-2,5-disilacyclopentane as the quenching reagent which furnished **40** in 69% yield.

In more detail, the amine-terminated poly(isoprene) **40** was prepared by a living anionic polymerization of isoprene initiated with *n*-butyl lithium in THF starting at  $-78^{\circ}\text{C}$  and warming to  $0^{\circ}\text{C}$ , followed by a quenching with the silyl-protected 3-bromo-propylamine derivative. The degree of polymerization was controlled by the monomer/initiator ratio which was typically chosen to be 9:1 leading to an average degree of polymerization  $\bar{P}_n \approx 9\text{--}10$ . A ratio of 1,4- to 1,2-addition of approximately 1:4 (according to  $^1\text{H}$  NMR spectroscopy) was usually observed under the chosen conditions (Figure 34A). Hydrochloric acid was added to remove the protecting group, and the desired product was obtained after a basic aqueous workup followed by column chromatography to remove minor amounts of unfunctionalized material in yields of up to 69% on a 20 g scale.

In order to avoid side reactions in subsequent transformations, the remaining double bonds were removed by a high pressure hydrogenation of **40** in toluene/ethanol (75:5 v/v) solution (Scheme 4). Palladium on charcoal was added as the catalyst, and a  $\text{H}_2$  pressure of 100 bar was applied. Depending on the catalyst quality, the reaction was complete after 3–10 days. The purification of the material was achieved by filtering the mixture through a layer of Celite covered with a second layer of activated



**Scheme 4:** Removal of the olefins from **40** by high pressure hydrogenation. *Reagents and Conditions:* 8 mol% Pd/C, 100 bar H<sub>2</sub>, 80 °C, toluene/EtOH, 3–10 days.

carbon in a glass filter frit. This plug was rinsed carefully with dichloromethane (DCM), which is a much better solvent for the poly(isoprene) as compared to toluene. After removal of the solvents, nearly quantitative amounts of **41** were obtained. It was found that the double bonds resulting from the 1,4-addition were easily removed under the chosen conditions whereas it was difficult to entirely hydrogenate the terminal olefins originating from the 1,2-additions. Therefore, a small amount (<1%) of olefins typically remained in the polymers and gave rise to a signal in the <sup>1</sup>H NMR at a value of 4.6–4.8 ppm (Figure 34B).

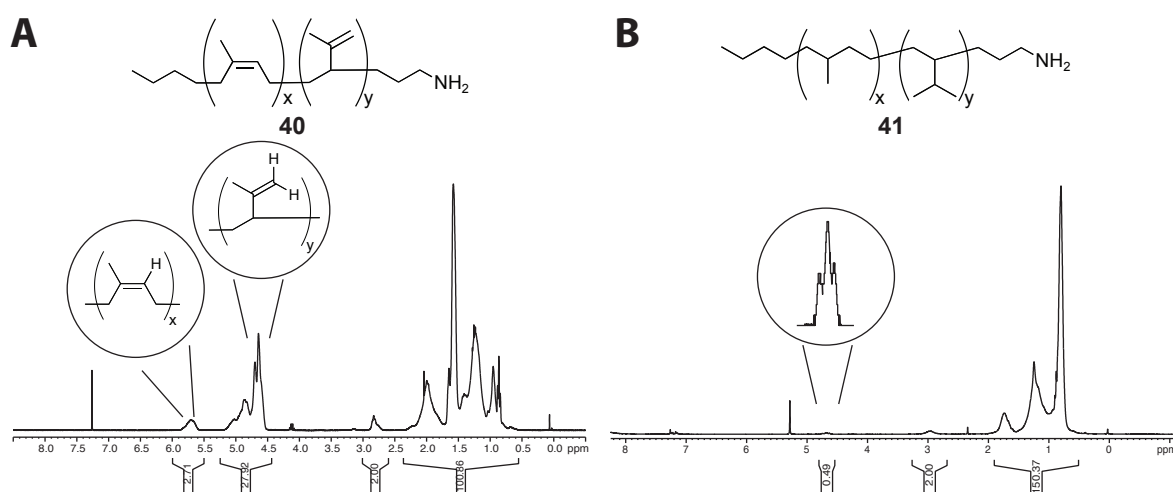
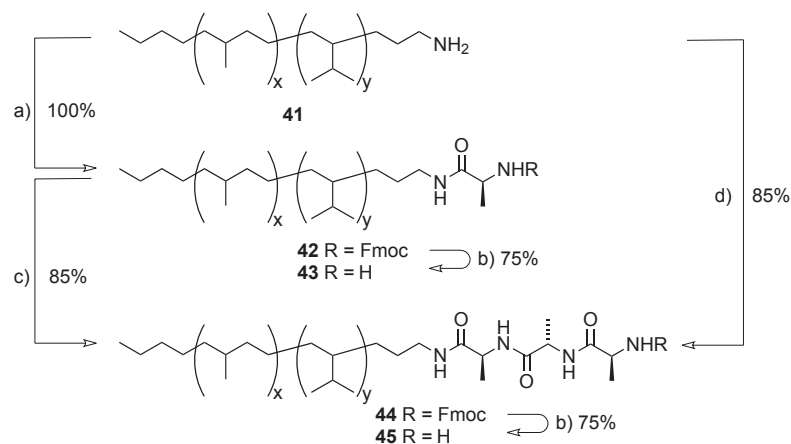


**Figure 34:** A) The relative intensities of the different olefin signals in the <sup>1</sup>H NMR allowed for an estimation of the ratio of 1,2- and 1,4-addition reactions during the formation of the polymer, B) these signals nearly completely disappeared after the hydrogenation, indicating that only a minor amount of terminal olefins was left.

The oligopeptide sequence was introduced by peptide coupling reactions between different amino acid or oligopeptide building blocks and **41** (Scheme 5). Thus, *N*-(9-fluorenylmethyloxycarbonyl)-L-alanine was attached to the polymer segment by an EDCI/HOBt-promoted peptide coupling reaction. An optimized protocol previously developed in the Schlüter group was applied.<sup>175</sup> Thus, the transformation of the carboxylic acid to the active ester intermediate was started by the addition of HOBt followed by the highly reactive EDCI at low temperature (−25 °C) in a mixture of dimethylformamide (DMF) and DCM. The mixture was allowed to reach room temperature while the reaction was monitored by thin layer chromatography (TLC). Upon

completion of the reaction, the solution was combined with a DCM solution containing the amine component and diisopropylethylamine (DIEA) at  $-40^{\circ}\text{C}$ . Depending on the quality of the starting materials, this protocol furnished yields ranging from 80% to 100% after an acidic aqueous workup. Therefore, the Fmoc-L-alanine functionalized polymer coil segment **42** typically did not require any further purification by column chromatography since the reaction could be driven to quantitative conversion by using a small excess of the amino acid derivative.



**Scheme 5:** The synthesis of the oligopeptide functionalized polymer coil intermediates was achieved by solution phase peptide synthesis. *Reagents and Conditions:* a) *N*-(9-fluorenylmethyloxycarbonyl)-L-alanine, EDCI/HOBt, TEA, DCM/DME,  $-40^{\circ}\text{C} \rightarrow \text{r.t.}$ ; b) piperidine, chloroform; c) Fmoc-Ala<sub>2</sub>-OH, PyBOP, DIEA, DCM/DME, r.t.; d) Fmoc-Ala<sub>3</sub>-OH, PyBOP, DIEA, DCM/DME, r.t.

The base-labile Fmoc protecting group was then removed by treating **42** with piperidine in  $\text{CHCl}_3$ , and a purification by column chromatography gave rise to pure **43** in yields of 75 to 80%. Subsequently, **43** was subjected to a PyBOP-promoted peptide coupling with **36** to give **44** in 85% yield after column chromatography. This coupling protocol was chosen because the EDCI couplings require a tedious preparation of the synthesis due to the elaborate temperature protocol, whereas a simple aqueous workup is sufficient afterwards. The PyBOP couplings, on the other hand, are very convenient in terms of the ease of the protocol and a less pronounced sensitivity against water in the reaction mixture. However, a purification by column chromatography is almost always necessary which is exacerbated by the often difficult removal of the phosphorous-containing side product. The use of PyBOP was possible in this case because the Fmoc-protected oligopeptide functionalized hydrogenated poly(isoprene) derivatives had  $R_f$  values as high as 0.9 in DCM/MeOH (10:1) mixtures compared to values of  $R_f$  0.3 found for the PyBOP side products. Again, the Fmoc-group was removed by treatment with piperidine to give the intermediate **45** in 75% yield after purification by column chromatography. This synthetic strategy worked out acceptably well with an overall yield of 48% over

four steps with respect to the initially used amount of polymer coil. However, a reduction of the number of synthetic steps was still desirable. For this purpose, the trimeric building block **39** was reacted directly with the amine terminated, hydrogenated poly(isoprene) **41** in a PyBOP-promoted peptide coupling reaction. As expected, the solubility of the *in situ* formed active ester turned out to be an issue. Thus, the reaction mixture needed to contain a higher DMF content to avoid its precipitation during the reaction. The yield of the reaction was 85% after purification, just as in the case of the dipeptide building block. However, the overall yield after the final removal of the Fmoc group from **44** could be increased from 48% to 64% due to the shorter reaction sequence. Additionally, the time needed to prepare the crucial intermediate **45** could be reduced to three days, because all other building blocks were easily prepared on a large scale and were, thus, available at all times.

### 3.1.4 Characterization of the Oligopeptide-Polymer Conjugates

The oligopeptide-polymer conjugates described so far were characterized by  $^1\text{H}$  NMR, matrix assisted laser desorption ionization - time of flight (MALDI-TOF) mass spectrometry and elemental analysis.

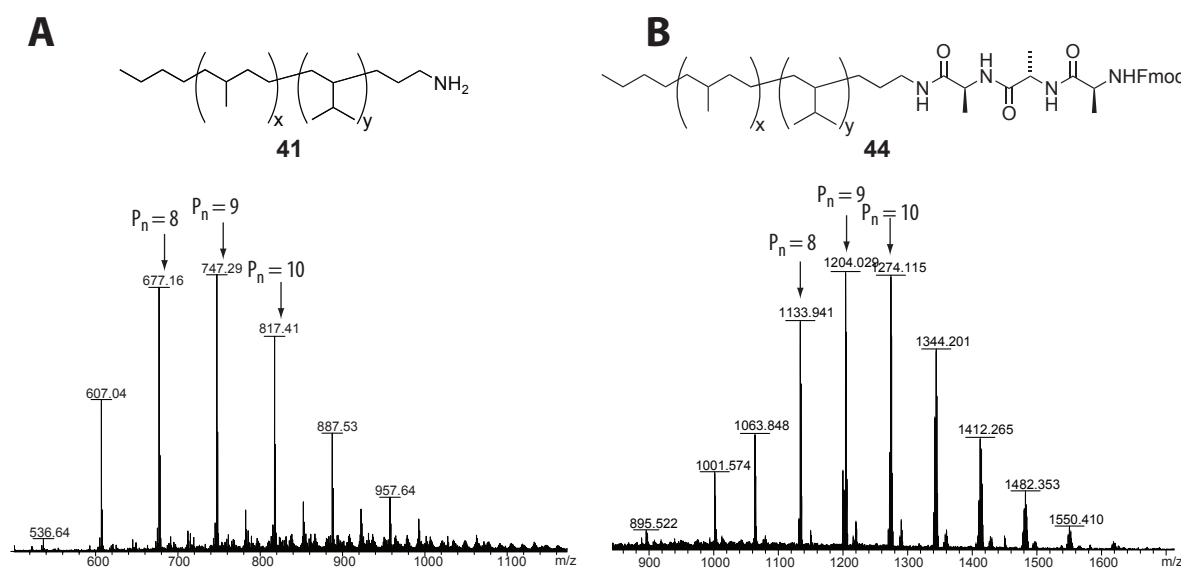


**Figure 35:** Representative MALDI-TOF MS spectra of A) **41** and B) **44** showing series of molecular ion peaks separated by the mass of the repeat unit ( $\text{C}_5\text{H}_{10}$ ). A second and a third series tended to appear in some spectra which were caused by sodium or potassium adducts. The maximum of intensity was found at  $\bar{P}_n = 9$ , and the distribution appeared to be narrow. Both properties were not affected by the involved synthesis and purification steps involved.

Attempts to determine the molecular weights by means of gel permeation chromatography (GPC) were hampered by the fact that all compounds featuring a free amine functionality were not eluted at all. In case of the Fmoc-protected derivatives, the GPC traces were nearly indistinguishable due to



the low molecular weights that were close to the calibration limit of the GPC instrument used in our group and the small relative molecular weight difference. The determination of the molecular weight distribution was, nevertheless, possible by MALDI-TOF MS in combination with the Polytool® software by Bruker (Figure 35). It turned out to be problematic to obtain good spectra from the amine-terminated poly(isoprene) **40** as well as the alanine-substituted derivative **43** because these compounds could only hardly be ionized by the matrix. However, electrospray ionization (ESI) spectra confirmed that also these compounds had the expected average molecular weights. Unfortunately, no complete molecular weight analysis was possible with spectra measured on the ESI spectrometer due to software limitations.

**Table 3.1:** Molecular weight determination of the poly(isoprene) building blocks.

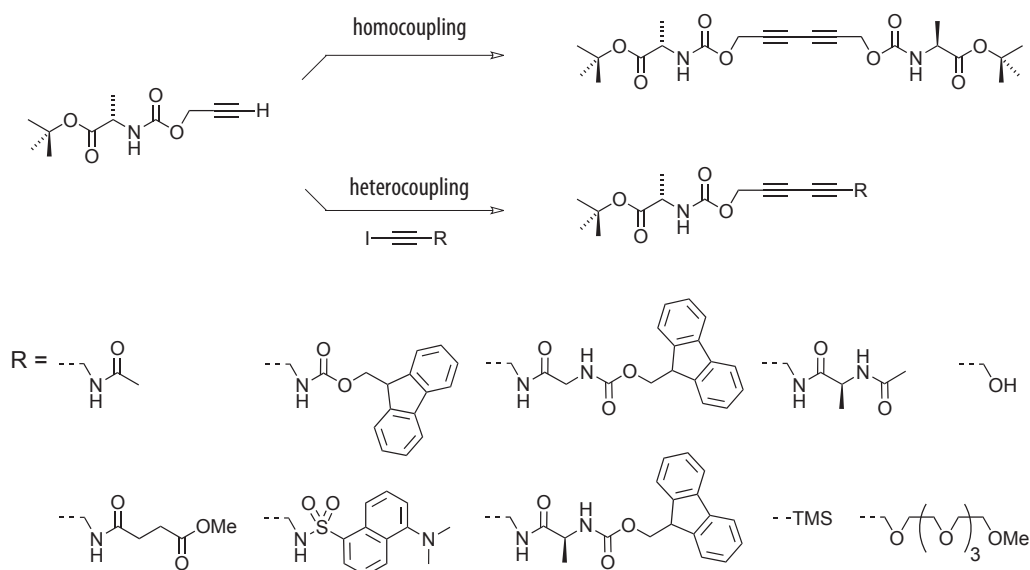
Compound	Calculated <sup>a</sup>	<sup>1</sup> H NMR <sup>b</sup>	MALDI MS		
	$\bar{M}_n$	$\bar{M}_n$ ( $\bar{P}_n$ )	$M_p$ ( $P_p$ ) <sup>c</sup>	$\bar{M}_n$ ( $\bar{P}_n$ ) <sup>d</sup>	PDI <sup>d</sup>
<b>40</b>	728	1244 (16.6)	728 (9)	n.d.	n.d.
<b>41</b>	746	1070 (13.7)	747 (9)	760 (9.1)	1.016
<b>42</b>	1040	1200 (11.3)	1063 (9)	1100 (9.5)	1.012
<b>43</b>	818	870 (9.8)	818 (9)	n.d.	n.d.
<b>44</b>	1182	1370 (11.7)	1204 (9)	1220 (9.2)	1.007
<b>45</b>	960	1220 (12.7)	1053 (10)	1060 (10.1)	1.010

<sup>a</sup>Calculated molecular weights assuming that the poly(isoprene) segments had an average degree of polymerization of  $\bar{P}_n = 9$ , according to the monomer/initiator ratio [isoprene]/[BuLi] = 9 employed in the initial anionic isoprene polymerization. <sup>b</sup>Average molecular weight determined by comparison of the intensities of the CH<sub>2</sub>NHR proton signals vs. the aliphatic poly(isoprene) proton signals. <sup>c</sup>([M+H]<sup>+</sup>) for **41**, ([M+Na]<sup>+</sup>) for **42**, **44** and **45**. <sup>d</sup>Number average molecular weight  $\bar{M}_n$  and polydispersity index PDI as calculated with the Polytool software package by Bruker.

The maximum degree of polymerization was found to be between  $\bar{P}_n = 9$ -10, and the molecular weight distribution was very narrow with typical polydispersity index (PDI) values of around 1.01. Although one has to admit that this method underestimates the polydispersity but the trend towards smaller PDIs with an increasing weight of the monodisperse segment in the molecule could clearly be extracted from the molecular weight data (Table 3.1).

### 3.1.5 Diacetylene Building Blocks

We decided to synthesize the diacetylene building blocks in Sonogashira<sup>176</sup> and Hay<sup>177</sup> type acetylene coupling reactions, since the mild conditions are compatible with various functional groups. Therefore, terminal acetylenes comprising a carbamate linker as well as haloacetylenes bearing various end groups were prepared (Scheme 6).

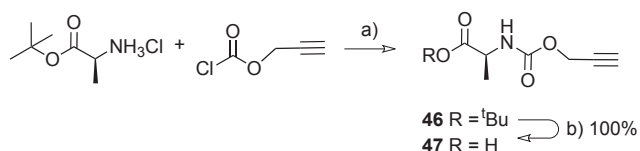


**Scheme 6:** Overview of the different functionalized diacetylene building blocks obtained in acetylene homo- and heterocoupling reactions.

#### 3.1.5.1 Synthesis of Propargyl Carbamates

The synthesis of the terminal acetylene unit started with the preparation of the propargyl carbamate **46** by reaction of L-alanine *tert*-butyl ester hydrochloride with propargyl chloroformate according to a literature procedure (Scheme 7).<sup>178</sup> The amine-component was dissolved in a mixture of DCM and triethylamine (TEA). A small excess of the chloroformate was then added slowly at 0 °C, and the reaction progress was monitored by TLC. Upon completion, the triethylamine hydrochloride was removed by an acidic aqueous workup, and no further purification of the product **46** was required after removal of the solvent *in vacuo*. In order to cleave the *tert*-butyl ester, **46** was treated with TFA in DCM. The corresponding carboxylic acid derivative **47** was obtained in quantitative yield after concentrating the reaction mixture at the rotary evaporator.

It is possible to obtain this building block directly by a treatment of L-alanine with propargyl chloroformate in aqueous NaOH solution.<sup>178</sup> However, only relatively poor yields were obtained so that

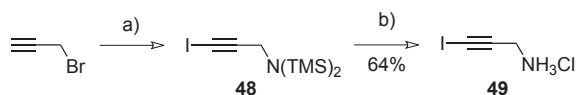


**Scheme 7:** Synthesis of propargyl carbamates **46** and **47** for the introduction of a carbamate linker between the oligopeptide and the diacetylene. *Reagents and Conditions:* a) TEA, DCM, 0 °C; b) TFA, DCM.

this procedure was not pursued any further and the more expensive alanine *tert*-butyl ester derivative was used for the preparation of the terminal acetylene derivative in the subsequent acetylene coupling reactions.

### 3.1.5.2 Synthesis of Haloacetylene Derivatives

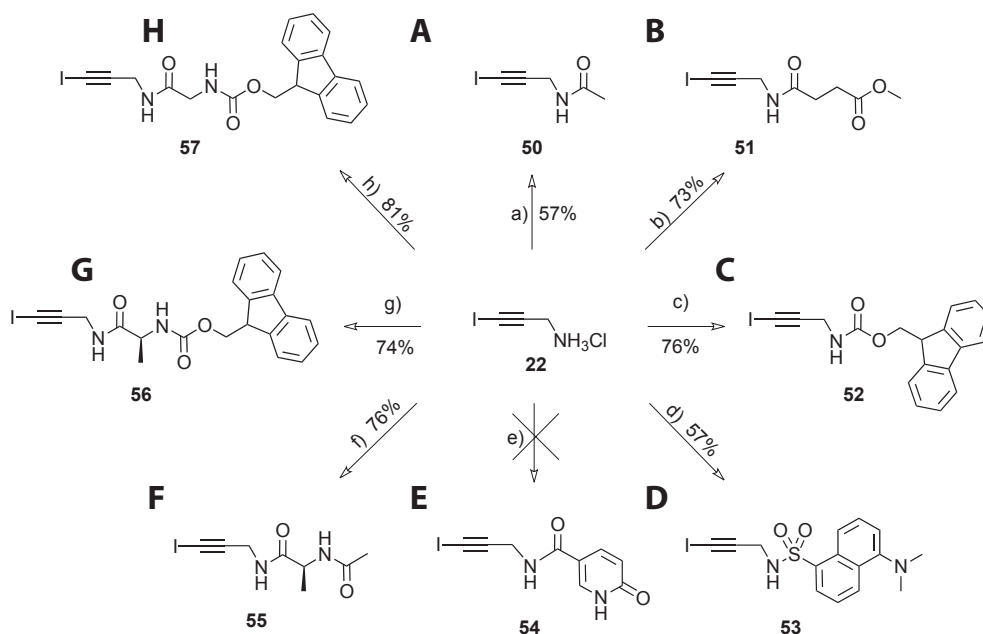
A variety of haloacetylene derivatives bearing different end groups was prepared. We decided to use iodinated derivatives due to their high reactivity in the Sonogashira reaction.<sup>179</sup> The direct iodination of propargylamine failed, most likely due to a halogenation of the unprotected amine functionality.<sup>174</sup> Instead, the hydrochloride salt of the iodinated propargylamine **49** was obtained in a simple one-pot procedure from commercially available propargyl bromide by adapting a previously published procedure for the preparation of other propargyl and vinyl compounds carrying silylated amine functionalities (Scheme 8).<sup>180</sup> Thus, propargyl bromide was added to a solution of 2 equivalents of lithium hexamethyldisilazide (LHMDS) in Et<sub>2</sub>O at -78 °C. After warming to room temperature, I<sub>2</sub> was added at -78 °C. An aqueous workup and the removal of excess hexamethyldisilazane (HMDS) by distillation afforded the crude silylated iodopropargylamine **48** which was subjected to alcoholysis in freshly prepared anhydrous HCl in a mixture of MeOH and DCM (1:1) without further purification. The hydrochloride salt precipitated immediately and could be easily filtered off to obtain **49** in 64% yield on a multiple gram scale.



**Scheme 8:** Synthesis of the iodoacetylene building block **49**. *Reagents and Conditions:* a) 2 eq LHMDS, 2. I<sub>2</sub>, Et<sub>2</sub>O, -78 °C → r.t.; b) HCl in MeOH/DCM.

This building block allowed for the facile synthesis of a variety of amide, carbamate and sulfonamide containing derivatives (Scheme 9). For instance, the treatment of **49** with a large excess of acetic anhydride in TEA basic DCM furnished the acetylated derivative **50** after basic aqueous workup and column chromatography in 57% yield (Scheme 9A). Furthermore, the iodopropargylamine derivative **49** was treated with methyl succinyl chloride in DCM at 0 °C using DIEA as the

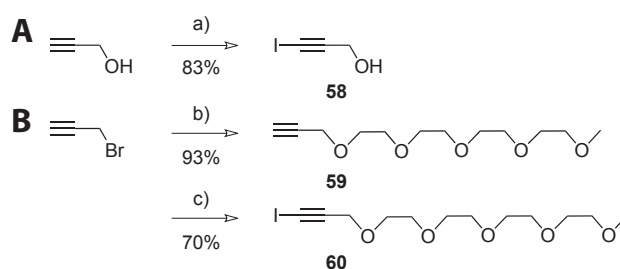
base (Scheme 9B). The latter was used because it forms a DCM-soluble hydrochloride while the TEA adduct sometimes tends to form gels at low temperature. After the slow addition of the acid chloride, the reaction was stirred until TLC indicated a complete conversion of the starting materials. After removal of the base by an acidic aqueous workup, the product **51** was obtained by column chromatography in 73% yield. Some product may have been lost in the aqueous phase but the main reason for this comparably low yield was the low purity of the commercially obtained acid chloride. In an analogous reaction, the Fmoc-protected building block **52** was prepared (Scheme 9C). Thus, **49** was treated with 9-fluorenylmethyloxycarbonyl chloride in DCM under basic conditions at 0 °C. The product precipitated in the separating funnel during an attempted aqueous workup due to the partial removal of the base from the organic phase. Thus, the material was directly recrystallized from DCM in later reactions to obtain the desired product in 76% yield. Additionally, a sulfonamide derivative **53** was prepared by treating **49** with *N*-5-dimethylamino-1-naphthalenesulfonyl chloride again in DIEA basic DCM (Scheme 9D). According to TLC, several side products formed during the synthesis. Therefore, the product was purified by column chromatography, and only 57% of the pure product were obtained.



**Scheme 9:** Preparation of various iodoacetylene derivatives from **49**. *Reagents and Conditions:* a) acetic anhydride, TEA, DCM; b) methyl succinyl chloride, DCM, DIEA, 0 °C; c) Fmoc-chloride, DCM, DIEA, 0 °C; d) Dansyl-chloride, DCM, DIEA, 0 °C; e) 6-hydroxynicotinic acid, PyBOP, DCM, DME, DIEA; f) *N*-Acetyl-L-alanine, PyBOP, DCM, DME, DIEA, 0 °C; g) *N*-(9-fluorenylmethyloxycarbonyl)-L-alanine, PyBOP, DCM, DME, DIEA, 0 °C; h) *N*-(9-fluorenylmethyloxycarbonyl)-glycine, PyBOP, DCM, DME, DIEA, 0 °C.

Derivative **49** was also used in standard peptide coupling reactions with carboxylic acid derivatives. One such attempt was carried out with 6-hydroxynicotinic acid. However, the reaction failed due to the complete insolubility of the starting material even in hot DMF so that the nicotinic acid derivative **54** was not obtained (Scheme 9E). Reactions using commercially available amino acid derivatives such as *N*-acetyl-L-alanine worked much better (Scheme 9F). Thus, the corresponding iodoacetylene derivative **55** was prepared by a PyBOP promoted peptide coupling and was obtained after an aqueous workup and column chromatography in 76% yield. Similarly, the Fmoc-protected derivatives **56** and **57** were prepared (Scheme 9G,H). Both derivatives were obtained in PyBOP promoted peptide couplings between **49** and Fmoc-protected amino acid building blocks *N*-(9-fluorenylmethyloxycarbonyl)-L-alanine and *N*-(9-fluorenylmethyloxycarbonyl)-glycine, respectively. The alanine derivative was obtained in 74% yield after recrystallization from DCM, whereas the glycine compound gave a yield of 81%.

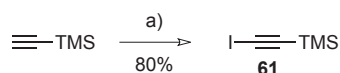
Further iodoacetylene building blocks were prepared that were derivatives of propargyl alcohol (Scheme 10A). The latter was, therefore, directly iodinated according to a protocol developed in our group,<sup>181</sup> which involved a treatment with KOH in methanolic solution followed by the addition of I<sub>2</sub>. The iodinated product **58** was obtained in 83% yield on a 40 g scale after extraction of the neutralized reaction mixture with Et<sub>2</sub>O. This derivative turned out to be tremendously irritant to the skin and, thus, the exposure of tiniest amounts already led to first itchy and later hurting wounds on the hands and, therefore, a very careful handling of the substance was essential.



**Scheme 10:** Synthesis of the iodinated propargyl alcohol **58** as well as the tetraethylene glycol functionalized building block **60**. *Reagents and Conditions:* a) 1. KOH (4 eq), I<sub>2</sub>, MeOH, r.t., 16 h; 2. HCl, Et<sub>2</sub>O extraction; b) tetraethyleneglycol monomethyl ether, NaH, THF, 0 °C, 16 h; c) 1. KOH (4 eq), I<sub>2</sub>, MeOH, r.t., 16 h; 2. HCl, CHCl<sub>3</sub> extraction.

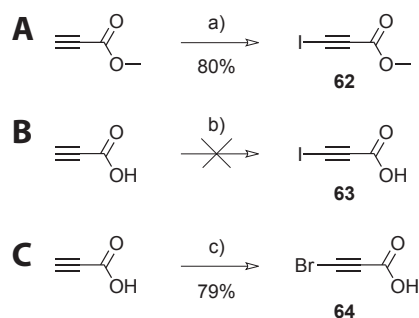
A related building block, i. e., an iodoacetylene that was equipped with a tetra(ethylene glycol) chain, was also prepared (Scheme 10B). Thus, tetra(ethylene glycol) monomethyl ether was subjected to a Williamson etherification reaction with propargyl bromide using NaH as the base. The propargyl ether **59** was obtained in 93% yield and iodinated under the same conditions as in the case of **58** to give **60** in 70% yield after column chromatography.

Additionally, a TMS terminated building block **61** was prepared starting from trimethylsilylacetylene (Scheme 11). Although this compound is commercially available, we prepared it by ourselves because of its enormous price. It was obtained by treating TMS-acetylene with *n*-butyl lithium at low temperature followed by quenching of the anion with elemental I<sub>2</sub>. The pure material was obtained in 80% yield after a distillation at reduced pressure.



**Scheme 11:** Synthesis of building block **61** exhibiting a trimethylsilyl group. *Reagents and Conditions:* a) 1. *n*-butyl lithium, THF, -78 °C → 0 °C; 2. I<sub>2</sub>, -78 °C → r.t., 16 h, distillation.

Finally, we prepared a different class of haloacetylenes that were equipped with a carbonyl group in direct conjugation to the triple bond (Scheme 12). Starting from propiolic acid methyl ester, the corresponding iodoacetylene **62** was prepared according to a procedure published for the iodination of another base-labile terminal acetylene (Scheme 12A).<sup>182</sup> Thus, propiolic acid methyl ester was treated with *N*-iodosuccinimide (NIS) in acetone catalyzed by AgNO<sub>3</sub>. After completion of the reaction, ice was added to the reaction mixture. The latter was then extracted with Et<sub>2</sub>O, and the obtained material was further purified by sublimation under high vacuum to obtain **62** in 80% yield.



**Scheme 12:** Synthesis of the halogenated propiolic acid derivatives **62**, **63** and **64**. *Reagents and Conditions:* a) AgNO<sub>3</sub>, NIS, acetone, 2.5 h, r.t., sublimation; b) aqueous KOH, I<sub>2</sub>, 0 °C, 30 min; c) aqueous KOH, Br<sub>2</sub>, 0 °C, 30 min.

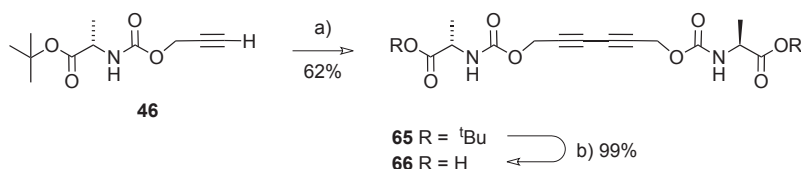
A procedure for the chlorination and bromination of propiolic acid<sup>183</sup> was adapted to the synthesis of an analogous iodinated compound (Scheme 12B). Unfortunately, the attempt failed due to the very low solubility of I<sub>2</sub> in aqueous KOH solution and the associated slow formation of hypoiodite, the crucial reactant in this transformation. However, the described protocol for the synthesis of the brominated derivative could be reproduced perfectly. Thus, an aqueous KOH solution was prepared,

and Br<sub>2</sub> was added to form a hypobromite solution. This could easily be followed due to the accompanied decolorization of the reaction mixture. Propiolic acid was then added, and the reaction mixture was neutralized and extracted with Et<sub>2</sub>O after a reaction time of 30 min. After recrystallization of the crude material from hot hexanes, pure **64** was obtained in a yield of 79%. The material was, similar to the iodinated propargyl alcohol derivative, an outmost aggressive compound. In addition to its escharotic properties it was also lachrymatory. These characteristics were described in a very figurative fashion already in the original literature from 1935.<sup>183</sup>

With the presented diverse set of haloacetylene compounds **a**, likewise, extensive collection of diacetylene derivatives was synthesized as described in the following section.

### 3.1.5.3 Synthesis of Amino Acid Functionalized Diacetylene Compounds

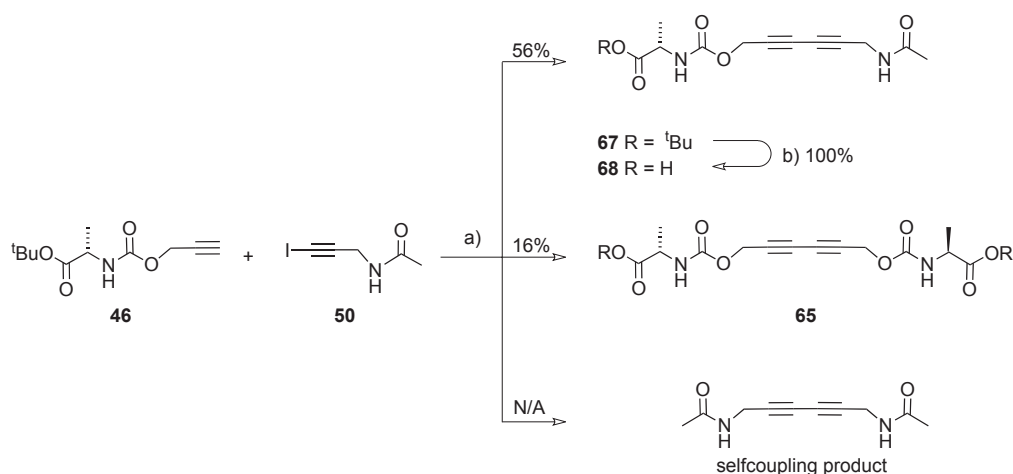
As illustrated in Scheme 6, we performed acetylene homo- and heterocoupling reactions in order to obtain the diacetylene derivatives. Starting from **46**, we prepared the symmetric diacetylene derivative **65** (Scheme 13). Thus, **46** was subjected to a homocoupling reaction using the Hay protocol,<sup>177</sup> i. e., by using CuCl and tetramethylethylenediamine (TMEDA) as the catalyst system. After bubbling air through the characteristically green acetone solution for three hours, the catalyst was removed by filtering the reaction mixture through a plug of silica gel. The oily crude product partially crystallized in the course of several days giving rise to pure **65** in a yield of 62%. The subsequent removal of both ester functions with TFA gave the dicarboxylic acid **66** in 99% yield without any problems.



**Scheme 13:** Preparation of the symmetric building block **65** under Hay conditions and its conversion to the dicarboxylic acid derivative **66**. *Reagents and Conditions:* a) TMEDA, CuCl, air, acetone, room temperature; b) TFA, DCM.

All unsymmetric diacetylenes were prepared using the Sonogashira protocol<sup>176</sup> using standardized conditions. Dry THF was used as the solvent, diisopropylamine (DIPA) as the base and a catalyst system of 10 mol% CuI and 2 mol% PdCl<sub>2</sub>(PPh<sub>3</sub>)<sub>2</sub> at 0 °C. Even at that temperature, the reaction was typically very fast with complete conversions already reached after 30 min according to TLC. The inevitable formation of the homo- and selfcoupling side products which typically had R<sub>f</sub> values similar to the starting materials made an unambiguous determination of the completion of the reaction

difficult. Therefore, the reaction times were usually chosen to exceed 3 h. We typically found that the oxidative homocoupling of the propargyl carbamate was faster than the selfcoupling of the halogenated acetylenes. In order to suppress the former reaction, a reductive  $N_2$  atmosphere containing 10% of  $H_2$  was applied. However, no substantial improvements could be achieved with that method and it was not pursued any further. Another alternative to increase the yield of the heterocoupling product was to use an excess (typically 1.2 eq) of the iodinated compounds. By taking these measures, the unsymmetric products were formed in acceptable yields between 45 and 61%.

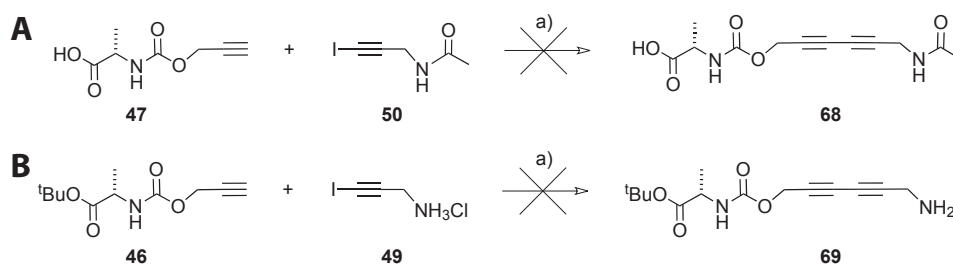


**Scheme 14:** Synthesis of the acetamidomethyl-functionalized diacetylene building blocks **67** and **68** and the formation of homocoupling and selfcoupling side products. *Reagents and Conditions:* a)  $PdCl_2(PPh_3)_2$  (2 mol%), CuI (10 mol%), DIPA, THF,  $0^\circ C$ ; b) trifluoroacetic acid, DCM.

The reaction of acetamidomethyl-functionalized iodoacetylene **50** with terminal acetylene **46** (Scheme 14) was stirred for 3 h until the reaction mixture only contained the desired heterocoupling product **67** ( $R_f$ : 0.5, DCM/MeOH 10:1) and the symmetric side products, i. e., the homocoupling product **65** ( $R_f$ : 0.8, DCM/MeOH 10:1) as well as the selfcoupling product exhibiting two acetamido groups ( $R_f$ : 0.2, DCM/MeOH 10:1). Thus, a separation by column chromatography was unproblematic and **67** could be isolated in a yield of 56%. Also **65** could be obtained in 16% yield whereas the selfcoupling product was not isolated. The subsequent removal of the *tert*-butyl ester with TFA furnished the free carboxylic acid derivative **68** in quantitative yield. The TFA was carefully removed by repeated co-evaporation with  $CHCl_3$  followed by a rigorous drying in HV.

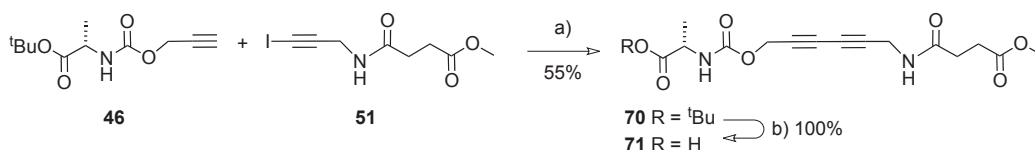
An analogous reaction was carried out using terminal acetylene **47** which comprised a free carboxylic acid function (Scheme 15A). However, no desired product could be isolated which may be attributed to the presence of the acid functionality that would be deprotonated under the chosen conditions and may, thus, deactivate the copper catalyst by complex formation.





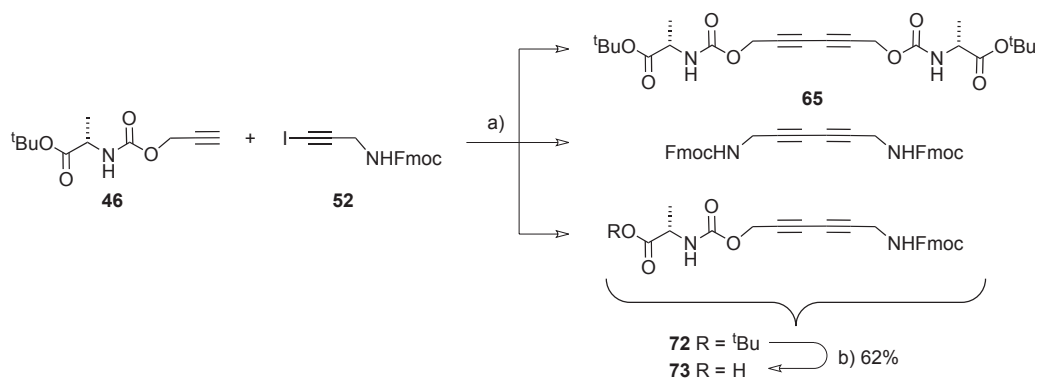
**Scheme 15:** Attempted direct synthesis of diacetylene building blocks exhibiting a free carboxylic acid or amine function. *Reagents and Conditions:* a)  $\text{PdCl}_2(\text{PPh}_3)_2$  (2 mol%), CuI (10 mol%), DIPA, THF,  $0^\circ\text{C}$ .

Similarly, a reaction of iodopropargylamine **49** with **46** only yielded a black tar with no hint of the product **69** (Scheme 15B). The presence of the primary amine may be responsible for that phenomenon as well as the instability of the product. The latter would be in agreement with previous findings in our group<sup>174</sup> where a phthalimide-protected aminomethyl-functionalized diacetylene derivative could not be deprotected by a simple hydrazinolysis, obviously due to the instability of the product.



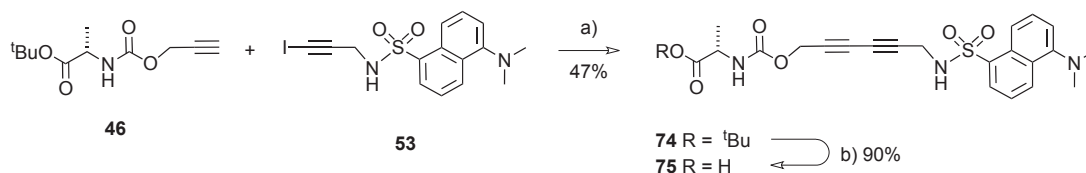
**Scheme 16:** Synthesis of the succinic acid methyl ester functionalized diacetylene building blocks **70** and **71**. *Reagents and Conditions:* a)  $\text{PdCl}_2(\text{PPh}_3)_2$  (2 mol%), CuI (10 mol%), DIPA, THF,  $0^\circ\text{C}$ ; b) trifluoroacetic acid, DCM, r.t.

As a consequence, we only used **46** in the following heterocoupling reactions with the other iodinated derivatives. The reaction of the succinyl ester derivative **51** worked comparably well, and the product **70** was obtained in 55% yield after an acidic aqueous workup followed by a purification by column chromatography (Scheme 16). The homocoupling product **65** could typically be isolated as well whereas the selfcoupling product was not isolated since it was the last material to be eluted from the column and not a useful material. The purification was, nevertheless, tedious in this case because the  $R_f$  value of **70** and the remainders of the palladium catalyst happened to be nearly identical in any chosen eluent mixture and, therefore, the obtained material tended to be not perfectly pure. It was, however, possible to purify the material completely after the subsequent *tert*-butyl ester deprotection since the obtained carboxylic acid derivative **71** was much more polar and could be separated by column chromatography if necessary. The yield of the deprotection reaction was usually close to quantitative.



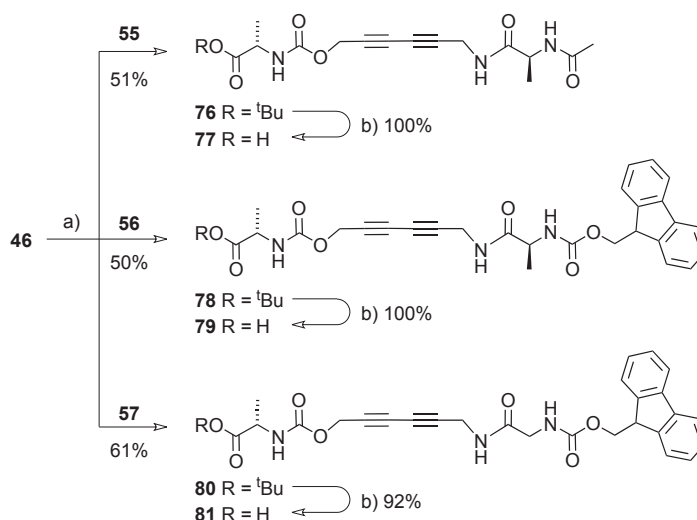
**Scheme 17:** Synthesis of the diacetylene building blocks **72** and **73**. The heterocoupling reaction resulted in an intractable ternary mixture that could only be purified after the TFA deprotection step. *Reagents and Conditions:* a)  $\text{PdCl}_2(\text{PPh}_3)_2$  (2 mol%), CuI (10 mol%), DIPA, THF, 0 °C; b) trifluoroacetic acid, DCM.

The heterocoupling of derivative **52** turned out to be a complete disaster because all three products were always eluted virtually simultaneously from a silica gel column irrespective of its size or the solvent system applied. Even solvent mixtures like pentane/ $\text{Et}_2\text{O}$  were applied but without re-sounding success. The removal of the heterocoupling derivative by recrystallization of the ternary mixture from DCM was the only improvement that could be achieved but the remaining two compounds could not be separated by chromatography. A reasonable way of purification was found to be possible only after the ester deprotection with TFA since the components of the mixture were differently affected by the acid treatment. First, the selfcoupling product featuring two Fmoc groups did not change at all in polarity ( $R_f$ : 0.8,  $\text{CH}_2\text{Cl}_2/\text{MeOH}$  10:1); secondly, the heterocoupling product was transformed into the corresponding carboxylic acid derivative **73** ( $R_f$ : 0.2,  $\text{CH}_2\text{Cl}_2/\text{MeOH}$  10:1), and, finally, the initial homocoupling product exhibited two acid functions after the reaction ( $R_f$ : 0,  $\text{CH}_2\text{Cl}_2/\text{MeOH}$  10:1). The targeted diacetylene derivative **73** could, therefore, be obtained by column chromatography in 62% which can be regarded as the lower limit of the yield of the heterocoupling reaction.



**Scheme 18:** Synthesis of diacetylene building blocks **74** and **75**. *Reagents and Conditions:* a)  $\text{PdCl}_2(\text{PPh}_3)_2$  (2 mol%), CuI (10 mol%), DIPA, THF, 0 °C; b) trifluoroacetic acid, DCM.

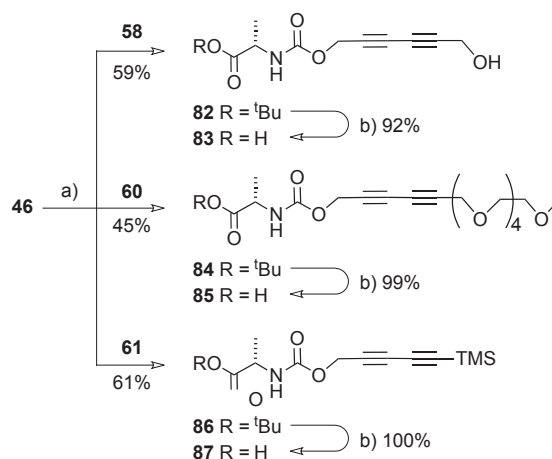
The reaction towards the diacetylene derivative **74** featuring the Dansyl group was, on the other hand, successful (Scheme 18), although the heterocoupling product was obtained in a fairly poor yield of 47%. Also the subsequent ester cleavage worked well and furnished **75** in 90% yield.



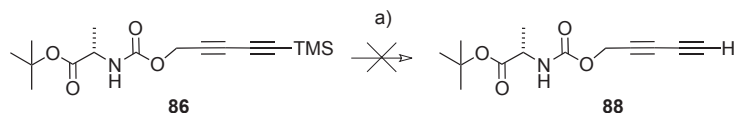
**Scheme 19:** Synthesis of the diacetylene building blocks **76**, **78** and **80** featuring two N–H···O=C hydrogen-bonds and their conversion into the free carboxylic acid derivatives **77**, **79** and **81**. *Reagents and Conditions:* a) PdCl<sub>2</sub>(PPh<sub>3</sub>)<sub>2</sub> (2 mol%), CuI (10 mol%), DIPA, THF, 0 °C; b) trifluoroacetic acid, DCM.

The heterocoupling reactions between **46** and the iodinated compounds **55**, **56** and **57** bearing a protected amino acid in the end group, were as successful as the previous heterocoupling reactions (Scheme 19). The initial concerns about the solubility of the reactants turned out to be unsubstantiated since these compounds dissolved quite well in THF. Only the acetylated derivative **55** was not well soluble and the reactions had to be carried out at higher dilution. The unsymmetric products **76**, **78** and **80** were obtained as pure crystalline materials in 51%, 50% and 61% yield, respectively, after column chromatography. Usually, the homocoupling derivative **65** could also be isolated easily. The subsequent cleavage of the *tert*-butyl ester functions worked very well with quantitative yields in the first two cases and 92% in the reaction of the glycine derivative.

The preparation of the diacetylene compounds that were not based on the propargylamine motif proceeded with varying success (Scheme 20). While the hydroxymethyl-terminated derivative **82** was obtained in a yield of 59% with an additional 39% of the homocoupling product **65**, the tetra(ethylene glycol)-functionalized molecule gave the overall lowest yield of only 45% of the heterocoupling product **84**. This was perhaps due to a fast selfcoupling reaction which produced 39% of the corresponding side product. Also, the purification was difficult since the different molecules were not well-separable by column chromatography due to their oligo(ethylene glycol) group and, therefore, some material was lost. The silylated derivative **86**, on the other hand, gave the highest yields of 61% in a smooth reaction that could easily be followed by TLC. In this case, the selfcoupling product, 1,4-bis(trimethylsilyl)butadiyne, were isolated as well. After a treatment of the heterocoupling products with TFA, the corresponding carboxylic acid derivatives could be isolated in 92% (**83**), 99% (**85**) as well as in quantitative yield in the case of **87**.



**Scheme 20:** Synthesis of the hydroxymethyl-, tetra(ethylene glycol)- and TMS-functionalized diacetylene building blocks **82**, **84** and **86** and their conversion into the free carboxylic acid derivatives **83**, **85** and **87** respectively. *Reagents and Conditions:* a) PdCl<sub>2</sub>(PPh<sub>3</sub>)<sub>2</sub> (2 mol%), CuI (10 mol%), DIPA, THF, 0 °C; b) trifluoroacetic acid, DCM.



**Scheme 21:** Attempted preparation of a terminal diacetylene building block. The reaction failed due to an unprecedented polymerization of the diacetylene in solution due to the attack of a nucleophile. *Reagents and Conditions:* a) TBAF, THF, 0 °C.

In order to obtain access to the terminal diacetylene building block **88**, an attempt was made to remove the silyl protection group from **86**. A typical method to remove a TMS function from a terminal acetylene is the treatment with tetrabutylammonium fluoride (TBAF) at low temperature. Thus, the TMS-equipped diacetylene derivative **86** was dissolved in THF, and TBAF was added at 0 °C. To our big surprise, the reaction mixture immediately attained a red color that intensified and turned violet later. After several hours, the reaction mixture turned brown, indicating that the species responsible for the color had disappeared or decomposed. The <sup>1</sup>H NMR of the reaction mixture did not contain any peaks associated with a silyl group, and it seemed as if we had mainly obtained the desired product. However, the latter turned out to be highly unstable and decomposed in very short times to a brown to black material. A UV spectrum of the violet reaction mixture (Figure 36) was interpreted in terms of a poly(diacetylene) formation. However, the color disappeared again over time spans of one to two hours. The result may indicate the unprecedented polymerization of a diacetylene in solution started by the attack of a fluoride as a nucleophile. We investigated some other nucleophiles like cyanide or methoxy anions but no such reaction occurred again. The fact that the polymer was unstable and that no systematic investigation seemed to be possible within a short time frame made us postpone a closer examination of this phenomenon.

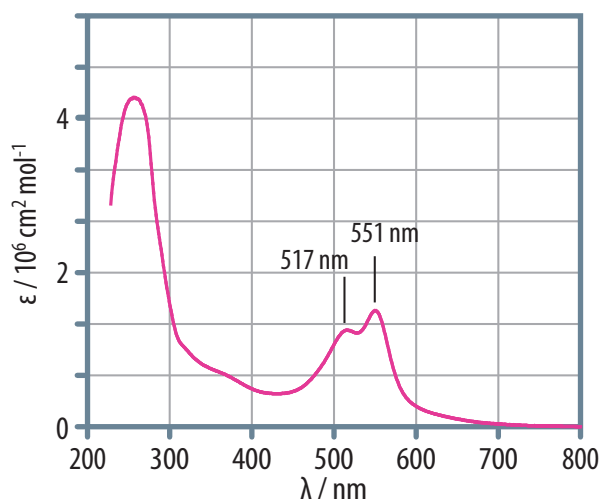
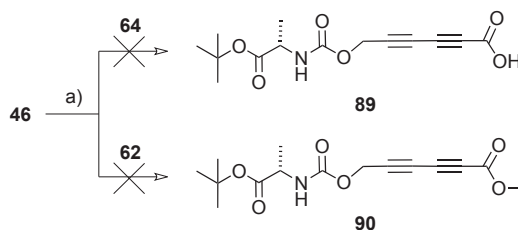


**Figure 36:** The UV spectrum of the reaction mixture of the TBAF deprotection of **86** measured shortly after the addition of the fluoride salt. The maxima at 517 and 551 nm clearly indicate the formation of a poly(diacetylene) backbone.

The heterocouplings of the haloacetylenes **64** and **62** with building block **46** failed, yielding an intractable black tar (Scheme 22) with no hint of the desired products **89** and **90**. In the case of the free carboxylic acid derivative **64**, we attributed the result to a possible complexation of the copper catalyst which we had already encountered in the case of **47** (*vide supra*). The unsuccessful reaction of the methyl ester derivative could, however, not be explained along these lines and remained elusive.



**Scheme 22:** Attempted synthesis of the CO<sub>2</sub>H- and CO<sub>2</sub>Me-terminated diacetylene building blocks **89** and **90** respectively. *Reagents and Conditions:* a) PdCl<sub>2</sub>(PPh<sub>3</sub>)<sub>2</sub> (2 mol%), CuI (10 mol%), DIPA, THF, 0 °C; b) trifluoroacetic acid, DCM.

In summary, the preparation of the diacetylenes worked with varying success. It completely failed if reagents with free amine or carboxylic acid functions were applied as well as when a carbonyl group was present in conjugation to the triple bonds. In all other cases, the desired heterocoupling product could be isolated in acceptable yields between 45% and 61% (Table 3.2) although the separation of the inevitably formed side products was often an issue. We were, nevertheless, able to prepare a satisfactory large set of diacetylene building blocks that can be used in the subsequent preparation of the macromonomers.

**Table 3.2:** Summary of isolated yields obtained in the heterocoupling- and ester deprotection reactions.

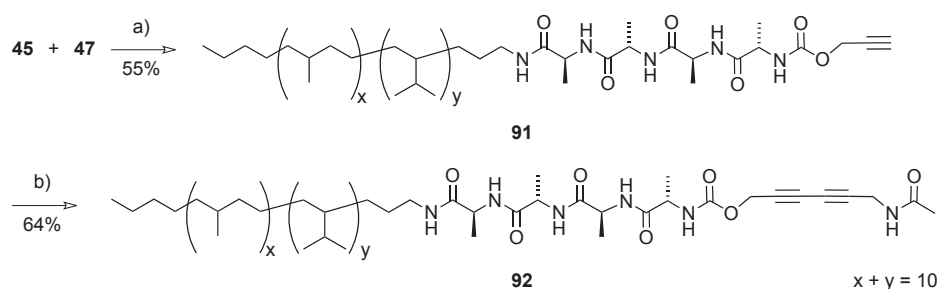
Iodoacetylene	Isolated yields in %			
	Hetero-	Homo-	Selfcoupling	TFA deprotection
<b>49</b>	–	–	–	–
<b>50</b>	56	16	not isolated	100
<b>51</b>	55	17	not isolated	100
<b>52</b>		ternary mixture		62
<b>53</b>	47	not isolated	not isolated	90
<b>55</b>	51	23	not isolated	100
<b>56</b>	50	23	not isolated	100
<b>57</b>	61	not isolated	not isolated	92
<b>58</b>	59	39	not isolated	92
<b>60</b>	45	24	39	99
<b>61</b>	61	not isolated	10	100
<b>62</b>	–	–	–	–
<b>64</b>	–	–	–	–

### 3.1.6 Preparation of the Macromonomers

#### 3.1.6.1 Divergent Route

Starting from the oligopeptide-polymer conjugate **45** a variety of diacetylene macromonomers were prepared. We wanted to explore both a divergent as well as a convergent route to optimize the results. The former started with an EDCI/HOBt-promoted peptide coupling of **47** and **45** (Scheme 23). After the aqueous workup, the obtained oligopeptide-polymer conjugate **91** was purified by column chromatography using DCM/MeOH mixtures as the eluent. The purification was hampered by the strong tendency of **91** to form gels in the solvent, so that the pure product was obtained in only 55% yield. The formation of the diacetylene-functionalized macromonomer was completed by a Sonogashira type heterocoupling reaction between iodoacetylene **50** and **91**. In order to avoid problems during the purification, a large excess (3.5 equivalents) of the iodinated compound was used to sup-

press the formation of the homocoupling product. The two starting materials were dissolved in a mixture of THF and DCM which served to solubilize the oligopeptide-polymer conjugate. The other parameters, i. e., the use of diisopropylamine as the base, the degassing of the reaction mixture as well as the amount of used catalysts were equal to the heterocouplings of low molecular weight compounds described above. The reaction was stirred over night since the reaction was carried out at high dilution due to the gel-forming properties of **91**. The solvents were removed, and the crude material was purified by a tedious procedure of repeated column chromatography runs, since the inevitably formed low molecular weight selfcoupling side product had an  $R_f$  value similar to the macromonomer **92**. However, after several purification runs, the  $^1\text{H}$  NMR showed the expected signal intensities, and **92** was obtained in 64% yield in an almost colorless form. The yield had decreased because the product was light-sensitive judged from the red color the sample attained when stored in daylight or in the bulk. Hence, the supposedly polymeric material was lost in the repeated purification steps.



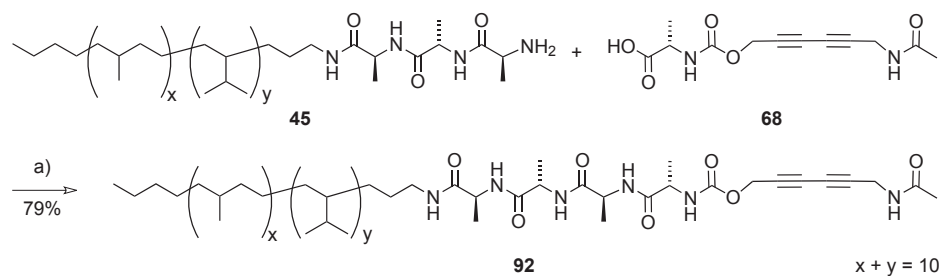
**Scheme 23:** Synthesis of macromonomer **92** by a divergent route. *Reagents and Conditions:* a) EDCI/HOBt, TEA, DCM/DMF,  $-40^\circ\text{C} \rightarrow \text{r.t.}$ , 16 h. b) **50** (3.5 eq),  $\text{PdCl}_2(\text{PPh}_3)_2$  (2 mol%), CuI (10 mol%), DIPA, THF, DCM, 16 h, r.t.

In summary, the macromonomers can be prepared by a divergent route. However, the purification issues and the low yield over two steps (35%) rendered this strategy unattractive. Furthermore, the possible impurities, e. g., the low molecular weight selfcoupling product, that could potentially interfere with the hydrogen-bonding of the oligopeptide segment made us abandon this pathway.

### 3.1.6.2 Convergent Route

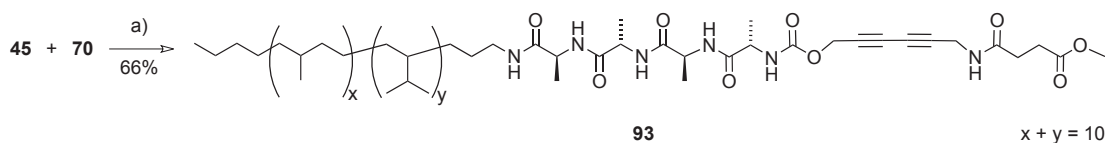
In the convergent route, the macromonomers were completed by a final peptide coupling reaction starting from **45** and the corresponding prefabricated diacetylene building blocks. Thus, **68** was subjected to an EDCI/HOBt promoted peptide coupling reaction with **45**. The active ester intermediate was prepared at low temperature while the amine component was dissolved in a large amount of DCM ( $<10\text{gL}^{-1}$ ) in a separate flask. The two components were combined at  $-40^\circ\text{C}$  and the reaction stirred over night. The reaction mixture had a slightly pink to purple color indicating that

a poly(diacetylene) had partially been formed already during the reaction. The water-soluble side products from the coupling reagents were removed by an acidic aqueous workup, the solvents were evaporated, and a reddish colored crude product was obtained. The latter was purified by column chromatography using a mixture of  $\text{CHCl}_3$  and MeOH which was found to be a much better eluent system as compared to DCM-containing mixtures. Consequently, the macromonomer **92** was obtained in a yield of 79%. The material seemed to polymerize in solution upon exposure to daylight and also in the dark when stored in bulk. Therefore, we stored the material at  $-25^\circ\text{C}$  in DCM solution to prevent a premature polymerization of the material.



**Scheme 24:** Synthesis of macromonomer **92** by a convergent route. *Reagents and Conditions:* a) EDCI/HOBt, TEA, DCM/DMF,  $-40^\circ\text{C} \rightarrow \text{r.t.}$ , 16h.

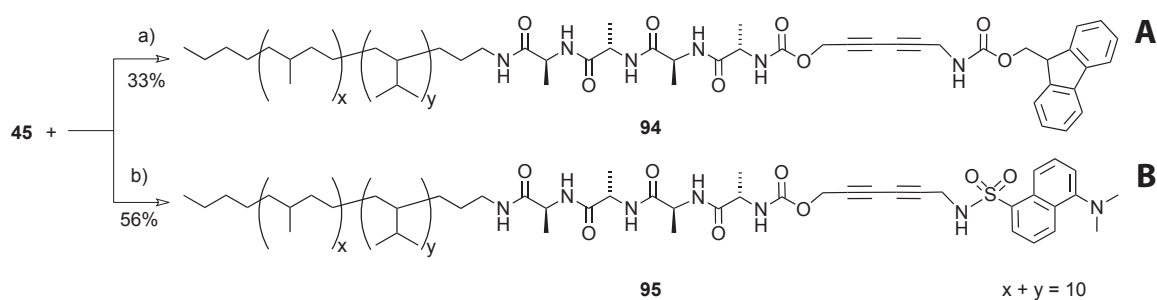
The obvious superiority of the convergent preparation pathway made us prepare all other macromonomers according to this strategy. Thus, the succinyl-terminated macromonomer **93** was obtained by coupling the oligopeptide-polymer conjugate **45** to the corresponding diacetylene building block **71** using the EDCI/HOBt protocol. The obtained target molecule **93** was very sensitive to daylight, and the workup had to be carried out as fast as possible, preferably in a dark room. Thus, an aqueous workup was skipped and the crude material was purified by column chromatography after a complete removal of DMF and TEA in HV. A solvent mixture of  $\text{CHCl}_3$ /MeOH 24:1 was the best compromise between a sufficient suppression of the macromonomers' aggregation and a good chromatographic separation. The pure macromonomer **93** was obtained in 66% yield with only minor losses due to premature polymerization (Scheme 25).



**Scheme 25:** A final EDCI/HOBt promoted peptide coupling yielded target molecule **93**. *Reagents and Conditions:* a) EDCI/HOBt, TEA, DCM/DMF,  $-40^\circ\text{C} \rightarrow \text{r.t.}$ , 16h.



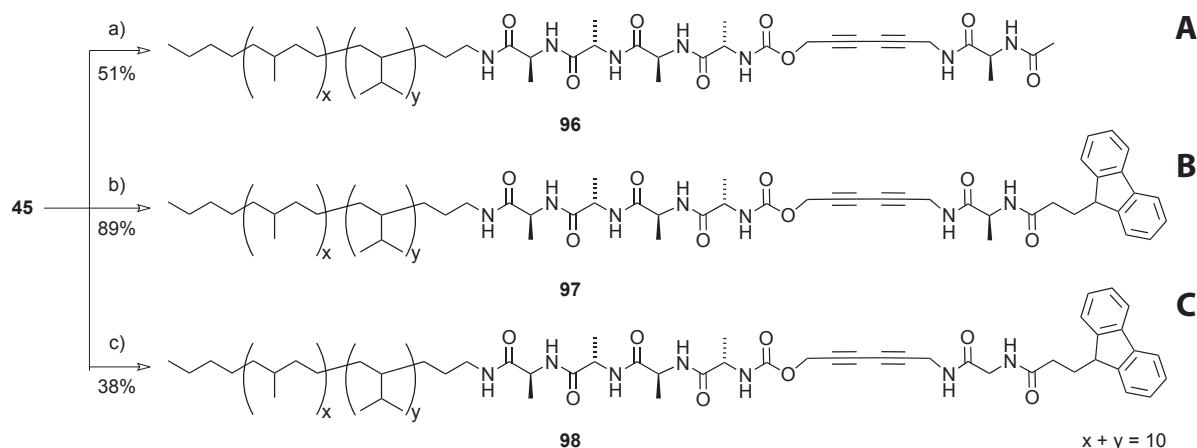
The preparation of the derivatives **94** and **95** was carried out only once in each case due to their poor polymerizabilities (Chapter 3.4). Macromonomer **94** was prepared from the corresponding diacetylene compound **73** and oligopeptide-polymer conjugate **45** using the EDCI/HOBt protocol (Figure 26A). However, an unexpectedly strong tendency of the product to gel the eluent used for the chromatography required repeated purification runs, reducing the yield to 33%. The Dansyl-functionalized derivative was obtained in a PyBOP promoted peptide coupling reaction using **45** as well as the diacetylene building block **75**. The relatively high  $R_f$  value and the missing tendency of the product to polymerize allowed for a good separation by column chromatography so that macromonomer **95** was obtained in a yield of 56% (Scheme 26B).



**Scheme 26:** Syntheses of target molecules **94** and **95**. *Reagents and Conditions:* a) **73**, EDCI/HOBt, TEA, DCM/DME,  $-40^{\circ}\text{C} \rightarrow \text{r.t.}$ , 16 h; b) **75**, PyBOP, DIEA, DCM/DME,  $0^{\circ}\text{C} \rightarrow \text{r.t.}$ , 16 h.

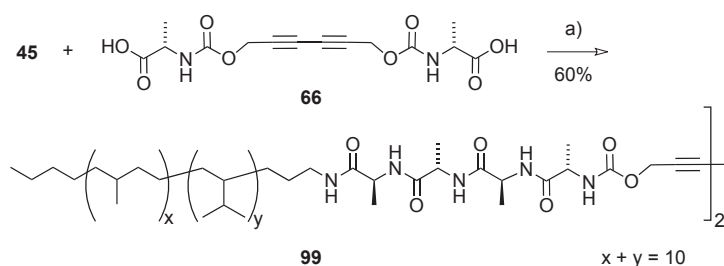
All target molecules featuring a protected amino acid derivative in the end group were prepared by the EDCI/HOBt-promoted reaction route. While derivative **96**, a very light-sensitive material, was finally obtained in 51% yield after a standard workup and purification procedure (Scheme 27A), macromonomer **97** was prepared in a much better yield of 89% in the best case (Scheme 27B). This was mainly due to a repeated synthesis of this compound because of its superior polymerization behavior (Chapter 3.4) and the ease of the purification of the diacetylene precursor **79**. Target compound **98**, on the other hand, was synthesized only once (Scheme 27C) since the subsequent topochemical polymerization was not very efficient. The yield in this single reaction was 38% which certainly could have been improved. The purification was exacerbated in all three cases by a very high reactivity in terms of premature diacetylene polymerizations. Even the reaction mixtures were typically found to be violet after stirring in the dark over night.

The same was true for the symmetric molecule **99** featuring two oligopeptide segments. The reaction mixture typically attained a red to purple color when the carboxylic acid building block **66** and two equivalents of the oligopeptide-substituted polymer **45** were subjected to a twofold EDCI/HOBt promoted peptide coupling reaction (Scheme 28). After purifying the violet crude material by column



**Scheme 27:** Synthesis of the macromonomers **96**, **97** and **98**. *Reagents and Conditions:* a) **77**, EDCI/HOBt, TEA, DCM/DME,  $-40^{\circ}\text{C} \rightarrow \text{r.t.}$ , 16 h; b) **79**, EDCI/HOBt, TEA, DCM/DME,  $-40^{\circ}\text{C} \rightarrow \text{r.t.}$ , 16 h; c) **81**, EDCI/HOBt, TEA, DCM/DME,  $-40^{\circ}\text{C} \rightarrow \text{r.t.}$ , 16 h.

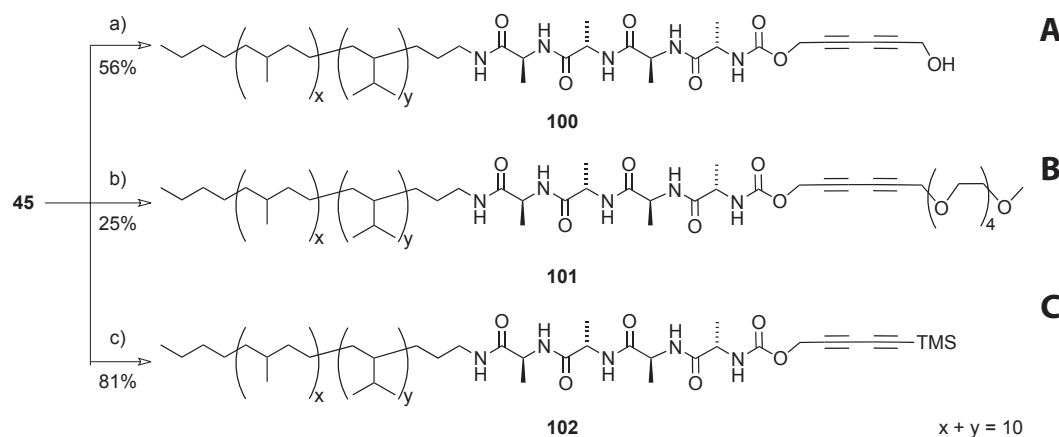
chromatography, **99** was obtained in a good yield of 60%, taking into account that a twofold reaction had to be achieved. One reason for the good yield may have been the very pure starting material **66** that was a fine crystalline powder and could, hence, easily be dried in HV.



**Scheme 28:** Preparation of the symmetric macromonomer **99**. *Reagents and Conditions:* a) EDCI/HOBt, TEA, DCM/DME,  $-40^{\circ}\text{C} \rightarrow \text{r.t.}$ , 16 h.

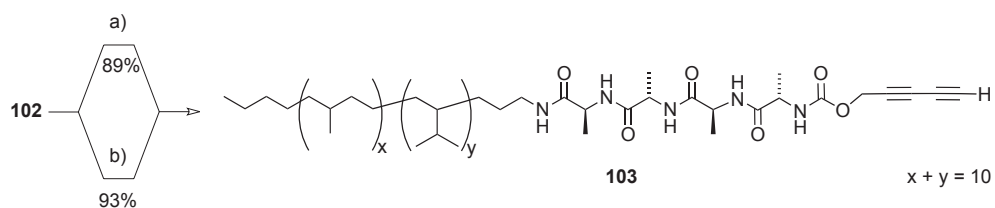
Varying results were obtained in the synthesis of the macromonomers **100**, **101** and **102** that featured a hydroxyl function, a tetra(ethylene glycol) moiety, or a TMS group in their end groups, respectively (Scheme 29). While **100** was obtained in a yield of 56% after the standard workup and purification procedure, the oligo(ethylene glycol)-equipped compound **101** was isolated in only 25% yield. A possible explanation could be the hygroscopic nature of the diacetylene precursor which would decrease the amount of peptide coupling promoter. The formation of the active ester intermediate during the peptide coupling reaction was difficult to follow by TLC and might not have been complete either. In any case, enough pure material was isolated to investigate its properties. By contrast, in the case of the TMS-substituted derivative **102**, the active ester formation could easily be followed by TLC since the silylated diacetylene derivatives gave rise to distinct spots that attained a character-

istic red color upon treatment with anisaldehyde solution. The corresponding macromonomer was, therefore, isolated in a very good yield of 81%.



**Scheme 29:** Syntheses of the macromonomers **100**, **101** and **102**. *Reagents and Conditions:* a) **83**, EDCI/HOBt, TEA, DCM/DME,  $-40^{\circ}\text{C} \rightarrow \text{r.t.}$ , 16 h; b) **85**, EDCI/HOBt, TEA, DCM/DME,  $-40^{\circ}\text{C} \rightarrow \text{r.t.}$ , 16 h; c) **87**, EDCI/HOBt, TEA, DCM/DME,  $-40^{\circ}\text{C} \rightarrow \text{r.t.}$ , 16 h.

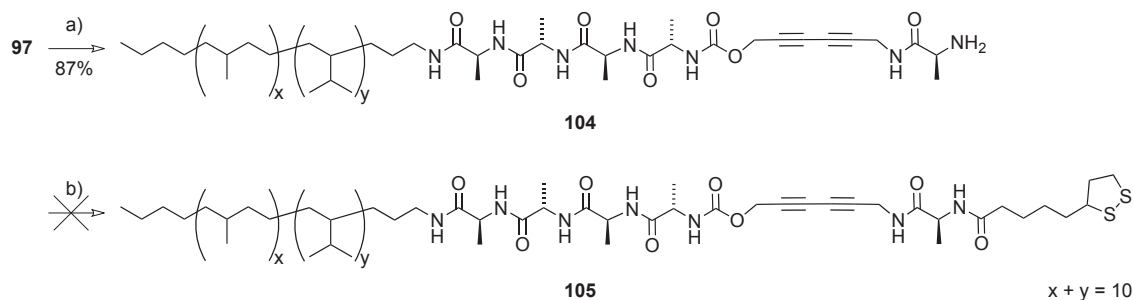
Finally, it was possible to remove the TMS group from **102** by a treatment with  $\text{K}_2\text{CO}_3$  in a mixture of DCM and MeOH. However, an untypical IR signature led to doubts about the nature and the stereochemical purity of the latter. Fortunately, the TBAF-promoted deprotection of **102** in a mixture of DCM and THF worked well, and macromonomer **103** was obtained in 93% yield after an aqueous workup and a subsequent purification by column chromatography (Scheme 30).



**Scheme 30:** Synthesis of the H-terminated macromonomer **103**. *Reagents and Conditions:* a)  $\text{K}_2\text{CO}_3$ , DCM/MeOH, r.t.; b) TBAF, DCM/THF,  $0^{\circ}\text{C} \rightarrow \text{r.t.}$

Starting from macromonomer **97**, the removal of the Fmoc-protecting group resulted in the free amine **104** which was found to be unstable, changing its color to a deep red when stored in the bulk. The purification by column chromatography had to be carried out with TEA as a co-eluent which turned out to be hard to remove. Thus, the intermediate was used without further purification in a peptide coupling reaction to thioctic acid (Scheme 31). The motivation for the introduction of sulfur atoms was a planned binding of gold nano clusters to the molecules. Unfortunately, the product **105**

turned out to be completely insoluble, and the characterization by  $^1\text{H}$  NMR spectroscopy as well as MALDI-TOF mass spectrometry remained inscrutable. This was further corroborated by an emerging smell of  $\text{H}_2\text{S}$  which led us to the conclusion that the material decomposed and/or cross-linked in terms of an opening and closing of disulfide bridges. For this reason, further investigations could not be carried out with this macromonomer.



**Scheme 31:** Cleaving the Fmoc-group from **97** yielded the unstable derivative **104** which was attempted to be further functionalized to **105**. *Reagents and Conditions:* a) piperidine,  $\text{CHCl}_3$ , r.t.; b) thioctic acid, EDCI/HOBt, TEA, DCM/DMF,  $-40^\circ\text{C} \rightarrow$  r.t.

### 3.1.6.3 Characterization of the Macromonomers

The macromonomers were typically characterized by  $^1\text{H}$  NMR spectroscopy, MALDI-TOF mass spectrometry, and combustion elemental analyses. The NMR spectra were heavily impaired by the aggregation of the oligopeptides resulting in a pronounced broadening of the aliphatic signals and a complete disappearance of all other signals. While the situation could partially be improved by using very dilute solutions at elevated temperatures, the amide and carbamate protons could still not be detected (Figure 37). The problem was solved to an acceptable extent by the addition of TFA as a hydrogen-bond breaking cosolvent. Typically 2% v/v were added to the  $\text{CDCl}_3$  solutions, leading to well-resolved aliphatic signals and the appearance of all signals belonging to the oligopeptide with matching intensities but poorly resolved fine structure. A comparison of the spectra of different macromonomers showed distinct changes well in line with what would have been expected. The signal of the  $\text{CH}_2\text{NH}$  group of the polymer coil appeared between 3.1–3.3 ppm and could be used to calibrate the integrals. This allowed for an estimate of the molecular weight of the poly(isoprene) segment and the purity of the materials by comparing the intensities to other known groups in the molecules.

A typical  $^1\text{H}$  NMR spectrum of the macromonomers can, thus, be described as follows. The hydrogenated poly(isoprene) polymer segment gave rise to a large signal at 0.6 to 1.9 ppm exhibiting a characteristic shape. The signals corresponding to the methyl groups of the alanines in the oligopeptide

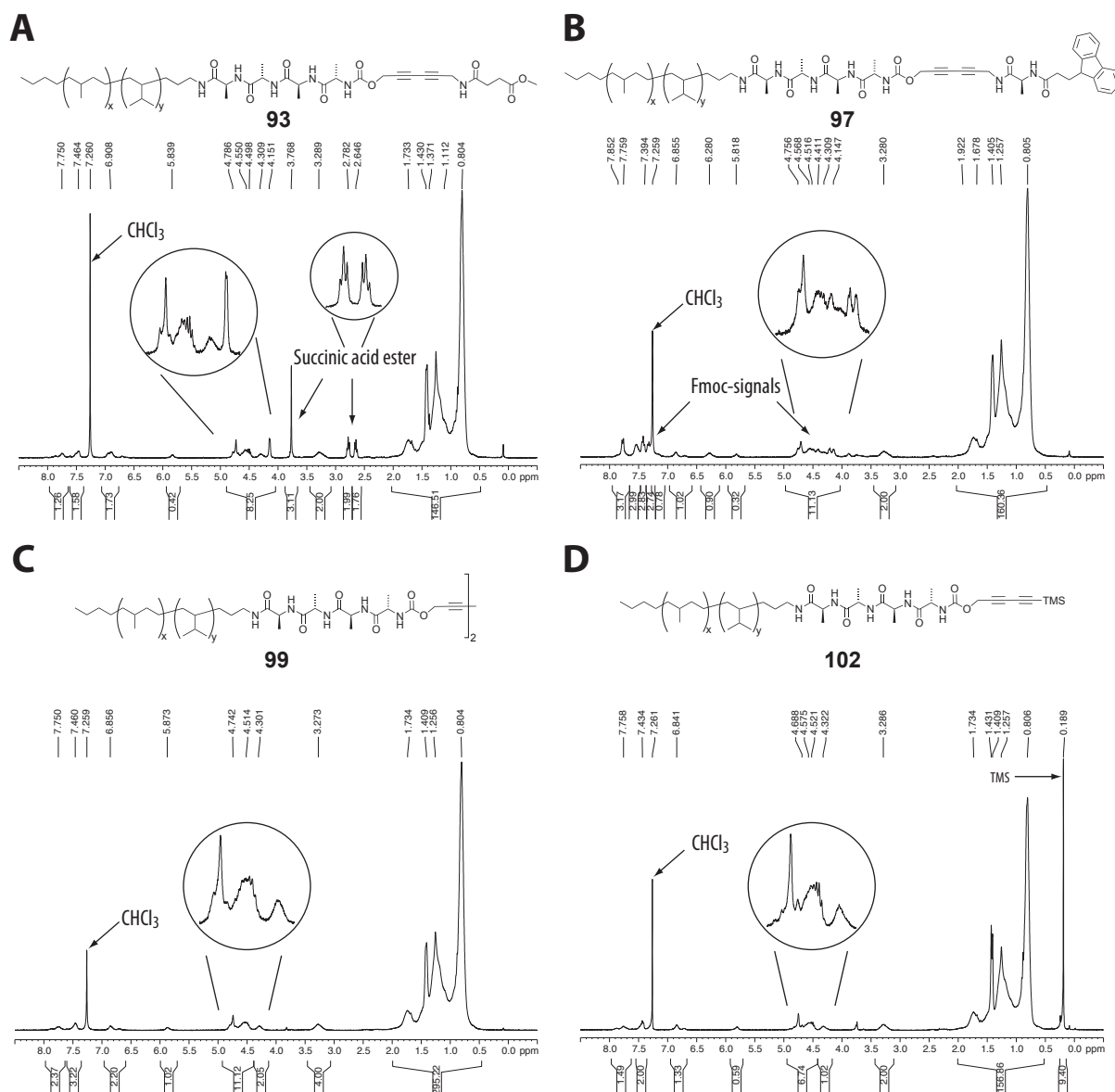


**Figure 37:** Representative  $^1\text{H}$  NMR spectra of macromonomers A) **93**; B) **96**; C) **99**; and D) **103**. The spectra show the aliphatic signals between 0.6 and 1.9 ppm, the signal of the last methylene group of the polymer segment at 3.1–3.3 ppm which was used as an “internal standard” for the molecular weight determination, the crucial region between 4 and 5 ppm, and the characteristic NH signals in the region from 5.8 to 7.8 ppm. Additionally, end group specific protons appear in all spectra as expected.

were buried under that signal and could not be detected. The aforementioned peak of the polymer’s  $\text{CH}_2\text{NH}$  group appeared at 3.1 to 3.3 ppm and its intensity was calibrated to two protons. Depending on the end group, the acetamide peaks (around 2.1 ppm) or signals corresponding to the succinic acid group (two triplets at 2.6 and 2.8 ppm) appeared in this region, as well. Signals corresponding to methyl esters or ethers (**93** or **101**) were typically observed between 3.5 and 4.0 ppm, as expected. The region between 4 and 5 ppm was typically not well-resolved because protons from residual olefin bonds, all chiral alanine protons, the methylene groups next to the diacetylenes, and also signals

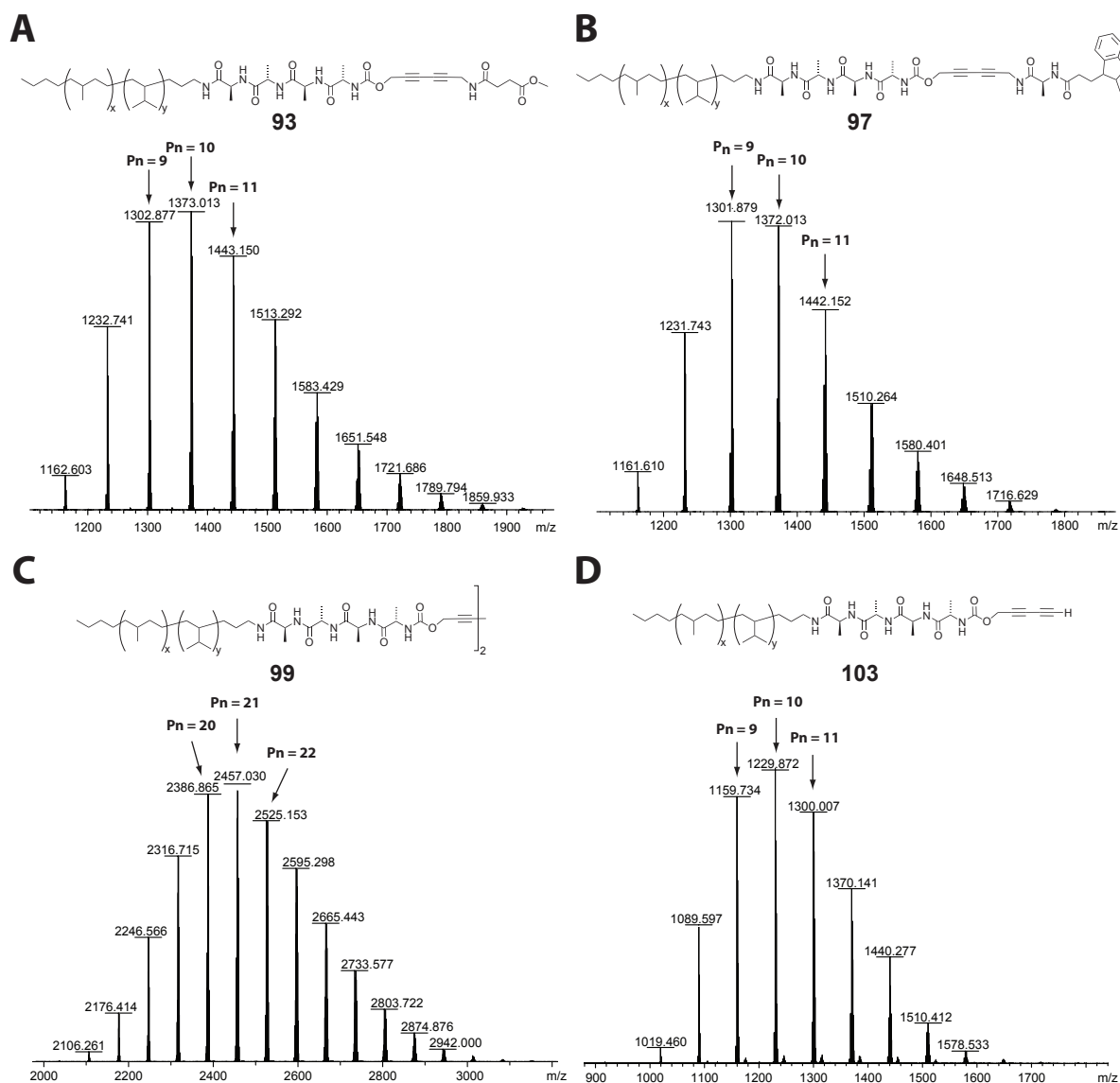


**Figure 38:** Representative MALDI-TOF MS spectra of A) **93**; B) **96**; C) **99**; and D) **103**. The spectra show series of peaks corresponding to sodium adducts of the molecules which are separated by the mass of the repeat unit ( $C_5H_{10}$ ). The overall shape of the distribution curves as well as the position of the maximum was very similar in all cases. Thus, the maximum was located at  $\bar{P}_n$  values around 10 in the cases of the unsymmetric diacetylene macromonomers, while the symmetric macromonomer **99** showed the maximum at 21 repeat units respectively.

from Fmoc groups (if present in the molecule) appeared here. The overall integration of these signal always gave the correct (expected) value. Depending on the hydrogenated poly(isoprene) batch, a signal caused by residual olefins at around 4.7 ppm was observed which, however, typically only had an intensity of 0.5 protons or less. The carbamate signal was usually located at 5.8 ppm but it was always found to be reduced in intensity, most likely due to a proton exchange with the TFA. The amide signals appeared as broad peaks between 6.8 and 7.8 ppm generally with a low intensity (due to the TFA), however, the number of the signals was always found to be correct. The evaluation of the amide

signals was sometimes hampered by the chloroform signal at 7.26 ppm and the appearance of aromatic signals in case of the Fmoc or Dansyl derivatives. The aromatic signals were found to give rise to correct integrations as compared to the other signals in the other regions of the spectra, as well. Finally, the TFA signal appeared at values around 11 ppm, depending on the amount of acid. If only small amounts of acid was added, the signal was found shifted toward the amide region due to an exchange with the NH protons.

**Table 3.3:** Molecular weight determination of the macromonomers.

Compound	Calculated <sup>a</sup>	<sup>1</sup> H NMR <sup>b</sup>	MALDI MS		
	M <sub>n</sub>	M <sub>n</sub> (P <sub>n</sub> )	M <sub>p</sub> (P <sub>p</sub> ) <sup>c</sup>	M <sub>n</sub> (P <sub>n</sub> ) <sup>d</sup>	PDI <sup>d</sup>
<b>92</b>	1278	1380 (11.4)	1301 (10)	1330 (10.4)	1.006
<b>93</b>	1349	1530 (12.2)	1373 (10)	1380 (10.1)	1.007
<b>94</b>	1458	1590	–	–	–
<b>95</b>	1469	1680	1492 (10)	1510 (10.2)	1.006
<b>96</b>	1350	1500 (11.7)	1302 (9)	1330 (9.4)	1.005
<b>97</b>	1529	1750 (13.2)	1552 (10)	1550 (10.0)	1.006
<b>98</b>	1515	1610	1537 (10)	–	–
<b>99</b>	2364	2679 (2 · 12.3)	2460 (21)	2385 (20.0)	1.002
<b>100</b>	1237	1290 (10.7)	1190 (9)	1190 (9.1)	1.006
<b>101</b>	1427	1460 (10.5)	1450 (10)	1470 (10.3)	1.005
<b>102</b>	1279	1500 (13.2)	1302 (10)	1310 (10.1)	1.007
<b>103</b>	1207	1360 (12.2)	1230 (10)	1240 (10.2)	1.008

<sup>a</sup>Calculated molar masses assuming that the poly(isoprene) segments had an average degree of polymerization of  $\bar{P}_n = 9$ , according to the monomer/initiator ratio [isoprene]/[BuLi] = 9 employed in the initial anionic isoprene polymerization. <sup>b</sup>Average molecular weight determined by comparison of the intensities of the CH<sub>2</sub>NHR proton signals and the aliphatic poly(isoprene) proton signals. <sup>c</sup>[M+H]<sup>+</sup> for **41**, [M+Na]<sup>+</sup> for **42**, **44** and **45**. <sup>d</sup>Number average molecular weight  $\bar{M}_n$  and polydispersity index (PDI) as calculated with the Polytool software package from Bruker.

The analysis by mass spectrometry was first attempted using the ESI MS technique. For this purpose, the macromonomers were dissolved in a mixture of DCM and MeOH and injected into the apparatus. The results were sometimes not easily reproducible because it was supposedly hard to ionize

the different species equally well. Therefore, additional tricks like the addition of acetic acid, silver salts, or sodium sources were attempted, allowing at for a characterization of the target structures. However, results from different measurements were still hard to compare with one another because the location of the signal with the highest intensity seemed to be more dependent on the experimental conditions rather than on the sample and, thus, an estimate of the molecular weight and the distribution of the latter was not reliable. The newly available MALDI-TOF equipment finally solved these problems after a suitable matrix system was found. Thus, the measurements were carried out using a *trans*-2-[3-(4-*tert*-butylphenyl)-2-methyl-2-propenylidene]malononitrile (DCTB) matrix with an additional Na<sup>+</sup> source, giving rise to well-resolved spectra (Figure 38). Furthermore, a software-based molecular weight analysis could be performed, yielding  $\overline{M}_n$ ,  $\overline{M}_w$  and PDI values which could not be obtained from GPC measurements because the material was not eluted at all.

The molecular weights as determined by NMR and MALDI-TOF (Table 3.3) matched the calculated values that had been obtained based on the monomer/initiator ratio used in the living anionic polymerization very well. The <sup>1</sup>H NMR data typically overestimated the molecular weight due to the comparison of the relatively small signal of the polymer's CH<sub>2</sub>NH group to the large aliphatic signal. The most intense peaks in the mass spectra, on the other hand, were always located at masses corresponding to a hydrogenated poly(isoprene) segment with 9 or 10 repeating units. Given that we used a monomer/initiator ration of 9:1, this experimental value can be considered as a good indication that the polymerization was well-controlled. This was further corroborated by the very small PDI values calculated by the software package which, admittedly, are typically underestimated in MS-based analyses, though.

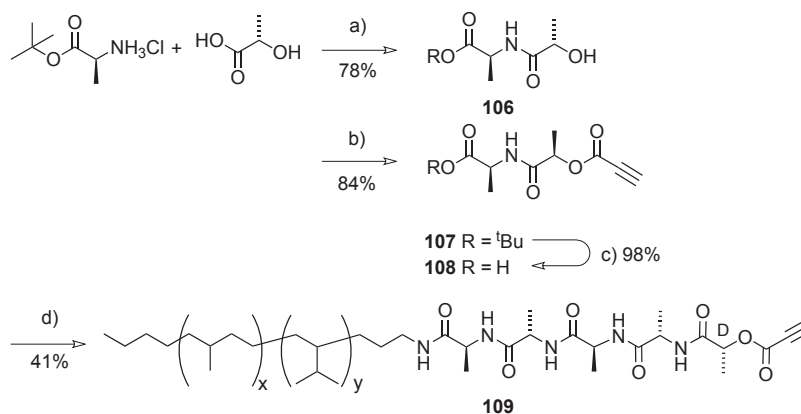
### 3.1.7 Variation of the Macromonomers

#### 3.1.7.1 Acceptor-Substituted Diacetylene Macromonomers

Macromonomers that have an acceptor substituent in direct conjugation to the diacetylene moiety may give rise to a different type of polymerization process. A propiolic acid lactic acid ester had been designed as a different linker for this purpose (Scheme 32). Thus, a peptide coupling between L-alanine *tert*-butyl ester hydrochloride and L-lactic acid was performed using the standard PyBOP coupling protocol. Due to the much higher nucleophilicity of the amine compared to the hydroxyl function, the latter did not have to be protected, and the reaction gave 78% of the desired product **106**. The subsequent esterification with propiolic acid turned out to be difficult since the latter tends to undergo various side reactions.<sup>184</sup> An attempted reaction promoted by EDCI/DPTS<sup>185</sup> did not work and, as the corresponding acid chloride was not commercially available and difficult to synthesize, a

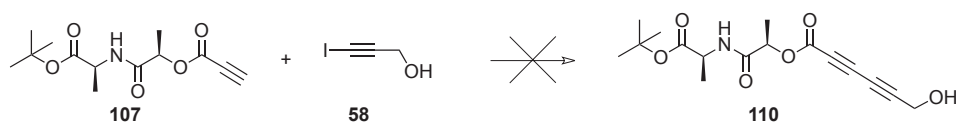


Mitsunobu reaction<sup>186</sup> was carried out. For this purpose, a solution of propiolic acid and diethyl azodicarboxylate (DEAD) in THF and a second solution of **106** and triphenylphosphane in the same solvent were prepared and combined. The product **107** was obtained in very good yield of 84% after column chromatography. However, the inevitable inversion of the configuration of the secondary alcohol led to the formation of a D-lactic acid ester in this case.



**Scheme 32:** Synthesis of the D-lactic acid spacer and its use in the preparation of a macromonomer precursor with an acceptor-substituted acetylene. *Reagents and Conditions:* a) PyBOP, DIEA, DCM/DMF 0 °C  $\rightarrow$  r.t.; b) propiolic acid, DEAD, PPh<sub>3</sub>; c) trifluoroacetic acid, DCM; d) PyBOP, DIEA, DCM/DMF 0 °C  $\rightarrow$  r.t.

The *tert*-butyl ester was cleaved in 98% yield with TFA, and the resulting carboxylic acid **108** was coupled to the oligopeptide-polymer conjugate **45** in a PyBOP promoted peptide coupling reaction. The low yield of only 41% was mainly due to purification issues associated with removing the PyBOP related side products. The product **109** turned out to be an efficient organogelator in DCM and CHCl<sub>3</sub>. That fact served as an indication that the self-assembly also worked in the case of molecules featuring the lactic acid linker.



**Scheme 33:** Attempted synthesis of a diacetylene equipped with the lactic acid ester linker. *Reagents and Conditions:* a) PdCl<sub>2</sub>(PPh<sub>3</sub>)<sub>2</sub> (2 mol%), CuI (10 mol%), DIPA, THF, 0 °C; b) trifluoroacetic acid, DCM.

In analogy to the convergent synthesis of the previously prepared macromonomers, a prefabrication of a diacetylene was thought to be the better pathway as compared to a heterocoupling to the oligopeptide-polymer conjugate **109**. Therefore, the propiolic acid ester derivative **107** was reacted with the iodinated propargyl alcohol **58** in a first test reaction using the standard Sonogashira reaction

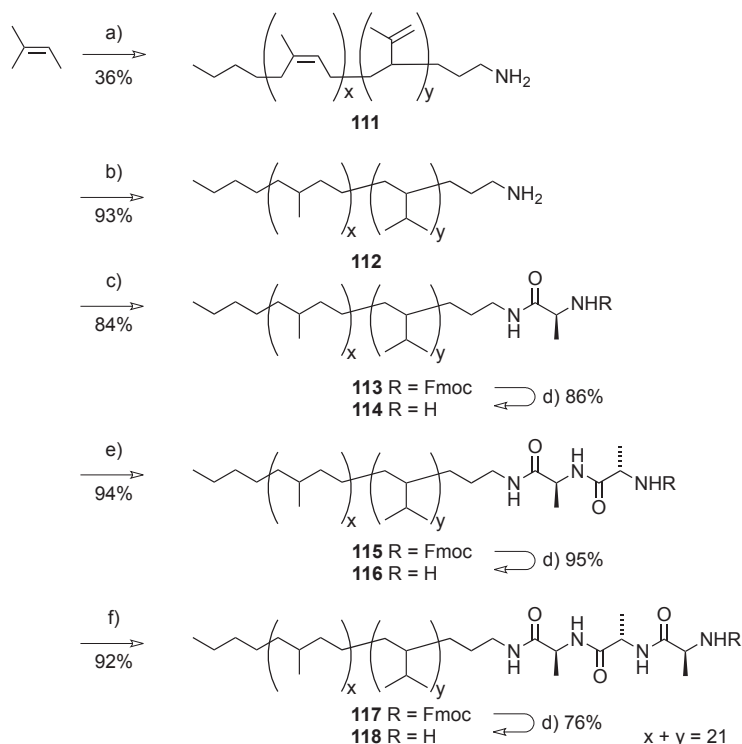
conditions (Scheme 33) but the reaction failed completely. Although the previous heterocoupling reactions that had been carried out with acceptor substituted acetylenes aimed at introducing carbonyl groups in direct conjugation to the triple bonds in the end groups had already failed as well (Section 3.1.5.3), we had hoped that the inversion of the substitution pattern (i. e., the haloacetylene did not contain the carbonyl group) would solve the problem. Since this was not the case, we did not attempt a heterocoupling reaction on the oligopeptide-polymer conjugate level with **109** and abandoned the synthesis of acceptor substituted diacetylene derivatives.

### 3.1.7.2 Variations of the Polymer and Oligopeptide Segments

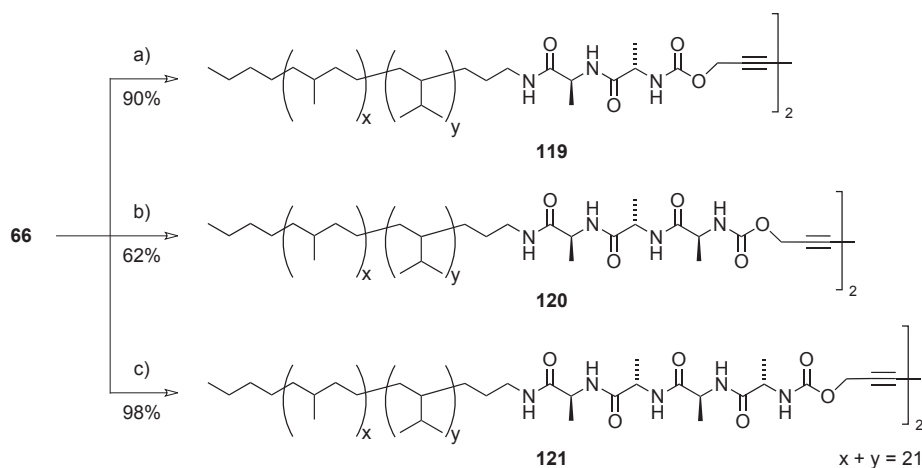
In order to broaden the scope of our investigations, we prepared macromonomers equipped with a longer hydrogenated poly(isoprene) segment. For this purpose, we synthesized an amine-terminated poly(isoprene) using a monomer/initiator ratio of 25:1. The reaction was carried out in analogy to the standard polymerization, i. e., the reaction was started by *n*-butyl lithium at 0 °C in THF and 1-(3-bromopropyl)-2,2,5,5-tetramethyl-1-aza-2,5-disilacyclopentane was used as quencher. Thus, **111** was obtained, however, in a reduced yield of 36% because the unexpectedly high  $R_f$  value of the product led to mixed fractions with minor amounts of unfunctionalized material during the chromatography. The MALDI-TOF analyses (not shown) indicated an average coil length of 21 repeat units. The subsequent hydrogenation of the olefins was more complicated compared to the shorter poly(isoprene) segments supposedly due to an increased tendency of the material to cover the activated carbon particles and, hence, the catalyst because of the increased molecular weight. Nevertheless, the double bonds could be removed to an extent of more than 98%, as estimated from the  $^1\text{H}$  NMR spectra.

The obtained hydrogenated poly(isoprene) segment **112** was then reacted with Fmoc-protected alanine building blocks of different lengths (Scheme 34), aiming at the subsequent preparation of target molecules with a variable length of the oligopeptide. The reactions were all carried out using PyBOP as the promoter. The yields of the reactions leading to **113**, **115** and **117** were generally very good with values from 84% to 92%. The subsequent removal of the Fmoc-group worked also well in all cases, furnishing derivatives **114**, **116** and **118** in yields from 76% to 95%.

In order to investigate the influence of the lengths of both the polymer segment and the oligopeptidesequence, we prepared symmetric molecules exhibiting di-, tri- and tetrapeptides by reacting diacetylene building block **66** with **114**, **116** and **118** (Scheme 35). These reactions were carried out using the EDCI/HOBt protocol and the corresponding symmetric target structures **119**, **120** as well as **121** could be obtained in 90%, 62% and 98% yield respectively. The comparably low yield in the second case was due to purification problems that occurred during column chromatography.

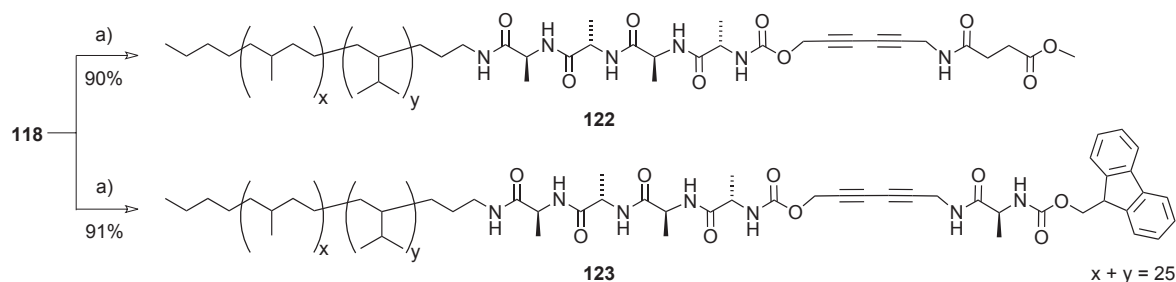


**Scheme 34:** Synthesis of a series of oligopeptide-polymer conjugates featuring a hydrogenated poly(isoprene) segment with an average number of repeat units  $\bar{P}_n = 21$  and a variable number of attached alanines (1-3). *Reagents and Conditions:* a) 1. *n*-butyl lithium, THF,  $-78^\circ\text{C}$ , 2. 1-(3-bromopropyl)-2,2,5,5-tetramethyl-1-aza-2,5-disilacyclopentane, 3. 25% HCl; b) 8 mol% Pd/C, 100 bar  $\text{H}_2$ ,  $80^\circ\text{C}$ , toluene/EtOH, 7-10 d; c) *N*-(9-fluorenylmethyloxycarbonyl)-L-alanine, PyBOP, DIEA, DCM/DME, r.t.; d) piperidine,  $\text{CHCl}_3$ , r.t.; e) **36**, PyBOP, DIEA, DCM/DME, r.t.; f) **39**, PyBOP, DIEA, DCM/DME, r.t.



**Scheme 35:** Macromonomers with a hydrogenated poly(isoprene) segment with  $\bar{P}_n = 21$  and differently long oligopeptide segments. *Reagents and Conditions:* a) EDCI/HOBt, TEA, DCM/DME,  $-40^\circ\text{C}$   $\rightarrow$  r.t.

Furthermore, analogues to macromonomers **93** and **94** were prepared that comprised a tetra-L-alanine sequence featuring the elongated polymer segment. For this purpose, the corresponding diacetylene building blocks **71** as well as **77** were peptide coupled to **118** in EDCI/HOBt promoted reactions (Scheme 36). The products **122** and **123** could be obtained in yields of 90% and 91%.



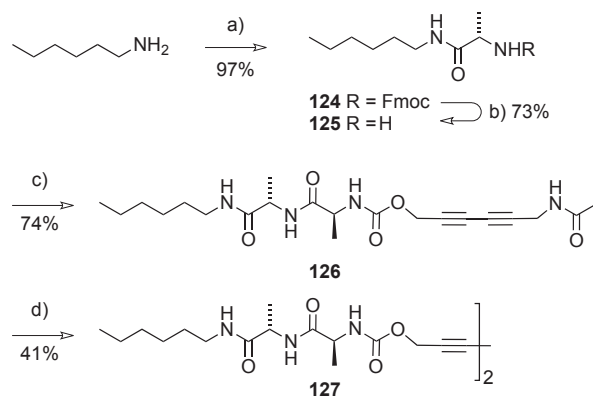
**Scheme 36:** Syntheses of macromonomers **122** and **123** that were equipped with the prolonged polymer segment. *Reagents and Conditions:* a) **71**, EDCI/HOBt, TEA, DCM/DME,  $-40^{\circ}\text{C} \rightarrow \text{r.t.}$ , 16h; b) **79**, EDCI/HOBt, TEA, DCM/DME,  $-40^{\circ}\text{C} \rightarrow \text{r.t.}$ , 16h.

### 3.1.8 Preparation of Model Compounds

The modular nature of the synthetic strategy allowed for the facile synthesis of monodisperse model compounds that were prepared to investigate the influence of the different elements in the chosen molecular architecture on the hierarchical structure formation and to obtain single-crystals that would allow for an investigation of the molecular arrangement of the diacetylenes in the oligopeptide array. Thus, we prepared simplified siblings of the original macromonomers that were equipped with hexyl or dodecyl substituents instead of the polymer coil, a di-alanine segment to which a selection of the prefabricated diacetylene building blocks was attached.

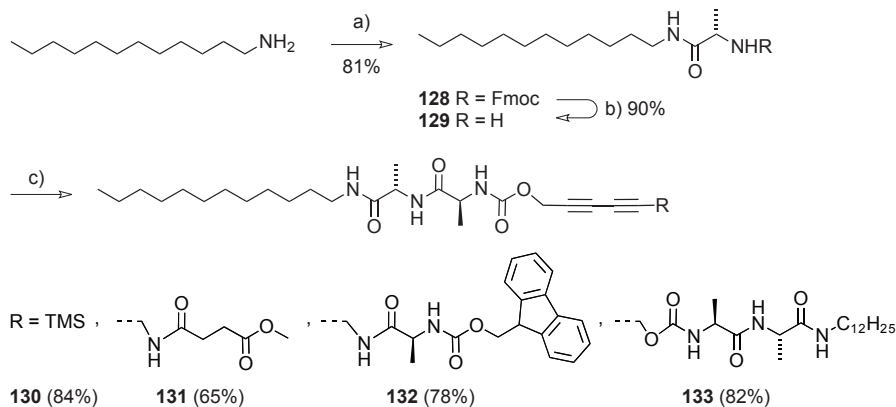
For this purpose, we coupled *N*-(9-fluorenylmethyloxycarbonyl)-L-alanine to hexylamine in a PyBOP promoted peptide coupling reaction yielding **124** in 97% yield (Scheme 37). The following deprotection of the amine furnished **125** in 73%. This building block was combined with the diacetylene building blocks **68** and **66** to obtain the model compounds **126** and **127** in 74% and 41% yield, respectively. These derivatives were found not to be recrystallizable since they only formed gels or polycrystalline material depending on the applied solvents. Alcohols as the solvents typically led to precipitation when the solutions were cooled after refluxing while THF or chlorinated solvents led to gelation already at low concentrations of the materials ( $\leq 2 \text{ g L}^{-1}$ ). However, also these solid precipitates or gels became violet upon exposure to daylight, indicating that a short range order in the system suitable for a topochemical polymerization was established, although three-dimensional crystallinity was not observed.

Inspired by investigations concerning the crystallization of di- and triacetylene compounds driven by phenyl-perfluorophenyl interactions which were carried out simultaneously in our group, we replaced the hexyl with a dodecyl chain since the latter proved to be much better suitable for crystallization attempts in the other study.<sup>187</sup> Thus, dodecylamine and *N*-(9-fluorenylmethyloxycarbonyl)-L-alanine were coupled to furnish **128** in 81% yield (Scheme 38). The subsequent removal of the protecting group led to **129** in 90% yield on a 5 g scale. In case of the dodecyl-substituted model com-

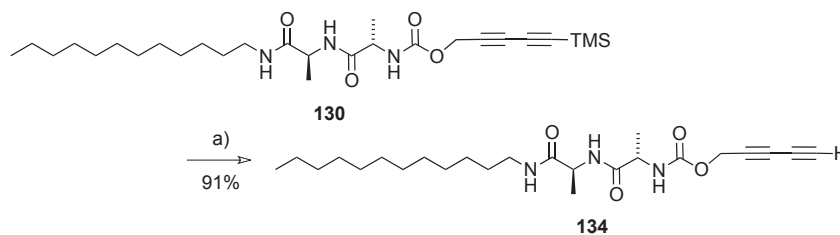


**Scheme 37:** Derivatives **126** and **127** were equipped with hexyl substituents. *Reagents and Conditions:* a) *N*-(9-fluorenylmethyloxycarbonyl)-L-alanine, PyBOP, DIEA, DCM/DME, r.t.; b) piperidine,  $\text{CHCl}_3$ , r.t.; c) **68**, PyBOP, DIEA, DCM/DME, r.t.; d) **66**, PyBOP, DIEA, DCM/DME, r.t.

pounds, we prepared a wider range of structures using diacetylene building blocks **87**, **71**, **79** and **66** in peptide coupling reactions with **129**. The peptide coupling reactions were advantageously carried out using PyBOP as the promoter since the products could be precipitated from water while all side products remained in solution. Thus, the reactions gave **130** (84%), **131** (65%), **132** (78%), and **133** (82%) in good yields. Derivative **134**, a terminal diacetylene, was obtained in 91% yield by treating **130** with  $\text{AgNO}_3$ , a mild reaction pathway to remove silyl protecting groups from terminal acetylenes (Scheme 39).<sup>182</sup>



**Scheme 38:** Model compounds **130–134** were prepared that featured a dodecyl substituent to improve the crystallizability. *Reagents and Conditions:* a) *N*-(9-fluorenylmethyloxycarbonyl)-L-alanine, PyBOP, DIEA, DCM/DME, r.t.; b) piperidine,  $\text{CHCl}_3$ , r.t.; c) diacetylene building blocks **71**, **79**, **87**, or **66**, PyBOP, DIEA, DCM/DME, r.t.



**Scheme 39:** The TMS-functionalized model compound **130** was converted into the terminal diacetylene **134**.  
*Reagents and Conditions:* a) 1. AgNO<sub>3</sub>, EtOH, MeOH, H<sub>2</sub>O; 2. KI.

### 3.1.9 Conclusions

In summary, a highly modular and efficient synthetic strategy has been developed that makes use of the prefabrication of oligopeptide, polymer and diacetylene building blocks which can be assembled to the macromonomers in either a divergent or convergent route. The available building blocks were used to prepare a large variety of macromonomers that featured different end groups as well as polymer and oligopeptide segments of different lengths. Furthermore, monodisperse model compounds were straightforwardly prepared that can be regarded as simplified siblings of the macromonomers. The end groups were chosen with their ability to influence the  $\beta$ -sheet formation in mind. Thus, the macromonomers as well as the model compounds can be grouped according to their different number and pattern of N–H $\cdots$ O=C hydrogen-bonds (Table 3.4), which are considered to be the main factors for controlling the formation of  $\beta$ -sheet aggregates as well as the internal  $\beta$ -strand orientation within these aggregates.

**Table 3.4:** Hydrogen-bonding pattern of the macromonomers and model compounds.

	Number of N–H $\cdots$ O=C hydrogen-bonds in the end group				
	0	1	2	3	5
Macromonomer	<b>100,</b> <b>101, 102,</b> <b>103</b>	<b>92, 93,</b> <b>94, 95,</b> <b>122</b>	<b>96,</b> <b>97, 98,</b> <b>123</b>	–	<b>99</b>
Model compound	<b>130, 134</b>	<b>126, 131</b>	<b>132</b>	<b>127, 133</b>	–

## 3.2 Secondary and Higher Structure Formation

### 3.2.1 IR Spectroscopic Investigations

Infrared spectroscopy is a powerful tool for the elucidation of the secondary structures of oligo- and polypeptides because the frequencies of the different vibrations in the amide function highly depend on their conformation and mode of aggregation. Consequently, there are distinct regions in the spectra containing information about the secondary structures of the oligopeptides:

- the amide A ( $\nu_{\text{NH}}$ ) region located between 3400-3200  $\text{cm}^{-1}$
- the amide I ( $\nu_{\text{C=O}}$ ) region at 1700-1600  $\text{cm}^{-1}$
- the amide II region around 1550-1500  $\text{cm}^{-1}$
- and the amide III region between 1300-1200  $\text{cm}^{-1}$

IR spectroscopy has been widely used to investigate protein secondary structures in the literature. However, one has to note that conflicting and contradictory assignments of IR bands to certain secondary structures are abundant.<sup>188-190</sup> Therefore, the following conclusions have to be drawn with care, even more so as we investigated the model compounds and oligopeptide-polymer conjugates in organic media as opposed to most literature examples that were obtained in aqueous solutions or in the bulk.

#### 3.2.1.1 Secondary Structures of the Model Compounds

The model compounds equipped with dodecyl chains were dissolved in  $\text{CHCl}_3$  or DCM and investigated by IR spectroscopy using a solution phase cuvette (Figure 39). It was found, that **131** formed mechanically weak gels in DCM and **132** as well as **133** gave rise to gels in  $\text{CHCl}_3$  already at low concentrations. These gels were, however, homogeneous and could be investigated by IR spectroscopy without any problems. The IR spectra of the TMS-functionalized model compound **130**, which comprised 3+0 N-H $\cdots$ O=C hydrogen-bonding sites and was well-soluble in  $\text{CHCl}_3$ , revealed an amide A absorption at 3430  $\text{cm}^{-1}$ , i. e., far above the upper limit of 3300  $\text{cm}^{-1}$  usually observed in the case of a  $\beta$ -sheet arrangement. Only a small band observed at 3309  $\text{cm}^{-1}$  points at a low degree of  $\beta$ -sheet formation. The amide I region contained two peaks at 1725 and 1667  $\text{cm}^{-1}$  that could be assigned to the carbamate and the peptide  $\nu_{\text{C=O}}$  vibrations, respectively. It is important to note that a carbamate absorption significantly beyond 1700  $\text{cm}^{-1}$  can be ascribed to a non-hydrogen-bonded state, and that the observed amide I absorption proved that the molecules mainly attained random coil secondary

structures. The amide II region contained only one absorption at  $1503\text{ cm}^{-1}$ . Unfortunately, a detailed analysis of the amide III region was not possible because of the presence of artefacts in that region of the IR spectra due to the subtraction of the solvent background spectra. The observed bands, together with the fact that no gel formation occurred, nevertheless, strongly suggested that model compound **130** did not aggregate into  $\beta$ -sheets. Derivative **134**, which featured the same number and pattern of hydrogen-bonding sites, showed a strikingly similar IR signature. The main amide A absorption was observed at  $3308\text{ cm}^{-1}$  accompanied by a smaller band at  $3423\text{ cm}^{-1}$ , and the IR absorptions in the amide I and II regions were found at  $1722$ ,  $1663$  and  $1515\text{ cm}^{-1}$ , respectively. These findings and the lack of gel formation in  $\text{CHCl}_3$  showed that (i)  $\beta$ -sheet formation was still not the predominant process, (ii) the carbamate was in a non-hydrogen-bonded state, and (iii) the molecule predominantly attained a random coil conformation.

Likewise, the IR spectra of **131** in  $\text{CHCl}_3$  exhibited amide A absorptions at  $3434$  and  $3314\text{ cm}^{-1}$  and two almost equally strong bands at  $1730$  and  $1675\text{ cm}^{-1}$  which can be assigned to the ester as well as the carbamate  $\nu_{\text{C=O}}$  vibrations and the amide and peptide  $\nu_{\text{C=O}}$  vibrations, respectively. As for **130** and **134**, the positions of these absorptions proved that the molecules were (i) not aggregated and (ii) the peptide was mainly in a random coil conformation. Interestingly, however, the IR signature of **131** changed drastically when the weak gel in DCM was investigated. The amide A region was now dominated by an absorption located at  $3285\text{ cm}^{-1}$ , well in line with aggregated  $\beta$ -sheet type secondary structures. Two additional, smaller bands at  $3352$  and  $3427\text{ cm}^{-1}$  indicated that a certain fraction of molecules remained in a non-aggregated state. The main absorption band in the amide I region was located at  $1641\text{ cm}^{-1}$ , and a smaller band was observed at  $1676\text{ cm}^{-1}$ . While the latter absorption was consistent with the presence of molecules in a random coil conformation, the former amide I absorption happened to closely match the calculated value of  $1637\text{ cm}^{-1}$  for the hypothetical infinite, single, parallel  $\beta$ -sheet<sup>191,192</sup> as well as the experimental value observed in a tripeptide that was found to form a parallel  $\beta$ -sheet-like crystal structure.<sup>193</sup> Apparently, in DCM, model compound **131** showed a tendency to form  $\beta$ -sheets, but the degree of order was not very high. Of course, the observed amide I band alone may not be conclusive, as it is curiously shifted away from the typical values reported for antiparallel  $\beta$ -sheet type secondary structures at  $1625$ – $1630\text{ cm}^{-1}$  and may also be assigned to other types of secondary structures. However, the absorptions of the ester and the carbamate function were separated into two bands at  $1734$  and  $1706\text{ cm}^{-1}$ , respectively. The latter value is clearly indicative of carbamates in a hydrogen-bonded array, as had previously been reported by Mutter *et al.*<sup>171</sup> And, finally, the amide II region revealed two peaks at  $1543$  and  $1503\text{ cm}^{-1}$ . Similar to the amide I absorptions, the former value exactly matched the value calculated for a single, parallel  $\beta$ -sheet,<sup>191,192</sup> and the latter value proved the presence of molecules in a random coil conformation. In conclusion, the



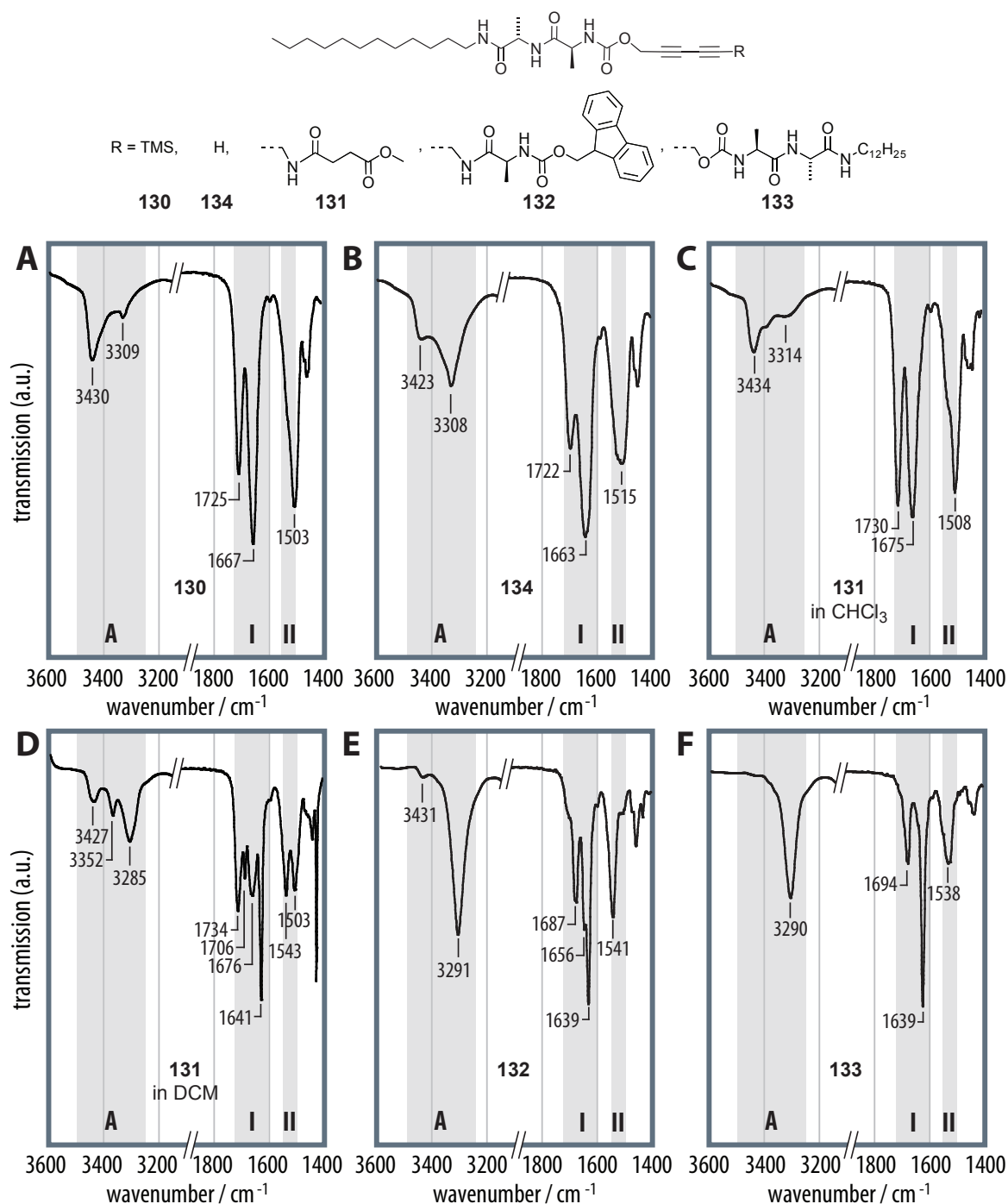


**Figure 39:** The IR spectra of the model compounds showed a clear trend: *A,B*) Derivatives **130** and **134** did not aggregate at all in  $\text{CHCl}_3$ . *C*) The same was true for **131** in the good solvent  $\text{CHCl}_3$ ; however, *D*) the formation of minor amounts of parallel  $\beta$ -sheets were observed in DCM. *E*) Model compound **132** clearly only formed parallel  $\beta$ -sheets with only very small amounts of unordered structures; *F*) A nearly perfect parallel  $\beta$ -sheet aggregation was found in the case of the symmetric molecule **133**.

amide A, carbamate, amide I, and amide II absorptions together converged into a consistent picture. Apparently, model copound **131** with its 3+1 hydrogen-bonding sites was just on the border of being able to aggregate, as it predominantly remained disordered in the more polar  $\text{CHCl}_3$  as the solvent but formed the desired  $\beta$ -sheet type aggregates in DCM, at least, to a certain extent.

The above interpretation and assignment of the IR absorptions was then further corroborated by the IR spectra of **132** and **133** comprising 3+2 and 3+3 hydrogen-bonding sites forming better-ordered  $\beta$ -sheet aggregates and, accordingly, featured clearer and more straightforwardly interpretable IR signatures. Particularly helpful in this context is the fact that model compound **133** can only give rise to parallel as opposed to antiparallel  $\beta$ -sheets due to its symmetry. The IR spectrum of **132** in  $\text{CHCl}_3$  exhibited a  $\nu_{\text{NH}}$  vibration at  $3291\text{ cm}^{-1}$  with only a minor shoulder at  $3431\text{ cm}^{-1}$ , and the amide A region of **133** showed a single sharp band at  $3290\text{ cm}^{-1}$ , consistent with predominantly aggregated N–H bonds. The amide I regions of both **132** and **133** were dominated by a band at  $1639\text{ cm}^{-1}$ , almost exactly matching the expected value of  $1637\text{ cm}^{-1}$  for a parallel  $\beta$ -sheet.<sup>191–193</sup> The carbamate bands were now observed at  $1687\text{ cm}^{-1}$  (**132**) and  $1694\text{ cm}^{-1}$  (**133**), both consistent with Mutter’s observations concerning aggregated carbamate functions and, thus, confirming the presence of highly ordered parallel  $\beta$ -sheet aggregates. It is, hence, important to acknowledge that, in this particular case, the band observed at around  $1690\text{ cm}^{-1}$  does not originate from the presence of antiparallel  $\beta$ -sheet structures (which were reported to exhibit a band at  $1690$  to  $1692\text{ cm}^{-1}$ )<sup>171,191,194</sup> but from the carbamate groups present in the molecules. Finally, the single amide II absorption bands located at  $1541\text{ cm}^{-1}$  (**132**) and  $1538\text{ cm}^{-1}$  (**133**) strongly supported the presence of parallel  $\beta$ -sheet aggregates, since the values again matched the calculated ones very well.

### 3.2.1.2 Secondary Structures of the Macromonomers 92–103

Macromonomers **92–103** were dissolved in DCM or  $\text{CHCl}_3$  (typically at concentrations of  $3\text{ g L}^{-1}$ ) and investigated by solution state IR spectroscopy in analogy to the model compounds (Table 3.5, Figure 40–Figure 42). With the exception of the TMS-functionalized macromonomer **102** and the oligo(ethylene oxide)-equipped derivative **101**, all macromonomers showed the predominant formation of  $\beta$ -sheet secondary structures together with varying proportions of unordered structures, as judged from the main amide A vibrations below  $3300\text{ cm}^{-1}$ , the main amide I absorptions at values of  $1625$  to  $1630\text{ cm}^{-1}$ , as well as the amide II absorptions located between  $1528$  to  $1541\text{ cm}^{-1}$ . Unfortunately, the amide III region was not interpretable again due to the presence of artefacts from the solvent subtraction. However, a detailed comparison of the remaining regions and a comparison to the model compounds allowed to identify systematic and distinct differences between the various macromonomers, allowing to differentiate three groups of molecules with dissimilar IR signatures.

The first group comprised the derivatives **92**, **93**, **96**, **97** as well as the symmetric molecule **99** ( $5+x$  hydrogen bonds;  $x = 1, 2, 5$ ). Their IR spectra indicated a particularly high content of defined  $\beta$ -sheet secondary structures (Figure 40). In particular, there was only one band for the amide A absorption which appeared in a narrow interval between  $3283$  and  $3290\text{ cm}^{-1}$  in all cases; only macromonomer

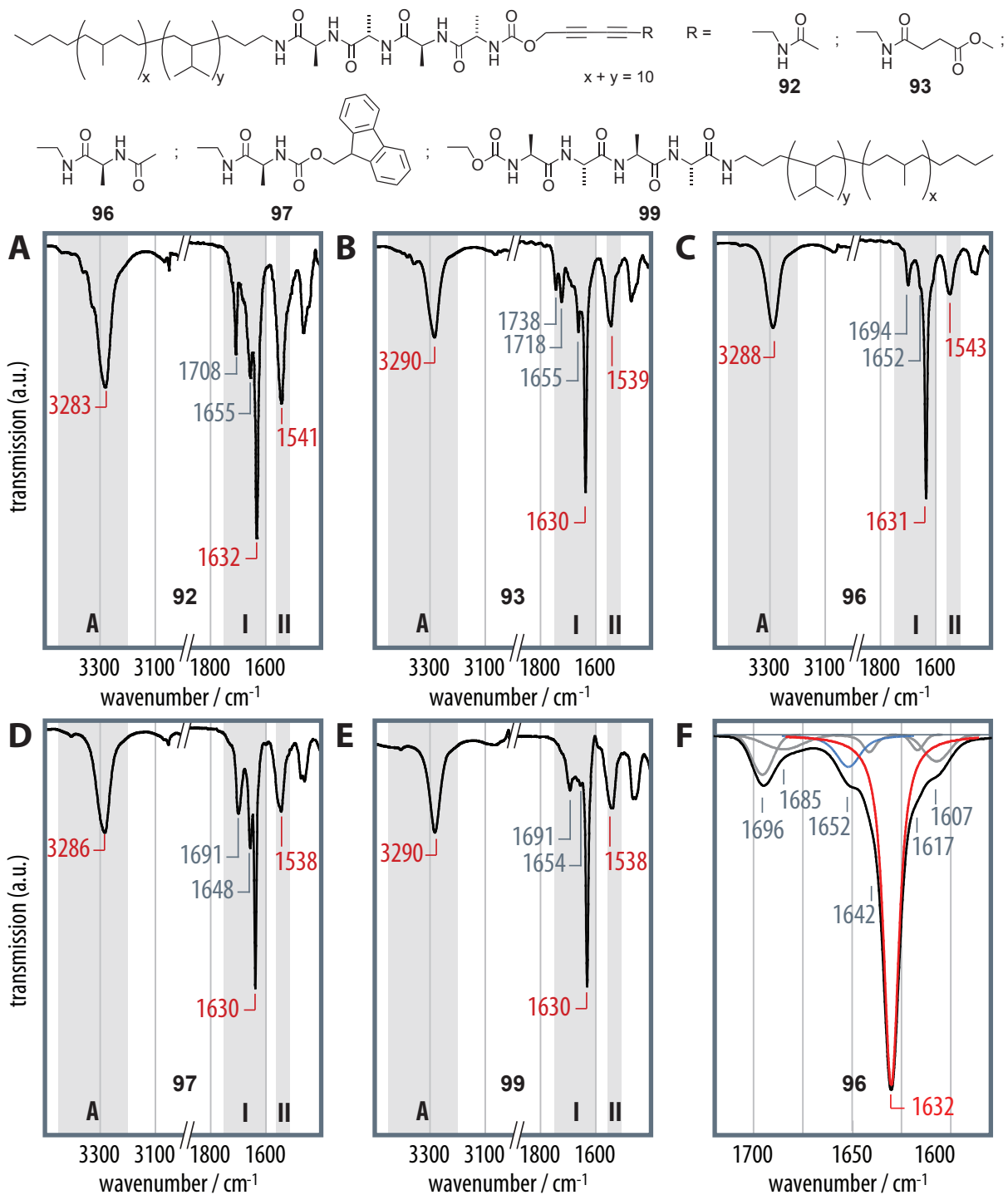


**Figure 40:** IR spectra of macromonomers **92**, **93**, **96**, **97** as well as **99**. All spectra showed only one amide A absorption below 3300 cm<sup>-1</sup>, a main amide I band in a very narrow range between 1630 and 1632 cm<sup>-1</sup>, as well as an amide II band at values between 1538 to 1543 cm<sup>-1</sup>, allowing for the conclusion that all these macromonomers formed parallel  $\beta$ -sheets. A representative peak fitting of the amide I region of **96** supports this assignment.

**92** exhibited a small shoulder at 3330 cm<sup>-1</sup>. The amide I region showed a very sharp and clearly predominating peak at 1630 to 1632 cm<sup>-1</sup> which, e.g., had a width at half-height of about 11 cm<sup>-1</sup> and

**Table 3.5:** The IR signatures proved that all macromonomers except **101** and **102** formed  $\beta$ -sheet type secondary structures. The combination of the amide A, amide I, carbamate as well as amide II vibrations allowed to identify the formation of parallel  $\beta$ -sheets in the case of **92**, **93**, **96**, **97** and **99**. Macromonomers **100** and **103** formed antiparallel  $\beta$ -sheets.

Compound	Amide A $\text{cm}^{-1}$	Amide I / NHC(O)O $\text{cm}^{-1}$	Amide II $\text{cm}^{-1}$
<b>92</b>	3283	1708, 1655, <b>1632</b>	1541
<b>93</b>	3290	1738, 1718, 1655, <b>1630</b>	1539
<b>94</b>	3291	1722, <b>1681</b> , 1654, <b>1631</b>	1534
<b>95</b>	3291	1718, 1694, <b>1666</b> , <b>1630</b>	1528
<b>96</b>	3288	1694, 1652, <b>1630</b>	1543
<b>97</b>	3296	1691, 1648, <b>1630</b>	1538
<b>99</b>	3290	1691, 1654, <b>1630</b>	1538
<b>100</b>	3427, 3348, <b>3274</b>	1715, <b>1672</b> , <b>1625</b>	1529
<b>101</b>	<b>3418</b> , <b>3354</b> , 3293	1723, <b>1673</b> , 1630, <b>1606</b>	1527, 1508
<b>102</b>	3418, 3355, <b>3277</b>	1718, <b>1673</b> , 1627, <b>1606</b>	1523, 1504
<b>103</b>	3331, <b>3271</b>	1713, 1676, 1655, <b>1626</b>	1531

accounted for 70% of the total peak area in the case of **96** as suggested by a peak fitting (Figure 40F). These very consistent amide I absorptions are, in fact, remarkable given the fact that they were exactly in the range of values experimentally determined for poly(L-alanine) and other examples of  $\beta$ -sheet forming poly(amino acid)s,<sup>194</sup> and they were close to the calculated value for an infinite parallel  $\beta$ -sheet, as well.<sup>191-193</sup> The main amide II absorptions of these macromonomers were observed at values from 1538 to 1543  $\text{cm}^{-1}$ , which did not match the corresponding experimental value for antiparallel poly(L-alanine) of 1524  $\text{cm}^{-1}$  at all.<sup>195,196</sup> However, they came, again, strikingly close to calculated and experimental values of some crystalline examples of oligopeptides aggregated in parallel  $\beta$ -sheets.<sup>193</sup> Furthermore, the non-peptidic carbamate bands showed a very interesting behaviour in so far as the band was shifted from a value above 1700  $\text{cm}^{-1}$  in the cases of derivatives **92** and **93** having 5+1 hydrogen-bonds to a constant value of 1691  $\text{cm}^{-1}$  when 5+2 or 5+5 hydrogen-bonds were formed. This was well in agreement with the spectra observed for the model compounds as well as

with the reports by Mutter *et al.* for water-soluble oligopeptide-PEO conjugates.<sup>171</sup> The overall remarkably clear IR signatures may, in part, originate from the short oligopeptide segments and the use of an organic solvent which may have restricted the structural dynamics of the hydrogen-bonded aggregates. Nevertheless, the secondary structure assignment appeared to be more straightforward here than in literature examples of similar oligopeptide conjugates<sup>124,125</sup> where only second derivative analyses allowed for an assignment. This qualitative difference may indicate a comparably high degree of internal order resulting from the chosen molecular architecture.

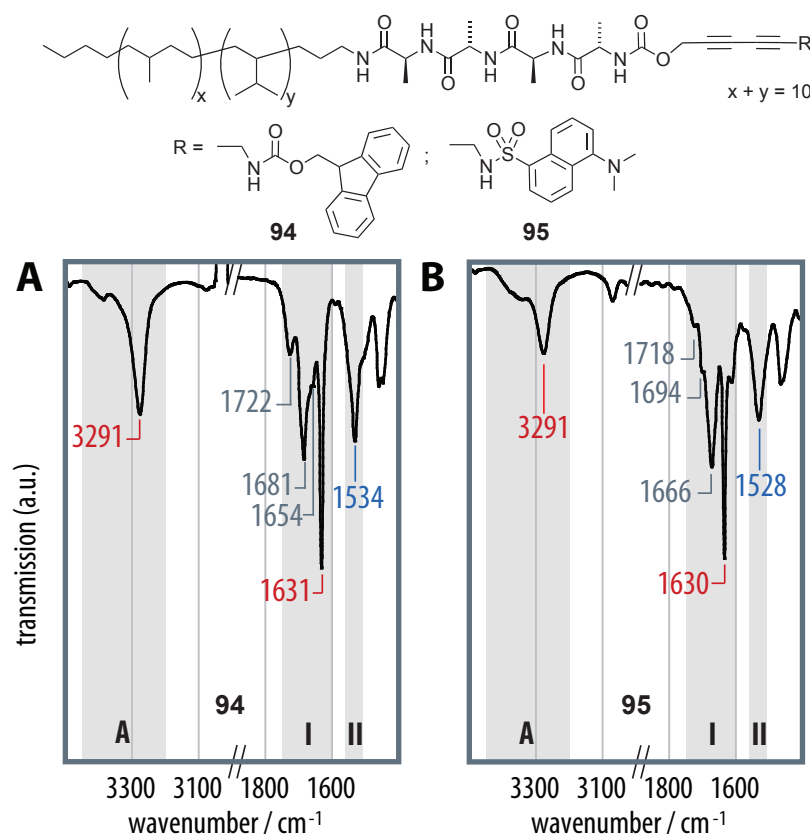


**Figure 41:** The IR spectra of macromonomers **94** and **95** showed a less ideal secondary structure formation. While, generally,  $\beta$ -sheet structures were formed, the strong absorptions at 1666 and 1681  $\text{cm}^{-1}$ , respectively, indicated the existence of a large amount of unordered structures in these two cases, as do the carbamate bands at 1722 and 1718  $\text{cm}^{-1}$ .

The second group of macromonomers comprising the Fmoc-derivative **94** and the Dansyl-derivative **95** (5+1 hydrogen-bonding sites), showed a somewhat different signature (Figure 41). Their amide A region was dominated by a band at 3291  $\text{cm}^{-1}$ . However, **95** exhibited a shoulder at higher wavenumbers, indicating mixtures of different secondary structures. Both derivatives showed an amide I band located at 1630 and 1631  $\text{cm}^{-1}$ , respectively, which was exactly the value found in the previous five cases. However, the very strong signals at 1666  $\text{cm}^{-1}$  in the case of **95** and 1681  $\text{cm}^{-1}$  (with a shoulder at lower wavenumbers) in the spectrum of **94** clearly indicated the presence of large

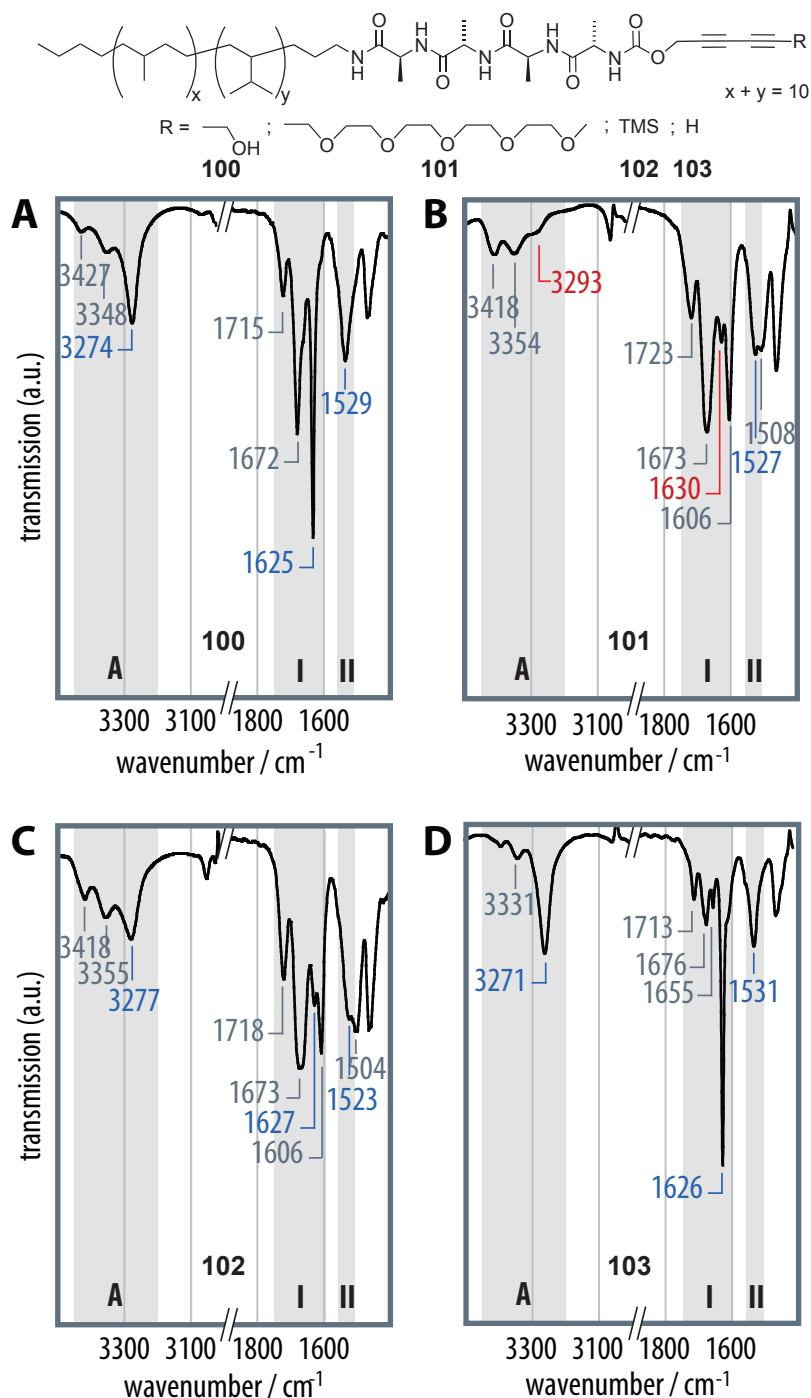


**Figure 42:** IR spectra of macromonomers **100–103** showed a different behavior compared to the previously discussed derivatives. While the terminal diacetylene clearly attained an antiparallel arrangement, **100** seemed to also contain unordered structures. In the case of **101** and **102**, a predominant formation of only unordered structures can be inferred from their IR spectra.

amounts of random coil secondary structures. The analysis of the carbamate vibration corroborated the assumption that mixtures of different secondary structures were present because in the spectrum of **94**, one corresponding band was found at  $1722 \text{ cm}^{-1}$ , indicative of a non-hydrogen-bonded state, whereas the band at  $1681 \text{ cm}^{-1}$  could be caused by aggregated carbamates, as well. In the case of

**95**, the spectrum was similar since, again, two peaks at  $1718\text{ cm}^{-1}$  and  $1694\text{ cm}^{-1}$  may be interpreted in terms of partially aggregated and non-aggregated carbamates. The amide II bands at  $1534$  and  $1528\text{ cm}^{-1}$  were, on the other hand, in agreement with  $\beta$ -sheet type structures.

The third group of macromonomers encompassed **100-103**. These compounds did not contain any  $\text{N-H}\cdots\text{O}=\text{C}$  hydrogen-bonds in their end groups (i. e., a total of  $5+0$  hydrogen-bonds) and showed distinctly different IR spectra. This ensemble could be further subdivided into two more groups. First, the derivatives **100** and **103** exhibited amide A absorption bands shifted to lower wavenumbers of  $3274\text{ cm}^{-1}$  and  $3271\text{ cm}^{-1}$  while both of them also showed minor absorptions above  $3300\text{ cm}^{-1}$ . The main amide I absorptions were now observed at  $1625$  and  $1626\text{ cm}^{-1}$ , and the amide II absorptions were located at values of  $1529$  and  $1531\text{ cm}^{-1}$ , respectively. In this context, it should be noted that Chirgadze *et al.*<sup>191,192</sup> also calculated the IR amide I absorption for an infinite, antiparallel single  $\beta$ -sheet to be  $1626\text{ cm}^{-1}$ , i. e., exactly the value obtained for **100** and **103** as well as other examples of self-assembled oligopeptides such as Boden's oligopeptides designed to self-assemble into discrete antiparallel single  $\beta$ -sheet tapes and ribbons.<sup>82-84,106,107</sup> Furthermore, the amide II bands of **103** and **100** also matched the expected and reported values for antiparallel oligo- and polypeptides more closely. The remaining macromonomers **102** and **101** exhibited less clear IR spectra suggesting the presence of mixtures of different secondary structures with only minor fractions of  $\beta$ -sheets, as could be inferred from their amide A regions that contained three absorption bands in each case. Also numerous amide I bands were present which were dominated by a band located at  $1673\text{ cm}^{-1}$  and a smaller band at  $1606\text{ cm}^{-1}$  in both cases. Only **101** exhibited a small band at  $1630\text{ cm}^{-1}$ , indicative of minor amounts of parallel  $\beta$ -sheets present in solution. The amide II region contained additional bands at  $1504$  and  $1508\text{ cm}^{-1}$ , respectively, which did not occur in the other cases as well.

### 3.2.1.3 Macromonomers with Longer Polymer Segments

The IR spectra of macromonomers **119-123**, which featured longer polymer segments exhibited very broad amide A bands located between values of  $3413$  to  $3416\text{ cm}^{-1}$ , i. e., far above  $3300\text{ cm}^{-1}$  (Figure 43). Only **121** featured a band at  $3306\text{ cm}^{-1}$  close to the region where  $\beta$ -sheet absorptions would be expected. The amide I regions showed a strong band between  $1722$  and  $1729\text{ cm}^{-1}$  which can be assigned to the carbamate functions in a non-hydrogen-bonded state. The dominating band in the amide I range was observed between  $1671$  and  $1677\text{ cm}^{-1}$ , indicative of random coil secondary structures for all derivatives, and only minor bands located at  $1629$  to  $1637\text{ cm}^{-1}$  proved a small extent of  $\beta$ -sheet formation. The amide II absorptions, finally, occurred between  $1496$  and  $1505\text{ cm}^{-1}$ .

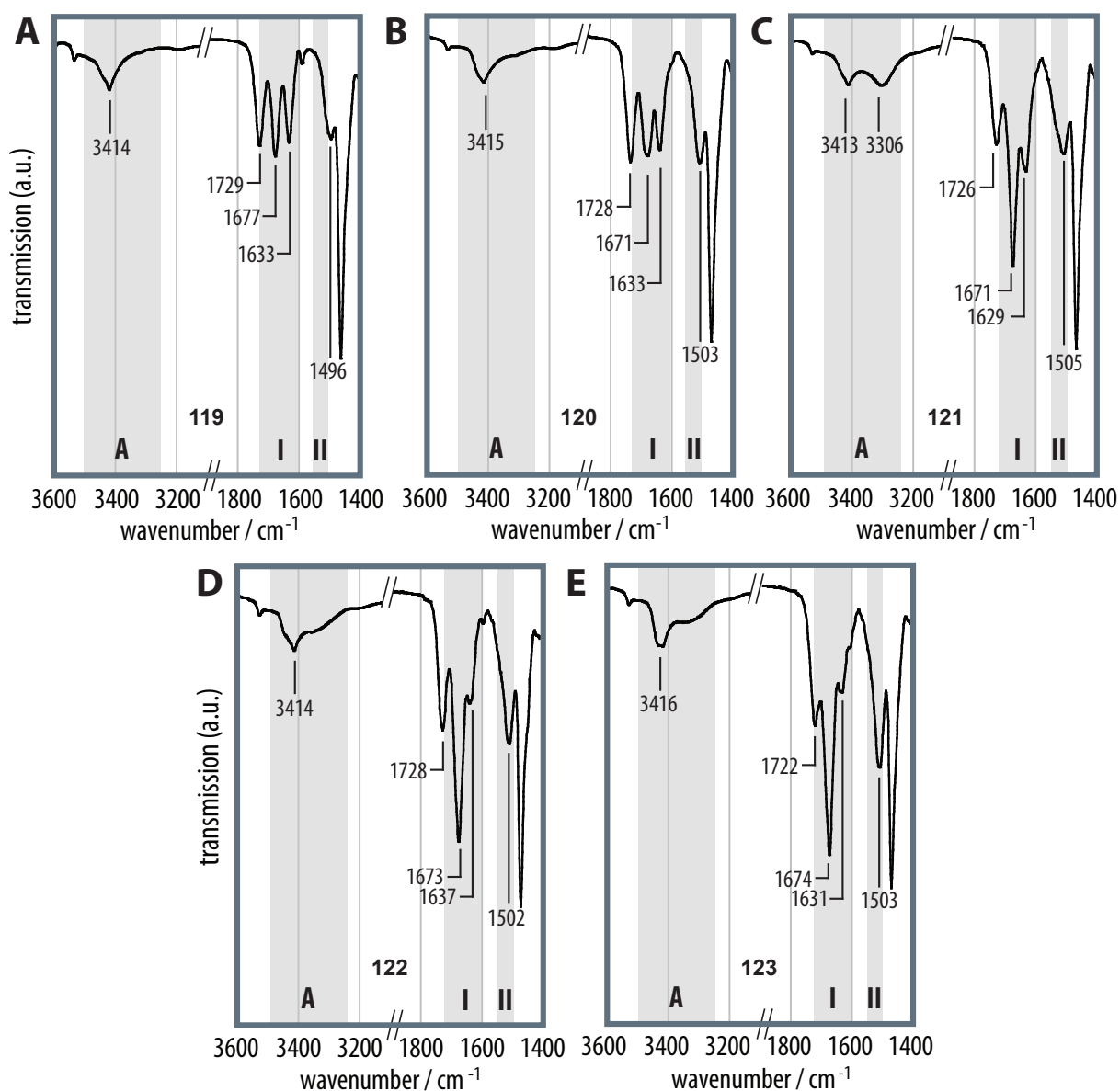


**Figure 43:** IR spectra of compounds 119–123 in DCM solution were indicative of non-hydrogen-bonded carbamate groups, and random coil secondary structures.

### 3.2.1.4 The Hydrogen-Bonding Pattern Controls the Secondary Structure Formation

From the above discussion of the IR spectra, it may be concluded that the hydrogen-bonding pattern decisively controlled the secondary structure formation. The model compounds showed that 3+1 non-equidistantly spaced N–H $\cdots$ O=C hydrogen-bonds can be regarded as the lower limit for a  $\beta$ -sheet formation. However, only minor changes of the solvent polarity (from CHCl<sub>3</sub> to DCM) were enough to suppress the aggregation. The only possible alignment of the  $\beta$ -strands was parallel because the relative energy difference to the antiparallel arrangement was comparably large in these cases. The use of 3+2 hydrogen-bonds can be assumed to be the lower limit for a *reliable* parallel  $\beta$ -sheet formation even in the better solvent CHCl<sub>3</sub>.



In the case of the macromonomers featuring a hydrogenated poly(isoprene) segment with an average degree of polymerization  $\bar{P}_n = 10$ , the different hydrogen-bonding patterns led to clearly distinct secondary structures. Thus, the macromonomers **92** and **93** (5+1 hydrogen-bonds), **96** and **97** (5+2 hydrogen-bonds) as well as **99** (5+5 hydrogen-bonds) did not only display a very high degree of  $\beta$ -sheet secondary structure formation; the IR spectra were also found to be consistent with a parallel  $\beta$ -strand orientation within the  $\beta$ -sheets. By additionally taking the shift of the carbamate absorption as well as the overall cleaner spectra of the derivatives with 5+2 and 5+5 hydrogen-bonds into account, a clear trend toward higher ordered parallel  $\beta$ -sheets can be assumed in these cases. The derivatives **95** and **94** (5+1 hydrogen-bonds) seemed to predominantly form  $\beta$ -sheet type structures. However, the amide A as well as the main amide I absorptions were consistent with a mixture of a parallel arrangement and random coil structures, while the amide II bands, again, indicated the formation of  $\beta$ -sheet type aggregates. Thus, the influence of the bulky aromatic residues seemed to be detrimental for a consistently ordered alignment of these molecules. By contrast, macromonomers **100** and **103** (5+0 hydrogen-bonds) were found to favor a predominantly antiparallel  $\beta$ -sheet secondary structure combined with an overall higher proportion of other secondary structures such as random coil conformations in the case of **100**. Finally, the derivatives **101** and **102** (5+0 hydrogen-bonds) clearly showed a majority of random coil structures with only minor amounts of parallel as well as antiparallel  $\beta$ -sheet structures.

All these considerations become, however, obsolete if a too long polymer segment is attached to the oligopeptides as in the case of derivatives **119–123**. Here, the apparently very sensitive system was completely dominated by the properties of the polymer segments, i. e., the macromonomers were simply dissolved and did not show any tendency to aggregate anymore.

In summary, the degree of primary structure control over the type of secondary structures is remarkable, given the very close structural relation between the different macromonomers. Apparently, the presence or absence of additional N–H $\cdots$ O=C hydrogen-bonding sites in the end groups as well as the length of the polymer segment (or aliphatic substituent) were the main factors that controlled the type of secondary structure. This interpretation can be rationalized by assuming that, normally, an antiparallel  $\beta$ -strand orientation should be preferred due to the more optimal hydrogen-bond geometries, the cancellation of the molecules' dipole moment components in  $\beta$ -strand direction, and the more favorable alternating placement of the bulky grafted polymer chains (or dodecyl substituents). In the cases of macromonomers **92–97** and **99**, as well as the model compounds **131** and **132**, however, these factors appear to be overcompensated by the presence of non-equidistantly placed N–H $\cdots$ O=C hydrogen-bonding sites, because the maximum number of 5+x or 3+x hydrogen-bonds can only be achieved in a parallel  $\beta$ -strand orientation.

### 3.2.2 Solid State NMR Investigations

In order to corroborate the results and interpretations of the IR measurements, an investigation of the secondary structure formation of the macromonomers by means of sophisticated solid state NMR techniques was carried out in collaboration with the group of Prof. Beat Meier. The aim of the planned experiments was to unambiguously prove that derivatives having additional N–H···O=C hydrogen-bonding sites in the end group formed parallel  $\beta$ -sheets while the others preferred an antiparallel arrangement. Furthermore, a close insight into the conformation of the oligopeptides in the  $\beta$ -sheets was to be obtained. Two different types of experiments were planned. First, Rotational Echo Double Resonance (REDOR)<sup>197</sup> spectroscopy allows for the determination of distances between two different spin systems such as  $^{13}\text{C}$  and  $^{15}\text{N}$  nuclei by using magic angle spinning (MAS) and cross polarization (CP) techniques.<sup>197</sup> This technique has successfully been applied to study the secondary structure formation of natural polypeptides<sup>197</sup> as well as synthetic oligo- $\beta$ -peptides.<sup>198</sup> The second method, double-quantum single-quantum correlation spectroscopy (DOQSY), aims at the measurement of torsion angles between two equivalent spin systems ( $^{13}\text{C}$ – $^{13}\text{C}$ ) either positioned in two neighboring molecules or within the same. This static solid state NMR technique has been developed for the measurement of torsion angles in polymers<sup>199</sup> and was applied for the elucidation of the internal structure of partially labeled spider silk.<sup>200–202</sup> Due to the low natural abundance of  $^{13}\text{C}$  and  $^{15}\text{N}$  nuclei, the synthesis of isotope-labeled macromonomers was required for both techniques.

#### 3.2.2.1 $^{13}\text{C}$ - and $^{15}\text{N}$ -Labeled Analogues to Macromonomers **92** and **103**

Macromonomer **92** as the simplest derivative with a predominantly parallel  $\beta$ -sheet secondary structure was chosen for the first DOQSY experiments. The carbonyl group of the fourth amino acid was chosen to be  $^{13}\text{C}$ -labelled, although this was synthetically very demanding. The rationale was that if the molecules aligned in a parallel fashion, the corresponding C=O groups would be closely packed at the intersheet distance of 4.8 Å, whereas an antiparallel arrangement would place the two spins at an estimated distance of 9.8 Å, i. e., as far apart as possible in the tetrapeptide (Figure 44).

In order to introduce the labeled carbonyl group at the chosen position, the less efficient divergent synthesis had to be pursued because only the [1- $^{13}\text{C}$ ]-labeled L-alanine was commercially available. The latter was reacted with propargyl chloroformate in aqueous NaOH solution at low temperature and a constant pH 9 (Scheme 40). While the test reaction with non-labeled L-alanine gave 75% yield on a 2 g scale, the labeled derivative **135** could only be obtained in 44% yield on a much smaller scale. However, enough pure material was obtained to continue the synthesis.

In the next step, the propargyl carbamate **135** was coupled to the oligopeptide-polymer conjugate **45** in an EDCI/HOBt promoted peptide coupling reaction. Although the product **136** was a very

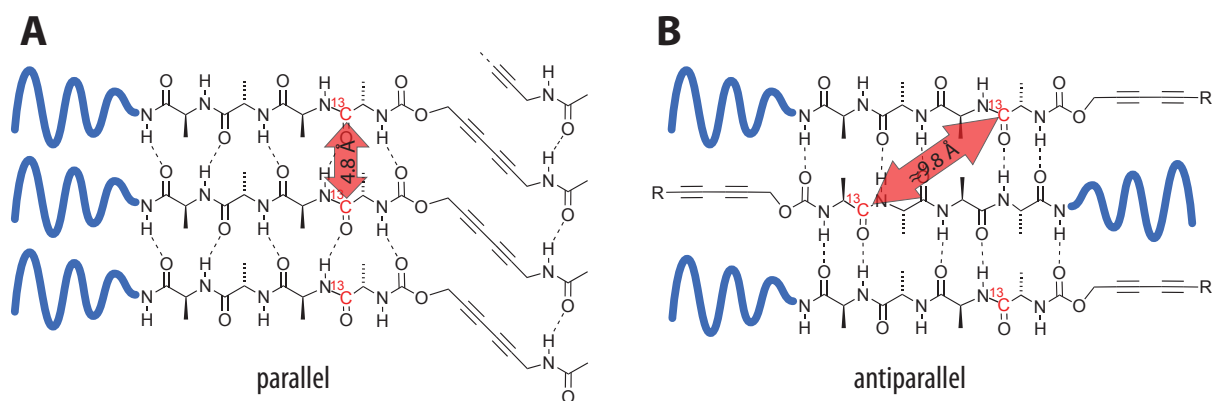
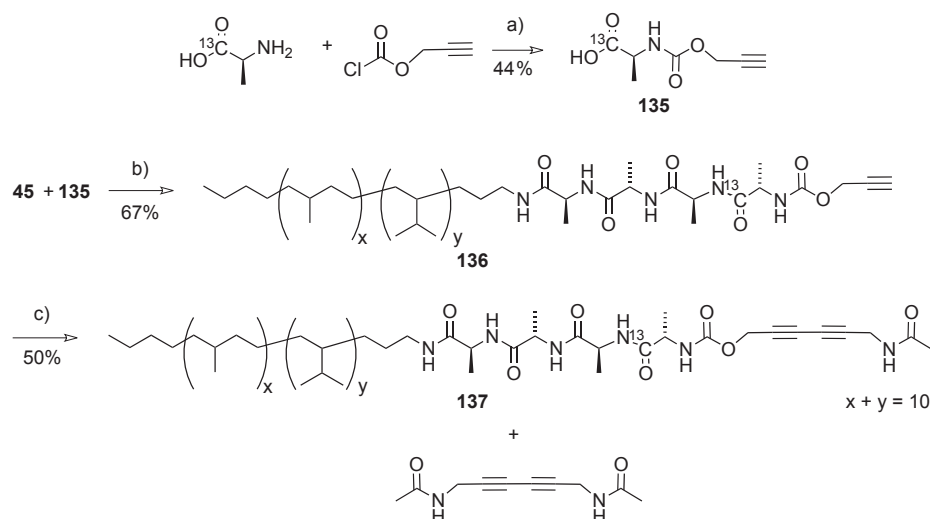


**Figure 44:** Schematic drawing of macromonomer **137**  $^{13}\text{C}$ -labeled at the fourth amino acid in a parallel  $\beta$ -sheet arrangement. This places the spins at a distance of approximately 4.8 Å. In an antiparallel arrangement, the distance is much larger, with approximately 9.8 Å.



**Scheme 40:** Preparation of the  $^{13}\text{C}$ -labeled macromonomer **137**. *Reagents and Conditions:* a) 1 N NaOH solution, 15 °C; b) EDCI/HOBt, TEA, DCM/DMF, -40 °C  $\rightarrow$  r.t.; c) 10 eq **50**,  $\text{PdCl}_2(\text{PPh}_3)_2$  (2 mol%), CuI (10 mol%), DIPA, THF/DCM, 0 °C.

strong organo-gelator, it was obtained in a yield of 67% (Scheme 40). In order to complete the synthesis of the target molecule, a final Sonogashira coupling was carried out using an even larger excess (10 equivalents) of the iodoacetylene compound **50** as compared to the original preparation. Thus, the formation of the homocoupling product was completely suppressed, and only the low molecular weight selfcoupling product had to be removed by repeated column chromatography runs. The final yield of 50% was, therefore, acceptable.

The results of the first DOQSY experiments carried out on a sample of **137** (not shown) were very promising since a strong signal could be recorded hinting at a parallel orientation of the molecules. Therefore, a  $^{15}\text{N}$ -labeled sibling for a REDOR experiment was prepared which was to prove the parallel arrangement directly, by measuring the  $^{13}\text{C} - ^{15}\text{N}$  distance (Figure 45).

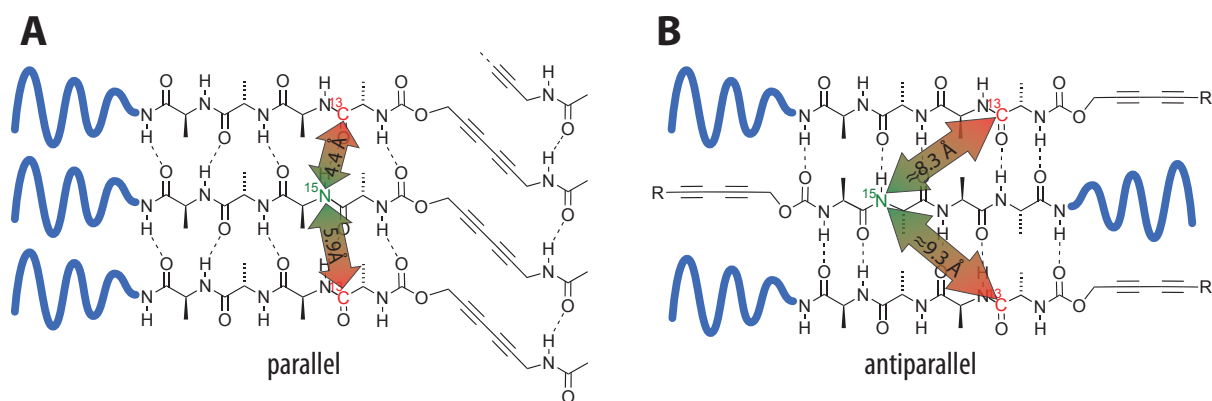
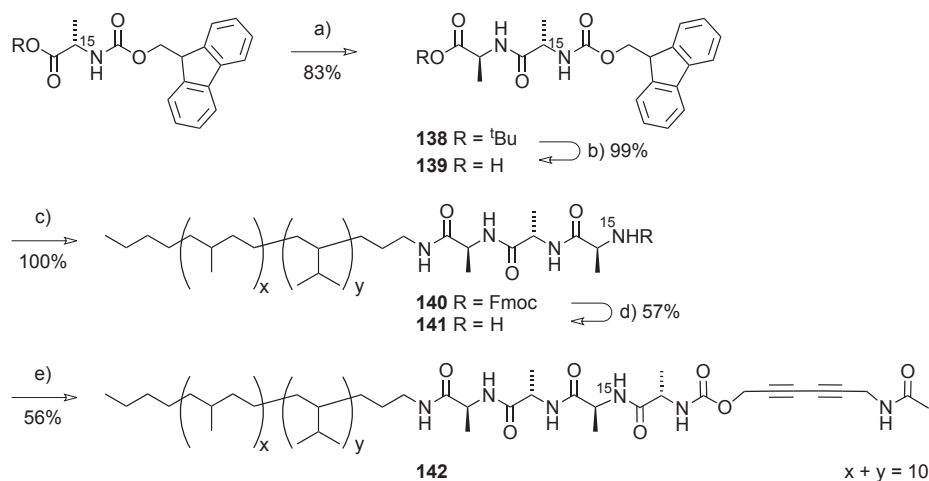


**Figure 45:** A) Schematic drawing of the distances between the  $^{13}\text{C}$ - and the  $^{15}\text{N}$ -labels in a parallel arrangement of the *N*-acetylated macromonomers **137** and **142**. B) For an antiparallel arrangement, these distances would be much larger.



**Scheme 41:** Preparation of the  $^{15}\text{N}$ -labeled macromonomer **142**. *Reagents and Conditions:* a) H-Ala-O<sup>t</sup>Bu, PyBOP, DCM, DIEA, 0 °C; b) TFA, DCM; c) **43**, EDCI/HOBt, TEA, DCM/DME, -40 °C → r.t.; d) piperidine, CHCl<sub>3</sub>; e) **68**, EDCI/HOBt, TEA, DCM/DME, -40 °C → r.t.

A suitable position of the  $^{15}\text{N}$  label was the nitrogen atom of the third amino acid, since this would result in a very close distance to the carbon label of a neighboring molecule in case of a parallel  $\beta$ -sheet-alignment. The synthesis was straightforward because the  $^{15}\text{N}$ -labeled, Fmoc-protected alanine derivative was commercially available and, hence, the more efficient convergent route could be pursued (Scheme 41).

Accordingly,  $^{15}\text{N}$ -labeled *N*-(9-fluorenylmethyloxycarbonyl)-L-alanine was coupled to L-alanine *tert*-butyl ester hydrochloride in a PyBOP-promoted peptide coupling furnishing the product **138** in 83% yield. The following *tert*-butyl ester deprotection with TFA worked with almost quantitative yield. In the next step, the labeled alanine dimer **139** was coupled to the hydrogenated poly(isoprene) building block **43** carrying already one alanine in an EDCI promoted reaction to give **140**. In order not to lose too much of this valuable material, only a minor amount was purified for analytical purposes. The main amount was used without further purification since the TLC and NMR had shown no ma-

for impurities after the acidic aqueous workup. The Fmoc-group was removed with piperidine, and the free amine derivative **141** was obtained in 57% yield. In the final step, **141** was reacted with the prefabricated diacetylene building block **68** in an EDCI promoted coupling resulting in an acceptable yield of 56% after repeated column chromatography.

For the REDOR measurement, a 1:1 mixture of the  $^{15}\text{N}$ - and the  $^{13}\text{C}$ -labeled molecules **142** and **137** was needed. Therefore, equal amounts were dissolved in a small amount of DCM, and the solution was heated and ultrasonicated for several minutes. Then, the sample was freeze-dried to remove the solvent. The obtained REDOR data could be fitted best assuming the presence of two  $^{13}\text{C} - ^{15}\text{N}$  distances of 4.4 as well as 5.9 Å, as would be expected in a parallel  $\beta$ -sheet arrangement with all amino acids aligned in register (Figure 46). It could be proved that more than 90% of the molecules were aligned in a parallel mode of aggregation when a more detailed model was applied.

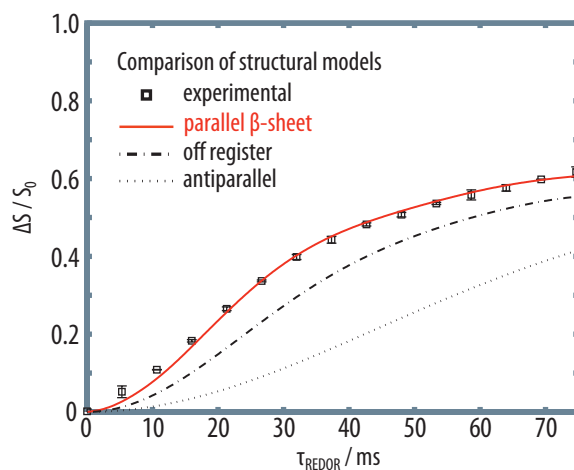


**Figure 46:** Analysis of the REDOR data revealed the existence of predominantly parallel  $\beta$ -sheet type arrangements, whereas an antiparallel alignment or an off-register placement of the amino acids could be excluded.

As the results of the first REDOR experiments were very promising, an improved molecular design was developed that would allow for a direct determination of the parallel or antiparallel  $\beta$ -sheet alignment. Furthermore, the synthetic complexity would be substantially reduced if one did not have to prepare two differently labeled molecules of any kind but rather only one  $^{15}\text{N}$ - and  $^{13}\text{C}$ -labeled derivative. As a result, we chose to include a  $^{13}\text{C}$ -label at the carbonyl function of the second alanine and a  $^{15}\text{N}$ -label in the third amino acid (Figure 47).

The REDOR measurements are also affected by the intramolecular interactions of the two labels. However, this distance is constant with a value of approximately 6.2 Å and can, thus, be taken into account during the data analysis. The intermolecular interactions would be clearly different in the two cases (Figure 47). Potential  $^{13}\text{C} - ^{13}\text{C}$  correlations in the DOQSY experiment would be stronger in the

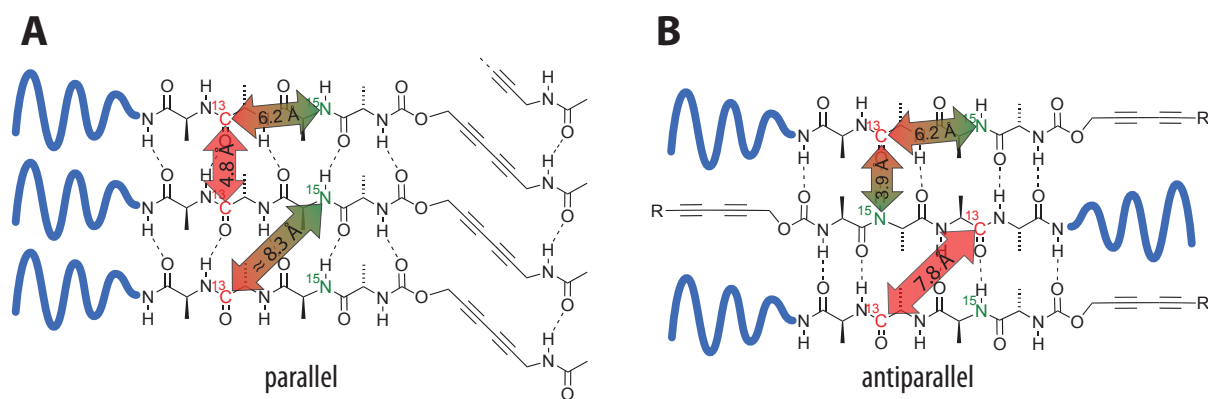


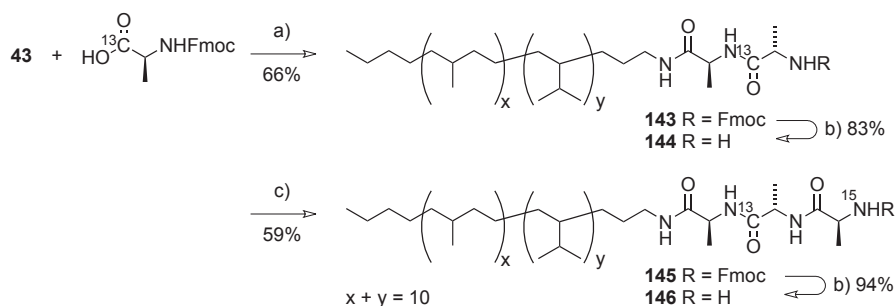
**Figure 47:** Schematic drawing of the various inter-spin distances in a parallel or an antiparallel arrangement of the  $^{15}\text{N}$ - and  $^{13}\text{C}$ -labeled macromonomer **147**. While the inter-strand  $^{13}\text{C}$ - $^{13}\text{C}$  interaction would be dominant in the first case, the closest contact in the second case would be a  $^{13}\text{C}$ - $^{15}\text{N}$  interaction. Thus, either DOQSY or REDOR experiments would prove the alignment of the macromonomers.

parallel arrangement though, allowing for an unambiguous assignment of the  $\beta$ -sheet arrangements.

These considerations implied the synthesis of different target molecules aimed at a parallel or an antiparallel self-assembly. A sequential strategy appeared to be most convenient since the  $^{13}\text{C}$ - and  $^{15}\text{N}$ -labeled Fmoc-protected L-alanines can be applied. Thus,  $^{13}\text{C}$ -labeled *N*-(9-fluorenylmethyloxycarbonyl)-L-alanine was coupled in an EDCI-promoted peptide coupling reaction to polymer building block **43**. Unfortunately, the reaction did not run as smoothly as usual, leading to an incomplete reaction. The required column chromatography furnished the clean product **143** in only 66% yield (Scheme 42). The following removal of the protecting group gave **144** in a good yield of 83% after column chromatography. In order to connect the  $^{15}\text{N}$ -labeled amino acid, the corresponding Fmoc-protected amino acid building block was reacted under the same conditions as before. The EDCI coupling was, again, not quantitative which may be explained by the generally much smaller reaction scales as compared to the non-labeled compounds. Consequently, the presence of minor amounts of moisture in the system may have a higher impact. The desired product **145** was, nevertheless, isolated in 59% yield after column chromatography. The subsequent Fmoc-deprotection proceeded very well, yielding the crucial intermediate **146** in an excellent 94% yield.

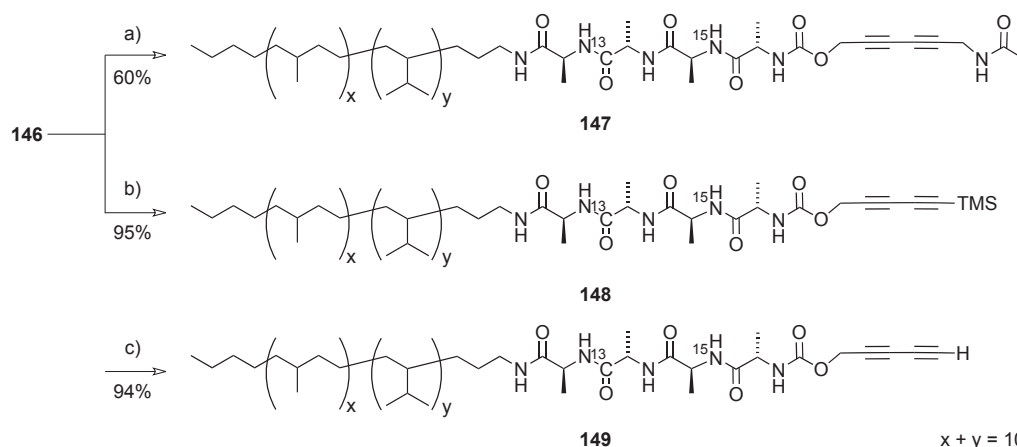
Starting from **146**, three different target molecules were prepared (Scheme 43). First of all, an acetamidomethyl functionalized derivative was prepared by attaching the corresponding diacetylene derivative **68**. The reaction gave **147** in a satisfactory yield of 60% after repeated column chromatography.

In order to get access to a molecule which we envisioned to self-assemble into an antiparallel  $\beta$ -sheet, we decided to prepare the H-terminated derivative **149**. Therefore, we first synthesized the TMS-substituted derivative **148** from building blocks **87** and **146**. By using 1.5 equivalents of



**Scheme 42:** Preparation of intermediate **146**. *Reagents and Conditions:* a) EDCI/HOBt, TEA, DCM/DME,  $-40^\circ\text{C} \rightarrow \text{r.t.}$ , 16h; b) piperidine,  $\text{CHCl}_3$ ; c)  $^{15}\text{N}$ -labeled *N*-(9-fluorenylmethyloxycarbonyl)-L-alanine, EDCI/HOBt, TEA, DCM/DME,  $-40^\circ\text{C} \rightarrow \text{r.t.}$ , 16h.

the carboxylic acid component, a nearly quantitative yield of 95% was achieved after repeated column chromatography. The subsequent removal of the silyl group was achieved by using TBAF as in the case of the non-labeled derivative. The product **149** was isolated in 94% yield after column chromatography.



**Scheme 43:** Preparation of the  $^{13}\text{C}$ - and  $^{15}\text{N}$ -labeled macromonomers **147**, **148** and **149**. *Reagents and Conditions:* a) **68**, EDCI/HOBt, TEA, DCM/DME,  $-40^\circ\text{C} \rightarrow \text{r.t.}$ ; b) **87**, EDCI/HOBt, TEA, DCM/DME,  $-40^\circ\text{C} \rightarrow \text{r.t.}$ ; c) TBAF, DCM/THF,  $0^\circ\text{C} \rightarrow \text{r.t.}$

Target molecules **147** and **149** were dissolved in DCM, heated and ultrasonicated prior to a freeze-drying procedure. The DOQSY experiment carried out with a sample of **147** showed a “diagonal” distribution of the intensities (Figure 48A). This allowed for the conclusion that the tensors of the labeled carbonyl groups of neighboring molecules were virtually parallel, i. e., the C=O bonds pointed to the same direction in space. The signal intensity was a clear indication of a parallel arrangement which was corroborated by a REDOR measurement (not shown). Furthermore, the intensity distribution was narrow, indicating a high intermolecular order.

Derivative **149** was designed to form antiparallel  $\beta$ -sheet secondary structures, as had been shown by IR spectroscopy for the non-labelled derivative. The REDOR experiment carried out with this macromonomer (Figure 48B) was fitted with two models. The first one was based on two spins only and assumed three different  $^{13}\text{C}$ - $^{15}\text{N}$  distances of 4.1, 5.1, or 6.1 Å. At short dephasing times ( $\leq 20$  ms) the fit for the shortest assumed distance was already acceptable indicating that the  $\beta$ -sheets were antiparallel. An overall much better fit was obtained, however, when a three spin system, i. e., two  $^{15}\text{N}$  and one  $^{13}\text{C}$  atoms, was considered. The best fit was produced assuming two  $^{13}\text{C}$ - $^{15}\text{N}$  distances of 4.04 and 6.05 Å and a C-N-N-angle of  $10^\circ$  which is well in line with one intermolecular distance (4.04 Å) and one intramolecular distance at about 6 Å. In conclusion, the antiparallel alignment of macromonomer **149** was unambiguously proved by the experiment.

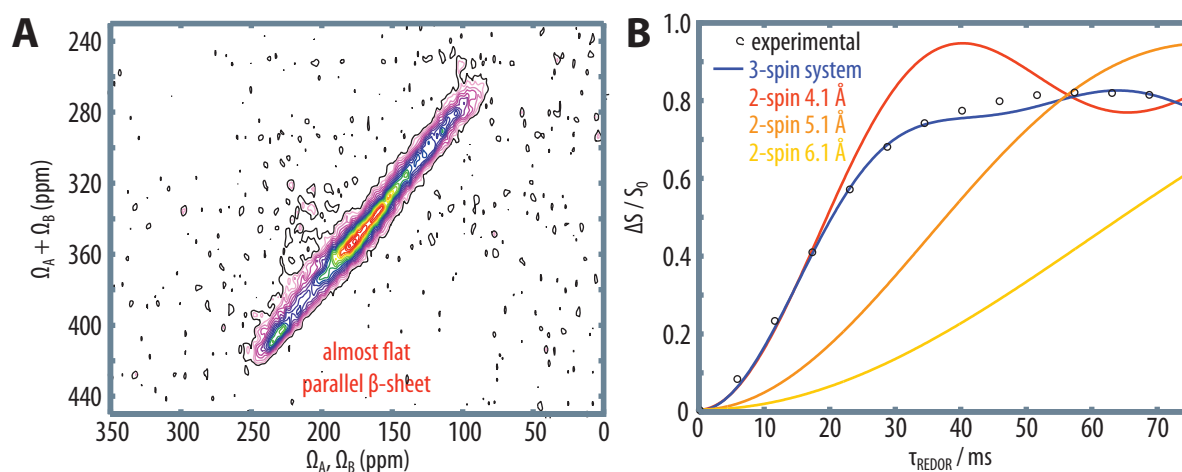


**Figure 48:** A) The DOQSY experiment carried out with **147** showed a “diagonal” intensity distribution indicating a parallel alignment of C=O bonds in neighboring molecules. B) The REDOR spectrum of **149** unambiguously proved an antiparallel  $\beta$ -strand alignment in the  $\beta$ -sheet.

### 3.2.2.2 Investigations on $^{13}\text{C}$ -Labeled Analogues to Macromonomer **93**

In order to elucidate the geometry of the  $\beta$ -sheets in more detail, i. e., the torsion angles between the different carbonyl groups within one molecule and between corresponding C=O groups of neighboring molecules, a completely different set of target structures was needed. All these aspects were to be determined by DOQSY experiments, only requiring the introduction of  $^{13}\text{C}$ -labels. Thus, molecules with two  $^{13}\text{C}$ -labeled carbonyl groups in adjacent amino acids were synthesized for the determination of the intramolecular torsion angles (Table 3.6).

The labeled Fmoc-protected alanine trimers **150**, **151**, **152**, **153**, and **154** were prepared via solid phase peptide synthesis in the Meier group. These were then reacted with amine-functionalized hy-



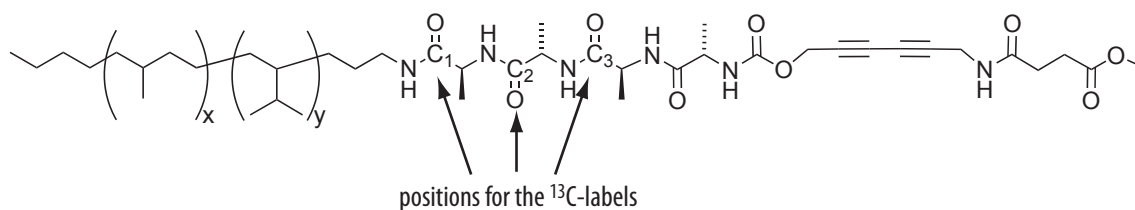


**Figure 49:** The <sup>13</sup>C-labels were incorporated in the carbonyl groups of the first three amino acids.

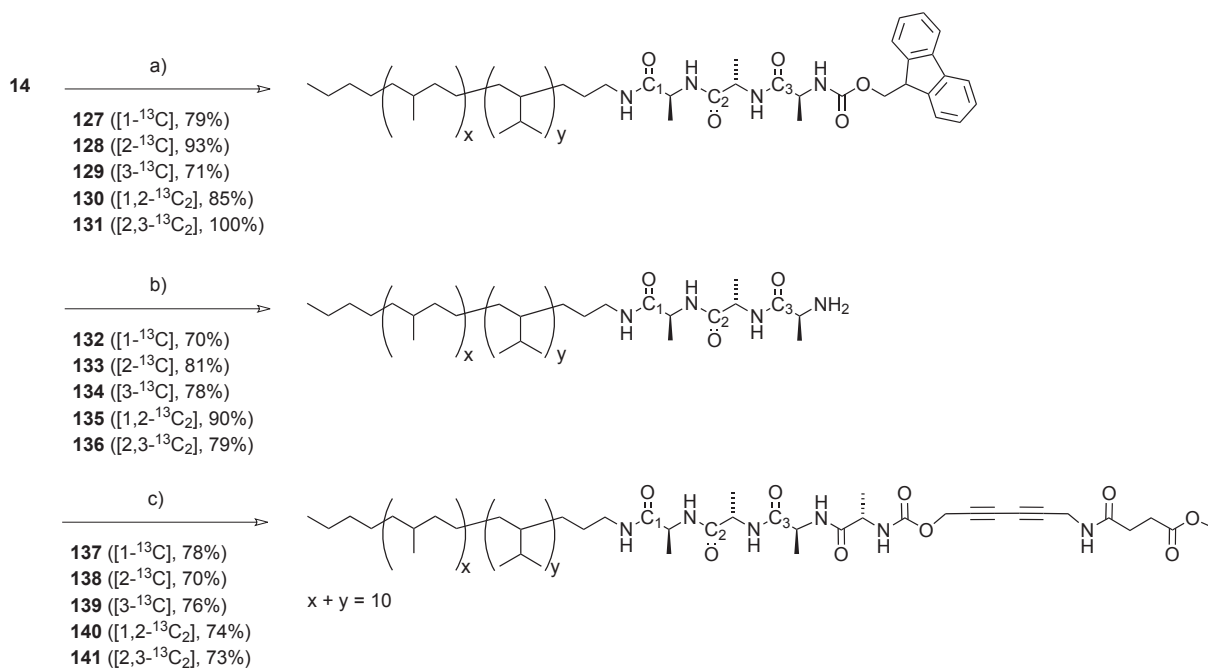
**Table 3.6:** Schematic overview of the <sup>13</sup>C-labeled macromonomers aimed at the determination of the inter- and intramolecular torsion angles by means of DOQSY NMR experiments. Derivatives with a <sup>13</sup>C-label in the fourth amino acid have not been prepared due to the associated synthetic difficulties.

Target Molecule	Amino acid Position			
	1	2	3	4
<b>165</b>	X	–	–	–
<b>166</b>	–	X	–	–
<b>167</b>	–	–	X	–
<b>168</b>	X	X	–	–
<b>169</b>	–	X	X	–

drogenated poly(isoprene) **41** in PyBOP-promoted peptide coupling reactions. While the derivatives carrying only one label were used as obtained from the peptide synthesizer, the doubly labeled compounds **153** and **154** were “diluted” to a concentration of 33 mol% with non-labeled alanine trimer **39** in order to avoid too many intermolecular <sup>13</sup>C–<sup>13</sup>C close contacts, which would render the analysis of the data too complex. The reactions were carried out on a scale of typically 60 to 70 mg of the trialanine building block, leading to yields ranging from 71 to 100%.

The subsequent cleavage of the protecting group was also successful in all cases, furnishing yields of 70 to 90% after column chromatography. The final peptide coupling was carried out using 2 equivalents of the diacetylene component **71** and 2.5 equivalents of both EDCI and HOBt to ensure a complete conversion. The obtained yields after two column chromatography runs were 70 to 78% which were good given the strong tendency of the target molecules to polymerize during the purification at daylight.

Samples of the five target structures **165**, **166**, **167**, **168**, and **169** were prepared by ultrasonication and heating of rather concentrated solutions followed by a lyophilization. The one-dimensional



**Scheme 44:** Preparation of various labeled macromonomers **165–169** for use in the DOQSY-based torsion angle measurements. *Reagents and Conditions:* a) Labeled Fmoc-protected alanine trimer **150–154**, PyBOP, DIEA, DCM/DME, 0 °C; b) piperidine,  $\text{CHCl}_3$ ; c) diacetylene building block **71**, EDCI/HOBt, TEA, DCM/DME,  $-40^\circ\text{C} \rightarrow \text{r.t.}$ , 16 h

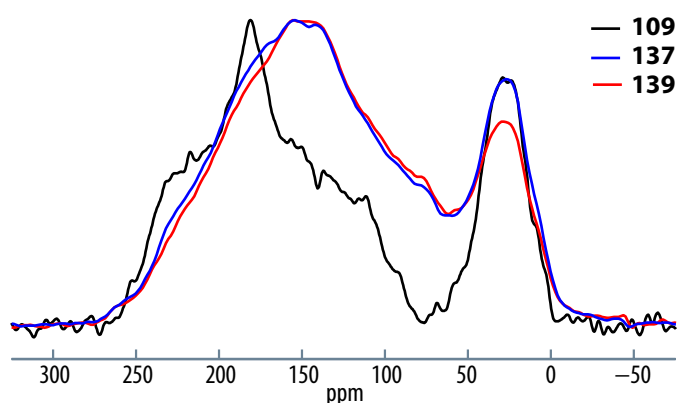


**Figure 50:** Representative one-dimensional  $^{13}\text{C}$  solid state NMR spectra showing that the quality of samples prepared for the current investigations was inferior to the one obtained from macromonomer **137**. In the latter case, the line shape was characteristic for an oriented sample while the new spectra were astonishingly featureless indicative of a low order in the samples.

spectra of all these derivatives were, however, inferior in quality as compared to **147** carrying the acetamidomethyl end group (Figure 50). In the latter case, the corresponding spectrum showed a characteristic line shape while the spectra of the analogues of macromonomer **93** exhibited rather featureless line shapes. Obviously, the sample preparation was suboptimal, a fact that should be considered in the following discussion of the two-dimensional spectra.

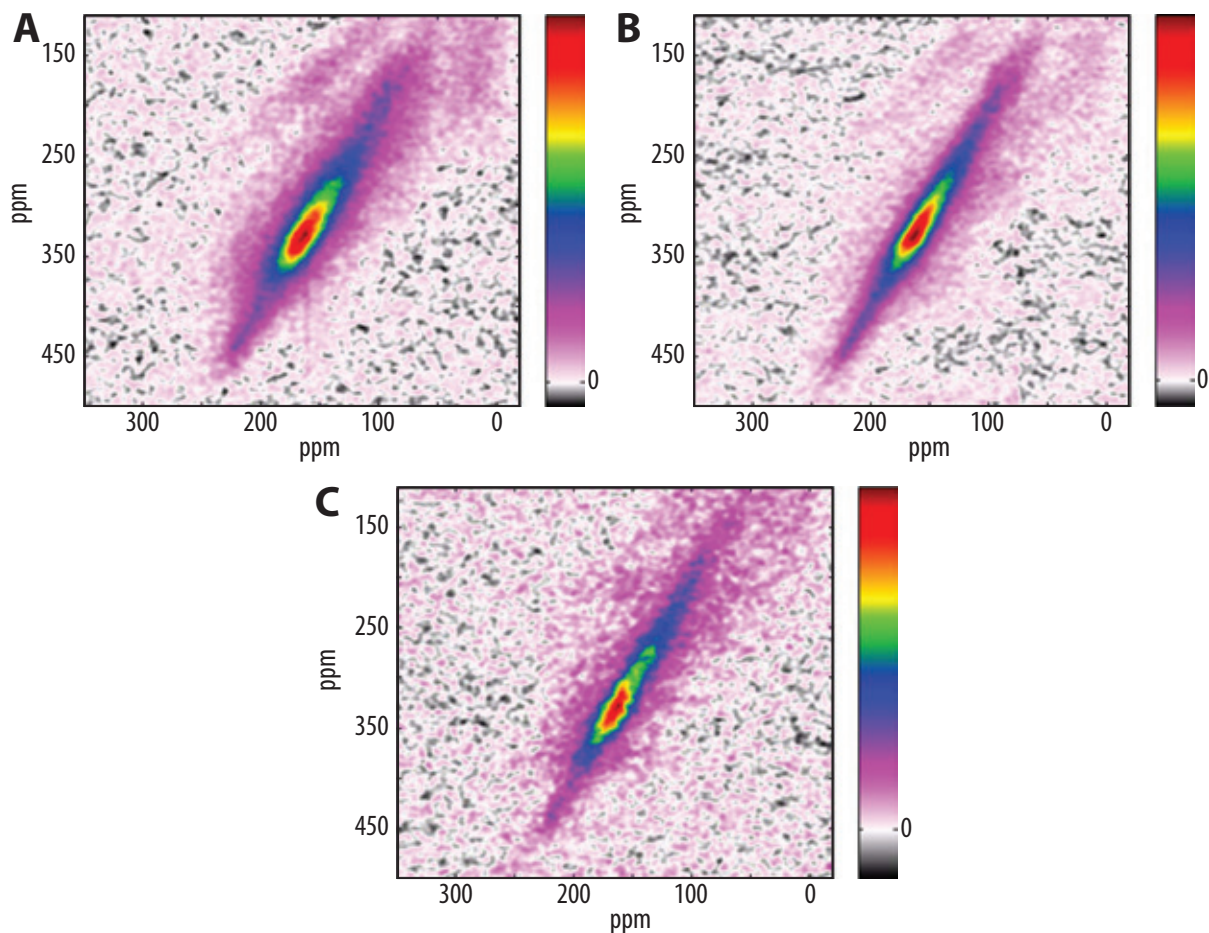


**Figure 51:** A) The DOQSY spectrum of derivative **165** showed a relatively broad diagonal intensity distribution. Consequently, a parallel arrangement of the C=O tensors in space may be assumed, although a considerable amount of disorder was present. B) Macromonomer **166** showed a similar spectrum but the molecular order was higher concluded from the narrower line width. C) This trend continued with macromonomer **167**. Unfortunately, the signal to noise ratio was worse in this case caused by a suboptimal experimental setup.

The DOQSY spectra of the singly  $^{13}\text{C}$ -labeled compounds **165**, **166** and **167** (Figure 51) were, nevertheless, well resolved. They all exhibited a diagonal intensity distribution indicative of a parallel orientation of the carbonyl tensors in space. Interestingly, the internal order as measured from the width of the intensity distribution increased from amino acid position one to three, as one would intuitively have expected. In more detail, the spectrum of derivative **165** was rather broad (Figure 51A) while **166** gave a much narrower distribution (Figure 51B). This trend continued in the DOQSY spectrum of **167**, although the signal-to-noise ratio was a little worse (Figure 51C) due to suboptimal measurement parameters chosen in this case. This caused an optical impression of a broader distribution, but a thorough data analysis revealed the contrary.

The investigation of the twofold  $^{13}\text{C}$ -labeled macromonomers **168**, and **169**, aiming at a measurement of the intramolecular orientation of neighboring carbonyl groups, was more complicated. The obtained spectra (Figure 52) had a completely different shape which had been expected since the

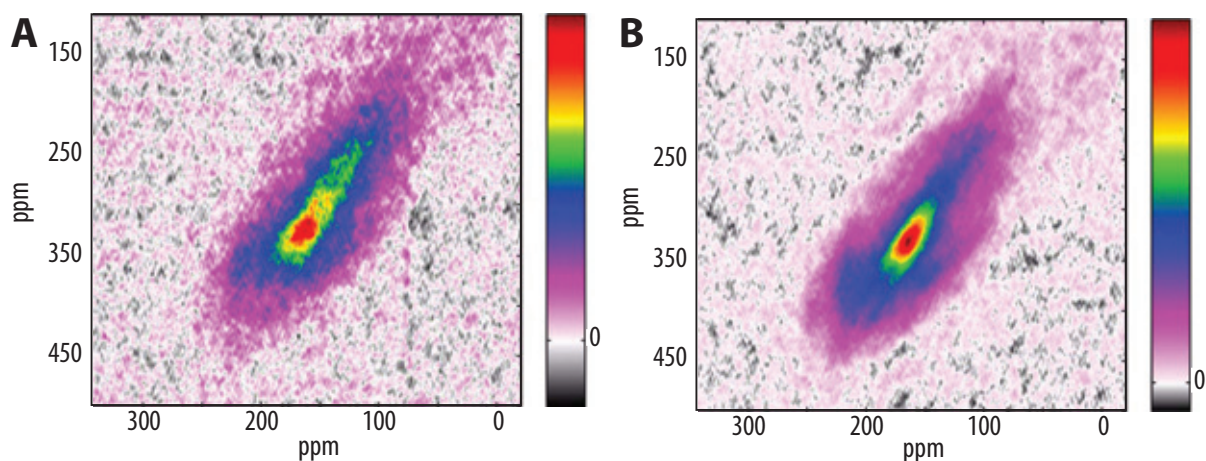


**Figure 52:** A) The DOQSY spectrum of macromonomer **168** showed an intensity distribution that could not be fitted to any model yet. B) The spectrum of **169** gave a spectrum typical for a  $\beta$ -sheet type secondary structure.

distance and relative orientation of two adjacent C=O bonds within a molecule is substantially different as compared to the previously investigated intermolecular cases. The spectrum obtained from compound **169** labeled at the second and third amino acids could be well fitted using a model that assumed a  $\beta$ -sheet configuration as it had been applied in earlier studies dealing with the elucidation of the internal structure of spider silk.<sup>202</sup> In more detail, the torsion angles  $\phi$  and  $\psi$  typically used to describe  $\beta$ -sheet configurations were found at values around  $-135$  as well as  $150^\circ$  well in line with  $\beta$ -sheet type secondary structures.

Unfortunately, things were different in case of **168** (Figure 52A) because no fit has been found yet that can explain the obtained spectrum. The relatively low signal-to-noise ratio as well as a questionable result of an elemental analysis of the corresponding tripeptide building block that had been used in the synthesis of the target compound were indicative of a problem with the purity of the sample. For this reason, the preparation of the material is currently being repeated, and the DOQSY results are to be regarded as preliminary.

### 3.2.3 Electron and X-ray Diffraction

The short-range order of the  $\beta$ -sheet arrays should be detectable by diffraction techniques although they are embedded in an amorphous matrix formed by the poly(isoprene) segments. Thus, we performed X-ray diffraction experiments on small pieces of samples obtained by a slow evaporation of macromonomer solutions under slow rotation of the rotary evaporator. In order not to disturb the internal order too much, the formed film was cut from the surface of the round bottom flask using a scalpel. The diffraction patterns obtained from different macromonomers (Figure 53) were virtually identical. The integrated and angle averaged X-ray diagrams all showed a peak corresponding to a

crystalline packing distance of 4.6 Å, as one would expect for a  $\beta$ -sheet structure. Model compound **133** showed the same peak, however, the spectrum contained more sharp peaks due to an overall higher crystalline order.

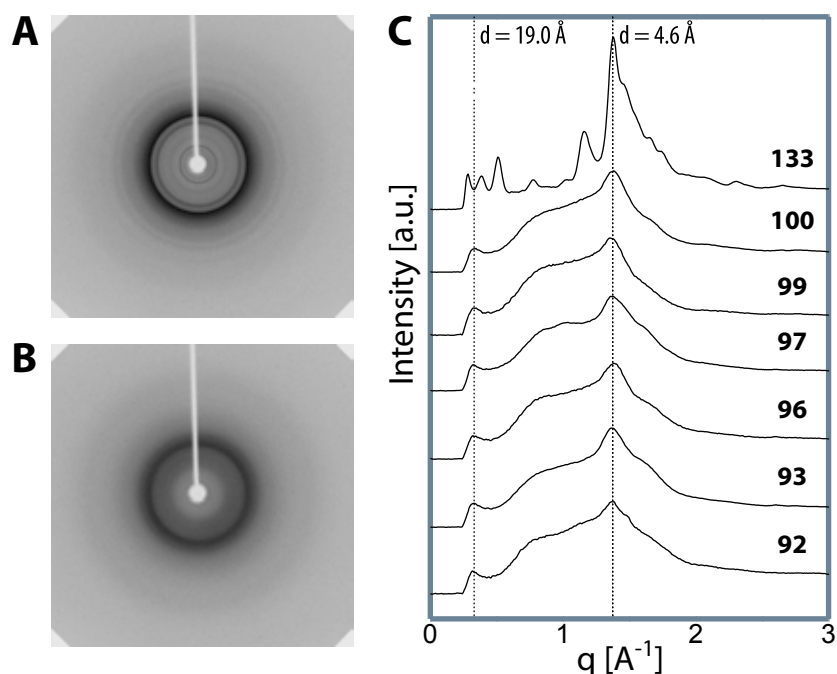


**Figure 53:** A) The X-ray diffractogram of model compound **133** showed some sharp circular reflections indicative of a crystalline order. B) Representative X-ray diffractogram of one macromonomer (**97**) indicative of low crystallinity and; C) the corresponding integrated and angle-averaged X-ray diagrams of several macromonomers and a model compound. The latter showed a higher crystallinity, whereas all the oligopeptide-polymer conjugates had very similar diffraction diagrams with a peak at 4.6 Å typical for a  $\beta$ -sheet.

During transmission electron microscopy (TEM) measurements on our system, selected area electron diffraction (SAED) was also carried out on one sample (Figure 54). In order to obtain good results, a sample on a TEM grid was obtained by drop-casting from a concentrated solution of macromonomer **92**, in order to cover the grid with a multilayer film of material. The diffractograms were stable for only a few seconds since the electron beam quickly “burnt” all material under a loss of the crystalline order, leading to a rapid disappearance of the diffraction pattern. Thus, the grid was blindly moved to a random position, and the diffraction image was taken as fast as possible. Nevertheless, the diffractograms were reproducible. The resulting analysis of the data revealed a doublet of reflections corresponding to crystalline packing distances of 4.59 and 4.76 Å which proved the  $\beta$ -sheet packing. The additional peaks at 4.25 and 8.04 Å were also typical of such oligopeptide systems, as had been previously reported.<sup>124,125,203</sup>

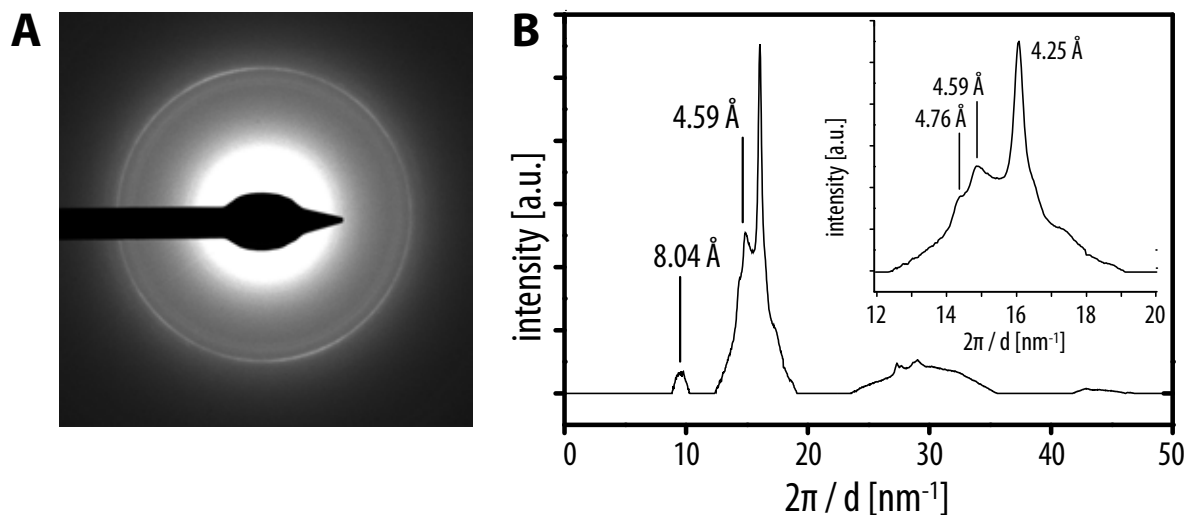


**Figure 54:** A) Electron diffractogram of a multilayer film of **92** on a TEM grid. The circular diffractions are clearly visible. B) the subsequent integration of the diffractogram showed a doublet of reflections at spacings of 4.59 and 4.76 Å, indicative of a  $\beta$ -sheet secondary structure.

## 3.2.4 Gelation Experiments

### 3.2.4.1 Organogels from the Model Compounds

The monodisperse model compounds **126**, **127** as well as **130-134** had initially been designed to grow single-crystals in order to elucidate the geometry of the diacetylenes in the oligopeptide array by X-ray diffraction. It was, however, impossible to obtain crystals from any of the structures since they rather formed gels in various solvents. In the cases of **130-134**, we, thus, attempted to dissolve the model compounds in solvents such as DCM,  $\text{CHCl}_3$ , THF or cyclohexane typically at a concentration of  $1 \text{ g L}^{-1}$ . While the TMS-terminated molecule **130** yielded clear solutions in all these solvents without any gel formation even at concentrations up to  $45 \text{ g L}^{-1}$ , **134** was found to be practically insoluble in cyclohexane while it was still well-soluble in the other solvents. During attempts to dissolve the material in hot cyclohexanes, the mixture became orange brown most likely due to thermal degradation, i. e., a random cross-linking of the terminal diacetylenes. This kind of instability was also observed when solutions in the other solvents were heated. **131** exhibiting 3+1  $\text{N-H}\cdots\text{O}=\text{C}$  hydrogen-bonds was found to form gels in pure DCM at a concentration of  $1 \text{ g L}^{-1}$ , in good agreement with the IR investigations. Analogous to literature examples of diacetylene-containing organogelators that had been topochemically polymerized,<sup>168</sup> the gels were subjected to UV irradiation. The gel immediately attained a red-violet color indicative of a successful polymerization. The non-polymerized gel was found to be mechanically stable up to the boiling point of DCM (Figure 55). No gels were formed in  $\text{CHCl}_3$  or THF at the same concentration and the obtained clear solutions did not undergo polymerizations upon heating or irradiation.

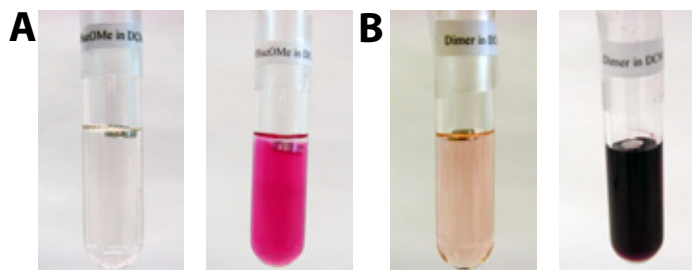


**Figure 55:** Representative pictures of gels from A) **131** and; B) **133** before and after polymerization. The Al-discs proved the stability of the transparent gels, which was not influenced by the polymerization.

An overall similar behaviour was found in the case of model compound **132** exhibiting 3+2 N–H···O=C hydrogen-bonds, which, on the one hand, could not be dissolved in cyclohexane while, on the other hand, THF dissolved the material without any problem. In the cases of DCM and CHCl<sub>3</sub>, weak gels were formed at a concentration of 1 gL<sup>-1</sup> which were stable only up to 35 °C in the case of DCM. Upon irradiation, the gels were destroyed due to a precipitation of violet polymeric material.

The observed general trend of solubilities and gelation abilities continued when the symmetric derivative **133** with 3+3 hydrogen bonds was investigated. It was completely insoluble in cyclohexane but it formed stable gels in DCM, CHCl<sub>3</sub> and even in THF already at concentrations of 0.5 gL<sup>-1</sup>. The gels in THF were very reactive toward the topochemical polymerization, since they became dark violet even when they were stored in the dark over night. Moreover, these gels tended to shrink dramatically upon polymerization. Gels formed in chlorinated solvents were stable up to the boiling points of the respective solvents. Upon UV irradiation, the gels became dark violet which was a clear indication of an efficient topochemical polymerization.

#### 3.2.4.2 Gelation Properties of the Macromonomers 92-103

The macroscopic properties of the macromonomers to function as organogelators turned out to be significantly different from those of the model compounds. Thus, macromonomers **92**, **93**, and **96** gave rise to viscous solutions but did not form gels at all in DCM and other chlorinated solvents at room temperature, even at concentrations of up to 30 gL<sup>-1</sup>. Only at low temperatures, solutions of **92** and **96** in DCM at concentrations above 5 gL<sup>-1</sup> formed mechanically weak gels with gelation temperatures of approximately  $-7 \pm 3$  °C and  $-8 \pm 2$  °C, respectively as measured by, again, placing an Al-disc on top of the gels (Figure 56). DCM solutions of **93** remained viscous even at temperatures of  $-30$  °C and below when the macromonomer began to precipitate.

By contrast, **100** and **103** were found to be efficient organogelators, forming mechanically stable gels at concentrations of 3 gL<sup>-1</sup> and below, with gelation temperatures of  $69 \pm 1$  °C and  $52 \pm 2$  °C, respectively. The difference of more than 60° in gelation temperatures is surprising, given

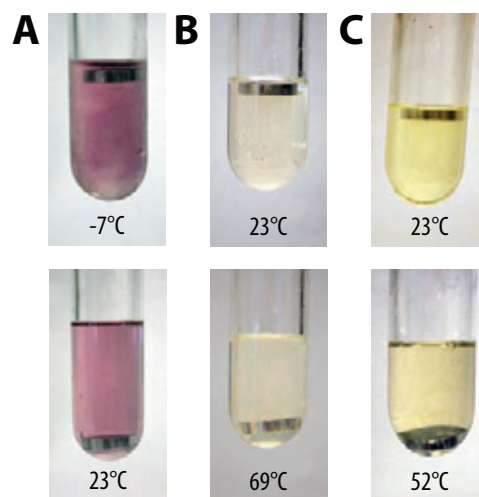


**Figure 56:** Representative pictures of gels formed from A) **92**; B) **100** and C) **103** before and after heating. The Al-discs proved the stability of the gels at lower temperatures. In case of **92**, the gel had a violet color due to premature poly(diacetylene) formation in the daylight.

the close structural relation of the investigated macromonomers. Furthermore, the observed trend in the mechanical stability of the gels and the transition temperatures appeared to contradict the macromonomers' tendency toward aggregation into  $\beta$ -sheet secondary structures, since **92**, **93** and **96** showed cleaner IR signatures with higher contents of  $\beta$ -sheet secondary structures. This behavior could, however, be understood with the help of SFM imaging (Section 3.2.6), which revealed a much higher degree of order within the aggregates formed by the macromonomers aligning in parallel  $\beta$ -sheets as opposed to the macromonomers that attained an antiparallel arrangement.

### 3.2.5 Imaging of Higher Structures by Transmission Electron Microscopy

The first attempts to image the supramolecular aggregates formed by the macromonomers were made by transmission electron microscopy (TEM) at the electron microscopy center at ETH on a transmission electron microscope that was operating at an acceleration voltage of 100 kV. Copper grids coated with a layer of a few nanometers of amorphous carbon were used as the substrates, and samples were prepared by drop-casting dilute solutions of macromonomer **92** at typical concentrations of 0.01 and 0.03 gL<sup>-1</sup>. The TEM images showed remarkably straight fibrillar features of several micrometers in length and variable widths (Figure 57). This appeared to be caused by lateral aggregation, and the width of the constituting fibrils was estimated to be below 20 nm. However, the contrast in the TEM images was poor which became an increasing problem with enhanced magnification (Figure 57B).

In order to address the problem of the weak contrast, we attempted to stain the samples with various reagents, e. g., aqueous uranyl acetate or osmium tetroxide solutions as well as pure ruthenium



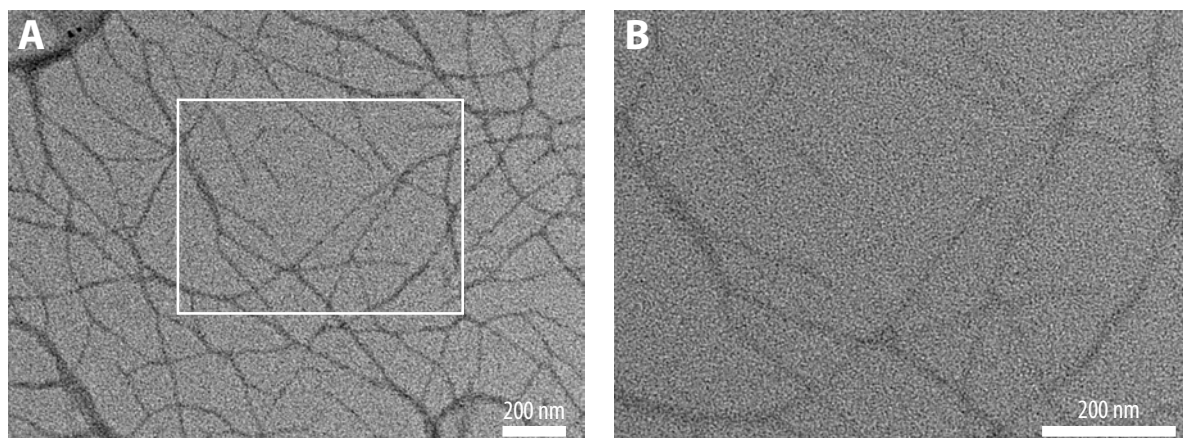


**Figure 57:** A) TEM image of a sample of **92**. Fibrillar features of different widths were observed the narrowest of which were estimated to be less than 20 nm wide. Typically, these structures were several hundred nanometers long and remarkably straight; B) At higher magnification, the contrast to the carbon background became too poor to allow for a further analysis of the interior structure.

tetroxide. Unfortunately, all attempts failed, and only virtually unchanged images were obtained that were, if at all, contaminated by unspecifically distributed staining material.

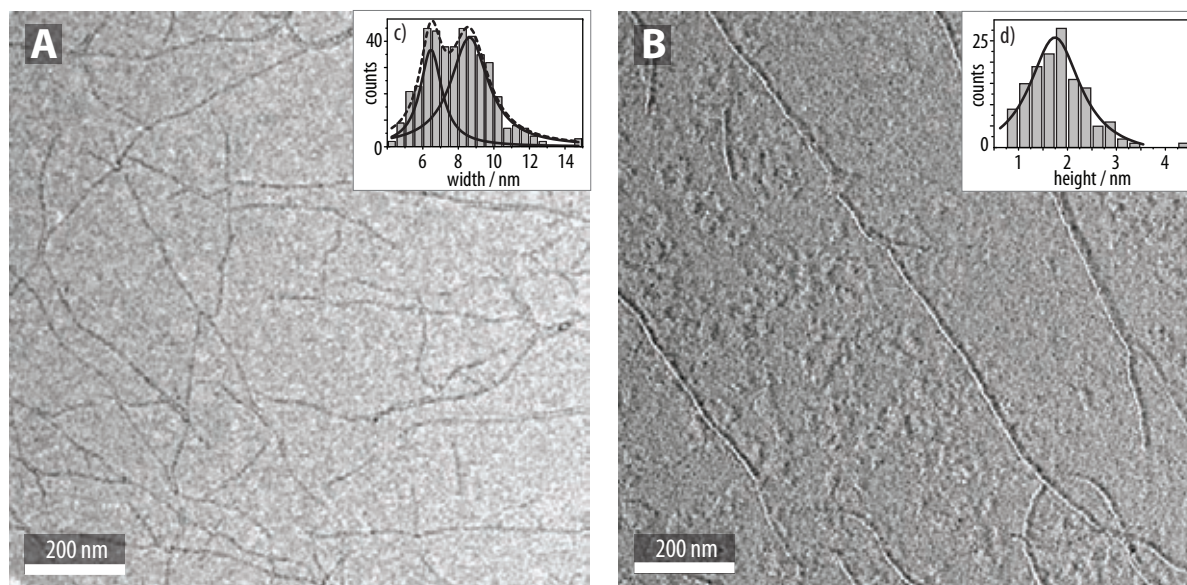


**Figure 58:** A) TEM image of a sample of **92** measured on a 200 kV TEM instrument at the Max Planck Institute for Polymer Research in Mainz, Germany, allowing for filtering of inelastically scattered electrons which gave rise to a better contrast as well as resolution. Again, long and straight fibrillar features were visible that seemed to have a uniform width. B) Image of a carbon-shadowed TEM grid, allowing for an estimate of the height of the structures due to a measurement of the “shadows” (light) caused by the fibrils.

TEM images obtained in collaboration with Dr. Ingo Lieberwirth at the Max Planck Institute for Polymer Research in Mainz, Germany, exhibited an improved contrast even without staining due to

filtering of inelastically scattered electrons. Again, the images showed straight fibrils that extended over several micrometers in many cases (Figure 58A). The quality of the images allowed for a statistical analysis of the fibrils' width which revealed a bimodal distribution centered at maxima located at  $6.5 (\pm 1.4)$  nm and  $8.7 (\pm 2.5)$  nm (Figure 58A inset). For the first time, this exact analysis allowed to establish that the width of the supramolecular aggregates was on the order of the macromonomers' molecular length of approximately 6 to 7 nm.

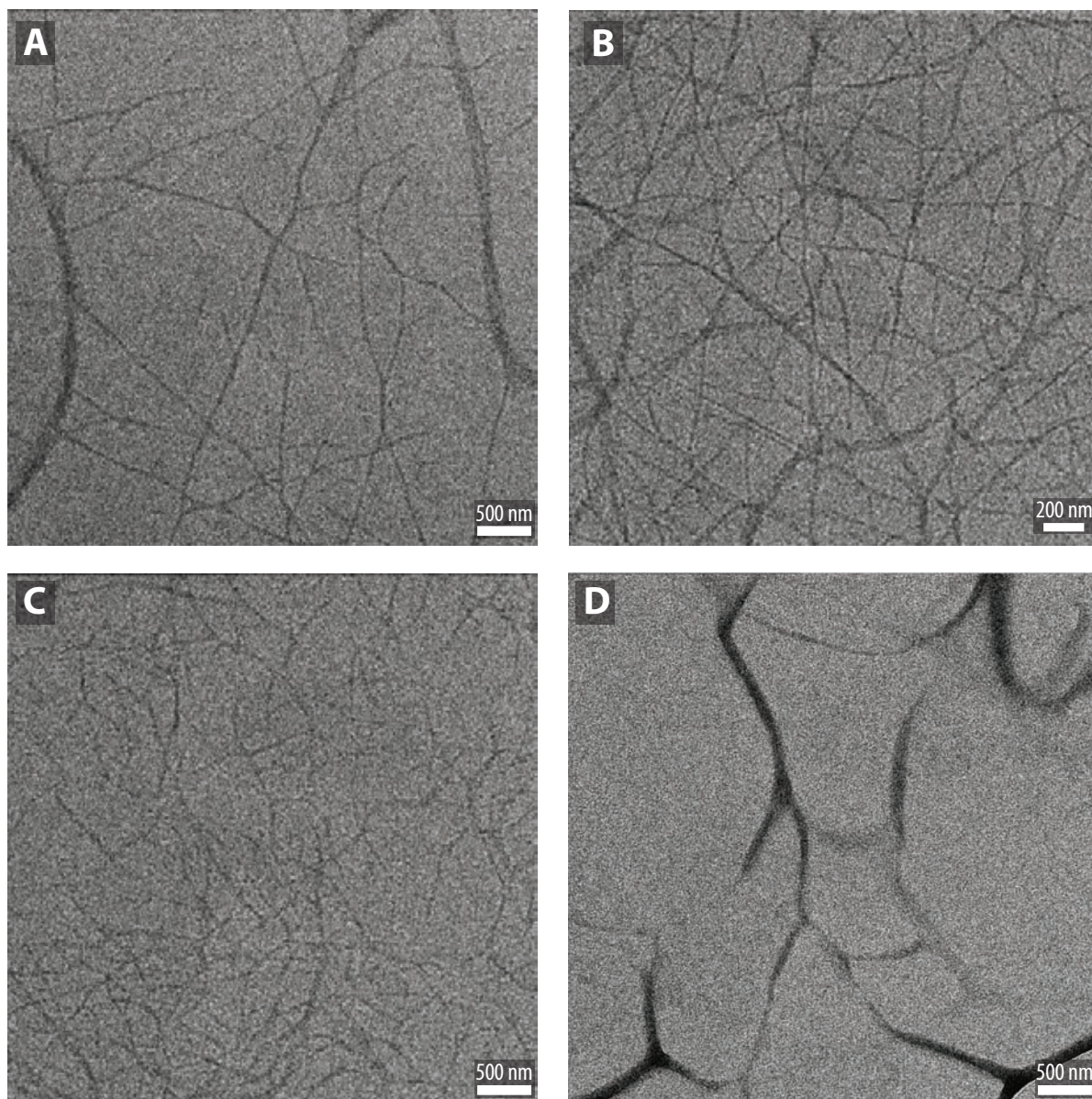


**Figure 59:** TEM images measured on a 120 kV instrument at the Max Planck Institute for Colloids and Interfaces in Golm, Germany, allowing for the filtering of inelastically scattered electrons of *A*) a sample of **93** showing the expected very long and straight fibrillar features; *B*) derivative **96** formed similar aggregates, while *C*) **99** formed much shorter features that, furthermore, gave rise to much less contrast; *D*) macromonomer **100** (as well as **101**, **102**, **103**) exhibited large ill-defined aggregates of organic material.

In order to also extract height information from a transmission experiment, samples were prepared using the carbon-shadowing method. For this purpose, a graphite electrode is evaporated in an arc discharge. The generated carbon nano particles cover the surface of TEM grids so that objects on the grids cause a carbon shadow the dimensions of which directly translate into the height of the former. The resulting unequal distribution of carbon can then be resolved in the TEM measurements due to differences in contrast (Figure 58B). In the case of macromonomer **92** a statistical analysis of the shadow widths (Figure 58B inset) resulted in a monomodal distribution centered at a value of  $1.7 (\pm 1.3)$  nm. Obviously, the aggregates can be described as flat objects having a uniform height whether being laterally aligned or isolated. If these dimensions represented those of the aggregates in solution (implying tape- or ribbon-like structures) or if the structures collapsed on the surface under the given conditions (surface forces, ultra-high vacuum) and were, thus, only “projections” of the original geometry remained unclear. However, the determined height was approximately twice the value one would expect for a single  $\beta$ -sheet.

TEM images of macromonomer **93** obtained in collaboration with Dr. Jürgen Hartmann at the Max Planck Institute for Colloids and Interfaces in Golm, Germany, revealed similar structures as compared to derivative **92** upon a qualitative inspection of the images (Figure 59A). The same was true for macromonomer **96** (Figure 59B). By contrast, the aggregates formed by the symmetric derivative **99** (Figure 59C) gave less contrast despite its nearly doubled molecular weight. The obtained fibrils seemed to be much shorter, as well. As may be anticipated considering the results from the IR investigations, the macromonomers **101** and **102** that were supposedly unordered in solution showed only large drying artifacts of organic material. The same was observed for derivatives **100** and **103** that are supposedly arranged in antiparallel  $\beta$ -sheets (Figure 59D). Apparently, the aggregates formed by antiparallel  $\beta$ -sheet arrangements can not be resolved by TEM.

## 3.2.6 Imaging of Higher Structures by Scanning Force Microscopy

### 3.2.6.1 Supramolecular Polymers from the Macromonomers

In order to study the aggregates formed by the self-assembly of the macromonomers in more detail, SFM imaging was carried out in a close collaboration with the group of Prof. Jürgen P. Rabe at the Humboldt University Berlin. Thus, images of a sample of macromonomer **92** ( $5+1$  N-H $\cdots$ O=C hydrogen-bonds) spin-coated onto highly oriented pyrolytic graphite (HOPG) from dilute DCM solution confirmed the existence of fibrillar features, as already observed in the TEM images. The resolution of the images was high enough to allow for an examination of the internal structure of the fibrils. These were obviously helical in nature, exhibiting a right-handed twist (Figure 60). The un-

ordered material that appeared in the background of these images was found to cover the graphite surface completely and could later be identified as a monolayer of the macromonomer itself. This phenomenon did not occur when the HOPG substrates were first covered with an amphiphilic monolayer (tricontanoic acid or stearyl amine).

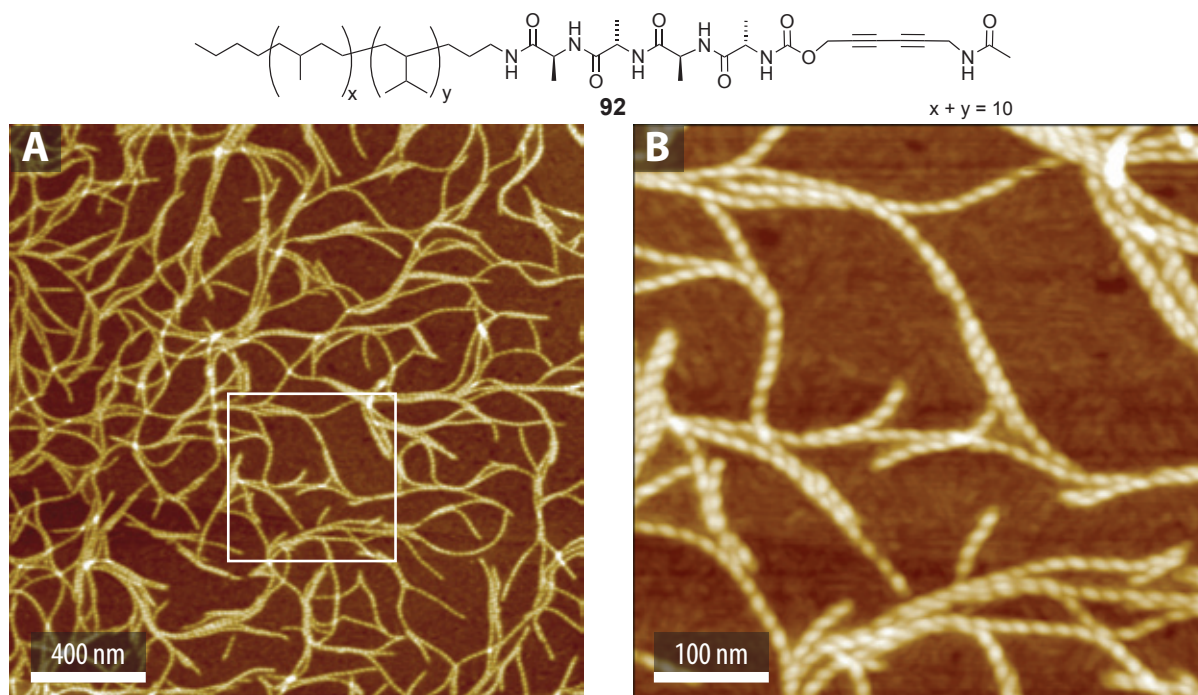


**Figure 60:** SFM images of macromonomer **92** spin-coated on HOPG from a DCM solution revealed fibrillar features with lengths of several hundred nanometers and a right-handed helical fine structure; a monolayer of unordered material is visible in the background.

The reproducibility of the images was very high, and virtually the same results were obtained from different solutions using different concentrations, solvents (DCM,  $\text{CHCl}_3$ ) or substrates. Several instances (Figure 61B) allowed to identify the double-helical nature of the fibrils that were obviously made up of two flat, featureless “ribbon” substructures. In order to extract more geometrical information from the images, height profiles along the contour of the fibrils (Figure 61A) as well as cross-sections of the latter were investigated. A histographical analysis of a large number of such measurements allowed for the determination of the apparent height of the features which was found to be  $4.7 (\pm 0.5)$  nm. The apparent width was measured to be on the order of 18 nm. However, this value had to be corrected for the radius of the SFM tip which is on the order of 10 nm, resulting in an estimated corrected width of 5-6 nm. Thus, the cross-section seemed to be close to circular. The evaluation of the periodical pattern of the contour gave an identity period of  $17.8 (\pm 1.7)$  nm, translating into a helix pitch of approximately 36 nm, taking the double-helical nature into account. From the helix pitch and the helix angle of approximately  $55^\circ$ , the width of the ribbon substructures was

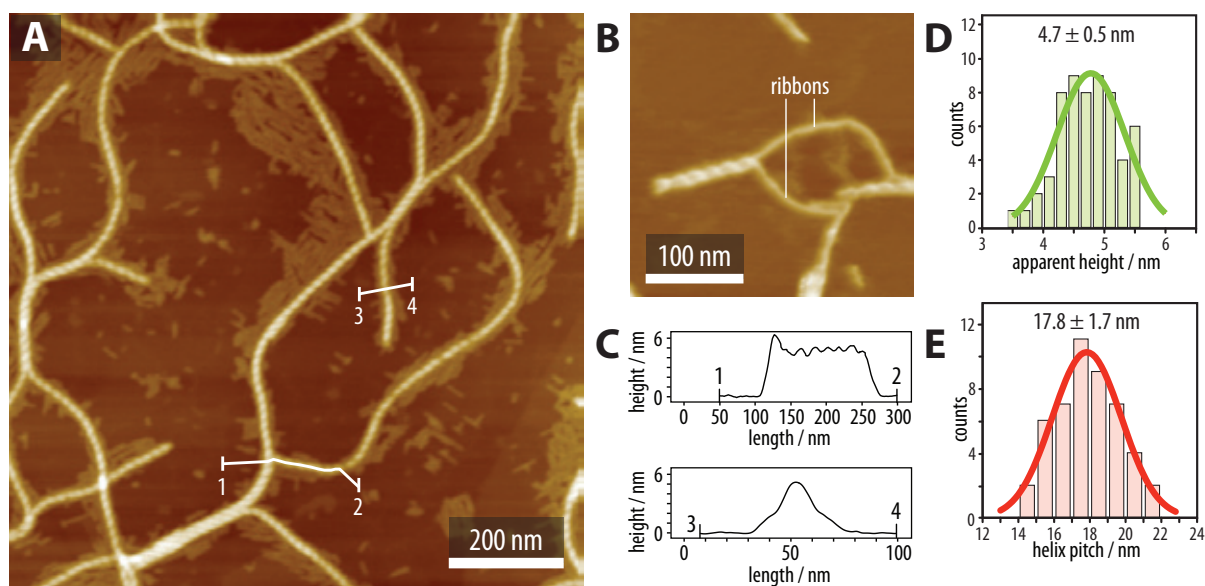


**Figure 61:** A) The helical structures formed by **92** were observed reproducibly; spin-coating from more dilute solutions onto HOPG led to a decreased amount of features allowing for an easier measurement of single objects. B) Two flat “ribbon” structures come together to form a double-helical fibril. C) Representative height profiles of (top) the contour of an aggregate and (bottom) the cross-section of the latter both measured along the indicated pathways. D) Histogramical analysis of the height resulting in an average height of  $4.7 \pm 0.5$  nm. E) Histogramical analysis of the helix pitch giving an average pitch of  $17.8 \pm 1.7$  nm for a half-turn of the double-helical aggregate.

estimated to be roughly 10-14 nm which would be about twice the molecules’ extended length of the macromonomer of 6-7 nm.

SFM images of macromonomer **93** (5+1 hydrogen-bonds) (Figure 62) showed strikingly similar helical fibrillar structures. The fibrils obtained in this case were extremely long, some extending over several dozens of micrometers, running diagonal through an entire image, and preventing the localization of their ends. At the same time, they appeared to be more rigid than those fibrils obtained from derivative **92**. They also had a close to circular cross-section and a uniform diameter, with an apparent height of  $5.7 (\pm 0.4)$  nm and an estimated width of about 6 nm (again, corrected for the SFM tip radius). Most of the fibrils exhibited a periodic fine structure suggesting that they were right-handed helices with a periodicity of  $18.6 (\pm 0.9)$  nm (helix pitch of about 37 nm). Thus, while no instances could be found that would unambiguously prove their double-helical nature, this assumption may still be regarded as reasonable given the close structural relation to macromonomer **92** both in terms of their molecular and their nanoscopic structure.

It should, however, also be noted that some features formed by **93** did not show any helical fine structure at all (Figure 62C), although they were otherwise more or less indistinguishable from the helical ones judging from their height, width, length, curvature and general appearance (Figure 63). This qualitative conclusion could be corroborated by a thorough analysis and comparison of “aver-

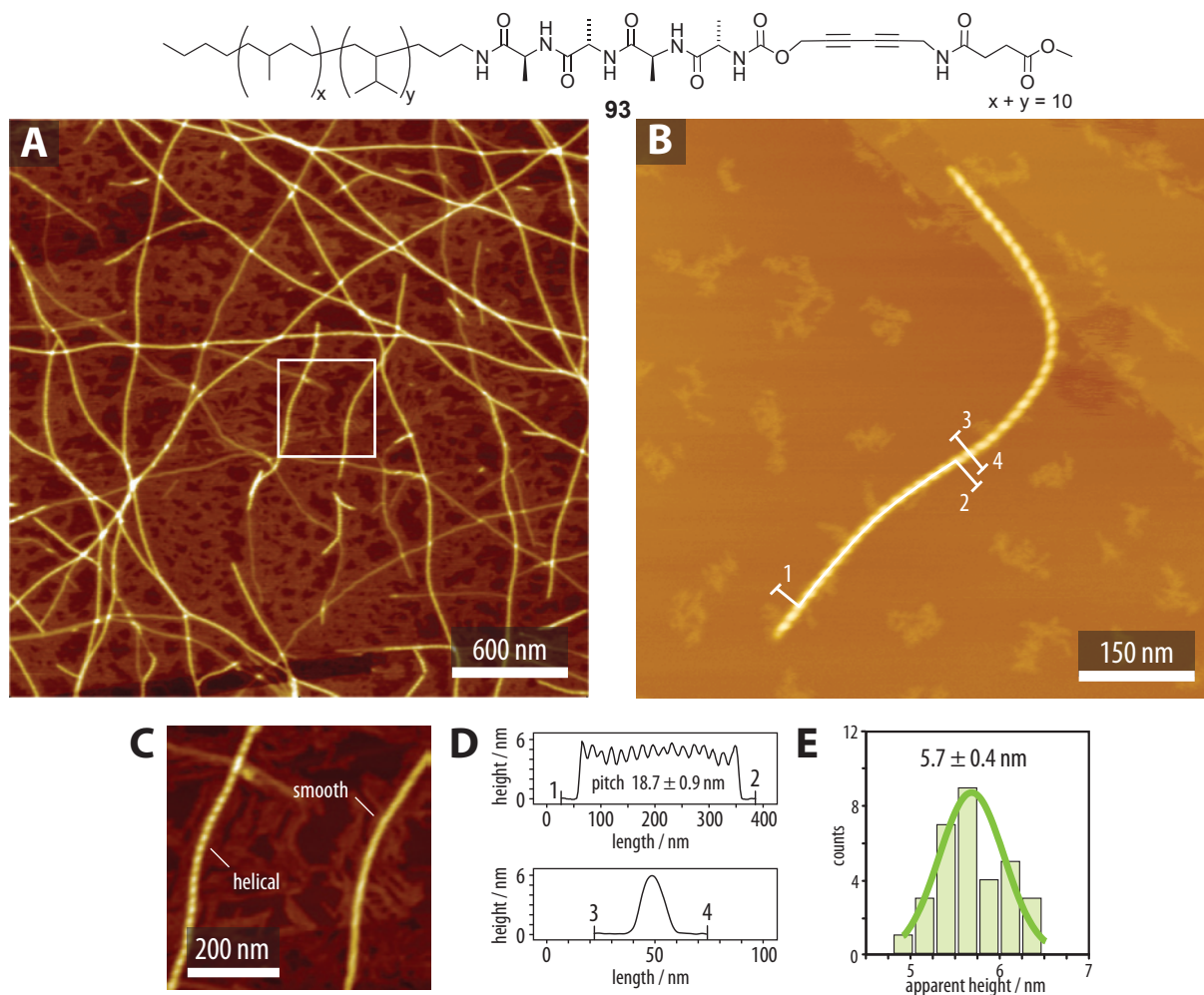


**Figure 62:** A) Macromonomer **93** gave also rise to fibrillar features that were several dozens of micrometers long and seemed to be more rigid as compared to the aggregates formed by **92**; B) A close-up of the structures again proved a right-handed helical fine structure; C) A close-up of image A reveals the presence of helical as well as smooth fibrils; D) An identity period of  $18.7 (\pm 0.9)$  nm was extracted from height profiles of the fibrils' contour giving rise to a helix pitch of twice this value assuming a double-helical nature of the fibrils; E) A histogramical analysis of the height taken from many measured cross-sections revealed a height of  $5.7 (\pm 0.4)$  nm.

age profiles" (Figure 63D-G) of the helices formed from macromonomer **92** as well as both the helical and the smooth aggregates from derivative **93**. These "average profiles" were obtained by aligning the maxima of different cross-sectional profiles taken from different locations along the fibrils, different fibrils of each type, as well as different images of the same macromonomer followed by an averaging of the curves. Although such a procedure can only serve as a coarse comparison, it provided a clear indication that the three different types of aggregates were also very similar from a quantitative perspective with respect to their average height and apparent width at half-height. Furthermore, the assumption that their cross-sections were approximately circular was very well consistent with the results in all three cases. The missing fine-structure, however, could not be explained.

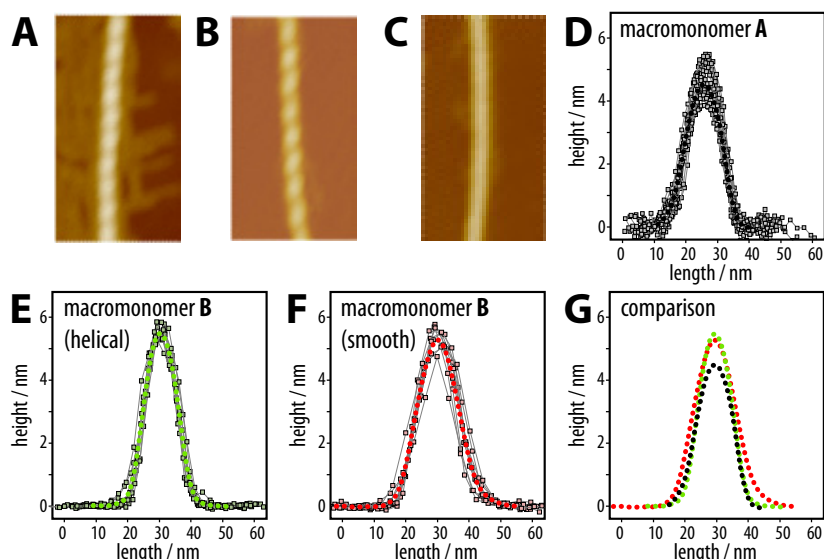


**Figure 63:** A-C) The helical fibrils obtained from **92** and **93** as well as the smooth features only obtained in the case of **93**. D-G) The corresponding height analyses showed an overall very similar appearance with close to circular cross-sections and a diameter of 5-6 nm (after correction for the tip radius) in all cases.

Similar to **92** and **93**, macromonomer **96** (5+2 N-H $\cdots$ O=C hydrogen-bonds) was found to self-assemble into helical fibrillar features (Figure 64) which also extended over several micrometers. The aggregates again appeared to be more rigid as compared to fibrils formed from **92** but they exhibited an apparent height and estimated width very similar to fibrils found in the former cases. In contrast to **92** and **93**, macromonomer **96** formed uniform left-handed single helices with a much more complex periodic fine structure. In contrast to the supposedly double-helical aggregates formed by the macromonomers having 5+1 N-H $\cdots$ O=C hydrogen-bonds, these single helices showed a significantly smaller tendency to form double-helical bundles that were, nevertheless, occasionally observed (Figure 64G).

Height profiles, cross-sectional profiles, as well as height and phase images helped to identify a periodic pattern with an identity period of 121 ( $\pm$  17.6) nm in which shorter, elevated “turns” were followed by two longer, lower segments that were separated by a second type of “twists”. The latter were less clearly distinguishable in the height images and, contrary to the turns, exhibited a dark line running through their centers diagonal to the axis of the aggregate in the phase images. Additionally, a minor population of very similar left-handed helical aggregates (not shown) was observed which only comprised the first type of “turns” spaced at 60 ( $\pm$  8) nm, i. e., more or less exactly half the identity period of the predominant type of fibrils. It remained unclear whether these aggregates were, indeed, a second population or just different variants or projections of the same type of aggregates. The turns’ height was determined to be 5.3 ( $\pm$  0.9) nm, and their length in the direction of the aggregate axis was estimated to be on the order of 18 nm (Figure 65). An averaging of cross-sectional profiles for the





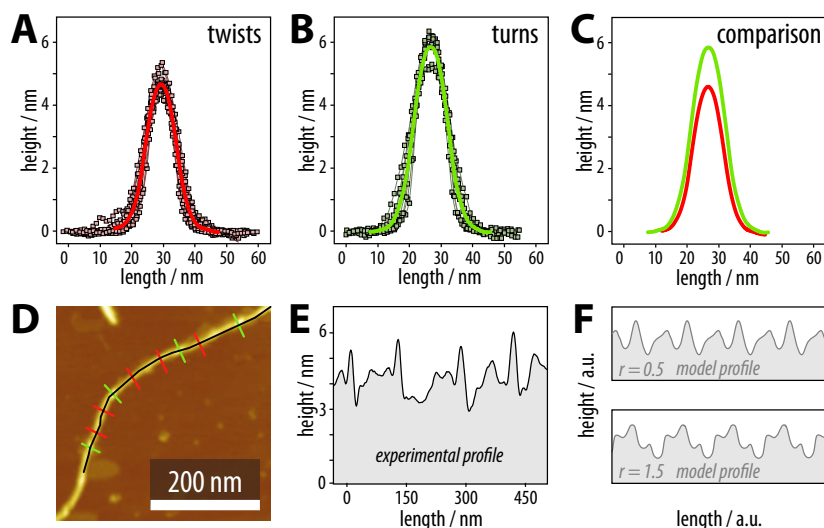


**Figure 65:** *A)* The average height of the “twists” was lower than *B)* the height of the “turns”, as can clearly be seen from *C)* a direct comparison of the average curves. *D)* The height image showed the cross-sections taken at the “twists” and “turns”. *E)* The experimental height profile along a fibril was *F)* strongly reminiscent of modeled height profiles of “bent and twisted” single-helices with an ellipsoidal cross-section ( $r$  = ratio of bending and twisting periodicity).

height profiles were well-reproduced. Consequently, the aggregates formed from macromonomer **96** were tentatively interpreted as bent and twisted left-handed helical ribbons.

While the derivatives **92** and **93** (5+1 N–H $\cdots$ O=C hydrogen-bonds) formed very similar aggregates, exactly the same was true in the cases of the macromonomers **96** and **97** (5+2 N–H $\cdots$ O=C hydrogen-bonds). Thus, SFM images taken from samples of macromonomer **97** (Figure 66) revealed the presence of fibrillar features extending over several micrometers, the majority of which were left-handed helically twisted ribbons very similar to those observed for derivative **96**. The aggregates also exhibited a complex periodic fine structure in which sharp helix “turns” alternated with broader “twists” having a periodicity of 113.8 ( $\pm$  18.8) nm. In this case, a minor population of likewise left-handed helical ribbons with a similar width and height, but a more tightly wound helical fine structure was observed (Figure 66E) that only featured helix “turns” spaced at a distance of 64.2 ( $\pm$  6.1) nm. The major population of left-handed helical ribbons had a height of 7.7 ( $\pm$  0.7) nm measured at the helix “turns” and an apparent width of 17.4 ( $\pm$  1.7) nm (not corrected for the SFM tip radius).

Interestingly, some ribbons could be found that were unwound at their ends (Figure 67) allowing, for the first time, to unambiguously prove that also these structures were indeed constituted from two flat substructures with a height of (3.1  $\pm$  0.4) nm and an estimated width of the two species of 16.9 ( $\pm$  1.2 nm) (without correction for the SFM tip radius). This would be commensurate with the dimensions of single  $\beta$ -sheet tapes formed by macromonomer **97** having an extended molecular length of 6-8 nm.

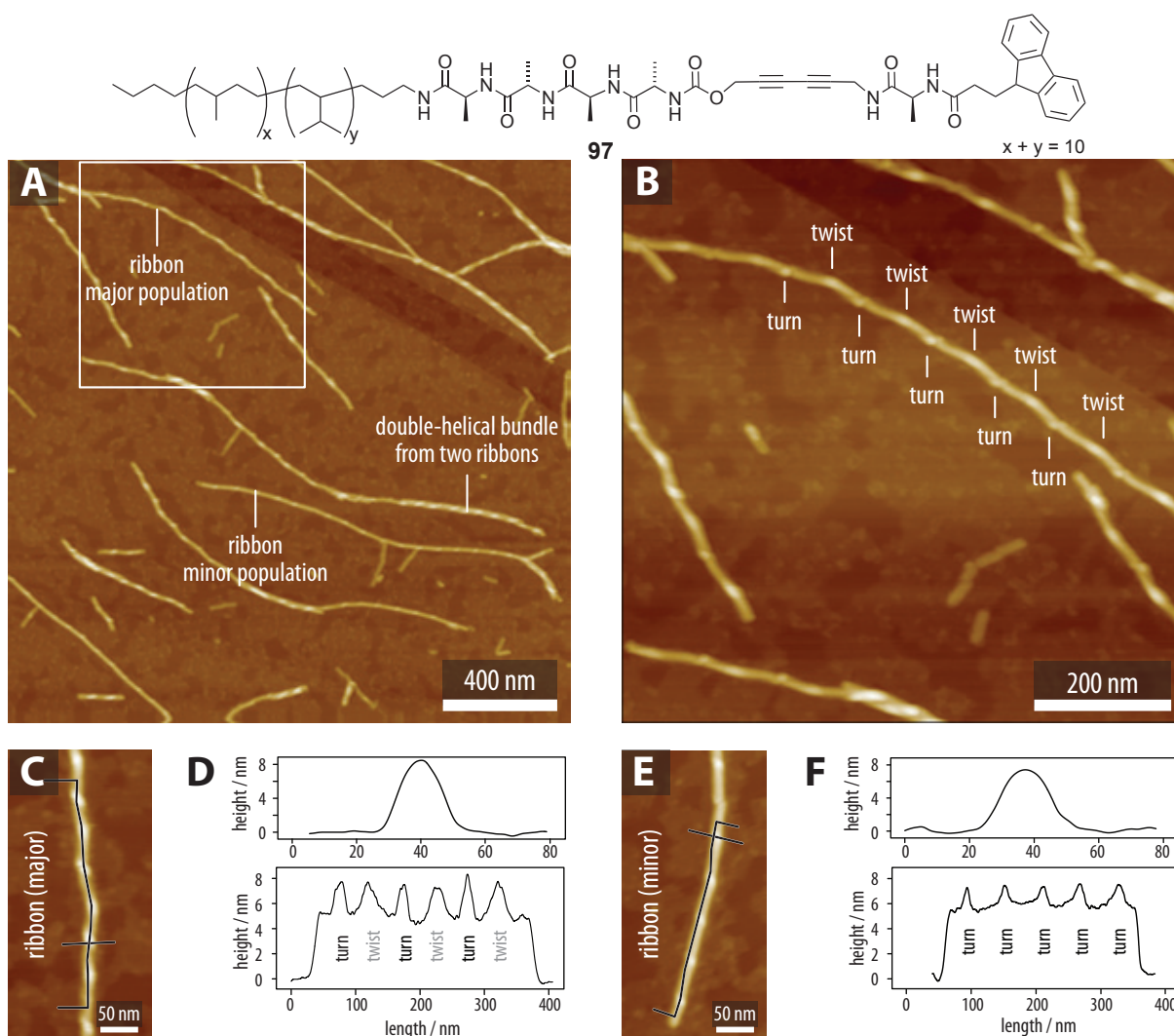


**Figure 66:** *A,B*) SFM images of macromonomer **97** on a monolayer of flat lying stearyl amine on HOPG showed left-handed helical ribbons that only occasionally formed double helices and occurred in two populations. *C,D*) The major population exhibited a periodic fine structure with an identity period of  $113.8 (\pm 18.8)$  nm, where sharp features reminiscent of helix “turns” alternated with broader “twists”. *E,F*) The minor population of ribbons only exhibited left-handed helix “turn” features placed at a distance of  $64.2 (\pm 6.1)$  nm.

In SFM images of macromonomer **99** (5+5 N–H $\cdots$ O=C hydrogen-bonds) spin-coated onto HOPG from DCM solutions, several micrometers long and comparably rigid fibrillar aggregates were observed, as well (Figure 68). This time, however, these aggregates appeared to be broad, flat tapes with an apparent height of  $2.5 (\pm 0.3)$  nm and an approximate width on the order of 7 nm, i. e., less than the molecules’ extended length of 11–12 nm. These width measurements were carried out at positions where multiple tapes aligned laterally (Figure 68A,D) so that it is plausible to assume that the hydrogenated poly(isoprene) coil segments of adjacent tapes partially merged, giving rise to an underestimation of the width. In some of the phase images (Figure 68D), a faint dark line was visible along the middle of the tapes probably caused by the “hard” oligopeptide core which suggested that they had a dumbbell-shaped cross-section. In some cases, several of these tapes gave rise to features

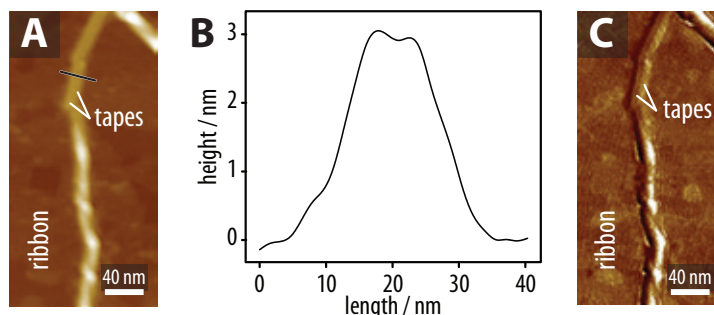


**Figure 67:** A, C) Some instances in height as well as phase images directly proved that the helical “ribbons” consisted of two flat substructures. B) A height profile measured across the two tapes clearly showed two maxima. The combined apparent width of the two species was found to be  $16.9 (\pm 1.2 \text{ nm})$  (without correction for the SFM tip radius) while each had a height of  $3.1 (\pm 0.4 \text{ nm})$ . This would be commensurate with the dimensions of single  $\beta$ -sheet tapes formed from macromonomer **97** having an extended molecular length of 6-8 nm.

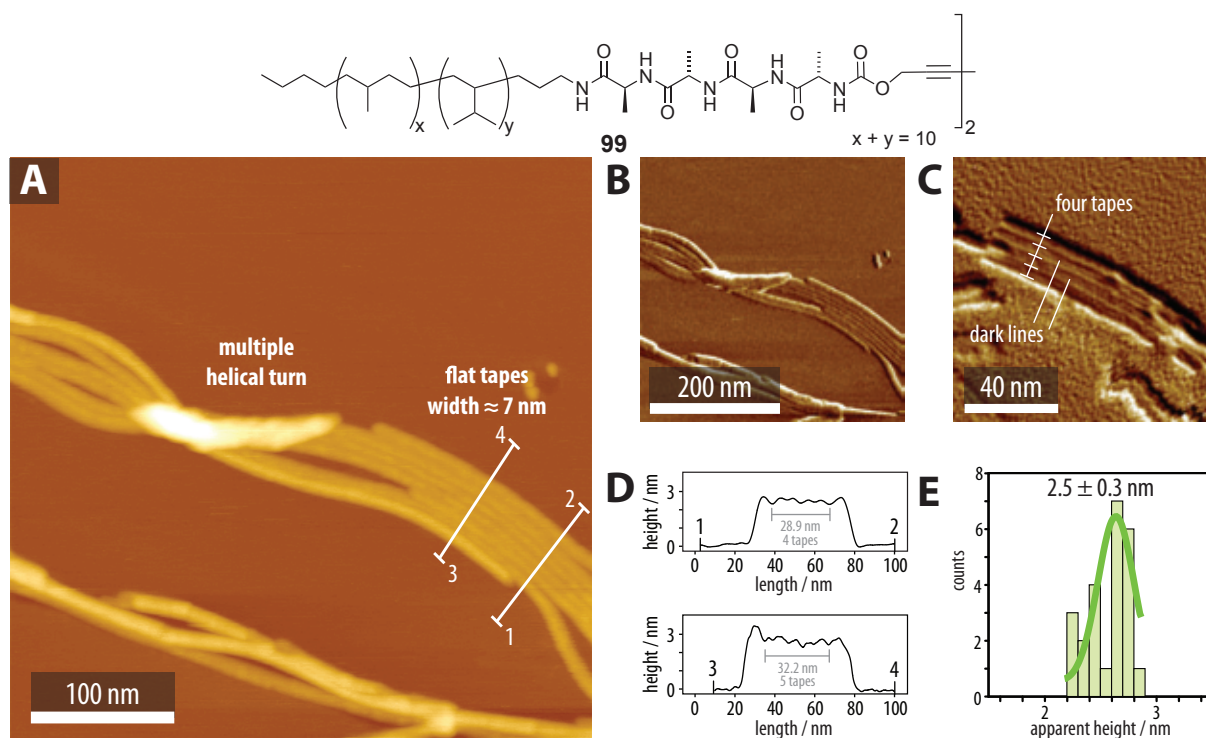


**Figure 68:** A) The symmetric derivative **99** formed flat tapes that typically aligned laterally and occasionally formed multiple-helical turns; B) These tapes and turns were also clearly visible in a phase image; C) Upon zooming into the phase image, faint dark lines in the middle of the tapes became visible, indicating a “hard” core; D) Height profiles measured across four or five laterally aligned tapes allowed for an estimate of the width of the tapes (7 nm); E) Histogramical analysis of the height taken from many measured cross-sections giving a value of  $2.5 (\pm 0.3 \text{ nm})$ .

that looked like multiple-helical turns. This was even more pronounced in images taken on substrates that were coated with tricontanoic acid prior to spin-coating of the macromonomer solution.

The macromonomers that were shown to self-assemble via an antiparallel  $\beta$ -sheet formation were hard to image using SFM. Target molecule **103** as well as derivative **100** gave rise to fibrillar features

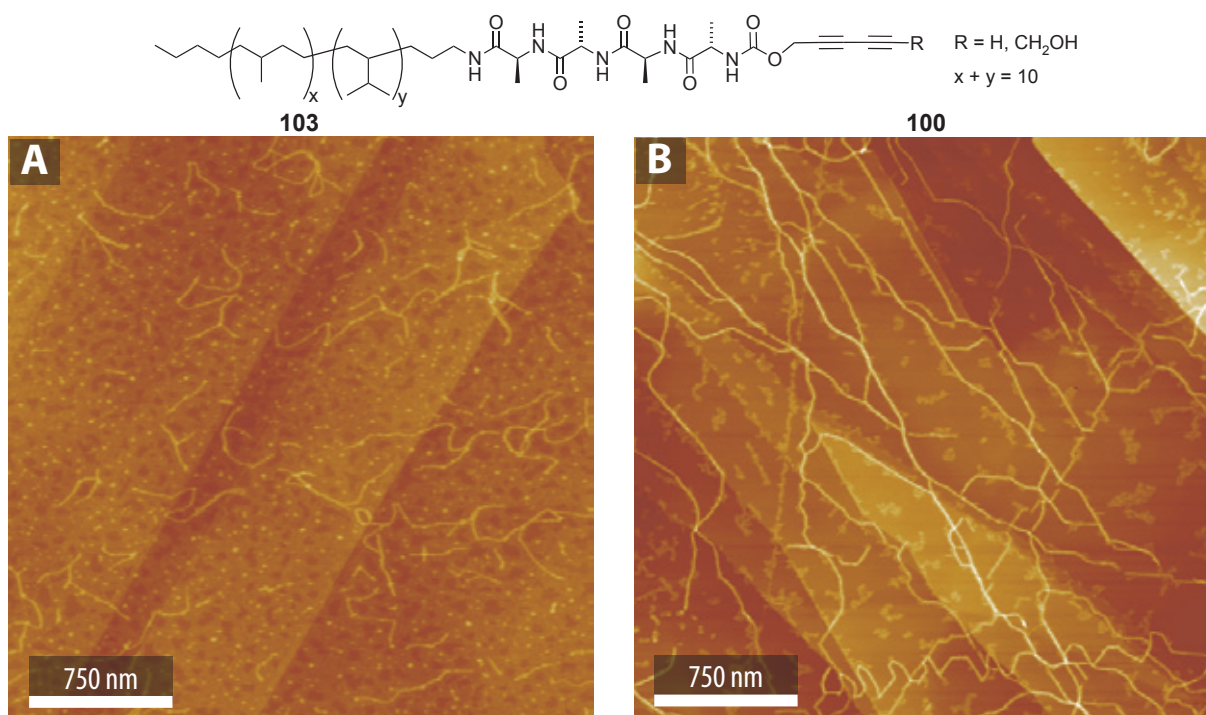


**Figure 69:** It was hard to find fibrillar material in case of the macromonomers that were not able to form  $N-H \cdots O=C$  hydrogen-bonds with their end groups. *A*) Only the H-terminated molecule **103** and; *B*) derivative **100** formed very thin and flexible fibrillar features that only occasionally give rise to helical features.

which appeared to be much thinner and more flexible than those formed from, e. g., **99** (Figure 69). Additionally, they only occasionally formed helical features but by far not as regularly as the other derivatives. Furthermore, substantial amounts of non-fibrillar material were visible in both cases, as well, even when the HOPG surface had been treated with an amphiphile prior to spin-coating the sample solutions. This observation implied that these macromonomers exhibited a significantly smaller tendency to aggregate into fibrillar features and that the latter were less stable. This interpretation is well in agreement with the IR and TEM results as well as our expectations, since only 5  $N-H \cdots O=C$  hydrogen-bonds are available. Finally, in SFM images of the TMS- as well as the tetra(ethylene glycol)-substituted derivatives **102** and **101**, respectively (not shown), mostly non-fibrillar material was observed. This was well in agreement with the corresponding IR spectra that suggested a predominantly random coil secondary structure. In summary, fibrillar aggregates were obtained from macromonomers **92**, **93**, **96**, **97**, **99**, **100** as well as **103** that had been found to attain  $\beta$ -sheet type secondary structures. However, the five derivatives that had been found to favor a parallel  $\beta$ -strand orientation (**92**, **93**, **96**, **97**, **99**) exhibited a significantly higher propensity to aggregate into fibrillar features, and the obtained self-assembled structures were much better defined. Apparently, the formation of hierarchical structures as well as the exact nature of the latter were also controlled by the presence and the number of  $N-H \cdots O=C$  hydrogen-bonding sites in the molecules' end groups.

### 3.2.6.2 SFM Images of Organogels from the Model Compounds

SFM investigations of solutions or gels of the model compounds confirmed the results of their corresponding IR measurements and helped to understand the macroscopic gelation behavior. Thus, no aggregates of any kind were observed in SFM images from **130** and **134** since the molecules were obviously well dissolved. In the case of **131**, samples spin-coated from DCM gave rise to several hundred nanometer long fibrillar aggregates with non-uniform appearance and tendency to form larger “clumps” (Figure 70A) whereas no features were obtained from samples dissolved in  $\text{CHCl}_3$ . Derivative **132** was found to form comparable structures, however, they were shorter and seemed to be more rigid (Figure 70B). These results were in well agreement with the observed stabilities of the gels but contradictory to the IR investigations that proved a much better  $\beta$ -sheet formation of **132**.

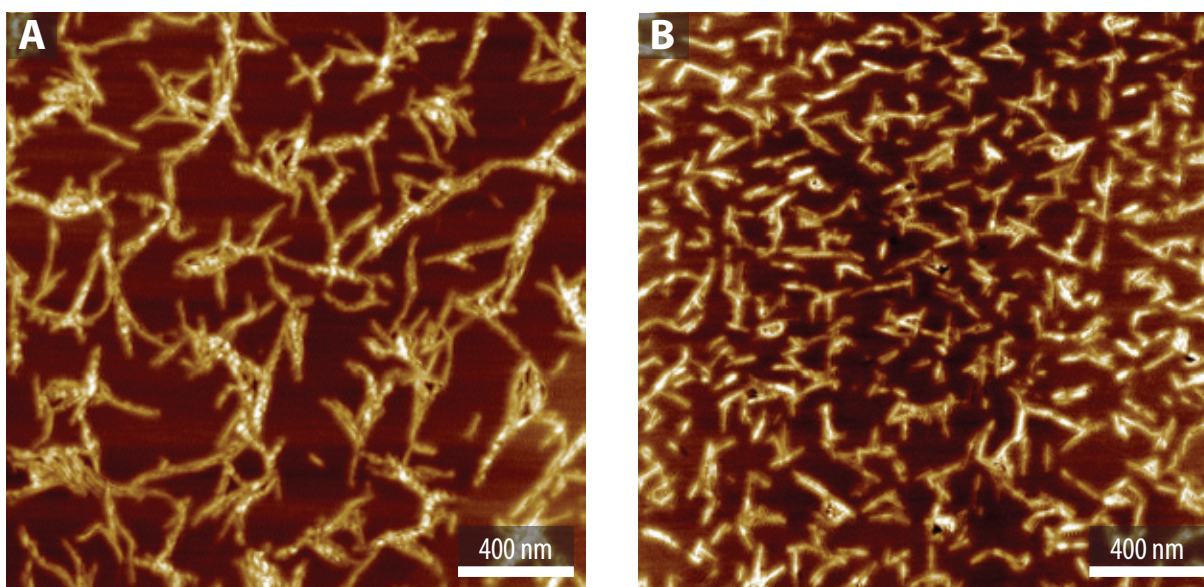


**Figure 70:** A) SFM images of model compound **131** on HOPG showed several hundred nanometer long fibrillar features. B) Derivative **132** formed similar features which were, however, much shorter (100-200 nm).

The symmetric derivative **133** showed a completely different behavior, forming several micrometer long helical fibrils (Figure 71). The latter had variable diameters and showed a strong tendency to entwine. While these results are, again, in complete agreement with the gel stability as well as the clean IR signatures, they also highlight the similarities and differences in comparison to the macromonomers. Apparently, the 3+3  $\text{N-H}\cdots\text{O=C}$  hydrogen-bonds led to the formation of stable fibrils in analogy to the macromonomers, which were found to form such aggregates starting from 5+1 hydrogen-bonds. The fibrils formed by **133** were, however, far from uniform. They tended to align laterally, entwined and exhibited various diameters and had, thus, to be regarded as vesicular or micellar structures as opposed to well-defined supramolecular polymers. This observation al-

lowed to explain the gel formation in this case, whereas the highly ordered structures formed by the macromonomers were not able to support gels highlighting the important influence of the polydisperse polymer segment on the self-assembly process. These results are well in line with the results obtained from investigations concerning the self-assembly of oligopeptides and their polymer conjugates (Section 1.2).

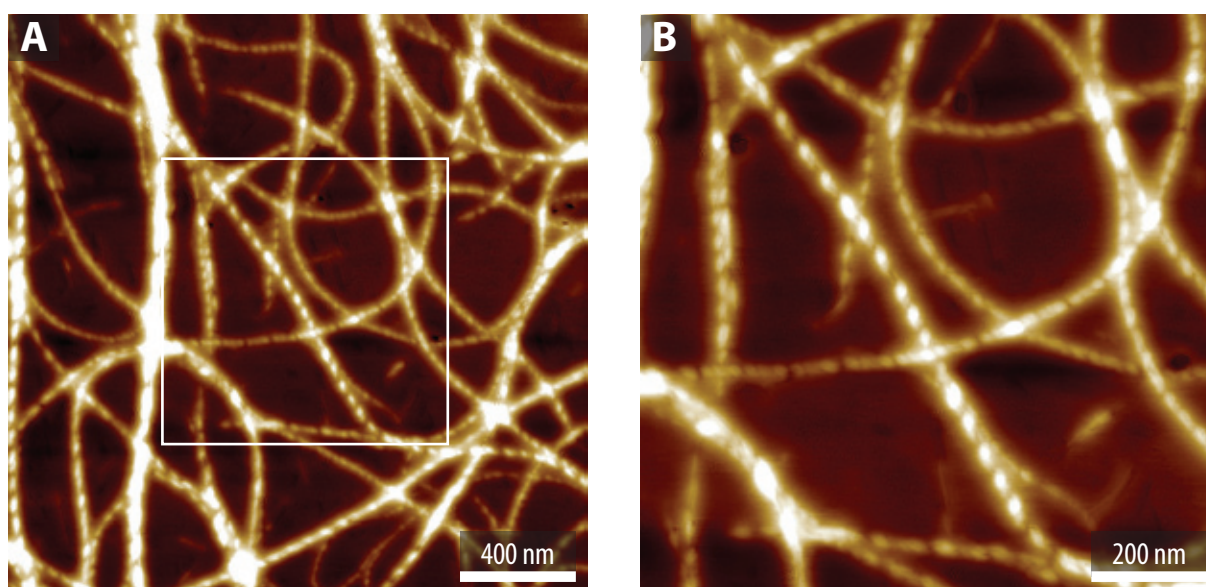


**Figure 71:** A) Solutions of **133** spin-coated on HOPG resulted in a variety of helical fibrils extending over several micrometers. Their widths were far from uniform and corresponded to multiples of the extended lengths of their constituting molecules. B) A close up of the image further confirmed the non-uniformity of the helical features.

### 3.2.7 Further Investigations Concerning the Higher Structure Formation

An investigation of the supramolecular aggregates in solution was also attempted by using cryo-TEM and light scattering techniques. As cryo-TEM is typically performed in water, our system could not be properly investigated because we were restricted to the use of chlorinated solvents. Initial light scattering attempts have been carried out with the help of the group of Prof. Manfred Schmidt at the Johannes Gutenberg University in Mainz, Germany, but the results of experiments carried out with solutions of macromonomer **92** were not straightforwardly interpretable. Apparently, the mixture of different structures in solution or their dimensions rendered a fitting of the data impossible. A repetition of the experiments using other macromonomers has not been carried out to date.

### 3.3 Model for the Self-Assembly of Macromonomers 92-103

The observed secondary and higher structure formation of the different macromonomers in organic solution which has been described in the previous sections was obviously influenced by the presence and the number of additional N-H $\cdots$ O=C hydrogen-bonding sites in their end groups and by the presence of the flexible, polydisperse and hydrophobic polymer segments. Therefore, it is certainly desirable to rationalize the exact relation between the molecular structure, the nature of the secondary structures, and the type of the fibrillar aggregates, in order to develop a set of guidelines for the preparation of  $\pi$ -conjugated polymers with a predictable hierarchical structure in the future. This goal was accomplished in analogy to and extension of the model for the step-wise, hierarchical self-organization of designed oligopeptides in protic solvents into uniform tapes, ribbons, fibrils, and fibers in protic solvents proposed by Boden, Fishwick and coworkers.<sup>82-84,106,107</sup> As discussed in detail in section 1.2.2, a short oligopeptide in  $\beta$ -strand conformation as the basic chiral, right-handed twisted rodlike unit should be expected to form single antiparallel  $\beta$ -sheet *tapes* which typically bend into left-handed helices (Figure 72). The formation of left-handed helical twisted *ribbons* (double tapes) serves to hide hydrophobic  $\beta$ -sheet surfaces in the case of amphiphilic  $\beta$ -sheets. The mutual attraction of the ribbon surfaces then leads to further  $\beta$ -sheet stacking into left-handed helical twisted *fibrils*, and the attraction of the fibrils' edges causes a bundeling of the fibrils into left-handed helical *fibers*. Thus, it is the inherent helicity of the  $\beta$ -sheet-based fibrillar aggregates (or, more precisely, the interplay of aggregation enthalpy and the elastic energetic penalty associated with readjusting the helix geometry upon aggregation) that will prohibit an unlimited aggregation and guide the system to form well-defined aggregates with a finite number of constituent tapes and a finite width on every level of self-organization. The formation of higher aggregates may, for example, be further suppressed by introducing additional non-covalent interactions such as electrostatic repulsion induced by charged side chains.

This remarkably intuitive general model is also applicable to the self-assembly of the oligopeptide-based macromonomers if the particularities of their molecular architecture as well as the differences in the conditions for self-organization are acknowledged. Most importantly, the self-assembly of the macromonomers was performed in organic solution so that, due to the absence of competition from the solvent, hydrogen-bonding responsible for the aggregation into  $\beta$ -sheets should be stronger. At the same time, any hydrophobic interactions responsible for the mutual attraction of  $\beta$ -sheets should be noticeably reduced. Secondly, the attachment of an amorphous and flexible hydrophobic polymer segment introduces a strong element of phase segregation and a source of molecular disorder both uncommon in the realm of pure oligopeptides. Thirdly, the macromonomers contain a diacetylene moiety integrated into the oligopeptide segment which may be regarded as a rigid spacer resulting in

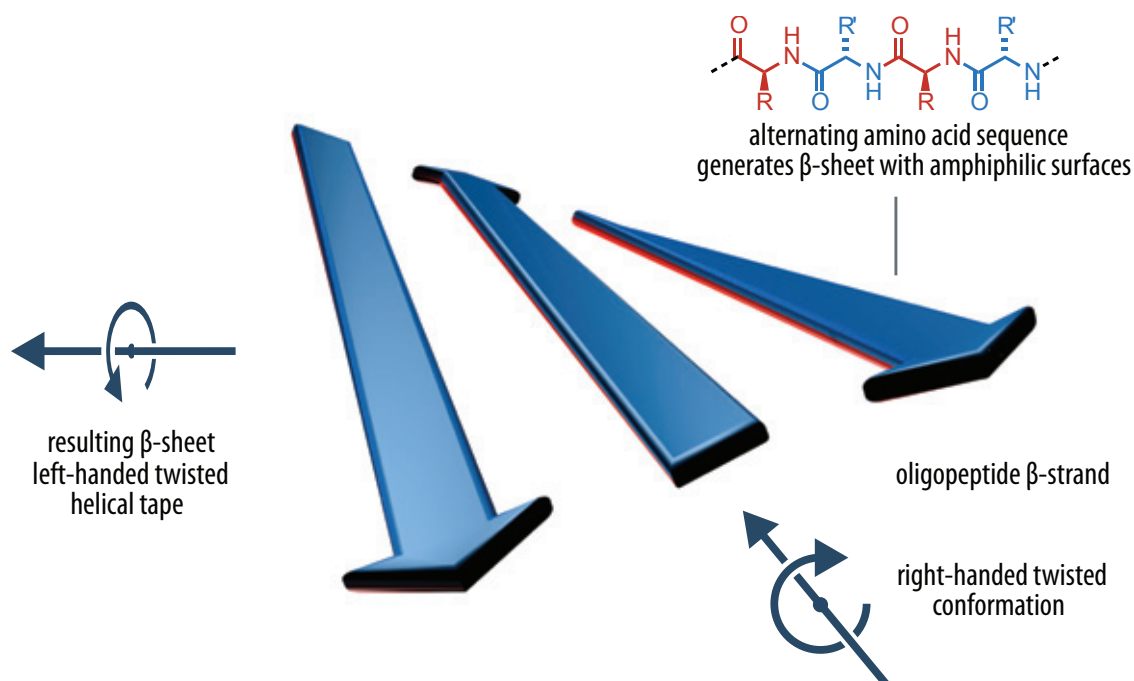


**Figure 72:** An oligopeptide  $\beta$ -strand (twisted arrow) has a right-handed twist due to the L-chirality of the amino acids. Consequently, a resulting  $\beta$ -sheet tape *must* exhibit a left-handed twist to allow for an optimal hydrogen-bonding (alignment of the arrow's edges).

a non-equidistant placement of the  $\text{N-H}\cdots\text{O=C}$  hydrogen-bonding sites in the core and in the end group. The formation of comparably stable tapes (single  $\beta$ -sheets) can straightforwardly be assumed as the first step of self-organization for all macromonomers in organic solution. The main difference between the macromonomers is the unambiguously proved fact that the tapes of macromonomers with 5+1, 5+2 and 5+5  $\text{N-H}\cdots\text{O=C}$  hydrogen-bonds typically feature a parallel  $\beta$ -strand orientation while the others favored an antiparallel alignment of the  $\beta$ -strands. As a consequence, the former  $\beta$ -sheets exhibit a residual dipole moment component perpendicular to the tape axis (in  $\beta$ -strand direction) (Figure 73).<sup>109</sup> In addition, the odd number of  $\text{N-H}\cdots\text{O=C}$  hydrogen-bonds will also cause a residual dipole moment component parallel to the tape axis. The impact of the additional hydrogen-bonding sites in the macromonomers' end groups is hard to predict as their orientation relative to the others is not known.

Consequently, the formation of antiparallel  $\beta$ -sheets from macromonomers **100** and **103** can be regarded as an apolar mode of self-assembly in the sense that the dipole moment components of the oligopeptide strands perpendicular to the tape axis are cancelled out and both edges of the tape are lined with polymer segments grafted to the oligopeptide strands in an alternating fashion (Figure 73, Figure 74B). In this way, the whole tape is conveniently wrapped into a “cushion” of the polymer segments and, thus, shielded from the hydrophobic environment. The latter factor may also be assumed



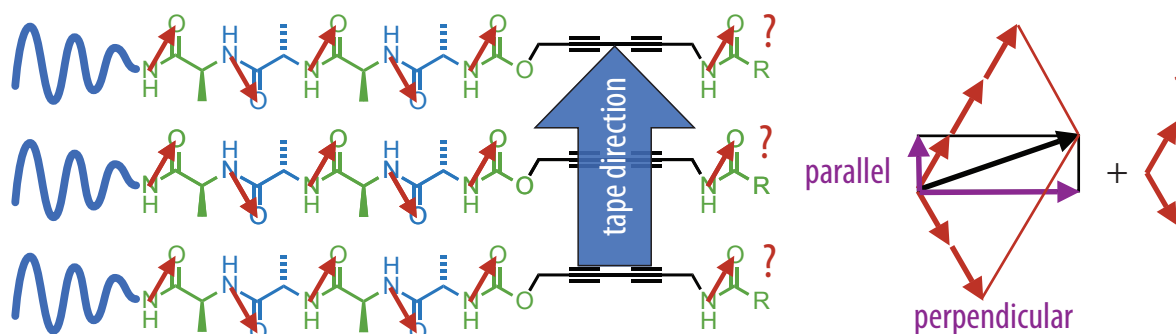


**Figure 73:** Parallel  $\beta$ -sheets exhibit a residual dipole moment component in  $\beta$ -strand direction (perpendicular to the tape direction). Additionally, there will also be a dipole moment parallel to the tape direction in case of an odd number of amide bonds. The relative orientation of additional amide bonds in the end group is not clear.

to prohibit any further stacking of the single  $\beta$ -sheet tapes into ribbons or higher aggregates. Consistent with the SFM results and in analogy to the model of Boden and Fishwick, the tapes formed from macromonomers **100** and **103** should have only little incentive to bend into helices because both  $\beta$ -sheet surfaces and the environment are hydrophobic.

Similarly, the symmetric macromonomer **99** forms tapes via an apolar mode of self-assembly (Figure 74A). While the  $\beta$ -strand orientation has been proved to be parallel, it must be taken into account that the oligopeptide segments covalently attached to the central diacetylene unit have opposite directionality so that the tapes actually consist of two parallel  $\beta$ -sheet domains with opposite  $\beta$ -strand orientation. Hence, the dipole moment components perpendicular to the tape axis are cancelled out and both tape edges are equally lined with the grafted polymer segments such that, with the same reasoning as presented above, a further self-organization into ribbons or higher aggregates is unfavorable. The tapes formed from **99** should only have a small tendency to bend into helices for the same reasons as **100** and **103** but, of course, be wider and more rigid due to the constituent molecules' dimensions and the doubled number of hydrogen-bonds.

The situation is different in the case of macromonomers **92**, **93**, **96**, and **97** in one important aspect. The formation of tapes via parallel  $\beta$ -sheet formation is a *polar* mode of self-assembly in these cases because of the residual dipole moment components. Furthermore, all polymer segments are grafted to the *same* edge of the tape while the other one is bare. In addition to the resulting steric mismatch between the tapes' edges, a simple molecular model shows that the chosen chain length of the polymer segments ( $x + y \approx 10$ ) is not sufficient to completely wrap the tapes and, thus, shield the polar cores from the hydrophobic environment. The combination of all of these factors supposedly results in the formation of ribbons (double tapes) from two (partially) stacked tapes with opposite  $\beta$ -strand orientation (Figure 74D), which would also explain the observed width of more than the

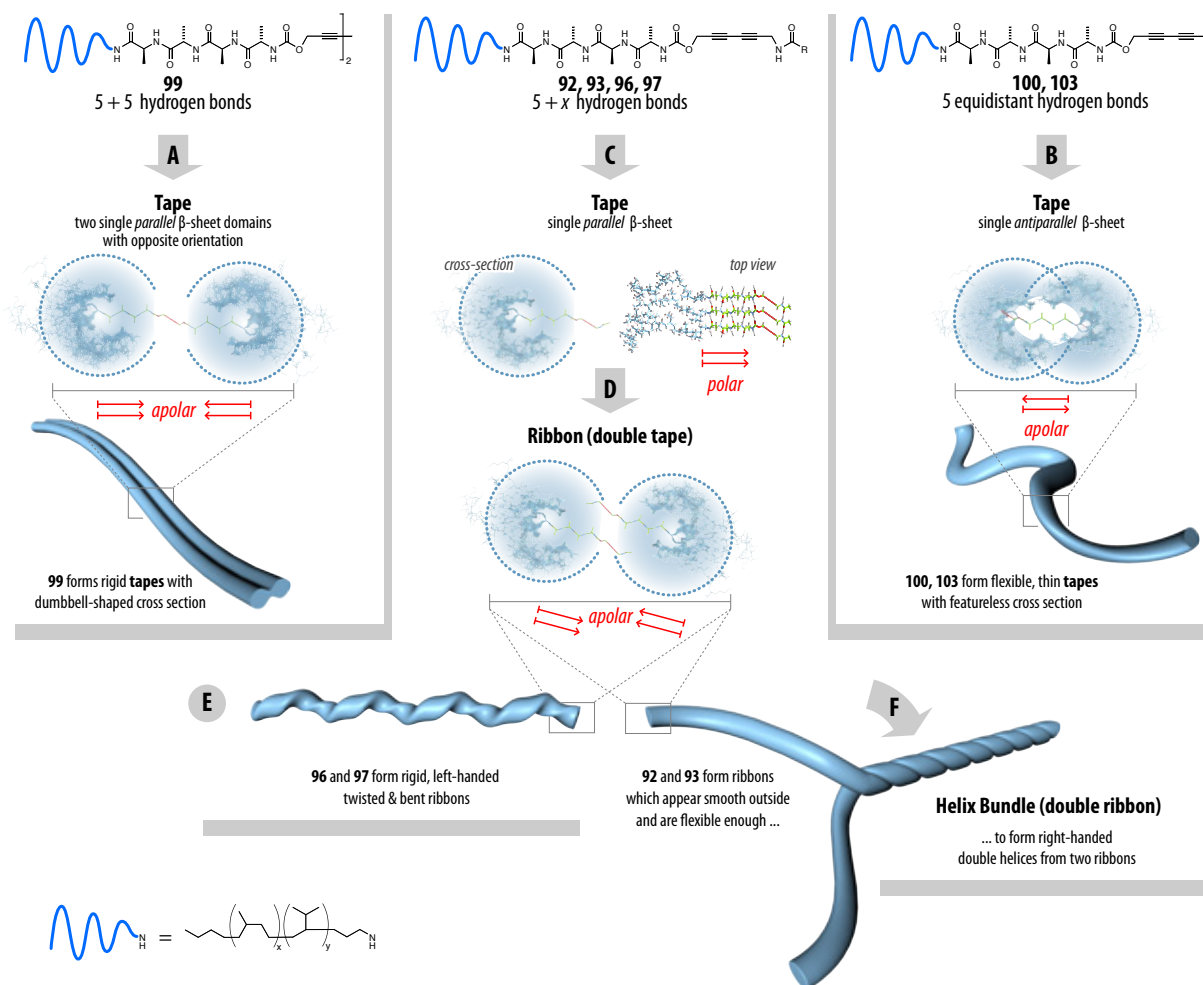


**Figure 74:** Schematic outline of the proposed model for the hierarchical self-organization of the macromonomers. *A)* **99** forms single parallel  $\beta$ -sheets, resulting in tapes with dumbbell-shaped cross-sections. *B)* **100** and **103** aggregate into single antiparallel  $\beta$ -sheets yielding flexible, featureless tapes. *C)* Tapes obtained by parallel  $\beta$ -sheet formation from **92**, **93**, **96**, and **97** are polar structures which *D)* further self-organize into ribbons. *E)* Left-handed twisted and bent ribbons from **96** and **97** are rigid, and only occasionally form helix bundles, in contrast to *F)* ribbons from **92** and **93** which are flexible enough to aggregate into double-helical bundles. Red arrows indicate the directionality of the peptide strands and also the net dipole moment components in strand direction (perpendicular to the tapes).

molecules' extended lengths. In this arrangement, the dipole moment components perpendicular to the axes of the constituent tapes would, again, be cancelled out and the whole ribbon structure would be wrapped with the aliphatic polymer segments from both sides, hiding the two  $\beta$ -sheet tapes inside.

Thus, the formation of left-handed single-helical ribbons from macromonomers **96** and **97** is analogous to the model proposed by Boden and Fishwick. As schematically illustrated in Figure 74 E, their observed complex fine structure may straightforwardly be attributed to result from bent and twisted ribbons with an approximately ellipsoidal cross-section, which is consistent with the tentative interpretation of the height profiles in the SFM images.

By contrast, the aggregates formed from **92** and **93** were right-handed double-helices formed from two ribbon substructures. The latter did not show a periodic fine structure like the ribbons formed from **96** or **97**, and they were obviously much more flexible. Both may be seen as a consequence of the fact that **92** and **93** are one peptide residue shorter so that the  $\beta$ -sheets are narrower and potentially less rigid so that any (left-handed) helicity of the tapes is concealed by the soft polymer shell around it. While, formally, the resulting double helices can be regarded as fibrils because they are constructed from two ribbons, the mechanism of fibril formation would be entirely different from the one described by Boden and Fishwick. As in the case of the other macromonomers, the soft polymer shells covering the ribbons from **92** and **93** will prevent fibril formation via  $\beta$ -sheet stacking; but interactions between them may promote the formation of superstructures in order to minimize the interface with the solvent. The resulting superstructures should, therefore, rather be referred to as helix bundles (Figure 74F). The reason for the right-handedness, however, is unknown.

This model has decisive implications concerning the planned UV-induced polymerization of the diacetylenes. The  $\beta$ -sheet tapes formed by **99** comprise exactly one array of diacetylenes and should, hence, be converted into a single-stranded poly(diacetylene) upon UV irradiation. Macromonomers **96** and **97** which formed left-handed *single-helical* ribbons that supposedly comprised two  $\beta$ -sheet tapes should, on the other hand, furnish *double-helical*  $\pi$ -conjugated polymers. Finally, macromonomers **92** as well as **93** that were shown to form right-handed double-helical helix bundles that consisted of a total of four laminated  $\beta$ -sheet tapes and the same number of polymerizable diacetylene arrays are expected to give rise to *quadruple-helical* poly(diacetylene)s exhibiting an opposite helix-sense as compared to the other poly(diacetylene)s.

### 3.4 UV Induced Topochemical Polymerization

The results concerning the controlled secondary and higher structure formation of the newly designed oligopeptide-polymer conjugates **92-103** as well as the initial polymerization results of the gels formed by model compounds **131-133** were promising with respect to the desired detailed study of the polymerization behavior that will be presented in the current section.

#### 3.4.1 Polymerization of the Macromonomers 92-103

An initial polymerization experiment was carried out with DCM solutions of **92** in UV cuvettes using a medium pressure Hg lamp exhibiting a broad emission spectrum (Figure 75). Before the irradiation, the solution was clear and colorless but attained an intense purple color almost instantaneously after

the irradiation was started. The color continued to intensify for a period of 5 min accompanied by a color change to a more reddish tone. From that point on, however, the strong UV irradiation seemed to destroy the just formed chromophores and obviously the solutions were “bleached”. After 20 min, the solution was orange and a prolonged UV-treatment led to a brownish colored reaction mixture.

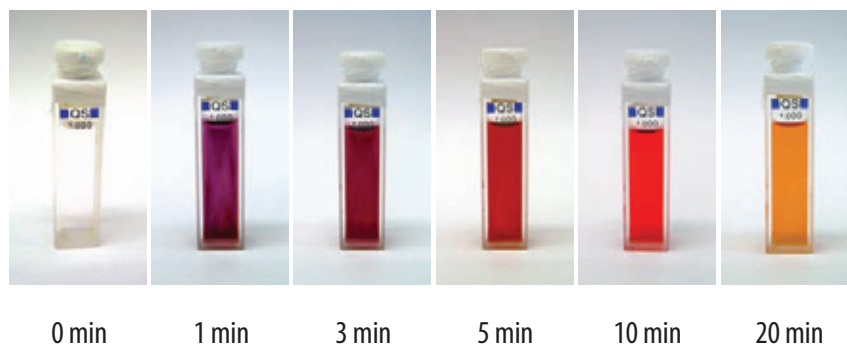


**Figure 75:** The solution of **92** in DCM attained a deep violet color almost instantaneously. The color intensified and changed to a more reddish tone after 5 min before the strong UV irradiation started to “bleach” the color.

In order to investigate the process spectroscopically, we measured UV-vis spectra after different time intervals (Figure 76). The obtained spectra showed a broad absorption starting at roughly 650 nm. Two main absorption bands located at 574 and 544 nm increased in intensity over time. This process was accompanied by a movement of the maxima toward shorter wavelengths. Below 500 nm, a featureless absorption was observed that had a minimum around 350 to 400 nm which, however, increased dramatically with irradiation time. After 5 min of UV-treatment, the highest extinction coefficient  $\epsilon_{\max} = 2 \cdot 10^6 \text{ cm}^2 \text{ mol}^{-1}$  at 516 nm was reached (normalized by the average molar mass of the macromonomer). The spectra obtained after longer irradiation times showed a drop in the intensities of the absorption bands above 500 nm, and after 20 min, the spectrum was more or less featureless showing a very high absorption below 400 nm, indicative of a photo-oxidative chain scission process described by Wenz *et al.*<sup>204</sup> In conclusion, the topochemical polymerization was successful but the chosen reaction conditions were inappropriate and had to be improved.

In order to optimize the setup, we exchanged the light source to a 250W Ga doped Hg lamp (Figure 77) exhibiting an emission spectrum featuring discrete main bands at 254 nm, 300 nm, 366 nm, 408 nm, 422 nm, 555 nm, and 580 nm. Secondly, the polymerization solutions were placed into a thermostated Schlenk reactor to allow for an exclusion of O<sub>2</sub> (Figure 77B).

The polymerization reactions using the new setup were carried out in DCM as the solvent since it is more inert against UV irradiation. In order to obtain reproducible results, stock solutions of the macromonomers in DCM were prepared, typically at concentrations of 5 or 10 gL<sup>-1</sup> and stored in the

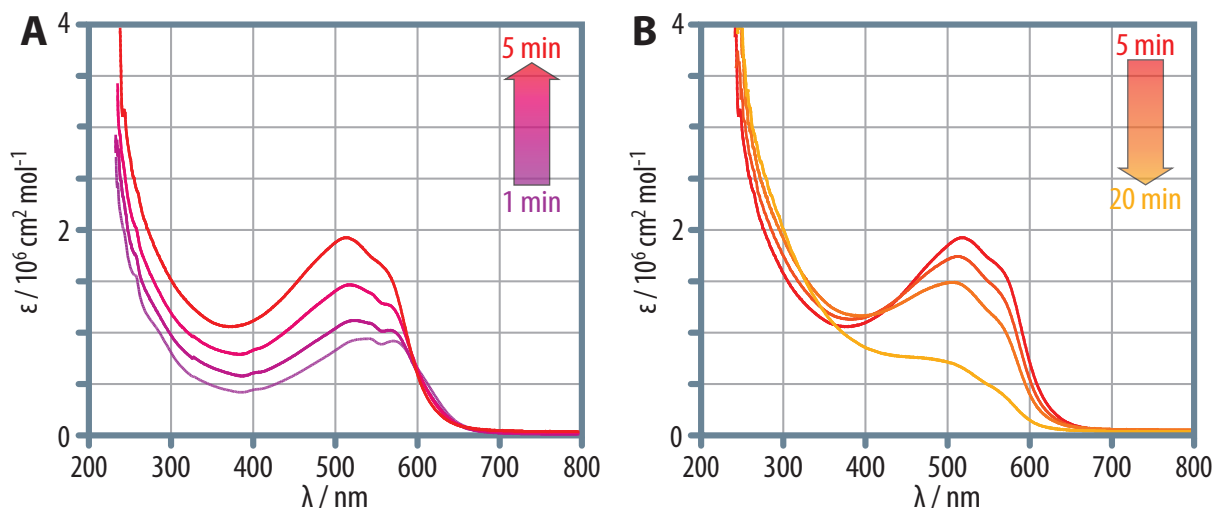


**Figure 76:** UV-vis spectra of the polymerization solution at different irradiation times *A*) first showed increasing absorption bands between 500 and 600 nm that were assigned to the poly(diacetylene) backbone formed during the reaction. *B*) After longer irradiation times, these bands decreased at the expense of a strong increase of absorptions below 400 nm, indicating a photo-oxidative polymer degradation.

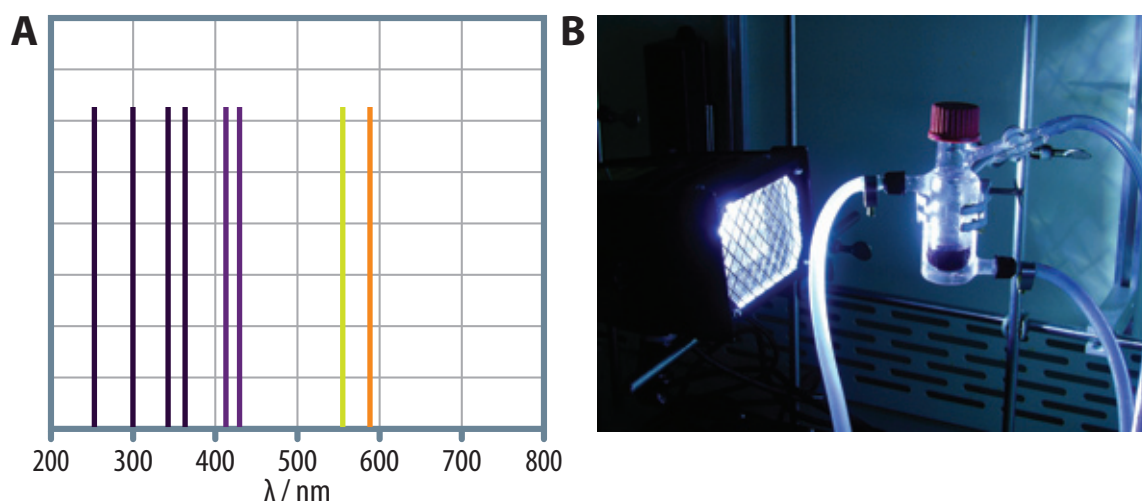


**Figure 77:** *A*) Schematic emission spectrum of the UV lamp; *B*) The setup of the UV polymerizations: the quartz glass Schlenk flask could be equipped with an inert  $\text{N}_2$  atmosphere, was thermostated and placed at a variable distance from the UV lamp. The macromonomer solution was irradiated (violet solution) and samples could be taken by opening the GL cap in the  $\text{N}_2$  counter current.

dark in the freezer. These stock solutions were heated to room temperature and ultrasonicated for several minutes to ensure a homogeneous distribution of the material. A sample was taken and diluted in more DCM to the desired concentration. The reaction solution was then degassed by three freeze-pump-thaw cycles, transferred to the reaction vessel, and thermostated to the desired temperature for 15 min before the UV-irradiation was started. The reactor was opened in  $\text{N}_2$  counter current and samples were taken at different time intervals. Due to the high extinction coefficient of the  $\pi$ -conjugated polymer backbone, the samples were further diluted before the UV-vis spectra were

measured. Thus, small samples of several hundred microliters were transferred to volumetric flasks (1-5 mL) using a microliter syringe, and then diluted to a concentration of  $0.25 \text{ gL}^{-1}$ .

Several test polymerizations with the various macromonomers at different concentrations ( $0.1\text{--}10 \text{ gL}^{-1}$ ), temperatures [ $-20^\circ\text{C}$  to  $+30^\circ\text{C}$ ] and irradiation times revealed that optimal polymerization results, judged from the highest extinction coefficients and the general shape of the spectra, were obtained by irradiating solutions with a concentration of  $1 \text{ gL}^{-1}$  for 2 h at  $0^\circ\text{C}$ .<sup>205</sup> Although the reaction was generally faster at elevated temperatures, a pronounced evaporation of the volatile DCM caused an increase in concentration and, thus, the extinction coefficients measured in UV spectroscopy became unreliable. Thus, all macromonomers were polymerized under “standard conditions” at  $0^\circ\text{C}$  to obtain comparable results.

The poly(diacetylene) formed by macromonomer **92** exhibited a main absorption band located at 518 nm with a shoulder to higher wavelengths at  $\approx 580 \text{ nm}$  (Figure 78A). The maximum extinction reached a value of  $2.75 \cdot 10^6 \text{ cm}^2 \text{ mol}^{-1}$  after 2 h of irradiation. The most important improvement in comparison to the initial experiment (*vide supra*) could be observed in the spectral region below 400 nm. Although, still, a pronounced increase in absorption was observed in that region, the polymer was found to be much more stable to photo-oxidative degradation.

Macromonomer **93** with the same amount of  $\text{N-H}\cdots\text{O}=\text{C}$  hydrogen-bonds was more reactive than **92** judged from the higher  $\epsilon_{\text{max}} = 4 \cdot 10^6 \text{ cm}^2 \text{ mol}^{-1}$  (Figure 78B) and a comparative plot of the extinction coefficients at the global maximum against time (Figure 78F). The global absorption maximum was located at 536 nm exhibiting a shoulder at about 500 nm. Additionally, a second clearly resolved peak at 584 nm was observed, indicative of the presence of a second poly(diacetylene) species that formed different spectroscopic aggregates. The higher reactivity of **93** was well in line with the results from IR spectroscopy and SFM imaging which had proved a better ordered secondary- and higher structure formation.

Macromonomer **96** featuring  $5+2 \text{ N-H}\cdots\text{O}=\text{C}$  hydrogen-bonds was highly reactive towards the topochemical polymerization as well (Figure 78C). The obtained spectra featured a well-resolved absorption band at 533 nm exhibiting a shoulder at 495 nm which could be assigned as vibrational fine structure with the help of Raman spectroscopy (Section 3.5.1). Toward higher wavelengths, a less pronounced shoulder was present but the spectra seemed to represent mainly only one poly(diacetylene) species. The reactivity was highly increased as compared to **92** and **93** since the UV bands grew much faster and  $\epsilon_{\text{max}}$  reached a value of almost  $6 \cdot 10^6 \text{ cm}^2 \text{ mol}^{-1}$  after 120 min of irradiation time.

The polymerization of macromonomer **97** worked generally well, as may be concluded from the corresponding series of UV-vis spectra (Figure 78D). Judged from the number of hydrogen-bonds, the IR spectra as well as the SFM images, one would expect a similar behavior as compared to **96**. How-

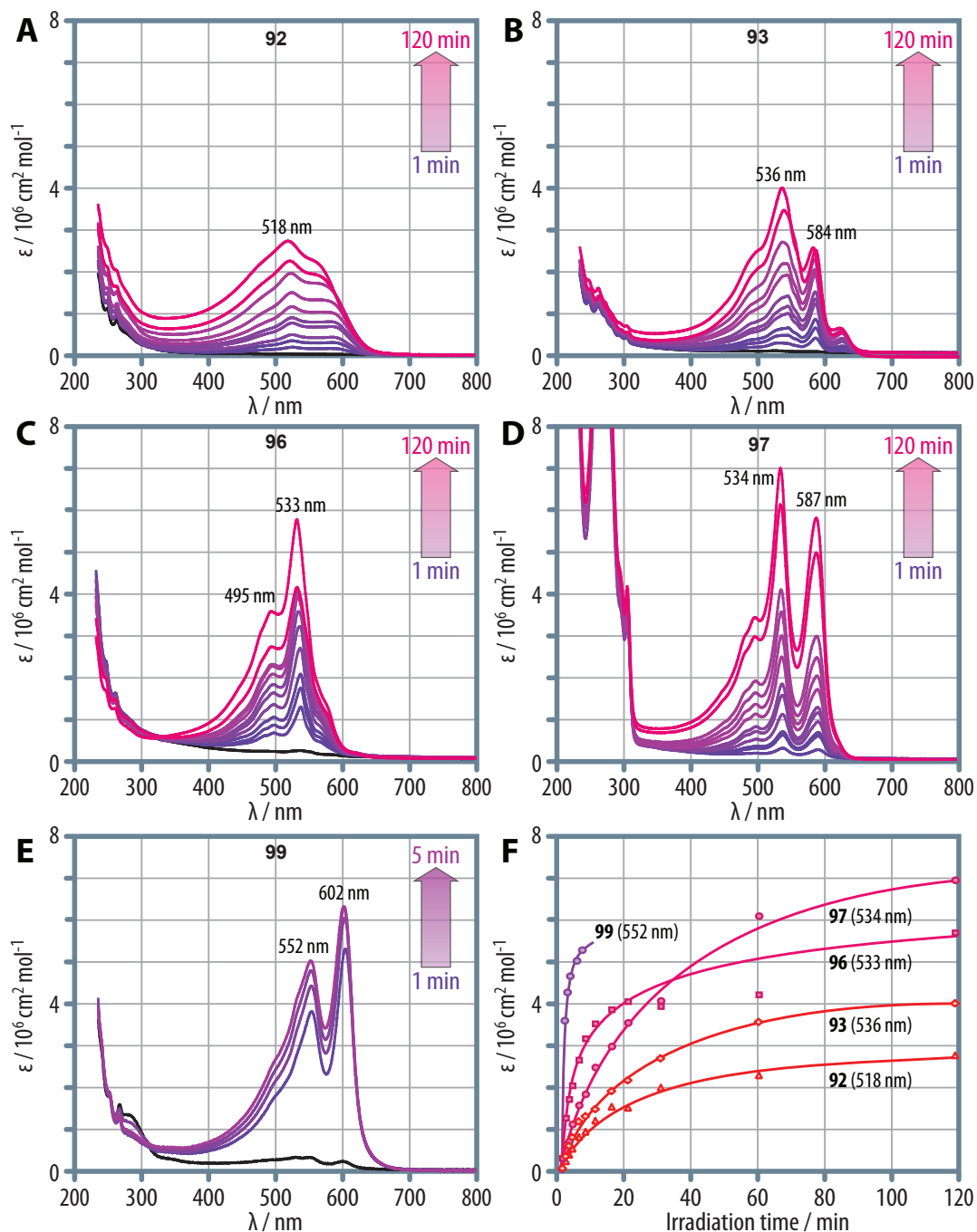


**Figure 78:** A) Macromonomer **92** had a global absorption maximum at 518 nm with  $\epsilon_{\text{max}} = 2.8 \cdot 10^6 \text{ cm}^2 \text{ mol}^{-1}$ . B) **93** reached a higher  $\epsilon_{\text{max}}$  with roughly  $4 \cdot 10^6 \text{ cm}^2 \text{ mol}^{-1}$  and showed a clear peak at 584 nm in addition to the main peak located at 536 nm. C) **96** reached nearly  $6 \cdot 10^6 \text{ cm}^2 \text{ mol}^{-1}$  exhibiting a main absorption at 533 nm. D) **97** reached an  $\epsilon_{\text{max}}$  of  $7 \cdot 10^6 \text{ cm}^2 \text{ mol}^{-1}$  at 534 nm but a second band at 587 nm was observed; E) **99** was polymerized at  $30^\circ\text{C}$ , however, also at elevated temperatures the polymeric material precipitated after 5 min of irradiation. Until then, a band at 552 nm reached  $5 \cdot 10^6 \text{ cm}^2 \text{ mol}^{-1}$ , and an even more intense signal at 602 nm was observed; F) Plots of  $\epsilon_{\text{max}}$  versus time revealing a structure reactivity relationship.

ever, a closer inspection of the polymerization revealed some particularities in this case. The initial reaction rate, i. e., the growth of the global absorption maximum, was notably reduced (Figure 78F) as compared to **96**. Nevertheless, the final conversion after 2 h was higher, leading to an extinction co-

efficient of the main band at 534 nm of  $7 \cdot 10^6 \text{ cm}^2 \text{ mol}^{-1}$ . Additionally, a second strong band located at 587 nm was present indicative of a second poly(diacetylene) species. Apparently, the presence of the Fmoc group which made the solution almost intransparent below 300 nm slowed down the reaction, but also led to a cleaner reaction to higher conversions. This observation made us use a “black bandpass filter” exhibiting a transparency window from 315 to 405 nm in subsequent reactions.

The symmetric derivative **99** with its 5+5 N–H $\cdots$ O=C hydrogen-bonds was expected to be highly reactive towards the topochemical polymerization extrapolated from the so far described results. The results of the polymerization confirmed these assumptions (Figure 78E,F). However, the polymeric material precipitated already after very short irradiation times. The initial reaction rate was by far the highest of all macromonomers, but the polymerization could only be followed within the first 5 min of the experiment. Two bands located at 552 and 602 nm dominated the corresponding UV-vis spectra and the extinction coefficients had reached 5 as well as  $6 \cdot 10^6 \text{ cm}^2 \text{ mol}^{-1}$ , respectively, already after that short irradiation time. The data are admittedly hard to compare because this reaction had been carried out at 30 °C to avoid the precipitation of the material, which was not successful. Apparently, the octapeptide core was not sufficiently hindered from stacking by the hydrogenated poly(isoprene) segments after polymerization.

In summary, all macromonomers that had been ascribed to form parallel  $\beta$ -sheets in solution based on the IR investigations were well-polymerizable. This fact can be regarded as the ultimate proof for the parallel arrangement since only in this way, a topochemical polymerization of the diacetylenes can be achieved. Furthermore, a clear structure-reactivity relation was observed, i. e., the more N–H $\cdots$ O=C hydrogen-bonding sites were located in the end groups the higher were the rate and conversion of the polymerization.

The macromonomers **100**, **101**, **102** as well as **103** that were proved to self-assemble in antiparallel  $\beta$ -sheets or unordered structures were, nevertheless, treated with UV light in solution under standardized conditions, i. e., without bandpass filter. Solutions of macromonomers **100-103** did not attain a violet or red color but rather stayed colorless or became, at most, slightly yellow. The UV-vis spectra (Figure 79) only showed a small increase in absorption below 400 nm which was interpreted in terms of a random cross-linking of the diacetylenes or a photo-oxidation of the latter. The highest reactivity was found for **101** which showed the highest increase in absorption at wavelengths up to 500 nm. This was well in line with the IR investigations that indicated the presence of minor amounts of parallel  $\beta$ -sheets in the case of **101** which may have led to the formation of  $\pi$ -conjugated oligomers.

In one occasion, it was possible to polymerize a solution of the hydroxyl-functionalized macromonomer **100** after it had been treated for several hours in the ultrasonicator (Figure 80). After several minutes of UV irradiation, an absorption band at 530 nm was formed exhibiting an extinc-



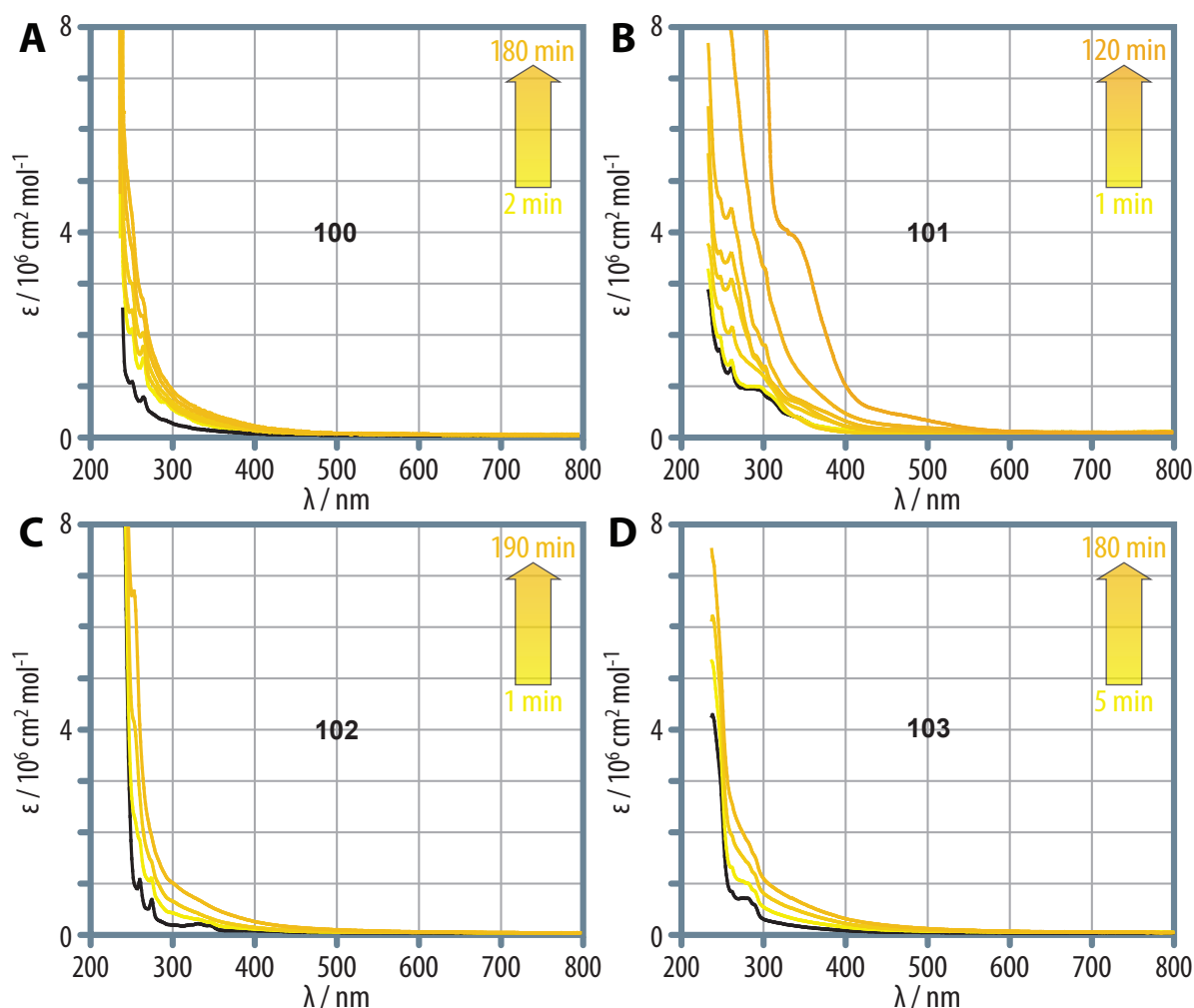


**Figure 79:** The macromonomers that were found to mainly form antiparallel  $\beta$ -sheets did not undergo a topochemical polymerization. A) **100** only showed a small increase of the absorption below 400 nm, indicative of a random cross-linking or photo-oxidation of the diacetylenes; B) **101** showed a stronger increase in absorption in the lower wavelength region indicating the formation of oligomers in agreement to the corresponding IR spectrum that indicated the presence of minor amounts of parallel  $\beta$ -sheets; C) **102** as well as D) **103** seemed to suffer from random cross-linking only.

tion coefficient of about  $1 \cdot 10^6 \text{ cm}^2 \text{ mol}^{-1}$ , before a quick degradation of the polymeric material occurred with prolonged irradiation times (not shown). Apparently, it had been possible to rearrange the molecules into a parallel  $\beta$ -sheet configuration, at least, to a small extent. This phenomenon was, unfortunately, not well-reproducible and, hence, not further investigated.

Macromonomers **94** and **95** were also subjected to UV irradiation (Figure 81). In case of **94**, almost no polymerization occurred even at an elevated temperature of  $50^\circ\text{C}$  (in 1,2-dichloroethane). This result is remarkable given the close structural relation to the other macromonomers with 5+1 N-H $\cdots$ O=C hydrogen-bonds and its sibling **97** having 5+2 hydrogen-bonds but it also underlines the power of the IR investigations that already indicated unordered structures in solution. Things were similar in the case of **95**. No polymerization occurred which was well in line with the corresponding

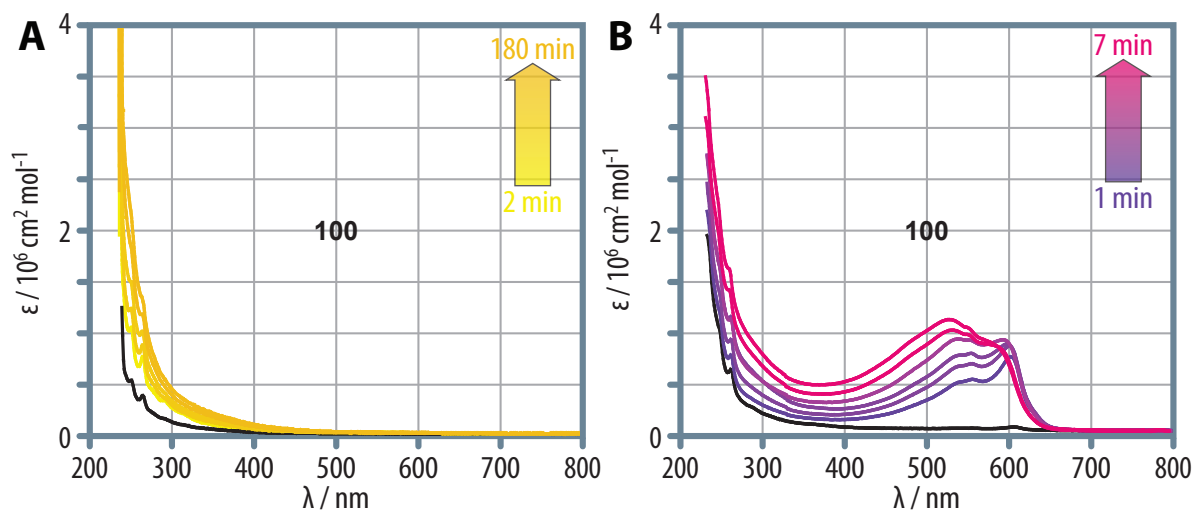


**Figure 80:** A) Macromonomer **100** could usually not be polymerized due to its antiparallel  $\beta$ -sheet arrangement; B) This was, however, partially changed by a treatment with ultrasound that was carried out for several hours once allowing for a limited formation of poly(diacetylene)s. This experiment was not well reproducible.

IR signature. This macromonomer was initially designed to act as a sensitizer for the polymerization of the diacetylenes which had been shown to work with other fluorescent dyes.<sup>206</sup> Thus, we mixed **95** with macromonomers **92** and **93** to test the effect on the polymerizability. Disappointingly, the reactions were significantly slowed down and showed no improvements of any kind. The decreased reactivity was explained by the absorption spectrum of **95** (Figure 81B), which showed strong absorption bands at 256 as well as 372 nm and, therefore, absorbed at UV wavelengths that initiate the topochemical polymerization.

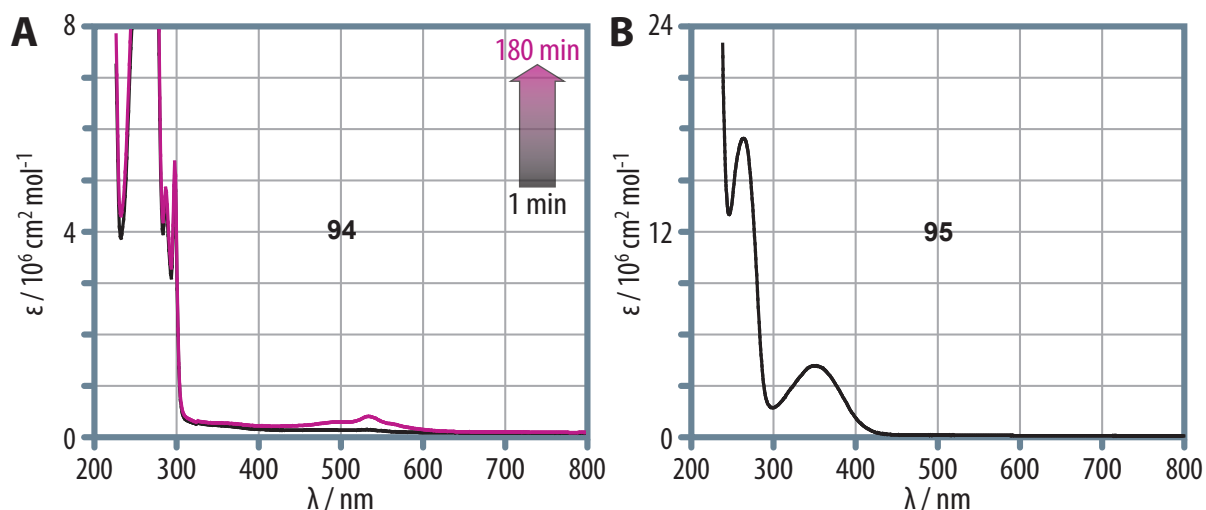


**Figure 81:** A) The UV-vis spectrum of a solution of **94** after 4 h of irradiation was almost unchanged as compared to the initial spectrum indicating a non-successful polymerization; B) UV-vis spectrum of macromonomer **95** in DCM. The absorptions of the Dansyl group at 256 as well as 372 nm hindered the polymerization of samples mixed with other macromonomers.

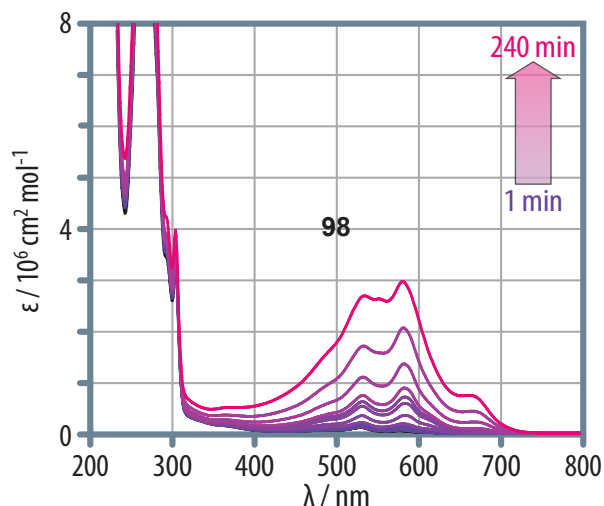


**Figure 82:** The polymerization of **98** was possible. However, compared to its sibling **97**, the reactivity was reduced and the spectrum contained several peaks indicative of mixtures of poly(diacetylene) species.

Finally, macromonomer **98** that was equipped with an achiral glycine residue was investigated. Although this derivative exhibited 5+2 hydrogen-bonding sites, a comparably low reactivity was observed (Figure 82). The maximum extinction coefficient reached only  $3 \cdot 10^6 \text{ cm}^2 \text{ mol}^{-1}$  even after 4 h of irradiation. The UV-vis signature was complicated, i. e., it contained three maxima at 535, 584 as well as 666 nm. Especially the last band was indicating a strong tendency of the conjugated polymers to form spectroscopic aggregates. Therefore, the investigations concerning this macromonomer were not intensified.

In summary, we were able to show that a topochemical polymerization was possible in solution, i. e., a transformation of the well-defined supramolecular polymers into  $\pi$ -conjugated polymers was successful whenever the oligopeptide-polymer conjugates formed parallel  $\beta$ -sheets. The latter was well-controlled by the introduction of different end groups that either were or were not equipped with  $\text{N-H}\cdots\text{O=C}$  hydrogen-bonding sites. The reactivity of the different macromonomers was directly related to the number and pattern of the hydrogen-bonds, i. e., derivatives having 5+0 bonds did not react at all (as they formed antiparallel  $\beta$ -sheets or random coil secondary structures). The macromonomers exhibiting 5+1 hydrogen-bonds (**92** and **93**) typically reacted well with the exception of compound **94**. **96** and **97** featuring 5+2  $\text{N-H}\cdots\text{O=C}$  hydrogen-bonds were highly reactive only outperformed by the symmetric derivative **99** having 5+5 hydrogen-bonding sites. All these results were perfectly in agreement with the results in IR spectroscopy, which strongly underlines the correctness of our assignments that were possible mostly due to the clear signatures and despite contradictory declarations of IR bands to secondary structures of oligo- and polypeptides in the literature.

### 3.4.2 Polymerization of the Model Compounds

In order to investigate the polymerization of the model compounds in the gel state, the process was followed with UV-vis spectroscopy, as well. Thus, thoroughly degassed DCM or  $\text{CHCl}_3$  solutions of the model compounds at typical concentrations of 0.5 to  $1 \text{ gL}^{-1}$  were treated with ultrasound, heated, and transferred directly into 2 mm quartz cuvettes (Figure 83). The latter were carefully closed to avoid the intrusion of oxygen as far as possible to ensure a smooth polymerization. The solutions formed gels in the cuvettes depending on the compounds, and UV spectra were measured before the UV-irradiation. Then, the samples were irradiated for 2 h.

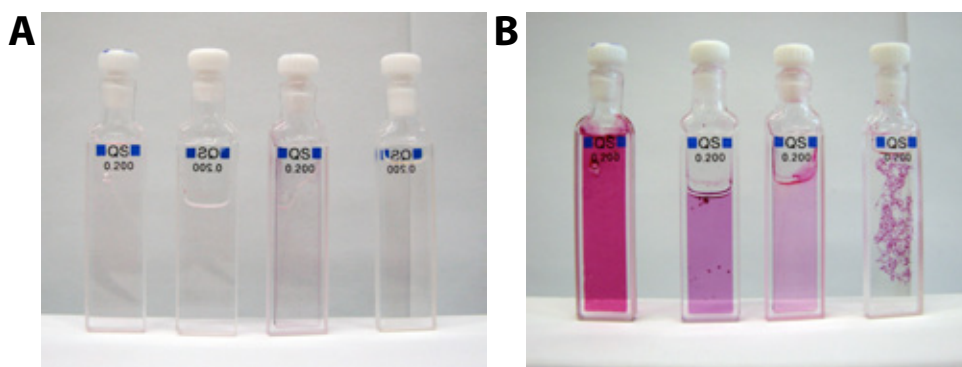


**Figure 83:** Photographs of *A*) gels of **133** in  $\text{CHCl}_3$  and DCM, as well as of **132**, and **131** in DCM (from left to right); *B*) the same samples after UV irradiation. It is interesting to note that the bubble in the leftmost cuvette ( $\text{CHCl}_3$  gel of **133**) was preserved whereas the gel formed by **132** (right) was destroyed due to a precipitation of the colored polymer.

In case of compound **130** (Figure 84A), no change in the UV-vis spectra was observed upon UV irradiation. In case of **134**, the spectra showed a broad featureless absorption below 500 nm indicative of a random cross-linking process that could also be observed in the solid state as well as during attempts to dissolve the material in the heat (Figure 84B). In contrast, DCM gels formed from model compound **131** (3+1 N-H $\cdots$ O=C hydrogen-bonds) were found to develop typical poly(diacetylene) absorption bands (Figure 84C). The global absorption maximum was located at 573 nm, and a second band was found at 528 nm, well resembling the spectra of the related macromonomer **93**. In accordance with the IR spectra,  $\text{CHCl}_3$  solutions of **131** neither formed gels nor were polymerizable by UV treatment. Repetitive attempts to irradiate gels formed from **132** all resulted in the precipitation of violet polymeric material that could not be dissolved again. Therefore, a UV-vis spectrum could not be recorded in this case. The gels formed from **133** having 3+3 hydrogen-bonds were stable during the polymerization process, and the corresponding spectra also exhibited the characteristic UV absorption bands. They were, however, much more intense. The normalized extinction coefficient was six to seven times higher as compared to **131**. The spectrum of the gel formed in DCM

showed a global absorption maximum at 534 nm with a shoulder at 495 nm. However, also two rather undefined bands appeared in the longer wavelength region peaking at 588 and 571 nm respectively. The spectrum of the  $\text{CHCl}_3$  gel also featured the peaks at 534 and 495 nm but the absorption maxima at the higher wavelength absorptions were much less pronounced. This could be interpreted in terms of a cleaner reaction giving rise to mainly only one poly(diacetylene) species in this case. The fact that the polymer material did not precipitate in this case may be explained with the help of SFM. The aggregates were very long and strongly entwined giving rise to a much stronger gel which could not be destroyed by the polymerization process.

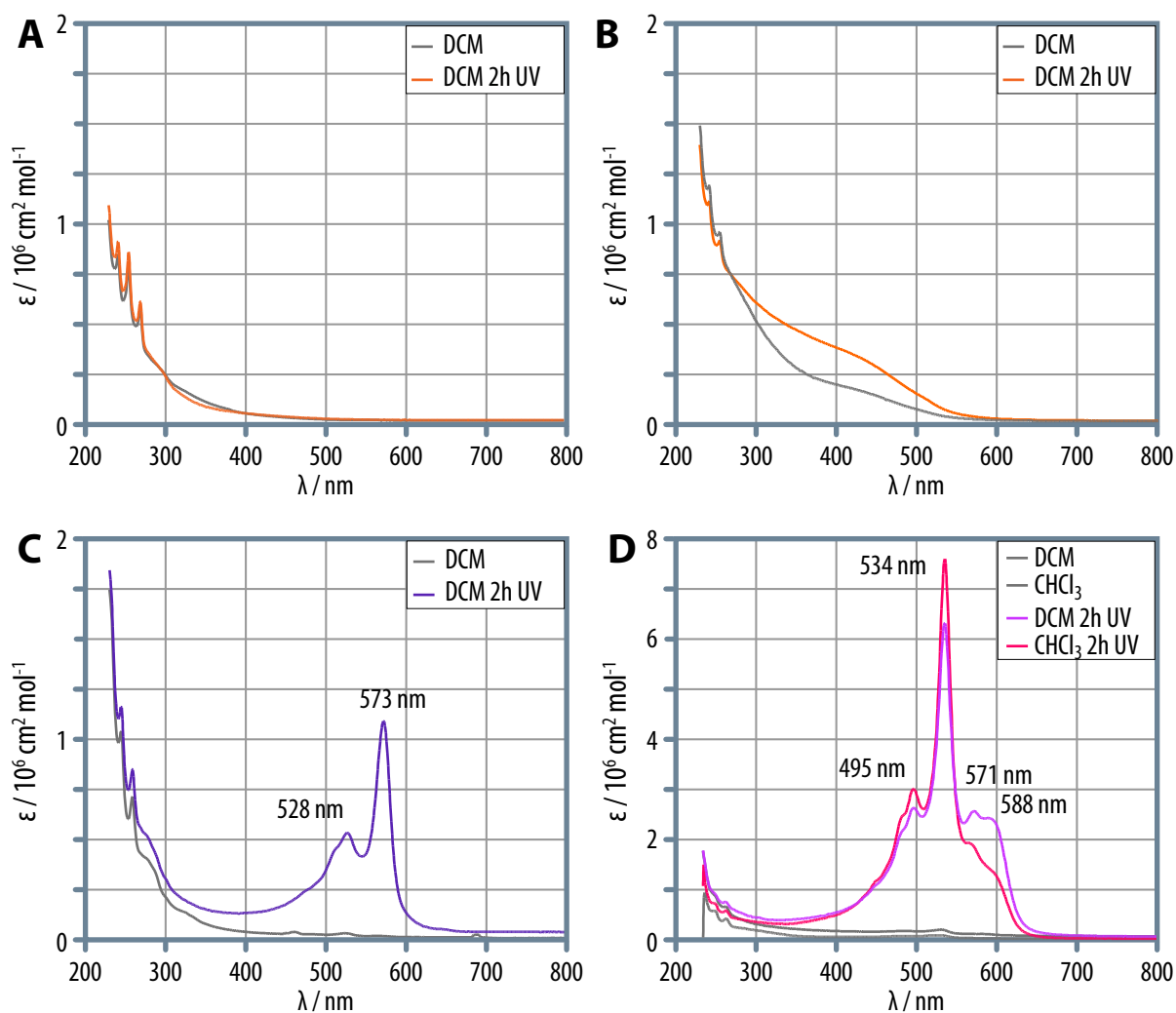


**Figure 84:** UV spectra of the different model compounds before and after 2 h of UV irradiation. A) The TMS terminated molecule **130** did not show any change in the UV spectrum upon UV irradiation; B) This was also true in the case of **134**; however, a featureless absorption below 500 nm appeared upon the UV treatment; C) The spectrum of derivative **131** exhibited the typical absorption maxima between 500 and 600 nm characteristic of a poly(diacetylene). D) The same was found in case of the symmetric molecule **133** but with a six to seven times higher intensity.

In summary, one can conclude that a topochemical polymerization of the dodecyl substituted derivatives was possible only in the gel state, whereas solutions of the material obviously were not. This is in sharp contrast to the behavior of the original macromonomers that indeed could be polymerized “in solution” due to their molecular design. The polydisperse coil segment led to a seclusion of the single aggregates whether they were tapes, ribbons or fibrils, and prevented a strong interaction of these aggregates and, consequently, the formation of a stable macroscopic gel. In case of the simpler model compounds, gel formation was observed whenever a  $\beta$ -sheet-like structure was formed, i. e., in all cases where a topochemical polymerization was possible.

### 3.4.3 Characterization of the Poly(diacetylene)s

The formation of the poly(diacetylene) backbones was already proved by their characteristic UV-vis spectra. Nonetheless, other spectroscopic techniques as well as imaging methods were used to obtain more information on conversions as well as molecular weights and properties of the poly(diacetylene)s.

#### 3.4.3.1 Spectroscopic Evidence for the Formation of Poly(diacetylene)s

The topochemical polymerization is typically proved by  $^{13}\text{C}$  NMR spectroscopy because the chemical shifts of the polymer backbone differ substantially from the purely  $sp$ -hybridized carbons of the diacetylene precursors. Thus, we polymerized a comparably large amount (100 mg) of macromonomer **92** and investigated it by means of solid state NMR spectroscopy before and after polymerization (Figure 85). The diacetylene functions of the macromonomer gave rise to four clearly resolved signals at 67.3, 69.9, 71.8 and 76.2 ppm. Additionally, the two methylene groups next to the  $sp$ -hybridized carbons could be assigned to signals at 49.5 as well as 54.1 ppm. After polymerization, the region of the diacetylene had lost in intensity, a new, admittedly very broad peak at 129.9 ppm appeared, and the methylene carbon signals were shifted upfield. The peak at 130 ppm could be assigned to the  $sp^2$ -hybridized carbons of the polymer backbone. A possible explanation for the broad line width of the poly(diacetylene) signals may be given by the apparently stiff backbone that is incorporated into the hydrogen-bonding array leading to long relaxation times.

Vibrational spectroscopic methods can be used to prove the conversion of the diacetylenes to poly(diacetylene)s, as well. While IR spectroscopy is not well suited for the determination of the vibrations of  $\text{C}\equiv\text{C}$  bonds due to the only small change in dipole moments,<sup>135,207</sup> Raman spectroscopy depends on a change in the polarizability and is, thus, able to detect vibrations of  $\text{C}\equiv\text{C}$  as well as  $\text{C}=\text{C}$  bonds.<sup>160,207,208</sup> Since the vibrational frequencies of monomers and polymers are distinctly different,

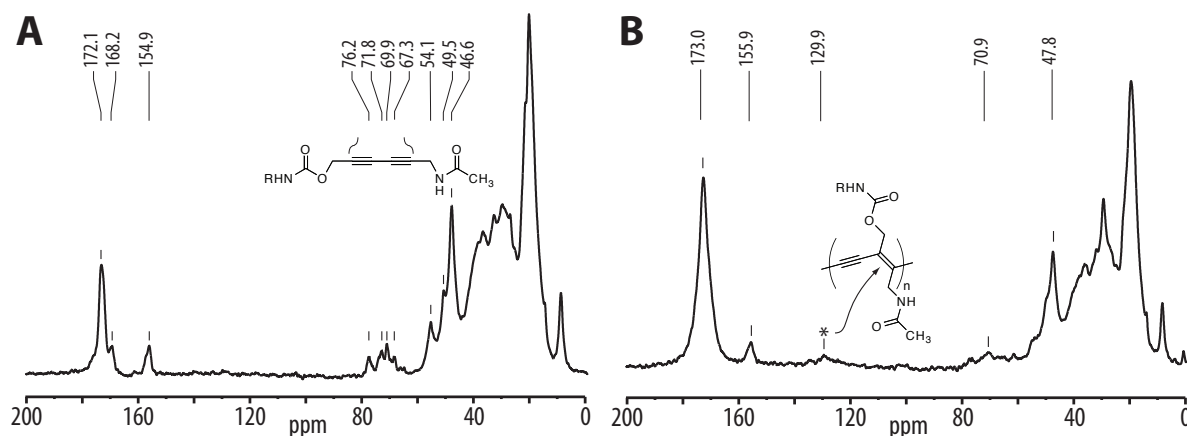


**Figure 85:** A) The solid state NMR spectra of macromonomer **92** showed the diacetylene signals between 67 and 76 ppm; B) After polymerization, these peaks have nearly disappeared and a new broad peak at 130 ppm has appeared that was assigned to the newly formed  $sp^2$ -hybridized carbons of the polymer backbone.

the transformation is straightforwardly detectable. A Raman spectrum of **92** in the solid state was found to contain an intense band at  $2261\text{ cm}^{-1}$  that was caused by the diacetylene vibration. After polymerization, two new peaks appeared at  $2114$  and  $1490\text{ cm}^{-1}$ , respectively, that represented the newly formed double and triple bonds of the polymer backbone (Figure 86). In case of **92**, a small monomer peak was still detectable. In the cases of **93**, **96** and **97** the conversions were quantitative as judged from the complete absence of monomer peaks in their Raman spectra (Section 3.5.1).

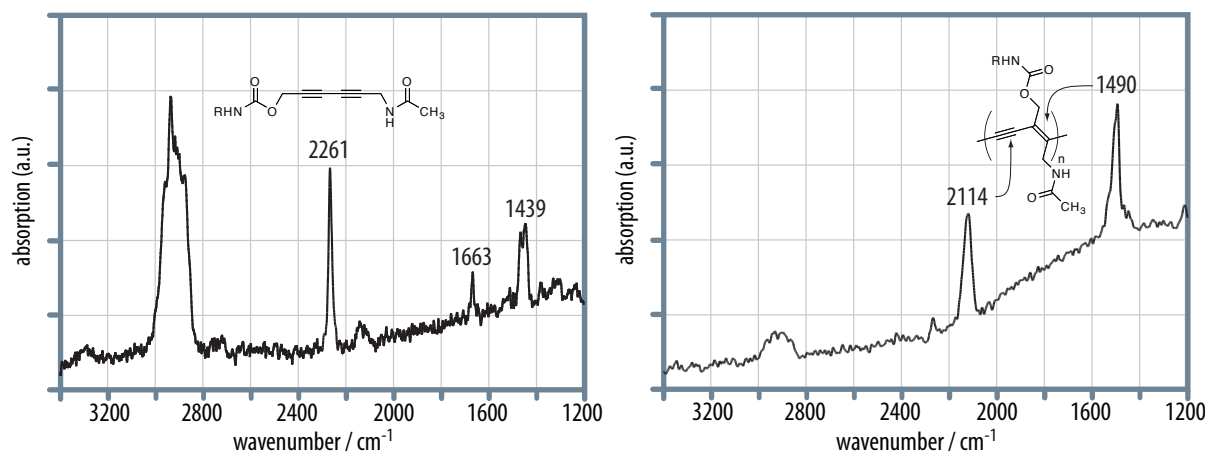


**Figure 86:** A) The solid state Raman spectrum of macromonomer **92** exhibited a strong peak at  $2261\text{ cm}^{-1}$  resulting from the diacetylene vibration. B) After polymerization, two new peaks at  $2114$  and  $1490\text{ cm}^{-1}$  were found caused by the poly(diacetylene) backbone. Only a small peak corresponding to the macromonomer remained at  $2261\text{ cm}^{-1}$ .

### 3.4.3.2 SFM Imaging on Polymerized Samples

SFM imaging was used to investigate the influence of the polymerization process on the self-assembled aggregates. For this purpose, polymerized samples of macromonomers **93**, **96** and **97** were imaged. In all cases, fibrillar features were observed that exhibited *exactly* the same superstructures as the non-polymerized materials. Thus, polymerized samples of **93** (**P93**) gave rise to right-handed helical aggregates with the same geometrical features as the sample before UV irradiation (Figure 87A). Analogously, polymerized **97** (**P97**) gave rise to left-handed single-helices exhibiting the same complex fine structure as the parent supramolecular assemblies.

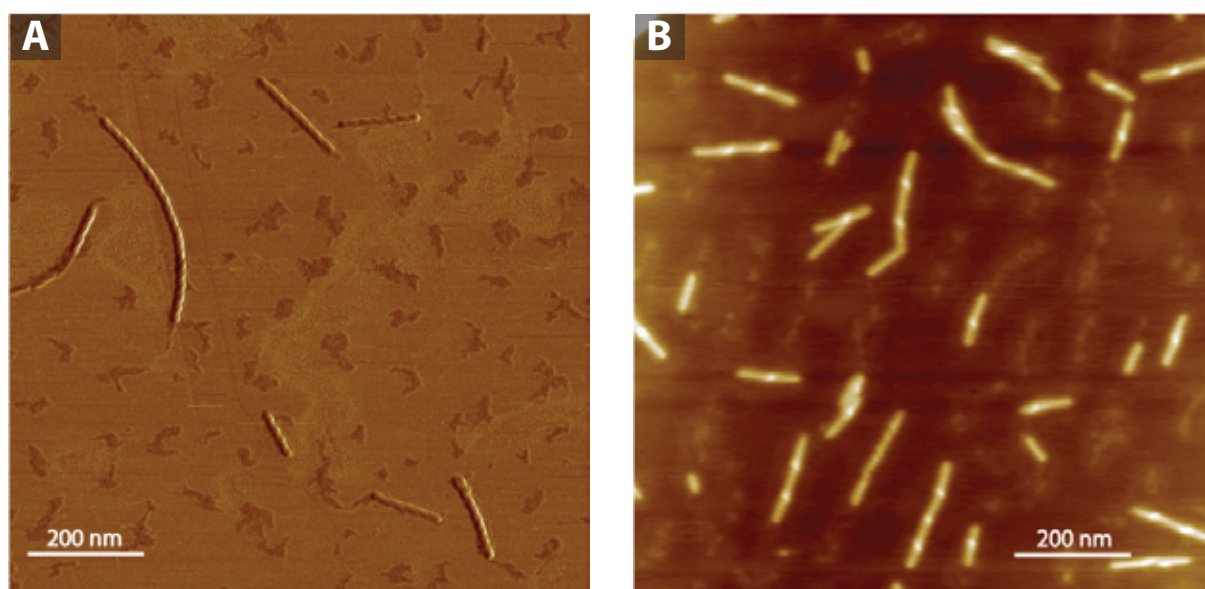


**Figure 87:** A) A SFM (phase) image of a sample of **P93** showed right-handed helical features with equal geometrical features as the fibrils obtained by the non-polymerized samples. B) A SFM (height) image of **P97** revealed the presence of left-handed single helices matching the parent supramolecular aggregates perfectly.

In order to prove the formation of the covalent polymer backbone in the nanoscopic structures, we treated solutions of **93** and **P93** with hexafluoroisopropanol (HFIP), a hydrogen-bond breaking cosolvent. This led to a complete deaggregation of the macromonomer in the non-irradiated solution so that no structures could be imaged at all. The covalently captured structures in the polymer solution, however, could not be dissolved and the corresponding SFM images showed helical, fibrillar features in addition to unordered material (Figure 88A). The polymer formation was then ultimately proved by “SFM manipulation”. While the supramolecular aggregates were easily destroyed by the SFM tip when the latter was moved over the surface in contact mode (Figure 88B), the polymerized fibrils stayed intact and could even be moved across the surface (Figure 88C,D). Apparently, the self-assembled structures had been stabilized dramatically due to the formation of chemical bonds.



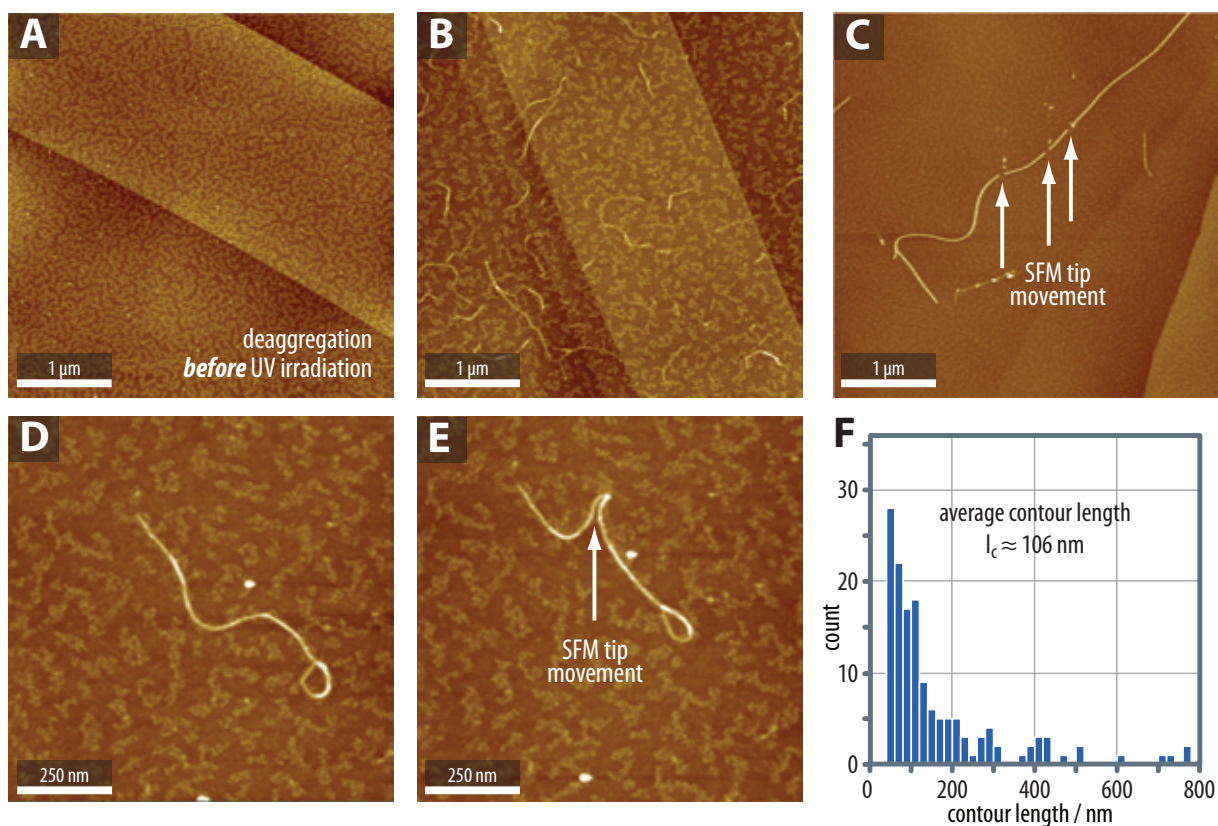


**Figure 88:** A) SFM image of a non-polymerized solution of **93** after the addition of HFIP as hydrogen-bond breaking cosolvent revealed that no fibrillar features remained in solution. B) An image of a polymerized **93** solution revealed the presence of fibrillar features; C) While a manipulation of the supramolecular polymers with the SFM tip destroyed the non-covalently connected polymers, D, E) a covalently captured fibril stayed intact upon the addition of HFIP and could be moved on the surface without destruction. F) A histogram analysis of the contour lengths of a large number of polymerized fibrillar features gave an average contour length of 106 nm.

SFM imaging also allowed for an estimation of the molecular weight of the polymers which had not been possible by GPC (the material was not eluted) or light scattering (the solutions could not be filtered). For this purpose, solutions of **P93** were treated with HFIP to dissolve the non-polymerized material, and a statistical relevant number of SFM images was recorded. A histogram analysis of the contour lengths of a large number of intact helical fibrils revealed an average length of 106 nm (Figure 88F), which translated into at least 200 repeating units given the poly(diacetylene) identity period of 4.91 Å.

In summary, the successful conversion of the supramolecular polymers into covalent macromolecules was unambiguously proved. Moreover, the polymerization was shown to proceed under retention of the previously attained hierarchical structures. According to the developed model for the hierarchical structure formation of the macromonomers (Section 3.3), this would translate into the formation of polymers with right-handed quadruple-helical quaternary structures in cases of **P92** and **P93**, whereas right-handed, double-helical poly(diacetylene)s were formed in the cases of **P96** and **P97**, as will be investigated in the next section.

## 3.5 Chiroptical Properties of the Poly(diacetylene)s

### 3.5.1 Evidence for Helical Poly(diacetylene)s in Solution

Circular dichroism (CD) spectroscopy is a powerful tool to confirm the presence of helical structures in solution and has already been used extensively for the determination of secondary structures of conjugated polymers like poly(acetylene)s<sup>59–63</sup> as well as poly(diacetylene)s.<sup>165,167,168</sup> While initial CD experiments on polymerized solutions of several macromonomers revealed a strong CD activity of both the poly(diacetylene) backbone and chromophores such as the Fmoc end groups, the results were not reproducible in so far that the sign and the intensity of the CD signals was changing from one measurement to the next even if the same sample was investigated (Figure 89).

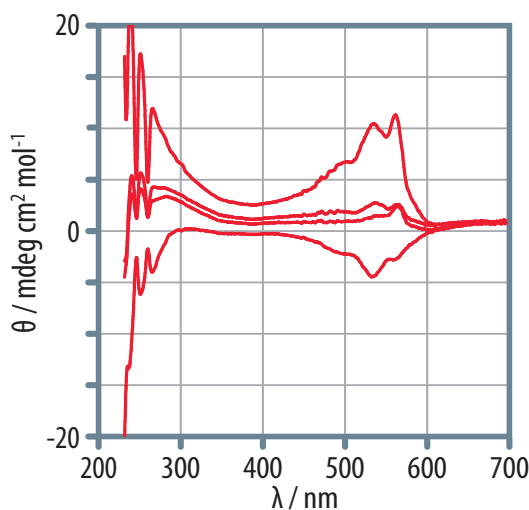


**Figure 89:** Representative CD spectra of the same sample of **P96** measured four times revealed that the spectra were not reproducible due to CIDS.

Obviously, the measurements were influenced by side-effects that were responsible for the “artifacts” in the spectra, most likely due to the circular intensity differential scattering (CIDS) effect.<sup>166,209</sup> The latter occurs whenever objects exhibiting sizes on the order of the wavelength of the incident light are present in solution. As well-ordered one-dimensional objects would not cause CIDS, large aggregates were apparently present in solution due to a suboptimal sample preparation, which had to be improved substantially. First of all, the CD spectra should be measured directly after polymerization to limit a post-polymerization aggregation of the fibrillar features in solution. Secondly, 1,2-dichloroethane (DCE) was used as the solvent instead of DCM in order to perform temperature-dependent measurements. Thirdly, the concentration was reduced to  $0.5 \text{ gL}^{-1}$  and the ultrasonication prior to the polymerizations was extended to at least 30 min at  $60^\circ\text{C}$  followed by an aging of the

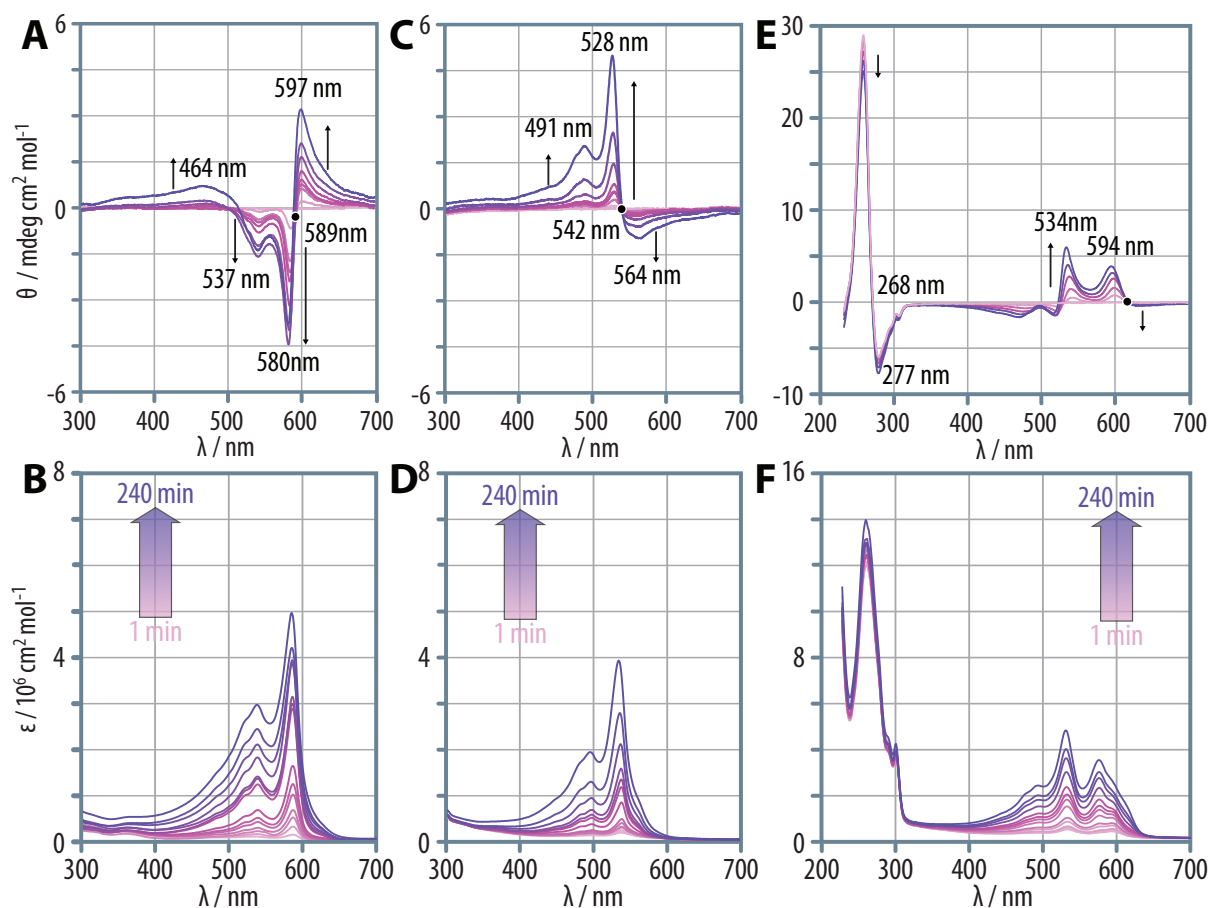


**Figure 90:** *A,B*) The polymerization of **93** was accompanied by the usual appearance of UV-vis absorption bands. A positive bisignate Cotton effect could be observed by CD spectroscopy right from the beginning of the reaction indicating a chiral environment of the poly(diacetylene) backbone. *C,D*) In the case of **96**, the CD signal exhibited a negative Cotton effect; *E,F*) The emerging UV-vis bands in the case of the polymerization of **P97** were more complicated and indicative of a mixture of PDA species; the corresponding CD spectra also showed a poorly developed negative Cotton effect for the highest wavelength absorption.

solution for at least 1 h. And finally, a black bandpass filter was used during the UV-induced polymerizations in order to limit photo-oxidative side reactions. The improved sample preparation led altogether to “cleaner” UV signatures already in the course of the polymerizations (Figure 90A-F). Accordingly, **P93** exhibited a global absorption maximum at 589 nm with a second, clearly resolved band at 540 nm. **P96** showed a nearly unchanged spectrum as compared to the DCM reactions exhibiting a main absorption at 535 nm accompanied by a second one at 496 nm. In comparison to **P93**, the spectra looked nearly congruent and blue-shifted by 54 nm. Finally, the spectra of **P97** featured the highest absorption at 534 nm with a shoulder around 495 nm but also a poorly resolved absorption peak at 587 nm. The final extinction maxima  $\epsilon_{\max}$  reached values between 4 and  $5 \cdot 10^6 \text{ cm}^2 \text{ mol}^{-1}$  after 2 h of irradiation time. In the associated series of CD measurements, strong signals in the absorption region of the polymer backbones as well as the Fmoc chromophore emerged right from the beginning of the irradiation and intensified over time. Consequently, the polymers were in a chiral environment. Most

interestingly, the CD signal of the polymer backbone of **P93** exhibited a positive bisignate Cotton effect with a zero-crossing at the position of the highest wavelength UV absorption maximum at 588 nm combined with a negative CD activity with a minimum close to the second UV absorption maximum at 536 nm. On the other hand, polymers **P96** and **P97** showed a negative bisignate Cotton effect near the respective positions of the highest wavelength absorptions (542 nm as well as 603 nm) and positive CD activities with a maximum close to the lower absorption bands. This was in perfect agreement with the SFM images that had shown a right-handed helicity for the fibrils formed by **93** while **96** and **97** self-assembled into left-handed helical ribbons. Obviously, the supramolecular structures present in solution were, at least, closely related to those observed in dried films.

Additionally, Raman spectra were measured that showed the poly(diacetylene) C=C and C≡C vibrational frequencies at 1506/2133 cm<sup>-1</sup> (**P93**), 1512/2139 cm<sup>-1</sup> (**P96**), and 1492/2116 cm<sup>-1</sup> (**P97**), respectively (Figure 91A-C). It was, thus, possible to identify the shorter wavelength absorptions in the UV spectra of **P93** and **P96** as vibronic fine-structures.<sup>210</sup> The spectra of **P97**, on the other hand, were more complicated, indicating that more than one species of poly(diacetylene)s was present in the polymer solutions as opposed to the other cases. Remembering the two different types of ribbons that were observed in SFM images of **97** (Figure 66) one might assume that these different types of aggregates were also present in solution yielding poly(diacetylene)s in different conformations.

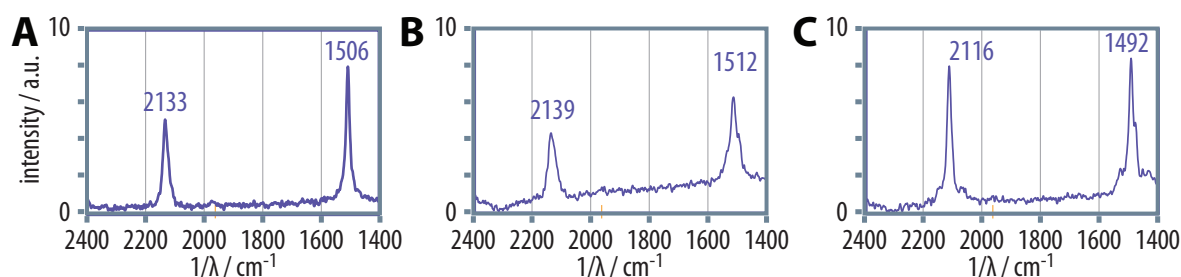


**Figure 91:** Raman spectra of A) **P93**; B) **P96** and C) **P97** in CHCl<sub>3</sub> proved the successful conversion to poly(diacetylene)s and did not contain any hint to monomeric materials. The vibrational frequencies allowed to analyse the UV-vis spectra.

We used the obtained Raman frequencies to calculate the effective conjugation length of the polymer backbone<sup>210</sup> using models developed for poly(diacetylene)s<sup>170</sup> as well as poly(acetylene)s.<sup>164</sup> The obtained values predicted highest wavelength absorptions between 433 and 472 nm in case the PDA model was used as well as 493 to 558 nm in the other. Both series of values were obviously not in agreement with the experimental data since the measured absorption bands were located at much higher wavelengths in all investigated cases. Obviously, these single-chain models were inapplicable to polymers **P93**, **P96** and **P97**. This assumption was further supported by the corresponding CD

spectra that exhibited signatures which perfectly coincided with the helix sense of the aggregates observed in SFM. More importantly, the *bisignate* nature of the CD signals of the polymer backbones can be interpreted to result from an excitonic coupling of several chromophores in all three cases.

In summary, the UV and CD spectra can only be explained if the formation of spectroscopic aggregates of the poly(diacetylene) backbones is assumed. This finding is well in line with the publication by Giesa *et al.*<sup>170</sup> who had demonstrated that  $\lambda_{\max} = 551$  nm represents the upper absorption limit of a single-chain poly(diacetylene) and that all higher absorptions needed a further explanation. Furthermore, the sign of the CD signals suggested that the superstructures found in the SFM images (Section 3.4.3.2) were converted into conjugated polymers under retention of their architectures and that our model of multiple helical assemblies was correct also in solution.

### 3.5.2 Comparison of Supramolecular Aggregates versus Covalent

#### Polymers

The Fmoc group in **97** gave rise to a strong UV signal at 264 nm accompanied by an intense CD activity. The latter fact in itself proved a chiral aggregation of the fluorenyl groups and, accordingly, the macromonomers in solution. While the intensity of the Fmoc group's UV signal was, of course, constant during the polymerization of **97**, its CD signal slightly decreased (Figure 90G). This fact may be the result of small geometrical changes during the polymerization since the inter-strand packing of 4.8 Å in the  $\beta$ -sheets was changed to the identity period of the poly(diacetylene) backbone which is 4.91 Å. Another explanation could be the stabilization of the  $\beta$ -sheet array because  $\beta$ -sheets themselves give rise to CD signals in the range of 180 to 240 nm. In case such a signal (which we could not measure directly due to the intransparency of chlorinated solvents below 230 nm) increased, the combined signal with the Fmoc chromophore would be changed as well.

The addition of hydrogen-bond breaking cosolvents such as TFA or HFIP to solutions of macromonomer **97** and **P97** led to a drastic decrease of the CD activity at 264 nm (Figure 92). In more detail, the addition of 0.1 vol% TFA completely erased the CD signal of the non-polymerized solution whereas 2 vol% of the much weaker reagent HFIP were needed. This experiment proved that the CD signal of the Fmoc-chromophore was not caused by the molecular chirality but rather by the chiral, supramolecular assembly of the chromophores. A treatment of the polymerized sample showed a distinctly different behavior. Here, more than 4 vol% of TFA were needed to cancel the CD signal. Obviously, the oligopeptide side chains were efficiently held together by the covalent polymer backbone. This became even clearer when HFIP was titrated to a solution of **P97**, since a complete loss of CD activity could not even be reached. The final CD signal still had 28% of the original intensity even after 20vol% of HFIP had been added.

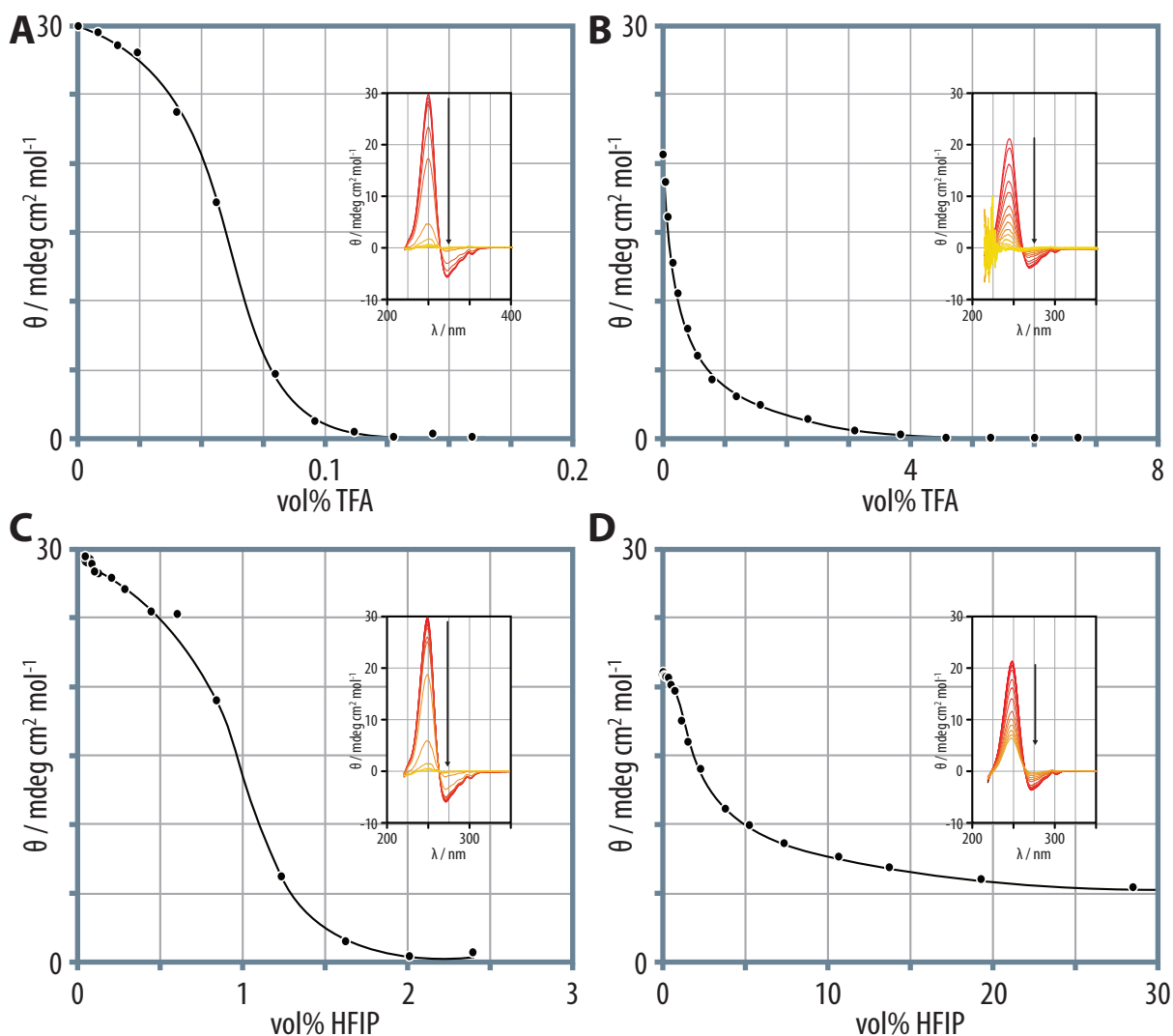


**Figure 92:** A) A titration of a solution of **97** with TFA led to a fast cancellation of the Fmoc group's CD signal; B) The same process required much more acid in the case of **P97**, indicative of a stabilization of the oligopeptide side chains due to the covalent capture. C, D) When HFIP was used as the cosolvent, much larger amounts were needed to erase the CD signal of the Fmoc group for the non-polymerized solution while the polymerized sample could not be deaggregated completely.

The thermal stability of the aggregates was investigated by slowly heating the sample in the CD spectrophotometer from 20 to 70 °C. The CD signal of the non-polymerized sample decreased dramatically by more than 50% (Figure 93A). Interestingly, cooling the solutions back to 20 °C did not lead to a recovery of the CD signal, even after aging of the solution for 24 h. Obviously, the molecular disorder in the aggregates was increased during the heating process which was not easily reversible at room temperature. This observation explains why a thorough sample preparation using ultrasonication is very important for a successful topochemical polymerization. When the polymerized sample was investigated under the same conditions, a much weaker effect on the Fmoc group's CD signal was observed (Figure 93D). Furthermore, the signal nearly reached its starting value directly after cooling

back to room temperature, although a weak hysteresis behavior was observed. The polymers' behavior resembled that of a mechanical spring in that a certain degree of disorder within the oligopeptide side chains may have been induced during the heating process, but the system immediately folded back into its original conformation upon cooling.

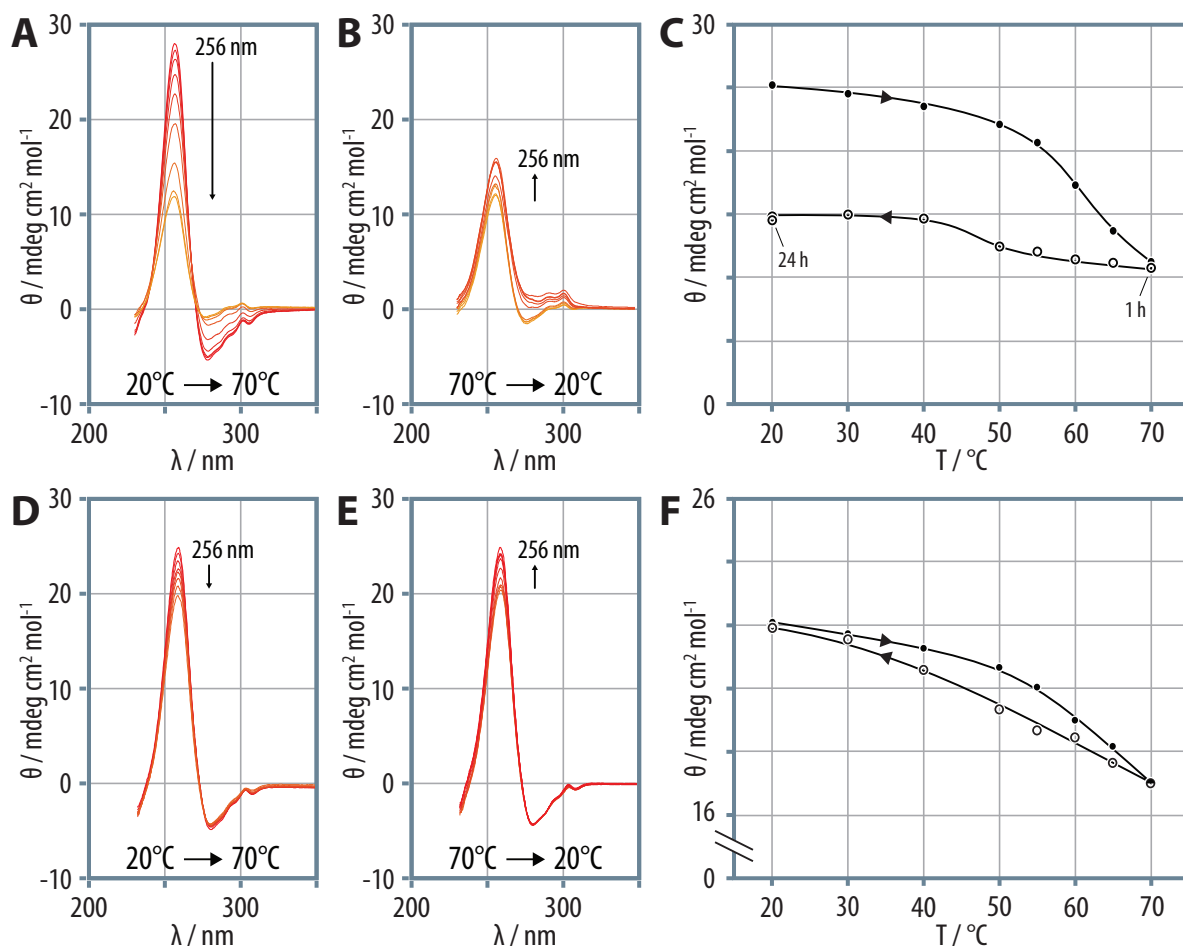


**Figure 93:** A) The CD activity of the Fmoc chromophore was substantially decreased by heating the sample from 20 to 70°C; B) Upon cooling back to 20°C, C) the signal intensity recovered only partially. D-F) The polymerized material showed a much weaker effect which was directly reversed upon cooling, showing only small hysteresis.

In summary, the oligopeptide side chains of the poly(diacetylene)s were apparently stabilized against a deaggregation by hydrogen-bond breaking cosolvents or a thermal denaturation as compared to the supramolecular aggregates prior to their covalent capture. Furthermore, the assumption that the topochemical polymerization of the diacetylenes in the self-assembled supramolecular polymers proceeded under retention of the previously attained hierarchical structures was strongly supported by CD spectroscopy. The appearance of a CD activity right from the beginning of the polymerization clearly proved the helical conformation of the polymer backbones. Furthermore, the op-

posite sign of the bisignate Cotton effect of, on the one hand, **P93** as well as **P96** and **P97** on the other hand was well in line with the SFM images showing an opposite helix-sense of the aggregates.

### 3.6 Solvatochromism and Conformational Transitions

During the denaturation experiments using TFA or HFIP, color transitions of the polymerized solutions from blue to yellow had been observed (Figure 94). This highly interesting behavior of poly(diacetylene)s (Section 1.3.3) deserved a systematic investigation.

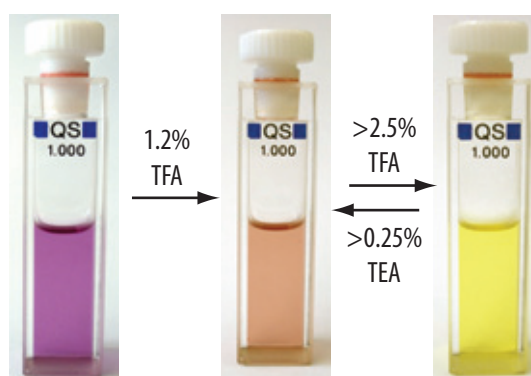


**Figure 94:** Photographs of the blue, red and yellow solutions of **P93**.

Thus, DCE solutions of **P93**, **P96** as well as **P97** were titrated with TFA or HFIP, and the resulting changes in the chiroptical properties were monitored by UV-vis, CD and Raman spectroscopy. All spectroscopic investigations were carried out using the same batch of polymerized solutions after 4 h of UV irradiation at 50 °C in DCE. Upon the addition of TFA, all polymer solutions showed two-step color changes from blue to red and then to yellow, and the corresponding UV spectra experienced significant hypsochromic shifts. These two solvatochromic transitions were, in all cases, associated with two isosbestic points (Figure 95).

Thus, the blue-purple solution of **P93** exhibited a highest wavelength UV absorption at 589 nm with a shoulder at 540 nm and experienced a hypsochromic shift to a spectroscopic “red state” upon the addition of about 1.2 vol% TFA. The global absorption maximum was shifted to 519 nm with a shoulder at 487 nm. A second hypsochromic transition to the yellow state was complete after the addition of 2.5 vol% TFA, leading to a featureless UV absorption with a maximum at 459 nm (Figure 95). The overall process exhibited two clear isosbestic points at 536 and 469 nm that implied the presence of two independent transitions involving three species.

Although solutions of **P96** attained a red-violet color after UV induced polymerization, also in this case, the deaggregation process proceeded in two consecutive steps. First, the spectroscopic



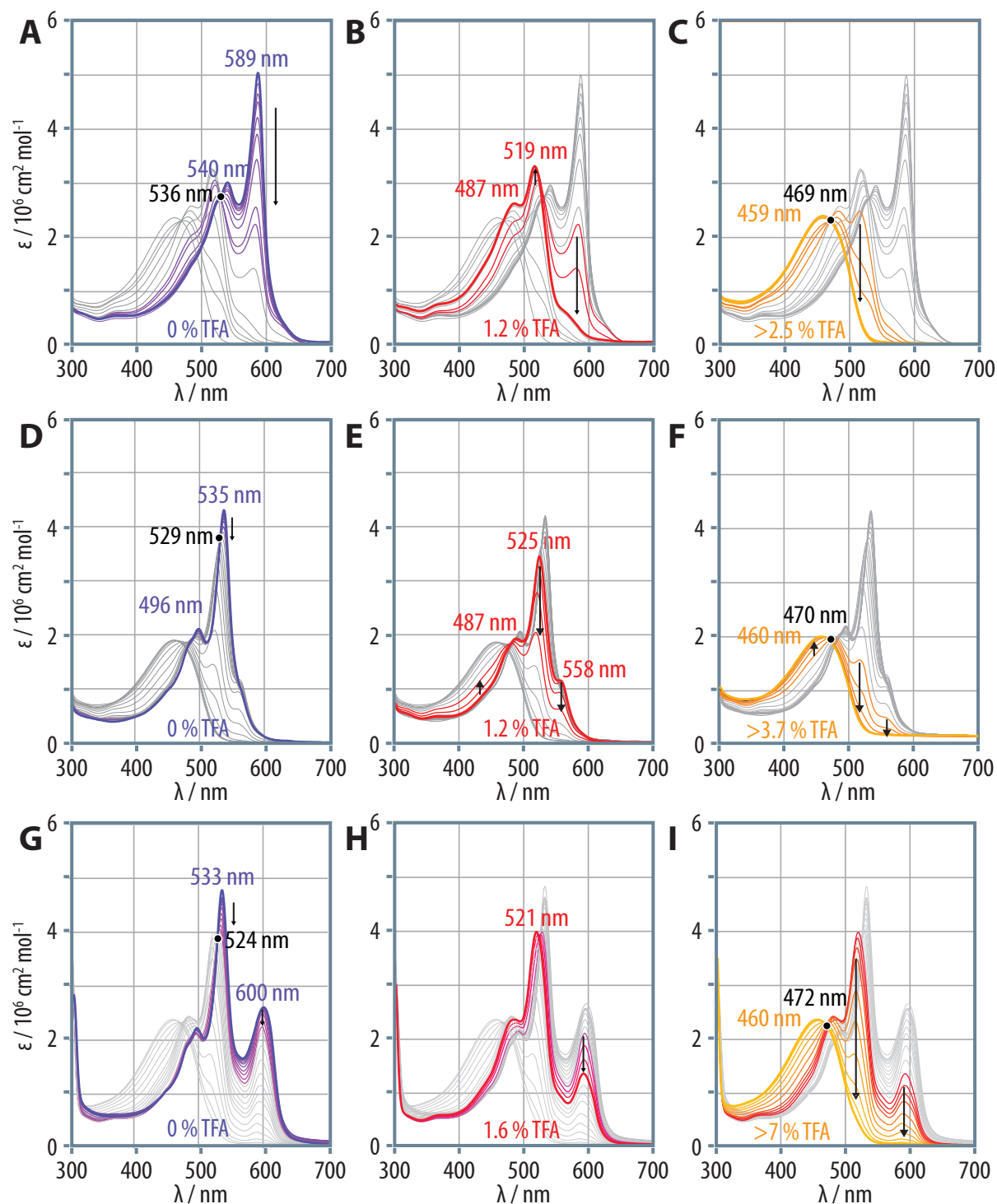


**Figure 95:** A-C) The UV-vis spectra of **P93** experienced a strong hypsochromic shift upon addition of TFA during the blue-red as well as the red-yellow transitions; both featured isobestic points; D-F) **P96** and; G-I) **P97** showed a similar behavior. The transitions were, however, not so distinct, especially in the latter case. The ultimately reached yellow form exhibited nearly identical spectra for all derivatives.

“blue state” with a highest wavelength UV absorption at 535 nm and a shoulder located at 495 nm was converted into a spectroscopic “red form” with the global absorption maximum at 525 nm together with two shoulders at 560 and 488 nm respectively at a volume fraction TFA of 1.2%. A yellow solution

exhibiting a featureless absorption band at 460 nm was then reached after the TFA content exceeded 3.1 vol% (Figure 95). Furthermore, the two isosbestic points at 529 and 469 nm indicated a distinct two-step process for the transition from blue to red to yellow.

The behavior of **P97** was similar although the transitions were not so clear since the blue-purple solution probably already contained a mixture of different spectroscopic species. This was further supported by the fact that the exact position and intensity of the highest wavelength absorption at 600 nm was hard to reproduce between different polymerization batches. Nevertheless, the titration of up to 1.6 vol% TFA triggered a color change to red which was reflected by a hypsochromic shift of the global UV maximum from 533 to 521 nm, and a 50% decrease of the UV absorption at 600 nm. The continued addition of TFA (7 vol%) led to the expected color transition from red to yellow, and a second hypsochromic shift from 521 to 460 nm (Figure 95) was observed. Again, two isosbestic points at 524 as well as 472 nm were supportive of a two-step process.

Spectroscopic transitions involving more than two species can be analyzed by plotting extinction ratios at fixed wavelengths chosen from the affected spectral regions. Thus, we chose the positions of the UV absorption maxima of the blue, red, and yellow form of **P93** (588/520 vs. 469/520), **P96** (534/524 vs. 460/524) and **P97** (588/520 vs. 469/520) and plotted them against the volume fraction of TFA (Figure 96). The consecutive and cooperative nature of the two transitions is obvious in the case of **P93**. At a TFA content of 0.9-1.2 vol%, the first transition was almost completed and the highest UV absorption intensity for the red form was observed, while the red-to-yellow transition had not yet started. By contrast, the conversions of polymers **P96** and **P97** proceeded much more gradually, and a coexistence of all three forms was observed over a wide range of TFA concentrations.

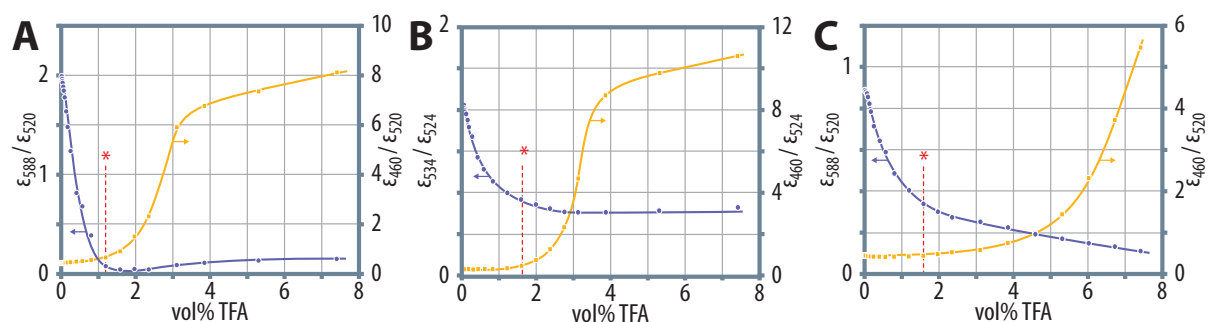


**Figure 96:** A) A plot of the extinction ratios at the UV absorption maxima revealed two clearly consecutive steps for the transition of **P93** while B,C) the processes in the case of **P96** and **P97** were more gradually, i. e., all species coexisted over a range of TFA concentrations. While the blue-to-red transition is depicted by blue curves, the yellow curves represent the second spectroscopic transition. The red asterisk denotes the cosolvent content at which the overall highest absorption for the red forms was observed.

We repeated similar experiments replacing the TFA by the much less acidic HFIP. While in principle, the same transitions were observed for **P93**, the second transition to yellow was not complete even at a HFIP content of 44 vol%. The isosbestic points were the same as in the TFA titration corroborating that the same solvatochromic transitions occurred. In the case of the other two polymers, the second transition was not even achieved while the first one showed the same isosbestic point as in the case of the TFA treatment. Apparently, the polymers were more stable due to the increased number of hydrogen-bonding sites.

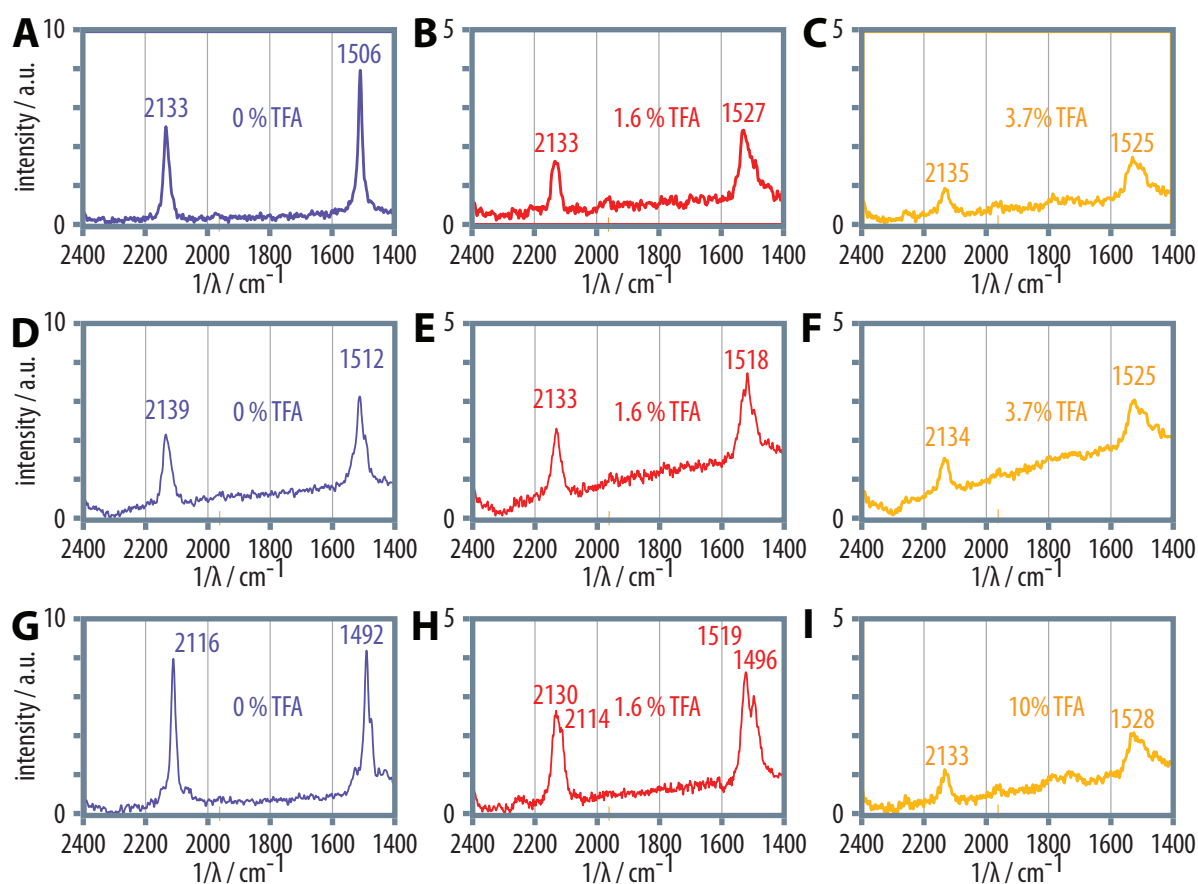


**Figure 97:** A-C) **P93** showed a marginal decrease in the double bond vibrational frequency from the blue to the red form, while the transition to the yellow form did not significantly influence the signal. The band of the triple bonds was almost unaffected during the whole process; D-F) **P96** showed a gradual decrease in the C=C vibration and also the C≡C band shifted a bit to lower wavenumbers; G-I) **P97** experienced the largest shifts in both bands during the blue-red transition. A mixture of bands was observed for the red form while the yellow state was nearly identical in all cases.

The solvatochromic transitions induced by TFA addition to solutions of all three polymers in  $\text{CHCl}_3$  were accompanied by an increase of the vibrational frequency of the C=C bonds, while the C≡C bonds did not show a continuous change in vibrational frequency as was observed by Raman spectroscopy. Thus, the double bond vibration of **P93** significantly changed during the transition from blue ( $1506\text{ cm}^{-1}$ ) to red ( $1527\text{ cm}^{-1}$ ). However, the second transition did not significantly affect

the position of the band at all ( $1525\text{ cm}^{-1}$ , Figure 97). The signal attributed to the  $\text{C}\equiv\text{C}$  bonds stayed at  $2133\text{ cm}^{-1}$  during the first transition and was also unaffected by the second one ( $2135\text{ cm}^{-1}$ ). **P96** showed a more gradual decrease of the vibrational frequencies from  $1512\text{ cm}^{-1}$  in the blue state to  $1518\text{ cm}^{-1}$  in the red state to finally reach a value of  $1525\text{ cm}^{-1}$  in the yellow state. The triple bonds encountered a slight change in this case ( $2139$  to  $2133\text{ cm}^{-1}$ ). During the red-to-yellow transition, however, the vibration was virtually constant ( $2134\text{ cm}^{-1}$ ). **P97** showed more complicated spectra. The blue solution exhibited signals at  $2116$  and  $1492\text{ cm}^{-1}$  for the triple and double bonds. Upon the addition of TFA, the  $\text{C}\equiv\text{C}$  vibration changed to  $2130\text{ cm}^{-1}$  while the other band was shifted to  $1519\text{ cm}^{-1}$ . Additionally, the peaks at  $2114$  and  $1496\text{ cm}^{-1}$  close to the initial values indicated the continuous presence of the blue species. Obviously, the two different species of PDAs that we had found in UV-vis spectroscopy were also clearly distinguishable with Raman spectroscopy. The yellow form of **P97** was nearly identical to the other yellow forms exhibiting bands at  $2133$  and  $1528\text{ cm}^{-1}$ .

The obtained Raman data was again used to calculate the effective conjugation lengths and the corresponding highest wavelength UV absorptions.<sup>210</sup> The poly(diacetylene)-based model predicted values for the highest wavelength absorptions from  $433$ - $472\text{ nm}$  (blue form),  $407$ - $422\text{ nm}$  (red form) and  $405$ - $410\text{ nm}$  (yellow form), whereas the polyene based model furnished values from  $493$ - $558\text{ nm}$  (blue),  $452$ - $476\text{ nm}$  (red) and  $449$ - $457\text{ nm}$ . Again, the polyene model explained the experimentally obtained values better, but still underestimated the highest wavelength absorption, especially, for the blue and red forms. Only the values obtained for the yellow state were reasonable. Furthermore, the Raman bands were only marginally shifted during most transitions; the accompanied hypsochromic shifts in the UV spectra were, however, considerable. Obviously, the single-chain models were not applicable to the blue and the red forms, and the color transitions were caused at least partially by aggregation phenomena. In consequence, the blue and the red form were considered as two different forms of spectroscopic aggregates of the PDA backbones that were transformed into one another by the addition of TFA or HFIP, whereas all superstructures are most likely completely deaggregated when the yellow state is reached.

Most importantly, the observed solvatochromic transitions were associated with drastic changes in the CD activity. Thus, the TFA titration of the blue solution of **P93** started with an almost complete loss of the positive bisignate Cotton effect at  $588\text{ nm}$  after  $0.6\text{ vol}\%$  of acid had been added (Figure 98). The continued addition of more TFA led, however, to the recurrence of a CD signal with a negative, bisignate Cotton effect and a zero crossing at the position of the highest wavelength absorption of the “red form” of **P93** at  $524\text{ nm}$ . A second positive CD signal was observed in the shoulder of the UV band located near  $487\text{ nm}$ . This reversion of the CD activity during the transition from the blue to the red form may be interpreted in terms of a helix-sense inversion. Thus, the right-handed helical

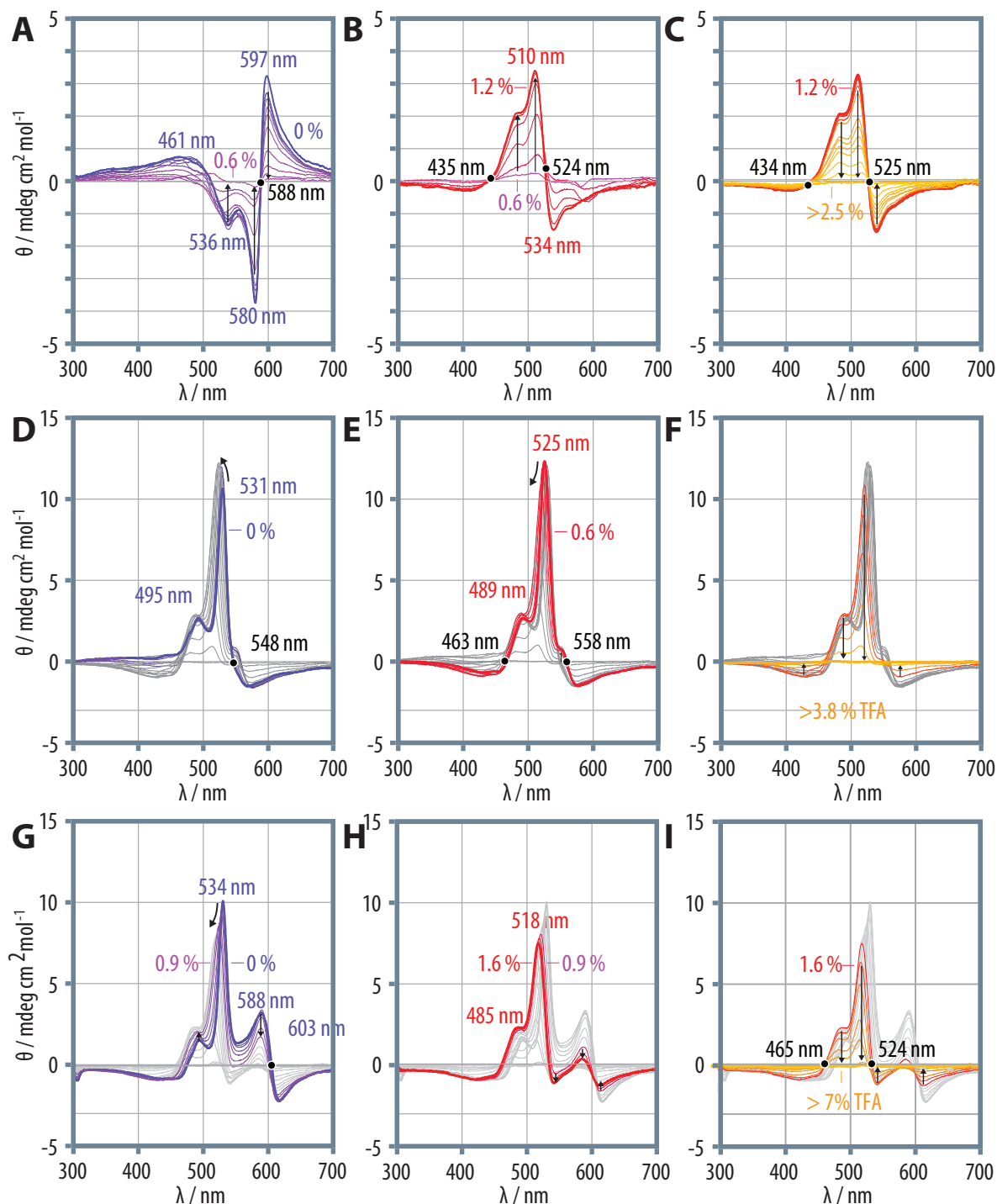


**Figure 98:** A) The titration of TFA to the blue DCE solutions of **P93** started with a complete loss of the bisignate positive Cotton effect; B,C) the continued addition of acid led first to the appearance of a bisignate negative CD activity in the red state and an ultimate loss of the signal in the yellow state; C-F) **P96** did not change the sign of the CD activity during the transformation to the red form but experienced a shift from 530 to 525 nm. The CD signal disappeared in the yellow form; G-I) A similar behavior was found for **P97**; however, the spectra were not so clear due to the mixture of PDA species in the blue form.

superstructures present in the blue state seemed to be converted into left-handed superstructure in the “red state”. The intermediate loss of CD activity which exhibited an isosbestic point at the zero

crossing at 588 nm could be explained by the coexistence of left and right-handed helices the circular dichroism of which annihilated each other at a certain point. During the second transition to the final yellow form, the CD activity continuously decreased until it completely disappeared at a cosolvent content of 2.5 vol%. Obviously, the helical superstructures in the “red form” were completely dissolved, resulting in a random coil conformation which was, of course, CD-inactive.

On the contrary, the supposedly left-handed helices that were present in the blue form of **P96** did not change their helix-sense during the transition to the red state since the negative unsymmetric Cotton effect just shifted from 535 to 530 nm while the overall peak shape did not vary at all upon TFA addition (0.6 vol%). In combination with the Raman data, the assumption that the blue state contained mainly only one species was still reasonable. Apparently, this aggregated species underwent a conformational transition to the red state under retention of a left-handed helicity. Upon further addition of TFA, the CD signal at 530 nm started to decrease. At 3.8 vol% TFA content, the yellow form was reached that, again, was completely CD-inactive, obviously due to a random coil conformation. The temporary coexistence of all the forms that was found during the UV study was, thus, also observed in the CD spectra.

The behavior of **P97** was less distinct since the initial state already contained a mixture of species. Thus, upon addition of the first 1.6 vol% TFA, the CD signal with a zero crossing at 603 nm lost in intensity while the global absorption maximum shifted from 534 to 518 nm simultaneously. However, the sign of the bisignate Cotton effect did not change its sign, indicating a conservation of the initial left-handed helix-sense during the transition to the red form. The rather unclear spectrum corroborated the assumption that still two species attaining different conformations were present, as already indicated by Raman spectroscopy. The entire process was, again, completed by the transition to the yellow form that was CD-inactive as in the previous examples.

We repeated the investigations by titrations using the weaker hydrogen-bond breaking HFIP. In summary, all results from the TFA series could be confirmed as far as the solvatochromic transitions were complete. **P93** showed an initial inversion of its CD signal exhibiting the same isosbestic points, and then nearly lost the CD activity. The other derivatives did not change their helix-sense during the blue-red transition. A completion of the final loss in CD activity could not be reached, as in the case of the UV experiments, because the transition to the “yellow form” was not complete.

Interestingly, the red-yellow solvatochromic transition and the associated helix-coil conversions were completely reversible upon the addition of bases such as  $K_2CO_3$ , basic ion exchange resins or triethylamine TEA (Figure 99). Thus, **P93** was first completely deaggregated by the addition of 1.6 vol% TFA and the subsequent addition of 0.4 vol% of TEA (2 drops) to the yellow solution instantaneously changed the color to red again. In the corresponding UV-vis spectrum, the featureless absorption at

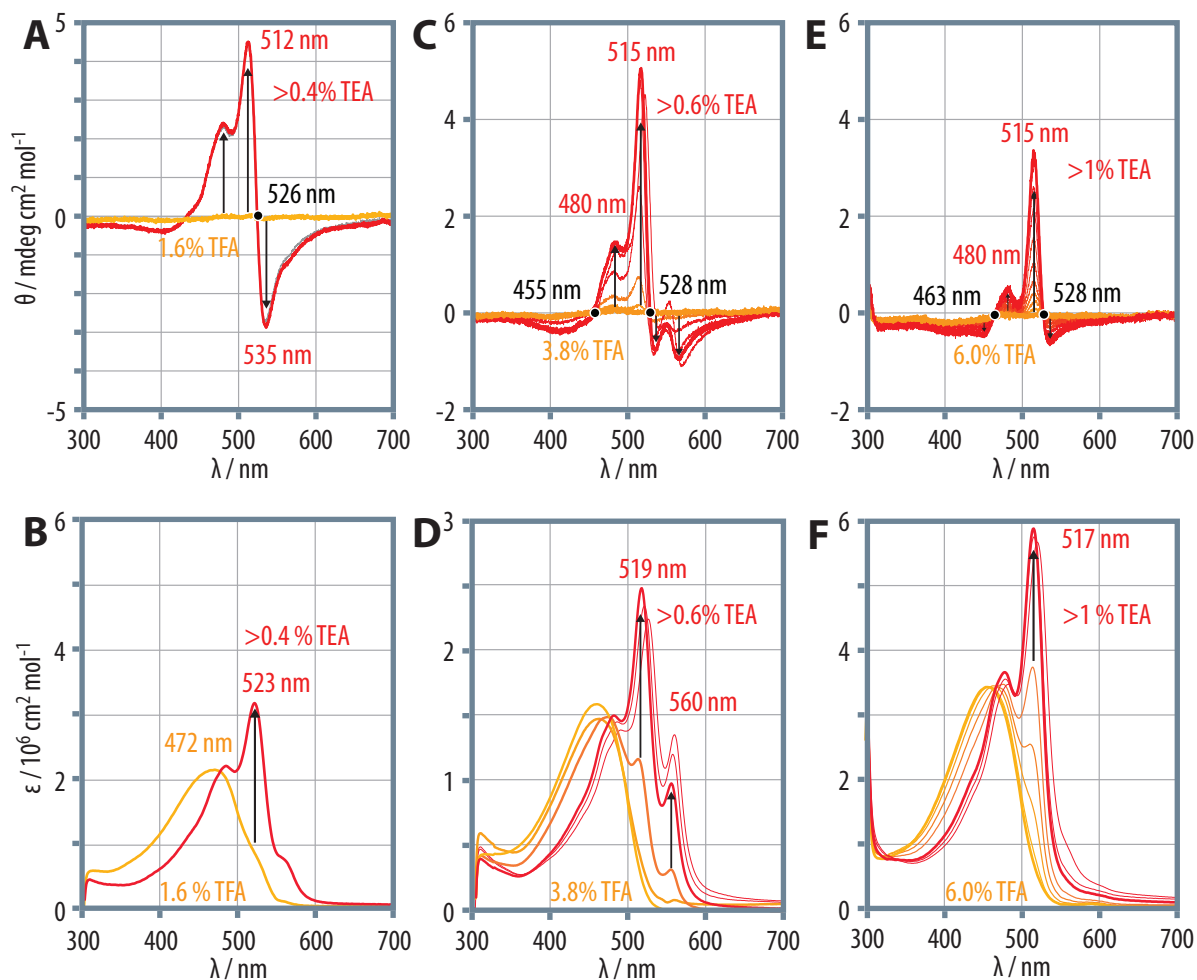


**Figure 99:** A, B) The addition of minor amounts of TEA to the yellow solution of **P93** recovered the “red state” in a pure form. The CD spectrum showed a clear bisignate negative Cotton effect and the UV-vis spectrum almost exactly matched the spectrum observed before for the red solution. C, D) Under similar conditions, **P96** as well as E, F) **P97** could be transformed step-wise to their “pure” red forms, giving rise to negative Cotton effects and cleaner UV-vis spectra than observed before.

472 nm experienced a pronounced bathochromic shift to 523 nm, and a shoulder appeared at 487 nm. Thus, the spectrum we had encountered for the “red state” during the previous transition was almost completely recovered, as well as the extinction coefficient. Following the same experiment with CD spectroscopy revealed that a recurrence of CD activity was observed, as well (Figure 99A,B). A clearly resolved, negative bisignate Cotton effect with a zero crossing at 526 nm appeared which was even more intense ( $\approx 50\%$  higher) than the one found for the “red state” during the initial transition. This may be explained by the exclusive presence of left-handed helical superstructures in this case, whereas the red solution obtained after the deaggregation of the “blue form” may still have contained right-handed species. The intensification may have been caused by a CIDS effect due to potential aggregation phenomena, as well. However, we did not find any further hints to such an effect, since the shape of the spectrum was in all other regards unsuspecting.

Analogous experiments were carried out with **P96** and **P97** which were converted into their “yellow states” by the addition of 3.8 as well as 6.0 vol% TFA. Upon addition of 0.6 and 1.0 vol% TEA, respectively, both polymers were transformed into their “red states”, giving rise to cleaner UV and CD spectra than observed for the mixed states during the deaggregation experiments (Figure 99C-E). **P96** exhibited a UV band at 525 nm having the same two shoulders at 560 nm to higher as well as at 495 nm to lower wavelengths which had already been present in the spectra of the red solutions before. The CD activity featured a negative bisignate Cotton effect with zero crossings at 455 as well as 528 nm and reached almost half the intensity as in the case of the TFA titration. This is well in line with the expectations, since the other two forms were not present this time. The UV-vis spectrum of the recovered red solution of poly(diacetylene) **P97** showed a global absorption maximum located at 523 nm which exhibited the known shoulder at 485 nm. In contrast to the spectrum of the “red form” that was recorded after the blue-red transition, the peak at higher wavelengths (600 nm) that had been ascribed to the “blue species” was now completely absent explaining the 50% increase in the extinction coefficient at 523 nm. Apparently, the “red form” was produced “in pure form” in this case, as well. The corresponding CD spectra showed a negative Cotton effect as in the cases of the other polymers this time containing zero crossings at 463 and 528 nm.

In the case of **P93**, we investigated the reversibility more in detail once again. The red solution obtained after the addition of TFA and TEA was, once again, treated with the acid (4.4 vol%) in order to reestablish the “yellow state”. The corresponding UV-vis spectrum exhibited a maximum located at 468 nm very close to the value obtained in the first deaggregation process. The subsequent drop-wise addition of TEA led to the formation of a shoulder at 522 nm in the UV-vis spectrum which became the global absorption maximum in the course of the experiment giving rise to an almost identical spectrum as compared to the red solution obtained after the first yellow-red transition. In conclusion, the red-to-yellow transition was completely reversible and the system could be switched back and forth multiple times.

The combination of the entire data that was collected in UV-vis, CD as well as Raman spectroscopy of **P93**, **P96** and **P97** suggested that the red and even more so the yellow forms of all polymers were remarkably similar. This rendered the assumption that all poly(diacetylene)s attained very similar conformational states after the initial blue-red transition very reasonable. Furthermore, the minor changes in the corresponding Raman spectra suggest that the observed hypsochromic shifts cannot be explained to result from a changed conjugation length *alone*. Obviously, the modified interactions between the poly(diacetylene) backbones that were caused by the deaggregation of the laminated  $\beta$ -sheet aggregates contributed to the entire effect. **P93** started from right-handed double-helical fibrils that in total contained four laminated poly(diacetylene) chains. During the first transition, these were



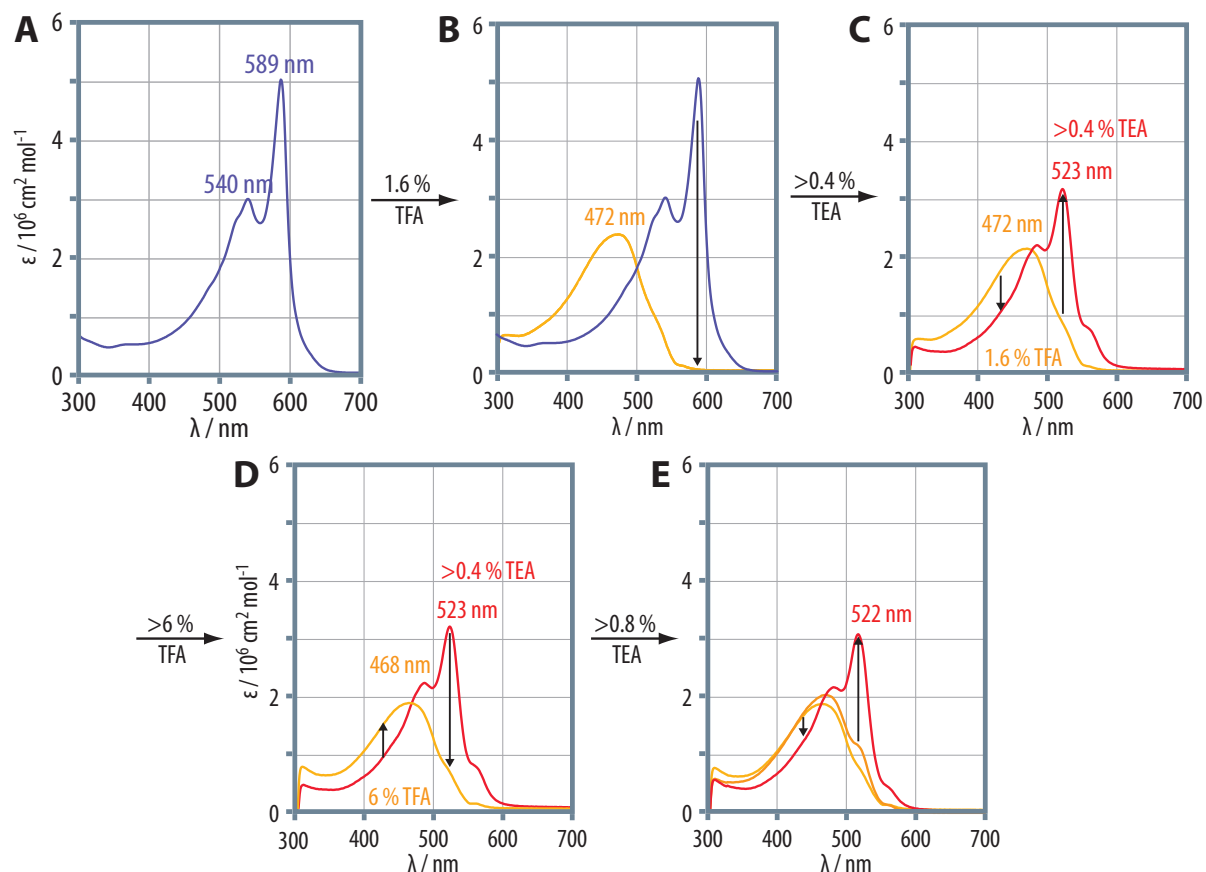


**Figure 100:** The addition of TFA to A) the blue solution of **P93** initiated the transition to B) the “yellow form”. Upon addition of TEA, C) the “red state” was recovered, which was D,E) completely reversible as shown by the repeated addition of more TFA and TEA.

converted into left-handed helical ribbons (two laminated polymer backbones) in a helix-helix transition by an unwinding of the two entwined ribbons. Finally, these ribbons were entirely dissolved to yield single poly(diacetylene) chains in a random coil conformation (Figure 101). By contrast, polymers **P96** and **P97** started from twisted and bent left-handed ribbons that were first converted into another type of left-handed laminated superstructures in a helix-helix transition. This process was, again, followed by a helix-coil transition into single chain random coils (Figure 101). Furthermore, the red-to-yellow transition was found to be completely reversible upon the addition of a base such as TEA. This process furnished the pure “red forms” of all three polymers exhibiting better-resolved CD as well as UV-vis spectra. Apparently, the random coil conformation present in the yellow solutions was transformed back into left-handed helical superstructures in an aggregated state. In conclusion, the hierarchically structured oligopeptide-functionalized poly(diacetylene)s prepared in the course of this Ph. D. thesis showed a rich folding behavior which only finds analogies in the realm of biopolymers. Furthermore, we were able to show that single-chain models only assuming a change of the effective conjugation length within the  $\pi$ -system of poly(diacetylene)s in the course of the sol-

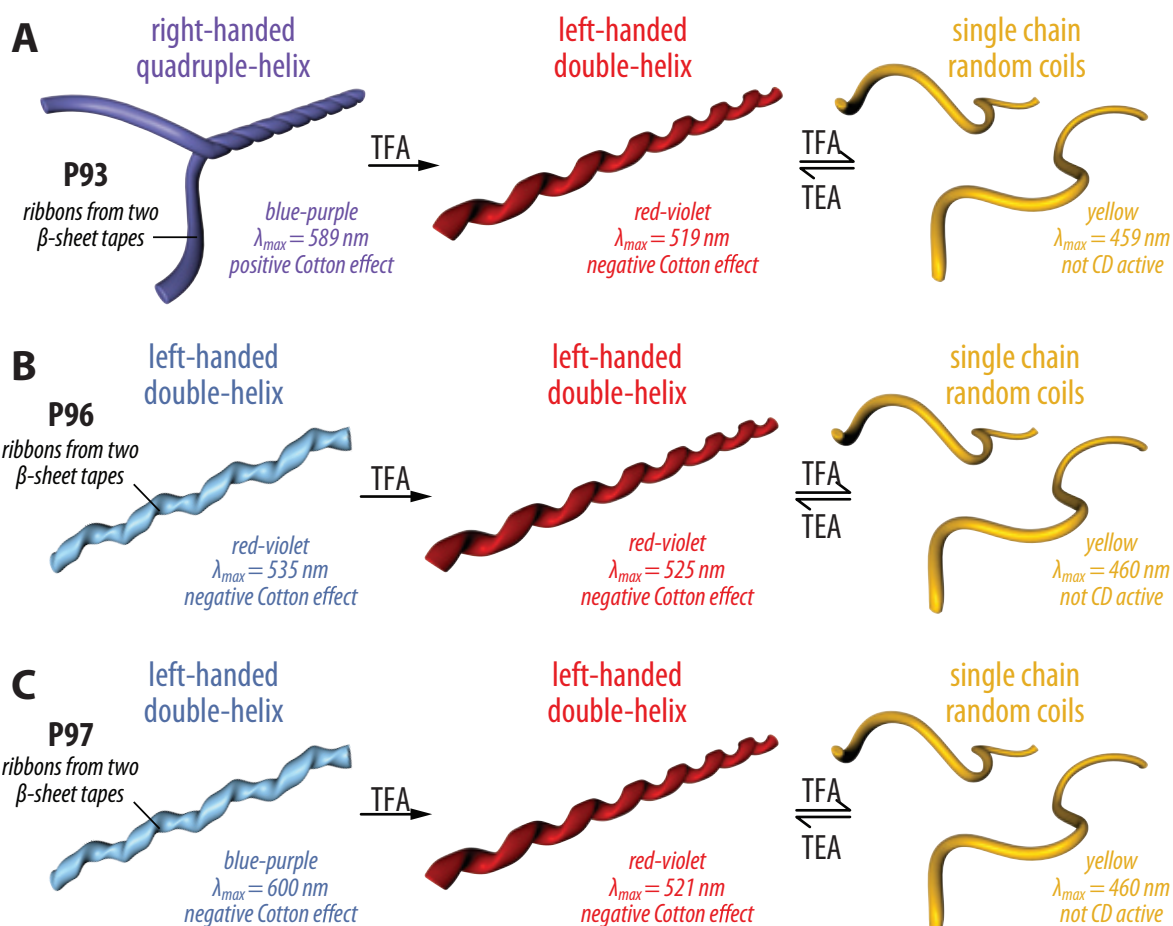


**Figure 101:** A) The blue form of **P93** was found to form right-handed quadruple helices (of  $\beta$ -sheet arrays) in the SFM and exhibited a positive Cotton effect. Upon addition of hydrogen-bond breaking cosolvents, a helix-helix transition under helix-sense inversion was concluded from a negative Cotton effect of the red form. The addition of more TFA (HFIP) led to a CD-inactive yellow form – a random coil structure. B,C) **P96** and **P97** started from a left-handed double helix featuring a negative Cotton effect and experienced a helix-helix transition followed by a helix-coil transition while going to the red and yellow forms. The latter could only be reached by the addition of TFA while HFIP was to weak a deaggregating agent.

vatochromic transitions are insufficient. Apparently, the formation of spectroscopic aggregates of several poly(diacetylene) chromophores has a decisive influence on the optical properties of the material, which could be shown because, in the present system, the aggregation state of the investigated poly(diacetylene)s was well-defined.

### 3.7 Synthesis of Higher Oligo(ethynylene)s

The successful arrangement and subsequent topochemical polymerization of the diacetylene moieties in the self-assembled supramolecular polymers described in the previous sections may be extended toward highly reactive oligo(ethynylene)s by bringing the latter into close proximity in order to use them as  $\pi$ -conjugated precursors for multi-stranded conjugated polymers or even graphite

nano-tapes. Nakanishi *et al.* have investigated the topochemical polymerization of oligoynes in the solid state<sup>211–214</sup> and found that tetra- as well as hexaynes that underwent a 1,4-polyaddition (Figure 102A,B) could be transformed into ladder polymers having a second poly(diacetylene) backbone in conjugation to the first one (Figure 102C) by heating the solid material. A postulated aromatization of such a highly unsaturated system was proposed; however, the spectroscopic evidence was scarce. A rationale for the supposedly failed polyaromatization may be that the required geometric rearrangements had not been possible in the crystalline state. If such a system could be introduced into the more flexible supramolecular polymers obtained from the self-assembly of oligopeptide-polymer conjugates, such a transformation may be more likely. But at least the formation of soluble double stranded poly(diacetylene)s should be possible which would be an attractive research goal in itself. In order to prepare such materials, macromonomers bearing tetra- as well as hexayne moieties were synthesized.

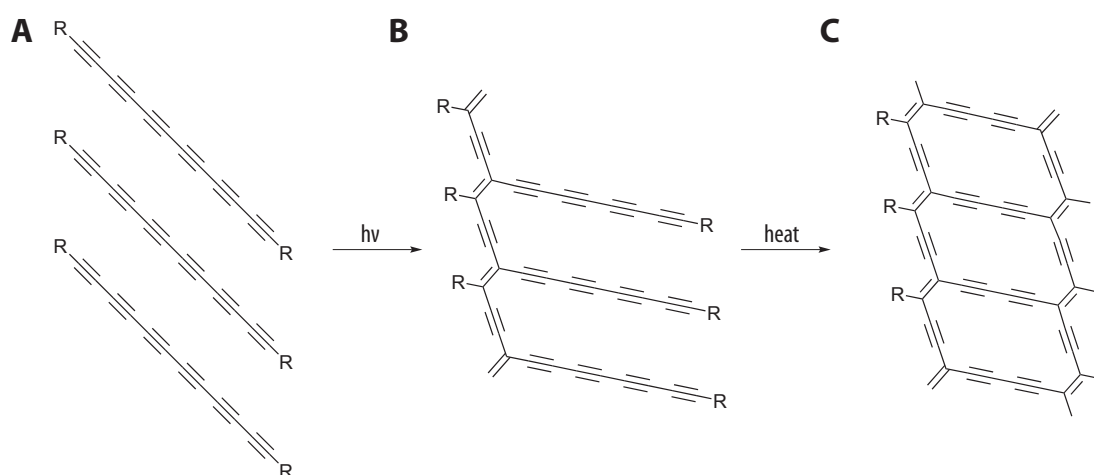
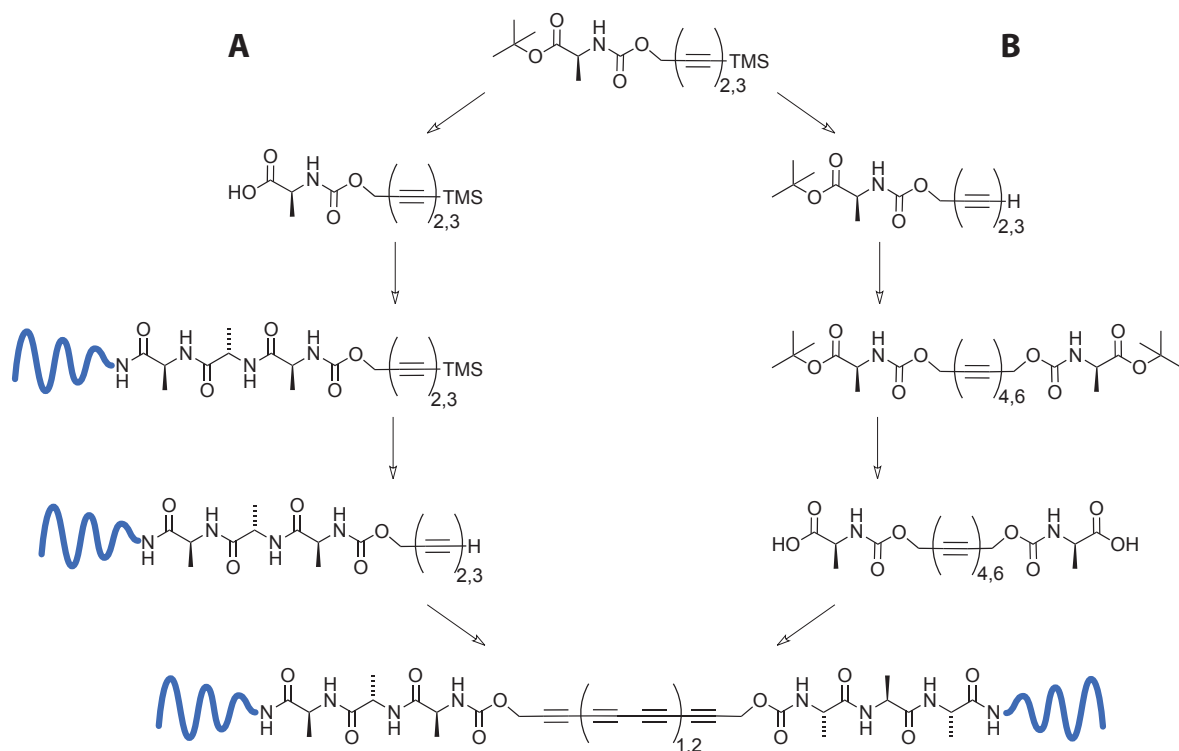


**Figure 102:** A) Hexaynes may undergo a 1,4-polyaddition furnishing B) a tetrayne-substituted poly(diacetylene). C) The latter was converted into a  $\pi$ -conjugated ladder polymer which was proposed to rearrange into a graphite-like structure in an aromatization reaction.<sup>213</sup>

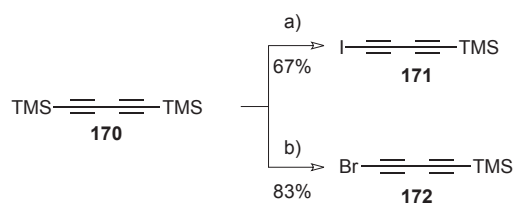
As the synthesis of higher oligoynes is problematic due to the inherent reactivity of the latter, we only planned the synthesis of symmetric target molecules which seemed accessible via two synthetic strategies. The first would require the prefabrication of a tetra- or hexayne which had to be suitably functionalized to allow for a subsequent attachment of the oligopeptide-polymer conjugate, while the second was based on the synthesis of macromonomers bearing terminal di- or triacetylenes which would be homocoupled in the final step (Scheme 45).

Amino acid functionalized terminal di- and triacetylenes were to be made in the beginning of any of the two routes. The TMS protected diacetylene **86** had already been prepared before and was,



**Scheme 45:** The desired oligoynes may be accessible by two possible pathways. *A)* The first strategy starts from TMS-terminated di- and triacetylene-functionalized alanine building blocks, which are first deprotected at the carboxylic acid function and then coupled to an oligopeptide-polymer conjugate. Then, the silyl group is removed to subsequently arrive at the target structures via a final acetylene homocoupling. *B)* The alternative route requires the removal of the TMS-group first followed by an acetylene homocoupling of the amino acid functionalized di- and triacetylenes to furnish prefabricated tetra- and hexayne species. These would then need to undergo the ester deprotection followed by a final peptide coupling to access the desired structures.

thus, available in our lab. The preparation of the corresponding triacetylene **173** required the prior synthesis of a halogenated diacetylene derivative for the Sonogashira reaction (Scheme 46).

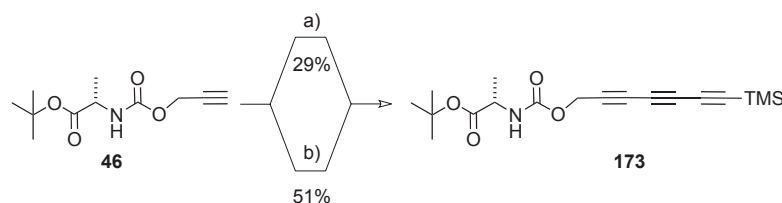


**Scheme 46:** Preparation of halogenated diacetylene derivatives **171** and **172** aimed at the synthesis of oligoynone precursors. *Reagents and Conditions:* *a)* 1. MeLi·LiI, Et<sub>2</sub>O, 16 h; 2. I<sub>2</sub>, -78 °C → r.t., over night; *b)* 1. MeLi·LiBr, Et<sub>2</sub>O, 16 h; 2. Br<sub>2</sub>, -78 °C → r.t., over night.

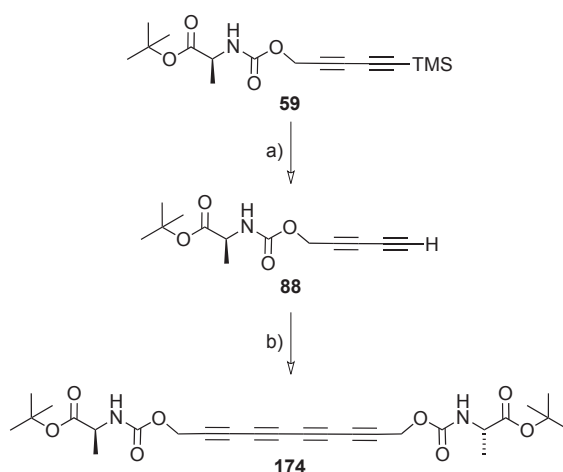
For this purpose, 1,4-bis(trimethylsilyl)butadiyne **170** was reacted with MeLi·LiI in case of the iodination reaction and with MeLi·LiBr in case of the bromination to be sure to obtain the correct halogenated target molecule **171** and **172**, respectively. The same Li-acetylide was formed as an interme-

diolate in both cases which was then quenched with the elemental halogens at low temperature. After an aqueous workup including a treatment with sat.  $\text{Na}_2\text{S}_2\text{O}_3$  solution to remove residual amounts of  $\text{I}_2$ , **171** was obtained as slightly brown crystalline needles. A purification was possible by a sublimation at reduced pressure, and colorless crystals were obtained in 67% yield. The synthesis of the brominated derivative **172** has been previously established in our lab.<sup>174</sup> The material was obtained as a dark brown oil that would only solidify in the freezer. A purification by column chromatography did not remove all impurities but an upper limit of the yield could be given with 83%.

The heterocoupling reaction between **46** and these halodiacetylenes was first attempted with the cleaner iodinated diacetylene. The yield of the heterocoupling product was very low with about 29% due to pronounced side reactions and formation of the homo- as well as the selfcoupling products. When the less reactive **172** was used instead, the product **173** was obtained in an acceptable yield of 51%.



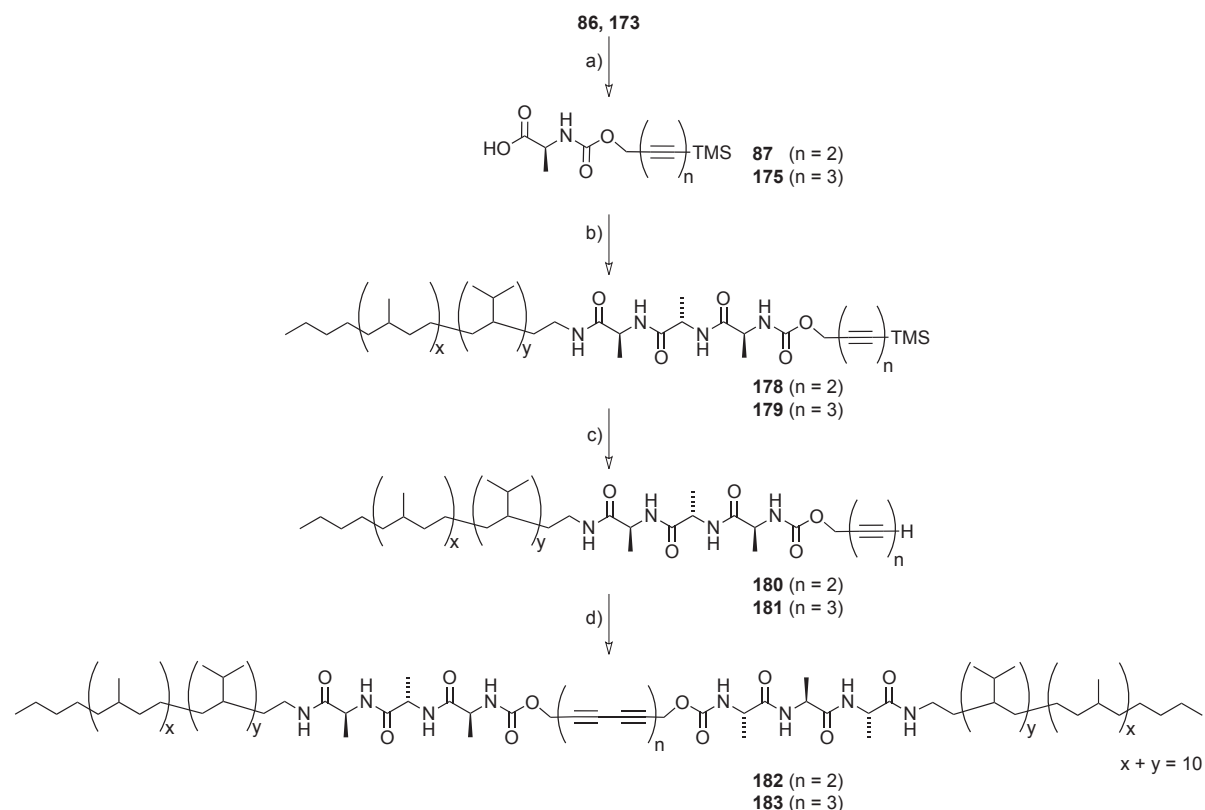
**Scheme 47:** Synthesis of the L-alanine-substituted triacetylene derivative **173**. *Reagents and Conditions:* a) **171**,  $\text{PdCl}_2(\text{PPh}_3)_2$  (2 mol%),  $\text{CuI}$  (10 mol%), DIPA, THF,  $0^\circ\text{C}$ , 3 h; b) **172**,  $\text{PdCl}_2(\text{PPh}_3)_2$  (2 mol%),  $\text{CuI}$  (10 mol%), DIPA, THF,  $0^\circ\text{C}$ , 3 h.



**Scheme 48:** Preparation of the symmetric alanine substituted tetrayne derivative **174**. *Reagents and Conditions:* a) 1.1 eq  $\text{AgOTf}$ , MeOH, EtOH,  $\text{H}_2\text{O}$ , 3 h, r.t.; b) TMEDA,  $\text{CuCl}$ , DCM,  $\text{O}_2$ , r.t.

The feasibility of the envisioned synthesis of amino acid substituted tetra- and hexaynes was to be tested by an acetylene homocoupling. Therefore, the TMS group had to be removed from derivative **86** first. As a removal with TBAF had led to an unusual diacetylene polymerization in solution before (Section 3.1.5.3), we used a milder Ag(I)-promoted methodology, instead.<sup>182</sup> Thus, the starting material was dissolved in a mixture of MeOH, EtOH and H<sub>2</sub>O followed by the addition of a stoichiometric amount of AgOTf. The reaction could easily be monitored by TLC, since the formed silver acetylide had an R<sub>f</sub> value of 0, while the spot of the starting material (R<sub>f</sub> = 0.5) slowly disappeared. After the completion of the reaction, a small excess of KI was added to force the silver to precipitate in the form of AgI while the terminal diacetylene is protonated. After workup and purification, it turned out, that the product **88** was very unstable. Thus, the reaction was repeated and **88** was used directly without purification (Scheme 48). The AgI was filtered off, the solvents were removed (especially the water) and the residue was taken up in dry DCM containing 4 Å molecular sieves. A second DCM solution including TMEDA and CuCl was prepared separately to form the Hay catalyst. Both solutions were combined and stirred over night under ambient atmosphere. A workup by column chromatography gave the tetrayne **174** as a yellowish oil that quickly attained a brown color and started to decompose before it could be characterized. Consequently, we refrained from removing the ester functions or synthesizing the corresponding hexayne species which would be even more elusive.

As this route seemed to be unfeasible, the alternative synthesis of oligopeptide-polymer conjugates equipped with a terminal di- or triacetylene was carried out (Scheme 49). Thus, the *tert*-butyl esters were removed from compounds **86** and **173** by treatment with TFA which furnished derivatives **87** and **175** in the usual nearly quantitative yields. For the first attempt, we decided to couple the obtained carboxylic acids to the hydrogenated poly(isoprene) segment **177** with an average number of repeat units  $\bar{P}_n = 9-10$  that was equipped with only two L-alanine residues. The potential final product would, hence, feature the polymer segment length found to be appropriate in the case of the diacetylene macromonomers but only 4+4 N-H...O=C hydrogen-bonds which seemed to be a good compromise. The EDCI coupling of the diacetylene derivative **87** to **177** proceeded as expected without any problems giving **178** in a yield of 70%. In case of the triacetylene derivative **179**, the TMS group was partially removed from the product already after the purification as could be concluded from the <sup>1</sup>H NMR spectrum. Nevertheless, both materials were treated with AgOTf in order to first remove the TMS group in case of **178** to arrive at the terminal diacetylene **180** and, secondly, complete the removal of the silyl group in the triacetylene case to obtain **181** as well. MALDI-TOF mass spectrometry proved the successful conversion in so far as the spectra contained a series of peaks with the expected masses. The triacetylene spectrum contained an additional series of signals with lower intensity roughly corresponding to the two and threefold molecular weight of the target structure that



**Scheme 49:** Synthesis of the tetra- and hexayne target molecules equipped with a modified oligopeptide-polymer conjugate. *Reagents and Conditions:* a) TFA, DCM; b) **177**, EDCI/HOBt, TEA, DCM/DMF,  $-40^\circ\text{C}$   $\rightarrow$  r.t.; c) 1.1 eq AgOTf, MeOH, EtOH,  $\text{H}_2\text{O}$ , 2 h, r.t., KI; b) TMEDA, CuCl, DCM, air, r.t., 4 days.

were difficult to explain. Also the  $^1\text{H}$  NMR spectra were not perfect as they contained two signals at 3.6 and 3.75 ppm that could not be assigned and were increasing with every purification step. Moreover, the signals of the terminal di- and triacetylene protons had a much too low intensity which could not be properly explained. Furthermore, the terminal triacetylene derivative was a brown material that certainly was not perfectly pure.

Nevertheless, we used the compounds to complete both target molecules **182** and **183** by an acetylene homocoupling under Hay conditions. The starting materials were dissolved in DCM and the prepared catalyst solution was added. The reaction was stirred for four days at ambient atmosphere to ensure a complete reaction. The materials were purified by repeated column chromatography and extractions with saturated  $\text{NH}_4\text{Cl}$  solution to remove the copper species. In case of **182**, the product was obtained in 73%. However, the material seemed to still contain minor amounts of copper concluded from a slightly green tinge. The  $^1\text{H}$  NMR spectrum still contained the unknown signals at 3.6 as well as 3.75 ppm but the diacetylene proton signal had completely disappeared as expected. Other than that, the signal of the methylene group next to the *sp*-hybridized carbons gave rise to a completely distorted signal that additionally had a much too low intensity. The same was true for

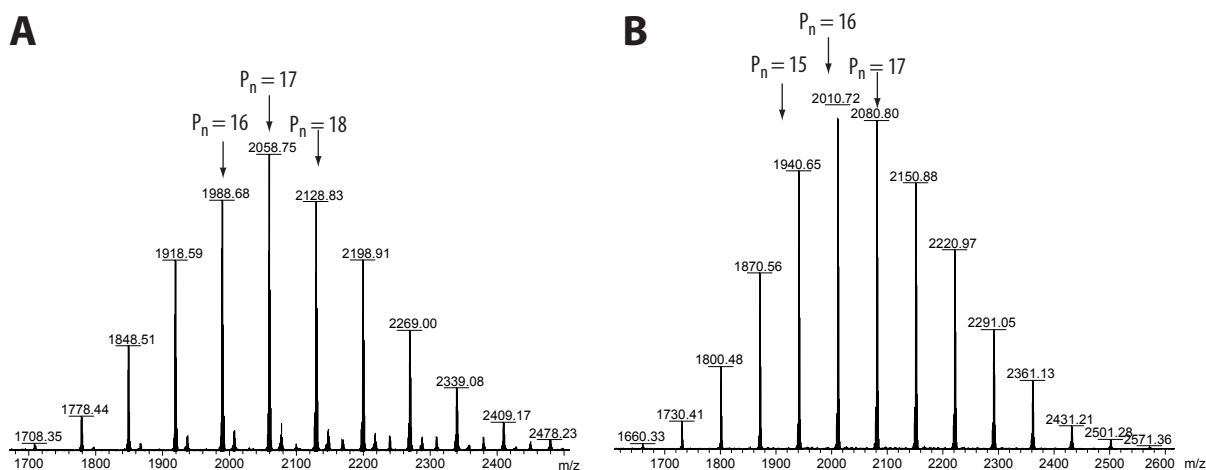


**Figure 103:** A) The MALDI-TOF spectrum of **182** featured the expected series of peaks. B) The spectrum of **183** contained a series corresponding to the correct masses, however, that had been already present in the spectrum of the starting material. A second series (not shown) at values corresponding to a threefold mass of **181** was also present.

compound **183**, however, all mentioned aspects were even worse. The MALDI-TOF spectra of **182** contained only one series of signals showing the correct molecular weight (Figure 103). The MALDI spectrum of **183** was similar to the starting material in so far as it contained signals belonging to the symmetric (dimeric) structure as well as a series that seemed to have the threefold molar mass with respect to **179**. One could conclude that, during the Ag-catalyzed reaction aimed at the removal of the TMS group, a partial homocoupling and other side reactions had already occurred.

In summary, a synthetic route has been established which, however, needs to be further optimized concerning the purification of the intermediates and the characterization of the target structures. Once that has been achieved, the self-assembly of the compounds needs to be investigated by IR spectroscopy as well as SFM imaging before a rearrangement of the oligoynes towards multiple stranded polymers or graphite-tape structures can be performed. Unfortunately, all these tasks could not be accomplished during this Ph. D. thesis and have to be postponed to the near future.





## Conclusions & Outlook



## 4 Conclusions and Outlook

In conclusion, the intended preparation of a new class of hierarchically structured  $\pi$ -conjugated polymers was successfully achieved by the novel “*self-assemble, then polymerize*” approach developed in the course of this thesis. The basis for the investigations was the elaboration of a highly modular and efficient synthetic strategy that made use of the prefabrication of oligopeptide, polymer and diacetylene building blocks which were then assembled to the final macromonomers preferably using a convergent route. Thus, it had been possible to prepare a large variety of macromonomers featuring different end groups as well as polymer- and oligopeptide-segments of different lengths in a short period of time. Furthermore, monodisperse model compounds were straightforwardly prepared to broaden the scope of the investigations.

The investigation of the macromonomers' secondary structures by solution phase IR spectroscopy and solid state NMR techniques revealed that the hydrogen-bonding pattern decisively controlled the secondary structure formation. Apparently, the presence or absence of additional N–H $\cdots$ O=C hydrogen-bonding sites in the end groups was the main factor that controlled the type of secondary structures. Thus, macromonomers exhibiting such additional N–H $\cdots$ O=C hydrogen-bonds gave rise to parallel  $\beta$ -sheets, while those without either formed antiparallel  $\beta$ -sheets or random coil structures. Apparently, the non-equidistant placement of the N–H $\cdots$ O=C hydrogen-bonds provided a sufficient driving force to favor parallel over antiparallel  $\beta$ -sheet formation.

The higher structure formation of the macromonomers as observed by transmission electron microscopy (TEM) and mainly scanning force microscopy (SFM) was dependent on the hydrogen-bonding pattern, as well. Thus, fibrillar aggregates were obtained from macromonomers that formed  $\beta$ -sheet type secondary structures, although a significantly higher propensity toward self-assembly into well-defined aggregates was found for the derivatives that favored a parallel  $\beta$ -strand orientation. The observed superstructures were identified as flat single-tapes, left-handed single-helices comprising two tape-like substructures, and right-handed double-helices, which consisted of four laminated  $\beta$ -sheet tapes in total. In comparison to the model compounds which only formed ill-defined one-dimensional aggregates, the aggregates from the macromonomers can be regarded as well-defined supramolecular polymers with a uniform diameter and a defined, finite number of strands, highlighting the importance of the polydisperse polymer segment for a controlled self-assembly.

The UV-induced topochemical polymerization of the diacetylenes was shown to be possible within the aggregates whenever the oligopeptide-polymer conjugates formed parallel  $\beta$ -sheets, as was proved by means of UV, NMR and Raman spectroscopy. Hence, the intended transformation of the well-defined supramolecular polymers into  $\pi$ -conjugated polymers under retention of the previously attained hierarchical structures was successful, as evidenced by SFM imaging and CD spectroscopy in solution.

A thorough investigation of the observed solvatochromism of the obtained poly(diacetylene)s induced by the addition of hydrogen-bond breaking cosolvents revealed that the distinct two-step color transitions were associated with defined conformational conversions. Thus, a helix-helix followed by a helix-coil transition was observed by CD spectroscopy. The final transition was found to be completely reversible upon the addition of a base. This rich folding behavior is remarkable for a synthetic polymer and finds analogies only in the realm of biopolymers.

In future investigations, the chosen molecular architecture based on oligopeptide-polymer conjugates may serve as a “universal” supramolecular scaffold for the preorganization of reactive moieties other than diacetylenes. For example, appropriately functionalized oligo(ethynylene)s may be used as molecular precursors for the preparation of soluble, nanostructured, multi-stranded  $\pi$ -conjugated polymers or even “graphite ribbons”.



## Experimental Part



## 5 Experimental Part

### 5.1 Instrumentation

**Solution Phase NMR spectroscopy** was carried out on a Bruker Avance 300 spectrometer operating at a frequency of 300.23 MHz for  $^1\text{H}$  and 75.49 MHz for  $^{13}\text{C}$  nuclei.

**Solid State CP-MAS  $^{13}\text{C}$  NMR** spectra were recorded on a Bruker Avance 500 spectrometer operating at a frequency of 125.72 MHz for  $^{13}\text{C}$  nuclei. The rotational frequency was typically chosen between 10 and 12.5 kHz.

**High Resolution Mass Spectra** were recorded on an Ionspec Ultima FTMS: 6211 HiRes-MALDI device, an Ionspec Ultima 494 HiRes-ESI-MS, a Bruker Daltonics Ultraflex II for MALDI-tof, and a Micromass Autospec device for HREI-MS. The measurements were carried out at the mass spectrometry service at the Institute of Organic Chemistry at ETH Zurich.

**Combustion Elemental Analyses** were carried out as service measurements at the Institute of Organic Chemistry at the Department of Chemistry and Applied Biosciences at ETH Zurich using a LECO CHN/900 instrument.

**UV-Vis spectra** were recorded on a Perkin-Elmer UV-20 spectrometer with a scan speed of 480 nm per minute using 1 cm quartz cuvettes from Hellma.

**CD spectra** were recorded on a JASCO-715 spectropolarimeter working at a scan speed of 50 nm per minute using 1 cm quartz cuvettes from Hellma.

**Solution or Gel Phase IR spectra** were recorded on a "Spectrum One" IR spectrometer from Perkin Elmer using a solution phase cuvette with KBr windows and a light path of 0.5 mm.

**Transmission Electron Microscopy (TEM)** was carried out at ETH Zurich using a FEI Tecnai Morgagni instrument operating at an acceleration voltage of 100 kV; in collaboration with the Max Planck Institute for Polymer Research in Mainz, Germany, using a FEI Tecnai F20 FEG device operating at an acceleration voltage of 200 kV; and in collaboration with the Max Planck Institute for Colloids and Interfaces in Golm, Germany, using a LEO Omega 912 device operating at an acceleration voltage of 120 kV.

**Scanning Force Microscopy (SFM)** was performed in collaboration with the group of Prof. Jürgen P. Rabe at Humboldt University Berlin, Germany. The images were obtained in tapping mode<sup>TM</sup> using a Multimode Microscope<sup>TM</sup> (Digital Instruments Inc., Santa Barbara, CA, USA). Olympus Micro Cantilevers were used with a typical resonance frequency of 300 and 70 kHz and a spring constant of  $42 \text{ N m}^{-1}$  and  $2 \text{ N m}^{-1}$ , respectively. The samples were prepared by spin-coating DCM or  $\text{CHCl}_3$  solutions of the macromonomers onto mica, HOPG or a monolayer of tricontanoic acid or stearyl amine on HOPG.<sup>215</sup> The correction of the observed fibrils' apparent width was calculated assuming a 9 nm tip radius, consistent with the manufacturer's specifications. As the apparent height of the fibrils appeared to have a slight dependence on the scanning conditions, all images for height analysis were taken under "soft" scanning conditions, with an amplitude damping of 10-20%. The apparent height was determined at the maxima of the fibrils' helical fine structure, and the height profiles were measured along the SFM fast scan direction to minimize the influence of thermal drift. The length and cross-section analysis was performed with a home-built software package. For SFM manipulation,<sup>216</sup> the feedback was switched off, the SFM tip was moved toward the surface by 20–30 nm and then laterally into the desired direction. SFM manipulation experiments were carried out using samples spin-coated onto a monolayer of octadecyl amine on HOPG. The amphiphile monolayers were used in order to fine tune the immobilization of isolated fibrils on the substrate. No apparent structural difference between fibrils deposited directly on HOPG or amphiphile monolayers was observed. Only fibrillar features longer than 40 nm were considered in the contour length distribution; for the average contour length determination, the distribution was extrapolated toward shorter contour lengths with a Schulz-Flory distribution.

## 5.2 Chromatography

**TLC Analyses** were performed on TLC plates from Macherey-Nagel (Alugramm® Sil G/UV<sub>254</sub>) or from Merck. UV-light (254 nm) or standard coloring reagents were used for detection.

**Column Chromatography** was conducted on Geduran® Silica gel Si 60 from Merck (40 – 60  $\mu\text{m}$ ).



## 5.3 General Procedures

**UV Polymerizations** were performed using a 250 W Ga-doped low pressure Hg lamp from UV-Light Technology, Birmingham, UK, using a “black bandpass filter” with a transparency window from 315 to 405 nm. The monomer solutions were thoroughly degassed in three freeze-pump-thaw cycles to remove O<sub>2</sub>. The solution was then transferred into a N<sub>2</sub> flushed, thermostated Schlenk flask equipped with a septum.

**Solvents and Reagents.** Unless otherwise noted, all reactions were carried out in dried Schlenk glassware in an inert N<sub>2</sub> atmosphere. All reagents were purchased as reagent grade and used without further purification. Solvents were purchased as reagent grade and distilled prior to use. Diethylether, toluene and THF were dried over sodium/benzophenone, dichloromethane over CaH<sub>2</sub>, and acetone was dried using P<sub>2</sub>O<sub>5</sub>. The solvents were freshly distilled and stored over molecular sieves prior to use.

**General Procedure for Sonogashira Couplings (Procedure A).** *N*-propargyloxycarbonyl-L-alanine *tert*-butyl ester **46**, 1.2 eq of the iodoacetylene compound and 4 eq of diisopropylamine were dissolved in dry THF. The solution was degassed in three freeze-pump-thaw cycles. After covering the flask with aluminum foil and cooling to 0 °C, PdCl<sub>2</sub>(PPh<sub>3</sub>)<sub>2</sub> (2.0 mol%) and CuI (10 mol%) were added. The brown solution was stirred for 2 to 12 h, followed by the removal of the solvent. The crude material was taken up in CH<sub>2</sub>Cl<sub>2</sub> followed by an aqueous workup, unless otherwise noted. The organic phase was dried over MgSO<sub>4</sub>, filtered, and concentrated *in vacuo*. The purification was carried out by column chromatography (silica gel) to separate the desired product from homo- and self-coupling side products.

**Procedure for the Deprotection of *tert*-Butyl Esters (Procedure B).** The *tert*-butyl ester derivatives were dissolved in dry CH<sub>2</sub>Cl<sub>2</sub>. Then, a large excess (≥13 eq) of trifluoroacetic acid (TFA) was added, and the solution was stirred for 3 to 16 h. The reaction was monitored by thin layer chromatography. After completion of the reaction, the solvents were removed *in vacuo*. The crude product was typically used in the next step without further purification.

**Procedure for the Deprotection of Fmoc-Protecting Groups (Procedure C).** The Fmoc-protected amine derivatives were dissolved in CHCl<sub>3</sub>. Then, a large excess (≥5 eq) of piperidine were added, and the solution was stirred over night. The reaction was monitored by thin layer chromatography. After completion of the reaction, the solvents were removed *in vacuo*. The crude product was typically purified by column chromatography.

**General Procedure for PyBOP-Promoted Peptide couplings (Procedure D).** The carboxylic acid derivative was dissolved in a mixture of dry  $\text{CH}_2\text{Cl}_2$  and dry DMF. The amine (1 eq) was added, as well as 4 eq of *N*-ethyl-diisopropylamine (DIEA). The resulting solution was cooled to  $0^\circ\text{C}$ , and 1.05 eq of (benzotriazol-1-yloxy)tripyrrolidinophosphonium hexafluorophosphate (PyBOP) was added in one portion. The cooling bath was removed, and the reaction mixture was stirred at room temperature for 3 to 16 h. The solvents were removed, and the obtained crude materials were purified by column chromatography, unless otherwise noted.

**General Procedure for EDCI/HOBt-Promoted Peptide couplings (Procedure E).** The carboxylic acid derivative was dissolved in a mixture of dry  $\text{CH}_2\text{Cl}_2$  and dry DMF. Then, 1.25 eq of 1-hydroxybenzotriazole (HOBt) were added, and the mixture was cooled to  $-25^\circ\text{C}$ . Then, 1.2 eq of 1-ethyl-3-(3-dimethyl-aminopropyl)carbodiimide hydrochloride (EDCI) were added, and the solution was stirred for 45 min at that temperature. The cooling bath was removed, and the reaction was allowed to reach room temperature while the formation of the active ester intermediate was monitored by thin layer chromatography (TLC). A second solution of the amine (1 eq) and 4 eq of triethylamine (TEA) in dry  $\text{CH}_2\text{Cl}_2$  was prepared. Both solutions were cooled to  $-40^\circ\text{C}$  and combined with a syringe. The reaction mixture was stirred over night, slowly warming up to approximately  $15^\circ\text{C}$ .

## 5.4 Syntheses

***N*-(9-Fluorenylmethyloxycarbonyl)-L-alanyl-L-alanine *tert*-Butyl Ester 35.** Following general procedure D, *N*-(9-fluorenylmethyloxycarbonyl)-L-alanine (6.22 g, 20 mmol) and L-alanine *tert*-butyl ester hydrochloride (3.63 g, 20 mmol) were dissolved in a mixture of dry  $\text{CH}_2\text{Cl}_2$  (100 mL) and dry DMF (50 mL). DIEA (10.34 g, 80 mmol) and PyBOP (10.92 g, 21 mmol) were added. The next day, the solution was diluted with more  $\text{CH}_2\text{Cl}_2$  (300 mL), washed twice with 1M HCl and once with sat. NaCl solution. The combined organic phases were dried over  $\text{MgSO}_4$ , filtered, and concentrated *in vacuo*. The crude product was purified by column chromatography (silica gel,  $\text{CH}_2\text{Cl}_2/\text{MeOH}$  25:1). **35** (7.78 g, 89%) was obtained as a colorless solid.

$^1\text{H}$  NMR (300.23 MHz,  $\text{CDCl}_3$ ):  $\delta$  = 1.38 (d,  $J$  = 7.2 Hz, 3H,  $\text{CHCH}_3$ ), 1.43-1.47 (m, 12H,  $\text{C}(\text{CH}_3)_3$ ,  $\text{CHCH}_3$ ), 4.22 (t,  $J$  = 7.2 Hz, 1H, fluorenyl CH), 4.38-4.51 (m, 4H, 2  $\text{CHCH}_3$ , Fmoc- $\text{CO}_2\text{CH}_2$ ), 5.79 (d,  $J$  = 7.8 Hz, 1H, carbamate NH), 6.88 (d,  $J$  = 6.9 Hz, 1H, NH), 7.31 (dt,  $J$  = 7.5 Hz, 1.5 Hz, 2H, aromatic H), 7.41 (t,  $J$  = 7.5 Hz, 2H, aromatic H), 7.61 (dd,  $J$  = 7.8 Hz, 2.7 Hz, 2H, aromatic H), 7.77 (d,  $J$  = 7.5 Hz, 2H, aromatic H).  $^{13}\text{C}$  NMR (75.49 MHz,  $\text{CDCl}_3$ ):  $\delta$  = 18.3, 19.0 (2  $\text{CHCH}_3$ ), 27.8 ( $\text{C}(\text{CH}_3)_3$ ), 47.0 (fluorenyl CH), 48.6, 50.3 (2  $\text{CHCH}_3$ ), 67.0 (Fmoc- $\text{CO}_2\text{CH}_2$ ), 81.9 ( $\text{C}(\text{CH}_3)_3$ ), 119.8, 125.0, 127.0, 127.6, 141.2,

143.7 (aromatic C), 155.8 (carbamate C=O), 171.8 (amide and ester C=O). Anal. calcd for C<sub>25</sub>H<sub>30</sub>N<sub>2</sub>O<sub>5</sub>: C, 68.47%; H, 6.90%; N, 6.39%; O, 18.24%; found: C, 68.22%; H, 7.00%; N, 6.33%; O, 18.46%. HRMS (ED): calcd for C<sub>25</sub>H<sub>30</sub>N<sub>2</sub>O<sub>5</sub>: ([M]<sup>+</sup>) 438.2150; found: 438.2149. R<sub>f</sub>: 0.7 (CH<sub>2</sub>Cl<sub>2</sub>/MeOH 10:1). m. p.: 67-69 °C.

***N*-(9-Fluorenylmethoxycarbonyl)-L-alanyl-L-alanine 36.** Following general procedure B, **35** (7.0 g, 15.96 mmol) was dissolved in CH<sub>2</sub>Cl<sub>2</sub> (60 mL). TFA (24.8 g, 217 mmol) was added, and the reaction mixture was stirred over night. The solvent was removed in HV, and the obtained crude product was recrystallized from CH<sub>2</sub>Cl<sub>2</sub>. The colorless precipitate was filtered and dried to give pure **36** (5.5 g, 90%).

<sup>1</sup>H NMR (300.23 MHz, DMSO-D<sub>6</sub>): δ = 1.39 (d, *J* = 6.3 Hz, 3H, CHCH<sub>3</sub>), 1.45 (d, *J* = 6.9 Hz, 3H, CHCH<sub>3</sub>), 4.19 (t, *J* = 6.9 Hz, 1H, fluorenyl CH), 4.36-4.59 (m, 4H, 2 CHCH<sub>3</sub>; Fmoc-CO<sub>2</sub>CH<sub>2</sub>), 6.19 (d, *J* = 7.0 Hz, 1H, NH), 7.30 (t, *J* = 7.2 Hz, 2H, aromatic *H*), 7.40 (t, *J* = 7.2 Hz, 2H, aromatic *H*), 7.56 (m, 2H, aromatic *H*), 7.75 (d, *J* = 7.5 Hz, 2H, aromatic *H*), 12.7 (bs, 1H, CO<sub>2</sub>H). <sup>13</sup>C NMR (75.49 MHz, DMSO-D<sub>6</sub>): δ = 17.4, 18.1 (2 CHCH<sub>3</sub>), 46.9 (fluorenyl CH), 48.4, 50.4 (2 CHCH<sub>3</sub>), 67.9 (Fmoc-CO<sub>2</sub>CH<sub>2</sub>), 120.0, 125.0, 127.1, 127.9, 141.3, 143.3 (aromatic C), 156.8 (carbamate C=O), 173.9 (amide C=O), 176.2 (acid C=O). Anal. calcd for C<sub>21</sub>H<sub>22</sub>N<sub>2</sub>O<sub>5</sub>: C, 65.96%; H, 5.80%; N, 7.33%; found: C, 65.97%; H, 5.88%; N, 7.32%. HRMS (ESI): calcd for C<sub>21</sub>H<sub>23</sub>N<sub>2</sub>O<sub>5</sub>: ([M+H]<sup>+</sup>) 383.4; found: 383.3. R<sub>f</sub>: 0.25 (CH<sub>2</sub>Cl<sub>2</sub>/MeOH 10:1). m. p.: 198-199 °C.

***L*-Alanyl-L-alanine *tert*-Butyl Ester 37.** Following general procedure C, **35** (6.20 g, 141.4 mmol) was dissolved in CHCl<sub>3</sub> (60 mL). Piperidine (6.02 g, 706.9 mmol) was added, and the reaction mixture was stirred at room temperature for 43 h. The crude product was purified by column chromatography (silica gel, CH<sub>2</sub>Cl<sub>2</sub>/MeOH 24:1 with 2% v/v TEA). **37** (2.7 g, 84%) was obtained as a slightly yellow oil.

<sup>1</sup>H NMR (300.23 MHz, CDCl<sub>3</sub>): δ = 1.22 (d, *J* = 6.9 Hz, 3H, CHCH<sub>3</sub>), 1.26 (d, *J* = 7.2 Hz, 3H, CHCH<sub>3</sub>), 1.34 (s, 9H, C(CH<sub>3</sub>)<sub>3</sub>), 1.52 (s, 2H, NH<sub>2</sub>), 3.40 (q, *J* = 6.9 Hz, 1H, CHCH<sub>3</sub>), 4.31 (qui, *J* = 7.2 Hz, 1H, CHCH<sub>3</sub>), 7.65 (d, *J* = 6.6 Hz, amide NH). <sup>13</sup>C NMR (75.49 MHz, CDCl<sub>3</sub>): δ = 18.5, 21.5 (2 CHCH<sub>3</sub>), 27.9 (C(CH<sub>3</sub>)<sub>3</sub>), 48.1 (CHCH<sub>3</sub>), 50.6 (CHCH<sub>3</sub>), 81.6 (C(CH<sub>3</sub>)<sub>3</sub>), 172.2 (carbamate C=O), 175.2 (amide C=O). Anal. calcd for C<sub>10</sub>H<sub>20</sub>N<sub>2</sub>O<sub>3</sub>: C, 55.53%; H, 9.32%; N, 12.95%; O, 22.19%; found: C, 55.77%; H, 9.32%; N, 12.83%. HRMS (MALDI): calcd for C<sub>10</sub>H<sub>21</sub>N<sub>2</sub>O<sub>3</sub>: ([M+H]<sup>+</sup>) 217.1547; found 217.1546. R<sub>f</sub>: 0.35 (CH<sub>2</sub>Cl<sub>2</sub>/MeOH 10:1).

***N*-(9-Fluorenylmethoxycarbonyl)-L-alanyl-L-alanyl-L-alanine *tert*-Butyl Ester 38.** Following general procedure D, *N*-(9-fluorenylmethoxycarbonyl)-L-alanine (5.05 g, 16.18 mmol) and

**37** (3.50 g, 16.18 mmol) were dissolved in a mixture of dry CH<sub>2</sub>Cl<sub>2</sub> (50 mL) and dry DMF (25 mL). DIEA (8.8 g, 64.72 mmol) and PyBOP (8.84 g, 17.0 mmol) were added. The next day, the solution was concentrated *in vacuo* and the crude product was recrystallized from CH<sub>2</sub>Cl<sub>2</sub>. **38** (6.65 g, 80%) was obtained as a colorless solid.

<sup>1</sup>H NMR (300.23 MHz, DMSO-D<sub>6</sub>): δ = 1.25 (m, 9H, 3 CHCH<sub>3</sub>), 1.39 (s, 9H, C(CH<sub>3</sub>)<sub>3</sub>), 4.1 (m, 2H, CHCH<sub>3</sub>, fluorenyl CH), 4.2-4.4 (m, 4H, 2 CHCH<sub>3</sub>, Fmoc-CO<sub>2</sub>CH<sub>2</sub>), 7.34 (t, *J* = 7.2 Hz, 2H, aromatic *H*), 7.43 (t, *J* = 7.2 Hz, 2H, aromatic *H*), 7.53 (d, *J* = 7.5 Hz, 1H, *NH*), 7.88 (m, 2H, aromatic *H*), 7.85-8.0 (m, 3H, 2 aromatic *H*, *NH*), 8.17 (d, 6.9 Hz, 1H, *NH*). <sup>13</sup>C NMR (75.49 MHz, DMSO-D<sub>6</sub>): δ = 17.9, 18.2, 18.8 (3 CHCH<sub>3</sub>), 27.9 (C(CH<sub>3</sub>)<sub>3</sub>), 47.1, 48.7, 49.3, 50.4 (fluorenyl-CH, 3 CHCH<sub>3</sub>), 67.0 (Fmoc-CO<sub>2</sub>CH<sub>2</sub>), 81.9 (C(CH<sub>3</sub>)<sub>3</sub>), 120.0, 125.0, 127.1, 127.7, 141.2, 143.8 (aromatic C), 156.2 (carbamate C=O), 171.9, 172.7 (ester, 2 amide C=O). Anal. calcd for C<sub>28</sub>H<sub>35</sub>N<sub>3</sub>O<sub>6</sub>: C, 65.99%; H, 6.92%; N, 8.25%; O, 18.84%; found: C, 66.07%; H, 6.89%; N, 8.22%; O, 18.91%. HRMS (ESI): calcd for C<sub>28</sub>H<sub>35</sub>N<sub>3</sub>O<sub>6</sub>Na ([M+Na]<sup>+</sup>) 532.2418; found 532.2420. R<sub>f</sub>: 0.75 (CH<sub>2</sub>Cl<sub>2</sub>/MeOH 10:1). m. p.: 192-193 °C.

***N*-(9-Fluorenylmethoxycarbonyl)-L-alanyl-L-alanyl-L-alanine 39.** Following general procedure B, **38** (5.0 g, 9.81 mmol) was dissolved in dry CH<sub>2</sub>Cl<sub>2</sub> (40 mL), and a large excess of TFA was added. The solution was stirred for 4 h, and the crude product was dried in HV. **39** (4.4 g, 99%) was obtained as a colorless crystalline material. No further purification was necessary before the next step.

<sup>1</sup>H NMR (300.23 MHz, DMSO-D<sub>6</sub>): δ = 1.19 (d, *J* = 7.2 Hz, 6H, 2 CHCH<sub>3</sub>), 1.24 (d, *J* = 7.5 Hz, 3H, CHCH<sub>3</sub>), 4.05 (m, 1H, fluorenyl CH), 4.1-4.4 (m, 5H, 3 CHCH<sub>3</sub>, Fmoc-CO<sub>2</sub>CH<sub>2</sub>), 7.31 (t, *J* = 7.2 Hz, 2H, aromatic *H*), 7.40 (t, *J* = 7.2 Hz, 2H, aromatic *H*), 7.50 (d, *J* = 7.5 Hz, 1H, *NH*), 7.70 (t, *J* = 6 Hz, 2H, aromatic *H*), 7.87 (d, *J* = 7.5 Hz, 2H, aromatic *H*), 7.92 (d, *J* = 6.6 Hz, 1H, *NH*), 8.08 (d, 6.9 Hz, 1H, *NH*). <sup>13</sup>C NMR (75.49 MHz, DMSO-D<sub>6</sub>): δ = 17.6, 18.7, 18.7 (3 CHCH<sub>3</sub>), 47.1, 47.9, 48.2, 50.4 (fluorenyl-CH, 3 CHCH<sub>3</sub>), 66.1 (Fmoc-CO<sub>2</sub>CH<sub>2</sub>), 120.6, 125.8, 127.6, 128.1, 141.2, 144.4 (aromatic C), 156.2 (carbamate C=O), 172.3, 172.6, 174.4 (acid, 2 amide C=O). HRMS (MALDI): calcd for C<sub>24</sub>H<sub>27</sub>N<sub>3</sub>O<sub>6</sub>Na ([M+Na]<sup>+</sup>) 476.1798; found 476.1796. R<sub>f</sub>: 0.2 (CH<sub>2</sub>Cl<sub>2</sub>/MeOH 10:1). m. p.: 206-208 °C.

**PI<sub>10</sub>-NH<sub>2</sub> 40.** Isoprene (26.5 g, 389.2 mmol) was freshly distilled from CaH<sub>2</sub> prior to use. A rigorously dried 500 mL Schlenk flask was filled with dry THF (120 mL), and *n*-butyl lithium (43.25 mmol, 1.6 M solution in hexanes) was added slowly via a syringe at -78 °C. Under vigorous stirring, isoprene was added via a syringe as fast as possible, leading to a yellow to orange color of the solution. The temperature was adjusted to 0 °C, the mixture was stirred for 10 min and then cooled again to -78 °C. Then, 1-(3-bromopropyl)-2,2,5,5-tetramethyl-1-aza-2,5-disilacyclopentane (15 g, 51.8 mmol)

was added via a syringe, causing an immediate decoloration. The cooling bath was removed, and the reaction mixture was stirred for 5 h at room temperature. Then, 2 M HCl (75 mL) was added, and stirring was continued over night. The mixture was concentrated *in vacuo*, taken up in CH<sub>2</sub>Cl<sub>2</sub>, washed twice with sat. NaHCO<sub>3</sub> solution and once with sat. NaCl solution. The combined organic phases were dried over MgSO<sub>4</sub>, filtered, and concentrated *in vacuo*. The crude product was purified by column chromatography (silica gel, gradient CH<sub>2</sub>Cl<sub>2</sub> → CH<sub>2</sub>Cl<sub>2</sub>/MeOH 5:1). The amine terminated poly(isoprene) **40** (21.50 g, 69%) was obtained as a slightly yellow oil.

<sup>1</sup>H NMR (300.23 MHz, CDCl<sub>3</sub>): δ = 0.8-2.2 (m, 100H, aliphatic *H*), 2.7-2.9 (m, 2H, CH<sub>2</sub>NH<sub>2</sub>), 4.6-5.2 (m, 28H, terminal olefin *H*), 5.6-5.9 (m, 3H, internal olefin *H*). Anal. calcd for C<sub>52</sub>H<sub>89</sub>N: C, 85.76%; H, 12.32%; N, 1.92%; found: C, 84.15%; H, 11.87%; N, 1.79%. HRMS (ESI): calcd for C<sub>52</sub>H<sub>90</sub>N: ([M+H]<sup>+</sup>) 728.7; found: 728.4. R<sub>f</sub>: 0.2 (CH<sub>2</sub>Cl<sub>2</sub>/MeOH 10:1).

**hPI<sub>10</sub>-NH<sub>2</sub> 41.** The amine-terminated poly(isoprene) **40** (9 g, 11.3 mmol) was dissolved in a mixture of toluene (75 mL) and EtOH (5 mL). The solution was transferred to a high pressure autoclave, and 8 mol% Pd on charcoal (3.7 g, 5% Pd/C, 52% H<sub>2</sub>O content) was added as the catalyst. The mixture was stirred at a H<sub>2</sub> pressure of 100 bar at 80 °C for 72 h. The hydrogenated amine terminated poly(isoprene) **41** was obtained as a slightly yellow oil in quantitative yield after filtration and removal of the solvent.

<sup>1</sup>H NMR (300.23 MHz, CDCl<sub>3</sub>): δ = 0.8-1.8 (m, 135H, aliphatic *H*), 2.9-3.1 (m, 2H, CH<sub>2</sub>NH<sub>2</sub>), 4.7 (m, 1H, residual olefin *H*). Anal. calcd for C<sub>52</sub>H<sub>107</sub>N: C, 83.67%; H, 14.45%; N, 1.88%; found: C, 77.40%; H, 13.43%; N, 1.45%. HRMS (MALDI): calcd for C<sub>52</sub>H<sub>108</sub>N: ([M+H]<sup>+</sup>) 747.421; found 747.29. R<sub>f</sub>: 0.15 (CH<sub>2</sub>Cl<sub>2</sub>/MeOH 10:1).

**hPI<sub>10</sub>-NH-Ala-Fmoc 42.** Following general procedure E, Fmoc-L-alanine (3.33 g, 10.67 mmol) was dissolved in a mixture of dry DMF (40 mL) and dry CH<sub>2</sub>Cl<sub>2</sub> (40 mL). HOBt (1.73 g, 12.8 mmol) and EDCI (2.56 g, 13.34 mmol) were added to form the active ester intermediate. A second solution containing **41** (8.7 g, 10.67 mmol) and TEA (4.32 g, 42.68 mmol) in dry CH<sub>2</sub>Cl<sub>2</sub> (250 mL) was prepared, and both solutions were combined. The next day, the solution was washed twice with 1M HCl and once with sat. NaCl solution. The combined organic phases were dried over MgSO<sub>4</sub>, filtered, and concentrated *in vacuo*. **42** was obtained quantitatively and was used in the next step without any further purification.

<sup>1</sup>H NMR (300.23 MHz, CDCl<sub>3</sub>): δ = 0.8-1.8 (m, 128H, aliphatic *H*, 1 CHCH<sub>3</sub>), 3.1-3.3 (m, 2H, CH<sub>2</sub>NHR), 4.2-4.3 (m, 2H, CHCH<sub>3</sub>, fluorenyl *CH*), 4.39 (d, *J* = 6.9 Hz, 2H, Fmoc-CO<sub>2</sub>CH<sub>2</sub>), 4.7 (m, 1H, residual olefin *H*), 5.5 (m, 1H, carbamate *NH*), 6.1 (m, 1H, amide *NH*), 7.31 (dt, *J* = 7.5 Hz, 1.0 Hz, 2H,

aromatic *H*), 7.38 (t,  $J = 7.5$  Hz, 2H, aromatic *H*), 7.58 (d,  $J = 7.2$  Hz, 2H, aromatic *H*), 7.75 (d,  $J = 7.5$  Hz, 2H, aromatic *H*). Anal. calcd for  $C_{70}H_{122}N_2O_3$ : C, 80.86%; H, 11.83%; N 2.69%; found: C, 81.17%; H, 12.02%; N, 2.39%. HRMS (MALDI): calcd for  $C_{70}H_{122}N_2O_3Na$ :  $([M+Na]^+)$  1061.935; found 1062.573.  $R_f$ : 0.75 ( $CH_2Cl_2/MeOH$  10:1).

**hPI<sub>10</sub>-NH-Ala-H 43.** Following general procedure C, **42** (11.8 g, 10.67 mmol) was dissolved in  $CHCl_3$  (100 mL) and piperidine (8.5 g, 100 mmol) was added. The next day, the solution was washed twice with sat.  $NaHCO_3$  solution and once with sat.  $NaCl$  solution. The combined organic phases were dried over  $MgSO_4$ , filtered, and concentrated *in vacuo*. The crude product was purified by column chromatography (silica gel,  $CH_2Cl_2/MeOH$  10:1). **43** (8.56 g, 90% over two steps) was obtained as a colorless oil.

$^1H$  NMR (300.23 MHz,  $CDCl_3$ ):  $\delta = 0.8$ -1.8 (m, 114H, aliphatic *H*, 1  $CHCH_3$ ), 3.2-3.3 (m, 2H,  $CH_2NHR$ ), 3.6-3.7 (m, 1H,  $CHCH_3$ ), 4.7 (m, 1H, residual olefin *H*), 6.5 (bs, 1H, amide *NH*). Anal. calcd for  $C_{55}H_{112}N_2O$ : C, 80.81%; H, 13.81%; N, 3.43%; found: C, 80.18%; H, 13.33%; N, 2.69%. HRMS (ESI): calcd for  $C_{55}H_{113}N_2O$ :  $([M+H]^+)$  817.9; found 817.6.  $R_f$ : 0.1 ( $CH_2Cl_2/MeOH$  10:1).

**hPI<sub>10</sub>-NH-Ala<sub>3</sub>-Fmoc 44.** From hPI<sub>10</sub>-NH-Ala-H **43**: Following general procedure D, **36** (3.24 g, 8.46 mmol) and **43** (7.5 g, 8.46 mmol) were dissolved in a mixture of dry  $CH_2Cl_2$  (120 mL) and dry DMF (60 mL). DIEA (4.38 g, 33.8 mmol) and PyBOP (4.62 g, 8.88 mmol) were added. In the course of the reaction, dry  $CHCl_3$  (200 mL) was added in order to prevent gel formation. The next day, the solvents were removed *in vacuo*, and the crude product was purified by column chromatography (silica gel,  $CHCl_3/MeOH$  20:1). **44** (9.0 g, 85%) was obtained as a colorless amorphous solid.

From hPI<sub>10</sub>-NH<sub>2</sub> **41**: Following general procedure D, **39** (1.36 g, 2.90 mmol) and **41** (2.37 g, 2.90 mmol) were dissolved in a mixture of dry  $CH_2Cl_2$  (90 mL) and dry DMF (30 mL). DIEA (1.13 g, 8.71 mmol) and PyBOP (1.58 g, 3.05 mmol) were added. After 3 h, the solvents were removed *in vacuo*, and the crude product was purified by column chromatography (silica gel,  $CHCl_3/MeOH$  20:1). **44** (3.09 g, 85%) was obtained as a colorless amorphous solid.

$^1H$  NMR (300.23 MHz,  $CDCl_3$ ):  $\delta = 0.8$ -1.8 (m, 131H, aliphatic *H*, 3  $CHCH_3$ ), 3.0-3.3 (m, 2H,  $CH_2NHR$ ), 4.2 (m, 1H, fluorenyl *CH*), 4.3-4.4 (m, 2H,  $NHCO_2CH_2$ ), 4.6-4.9 (m, 4H, 3  $CHCH_3$ , 1 residual olefin *H*), 6.5 (m, 1H, amide *NH*), 7.2 (m, 1H, amide *NH*), 7.25 (t,  $J = 7.5$  Hz, 2H, aromatic *H*), 7.35 (m, 2H, aromatic *H*), 7.6 (m, 2H, aromatic *H*), 7.75 (m, 3H, 2 aromatic *H*, amide *NH*) 8.2 (m, 1H, amide *NH*). Anal. calcd for  $C_{76}H_{132}N_4O_5$ : C, 77.23%; H, 11.26%; N, 4.74%; found: C, 77.71%; H, 11.14%; N, 4.46%. HRMS (MALDI): calcd for  $C_{76}H_{132}N_4O_5Na$ :  $([M+Na]^+)$  1204.010; found 1204.029.  $R_f$ : 0.4 ( $CH_2Cl_2/MeOH$  10:1).

**hPI<sub>10</sub>-NH-Ala<sub>3</sub>-H 45.** Following general procedure C, **44** (8.75 g, 7.0 mmol) was dissolved in CHCl<sub>3</sub> (100 mL), and piperidine (8.5 g, 100 mmol) was added. The next day, the solution was washed twice with sat. NaHCO<sub>3</sub> solution as well as once with sat. NaCl solution. The combined organic phases were dried over MgSO<sub>4</sub>, filtered, and concentrated *in vacuo*. The oily crude product was purified by column chromatography (silica gel, gradient CH<sub>2</sub>Cl<sub>2</sub>/MeOH 24:1 → CH<sub>2</sub>Cl<sub>2</sub>/MeOH 5:1). The product **45** (5.85 g, 75%) was obtained as a colorless amorphous solid.

<sup>1</sup>H NMR (300.23 MHz, CDCl<sub>3</sub>): δ = 0.8-1.8 (m, 149H, aliphatic *H*, 3 CHCH<sub>3</sub>), 3.1-3.3 (m, 2H, CH<sub>2</sub>NHR), 3.55 (m, 1H, CHCH<sub>3</sub>), 4.45 (m, 2H, CHCH<sub>3</sub>), 4.7 (m, 1H, residual olefin *H*), 6.5 (m, 1H, amide *NH*), 7.1 (m, 1H, amide *NH*), 7.85 (m, 1H, amide *NH*). Anal. calcd for C<sub>61</sub>H<sub>122</sub>N<sub>4</sub>O<sub>3</sub>: C, 76.35%; H, 12.81%; N, 5.84%; found: C, 76.68%; H, 12.73%; N, 5.20%. HRMS (MALDI): calcd for C<sub>66</sub>H<sub>132</sub>N<sub>4</sub>O<sub>3</sub>Na: ([M+Na]<sup>+</sup>) 1052.020; found 1052.662. R<sub>f</sub>: 0.1 (CH<sub>2</sub>Cl<sub>2</sub>/MeOH 10:1).

***N*-Propargyloxycarbonyl-L-alanine *tert*-Butyl Ester 46.** L-Alanine *tert*-butyl ester hydrochloride (3.30 g, 18.15 mmol) was dissolved in dry CH<sub>2</sub>Cl<sub>2</sub> (50 mL). TEA (3.86 g, 38.12 mmol) was added, which led to the precipitation of its hydrochloride. The mixture was cooled to -78 °C and propargyl chloroformate (2.15 g, 18.15 mmol) was added dropwise. The solution was stirred for 1 h at -78 °C, for 2 h at 0 °C, and then allowed to warm up to room temperature. The organic phase was washed with water and sat. NaCl solution, dried over MgSO<sub>4</sub>, filtered, and concentrated *in vacuo*. **46** (3.87 g, 93%) was obtained as a colorless oil, and no further purification was necessary.

<sup>1</sup>H NMR (300.23 MHz, CDCl<sub>3</sub>): δ = 1.32 (d, *J* = 7.2 Hz, 3H, CHCH<sub>3</sub>), 1.41 (s, 9H, C(CH<sub>3</sub>)<sub>3</sub>), 2.44 (t, *J* = 2.5 Hz, 1H, C≡CH), 4.18 (m, 1H, CHCH<sub>3</sub>), 4.63 (m, 2H, NHCO<sub>2</sub>CH<sub>2</sub>), 5.6 (d, *J* = 6.6 Hz, 1H, *NH*). <sup>13</sup>C NMR (75.49 MHz, CDCl<sub>3</sub>): δ = 18.6 (CHCH<sub>3</sub>), 27.9 (C(CH<sub>3</sub>)<sub>3</sub>), 50.2 (CHCH<sub>3</sub>), 52.4 (NHCO<sub>2</sub>CH<sub>2</sub>), 74.7 (C≡CH), 78.2 (C≡CH), 81.8 (C(CH<sub>3</sub>)<sub>3</sub>), 154.6 (carbamate C=O), 171.9 (ester C=O). Anal. calcd for C<sub>11</sub>H<sub>17</sub>NO<sub>4</sub>: C, 58.14%; H, 7.54%; N, 6.16%; found: C, 57.85%; H, 7.50%; N, 6.14%. HRMS (EI): calcd for C<sub>7</sub>H<sub>9</sub>NO<sub>3</sub>: ([M-C<sub>4</sub>H<sub>9</sub>O]<sup>+</sup>) 154.0499; found: 154.0501. R<sub>f</sub>: 0.7 (CH<sub>2</sub>Cl<sub>2</sub>/MeOH 10:1).

***N*-Propargyloxycarbonyl-L-alanine 47.** From *N*-propargyloxycarbonyl-L-alanine *tert*-butyl ester **46**: Following general procedure B, **46** (1.02 g, 4.51 mmol) was dissolved in dry CH<sub>2</sub>Cl<sub>2</sub> (15 mL), and the solution stirred over night. **47** (0.77 g, 100%) was obtained as a colorless oil. A further purification was not necessary before the next step.

From L-alanine: L-Alanine (1.02 g, 11.45 mmol) was dissolved in 1N NaOH solution (11.5 mL). The mixture was cooled to 15 °C, and propargyl chloroformate (2.71 g, 22.44 mmol) was added. After 30 min, more NaOH solution was added to adjust the pH to 9. The solution was cooled to 0 °C after stirring over night. The solution was extracted twice with Et<sub>2</sub>O. NaCl and 3N HCl were added to the

aqueous phase to adjust the pH to 1. The solution was extracted three times with CH<sub>2</sub>Cl<sub>2</sub>. The combined CH<sub>2</sub>Cl<sub>2</sub>-phases were dried over Na<sub>2</sub>SO<sub>4</sub>, filtered, and concentrated *in vacuo*. **47** (1.44 g, 75%) was obtained as a slightly yellow oil.

<sup>1</sup>H NMR (300.23 MHz, DMSO-D<sub>6</sub>): δ = 1.26 (d, *J* = 7.2 Hz, 3H, CHCH<sub>3</sub>), 3.42 (t, *J* = 2.4 Hz, 1H, C≡CH), 4.02 (m, 1H, CHCH<sub>3</sub>), 4.67 (m, 2H, NHCO<sub>2</sub>CH<sub>2</sub>), 7.67 (d, *J* = 7.5 Hz, 1H, NH), 10.0 (bs, 1H, CO<sub>2</sub>H). <sup>13</sup>C NMR (75.49 MHz, DMSO-D<sub>6</sub>): δ = 17.5, (CHCH<sub>3</sub>), 49.7 (CHCH<sub>3</sub>), 52.0 (NHCO<sub>2</sub>CH<sub>2</sub>), 77.5 (C≡CH), 79.6 (C≡CH), 155.5 (carbamate C=O), 174.7 (acid C=O). Anal. calcd for C<sub>7</sub>H<sub>9</sub>NO<sub>4</sub>: C, 49.12%; H, 5.30%; N, 8.18%; found: C, 48.94%; H, 5.30%; N, 8.08%. HRMS (ESI): calcd for C<sub>7</sub>H<sub>10</sub>NO<sub>4</sub>: ([M+H]<sup>+</sup>) 172.2; found: 172.3. R<sub>f</sub>: 0.2 (CH<sub>2</sub>Cl<sub>2</sub>/MeOH 10:1).

**3-Iodopropargylamine Hydrochloride 49.** Hexamethyldisilazane (9.68 g, 60 mmol) was dissolved in Et<sub>2</sub>O (30 mL) at 0 °C, and *n*-butyl lithium (60 mmol, 1.6 M solution in hexanes) was added slowly. The mixture was allowed to reach room temperature and stirred for another 30 min. The flask was covered with aluminum foil, the solution was cooled to -78 °C, and propargyl bromide (3.57 g, 30 mmol) in dry Et<sub>2</sub>O (20 mL) was added dropwise. The reaction mixture was allowed to reach room temperature again and stirred for 2 h. Then, I<sub>2</sub> (7.61 g, 30 mmol) was added at -78 °C, and the reaction mixture was stirred at room temperature over night. The reaction was quenched by washing with sat. Na<sub>2</sub>S<sub>2</sub>O<sub>3</sub> solution. The organic phase was dried over MgSO<sub>4</sub>, filtered, and concentrated *in vacuo* at room temperature. Residual hexamethyldisilazane was distilled off the crude mixture at 0 °C (4·10<sup>-2</sup> mbar). The remaining crude 3-iodo-*N,N*-bis(trimethylsilyl)propargylamine **48** (9.17 g, 80%), a slightly orange oil, was deprotected without further purification. For this purpose, acetyl chloride (7.85 g, 100 mmol) was dissolved in dry MeOH (25 mL) at 0 °C in order to generate anhydrous HCl in MeOH. The solution was stirred for 30 min at room temperature and diluted with CH<sub>2</sub>Cl<sub>2</sub> (25 mL). The protected amine derivative **48** (6.0 g, 18.4 mmol) was added at 0 °C, and a fine brown precipitate formed instantly. The precipitate was filtered off and dried *in vacuo*. **49** (3.21 g, 80%) was obtained as a slightly brown powder.

<sup>1</sup>H NMR (300.23 MHz, DMSO-D<sub>6</sub>): δ = 3.79 (s, 2H, CH<sub>2</sub>), 8.46 (s, 3H, NH<sub>3</sub>Cl). <sup>13</sup>C NMR (75.49 MHz, DMSO-D<sub>6</sub>): δ = 20.2 (C≡CI), 30.3 (CH<sub>2</sub>), 84.9 (C≡CI). HRMS (EI): calcd for C<sub>3</sub>H<sub>4</sub>IN: ([M-HCl]<sup>+</sup>) 180.9384; found 180.9383. m. p.: 168-169 °C (decomposition).

***N*-(3-Iodo-prop-2-ynyl)acetamide 50.** 3-Iodopropargylamine hydrochloride **49** (3.0 g, 13.8 mmol) was dissolved in a mixture of dry CH<sub>2</sub>Cl<sub>2</sub> (70 mL) and DIEA (8.91 g, 68.9 mmol). The reaction mixture was cooled to 0 °C, and acetic anhydride (14.1 g, 138 mmol) was added via a syringe. The flask was covered with aluminum foil, and the reaction mixture was stirred at room temperature



over night. The solution was diluted with  $\text{CH}_2\text{Cl}_2$ , and the organic phase was washed twice with sat.  $\text{NaHCO}_3$  solution and once with sat.  $\text{NaCl}$  solution. The organic phase was dried over  $\text{MgSO}_4$ , filtered, and concentrated *in vacuo* at room temperature in the dark. The crude material was purified by column chromatography (silica gel,  $\text{CH}_2\text{Cl}_2/\text{MeOH}$  100:1). **50** (1.76 g, 57%) was obtained as a slightly yellow crystalline solid.

$^1\text{H}$  NMR (300.23 MHz,  $\text{CDCl}_3$ ):  $\delta$  = 1.99 (s, 3H,  $\text{CH}_3$ ), 4.16 (d,  $J$  = 5.1 Hz, 2H,  $\text{CH}_2$ ), 6.29 (bs, 1H, NH).  $^{13}\text{C}$  NMR (75.49 MHz,  $\text{CDCl}_3$ ):  $\delta$  = -0.1 ( $\text{C}\equiv\text{C}$ ), 22.9 ( $\text{CH}_3$ ), 31.1 ( $\text{CH}_2$ ), 89.7 ( $\text{C}\equiv\text{C}$ ), 170.0 (amide  $\text{C}=\text{O}$ ). Anal. calcd for  $\text{C}_5\text{H}_6\text{INO}$ : C, 26.93%; H, 2.71%; I, 56.90%; N, 6.28%; found: C, 26.76%; H, 2.62%; I, 56.99%; N, 6.12%. HRMS (EI): calcd for  $\text{C}_5\text{H}_6\text{INO}$ : ( $[\text{M}]^+$ ) 222.9489; found 222.9488.  $R_f$ : 0.35 ( $\text{CH}_2\text{Cl}_2/\text{MeOH}$  10:1). m. p.: 104-106 °C.

***N*-(4-Methoxysuccinyl) 3-Iodopropargylamide 51.** 3-Iodopropargylamine hydrochloride **49** (3.04 g, 14 mmol) was dissolved in a mixture of dry  $\text{CH}_2\text{Cl}_2$  (60 mL) and DIEA (9.0 g, 70 mmol). The solution was cooled to 0 °C. Succinic acid monomethyl ester chloride (2.10 g, 14 mmol) was added dropwise, and the solution was stirred over night. After an acidic aqueous work-up, the organic solution was concentrated *in vacuo*. The crude product was purified by column chromatography (silica gel,  $\text{CH}_2\text{Cl}_2/\text{MeOH}$  50:1). **51** (2.96 g, 73%) was obtained as a colorless solid.

$^1\text{H}$  NMR (300.23 MHz,  $\text{DMSO}-d_6$ ):  $\delta$  = 2.37 (t,  $J$  = 6.3 Hz, 2H,  $\text{CH}_2$ ), 2.52 (t,  $J$  = 6.3 Hz, 2H,  $\text{CH}_2$ ), 3.58 (s, 3H,  $\text{CH}_3$ ), 3.97 (d,  $J$  = 5.4 Hz, 2H,  $\text{CH}_2\text{N}$ ), 8.32 (s, 1H, NH).  $^{13}\text{C}$  NMR (75.49 MHz,  $\text{DMSO}-d_6$ ):  $\delta$  = 8.1 ( $\text{C}\equiv\text{C}$ ), 29.0, 30.0, 30.2 (3  $\text{CH}_2$ ), 51.8 ( $\text{CH}_3$ ), 90.5 ( $\text{C}\equiv\text{C}$ ), 170.9, 173.2 (2  $\text{C}=\text{O}$ ). Anal. calcd for  $\text{C}_8\text{H}_{10}\text{INO}_3$ : C, 32.56%; H, 3.42%; N, 4.75%; I, 43.01%; found: C, 32.77%; H, 3.40%; I, 42.84%; N, 4.62%. HRMS (EI): calcd for  $\text{C}_8\text{H}_{10}\text{NO}_3\text{I}$ : ( $[\text{M}]^+$ ) 294.9700; found: 294.9700.  $R_f$ : 0.5 ( $\text{CH}_2\text{Cl}_2/\text{MeOH}$  10:1). m. p.: 104-105 °C.

***N*-(9-Fluorenylmethyloxycarbonyl) 3-Iodopropargylamine 52.** 3-Iodopropargylamine hydrochloride **49** (2.90 g, 13.3 mmol) was dissolved in a mixture of dry  $\text{CH}_2\text{Cl}_2$  (60 mL) and DIEA (9.10 g, 70.4 mmol). 9-Fluorenylmethyloxycarbonyl chloride (3.45 g, 13.3 mmol) was added at 0 °C, and the solution was stirred at room temperature over night. The solvents were removed *in vacuo*, and the crude material was recrystallized from  $\text{CH}_2\text{Cl}_2$ . **52** (4.10 g, 76%) was obtained as a colorless solid.

$^1\text{H}$  NMR (300.23 MHz,  $\text{DMSO}-d_6$ ):  $\delta$  = 3.93 (d,  $J$  = 5.4 Hz, 2H,  $\text{NHCH}_2$ ), 4.24 (m, 1H, fluorenyl-CH), 4.33 (d,  $J$  = 6.9 Hz, 2H,  $\text{Fmoc}-\text{CO}_2\text{CH}_2$ ), 7.34 (t,  $J$  = 7.2 Hz, 2H, aromatic H), 7.43 (t,  $J$  = 7.5 Hz, 2H, aromatic H), 7.70 (d,  $J$  = 7.2 Hz, 2H, aromatic H), 7.80 (t,  $J$  = 5.4 Hz, 1H, NH), 7.90 (d,  $J$  = 7.5 Hz, 2H, aromatic H).  $^{13}\text{C}$  NMR (75.49 MHz,  $\text{DMSO}-d_6$ ):  $\delta$  = 8.4 ( $\text{C}\equiv\text{C}$ ), 32.2 ( $\text{NHCH}_2$ ), 47.1 (fluorenyl-CH), 66.2 ( $\text{Fmoc}-\text{CO}_2\text{CH}_2$ ), 90.8 ( $\text{C}\equiv\text{C}$ ), 120.6, 125.6, 127.6, 128.1, 141.2, 144.3 (aromatic C), 156.4

(carbamate C=O). Anal. calcd for C<sub>18</sub>H<sub>14</sub>NO<sub>2</sub>I: C, 53.62%; H, 3.50%; N, 3.47%; I, 31.47%; found: C, 53.78%; H, 3.60%; N, 3.47%; I, 31.47%. HRMS (EI): calcd for C<sub>18</sub>H<sub>14</sub>NO<sub>2</sub>I: ([M]<sup>+</sup>) 403.0064; found: 403.0067. R<sub>f</sub>: 0.7 (CH<sub>2</sub>Cl<sub>2</sub>/MeOH 10:1). m. p.: 159-160 °C.

***N*-(5-Dimethylamino-1-naphthalenesulfonyl) 3-iodopropargylamide 53.** 3-Iodopropargylamine hydrochloride **49** (0.50 g, 2.3 mmol) was dissolved in a mixture of dry CH<sub>2</sub>Cl<sub>2</sub> (20 mL) and DIEA (0.74 g, 5.8 mmol). The solution was cooled to 0 °C and 5-dimethylamino-1-naphthalenesulfonyl chloride (0.68 g, 2.5 mmol) was added. The mixture was stirred for 20 min at 0 °C. The reaction was quenched by the addition of MeOH (10 mL). The resulting solution was washed twice with water. The organic phase was dried over MgSO<sub>4</sub>, filtered, and concentrated *in vacuo*. The crude product was purified by column chromatography (silica gel, CH<sub>2</sub>Cl<sub>2</sub>/MeOH 10:1). **53** (0.63 g, 57%) was obtained as a slightly brown powder.

<sup>1</sup>H NMR (300.23 MHz, DMSO-D<sub>6</sub>): δ = 2.85 (s, 6H, N(CH<sub>3</sub>)<sub>3</sub>), 3.86 (d, *J* = 6 Hz, 2H, NHCH<sub>2</sub>), 7.27 (d, *J* = 7.2 Hz, 1H, aromatic *H*), 7.62 (m, 2H, aromatic *H*), 8.15 (dd, *J* = 7.2 Hz, 1.2 Hz, 1H, aromatic *H*), 8.26 (d, *J* = 8.7 Hz, 1H, aromatic *H*), 8.36 (t, *J* = 6 Hz, 1H, amide *NH*), 8.5 (d, *J* = 8.7 Hz, 1H, aromatic *H*). <sup>13</sup>C NMR (75.49 MHz, DMSO-D<sub>6</sub>): δ = 10.0 (C≡C-I), 34.0 (NHCH<sub>2</sub>), 45.7 (N(CH<sub>3</sub>)<sub>2</sub>), 88.4 (C≡C-I), 115.5, 119.7, 124.0, 128.3, 129.2, 129.6, 129.7, 130.2, 136.4, 151.8 (aromatic C). Anal. calcd for C<sub>15</sub>H<sub>15</sub>IN<sub>2</sub>O<sub>2</sub>S: C, 43.49%; H, 3.65%; N, 6.76%; O, 7.72%; S, 7.74%; I, 30.63%; found: C, 43.66%; H, 3.52%; N, 6.70%; O, 7.76%; S, 7.56%; I, 30.80%. HRMS (EI): calcd for C<sub>15</sub>H<sub>15</sub>IN<sub>2</sub>O<sub>2</sub>S: ([M+H]<sup>+</sup>) 412.9816; found: 412.9816. R<sub>f</sub>: 0.7 (CH<sub>2</sub>Cl<sub>2</sub>/MeOH 10:1).

***N*-(*N'*-Acetyl-L-alanyl) 3-Iodopropargylamide 55.** 3-Iodopropargylamine hydrochloride **49** (1.66 g, 7.63 mmol) was dissolved in dry CH<sub>2</sub>Cl<sub>2</sub> (20 mL) and dry DMF (10 mL). *N*-Acetyl-L-alanine (1.02 g, 7.63 mmol) and DIEA (4.92 g, 38.2 mmol) were added. The reaction mixture was cooled to 0 °C, and PyBOP (3.98 g, 7.63 mmol) was added in one portion. The reaction was stirred at room temperature over night. The solvents were removed *in vacuo*, and the purification was carried out by column chromatography (silica gel, CH<sub>2</sub>Cl<sub>2</sub>/MeOH 24:1). **55** (1.80 g, 76%) was obtained as a colorless crystalline solid.

<sup>1</sup>H NMR (300.23 MHz, DMSO-D<sub>6</sub>): δ = 1.15 (d, *J* = 6.9 Hz, 3H, CHCH<sub>3</sub>), 1.82 (s, 3H, C(O)CH<sub>3</sub>), 3.96 (m, 2 H, CH<sub>2</sub>NH), 4.22 (m, 1H, CHCH<sub>3</sub>), 8.03 (d, *J* = 7.5 Hz, 1H, *NH*), 8.29 (t, *J* = 5.1 Hz, 1H, *NH*). <sup>13</sup>C NMR (75.49 MHz, DMSO-D<sub>6</sub>): δ = 8.2 (C≡C-I), 18.6 (CHCH<sub>3</sub>), 23.0 (C(O)CH<sub>3</sub>), 30.3 (CH<sub>2</sub>NH), 48.4 (CHCH<sub>3</sub>), 90.4 (C≡C-I), 169.4, 172.6 (2 amide C=O). Anal. calcd for C<sub>8</sub>H<sub>11</sub>IN<sub>2</sub>O<sub>2</sub>: C, 32.67%; H, 3.77%; I, 43.15%; N, 9.53%; found: C, 32.86%; H, 3.83%; I, 43.01%; N, 9.50%. HRMS (EI): calcd for C<sub>8</sub>H<sub>11</sub>IN<sub>2</sub>O<sub>2</sub>: ([M]<sup>+</sup>) 293.9860; found: 293.9861. R<sub>f</sub>: 0.4 (CH<sub>2</sub>Cl<sub>2</sub>/MeOH 10:1). m. p.: 173-174 °C.

***N*-[*N'*-(9-Fluorenylmethyloxycarbonyl)-L-alanyl] 3-Iodopropargylamide 56.** Following general procedure D, DIEA (9.69 g, 75 mmol) was dissolved in a mixture of dry CH<sub>2</sub>Cl<sub>2</sub> (60 mL) and dry DMF (20 mL). 3-Iodopropargylamine hydrochloride **49** (3.26 g, 15 mmol) and *N*-(9-fluorenylmethyloxycarbonyl)-L-alanine (4.67 g, 15 mmol) were added. At 0 °C, PyBOP (8.32 g, 16 mmol) was added, and the solution was stirred over night. After removal of the solvent, the crystalline product was washed with CH<sub>2</sub>Cl<sub>2</sub>. **56** (5.24 g, 74%) was obtained as colorless crystalline material.

<sup>1</sup>H NMR (300.23 MHz, DMSO-D<sub>6</sub>): δ = 1.21 (d, *J* = 7.2 Hz, 3H, CHCH<sub>3</sub>), 4.0-4.1 (m, 3H, CH<sub>2</sub>NH, fluorenyl CH), 4.2-4.4 (m, 3H, CHCH<sub>3</sub>, CO<sub>2</sub>CH<sub>2</sub>), 7.34 (t, *J* = 7.2 Hz, 2H, aromatic *H*), 7.43 (t, *J* = 7.2 Hz, 2H, aromatic *H*), 7.55 (d, *J* = 7.8 Hz, 1H, carbamate NH), 7.74 (t, *J* = 6.0 Hz, 2H, aromatic *H*), 7.90 (d, *J* = 7.5 Hz, 2H, aromatic *H*), 8.31 (t, *J* = 5.3 Hz, 1H, amide NH). <sup>13</sup>C NMR (75.49 MHz, DMSO-D<sub>6</sub>): δ = 8.4 (C≡Cl), 18.6 (CHCH<sub>3</sub>), 30.5 (CH<sub>2</sub>N), 47.2 (fluorenyl CH), 50.4 (CHCH<sub>3</sub>), 66.1 (CO<sub>2</sub>CH<sub>2</sub>), 90.4 (C≡Cl), 120.6, 125.8, 127.6, 128.1, 141.2, 144.3 (aromatic C), 156.2 (carbamate C=O), 172.8 (amide C=O). Anal. calcd for C<sub>21</sub>H<sub>19</sub>IN<sub>2</sub>O<sub>3</sub>: C, 53.18%; H, 4.04%; I, 26.76%; N, 5.91%; found: C, 52.89%; H, 4.34%; I, 26.57%; N, 5.77%. HRMS (EI): calcd for C<sub>21</sub>H<sub>19</sub>IN<sub>2</sub>O<sub>3</sub>: ([M]<sup>+</sup>) 474.0435; found: 474.0432. R<sub>f</sub>: 0.5 (CH<sub>2</sub>Cl<sub>2</sub>/MeOH 10:1). m. p.: 189-190 °C (decomposition).

***N*-[*N'*-(9-Fluorenylmethyloxycarbonyl)-glycyl] 3-Iodopropargylamide 57.** Following general procedure D, *N*-(9-fluorenylmethyloxycarbonyl)-glycine (2.68 g, 9.0 mmol) and **49** (1.96 g, 9.0 mmol) were dissolved in a mixture of dry CH<sub>2</sub>Cl<sub>2</sub> (30 mL) and dry DMF (10 mL). DIEA (6.65 g, 45.0 mmol) and PyBOP (4.92 g, 9.45 mmol) were added. The next day, the solution was concentrated *in vacuo*, and the product was washed with CH<sub>2</sub>Cl<sub>2</sub>. **57** (3.35 g, 81%) was obtained as a colorless solid.

<sup>1</sup>H NMR (300.23 MHz, DMSO-D<sub>6</sub>): δ = 3.62 (d, *J* = 6.3 Hz, 2H, Gly-CH<sub>2</sub>), 4.01 (d, *J* = 5.4 Hz, 2H, C≡CCH<sub>2</sub>NH), 4.27 (m, 3H, fluorenyl CH, Fmoc-CO<sub>2</sub>CH<sub>2</sub>), 7.34 (t, *J* = 7.2 Hz, 2H, aromatic *H*), 7.43 (t, *J* = 7.2 Hz, 2H, aromatic *H*), 7.57 (t, *J* = 6.0 Hz, 1H, NH), 7.73 (d, *J* = 7.2 Hz, 2H, aromatic *H*), 7.90 (d, *J* = 7.2 Hz, 2H, aromatic *H*), 8.32 (t, *J* = 5.4 Hz, 1H, NH). <sup>13</sup>C NMR (75.49 MHz, DMSO-D<sub>6</sub>): δ = 8.4 (C≡Cl), 30.3 (NHCH<sub>2</sub>), 43.8 (Gly-CH<sub>2</sub>), 47.1 (fluorenyl CH), 66.2 (Fmoc-CO<sub>2</sub>CH<sub>2</sub>), 90.4 (C≡Cl), 120.6, 125.7, 127.6, 128.1, 141.2, 144.3 (aromatic C), 157.0 (carbamate C=O), 169.4 (amide C=O). Anal. calcd for C<sub>20</sub>H<sub>17</sub>N<sub>2</sub>O<sub>3</sub>I: C, 52.19%; H, 3.72%; N, 6.09%, O, 10.43%; I, 27.57%; found: C, 52.20%; H, 3.78%; N, 6.00%. HRMS (ESI): calcd for C<sub>20</sub>H<sub>17</sub>N<sub>2</sub>O<sub>3</sub>I: ([M]<sup>+</sup>) 460.0279; found: 460.0281. R<sub>f</sub>: 0.8 (CH<sub>2</sub>Cl<sub>2</sub>/MeOH 10:1).

**3-Iodoprop-2-yn-1-ol 58.** Propargylic alcohol (16.0 g, 285.3 mmol) was dissolved in MeOH (400 mL). A solution of KOH (56.0 g, 1.0 mol) in H<sub>2</sub>O (100 mL) was prepared, cooled to 0 °C, and added

to the reaction mixture. I<sub>2</sub> (63.5 g, 250 mmol) was added in one portion, and the solution was stirred at room temperature over night. The reaction mixture was neutralized with 1M HCl and extracted with Et<sub>2</sub>O. The organic phase was washed with sat. Na<sub>2</sub>S<sub>2</sub>O<sub>3</sub> solution, dried over Na<sub>2</sub>SO<sub>4</sub>, filtered, and concentrated *in vacuo*. **58** (43.3 g, 83%) was obtained as a colorless solid material.

<sup>1</sup>H NMR (300.23 MHz, CDCl<sub>3</sub>): δ = 2.04 (t, *J* = 5.4 Hz, 1H, OH), 4.41 (d, *J* = 5.4 Hz, 2H, CH<sub>2</sub>). <sup>13</sup>C NMR (75.49 MHz, CDCl<sub>3</sub>): δ = 2.8 (C≡CI), 52.6 (CH<sub>2</sub>), 92.5 (C≡CI). Anal. calcd for C<sub>3</sub>H<sub>3</sub>IO: C, 19.80%; H, 1.66%; I, 69.74%; found: C, 19.85%; H, 1.64%; I, 69.77%. HRMS (EI): calcd for C<sub>3</sub>H<sub>3</sub>IO: ([M]<sup>+</sup>) 181.9233; found: 181.9236. R<sub>f</sub>: 0.7 (CH<sub>2</sub>Cl<sub>2</sub>/MeOH 10:1). m. p.: 42–43 °C.

**1-{2'''-{2''-[2'-(2-Methoxyethoxy)ethoxy]ethoxy}ethoxy}ethoxy}-3-iodoprop-2-yne 60.** In a thoroughly dried Schlenk flask, NaH (60% dispersion in mineral oil, 0.40 g, 10.0 mmol) was mixed with THF (100 mL), and the mixture was degassed in two freeze-pump-thaw cycles. Tetra(ethylene glycol) monomethyl ether (2.08 g, 10.0 mmol) was added at 0 °C, forming a suspension. The mixture was stirred for 30 min before propargyl bromide (80% in toluene, 2.23 g, 15 mmol) was added. Stirring was continued over night. The reaction mixture was concentrated *in vacuo* and taken up in Et<sub>2</sub>O. The organic phase was washed with H<sub>2</sub>O, dried over MgSO<sub>4</sub> and concentrated. 1-{2'''-{2''-[2'-(2-Methoxyethoxy)ethoxy]ethoxy}ethoxy}prop-2-yne (2.29 g, 93%) was obtained as a yellow liquid, which was directly used in the following step without further purification. For the iodination reaction, the tetra(ethylene glycol) derivative (2.12 g, 8.61 mmol) was dissolved in MeOH (50 mL). A solution of KOH (1.45 g, 25.84 mmol) in H<sub>2</sub>O (3 mL) was prepared, cooled to 0 °C, and added to the reaction mixture. After 10 min, I<sub>2</sub> (2.35 g, 9.25 mmol) was added in one portion, and the solution was stirred at room temperature over night. The solvent was removed *in vacuo*, and the residue was taken up in 1M HCl. The aqueous phase was extracted with CHCl<sub>3</sub>. The organic phase was washed with sat. Na<sub>2</sub>S<sub>2</sub>O<sub>3</sub> solution, dried over Na<sub>2</sub>SO<sub>4</sub>, filtered, and concentrated *in vacuo*. The crude material was purified by column chromatography (silica gel, CH<sub>2</sub>Cl<sub>2</sub>/MeOH 24:1). **60** (2.25 g, 70%) was obtained as a yellowish oil.

<sup>1</sup>H NMR (300.23 MHz, CDCl<sub>3</sub>): δ = 3.28 (s, 3H, CH<sub>3</sub>), 3.42–3.46 (m, 2H, CH<sub>2</sub>), 3.51–3.60 (m, 14 H, CH<sub>2</sub>), 4.24 (s, 2H, CH<sub>2</sub>C≡C). <sup>13</sup>C NMR (75.49 MHz, CDCl<sub>3</sub>): δ = 3.6 (C≡CI), 59.0, 60.0, 69.2, 70.3, 70.4, 70.5, 70.5, 70.5, 70.5, 71.9 (OCH<sub>2</sub>, OCH<sub>3</sub>), 90.4 (C≡CI). Anal. calcd for C<sub>12</sub>H<sub>21</sub>IO<sub>5</sub>: C, 38.72%; H, 5.69%; I, 34.10%; found: C, 38.82%; H, 5.47%; I, 34.20%. R<sub>f</sub>: 0.5 (CH<sub>2</sub>Cl<sub>2</sub>/MeOH 10:1).

**1-Iodo-2-trimethylsilylacetylene 61.** Trimethylsilylacetylene (1.96 g, 20.0 mmol) was dissolved in dry THF (25 mL). The solution was cooled to –78 °C and *n*-butyl lithium (1.6 M in hexanes, 20.0 mmol) was added. The reaction was stirred for 10 min, then heated to 0 °C and stirred for another 10 min. Then, the temperature was adjusted to –78 °C, and I<sub>2</sub> (5.10 g, 20.0 mmol) was added in

one portion. The flask was covered with aluminum foil, and the reaction mixture was stirred at room temperature over night. The solution was diluted with  $\text{CH}_2\text{Cl}_2$  and washed with sat.  $\text{Na}_2\text{S}_2\text{O}_3$  solution as well as water. The organic phase was dried over  $\text{MgSO}_4$ , filtered, and concentrated *in vacuo*. The purification of the crude material was carried out by distillation (20 mbar,  $70^\circ\text{C}$ ), and **61** (3.60 g, 80%) was obtained as a colorless liquid.

$^1\text{H}$  NMR (300.23 MHz,  $\text{CDCl}_3$ ):  $\delta = 0.18$  (s, 9H,  $\text{Si}(\text{CH}_3)_3$ ).  $^{13}\text{C}$  NMR (75.49 MHz,  $\text{CDCl}_3$ ):  $\delta = -0.1$  ( $\text{Si}(\text{CH}_3)_3$ ), 20.6 ( $\text{C}\equiv\text{C}$ ), 104.2 ( $\text{C}\equiv\text{C}$ ).  $R_f$ : 0.8 ( $\text{CH}_2\text{Cl}_2$ ).

**3-Iodopropiolic Acid Methyl Ester 62.** Propiolic acid methyl ester (1.0 g, 11.89 mmol) was dissolved in dry acetone (30 mL). *N*-Iodosuccinimide (4.0 g, 17.85 mmol) and  $\text{AgNO}_3$  (0.4 g, 2.35 mmol) were added. After 2.5 h, the reaction mixture was cooled to  $0^\circ\text{C}$ , and ice was added. The reaction mixture was extracted with  $\text{Et}_2\text{O}$ . The organic phase was dried over  $\text{MgSO}_4$ , filtered, and concentrated *in vacuo*. The obtained crude material was purified by sublimation ( $40^\circ\text{C}$ ,  $1\cdot 10^{-2}$  mbar). **62** (2.0 g, 80%) was obtained as a colorless crystalline material.

$^1\text{H}$  NMR (300.23 MHz,  $\text{CDCl}_3$ ):  $\delta = 3.80$  (s, 3H,  $\text{CH}_3$ ).  $^{13}\text{C}$  NMR (75.49 MHz,  $\text{CDCl}_3$ ):  $\delta = 14.8$  ( $\text{C}\equiv\text{C}$ ), 53.1 ( $\text{CH}_3$ ), 86.8 ( $\text{C}\equiv\text{C}$ ), 152.8 (ester  $\text{C}=\text{O}$ ). Anal. calcd for  $\text{C}_4\text{H}_3\text{IO}_2$ : C, 22.88%; H, 1.44%; I, 60.44%; found: C, 22.98%; H, 1.43%; I, 60.43%. HRMS (EI): calcd for  $\text{C}_4\text{H}_3\text{IO}_2$ : ( $[\text{M}]^+$ ) 201.9173; found 201.9175.  $R_f$ : 0.5 ( $\text{CH}_2\text{Cl}_2/\text{MeOH}$  10:1). m. p.:  $45^\circ\text{C}$ .

**3-Bromopropiolic Acid 64.** KOH (5.1 g, 90 mmol) was dissolved in  $\text{H}_2\text{O}$  (40 mL) at  $0^\circ\text{C}$ .  $\text{Br}_2$  (4.8 g, 30 mmol) was added to the aqueous solution. Another KOH (1.7 g, 30 mmol) solution in  $\text{H}_2\text{O}$  (10 mL) was prepared and cooled to  $0^\circ\text{C}$ , to which propiolic acid (2.1 g, 30 mmol) was added. Both solutions were combined and stirred for 30 min. The solution was acidified by the addition of 1M HCl and extracted four times with  $\text{Et}_2\text{O}$  and once with  $\text{CH}_2\text{Cl}_2$ . The combined organic phases were dried over  $\text{Na}_2\text{SO}_4$ , filtered, and concentrated *in vacuo*. **64** (3.52 g, 79%) was obtained by recrystallization from hot hexanes.

$^1\text{H}$  NMR (300.23 MHz,  $\text{CDCl}_3$ ):  $\delta = 11.5$  (bs, 1H,  $\text{CO}_2\text{H}$ ).  $^{13}\text{C}$  NMR (75.49 MHz,  $\text{CDCl}_3$ ):  $\delta = 56.6$  ( $\text{C}\equiv\text{CBr}$ ), 72.3 ( $\text{C}\equiv\text{CBr}$ ), 157.4 (acid  $\text{C}=\text{O}$ ). Anal. calcd for  $\text{C}_3\text{HBrO}_2$ : C, 24.19%; H, 0.68%; O, 21.48%; Br, 53.65%; found: C, 23.92%; H, 0.61%; O, 21.39%; Br, 53.83%. HRMS (EI): calcd for  $\text{C}_3\text{HBrO}_2$ : ( $[\text{M}]^+$ ) 147.9155; found: 147.9154.  $R_f$ : 0.2 ( $\text{CH}_2\text{Cl}_2/\text{MeOH}$  10:1). m. p.:  $84.5\text{--}85.5^\circ\text{C}$ .

**Hexa-2,4-diynylene-1,6-bis(oxycarbonyl-L-alanine *tert*-Butyl Ester) 65.** A solution of  $\text{CuCl}$  (0.66 g, 6.6 mmol) and TMEDA (1 mL, 6.6 mmol, 1 eq) in acetone (30 mL) was added to a solution of **46** (1.5 g, 6.6 mmol) in acetone (100 mL), and the resulting green mixture was stirred for 4 h at room temperature with dry air bubbling through the reaction mixture. A white precipitate formed which was

filtered and washed with cold acetone and afterwards dissolved and filtered again in boiling methanol to give **65** (0.93 g, 62%) as a colorless crystalline solid.

$^1\text{H}$  NMR (300.23 MHz,  $\text{CDCl}_3$ ):  $\delta$  = 1.31 (d,  $J$  = 7.2 Hz, 6H, 2  $\text{CHCH}_3$ ), 1.40 (s, 18H, 2  $\text{C}(\text{CH}_3)_3$ ), 4.16 (m, 2H, 2  $\text{CHCH}_3$ ), 4.67 (m, 4H, 2  $\text{NHCO}_2\text{CH}_2$ ), 5.59 (d,  $J$  = 7.5 Hz, 1H,  $\text{NH}$ ).  $^{13}\text{C}$  NMR (75.49 MHz,  $\text{CDCl}_3$ ):  $\delta$  = 18.6 (2  $\text{CHCH}_3$ ), 27.9 (2  $\text{CHCH}_3$ ), 50.3 (2  $\text{CHCH}_3$ ), 52.7 (2  $\text{NHCO}_2\text{CH}_2$ ), 70.2, 74.0 (diacetylene C), 81.9 (2  $\text{C}(\text{CH}_3)_3$ ), 154.5 (2 carbamate C=O), 171.9 (2 ester C=O). Anal. calcd for  $\text{C}_{22}\text{H}_{32}\text{N}_2\text{O}_8$ : C, 58.40%; H, 7.13%; N, 6.19%; found: C, 58.42%; H, 7.2%; N, 6.13%. HRMS (EI): calcd for  $\text{C}_{22}\text{H}_{32}\text{N}_2\text{O}_8$ :  $([\text{M}]^+)$  452.2153; found: 452.2195.  $R_f$ : 0.8 ( $\text{CH}_2\text{Cl}_2/\text{MeOH}$  10:1).

**Hexa-2,4-diynylene-1,6-bis(oxycarbonyl-L-alanine) 66.** Following general procedure B, **65** (0.45 g, 1.0 mmol) was dissolved in dry  $\text{CH}_2\text{Cl}_2$  (10 mL), a large excess of TFA was added, and the solution was stirred for 5 h. **66** (0.34 g, 99%) was obtained as a brown solid material. A further purification was not necessary before the next step.

$^1\text{H}$  NMR (300.23 MHz,  $\text{DMSO}-d_6$ ):  $\delta$  = 1.27 (d,  $J$  = 7.2 Hz, 6H, 2  $\text{CHCH}_3$ ), 4.00 (m, 2H, 2  $\text{CHCH}_3$ ), 4.77 (s, 4H, 2  $\text{CO}_2\text{CH}_2$ ), 7.76 (d,  $J$  = 7.8 Hz, 2H, 2  $\text{NH}$ ).  $^{13}\text{C}$  NMR (75.49 MHz,  $\text{DMSO}-d_6$ ):  $\delta$  = 17.5 (2  $\text{CHCH}_3$ ), 49.8 (2  $\text{CHCH}_3$ ), 52.4 (2  $\text{CO}_2\text{CH}_2$ ), 69.4, 76.3 (diacetylene C), 155.3 (carbamate 2 C=O), 174.6 (acid 2 C=O).  $R_f$ : 0.05 ( $\text{CH}_2\text{Cl}_2/\text{MeOH}$  10:1).

***N*-[6-(*N'*-Acetamido)hexa-2,4-diynyl-1-oxycarbonyl]-L-alanine *tert*-Butyl Ester 67.** Following general procedure A, **46** (0.65 g, 2.86 mmol) and *N*-(3-iodo prop-2-ynyl)acetamide **50** (0.8 g, 3.59 mmol) were dissolved in dry THF (30 mL). The solution was stirred over night. The purification was carried out by column chromatography (silica gel, gradient  $\text{CH}_2\text{Cl}_2/\text{MeOH}$  50:1  $\rightarrow$   $\text{CH}_2\text{Cl}_2/\text{MeOH}$  20:1). **67** (0.52 g, 56%) was obtained as a brownish solid.

$^1\text{H}$  NMR (300.23 MHz,  $\text{CDCl}_3$ ):  $\delta$  = 1.32 (d,  $J$  = 7.2 Hz, 3H,  $\text{CHCH}_3$ ), 1.41 (s, 9H,  $\text{C}(\text{CH}_3)_3$ ), 1.96 (s, 3H,  $\text{C}(\text{O})\text{CH}_3$ ), 4.05 (d,  $J$  = 5.4 Hz, 2 H,  $\text{CH}_2\text{NHAc}$ ), 4.15 (m, 1H,  $\text{CHCH}_3$ ), 4.67 (m, 2H,  $\text{NHCO}_2\text{CH}_2$ ), 5.63 (d,  $J$  = 7.5 Hz, 1H,  $\text{NH}$ ), 6.76 (m, 1H,  $\text{NH}$ ).  $^{13}\text{C}$  NMR (75.49 MHz,  $\text{CDCl}_3$ ):  $\delta$  = 18.4 ( $\text{CHCH}_3$ ), 22.7 ( $\text{C}(\text{O})\text{CH}_3$ ), 27.8 ( $\text{C}(\text{CH}_3)_3$ ), 29.5 ( $\text{CH}_2\text{NHAc}$ ), 50.2 ( $\text{CHCH}_3$ ), 52.8 ( $\text{NHCO}_2\text{CH}_2$ ), 66.8, 70.4, 72.3, 76.0 (diacetylene C), 82.0 ( $\text{C}(\text{CH}_3)_3$ ), 154.6 (carbamate C=O), 170.2 (amide C=O), 171.9 (ester C=O). HRMS (EI): calcd for  $\text{C}_{16}\text{H}_{22}\text{N}_2\text{O}_5$ :  $([\text{M}]^+)$  322.1524; found: 322.1523.  $R_f$ : 0.5 ( $\text{CH}_2\text{Cl}_2/\text{MeOH}$  10:1).

***N*-[6-(*N'*-Acetamido)hexa-2,4-diynyl-1-oxycarbonyl]-L-alanine 68.** Following general procedure B, **67** (0.86 g, 2.67 mmol) was dissolved in dry  $\text{CH}_2\text{Cl}_2$  (10 mL), a large excess of TFA was added, and the solution was stirred over night. **68** (0.71 g, 100%) was obtained as a brown amorphous material, and no further purification was carried out before the next step.

$^1\text{H}$  NMR (300.23 MHz,  $\text{CDCl}_3$ ):  $\delta$  = 1.40 (d,  $J$  = 7.2 Hz, 3H,  $\text{CHCH}_3$ ), 2.00 (s, 3H,  $\text{C(O)CH}_3$ ), 4.06 (d,  $J$  = 5.1 Hz, 2H,  $\text{CH}_2\text{NHAc}$ ), 4.26 (m, 1H,  $\text{CHCH}_3$ ), 4.68 (s, 2H,  $\text{NHCO}_2\text{CH}_2$ ), 5.77 (d,  $J$  = 7.5 Hz, 1H,  $\text{NH}$ ), 7.00 (m, 1H,  $\text{NH}$ ), 8.82 (bs, 1H,  $\text{CO}_2\text{H}$ ).  $^{13}\text{C}$  NMR (75.49 MHz,  $\text{CDCl}_3$ ):  $\delta$  = 18.4 ( $\text{CHCH}_3$ ), 22.6 ( $\text{C(O)CH}_3$ ), 29.7 ( $\text{CH}_2\text{NHAc}$ ), 49.7 ( $\text{CHCH}_3$ ), 52.9 ( $\text{NHCO}_2\text{CH}_2$ ), 67.0, 70.5, 72.6, 76.0 (diacetylene C), 154.8 (carbamate  $\text{C=O}$ ), 170.9 (amide  $\text{C=O}$ ), 174.9 (acid  $\text{C=O}$ ).  $R_f$ : 0.1 ( $\text{CH}_2\text{Cl}_2/\text{MeOH}$  10:1).

***N*-{6-[*N'*-(4-Methoxysuccinyl)amido]hexa-2,4-diyne-1-oxycarbonyl}-L-alanine *tert*-Butyl Ester **70**.** Following general procedure A, **46** (0.58 g, 2.55 mmol), **51** (0.92 g, 3.12 mmol) and the catalysts were dissolved in dry THF (30 mL). The solution was stirred for 4 h, and the solvents were removed *in vacuo*. Column chromatography (silica gel,  $\text{CH}_2\text{Cl}_2/\text{MeOH}$  20:1) afforded **70** (0.55 g, 55%) as a brownish solid material.

$^1\text{H}$  NMR (300.23 MHz,  $\text{CDCl}_3$ ):  $\delta$  = 1.33 (d,  $J$  = 7.2 Hz, 3H,  $\text{CHCH}_3$ ), 1.41 (s, 9H,  $\text{C}(\text{CH}_3)_3$ ), 2.48 (t,  $J$  = 6.7 Hz, 2H,  $\text{NHC(O)CH}_2$ ), 2.62 (t,  $J$  = 6.7 Hz, 2H,  $\text{CH}_2\text{CO}_2\text{CH}_3$ ), 3.63 (s, 3H,  $\text{OCH}_3$ ), 4.07 (d,  $J$  = 5.4 Hz, 2H,  $\text{CH}_2\text{NH}$ ), 4.16 (m, 1H,  $\text{CHCH}_3$ ), 4.67 (s, 2H,  $\text{CO}_2\text{CH}_2\text{C}\equiv\text{C}$ ), 5.61 (d,  $J$  = 7.5 Hz, 1H,  $\text{NH}$ ), 6.71 (t,  $J$  = 5.1 Hz, 1H,  $\text{NH}$ ).  $^{13}\text{C}$  NMR (75.49 MHz,  $\text{CDCl}_3$ ):  $\delta$  = 18.4 ( $\text{CHCH}_3$ ), 27.8 ( $\text{C}(\text{CH}_3)_3$ ), 29.1, 29.6, 30.4 ( $\text{CH}_2\text{NH}$ ,  $\text{CH}_2\text{CO}_2\text{CH}_3$ ,  $\text{NHC(O)CH}_2$ ), 50.3 ( $\text{CHCH}_3$ ), 51.8 ( $\text{OCH}_3$ ), 52.8 ( $\text{CO}_2\text{CH}_2\text{C}\equiv\text{C}$ ), 66.7, 70.5, 72.4, 76.3 (diacetylene C), 81.9 ( $\text{C}(\text{CH}_3)_3$ ), 154.7 (carbamate  $\text{C=O}$ ), 171.4, 171.9, 173.3 (2 ester  $\text{C=O}$ , amide  $\text{C=O}$ ). HRMS (EI): calcd for  $\text{C}_{19}\text{H}_{26}\text{N}_2\text{O}_7$ : ( $[\text{M}]^+$ ) 394.1735; found: 394.1733.  $R_f$ : 0.35 ( $\text{CH}_2\text{Cl}_2/\text{MeOH}$  10:1).

***N*-{6-[*N'*-(4-Methoxysuccinyl)amido]hexa-2,4-diyne-1-oxycarbonyl}-L-alanine **71**.** Following general procedure B, **70** (0.32 g, 0.8 mmol) was dissolved in dry  $\text{CH}_2\text{Cl}_2$  (10 mL), a large excess of TFA was added, and the solution was stirred over night. **71** (0.34 g, 100%) was obtained as a brown amorphous material. A further purification was not necessary before the next step.

$^1\text{H}$  NMR (300.23 MHz,  $\text{DMSO-}d_6$ ):  $\delta$  = 1.26 (d,  $J$  = 7.2 Hz, 3H,  $\text{CHCH}_3$ ), 2.39 (t,  $J$  = 6.6 Hz, 2H,  $\text{NHC(O)CH}_2$ ), 2.52 (t,  $J$  = 6.6 Hz, 2H,  $\text{CH}_2\text{CO}_2\text{CH}_3$ ), 3.58 (s, 3H,  $\text{OCH}_3$ ), 3.9-4.0 (m, 3H,  $\text{CH}_2\text{NH}$ ,  $\text{CHCH}_3$ ), 4.75 (s, 2H,  $\text{CO}_2\text{CH}_2\text{C}\equiv\text{C}$ ), 7.57 (d,  $J$  = 7.5 Hz, 1H,  $\text{NH}$ ), 8.43 (t,  $J$  = 5.4 Hz, 1H,  $\text{NH}$ ).  $^{13}\text{C}$  NMR (75.49 MHz,  $\text{DMSO-}d_6$ ):  $\delta$  = 17.5 ( $\text{CHCH}_3$ ), 29.0, 30.0 ( $\text{CH}_2\text{NH}$ ,  $\text{CH}_2\text{CO}_2\text{CH}_3$ ,  $\text{NHC(O)CH}_2$ ), 49.8 ( $\text{CHCH}_3$ ), 51.7 ( $\text{OCH}_3$ ), 52.4 ( $\text{CO}_2\text{CH}_2\text{C}\equiv\text{C}$ ), 65.7, 70.0, 74.2, 78.7 (diacetylene C), 155.3 (carbamate  $\text{C=O}$ ), 171.2, 173.2, 174.6 (ester  $\text{C=O}$ , amide  $\text{C=O}$ , acid  $\text{C=O}$ ).  $R_f$ : 0.1 ( $\text{CH}_2\text{Cl}_2/\text{MeOH}$  10:1).

***N*-{6-[*N'*-(9-Fluorenylmethyloxycarbonyl)amino]hexa-2,4-diyne-1-oxycarbonyl}-L-alanine *tert*-Butyl Ester **72**.** Following general procedure A, *N*-propargyloxycarbonyl-L-alanine *tert*-butyl ester (1.0 g, 4.4 mmol), **52** (2.1 g, 5.3 mmol) and the catalysts were dissolved in dry THF

(50 mL). The solution was stirred for 3 h, and the solvents were removed *in vacuo*. The crude material was purified by repeated column chromatography (silica gel, CHCl<sub>3</sub>/toluene 10:1) and preparative GPC (CHCl<sub>3</sub>). However, only mixtures of **72** and the homo- as well as heterocoupling side products were obtained.

HRMS (EI): calcd for C<sub>29</sub>H<sub>30</sub>N<sub>2</sub>O<sub>6</sub>: ([M]<sup>+</sup>) 502.2098; found 502.2085. R<sub>f</sub>: 0.75 (CH<sub>2</sub>Cl<sub>2</sub>/MeOH 10:1).

***N*-{6-[*N'*-(9-Fluorenylmethoxycarbonyl)amino]hexa-2,4-diynyl-1-oxycarbonyl}-L-**

**alanine 73.** Following general procedure B, **72** (1.8 g, impure) was dissolved in dry CH<sub>2</sub>Cl<sub>2</sub> (20 mL), a large excess of TFA was added, and the solution was stirred over night. The crude material was purified by column chromatography (silica gel, CH<sub>2</sub>Cl<sub>2</sub>/MeOH 10:1). **73** (1.0 g, 62%) was obtained as a nearly colorless material.

<sup>1</sup>H NMR (300.23 MHz, DMSO-D<sub>6</sub>): δ = 1.28 (d, *J* = 7.5 Hz, 3H, CHCH<sub>3</sub>), 3.95 (d, *J* = 5.7 Hz, 2H, NHCH<sub>2</sub>), 4.02 (m, 1H, CHCH<sub>3</sub>), 4.24 (t, *J* = 6.3 Hz, 1H, fluorenyl CH), 4.36 (d, *J* = 6.9 Hz, 2H, Fmoc-CO<sub>2</sub>CH<sub>2</sub>), 4.77 (m, 2H, NHCO<sub>2</sub>CH<sub>2</sub>), 7.34 (t, *J* = 7.2 Hz, 2H, aromatic *H*), 7.43 (t, *J* = 7.5 Hz, 2H, aromatic *H*), 7.70 (d, *J* = 7.5 Hz, 2H, aromatic *H*), 7.76 (d, *J* = 7.5 Hz, 1H, NH), 7.8-8.0 (m, 3H, aromatic *H*, NH). R<sub>f</sub>: 0.1 (CH<sub>2</sub>Cl<sub>2</sub>/MeOH 10:1).

***N*-{6-[*N'*-(5-Dimethylamino-1-naphthalenesulfonyl)amido)]hexa-2,4-diynyl-1-**

**oxycarbonyl}-L-alanine *tert*-Butyl Ester 74.** Following general procedure A, **46** (0.18 g, 0.81 mmol), **53** (0.46 g, 0.97 mmol) and the catalysts were dissolved in THF (30 mL). The solution was stirred over night, diluted with CHCl<sub>3</sub> (40 mL) and washed twice with sat. NaHCO<sub>3</sub> solution. The organic phase was dried over MgSO<sub>4</sub>, filtered, and concentrated *in vacuo*. The crude product was purified by column chromatography (silica gel, ethyl acetate/hexane 1:3). **74** (0.20 g, 47%) was obtained as a yellow powder.

<sup>1</sup>H NMR (300.23 MHz, DMSO-D<sub>6</sub>): δ = 1.39 (d, *J* = 7.2 Hz, 3H, CHCH<sub>3</sub>), 1.48 (s, 9H, C(CH<sub>3</sub>)<sub>3</sub>), 2.90 (s, 6H, N(CH<sub>3</sub>)<sub>2</sub>), 3.87 (d, *J* = 6.3 Hz, 2H, NHCH<sub>2</sub>), 4.24 (m, 1H, CHCH<sub>3</sub>), 4.62 (m, 2H, NHCO<sub>2</sub>CH<sub>2</sub>), 5.27 (bs, 1H, NH), 5.46 (m, 1H, NH), 7.21 (d, *J* = 7.5 Hz, 1H, aromatic *H*), 7.56 (m, 2H, aromatic *H*), 8.26 (m, 2H, aromatic *H*), 8.57 (d, *J* = 8.4 Hz, 1H, aromatic *H*). <sup>13</sup>C NMR (75.49 MHz, DMSO-D<sub>6</sub>): δ = 18.8 (CHCH<sub>3</sub>), 27.9 (C(CH<sub>3</sub>)<sub>3</sub>), 33.6 (NHCH<sub>2</sub>), 45.4 (N(CH<sub>3</sub>)<sub>2</sub>), 50.3 (CHCH<sub>3</sub>), 52.7 (NHCO<sub>2</sub>CH<sub>2</sub>), 68.2, 69.9, 72.9, 73.7 (diacetylene C), 82.2 (C(CH<sub>3</sub>)<sub>3</sub>), 115.2, 118.5, 123.2, 128.6, 129.7, 129.9, 129.9, 131.0, 134.1, 151.4 (aromatic C), 154.4 (carbamate C=O), 171.9 (ester C=O). Anal. calcd for C<sub>26</sub>H<sub>31</sub>N<sub>3</sub>O<sub>6</sub>S: C, 60.80%; H, 6.08%; N, 8.18%; found: C, 59.69%; H, 5.90%; N, 7.97%. R<sub>f</sub>: 0.5 (EtOAc/Hex 1:1).

***N*-{6-[*N'*-(5-Dimethylamino-1-naphthalenesulfonyl)amido)]hexa-2,4-diynyl-1-**

**oxycarbonyl}-L-alanine 75.** Following general procedure B, **74** (0.14 g, 0.27 mmol) was dissolved



in CH<sub>2</sub>Cl<sub>2</sub> (10 mL), a large excess of TFA was added, and the solution was stirred over night. **75** (0.11 g, 90%) was obtained as a dark amorphous substance. A further purification was not necessary before the next step.

<sup>1</sup>H NMR (300.23 MHz, DMSO-D<sub>6</sub>): δ = 1.27 (d, *J* = 7.5 Hz, 3H, CHCH<sub>3</sub>), 2.90 (s, 6H, N(CH<sub>3</sub>)<sub>2</sub>), 3.90 (d, *J* = 5.7 Hz, 2 H, NHCH<sub>2</sub>), 3.99 (m, 1H, CHCH<sub>3</sub>), 4.66 (m, 2H, NHCO<sub>2</sub>CH<sub>2</sub>), 7.35 (d, *J* = 7.5 Hz, 1H, aromatic *H*), 7.65 (m, 2H, aromatic *H*, *NH*), 7.74 (d, *J* = 7.5 Hz, 1H, aromatic *H*), 8.17 (d, *J* = 6.9 Hz, 1H, aromatic *H*), 8.31 (d, *J* = 8.7 Hz, 1H, aromatic *H*), 8.50 (m, 2H, aromatic *H*, *NH*). <sup>13</sup>C NMR (75.49 MHz, DMSO-D<sub>6</sub>): δ = 17.5 (CHCH<sub>3</sub>), 32.7 (NHCH<sub>2</sub>), 46.0 (N(CH<sub>3</sub>)<sub>2</sub>), 49.7 (CHCH<sub>3</sub>), 52.3 (NHCO<sub>2</sub>CH<sub>2</sub>), 66.9, 69.5, 74.6, 76.7 (diacetylene C), 116.0, 120.2, 124.3, 128.4, 129.2, 129.3, 129.5, 130.0, 136.1, 150.7 (aromatic C), 155.2 (carbamate C=O), 174.6 (ester C=O). R<sub>f</sub>: 0.3 (CH<sub>2</sub>Cl<sub>2</sub>/MeOH 10:1).

***N*-{6-[*N'*-(*N''*-Acetyl-L-alanyl)amido]hexa-2,4-diynyl-1-oxycarbonyl}-L-alanine *tert*-Butyl Ester **76**.** Following general procedure A, **46** (0.90 g, 3.96 mmol), **55** (1.4 g, 4.76 mmol) and the catalysts were dissolved in dry THF (30 mL). The solution was stirred over night. The purification was carried out by column chromatography (silica gel, gradient CH<sub>2</sub>Cl<sub>2</sub>/MeOH 50:1 → CH<sub>2</sub>Cl<sub>2</sub>/MeOH 20:1). **76** (0.80 g, 51%) was obtained as colorless solid material.

<sup>1</sup>H NMR (300.23 MHz, CDCl<sub>3</sub>): δ = 1.32 (d, *J* = 7.2 Hz, 3H, CHCH<sub>3</sub>), 1.33 (d, *J* = 7.5 Hz, 3H, CHCH<sub>3</sub>), 1.99 (s, 3H, C(O)CH<sub>3</sub>), 4.07 (d, *J* = 5.1 Hz, 2H, CH<sub>2</sub>NH), 4.18 (m, 1H, CHCH<sub>3</sub>), 4.58 (m, 1H, CHCH<sub>3</sub>), 4.68 (m, 2H, NHCO<sub>2</sub>CH<sub>2</sub>), 5.77 (d, *J* = 7.8 Hz, 1H, *NH*), 7.03 (d, *J* = 7.8 Hz, 1H, *NH*), 7.68 (m, 1H, *NH*). <sup>13</sup>C NMR (75.49 MHz, CDCl<sub>3</sub>): δ = 18.2, 18.3 (2 CHCH<sub>3</sub>), 23.0 (C(O)CH<sub>3</sub>), 27.9 (C(CH<sub>3</sub>)<sub>3</sub>), 29.7 (CH<sub>2</sub>NH), 48.7, 50.3 (2 CHCH<sub>3</sub>), 52.9 (NHCO<sub>2</sub>CH<sub>2</sub>), 67.1, 70.6, 72.6, 75.7 (diacetylene C), 82.1 (C(CH<sub>3</sub>)<sub>3</sub>), 154.7 (carbamate C=O), 170.6, 172.1, 172.6 (2 amide C=O, ester C=O). HRMS (EI): calcd for C<sub>19</sub>H<sub>27</sub>N<sub>3</sub>O<sub>6</sub>: ([M]<sup>+</sup>) 393.1895; found: 393.1896. R<sub>f</sub>: 0.5 (CH<sub>2</sub>Cl<sub>2</sub>/MeOH 10:1).

***N*-{6-[*N'*-(*N''*-Acetyl-L-alanyl)amido]hexa-2,4-diynyl-1-oxycarbonyl}-L-alanine **77**.** Following general procedure B, **76** (0.16 g, 0.40 mmol) was dissolved in dry CH<sub>2</sub>Cl<sub>2</sub> (10 mL), a large excess of TFA was added, and the solution was stirred for 5 h. **77** (0.13 g, 100%) was obtained as a brownish solid material. A further purification was not necessary before the next step.

<sup>1</sup>H NMR (300.23 MHz, DMSO-D<sub>6</sub>): δ = 1.18 (d, *J* = 7.2 Hz, 3H, CHCH<sub>3</sub>), 1.27 (d, *J* = 7.2 Hz, 3H, CHCH<sub>3</sub>), 1.84 (s, 3H, C(O)CH<sub>3</sub>), 3.9-4.1 (m, 3 H, CH<sub>2</sub>NH, CHCH<sub>3</sub>), 4.23 (m, 1H, CHCH<sub>3</sub>), 4.75 (s, 2H, NHCO<sub>2</sub>CH<sub>2</sub>), 7.76 (d, *J* = 7.5 Hz, 1H, *NH*), 8.08 (d, *J* = 7.2 Hz, 1H, *NH*), 8.40 (m, 1H, *NH*). <sup>13</sup>C NMR (75.49 MHz, DMSO-D<sub>6</sub>): δ = 17.5, 18.5 (2 CHCH<sub>3</sub>), 23.0 (C(O)CH<sub>3</sub>), 29.1 (CH<sub>2</sub>NH), 48.4, 49.7 (2 CHCH<sub>3</sub>), 52.4 (NHCO<sub>2</sub>CH<sub>2</sub>), 65.7, 70.1, 74.3, 78.7 (diacetylene C), 155.3 (carbamate C=O), 169.5, 172.8 (2 amide C=O), 174.6 (acid C=O). R<sub>f</sub>: 0.1 (CH<sub>2</sub>Cl<sub>2</sub>/MeOH 10:1).

***N*-{6-*[N'*-*[N''*-(9-Fluorenylmethyloxycarbonyl)-*L*-alanyl]amido}hexa-2,4-diynyl-1-oxycarbonyl}-*L*-alanine *tert*-Butyl Ester **78**.** Following general procedure A, **46** (1.53 g, 6.73 mmol), **56** (3.80 g, 8.01 mmol) and the catalysts were dissolved in THF (80 mL). The solution was stirred for 3 h, and an acidic aqueous workup was carried out. Flash column chromatography (silica gel, CH<sub>2</sub>Cl<sub>2</sub>/MeOH 50:1) afforded **78** (1.94 g, 50%) as slightly brown crystals.

<sup>1</sup>H NMR (300.23 MHz, CDCl<sub>3</sub>): δ = 1.36 (d, *J* = 6.9 Hz, 6H, 2 CHCH<sub>3</sub>), 1.46 (s, 9H, C(CH<sub>3</sub>)<sub>3</sub>), 4.11 (m, 2H, CH<sub>2</sub>NH), 4.2-4.3 (m, 3H, Fmoc-CO<sub>2</sub>CH<sub>2</sub>, fluorenyl CH), 4.4-4.5 (m, 2H, 2 CHCH<sub>3</sub>), 4.69 (m, 2H, CO<sub>2</sub>CH<sub>2</sub>C≡C), 5.44 (d, *J* = 6.6 Hz, 2H, NH), 6.62 (s, 1H, NH), 7.29 (dt, *J* = 1.2 Hz, 7.5 Hz, 2H, aromatic *H*), 7.39 (t, *J* = 7.5 Hz, 2H, aromatic *H*), 7.57 (d, *J* = 7.5 Hz, 2H, aromatic *H*), 7.75 (d, *J* = 7.5 Hz, 2H, aromatic *H*). <sup>13</sup>C NMR (75.49 MHz, CDCl<sub>3</sub>): δ = 18.5, 18.8 (2 CHCH<sub>3</sub>), 28.0 (C(CH<sub>3</sub>)<sub>3</sub>), 29.8 (CH<sub>2</sub>NH), 47.2 (fluorenyl CH), 50.3 (2 CHCH<sub>3</sub>), 52.9 (CO<sub>2</sub>CH<sub>2</sub>C≡C), 67.1, 67.4, 70.5, 72.7, 75.6 (diacetylene C, Fmoc-CO<sub>2</sub>CH<sub>2</sub>), 82.1 (C(CH<sub>3</sub>)<sub>3</sub>), 120.0, 125.0, 127.1, 127.8, 141.3, 143.7 (aromatic C), 154.5, 156.1 (2 carbamate C=O), 172.0, 172.1 (amide and ester C=O). Anal. calcd for C<sub>32</sub>H<sub>35</sub>N<sub>3</sub>O<sub>7</sub>: C, 67.00%; H, 6.15%; N, 7.33%; found: C, 66.72%; H, 6.19%; N, 7.08%. HRMS (MALDI): calcd for C<sub>32</sub>H<sub>35</sub>N<sub>3</sub>O<sub>7</sub>Na: ([M+Na]<sup>+</sup>) 596.2367; found: 596.2367. R<sub>f</sub>: 0.4 (CH<sub>2</sub>Cl<sub>2</sub>/MeOH 10:1).

***N*-{6-*[N'*-*[N''*-(9-Fluorenylmethyloxycarbonyl)-*L*-alanyl]amido}hexa-2,4-diynyl-1-oxycarbonyl}-*L*-alanine **79**.** Following general procedure B, **78** (0.52 g, 0.9 mmol) was dissolved in dry CH<sub>2</sub>Cl<sub>2</sub> (20 mL), a large excess of TFA was added, and the solution was stirred over night. **79** (0.59 g, 100%) was obtained as a brownish, crystalline material. A further purification was not necessary before the next step.

<sup>1</sup>H NMR (300.23 MHz, DMSO-D<sub>6</sub>): δ = 1.25 (m, 6H, 2 CHCH<sub>3</sub>), 4.03 (m, 4H, 2 CHCH<sub>3</sub>, CH<sub>2</sub>NH), 4.25 (m, 3H, Fmoc-CO<sub>2</sub>CH<sub>2</sub>, fluorenyl CH), 4.76 (s, 2H, CO<sub>2</sub>CH<sub>2</sub>C≡C), 7.32 (t, *J* = 7.2 Hz, 2H, aromatic *H*), 7.43 (t, *J* = 7.2 Hz, 2H, aromatic *H*), 7.57 (d, *J* = 7.5 Hz, 1H, NH), 7.74 (m, 3H, aromatic *H*, NH), 7.89 (d, *J* = 7.5 Hz, 2H, aromatic *H*), 8.43 (m, 1H, NH). <sup>13</sup>C NMR (75.49 MHz, DMSO-D<sub>6</sub>): δ = 17.5, 18.5 (2 CHCH<sub>3</sub>), 29.2 (CH<sub>2</sub>NH), 47.1 (fluorenyl CH), 49.8, 50.4 (2 CHCH<sub>3</sub>), 52.4 (CO<sub>2</sub>CH<sub>2</sub>C≡C), 65.77, 66.12, 70.08, 74.31, 78.64 (diacetylene C, Fmoc-CO<sub>2</sub>CH<sub>2</sub>), 120.6, 125.8, 127.5, 128.1, 141.2, 144.4 (aromatic C), 155.3, 156.2 (2 carbamate C=O), 172.9 (amide C=O), 174.6 (acid C=O). HRMS (MALDI): calcd for C<sub>28</sub>H<sub>27</sub>N<sub>3</sub>O<sub>7</sub>: ([M]<sup>+</sup>) 518.1922; found: 518.1922. R<sub>f</sub>: 0.1 (CH<sub>2</sub>Cl<sub>2</sub>/MeOH 10:1).

***N*-{6-*[N'*-*[N''*-(9-Fluorenylmethyloxycarbonyl)glycyl]amido}hexa-2,4-diynyl-1-oxycarbonyl}-*L*-alanine *tert*-Butyl Ester **80**.** Following general procedure A, **46** (0.45 g, 2.0 mmol), **57** (1.10 g, 2.4 mmol) and the catalysts were dissolved in dry THF (30 mL). The solution was stirred for 3 h, diluted with CH<sub>2</sub>Cl<sub>2</sub>, and an acidic workup was carried out. The organic phase was

dried over  $\text{MgSO}_4$ , filtered, and concentrated *in vacuo*. The crude product was purified by column chromatography (silica gel,  $\text{CH}_2\text{Cl}_2/\text{MeOH}$  20:1). **80** (0.68 g, 61%) was obtained as a slightly brown solid.

$^1\text{H}$  NMR (300.23 MHz,  $\text{CDCl}_3$ ):  $\delta$  = 1.39 (d,  $J$  = 7.2 Hz, 3H,  $\text{CHCH}_3$ ), 1.49 (s, 9H,  $\text{C}(\text{CH}_3)_3$ ), 3.90 (s, 2H, Gly- $\text{CH}_2$ ), 4.14 (m, 2H,  $\text{C}\equiv\text{CCH}_2\text{NH}$ ), 4.24 (m, 2H,  $\text{CHCH}_3$ , fluorenyl- $\text{CH}$ ), 4.48 (d,  $J$  = 6.9 Hz, 2H, Fmoc- $\text{CO}_2\text{CH}_2$ ), 4.73 (s, 2H,  $\text{NHCO}_2\text{CH}_2\text{C}\equiv\text{C}$ ), 5.65 (s, 1H,  $\text{NH}$ ), 6.59 (s, 1H,  $\text{NH}$ ), 7.33 (t,  $J$  = 7.2 Hz, 2H, aromatic  $H$ ), 7.42 (t,  $J$  = 7.2 Hz, 2H, aromatic  $H$ ), 7.61 (d,  $J$  = 7.2 Hz, 2H, aromatic  $H$ ), 7.78 (d,  $J$  = 7.2 Hz, 2H, aromatic  $H$ ).  $^{13}\text{C}$  NMR (75.49 MHz,  $\text{CDCl}_3$ ):  $\delta$  = 18.5 ( $\text{CHCH}_3$ ), 27.9 ( $\text{C}(\text{CH}_3)_3$ ), 29.6 ( $\text{NHCH}_2\text{C}\equiv\text{C}$ ), 47.1 (fluorenyl- $\text{CH}$ ), 50.4 (Gly- $\text{CH}_2$ ), 52.9 ( $\text{CHCH}_3$ ), 53.6 ( $\text{NHCO}_2\text{CH}_2$ ), 67.0 (Fmoc- $\text{CO}_2\text{CH}_2$ ), 67.1, 70.6, 72.8, 76.1 (diacetylene C), 82.0 ( $\text{C}(\text{CH}_3)_3$ ), 120.0, 125.1, 127.1, 127.7, 141.3, 143.8 (aromatic C), 154.8 (carbamate  $\text{C}=\text{O}$ ), 156.9 (carbamate  $\text{C}=\text{O}$ ), 169.6 (amide  $\text{C}=\text{O}$ ), 172.2 (ester  $\text{C}=\text{O}$ ). HRMS (ESI): calcd for  $\text{C}_{31}\text{H}_{33}\text{N}_3\text{O}_7\text{Na}([\text{M}+\text{Na}]^+)$  582.2211; found: 582.2210.  $R_f$ : 0.4 ( $\text{CH}_2\text{Cl}_2/\text{MeOH}$  10:1).

***N*-{6-[*N'*-[*N''*-(9-Fluorenylmethoxycarbonyl)glycyl]amido]hexa-2,4-diynyl-1-**

**oxycarbonyl]-L-alanine **81**.** Following general procedure B, **80** (0.4 g, 0.71 mmol) was dissolved in dry  $\text{CH}_2\text{Cl}_2$  (20 mL), a large excess of TFA was added, and the solution was stirred over night. The crude product was dried in HV and purified by column chromatography (silica gel,  $\text{CH}_2\text{Cl}_2/\text{MeOH}/\text{trifluoroacetic acid}$  199:10:1). **81** (0.33 g, 92%) was obtained as a brown solid material.

$^1\text{H}$  NMR (300.23 MHz,  $\text{DMSO}-d_6$ ):  $\delta$  = 1.25 (d,  $J$  = 7.2 Hz, 3H,  $\text{CHCH}_3$ ), 3.64 (s, 2H, Gly- $\text{CH}_2$ ), 4.03 (d,  $J$  = 5.1 Hz, 2H,  $\text{NHCH}_2\text{C}\equiv\text{C}$ ), 4.11 (m, 1H,  $\text{CHCH}_3$ ), 4.26 (m, 3H, fluorenyl- $\text{CH}$ , Fmoc- $\text{CO}_2\text{CH}_2$ ), 4.76 (s, 2H,  $\text{NHCO}_2\text{CH}_2$ ), 7.34 (t,  $J$  = 7.5 Hz, 2H, aromatic  $H$ ), 7.43 (t,  $J$  = 7.5 Hz, 2H, aromatic  $H$ ), 7.59 (t,  $J$  = 6.0 Hz, 1H,  $\text{NH}$ ), 7.73 (d,  $J$  = 7.5 Hz, 2H, aromatic  $H$ ), 7.90 (d,  $J$  = 7.5 Hz, 2H, aromatic  $H$ ), 8.42 (t,  $J$  = 5.4 Hz, 1H,  $\text{NH}$ ).  $^{13}\text{C}$  NMR (75.49 MHz,  $\text{DMSO}-d_6$ ):  $\delta$  = 17.5 ( $\text{CHCH}_3$ ), 29.0 ( $\text{NHCH}_2\text{C}\equiv\text{C}$ ), 47.1 (fluorenyl- $\text{CH}$ ), 49.8 ( $\text{CHCH}_3$ ), 52.4 ( $\text{CO}_2\text{CH}_2\text{C}\equiv\text{C}$ ), 55.3 (Gly- $\text{CH}_2$ ), 66.2 (Fmoc- $\text{CO}_2\text{CH}_2$ ), 65.7, 70.0, 74.3, 78.7 (diacetylene C), 120.6, 125.7, 127.5, 128.1, 141.2, 144.3 (aromatic C), 155.3, 157.0 (2 carbamate  $\text{C}=\text{O}$ ), 169.7 (amide  $\text{C}=\text{O}$ ), 174.6 (acid  $\text{C}=\text{O}$ ). HRMS (MALDI): calcd for  $\text{C}_{27}\text{H}_{25}\text{N}_3\text{O}_7\text{Na}([\text{M}+\text{Na}]^+)$  526.1585; found: 526.1588.  $R_f$ : 0.1  $\text{CH}_2\text{Cl}_2/\text{MeOH}$  10:1).

***N*-(6-Hydroxy-hexa-2,4-diynyl-1-oxycarbonyl)-L-alanine *tert*-Butyl Ester **82**.** Following general procedure A, **46** (1.02 g, 4.49 mmol), **58** (0.98 g, 5.39 mmol) and the catalysts were dissolved in dry THF (30 mL). The solution was stirred for 4 h. The purification was carried out by column chromatography (silica gel,  $\text{CH}_2\text{Cl}_2/\text{MeOH}$  24:1). **82** (0.74 g, 59%) was obtained as a yellowish oil.

$^1\text{H}$  NMR (300.23 MHz,  $\text{CDCl}_3$ ):  $\delta$  = 1.32 (d,  $J$  = 7.2 Hz, 3H,  $\text{CHCH}_3$ ), 1.41 (s, 9H,  $\text{C}(\text{CH}_3)_3$ ), 3.34 (s, 1H, OH), 4.16 (m, 1H,  $\text{CHCH}_3$ ), 4.26 (s, 2H,  $\text{CH}_2\text{OH}$ ), 4.71 (m, 2H,  $\text{NHCO}_2\text{CH}_2$ ), 5.64 (d,  $J$  = 7.5 Hz, 1H, NH).  $^{13}\text{C}$  NMR (75.49 MHz,  $\text{CDCl}_3$ ):  $\delta$  = 18.6 ( $\text{CHCH}_3$ ), 27.9 ( $\text{C}(\text{CH}_3)_3$ ), 50.3 ( $\text{CHCH}_3$ ), 51.0 ( $\text{CH}_2\text{OH}$ ), 53.0 ( $\text{NHCO}_2\text{CH}_2$ ), 69.1, 70.5, 73.4, 78.3 (diacetylene C), 82.2 ( $\text{C}(\text{CH}_3)_3$ ), 154.8 (carbamate C=O), 172.1 (ester C=O). Anal. calcd for  $\text{C}_{14}\text{H}_{19}\text{NO}_5$ : C, 59.78%; H, 6.81%; N, 4.98%; found: C, 59.98%; H, 6.89%; N, 5.12%. HRMS (EI): calcd for  $\text{C}_{14}\text{H}_{19}\text{NO}_5$ : ( $[\text{M}]^+$ ) 281.1258; found: 281.1258.  $R_f$ : 0.4 ( $\text{CH}_2\text{Cl}_2/\text{MeOH}$  24:1).

***N*-(6-Hydroxy-hexa-2,4-diynyl-1-oxycarbonyl)-L-alanine 83.** Following general procedure B, **82** (1.20 g, 4.27 mmol) was dissolved in dry  $\text{CH}_2\text{Cl}_2$  (15 mL), a large excess of TFA was added, and the solution was stirred for 4 h. The crude product was dried in HV. The carboxylic acid derivative **83** (0.90 g, 92%) was obtained as a brownish amorphous material, and no further purification was carried out before the next step.

$^1\text{H}$  NMR (300.23 MHz,  $\text{DMSO}-\text{D}_6$ ):  $\delta$  = 1.27 (d,  $J$  = 7.2 Hz, 3H,  $\text{CHCH}_3$ ), 3.18 (s, 1H, OH), 4.00 (m, 1H,  $\text{CHCH}_3$ ), 4.18 (s, 2H,  $\text{CH}_2\text{OH}$ ), 4.75 (s, 2H,  $\text{NHCO}_2\text{CH}_2$ ), 7.72 (d,  $J$  = 7.5 Hz, 1 H, NH).  $^{13}\text{C}$  NMR (75.49 MHz,  $\text{DMSO}-\text{D}_6$ ):  $\delta$  = 17.4 ( $\text{CHCH}_3$ ), 49.0 ( $\text{CHCH}_3$ ), 49.8 ( $\text{CH}_2\text{OH}$ ), 52.4 ( $\text{NHCO}_2\text{CH}_2$ ), 67.9, 70.0, 75.1, 81.1 (diacetylene C), 155.3 (carbamate C=O), 174.6 (acid C=O).  $R_f$ : 0.1 ( $\text{CH}_2\text{Cl}_2/\text{MeOH}$  10:1).

***N*-(6-{2''-{2''-[2'-(2-(Methoxyethoxy)ethoxy]ethoxy}ethoxy}hexa-2,4-diynyl-1-oxycarbonyl)-L-alanine tert-Butyl Ester 84.** Following general procedure A, **46** (0.31 g, 1.32 mmol), **60** (0.60 g, 1.61 mmol) and the catalysts were dissolved in dry THF (25 mL). The solution was stirred over night. The purification was carried out by column chromatography (silica gel,  $\text{CH}_2\text{Cl}_2/\text{MeOH}$  24:1). **84** (0.29 g, 45%) was obtained as a yellowish oil.

$^1\text{H}$  NMR (300.23 MHz,  $\text{CDCl}_3$ ):  $\delta$  = 1.30 (d,  $J$  = 7.2 Hz, 3H,  $\text{CHCH}_3$ ), 1.39 (s, 9H,  $\text{C}(\text{CH}_3)_3$ ), 3.30 (s, 3H,  $\text{OCH}_3$ ), 3.47 (m, 2H,  $\text{CH}_2\text{O}$ ), 3.55-3.65 (m, 14H,  $\text{CH}_2\text{O}$ ), 4.14 (m, 1H,  $\text{CHCH}_3$ ), 4.19 (s, 2H,  $\text{C}_4\text{CH}_2\text{O}$ ), 4.66 (m, 2H,  $\text{NHCO}_2\text{CH}_2$ ), 5.50 (d,  $J$  = 7.5 Hz, 1H, NH).  $^{13}\text{C}$  NMR (75.49 MHz,  $\text{CDCl}_3$ ):  $\delta$  = 18.7 ( $\text{CHCH}_3$ ), 27.9 ( $\text{C}(\text{CH}_3)_3$ ), 50.3 ( $\text{CHCH}_3$ ), 52.8 ( $\text{NHCO}_2\text{CH}_2$ ), 58.8 ( $\text{OCH}_3$ ), 58.9 ( $\text{CH}_2\text{O}$ ), 69.3 ( $\text{C}\equiv\text{C}$ ), 70.2-70.5 (6  $\text{CH}_2\text{O}$ ,  $\text{C}\equiv\text{C}$ ), 73.4, 76.0 ( $\text{C}\equiv\text{C}$ ), 82.0 ( $\text{C}(\text{CH}_3)_3$ ), 154.5 (carbamate C=O), 171.9 (ester C=O). HRMS (EI): calcd for  $\text{C}_{16}\text{H}_{28}\text{NO}_7$ : ( $[\text{M}-\text{C}_5\text{H}_9\text{O}_2]^+$ ) 370.1861; found: 370.1861.  $R_f$ : 0.5 ( $\text{CH}_2\text{Cl}_2/\text{MeOH}$  10:1).

***N*-(6-{2''-{2''-[2'-(2-(Methoxyethoxy)ethoxy]ethoxy}ethoxy}hexa-2,4-diynyl-1-oxycarbonyl)-L-alanine 85.** Following general procedure B, **84** (0.22 g, 0.47 mmol) was dissolved in dry  $\text{CH}_2\text{Cl}_2$  (10 mL), a large excess of TFA was added, and the solution was stirred for 5 h. **85** (0.19 g, 99%) was obtained as a brownish oil, and no further purification was carried out before the next step.

$^1\text{H}$  NMR (300.23 MHz,  $\text{CDCl}_3$ ):  $\delta$  = 1.38 (d,  $J$  = 6.9 Hz, 3H,  $\text{CHCH}_3$ ), 3.33 (s, 3H,  $\text{OCH}_3$ ), 3.52 (m, 2H,  $\text{CH}_2\text{O}$ ), 3.6-3.7 (m, 14H,  $\text{CH}_2\text{O}$ ), 4.22 (s, 2H,  $\text{C}\equiv\text{CCH}_2\text{O}$ ), 4.25 (m, 1H,  $\text{CHCH}_3$ ), 4.75 (m, 2H,  $\text{NHCO}_2\text{CH}_2$ ), 5.81 (d,  $J$  = 4.2 Hz, 1H,  $\text{NH}$ ), 8.4 (s, 1H,  $\text{CO}_2\text{H}$ ).  $^{13}\text{C}$  NMR (75.49 MHz,  $\text{CDCl}_3$ ):  $\delta$  = 18.5 ( $\text{CHCH}_3$ ), 50.0 ( $\text{CHCH}_3$ ), 52.9 ( $\text{NHCO}_2\text{CH}_2$ ), 58.8, 58.9 ( $\text{CH}_2\text{O}$ ), 69-71 (6  $\text{CH}_2\text{O}$ , 2 diacetylene C), 73.5, 76.0 (diacetylene C), 154.8 (carbamate  $\text{C}=\text{O}$ ), 176.5 (acid  $\text{C}=\text{O}$ ).  $R_f$ : 0.2 ( $\text{CH}_2\text{Cl}_2/\text{MeOH}$  10:1).

***N*-(5-Trimethylsilylpenta-2,4-diynyl-1-oxycarbonyl)-L-alanine *tert*-Butyl Ester 86.** Following general procedure A, **46** (0.98 g, 4.41 mmol), **61** (1.22 g, 5.35 mmol) and the catalysts were dissolved in dry THF (50 mL). The solution was stirred over night. The purification was carried out by column chromatography (silica gel,  $\text{CH}_2\text{Cl}_2$ ). **86** (0.85 g, 61%) was obtained as an orange oil.

$^1\text{H}$  NMR (300.23 MHz,  $\text{CDCl}_3$ ):  $\delta$  = 0.16 (s, 9H,  $\text{Si}(\text{CH}_3)_3$ ), 1.34 (d,  $J$  = 7.2 Hz, 3H,  $\text{CHCH}_3$ ), 1.44 (s, 9H,  $\text{C}(\text{CH}_3)_3$ ), 4.20 (m, 1H,  $\text{CHCH}_3$ ), 4.70 (m, 2H,  $\text{NHCO}_2\text{CH}_2$ ), 5.45 (d,  $J$  = 7.2 Hz, 1H,  $\text{NH}$ ).  $^{13}\text{C}$  NMR (75.49 MHz,  $\text{CDCl}_3$ ):  $\delta$  = -0.6 ( $\text{Si}(\text{CH}_3)_3$ ), 18.8 ( $\text{CHCH}_3$ ), 27.9 ( $\text{C}(\text{CH}_3)_3$ ), 50.3 ( $\text{CHCH}_3$ ), 52.8 ( $\text{NHCO}_2\text{CH}_2$ ), 71.2, 72.0, 87.1, 87.9 (diacetylene C), 82.1 ( $\text{C}(\text{CH}_3)_3$ ), 154.5 (carbamate  $\text{C}=\text{O}$ ), 171.9 (ester  $\text{C}=\text{O}$ ). Anal. calcd for  $\text{C}_{16}\text{H}_{25}\text{N}_2\text{O}_4\text{Si}$ : C, 59.41%; H, 7.79%; N, 4.33%; found: C, 59.40%; H, 8.04%; N, 4.31%. HRMS (EI): calcd for  $\text{C}_{16}\text{H}_{25}\text{N}_2\text{O}_4\text{Si}$ : ( $[\text{M}]^+$ ) 323.1547; found: 323.1546.  $R_f$ : 0.3 ( $\text{CH}_2\text{Cl}_2$ ).

***N*-(5-Trimethylsilylpenta-2,4-diynyl-1-oxycarbonyl)-L-alanine 87.** Following general procedure B, **86** (0.85 g, 2.6 mmol) was dissolved in dry  $\text{CH}_2\text{Cl}_2$  (10 mL), a large excess of TFA was added, and the solution was stirred over night. **87** (0.70 g, 100%) was obtained as a brown amorphous material, and no further purification was carried out before the next step.

$^1\text{H}$  NMR (300.23 MHz,  $\text{DMSO}-d_6$ ):  $\delta$  = 0.19 (s, 9H,  $\text{Si}(\text{CH}_3)_3$ ), 1.27 (d,  $J$  = 7.2 Hz, 3H,  $\text{CHCH}_3$ ), 4.01 (m, 1H,  $\text{CHCH}_3$ ), 4.76 (s, 2H,  $\text{NHCO}_2\text{CH}_2$ ), 7.74 (d,  $J$  = 7.5 Hz, 1H,  $\text{NH}$ ), 9.3 (bs, 1H,  $\text{CO}_2\text{H}$ ).  $^{13}\text{C}$  NMR (75.49 MHz,  $\text{DMSO}-d_6$ ):  $\delta$  = 0.3 ( $\text{Si}(\text{CH}_3)_3$ ), 17.5 ( $\text{CHCH}_3$ ), 49.7 ( $\text{CHCH}_3$ ), 52.3 ( $\text{NHCO}_2\text{CH}_2$ ), 70.3, 74.8, 87.6, 88.3 (diacetylene C), 155.3 (carbamate  $\text{C}=\text{O}$ ), 174.6 (acid  $\text{C}=\text{O}$ ). HRMS (EI): calcd for  $\text{C}_{12}\text{H}_{17}\text{NO}_4\text{Si}$ : ( $[\text{M}]^+$ ) 267.0921; found: 267.0923.  $R_f$ : 0.15 ( $\text{CH}_2\text{Cl}_2/\text{MeOH}$  10:1).

**hPI<sub>10</sub>-NH-Ala<sub>4</sub>-C(O)O-CH<sub>2</sub>-C≡C-H 91.** Following general procedure E, **47** (0.107 g, 0.60 mmol) was dissolved in a mixture of dry DMF (5 mL) and dry  $\text{CH}_2\text{Cl}_2$  (5 mL). HOBT (0.10 g, 0.66 mmol) and EDCI (0.15 g, 0.68 mmol) were added to form the active ester intermediate. A second solution containing **45** (0.6 g, 0.54 mmol) and TEA (0.73 g, 7.2 mmol) in dry  $\text{CH}_2\text{Cl}_2$  (100 mL) was prepared, and both solutions were combined. The next day, the solution was washed with 1M HCl and sat. NaCl solution. The combined organic phases were dried over  $\text{MgSO}_4$ , filtered, and concentrated *in vacuo*. The crude product was purified by column chromatography (silica gel,  $\text{CHCl}_3/\text{MeOH}$  10:1). The tar-

geted propargyl functionalized oligopeptide polymer conjugate **91** (0.38 g, 55%) was obtained as a colorless amorphous solid.

$^1\text{H}$  NMR (300.23 MHz,  $\text{C}_2\text{D}_2\text{Cl}_4$ , 120 °C):  $\delta$  = 0.8-1.8 (m, 145H, aliphatic *H*, 4  $\text{CHCH}_3$ ), 2.4 (s, 1H,  $\text{C}\equiv\text{CH}$ ), 3.0-3.2 (m, 2H,  $\text{CH}_2\text{NHR}$ ), 4.05 (m, 1H,  $\text{CHCH}_3$ ), 4.2-4.4 (m, 3H,  $\text{CHCH}_3$ ), 4.6 (m, 2H,  $\text{NHCO}_2\text{CH}_2$ ), 5.1 (s, 1H, carbamate *NH*), 6.2 (s, 1H, *NH*), 6.4 (s, 2H, *NH*). Anal. calcd for  $\text{C}_{73}\text{H}_{139}\text{N}_5\text{O}_6$ : C, 74.12%; H, 11.84%; N, 5.92%; found: C, 74.03%; H, 11.68%; N, 5.66%. HRMS (MALDI): calcd for  $\text{C}_{73}\text{H}_{139}\text{N}_5\text{O}_6\text{Na}$ :  $([\text{M}+\text{Na}]^+)$  1205.0623; found: 1205.847.  $R_f$ : 0.4 ( $\text{CHCl}_3/\text{MeOH}$  10:1).

**hPI<sub>10</sub>-NH-Ala<sub>4</sub>-C(O)O-CH<sub>2</sub>-C $\equiv$ C-C $\equiv$ C-CH<sub>2</sub>NHAc **92**.** *Divergent route from 50:* Following general procedure A, **91** (0.13 g, 0.11 mmol), **50** (0.08 g, 0.36 mmol) and the catalysts were dissolved in a mixture of  $\text{CHCl}_3$  (50 mL) and THF (50 mL). The reaction was stirred over night. The solvents were removed *in vacuo*, and the crude product was purified by repeated column chromatography (silica gel,  $\text{CHCl}_3/\text{MeOH}$  15:1). **92** (0.087 g, 64%) was obtained as a light-sensitive, colorless and amorphous solid.

*Convergent route from 68:* Following general procedure E, **68** (0.70 g, 2.63 mmol) was dissolved in a mixture of dry DMF (10 mL) and dry  $\text{CH}_2\text{Cl}_2$  (20 mL). HOBt (0.38 g, 2.81 mmol) and EDCI (0.53 g, 2.76 mmol) were added to form the active ester intermediate. A second solution containing **45** (1.50 g, 1.46 mmol) and TEA (1.0 g, 10.0 mmol) in dry  $\text{CH}_2\text{Cl}_2$  (100 mL) was prepared, and both solutions were combined. The next day, the solution was diluted with  $\text{CHCl}_3$  (100 mL) and washed with 1M HCl as well as sat. NaCl solution. The combined organic phases were dried over  $\text{MgSO}_4$ , filtered, and concentrated *in vacuo*. The crude product was purified by column chromatography (silica gel,  $\text{CHCl}_3/\text{MeOH}$  24:1). **92** (1.41 g, 79%) was obtained as a light-sensitive, slightly pink and amorphous solid.

$^1\text{H}$  NMR (300.23 MHz,  $\text{CDCl}_3$  / TFA 50:1):  $\delta$  = 0.6-1.9 (m, 139H, aliphatic *H*, 4  $\text{CHCH}_3$ ), 2.16 (s, 3H,  $\text{C(O)CH}_3$ ), 3.1-3.4 (m, 2H,  $\text{CH}_2\text{NHR}$ ), 4.1-4.2 (m, 2H,  $\text{CH}_2\text{NHAc}$ ), 4.2-4.3 (m, 1H,  $\text{CHCH}_3$ ), 4.5-4.9 (m, 5H, 3  $\text{CHCH}_3$ ,  $\text{NHCO}_2\text{CH}_2$ ), 5.81 (m, 1H, carbamate *NH*), 6.5-6.6 (m, 1H, *NH*), 6.8-7.0 (m, 1H, *NH*), 7.4-7.5 (m, 2H, 2 *NH*), 7.7-7.9 (m, 1H, *NH*). Anal. calcd for  $\text{C}_{78}\text{H}_{144}\text{N}_6\text{O}_7$ : C, 73.30%; H, 11.36%; N, 6.58%; found: C, 72.90%; H, 11.18%; N, 5.94%. HRMS (MALDI): calcd for  $\text{C}_{78}\text{H}_{144}\text{N}_6\text{O}_7\text{Na}$ :  $([\text{M}+\text{Na}]^+)$  1300.099; found: 1300.936.  $R_f$ : 0.3 ( $\text{CHCl}_3/\text{MeOH}$  10:1).

**hPI<sub>10</sub>-NH-Ala<sub>4</sub>-C(O)O-CH<sub>2</sub>-C $\equiv$ C-C $\equiv$ C-CH<sub>2</sub>NH-C(O)(CH<sub>2</sub>)<sub>2</sub>C(O)OMe **93**.** Following general procedure E, **71** (0.17 g, 0.41 mmol) was dissolved in a mixture of dry DMF (10 mL) and dry  $\text{CH}_2\text{Cl}_2$  (20 mL). HOBt (0.12 g, 0.9 mmol) and EDCI (0.12 g, 0.6 mmol) were added to form the active ester intermediate. A second solution containing **45** (0.4 g, 0.39 mmol) and TEA (0.2 g, 2.0 mmol) in dry  $\text{CH}_2\text{Cl}_2$  (100 mL) was prepared, and both solutions were combined. The next day, the solvent was

removed *in vacuo*, and the crude product was purified by repeated column chromatography (silica gel, CHCl<sub>3</sub>/MeOH 24:1). **93** (0.31 g, 66%) was obtained as a light-sensitive, amorphous solid.

<sup>1</sup>H NMR (300.23 MHz, CDCl<sub>3</sub> / TFA 50:1):  $\delta$  = 0.6-1.9 (m, 147H, aliphatic *H*, 4 CHCH<sub>3</sub>), 2.65 (t, *J* = 6.3 Hz, 2H, NHC(O)CH<sub>2</sub>), 2.78 (t, *J* = 6.0 Hz, 2H, CH<sub>2</sub>CO<sub>2</sub>CH<sub>3</sub>), 3.1-3.4 (m, 2H, CH<sub>2</sub>NHR), 3.77 (s, 3H, OCH<sub>3</sub>), 4.1-4.2 (m, 2H, CH<sub>2</sub>NH), 4.2-4.4 (m, 1H, CHCH<sub>3</sub>), 4.5-4.9 (m, 5H, 3 CHCH<sub>3</sub>, NHCO<sub>2</sub>CH<sub>2</sub>), 5.84 (s, 1H, carbamate NH), 6.8-7.0 (m, 2H, 2 NH), 7.4-7.6 (m, 2H, 2 NH), 7.7-7.9 (m, 1H, NH). Anal. calcd for C<sub>81</sub>H<sub>148</sub>N<sub>6</sub>O<sub>9</sub>: C, 72.06%; H, 11.05%; N, 6.22%; found: C, 72.72%; H, 11.13%; N, 5.67%. HRMS (MALDI): calcd for C<sub>81</sub>H<sub>148</sub>N<sub>6</sub>O<sub>9</sub>Na: ([M+Na]<sup>+</sup>) 1372.121; found: 1373.013. R<sub>f</sub>: 0.4 (CHCl<sub>3</sub>/MeOH 10:1).

**hPI<sub>10</sub>-NH-Ala<sub>4</sub>-C(O)O-CH<sub>2</sub>-C≡C-C≡C-CH<sub>2</sub>NH-Fmoc 94.** Following general procedure E, **73** (0.175 g, 0.4 mmol) was dissolved in a mixture of dry DMF (5 mL) and dry CH<sub>2</sub>Cl<sub>2</sub> (15 mL). HOBt (0.070 g, 0.50 mmol) and EDCI (0.10 g, 0.50 mmol) were added to form the active ester intermediate. A second solution containing **45** (0.41 g, 0.40 mmol) and TEA (0.20 g, 2.0 mmol) in dry CH<sub>2</sub>Cl<sub>2</sub> (100 mL) was prepared, and both solutions were combined. The next day, the solvents were removed *in vacuo*, and the crude product was purified by column chromatography (silica gel, CHCl<sub>3</sub>/MeOH 24:1). **94** (0.18 g, 33%) was obtained as a colorless amorphous solid.

<sup>1</sup>H NMR (300.23 MHz, CDCl<sub>3</sub> / TFA 50:1):  $\delta$  = 0.6-1.9 (m, 152H, aliphatic *H*, 4 CHCH<sub>3</sub>), 3.1-3.4 (m, 2H, CH<sub>2</sub>NHR), 4.0-4.1 (m, 2H, NHCH<sub>2</sub>), 4.2-4.4 (m, 2H, CHCH<sub>3</sub>, fluorenyl CH), 4.4-4.7 (m, 5H, 3 CHCH<sub>3</sub>, Fmoc-NHCO<sub>2</sub>CH<sub>2</sub>), 4.7-4.9 (m, 2H, NHCO<sub>2</sub>CH<sub>2</sub>), 5.8 (m, 1H, carbamate NH), 6.5-6.8 (m, 1H, Fmoc-NH), 6.8-6.9 (m, 1H, NH), 7.33 (t, *J* = 7.2 Hz, 2H, aromatic *H*), 7.4-7.5 (m, 3H, 2 aromatic *H*, NH), 7.5-7.6 (m, 3H, 2 aromatic *H*, NH), 7.7-7.9 (m, 3H, 2 aromatic *H*, NH). R<sub>f</sub>: 0.4 (CH<sub>2</sub>Cl<sub>2</sub>/MeOH 10:1).

**hPI<sub>10</sub>-NH-Ala<sub>4</sub>-C(O)O-CH<sub>2</sub>-C≡C-C≡C-CH<sub>2</sub>NH-dansyl 95.** Following general procedure D, **75** (0.11 g, 0.24 mmol) and **45** (0.20 g, 0.20 mmol) were dissolved in a mixture of dry DMF (10 mL), dry CH<sub>2</sub>Cl<sub>2</sub> (10 mL), and dry THF (15 mL). DIEA (0.92 g, 0.72 mmol) and PyBOP (0.13 g, 0.25 mmol) were added. The mixture was stirred for 5 h at room temperature in the dark. The solution was washed twice with water. The organic phase was dried over MgSO<sub>4</sub>, filtered, and concentrated *in vacuo*. The crude product was purified by repeated column chromatography (silica gel, gradient CH<sub>2</sub>Cl<sub>2</sub>/MeOH 30:1 → CH<sub>2</sub>Cl<sub>2</sub>/MeOH 5:1). **95** (0.16 g, 56%) was obtained as a colorless amorphous solid.

<sup>1</sup>H NMR (300.23 MHz, CDCl<sub>3</sub> / TFA 50:1):  $\delta$  = 0.8-1.9 (m, 148H, aliphatic *H*, 4 CHCH<sub>3</sub>), 3.2-3.4 (m, 2H, CH<sub>2</sub>NHR), 3.6 (s, 6H, N(CH<sub>3</sub>)<sub>2</sub>), 4.0 (s, 2H, NHCH<sub>2</sub>), 4.3 (m, 1H, CHCH<sub>3</sub>), 4.5-4.6 (m, 3H, CHCH<sub>3</sub>), 4.7 (m, 2H, NHCO<sub>2</sub>CH<sub>2</sub>), 5.9 (m, 1H, NH), 6.7 (m, 1H, NH), 7.4 (m, 1H, NH), 7.6 (m, 1H, NH), 7.8-7.9 (m, 3H, 1 NH, 2 aromatic *H*), 8.5 (m, 2H, aromatic *H*), 9.0 (m, 2H, aromatic *H*). HRMS (MALDI): calcd for C<sub>88</sub>H<sub>153</sub>N<sub>7</sub>O<sub>8</sub>SNa: ([M+Na]<sup>+</sup>) 1491.140; found: 1492.132.

**hPI<sub>10</sub>-NH-Ala<sub>4</sub>-C(O)O-CH<sub>2</sub>-C≡C-C≡C-CH<sub>2</sub>NH-AlaAc 96.** Following general procedure E, **77** (0.13 g, 0.39 mmol) was dissolved in a mixture of dry DMF (5 mL) and dry CH<sub>2</sub>Cl<sub>2</sub> (15 mL). HOBt (0.06 g, 0.44 mmol) and EDCI (0.10 g, 0.52 mmol) were added to form the active ester intermediate. A second solution containing **45** (0.3 g, 0.30 mmol) and TEA (0.2 g, 2.0 mmol) in dry CH<sub>2</sub>Cl<sub>2</sub> (100 mL) was prepared, and both solutions were combined. The next day, the solvent was removed *in vacuo* and the crude product was purified by repeated column chromatography (silica gel, CHCl<sub>3</sub>/MeOH 24:1). **96** (0.20 g, 51%) was obtained as a very light-sensitive, colorless and amorphous solid.

<sup>1</sup>H NMR (300.23 MHz, CDCl<sub>3</sub> / TFA 50:1): δ = 0.6-1.9 (m, 145H, aliphatic H, 4 CHCH<sub>3</sub>), 2.15 (s, 3H, C(O)CH<sub>3</sub>), 3.1-3.4 (m, 2H, CH<sub>2</sub>NHR), 4.1-4.2 (m, 2H, CH<sub>2</sub>NH), 4.2-4.4 (m, 1H, CHCH<sub>3</sub>), 4.5-4.9 (m, 6H, 4 CHCH<sub>3</sub>, NHCO<sub>2</sub>CH<sub>2</sub>), 5.82 (s, 1H, carbamate NH), 6.8-7.0 (m, 1H, NH), 7.1-7.3 (m, 1H, NH), 7.4-7.6 (m, 2H, NH), 7.7-7.9 (m, 2H, NH). Anal. calcd for C<sub>81</sub>H<sub>149</sub>N<sub>7</sub>O<sub>8</sub>: C, 72.11%; H, 11.13%; N, 7.27%; found: C, 71.82%; H, 11.11%; N, 6.48%. HRMS (MALDI): calcd for C<sub>76</sub>H<sub>139</sub>N<sub>7</sub>O<sub>8</sub>Na: ([M+Na]<sup>+</sup>) 1301.058; found: 1301.879. R<sub>f</sub>: 0.25 (CHCl<sub>3</sub>/MeOH 10:1).

**hPI<sub>10</sub>-NH-Ala<sub>4</sub>-C(O)O-CH<sub>2</sub>-C≡C-C≡C-CH<sub>2</sub>NH-Ala-Fmoc 97.** Following general procedure E, **79** (0.20 g, 0.39 mmol) was dissolved in a mixture of dry DMF (10 mL) and dry CH<sub>2</sub>Cl<sub>2</sub> (20 mL). HOBt (0.063 g, 0.47 mmol) and EDCI (0.11 g, 0.57 mmol) were added to form the active ester intermediate. A second solution containing **45** (0.4 g, 0.39 mmol) and TEA (0.20 g, 2.0 mmol) in dry CH<sub>2</sub>Cl<sub>2</sub> (100 mL) was prepared, and both solutions were combined. The next day, the solution was diluted with CHCl<sub>3</sub> (100 mL) and washed with sat. NaHCO<sub>3</sub> solution as well as sat. NaCl solution. The combined organic phases were dried over MgSO<sub>4</sub>, filtered, and concentrated *in vacuo*. The crude product was purified by column chromatography (silica gel, CHCl<sub>3</sub>/MeOH 24:1). **97** (0.53 g, 89%) was obtained as a light-sensitive, colorless amorphous solid.

<sup>1</sup>H NMR (300.23 MHz, CDCl<sub>3</sub> / TFA 50:1): δ = 0.6-1.9 (m, 160H, aliphatic H, 5 CHCH<sub>3</sub>), 3.1-3.4 (m, 2H, CH<sub>2</sub>NHR), 4.1-4.9 (m, 12H, 5 CHCH<sub>3</sub>, NHCH<sub>2</sub>, Fmoc-NHCO<sub>2</sub>CH<sub>2</sub>, NHCO<sub>2</sub>CH<sub>2</sub>, fluorenyl CH), 5.82 (m, 1H, carbamate NH), 6.2-6.4 (m, 1H, Fmoc-NH), 6.8-7.0 (m, 1H, NH), 7.1-7.3 (m, 1H, NH), 7.3-7.4 (m, 2H, aromatic H), 7.4-7.5 (m, 3H, 2 aromatic H, NH), 7.5-7.6 (m, 3H, 2 aromatic H, NH), 7.7-7.9 (m, 3H, 2 aromatic H, NH). Anal. calcd for C<sub>94</sub>H<sub>157</sub>N<sub>7</sub>O<sub>9</sub>: C, 73.83%; H, 10.35%; N, 6.41%; found: C, 73.40%; H, 10.43%; N, 5.88%. HRMS (MALDI): calcd for C<sub>94</sub>H<sub>157</sub>N<sub>7</sub>O<sub>9</sub>Na: ([M+Na]<sup>+</sup>) 1551.194; found: 1552.161. R<sub>f</sub>: 0.25 (CHCl<sub>3</sub>/MeOH 10:1).

**hPI<sub>10</sub>-NH-Ala<sub>4</sub>-C(O)O-CH<sub>2</sub>-C≡C-C≡C-CH<sub>2</sub>NH-Gly-Fmoc 98.** Following general procedure E, **81** (0.10 g, 0.20 mmol) was dissolved in a mixture of dry DMF (10 mL) and dry CH<sub>2</sub>Cl<sub>2</sub> (10 mL). HOBt (0.032 g, 0.24 mmol) and EDCI (0.046 g, 0.24 mmol) were added to form the active ester



intermediate. A second solution containing **45** (0.2 g, 0.2 mmol) and TEA (0.10 g, 1.0 mmol) in dry CH<sub>2</sub>Cl<sub>2</sub> (100 mL) was prepared, and both solutions were combined. The next day, the solution was diluted with CHCl<sub>3</sub> (100 mL) and washed with sat. NaHCO<sub>3</sub> solution as well as sat. NaCl solution. The combined organic phases were dried over MgSO<sub>4</sub>, filtered, and concentrated *in vacuo*. The crude product was purified by column chromatography (silica gel, CHCl<sub>3</sub>/MeOH 15:1). **98** (0.108 g, 38%) was obtained as a light-sensitive, colorless and amorphous solid.

<sup>1</sup>H NMR (300.23 MHz, CDCl<sub>3</sub> / TFA 50:1): δ = 0.6-1.9 (m, 140H, aliphatic H, 4 CHCH<sub>3</sub>), 3.1-3.4 (m, 2H, CH<sub>2</sub>NHR), 4.1-4.9 (m, 11H, 4 CHCH<sub>3</sub>, NHCH<sub>2</sub>, Fmoc-NHCO<sub>2</sub>CH<sub>2</sub>, NHCO<sub>2</sub>CH<sub>2</sub>, fluorenyl CH), 5.82 (m, 1H, carbamate NH), 6.8-7.0 (m, 1H, NH), 7.3-7.4 (m, 2H, aromatic H), 7.4-7.5 (m, 3H, 2 aromatic H, NH), 7.5-7.6 (m, 3H, 2 aromatic H, NH), 7.7-7.9 (m, 3H, 2 aromatic H, NH). HRMS (MALDI): calcd for C<sub>93</sub>H<sub>155</sub>N<sub>7</sub>O<sub>9</sub>Na: ([M+Na]<sup>+</sup>) 1537.178; found: 1537.023. (R<sub>f</sub>: 0.4 CH<sub>2</sub>Cl<sub>2</sub>/MeOH 10:1).

**(hPI<sub>10</sub>-NH-Ala<sub>4</sub>-C(O)O-CH<sub>2</sub>-C≡C-)<sub>2</sub> 99.** Following general procedure E, **66** (0.065 g, 0.2 mmol) was dissolved in a mixture of dry DMF (5 mL) and dry CH<sub>2</sub>Cl<sub>2</sub> (10 mL). HOBT (0.12 g, 0.89 mmol) and EDCI (0.16 g, 0.83 mmol) were added to form the active ester intermediate. A second solution containing **45** (0.4 g, 0.39 mmol) and TEA (0.20 g, 2.0 mmol) in dry CH<sub>2</sub>Cl<sub>2</sub> (150 mL) was prepared, and both solutions were combined. The next day, the solution was diluted with CHCl<sub>3</sub> (100 mL) and washed with sat. NaHCO<sub>3</sub> solution as well as sat. NaCl solution. The combined organic phases were dried over MgSO<sub>4</sub>, filtered, and concentrated *in vacuo*. The crude product was purified by column chromatography (silica gel, CHCl<sub>3</sub>/MeOH 24:1). **99** (0.277 g, 60%) was obtained as a light-sensitive, colorless and amorphous solid.

<sup>1</sup>H NMR (300.23 MHz, CDCl<sub>3</sub> / TFA 50:1): δ = 0.6-1.9 (m, 295H, aliphatic H, 8 CHCH<sub>3</sub>), 3.1-3.4 (m, 4H, 2 CH<sub>2</sub>NHR), 4.2-4.4 (m, 2H, 2 CHCH<sub>3</sub>), 4.5-4.9 (m, 10H, 6 CHCH<sub>3</sub>, 2 NHCO<sub>2</sub>CH<sub>2</sub>), 5.87 (m, 2H, 2 carbamate NH), 6.8-6.9 (m, 2H, 2 NH), 7.4-7.5 (m, 4H, 4 NH), 7.7-7.9 (m, 2H, 2 NH). Anal. calcd for C<sub>146</sub>H<sub>276</sub>N<sub>10</sub>O<sub>12</sub>: C, 74.18%; H, 11.77%; N, 5.93%; found: C, 74.21%; H, 11.68%; N, 5.30%. HRMS (MALDI): calcd for C<sub>151</sub>H<sub>286</sub>N<sub>10</sub>O<sub>12</sub>Na: ([M+Na]<sup>+</sup>) 2455.197; found: 2457.030. R<sub>f</sub>: 0.4 (CH<sub>2</sub>Cl<sub>2</sub>/MeOH 10:1).

**hPI<sub>10</sub>-NH-Ala<sub>4</sub>-C(O)O-CH<sub>2</sub>-C≡C-C≡C-CH<sub>2</sub>OH 100.** Following general procedure E, **83** (0.18 g, 0.80 mmol) was dissolved in a mixture of dry DMF (10 mL) and dry CH<sub>2</sub>Cl<sub>2</sub> (10 mL). HOBT (0.135 g, 1.00 mmol) and EDCI (0.198 g, 1.03 mmol) were added to form the active ester intermediate. A second solution containing **45** (0.6 g, 0.54 mmol) and TEA (0.73 g, 7.2 mmol) in dry CH<sub>2</sub>Cl<sub>2</sub> (150 mL) was prepared, and both solutions were combined. The next day, the solution was washed with 1M HCl and sat. NaCl solution. The combined organic phases were dried over MgSO<sub>4</sub>, filtered, and concentrated

*in vacuo*. The crude product was purified by column chromatography (silica gel, CH<sub>2</sub>Cl<sub>2</sub>/MeOH 24:1). **100** (0.40 g, 56%) was obtained as a colorless and amorphous solid.

<sup>1</sup>H NMR (300.23 MHz, CDCl<sub>3</sub> / TFA 50:1): δ = 0.6-1.9 (m, 132H, aliphatic H, 4 CHCH<sub>3</sub>), 3.1-3.4 (m, 2H, CH<sub>2</sub>NHR), 4.2-4.4 (m, 1H, CHCH<sub>3</sub>), 4.4-4.9 (m, 7H, 3 CHCH<sub>3</sub>, NHCO<sub>2</sub>CH<sub>2</sub>, CH<sub>2</sub>OH), 5.79 (m, 1H, carbamate NH), 6.8-6.9 (m, 1H, NH), 7.4-7.5 (m, 1H, NH), 7.5-7.6 (m, 1H, NH), 7.7-7.9 (m, 1H, NH). Anal. calcd for C<sub>76</sub>H<sub>141</sub>N<sub>5</sub>O<sub>7</sub>: C, 73.79%; H, 11.49%; N, 5.66%; found: C, 73.69%; H, 11.21%; N, 5.36%. HRMS (MALDI): calcd for C<sub>71</sub>H<sub>131</sub>N<sub>5</sub>O<sub>7</sub>Na: ([M+Na]<sup>+</sup>) 1188.995; found 1189.755. R<sub>f</sub>: 0.3 (CHCl<sub>3</sub>/MeOH 10:1).

**hPI<sub>10</sub>-NH-Ala<sub>4</sub>-C(O)O-CH<sub>2</sub>-C≡C-C≡C-CH<sub>2</sub>(O(CH<sub>2</sub>)<sub>2</sub>)<sub>4</sub>OMe 101.** Following general procedure E, **85** (0.17 g, 0.41 mmol) was dissolved in a mixture of dry DMF (10 mL) and dry CH<sub>2</sub>Cl<sub>2</sub> (10 mL). HOBT (0.06 g, 0.44 mmol) and EDCI (0.11 g, 0.57 mmol) were added to form the active ester intermediate. A second solution containing **45** (0.35 g, 0.34 mmol) and TEA (0.21 g, 2.07 mmol) in dry CH<sub>2</sub>Cl<sub>2</sub> (100 mL) was prepared, and both solutions were combined. The next day, the solution was concentrated *in vacuo* and the crude product was purified by column chromatography (silica gel, CHCl<sub>3</sub>/MeOH 24:1). **101** (0.12 g, 25%) was obtained as a colorless amorphous solid.

<sup>1</sup>H NMR (300.23 MHz, CDCl<sub>3</sub> / TFA 50:1): δ = 0.6-1.9 (m, 130H, aliphatic H, 4 CHCH<sub>3</sub>), 3.1-3.4 (m, 2H, CH<sub>2</sub>NHR), 3.50 (s, 3H, OCH<sub>3</sub>), 3.6-3.9 (m, 16H, OCH<sub>2</sub>), 4.2-4.9 (m, 8H, 4 CHCH<sub>3</sub>, NHCO<sub>2</sub>CH<sub>2</sub>, C≡CCH<sub>2</sub>O), 5.86 (m, 1H, carbamate NH), 6.8-6.9 (m, 1H, NH), 7.4-7.5 (m, 1H, NH), 7.5-7.6 (m, 1H, NH), 7.7-7.9 (m, 1H, NH). Anal. calcd for C<sub>85</sub>H<sub>159</sub>N<sub>5</sub>O<sub>11</sub>: C, 71.53%; H, 11.23%; N, 4.91%; found: C, 71.28%; H, 11.16%; N, 4.55%. HRMS (MALDI): calcd for C<sub>85</sub>H<sub>159</sub>N<sub>5</sub>O<sub>11</sub>Na: ([M+Na]<sup>+</sup>) 1449.193; found 1450.190. R<sub>f</sub>: 0.5 (CHCl<sub>3</sub>/MeOH 10:1).

**hPI<sub>10</sub>-NH-Ala<sub>4</sub>-C(O)O-CH<sub>2</sub>-C≡C-C≡C-TMS 102.** Following general procedure E, **87** (0.18 g, 0.67 mmol) was dissolved in a mixture of dry DMF (10 mL) and dry CH<sub>2</sub>Cl<sub>2</sub> (20 mL). HOBT (0.10 g, 0.74 mmol) and EDCI (0.16 g, 0.83 mmol) were added to form the active ester intermediate. A second solution containing **45** (0.4 g, 0.39 mmol) and TEA (0.22 g, 2.17 mmol) in dry CH<sub>2</sub>Cl<sub>2</sub> (150 mL) was prepared, and both solutions were combined. The next day, the solution was diluted with CHCl<sub>3</sub> (100 mL) and washed with sat. NaHCO<sub>3</sub> solution as well as sat. NaCl solution. The combined organic phases were dried over MgSO<sub>4</sub>, filtered, and concentrated *in vacuo*. The crude product was purified by column chromatography (silica gel, CH<sub>2</sub>Cl<sub>2</sub>/MeOH 24:1). **102** (0.40 g, 81%) was obtained as a colorless and amorphous solid.

<sup>1</sup>H NMR (300.23 MHz, CDCl<sub>3</sub> / TFA 50:1): δ = 0.19 (s, 9H, Si(CH<sub>3</sub>)<sub>3</sub>), 0.6-1.9 (m, 157H, aliphatic H, 4 CHCH<sub>3</sub>), 3.1-3.4 (m, 2H, CH<sub>2</sub>NHR), 4.2-4.4 (m, 1H, CHCH<sub>3</sub>), 4.5-4.9 (m, 5H, 3 CHCH<sub>3</sub>, NHCO<sub>2</sub>CH<sub>2</sub>),

5.8 (m, 1H, carbamate *NH*), 6.8-6.9 (m, 1H, *NH*), 7.4-7.5 (m, 2H, *NH*), 7.7-7.8 (m, 1H, *NH*). Anal. calcd for  $C_{78}H_{147}N_5O_6Si$ : C, 73.24%; H, 11.58%; N, 5.48%; found: C, 71.35%; H, 11.37%; N, 5.18%. HRMS (MALDI): calcd for  $C_{78}H_{147}N_5O_6SiNa$ :  $([M+Na]^+)$  1301.102; found: 1301.971.  $R_f$ : 0.5 ( $CH_2Cl_2/MeOH$  10:1).

**hPI<sub>10</sub>-NH-Ala<sub>4</sub>-C(O)O-CH<sub>2</sub>-C≡C-C≡C-H 103.** The TMS functionalized macromonomer **102** (0.21 g, 0.16 mmol) was dissolved in a mixture of  $CH_2Cl_2$  (50 mL) and THF (50 mL). The solution was cooled to 0 °C, and tetrabutylammonium fluoride trihydrate (0.055 g, 0.176 mmol) was added. The reaction mixture was stirred for 15 min, and the reaction was then quenched by an aqueous workup. After drying of the organic phase and removal of the solvent, an amorphous solid was obtained. The crude product was purified by column chromatography (silica gel,  $CHCl_3/MeOH$  24:1). **103** (0.18 g, 93%) was obtained as a colorless and amorphous solid.

$^1H$  NMR (300.23 MHz,  $CDCl_3$  / TFA 50:1):  $\delta$  = 0.6-1.9 (m, 147H, aliphatic *H*, 4  $CHCH_3$ ), 2.23 (s, 1H,  $C\equiv CH$ ), 3.1-3.4 (m, 2H,  $CH_2NHR$ ), 4.2-4.4 (m, 1H,  $CHCH_3$ ), 4.4-4.8 (m, 5H, 3  $CHCH_3$ ,  $NHCO_2CH_2$ ), 5.85 (m, 1H, carbamate *NH*), 6.8-6.9 (m, 1H, *NH*), 7.4-7.5 (m, 1H, *NH*), 7.5-7.6 (m, 1H, *NH*), 7.7-7.9 (m, 1H, *NH*). Anal. calcd for  $C_{75}H_{139}N_5O_6$ : C, 74.64%; H, 11.61%; N, 5.80%; found: C, 73.53%; H, 11.59%; N, 5.01%. HRMS (MALDI): calcd for  $C_{75}H_{139}N_5O_6Na$ :  $([M+Na]^+)$  1229.062; found: 1229.872.  $R_f$ : 0.5 ( $CH_2Cl_2/MeOH$  10:1).

**L-Lactyl-L-alanine *tert*-Butyl Ester 106.** Following general procedure D, L-lactic acid (1.47 g, 16.5 mmol) and L-alanine *tert*-butyl ester hydrochloride (3.01 g, 16.5 mmol) were dissolved in a mixture of dry  $CH_2Cl_2$  (60 mL) and dry DMF (30 mL). DIEA (6.7 g, 66 mmol) and PyBOP (9.45 g, 18.15 mmol) were added in one portion. The reaction was stirred at room temperature over night. The solution was diluted with  $CH_2Cl_2$ , washed twice with 1M HCl and once with sat. NaCl solution. The combined organic phases were dried over  $MgSO_4$ , filtered, and concentrated *in vacuo*. The crude product was purified by column chromatography (silica gel, ethyl acetate). The product **106** (2.80 g, 78%) was obtained as a colorless solid.

$^1H$  NMR (300.23 MHz,  $DMSO-D_6$ ):  $\delta$  = 1.23 (d,  $J$  = 6.6 Hz, 3H,  $CHCH_3$ ), 1.28 (d,  $J$  = 7.2 Hz, 3H,  $CHCH_3$ ), 1.41 (s, 9H,  $C(CH_3)_3$ ), 3.99 (q,  $J$  = 6.9 Hz, 1H,  $CHCH_3$ ), 4.18 (m, 1H,  $CHCH_3$ ), 7.69 (d,  $J$  = 7.2 Hz, 1H, *NH*).  $^{13}C$  NMR (75.49 MHz,  $DMSO-D_6$ ):  $\delta$  = 17.9, 21.35 (2  $CHCH_3$ ), 28.0 ( $C(CH_3)_3$ ), 48.2, 67.4 (2  $CHCH_3$ ), 80.9 ( $C(CH_3)_3$ ), 172.0 (amide  $C=O$ ), 174.6 (ester  $C=O$ ). Anal. calcd for  $C_{10}H_{19}NO_4$ : C, 55.28%; H, 8.81%; N, 6.45%; O, 29.46%; found: C, 55.11%; H, 9.00%; N, 6.28%; O, 29.69%. HRMS (EI): calcd for  $C_{10}H_{19}NO_4$ :  $([M]^+)$  217.1300; found: 217.1300.  $R_f$ : 0.5 (ethyl acetate). m.p.: 136-137 °C.

***N*-[*((S)*-2-Propioly]propanyl]-L-alanine *tert*-Butyl Ester **107**.**

The secondary alcohol **106** (1.5 g, 6.9 mmol) and triphenylphosphane (3.62 g, 13.8 mmol) were dissolved in dry THF (70 mL). Another solution containing diethyl azodicarboxylate (2.4 g, 13.8 mmol) and propiolic acid (0.97 g, 13.8 mmol) in dry THF (70 mL) was prepared. The first solution was added to the latter over a period of 60 min, and the reaction was stirred over night. The solvents were removed *in vacuo* and the crude product was purified by column chromatography (silica gel, ethyl acetate/hexanes 1:1). **107** (1.56 g, 84%) was obtained as a colorless solid.

$^1\text{H}$  NMR (300.23 MHz,  $\text{CDCl}_3$ ):  $\delta$  = 1.33 (d,  $J$  = 6.9 Hz, 3H,  $\text{CHCH}_3$ ), 1.42 (s, 9H,  $\text{C}(\text{CH}_3)_3$ ), 1.47 (d,  $J$  = 6.9 Hz, 1H,  $\text{CHCH}_3$ ), 3.06 (s, 1H,  $\text{C}\equiv\text{CH}$ ), 4.39 (m, 1H,  $\text{CHCH}_3$ ), 5.22 (q,  $J$  = 6.9 Hz, 1H,  $\text{CHCH}_3$ ), 6.75 (d,  $J$  = 7.2 Hz, 1H, *NH*).  $^{13}\text{C}$  NMR (75.49 MHz,  $\text{CDCl}_3$ ):  $\delta$  = 17.6, 18.3 (2  $\text{CHCH}_3$ ), 27.9 ( $\text{C}(\text{CH}_3)_3$ ), 48.6, 72.1 (2  $\text{CHCH}_3$ ), 74.0 ( $\text{C}\equiv\text{CH}$ ), 76.6 ( $\text{C}\equiv\text{CH}$ ), 82.2 ( $\text{C}(\text{CH}_3)_3$ ), 151.0 (propiolic ester  $\text{C}=\text{O}$ ), 168.6 (amide  $\text{C}=\text{O}$ ), 171.7 (ester  $\text{C}=\text{O}$ ). Anal. calcd for  $\text{C}_{13}\text{H}_{19}\text{NO}_5$ : C, 57.98%; H, 7.11%; N, 5.20%; O, 29.71%; found: C, 57.72%; H, 7.14%; N, 5.31%. HRMS (EI): calcd for  $\text{C}_{13}\text{H}_{19}\text{NO}_5$ :  $([\text{M}-\text{C}_4\text{H}_8]^+)$  214.0710; found: 214.0722.  $R_f$ : 0.7 ( $\text{CH}_2\text{Cl}_2/\text{MeOH}$  10:1). m. p.: 96-98 °C.

***N*-[*((S)*-2-Propioly]propanyl]-L-alanine **108**.**

Following general procedure B, **107** (0.40 g, 1.49 mmol) was dissolved in dry  $\text{CH}_2\text{Cl}_2$  (10 mL), a large excess of TFA was added, and the solution was stirred for 5 h. **108** (0.31 g, 98%) was obtained as a colorless crystalline material. No further purification was necessary before the next step.

$^1\text{H}$  NMR (300.23 MHz,  $\text{CDCl}_3$ ):  $\delta$  = 1.42 (d,  $J$  = 6.9 Hz, 3H,  $\text{CHCH}_3$ ), 1.50 (d,  $J$  = 6.9 Hz, 3H,  $\text{CHCH}_3$ ), 3.06 (s, 1H,  $\text{C}\equiv\text{CH}$ ), 4.53 (qui,  $J$  = 7.2 Hz, 1H,  $\text{CHCH}_3$ ), 5.26 (q,  $J$  = 6.6 Hz, 1H,  $\text{CHCH}_3$ ), 6.91 (d,  $J$  = 7.2 Hz, 1H, *NH*), 10.1 (bs, 1H,  $\text{CO}_2\text{H}$ ).  $^{13}\text{C}$  NMR (75.49 MHz,  $\text{CDCl}_3$ ):  $\delta$  = 17.6, 18.2 (2  $\text{CHCH}_3$ ), 48.0, 72.1 (2  $\text{CHCH}_3$ ), 74.0, 76.6 (acetylene C), 151.1 (propiolic ester  $\text{C}=\text{O}$ ), 169.1 (amide  $\text{C}=\text{O}$ ), 174.7 (acid  $\text{C}=\text{O}$ ). HRMS (EI): calcd for  $\text{C}_9\text{H}_{11}\text{NO}_5$ :  $([\text{M}]^+)$  213.0632; found: 213.0630.  $R_f$ : 0.3 ( $\text{CH}_2\text{Cl}_2/\text{MeOH}$  10:1). m. p.: 72-73 °C.

**hPI<sub>10</sub>-NH-Ala<sub>4</sub>-Lac-C(O)-C $\equiv$ C-H **109**.**

Following general procedure D, **108** (0.20 g, 0.94 mmol) and **45** (0.92 g, 0.84 mmol) were dissolved in a mixture of dry DMF (50 mL) and dry  $\text{CH}_2\text{Cl}_2$  (100 mL). DIEA (3.3 g, 2.55 mmol) and PyBOP (0.49 g, 0.94 mmol) were added. The next day, the solvents were removed *in vacuo*, and the crude product was purified by repeated column chromatography (silica gel,  $\text{CHCl}_3/\text{MeOH}$  25:1). The propiolic acid ester functionalized target molecule **109** (0.44 g, 41%) was obtained as a colorless amorphous solid.

$^1\text{H}$  NMR (300.23 MHz,  $\text{CDCl}_3$  / TFA 50:1):  $\delta$  = 0.6-1.9 (m, 151H, aliphatic *H*, 5  $\text{CHCH}_3$ ), 3.2-3.4 (m, 2H,  $\text{CH}_2\text{NHR}$ ), 3.63 (s, 1H,  $\text{C}\equiv\text{CH}$ ), 4.4-4.7 (m, 3H,  $\text{CHCH}_3$ ), 6.8 (m, 1H, *NH*), 7.5-8.0 (m, 3H,

*NH*). Anal. calcd for  $C_{75}H_{140}N_5O_7$ : C, 73.60%; H, 11.53%; N, 5.72%; found: C, 72.68%; H, 11.36%; N, 6.02%. HRMS (MALDI): calcd for  $C_{80}H_{151}N_5O_7Na$ : ( $[M+Na]^+$ ) 1317.151; found: 1312.081.  $R_f$ : 0.4 ( $CH_2Cl_2/MeOH$  10:1).

**PI<sub>25</sub>-NH<sub>2</sub> 111.** Isoprene (20.4 g, 300 mmol) was freshly distilled from  $CaH_2$  prior to use. A rigorously dried 250 mL Schlenk flask was filled with dry THF (120 mL), and *n*-butyl lithium (7.5 mL, 12 mmol) was added slowly via a syringe at  $-78^\circ C$ . Under vigorous stirring, isoprene was added via a syringe as fast as possible, leading to a yellow to orange color of the solution. The temperature was adjusted to  $0^\circ C$ , the mixture was stirred for 10 min and then cooled again to  $-78^\circ C$ . Then, 1-(3-bromopropyl)-2,2,5,5-tetramethyl-1-aza-2,5-disilacyclopentane (5 g, 17.8 mmol) was added via a syringe, causing an immediate decoloration. The cooling bath was removed, and the reaction mixture was stirred for 5 h at room temperature. Then, 2 M HCl (75 mL) was added, and stirring was continued over night. The mixture was concentrated *in vacuo*, taken up in  $CH_2Cl_2$ , washed twice with sat.  $NaHCO_3$  solution and once with sat. NaCl solution. The combined organic phases were dried over  $MgSO_4$ , filtered, and concentrated *in vacuo*. The crude product was purified by column chromatography ( $CH_2Cl_2/MeOH$  20:1). **111** (7.8 g, 36%) was obtained as a slightly yellow oil.

$^1H$  NMR (300.23 MHz,  $CDCl_3$ ):  $\delta$  = 0.6-2.1 (m, 100H, aliphatic *H*), 2.7-2.9 (m, 2H,  $CH_2NH_2$ ), 4.6-5.2 (m, 28H, terminal olefin *H*), 5.6-5.9 (m, 3H, internal olefin *H*). Anal. calcd for  $C_{52}H_{89}N$ : C, 85.76%; H, 12.32%; N, 1.92%; found: C, 84.15%; H, 11.87%; N, 1.79%.  $R_f$ : 0.4 ( $CH_2Cl_2/MeOH$  10:1).

**hPI<sub>25</sub>-NH<sub>2</sub> 112.** The amine-terminated poly(isoprene) **111** (7.7 g, 4.2 mmol) was dissolved in a mixture of toluene (75 mL) and EtOH (5 mL). The solution was transferred to a high pressure autoclave, and Pd on charcoal (3.0 g, 10% Pd/C, 50%  $H_2O$  content) was added as the catalyst. The mixture was stirred at a  $H_2$  pressure of 100 bar at  $80^\circ C$  for 10 d. After purification by a filtration of the reaction mixture through Celite and evaporation of the solvents, **112** (7.0 g, 93%) was obtained as slightly yellow oil.

$^1H$  NMR (300.23 MHz,  $CDCl_3$ ):  $\delta$  = 0.6-2.1 (m, 348H, aliphatic *H*), 2.7-2.9 (m, 2H,  $CH_2NH_2$ ), 4.6-4.8 (m, 2H, residual terminal olefin *H*). HRMS (MALDI): calcd for  $C_{52}H_{90}N$ : ( $[M+H]^+$ ) 728.7; found: 728.4.  $R_f$ : 0.6 ( $CH_2Cl_2/MeOH$  10:1).

**hPI<sub>25</sub>-NH-Ala-Fmoc 113.** Following general procedure D, **112** (1.50g, 0.8 mmol) and *N*-(9-fluorenylmethyloxycarbonyl)-L-alanine (0.30 g, 0.96 mmol) were dissolved in a mixture of DCM (20 mL) and DMF (5 mL). DIEA (0.52 g, 4.0 mmol) as well as PyBOP (0.53 g, 1.0 mmol) were added, and the reaction mixture stirred over night. The next day, the solvents were removed *in vacuo*, and

the crude product was purified by column chromatography (CH<sub>2</sub>Cl<sub>2</sub>/MeOH 24:1). **113** (1.46 g, 84%) was obtained as a colorless amorphous solid.

<sup>1</sup>H NMR (300.23 MHz, CDCl<sub>3</sub>): δ = 0.6-2.0 (m, 460H, aliphatic *H*, CHCH<sub>3</sub>), 3.1-3.3 (m, 1.2H, CH<sub>2</sub>NHR), 4.21 (t, *J* = 7.2 Hz, 1H, fluorenyl *CH*), 4.45 (d, *J* = 7.2 Hz, 2H, Fmoc-CO<sub>2</sub>CH<sub>2</sub>), 4.6-4.8 (m, 3H, 1 CHCH<sub>3</sub>, 2 residual olefin *H*), 5.8 (m, 0.25H, carbamate *NH*), 6.0 (m, 0.3H, amide *NH*), 7.31 (t, *J* = 7.5 Hz, 2H, aromatic *H*), 7.40 (t, *J* = 7.2 Hz, 2H, aromatic *H*), 7.60 (d, *J* = 7.2 Hz, 2H, aromatic *H*), 7.77 (d, *J* = 7.5 Hz, 2H, aromatic *H*). HRMS (MALDI): calcd for C<sub>70</sub>H<sub>122</sub>N<sub>2</sub>O<sub>3</sub>Na: ([M+Na]<sup>+</sup>) 1061.935; found 1062.573. R<sub>f</sub>: 0.9 (CH<sub>2</sub>Cl<sub>2</sub>/MeOH 10:1).

**hPI<sub>25</sub>-NH-Ala-H 114.** Following general procedure C, **113** (1.35g, 0.62 mmol) was dissolved in CHCl<sub>3</sub> (50 mL), and piperidine (0.27 g, 3.11 mmol) was added. The crude product was purified by column chromatography (gradient CH<sub>2</sub>Cl<sub>2</sub>/MeOH 24:1 → CH<sub>2</sub>Cl<sub>2</sub>/MeOH 9:1). **114** (1.03 g, 86%) was obtained as a colorless oil.

<sup>1</sup>H NMR (300.23 MHz, CDCl<sub>3</sub>): δ = 0.6-2.1 (m, 452H, aliphatic *H*, CHCH<sub>3</sub>), 3.0-3.3 (m, 2H, CH<sub>2</sub>NHR), 3.98 (m, 1H, CHCH<sub>3</sub>), 4.6-4.8 (m, 2H, residual olefin *H*). HRMS (MALDI): calcd for C<sub>70</sub>H<sub>122</sub>N<sub>2</sub>O<sub>3</sub>Na: ([M+Na]<sup>+</sup>) 1061.935; found 1062.573. R<sub>f</sub>: 0.5 (CH<sub>2</sub>Cl<sub>2</sub>/MeOH 10:1).

**hPI<sub>25</sub>-NH-Ala<sub>2</sub>-Fmoc 115.** Following general procedure D, **112** (1.50g, 0.8 mmol) and **36** (0.37 g, 0.96 mmol) were dissolved in a mixture of DCM (20 mL) and DMF (5 mL). DIEA (0.52 g, 4.0 mmol) as well as PyBOP (0.53 g, 1.0 mmol) were added, and the reaction mixture stirred over night. The next day, the solvents were removed *in vacuo*, and the crude product was purified by column chromatography (CH<sub>2</sub>Cl<sub>2</sub>/MeOH 24:1), **113** (1.70 g, 94%) was obtained as a colorless amorphous solid.

<sup>1</sup>H NMR (300.23 MHz, CDCl<sub>3</sub>): δ = 0.6-2.0 (m, 276H, aliphatic *H*, 2 CHCH<sub>3</sub>), 3.1-3.3 (m, 1.3H, CH<sub>2</sub>NHR), 4.0 (m, 0.3H, CHCH<sub>3</sub>), 4.22 (m, 1.7H, fluorenyl *CH*, CHCH<sub>3</sub>), 4.38 (m, 2H, Fmoc-CO<sub>2</sub>CH<sub>2</sub>), 4.6-4.8 (m, 2H, residual olefin *H*), 5.5 (m, 0.5H, carbamate *NH*), 7.31 (t, *J* = 7.5 Hz, 2H, aromatic *H*), 7.40 (t, *J* = 7.2 Hz, 2H, aromatic *H*), 7.60 (m, 2H, aromatic *H*), 7.77 (d, *J* = 7.5 Hz, 2H, aromatic *H*). HRMS (MALDI): calcd for C<sub>70</sub>H<sub>122</sub>N<sub>2</sub>O<sub>3</sub>Na: ([M+Na]<sup>+</sup>) 1061.935; found 1062.573. R<sub>f</sub>: 0.9 (CH<sub>2</sub>Cl<sub>2</sub>/MeOH 10:1).

**hPI<sub>25</sub>-NH-Ala<sub>2</sub>-H 116.** Following general procedure C, **115** (1.60 g, 0.71 mmol) was dissolved in CHCl<sub>3</sub> (50 mL), and piperidine (0.30 g, 3.57 mmol) was added. The crude product was purified by column chromatography (gradient CH<sub>2</sub>Cl<sub>2</sub>/MeOH 24:1 → CH<sub>2</sub>Cl<sub>2</sub>/MeOH 9:1). **114** (1.36 g, 95%) was obtained as a colorless amorphous solid.

$^1\text{H}$  NMR (300.23 MHz,  $\text{CDCl}_3$ ):  $\delta$  = 0.6-2.2 (m, 400H, aliphatic  $H$ , 2  $\text{CHCH}_3$ ), 3.0-3.3 (m, 2H,  $\text{CH}_2\text{NHR}$ ), 4.0-5.0 (m, 4H, 2  $\text{CHCH}_3$ , residual olefin  $H$ ), 6.1 (m, 0.3H, amide  $\text{NH}$ ). HRMS (MALDI): calcd for  $\text{C}_{70}\text{H}_{122}\text{N}_2\text{O}_3\text{Na}$ : ( $[\text{M}+\text{Na}]^+$ ) 1061.935; found 1062.573.  $R_f$ : 0.5 ( $\text{CH}_2\text{Cl}_2/\text{MeOH}$  10:1).

**hPI<sub>25</sub>-NH-Ala<sub>3</sub>-Fmoc 117.** Following general procedure D, **112** (1.50g, 0.8 mmol) and **39** (0.44 g, 0.96 mmol) were dissolved in a mixture of DCM (20 mL) and DMF (5 mL). DIEA (0.52 g, 4.0 mmol) as well as PyBOP (0.53 g, 1.0 mmol) were added, and the reaction mixture stirred over night. The next day, the solvents were removed *in vacuo*, and the crude product was purified by column chromatography ( $\text{CH}_2\text{Cl}_2/\text{MeOH}$  24:1). **113** (1.70 g, 92%) was obtained as a colorless amorphous solid.

$^1\text{H}$  NMR (300.23 MHz,  $\text{CDCl}_3$ ):  $\delta$  = 0.6-2.0 (m, 455H, aliphatic  $H$ , 3  $\text{CHCH}_3$ ), 3.1-3.3 (m, 1.2H,  $\text{CH}_2\text{NHR}$ ), 4.0-4.3 (m, 1.8H, fluorenyl  $\text{CH}$ ,  $\text{CHCH}_3$ ), 4.4-4.6 (m, 3H,  $\text{CHCH}_3$ , Fmoc- $\text{CO}_2\text{CH}_2$ ), 4.6-4.8 (m, 2.7H,  $\text{CHCH}_3$ , residual olefin  $H$ ), 5.4 (m, 0.6H, carbamate  $\text{NH}$ ), 6.5 (m, 0.3H, amide  $\text{NH}$ ), 7.31 (t,  $J$  = 7.2 Hz, 2H, aromatic  $H$ ), 7.40 (t,  $J$  = 7.5 Hz, 2H, aromatic  $H$ ), 7.60 (m, 2H, aromatic  $H$ ), 7.77 (d,  $J$  = 7.5 Hz, 2H, aromatic  $H$ ). HRMS (MALDI): calcd for  $\text{C}_{70}\text{H}_{122}\text{N}_2\text{O}_3\text{Na}$ : ( $[\text{M}+\text{Na}]^+$ ) 1061.935; found 1062.573.  $R_f$ : 0.9 ( $\text{CH}_2\text{Cl}_2/\text{MeOH}$  10:1).

**hPI<sub>25</sub>-NH-Ala<sub>3</sub>-H 118.** Following general procedure C, **117** (1.51g, 0.66 mmol) was dissolved in  $\text{CHCl}_3$  (50 mL), and piperidine (0.28 g, 3.28 mmol) was added. The crude product was purified by column chromatography (gradient  $\text{CH}_2\text{Cl}_2/\text{MeOH}$  24:1  $\rightarrow$   $\text{CH}_2\text{Cl}_2/\text{MeOH}$  9:1). **114** (1.05 g, 76%) was obtained as a colorless oil.

$^1\text{H}$  NMR (300.23 MHz,  $\text{CDCl}_3$ ):  $\delta$  = 0.6-2.2 (m, 470H, aliphatic  $H$ , 3  $\text{CHCH}_3$ ), 3.0-3.3 (m, 2H,  $\text{CH}_2\text{NHR}$ ), 4.0-4.2 (m, 1.3H, 1  $\text{CHCH}_3$ ), 4.4-4.6 (m, 1.3H, 1  $\text{CHCH}_3$ ), 4.6-4.9 (m, 3H, 1  $\text{CHCH}_3$ , residual olefin  $H$ ). HRMS (MALDI): calcd for  $\text{C}_{70}\text{H}_{122}\text{N}_2\text{O}_3\text{Na}$ : ( $[\text{M}+\text{Na}]^+$ ) 1061.935; found 1062.573.  $R_f$ : 0.5 ( $\text{CH}_2\text{Cl}_2/\text{MeOH}$  10:1).

**(hPI<sub>25</sub>-NH-Ala<sub>2</sub>-C(O)O-CH<sub>2</sub>-C $\equiv$ C-)<sub>2</sub> 119.** Following general procedure E, **66** (0.017 g, 0.05 mmol) was dissolved in a mixture of dry DMF (4 mL) and dry  $\text{CH}_2\text{Cl}_2$  (8 mL). HOBt (0.021 g, 0.16 mmol) and EDCI (0.030 g, 0.16 mmol) were added to form the active ester intermediate. A second solution containing **114** (0.20 g, 0.10 mmol) and TEA (0.031 g, 0.30 mmol) in dry  $\text{CH}_2\text{Cl}_2$  (40 mL) was prepared, and both solutions were combined. The next day, the solvents were removed *in vacuo*, and the crude material was purified by column chromatography (silica gel,  $\text{CHCl}_3/\text{MeOH}$  24:1). **119** (0.195 g, 90%) was obtained as a colorless amorphous solid.

$^1\text{H}$  NMR (300.23 MHz,  $\text{CDCl}_3$ ):  $\delta$  = 0.5-2.2 (m, 2444H, aliphatic  $H$ , 4  $\text{CHCH}_3$ ), 3.0-3.3 (m, 4H,  $\text{CH}_2\text{NHR}$ ), 4.0-4.1 (m, 2H, 2  $\text{CHCH}_3$ ), 4.2-4.3 (m, 4H, 2  $\text{CHCH}_3$ ), 4.6-4.9 (m, 25H, 2  $\text{CO}_2\text{CH}_2$ , residual

olefin *H*), 5.5 (m, 4H, 2 carbamate *NH*), 6.8 (m, 2H, 2 amide *NH*), 7.0 (m, 4H, 4 amide *NH*).  $R_f$ : 0.8 (CH<sub>2</sub>Cl<sub>2</sub>/MeOH 10:1).

**(hPI<sub>25</sub>-NH-Ala<sub>3</sub>-C(O)O-CH<sub>2</sub>-C≡C-)<sub>2</sub> 120.** Following general procedure E, **66** (0.017 g, 0.05 mmol) was dissolved in a mixture of dry DMF (4 mL) and dry CH<sub>2</sub>Cl<sub>2</sub> (8 mL). HOBt (0.020 g, 0.15 mmol) and EDCI (0.029 g, 0.15 mmol) were added to form the active ester intermediate. A second solution containing **116** (0.20 g, 0.10 mmol) and TEA (0.03 g, 0.30 mmol) in dry CH<sub>2</sub>Cl<sub>2</sub> (40 mL) was prepared, and both solutions were combined. The next day, the solvents were removed *in vacuo*, and the crude material was purified by column chromatography (silica gel, CHCl<sub>3</sub>/MeOH 24:1). **120** (0.133 g, 62%) was obtained as a colorless amorphous solid.

<sup>1</sup>H NMR (300.23 MHz, CDCl<sub>3</sub>):  $\delta$  = 0.5-2.2 (m, 2604H, aliphatic *H*, 6 CHCH<sub>3</sub>), 3.0-3.3 (m, 4H, CH<sub>2</sub>NHR), 4.0-4.3 (m, 2.8H, 2 CHCH<sub>3</sub>), 4.3-4.6 (m, 6H, 4 CHCH<sub>3</sub>), 4.6-4.9 (m, 27H, 2 CO<sub>2</sub>CH<sub>2</sub>, residual olefin *H*), 5.4 (m, 2H, 2 carbamate *NH*), 6.8 (m, 1H, 2 amide *NH*).  $R_f$ : 0.8 (CH<sub>2</sub>Cl<sub>2</sub>/MeOH 10:1).

**(hPI<sub>25</sub>-NH-Ala<sub>4</sub>-C(O)O-CH<sub>2</sub>-C≡C-)<sub>2</sub> 121.** Following general procedure E, **66** (0.016 g, 0.05 mmol) was dissolved in a mixture of dry DMF (4 mL) and dry CH<sub>2</sub>Cl<sub>2</sub> (8 mL). HOBt (0.019 g, 0.14 mmol) and EDCI (0.029 g, 0.15 mmol) were added to form the active ester intermediate. A second solution containing **118** (0.20 g, 0.10 mmol) and TEA (0.029 g, 0.29 mmol) in dry CH<sub>2</sub>Cl<sub>2</sub> (40 mL) was prepared, and both solutions were combined. The next day, the solvents were removed *in vacuo*, and the crude material was purified by column chromatography (silica gel, CHCl<sub>3</sub>/MeOH 24:1). **121** (0.210 g, 98%) was obtained as a colorless amorphous solid.

<sup>1</sup>H NMR (300.23 MHz, CDCl<sub>3</sub>):  $\delta$  = 0.5-2.2 (m, 2620H, aliphatic *H*, 8 CHCH<sub>3</sub>), 3.0-3.3 (m, 4H, CH<sub>2</sub>NHR), 4.0-5.0 (m, 39H, 8 CHCH<sub>3</sub>, residual olefin *H*).  $R_f$ : 0.8 (CH<sub>2</sub>Cl<sub>2</sub>/MeOH 10:1).

**hPI<sub>25</sub>-NH-Ala<sub>4</sub>-C(O)O-CH<sub>2</sub>-C≡C-C≡C-CH<sub>2</sub>NH-C(O)(CH<sub>2</sub>)<sub>2</sub>C(O)OMe 122.** Following general procedure E, **71** (0.049 g, 0.14 mmol) was dissolved in a mixture of dry DMF (4 mL) and dry CH<sub>2</sub>Cl<sub>2</sub> (8 mL). HOBt (0.023 g, 0.17 mmol) and EDCI (0.035 g, 0.18 mmol) were added to form the active ester intermediate. A second solution containing **118** (0.30 g, 0.14 mmol) and TEA (0.073 g, 0.72 mmol) in dry CH<sub>2</sub>Cl<sub>2</sub> (40 mL) was prepared, and both solutions were combined. The next day, the solvents were removed *in vacuo*, and the crude material was purified by column chromatography (silica gel, CHCl<sub>3</sub>/MeOH 24:1). **122** (0.31 g, 90%) was obtained as a colorless amorphous solid.

<sup>1</sup>H NMR (300.23 MHz, CDCl<sub>3</sub>):  $\delta$  = 0.5-2.2 (m, 588H, aliphatic *H*, 4 CHCH<sub>3</sub>), 2.55 (t,  $J$  = 6.9 Hz, 2H, NHC(O)CH<sub>2</sub>), 2.71 (t,  $J$  = 6.9 Hz, 2H, CH<sub>2</sub>CO<sub>2</sub>CH<sub>3</sub>), 3.0-3.3 (m, 0.7H, CH<sub>2</sub>NHR), 3.72 (s, 3H, OCH<sub>3</sub>), 4.0-4.2 (m, 3H, 1 CHCH<sub>3</sub>, CH<sub>2</sub>NH), 4.2-4.6 (m, 3H, 3 CHCH<sub>3</sub>), 4.6-4.9 (m, 5H, 2 CO<sub>2</sub>CH<sub>2</sub>, residual



olefin *H*), 5.6-5.7 (m, 0.2H, 1 carbamate *NH*), 6.4 (m, 0.3H, 1 amide *NH*), 6.8-7.0 (m, 1.2H, 2 amide *NH*). *R*<sub>f</sub>: 0.7 (CH<sub>2</sub>Cl<sub>2</sub>/MeOH 10:1).

**hPI<sub>25</sub>-NH-Ala<sub>4</sub>-C(O)O-CH<sub>2</sub>-C≡C-C≡C-CH<sub>2</sub>NH-Ala-Fmoc 123.** Following general procedure E, **79** (0.075 g, 0.14 mmol) was dissolved in a mixture of dry DMF (4 mL) and dry CH<sub>2</sub>Cl<sub>2</sub> (8 mL). HOBt (0.023 g, 0.17 mmol) and EDCI (0.035 g, 0.18 mmol) were added to form the active ester intermediate. A second solution containing **118** (0.30 g, 0.14 mmol) and TEA (0.073 g, 0.72 mmol) in dry CH<sub>2</sub>Cl<sub>2</sub> (40 mL) was prepared, and both solutions were combined. The next day, the solvents were removed *in vacuo*, and the crude material was purified by column chromatography (silica gel, CHCl<sub>3</sub>/MeOH 24:1). **123** (0.34 g, 91%) was obtained as a colorless amorphous solid.

<sup>1</sup>H NMR (300.23 MHz, CDCl<sub>3</sub>): δ = 0.5-2.2 (m, 334, aliphatic *H*, 4 CHCH<sub>3</sub>), 3.0-3.3 (m, 0.4H, CH<sub>2</sub>NHR), 4.0-5.0 (m, 11H, 5 CHCH<sub>3</sub>, NHCH<sub>2</sub>, Fmoc-NHCO<sub>2</sub>CH<sub>2</sub>, NHCO<sub>2</sub>CH<sub>2</sub>, fluorenyl *CH*), 5.6-5.7 (m, 0.5H, 2 carbamate *NH*), 6.8-7.1 (m, 0.5H, 2 amide *NH*), 7.3-7.4 (m, 3H, aromatic *H*, *NH*), 7.4-7.5 (m, 3H, 2 aromatic *H*, *NH*), 7.5-7.8 (m, 3H, 2 aromatic *H*, *NH*), 7.8-7.9 (m, 2H, 2 aromatic *H*). *R*<sub>f</sub>: 0.7 (CH<sub>2</sub>Cl<sub>2</sub>/MeOH 10:1).

***N*-(9-Fluorenylmethyloxycarbonyl)-L-alanine Hexylamide 124.** Following general procedure D, *N*-(9-fluorenylmethyloxycarbonyl)-L-alanine (2.0 g, 6.4 mmol) and hexylamine (0.7 g, 6.4 mmol) were dissolved in a mixture of dry CH<sub>2</sub>Cl<sub>2</sub> (90 mL) and dry DMF (45 mL). DIEA (3.3 g, 25.6 mmol) and PyBOP (3.5 g, 6.7 mmol) were added, and the reaction mixture was stirred over night. The solution was concentrated *in vacuo*, and the crude product was purified by column chromatography (silica gel, CH<sub>2</sub>Cl<sub>2</sub>/MeOH 24:1). **124** (2.5 g, 97%) was obtained as a colorless solid.

<sup>1</sup>H NMR (300.23 MHz, CDCl<sub>3</sub>): δ = 0.85 (t, *J* = 6.9 Hz, 3H, CH<sub>3</sub>), 1.2-1.6 (m, 11H, (CH<sub>2</sub>)<sub>4</sub>CH<sub>3</sub>, CHCH<sub>3</sub>), 3.21 (m, 2H, NHCH<sub>2</sub>), 4.1-4.3 (m, 2H, fluorenyl-*CH*, CHCH<sub>3</sub>), 4.36 (d, *J* = 6.9 Hz, 2H, Fmoc-CO<sub>2</sub>CH<sub>2</sub>), 5.67 (d, *J* = 6.9 Hz, 1H, *NH*), 6.37 (br s, 1H, *NH*), 7.29 (t, *J* = 7.5 Hz, 2H, aromatic *H*), 7.38 (t, *J* = 7.5 Hz, 2H, aromatic *H*), 7.56 (d, *J* = 7.5 Hz, 2H, aromatic *H*), 7.74 (d, *J* = 7.5 Hz, 2H, aromatic *H*). <sup>13</sup>C NMR (75.49 MHz, CDCl<sub>3</sub>): δ = 14.0 (CH<sub>3</sub>), 19.0 (CHCH<sub>3</sub>), 22.5, 26.5, 29.5, 31.4 (4 CH<sub>2</sub>), 39.6 (NHCH<sub>2</sub>), 47.1 (fluorenyl-*CH*), 50.6 (CHCH<sub>3</sub>), 67.1 (Fmoc-CO<sub>2</sub>CH<sub>2</sub>), 120.0, 125.1, 127.1, 127.8, 141.3, 143.8 (aromatic C), 156.1 (carbamate C=O), 172.2 (amide C=O). Anal. calcd for C<sub>24</sub>H<sub>30</sub>N<sub>2</sub>O<sub>3</sub>: C, 73.07%; H, 7.66%; N, 7.10%; found: C, 73.23%; H, 7.61%; N, 6.96%. HRMS (EI): calcd for C<sub>24</sub>H<sub>30</sub>N<sub>2</sub>O<sub>3</sub>: ([M]<sup>+</sup>) 394.2251; found 394.2281. *R*<sub>f</sub>: 0.6 (CH<sub>2</sub>Cl<sub>2</sub>/MeOH 10:1).

**L-Alanine Hexylamide 125.** Following general procedure C, **124** (2.5 g, 6.34 mmol) was dissolved in CHCl<sub>3</sub> (50 mL), and piperidine (6.7 g, 79 mmol) was added. The next day, the reaction mixture was

washed twice with sat. NaHCO<sub>3</sub> solution and once with sat. NaCl solution. The combined organic phases were dried over MgSO<sub>4</sub>, filtered, and concentrated *in vacuo*. The crude product was purified by column chromatography (silica gel, CH<sub>2</sub>Cl<sub>2</sub>/MeOH/triethylamine 70 : 2: 1). **125** (0.8 g, 73%) was obtained as a yellowish oil.

<sup>1</sup>H NMR (300.23 MHz, CDCl<sub>3</sub>): δ = 0.76 (t, *J* = 6.6 Hz, 3H, CH<sub>3</sub>), 1.1-1.3 (m, 9H, 3 CH<sub>2</sub>, CHCH<sub>3</sub>), 1.37 (m, 2H, CH<sub>2</sub>), 1.6 (s, 2H, NH<sub>2</sub>), 3.10 (q, *J* = 6.6 Hz, 2H, NHCH<sub>2</sub>), 3.36 (q, *J* = 6.9 Hz, 1H, CHCH<sub>3</sub>) 7.29 (bs, 1H, NH). <sup>13</sup>C NMR (75.49 MHz, CDCl<sub>3</sub>): δ = 13.9 (CH<sub>3</sub>), 21.7 (CHCH<sub>3</sub>), 22.4, 26.5, 29.5, 31.4 (4 CH<sub>2</sub>), 39.0 (NHCH<sub>2</sub>), 50.7 (CHCH<sub>3</sub>), 175.5 (amide C=O). HRMS (EI): calcd for C<sub>9</sub>H<sub>20</sub>N<sub>2</sub>O: ([M]<sup>+</sup>) 172.1570; found 172.1570. R<sub>f</sub>: 0.2 (CH<sub>2</sub>Cl<sub>2</sub>/MeOH 10:1).

***N*-[6-(*N'*-Acetamido)hexa-2,4-diynyl-1-oxycarbonyl]-L-alanyl-L-alanine Hexylamide**

**126.** Following general procedure E, **68** (0.24 g, 1.0 mmol) was dissolved in a mixture of dry DMF (10 mL) and dry CH<sub>2</sub>Cl<sub>2</sub> (30 mL). HOBt (0.18 g, 1.33 mmol) and EDCI (0.33 g, 1.72 mmol) were added to form the active ester intermediate. A second solution containing **125** (0.21 g, 1.22 mmol) and TEA (0.40 g, 4.0 mmol) in dry CH<sub>2</sub>Cl<sub>2</sub> (50 mL) was prepared, and both solutions were combined. The solution was washed twice with 1M HCl and once with sat. NaCl solution. The combined organic phases were dried over MgSO<sub>4</sub>, filtered, and concentrated *in vacuo*. The crude material was purified by column chromatography (silica gel, CHCl<sub>3</sub>/MeOH 24:1). **127** (0.28 g, 74%) was obtained as an amorphous solid.

<sup>1</sup>H NMR (300.23 MHz, DMSO-D<sub>6</sub>): δ = 0.87 (t, *J* = 6.6 Hz, 3H, CH<sub>3</sub>), 1.1-1.5 (m, 14H, 2 CHCH<sub>3</sub>, (CH<sub>2</sub>)<sub>4</sub>CH<sub>3</sub>), 1.84 (s, 3H, C(O)CH<sub>3</sub>), 3.04 (m, 2H, NH(CH<sub>2</sub>)(CH<sub>2</sub>)<sub>4</sub>CH<sub>3</sub>), 3.98 (C≡CCH<sub>2</sub>NH), 4.05 (m, 1H, CHCH<sub>3</sub>), 4.21 (m, 1H, CHCH<sub>3</sub>), 4.74 (m, 2H, NHCO<sub>2</sub>CH<sub>2</sub>), 7.62 (d, *J* = 7.5 Hz, 1H, NH), 7.75 (t, *J* = 5.4 Hz, 1H, NH), 7.93 (d, *J* = 7.8 Hz, 1H, NH), 8.36 (t, *J* = 5.4 Hz, 1H, NH). R<sub>f</sub>: 0.4 (CH<sub>2</sub>Cl<sub>2</sub>/MeOH 10:1).

**Hexa-2,4-diynylene-1,6-bis(oxycarbonyl-L-alanyl-L-alanine Hexylamide) 127.** Following general procedure E, **66** (0.31 g, 0.92 mmol) was dissolved in a mixture of dry DMF (10 mL) and dry CH<sub>2</sub>Cl<sub>2</sub> (30 mL). HOBt (0.38 g, 2.81 mmol) and EDCI (0.53 g, 2.80 mmol) were added to form the active ester intermediate. A second solution containing **125** (0.32 g, 1.83 mmol) and TEA (0.56 g, 5.5 mmol) in dry CH<sub>2</sub>Cl<sub>2</sub> (50 mL) was prepared, and both solutions were combined. The solution was washed twice with 1M HCl and once with sat. NaCl solution. The combined organic phases were dried over MgSO<sub>4</sub>, filtered, and concentrated *in vacuo*. The crude material was purified by column chromatography (silica gel, CHCl<sub>3</sub>/MeOH 24:1). **127** (0.25 g, 41%) was obtained as an amorphous solid.

<sup>1</sup>H NMR (300.23 MHz, DMSO-D<sub>6</sub>): δ = 0.86 (t, *J* = 6.6 Hz, 6H, 2 CH<sub>3</sub>), 1.1-1.5 (m, 28H, 4 CHCH<sub>3</sub>, 2 (CH<sub>2</sub>)<sub>4</sub>CH<sub>3</sub>), 3.03 (m, 4H, 2 NH(CH<sub>2</sub>)(CH<sub>2</sub>)<sub>4</sub>CH<sub>3</sub>), 4.05 (m, 2H, 2 CHCH<sub>3</sub>), 4.21 (m, 2H, 2 CHCH<sub>3</sub>), 4.77

(m, 4H, 2 NHCO<sub>2</sub>CH<sub>2</sub>), 7.64 (d, *J* = 7.2 Hz, 2H, *NH*), 7.77 (t, *J* = 5.1 Hz, 2H, *NH*), 7.96 (d, *J* = 7.5 Hz, 2H, *NH*). R<sub>f</sub>: 0.4 (CH<sub>2</sub>Cl<sub>2</sub>/MeOH 10:1).

***N*-(9-Fluorenylmethyloxycarbonyl)-L-alanine Dodecylamide 128.** Following general procedure D, dodecylamine (3.22 g, 17.37 mmol) and *N*-(9-fluorenylmethyloxycarbonyl)-L-alanine (5.52 g, 17.73 mmol) were dissolved in a mixture of dry CH<sub>2</sub>Cl<sub>2</sub> (90 mL) and dry DMF (30 mL). DIEA (6.7 g, 52.60 mmol) and PyBOP (9.4 g, 18.07 mmol) were added, and the reaction mixture was stirred over night. The organic phase was washed with sat. NaHCO<sub>3</sub> solution, 1M HCl and sat. NaCl solution, dried over MgSO<sub>4</sub>, filtered, and concentrated *in vacuo*. The crude material was purified by column chromatography (silica gel, gradient CH<sub>2</sub>Cl<sub>2</sub>/MeOH 24:1 → CH<sub>2</sub>Cl<sub>2</sub>/MeOH 10:1). **128** (5.83 g, 81%) was obtained as a colorless solid material.

<sup>1</sup>H NMR (300.23 MHz, CDCl<sub>3</sub>): δ = 0.89 (t, *J* = 6.9 Hz, 3H, (CH<sub>2</sub>)<sub>11</sub>CH<sub>3</sub>), 1.2-1.35 (m, 18H, (CH<sub>2</sub>)<sub>9</sub>CH<sub>3</sub>), 1.38 (d, *J* = 6.9 Hz, 3H, CHCH<sub>3</sub>), 1.44 (m, 2H, CH<sub>2</sub>(CH<sub>2</sub>)<sub>9</sub>CH<sub>3</sub>), 3.22 (m, 2H, NHCH<sub>2</sub>(CH<sub>2</sub>)<sub>10</sub>CH<sub>3</sub>), 4.15-4.3 (m, 2H, CHCH<sub>3</sub>, fluorenyl CH), 4.37 (d, *J* = 6.9 Hz, 2H, CO<sub>2</sub>CH<sub>2</sub>), 5.63 (d, *J* = 7.2 Hz, 1H, *NH*), 6.30 (bs, 1H, *NH*), 7.29 (t, *J* = 7.5 Hz, 2H, aromatic *H*), 7.39 (t, *J* = 7.5 Hz, 2H, aromatic *H*), 7.57 (d, *J* = 7.2 Hz, 2H, aromatic *H*), 7.75 (d, *J* = 7.5 Hz, 2H, aromatic *H*). <sup>13</sup>C NMR (75.49 MHz, CDCl<sub>3</sub>): δ = 14.1 ((CH<sub>2</sub>)<sub>11</sub>CH<sub>3</sub>), 18.9 (CHCH<sub>3</sub>), 22.7, 26.9, 29.3, 29.4, 29.5, 29.6, 29.7, 31.9 (10 CH<sub>2</sub>), 39.6 (NHCH<sub>2</sub>(CH<sub>2</sub>)<sub>10</sub>CH<sub>3</sub>), 47.1 (fluorenyl CH), 50.6 (CHCH<sub>3</sub>), 67.1 (CO<sub>2</sub>CH<sub>2</sub>), 120.0, 125.0, 127.1, 127.8, 141.3, 143.8 (aromatic C), 156.1 (carbamate C=O), 172.2 (amide C=O). Anal. calcd for C<sub>30</sub>H<sub>42</sub>N<sub>2</sub>O<sub>3</sub>: C, 75.28%; H, 8.84%; N, 5.85%; found: C, 75.15%; H, 8.84%; N, 5.93%. HRMS (EI): calcd for C<sub>30</sub>H<sub>42</sub>N<sub>2</sub>O<sub>3</sub>: ([M]<sup>+</sup>) 478.3190; found: 478.3200. R<sub>f</sub>: 0.75 (CH<sub>2</sub>Cl<sub>2</sub>/MeOH 10:1). m. p.: 136-137 °C.

**L-Alanine Dodecylamide 129.** Following general procedure C, **128** (5.63 g, 12.17 mmol) was dissolved in CHCl<sub>3</sub> (40 mL), and piperidine (8 mL, 81 mmol) was added. The solvents were removed *in vacuo* and the crude material was purified by column chromatography (silica gel, CH<sub>2</sub>Cl<sub>2</sub>/MeOH 24:1). **129** (2.82 g, 90%) was obtained as a colorless solid material.

<sup>1</sup>H NMR (300.23 MHz, CDCl<sub>3</sub>): δ = 0.85 (t, *J* = 6.9 Hz, 3H, (CH<sub>2</sub>)<sub>11</sub>CH<sub>3</sub>), 1.15-1.35 (m, 18H, (CH<sub>2</sub>)<sub>9</sub>CH<sub>3</sub>), 1.30 (d, *J* = 6.9 Hz, 3H, CHCH<sub>3</sub>), 1.48 (m, 2H, CH<sub>2</sub>(CH<sub>2</sub>)<sub>9</sub>CH<sub>3</sub>), 1.95 (bs, 2H, NH<sub>2</sub>), 3.20 (q, *J* = 6.6 Hz, 2H, NHCH<sub>2</sub>(CH<sub>2</sub>)<sub>10</sub>CH<sub>3</sub>), 3.44 (m, 1H, CHCH<sub>3</sub>), 7.29 (bs, 1H, *NH*). <sup>13</sup>C NMR (75.49 MHz, CDCl<sub>3</sub>): δ = 14.1 ((CH<sub>2</sub>)<sub>11</sub>CH<sub>3</sub>), 21.7 (CHCH<sub>3</sub>), 22.6, 26.9, 29.3, 29.5, 29.5, 29.6, 31.9 (10 CH<sub>2</sub>), 39.1 (NHCH<sub>2</sub>(CH<sub>2</sub>)<sub>10</sub>CH<sub>3</sub>), 50.7 (CHCH<sub>3</sub>), 175.7 (amide C=O). HRMS (EI): calcd for C<sub>15</sub>H<sub>32</sub>N<sub>2</sub>O: ([M]<sup>+</sup>) 256.2509; found: 256.2507. R<sub>f</sub>: 0.2 (CH<sub>2</sub>Cl<sub>2</sub>/MeOH 10:1). m. p.: 54-55 °C.

***N*-(5-Trimethylsilylpenta-2,4-diylnyl-1-oxycarbonyl)-L-alanyl]-L-alanine Dodecylamide 130.** Following general procedure D, **129** (0.148 g, 0.58 mmol) and **87** (0.15 g, 0.56 mmol) were

dissolved in a mixture of dry  $\text{CH}_2\text{Cl}_2$  (30 mL) and dry DMF (5 mL). DIEA (0.30 g, 2.32 mmol) and PyBOP (1.06 g, 2.04 mmol) were added, and the solution was stirred at room temperature over night. The next day, the solvents were removed *in vacuo*. The crude material was dissolved in a 1:1 mixture of THF (5 mL) and MeOH (5 mL), and purified by precipitation in water (120 mL). The precipitate was filtered off and dried in HV. **130** (0.24 g, 84%) was obtained as a slightly brown material.

$^1\text{H}$  NMR (300.23 MHz,  $\text{CDCl}_3$ ):  $\delta$  = 0.19 (s, 9H,  $\text{Si}(\text{CH}_3)_3$ ), 0.88 (t,  $J$  = 6.6 Hz, 3H,  $(\text{CH}_2)_{11}\text{CH}_3$ ), 1.25 (bs, 18H,  $(\text{CH}_2)_9\text{CH}_3$ ), 1.38 (d,  $J$  = 6.9 Hz, 6H, 2  $\text{CHCH}_3$ ), 1.50 (m, 2H,  $\text{CH}_2(\text{CH}_2)_9\text{CH}_3$ ), 3.24 (m, 2H,  $\text{NHCH}_2(\text{CH}_2)_{10}\text{CH}_3$ ), 4.26 (m, 1H,  $\text{CHCH}_3$ ), 4.44 (m, 1H,  $\text{CHCH}_3$ ), 4.74 (s, 2H,  $\text{NHCO}_2\text{CH}_2$ ), 5.55 (d,  $J$  = 7.5 Hz, 1H,  $\text{NH}$ ), 6.27 (m, 1H,  $\text{NH}$ ), 6.78 (d,  $J$  = 7.2 Hz, 1H,  $\text{NH}$ ).  $^{13}\text{C}$  NMR (75.49 MHz,  $\text{CDCl}_3$ ):  $\delta$  = 0.5 ( $\text{Si}(\text{CH}_3)_3$ ), 14.1 ( $(\text{CH}_2)_{11}\text{CH}_3$ ), 18.6, 19.0 (2  $\text{CHCH}_3$ ), 22.7, 26.9, 29.3, 29.3, 29.4, 29.6, 29.6, 31.9 (10  $\text{CH}_2$ ), 39.7 ( $\text{NHCH}_2(\text{CH}_2)_{10}\text{CH}_3$ ), 49.0, 50.8 (2  $\text{CHCH}_3$ ), 53.1 ( $\text{NHCO}_2\text{CH}_2$ ), 71.4, 71.7, 86.9, 88.2 (diacetylene C), 155.0 (carbamate C=O), 171.8 (amide C=O) 172.0 (amide C=O). Anal. calcd for  $\text{C}_{27}\text{H}_{47}\text{N}_3\text{O}_4\text{Si}$ : C, 64.12%; H, 9.37%; N, 8.31%; found: C, 64.16%; H, 9.22%; N, 8.59%. HRMS (MALDI): calcd for  $\text{C}_{27}\text{H}_{47}\text{N}_3\text{O}_4\text{SiNa}$ :  $([\text{M}+\text{Na}]^+)$  528.3234; found: 528.3228.  $R_f$ : 0.6 ( $\text{CH}_2\text{Cl}_2/\text{MeOH}$  10:1).

***N*-{6-[*N'*(4-Methoxysuccinyl)amido]hexa-2,4-diynyl-1-oxycarbonyl}-L-alanyl-L-alanine Dodecylamide **131**.** Following general procedure D, **129** (0.23 g, 0.88 mmol) and **71** (0.30 g, 0.88 mmol) were dissolved in a mixture of dry  $\text{CH}_2\text{Cl}_2$  (30 mL) and dry DMF (5 mL). DIEA (0.46 g, 3.56 mmol) and PyBOP (0.50 g, 0.96 mmol) were added, and the solution was stirred at room temperature over night. The next day, the solvents were removed *in vacuo*. The crude material was dissolved in a 1:1 mixture of THF (10 mL) and MeOH (10 mL), and purified by precipitation in water (120 mL). The precipitate was filtered off and dried in HV. **131** (0.36 g, 65%) was obtained as a slightly brown solid material.

$^1\text{H}$  NMR (300.23 MHz,  $\text{DMSO-}d_6$ ):  $\delta$  = 0.86 (t,  $J$  = 6.9 Hz, 3H,  $(\text{CH}_2)_{11}\text{CH}_3$ ), 1.1-1.5 (m, 26H,  $(\text{CH}_2)_{10}\text{CH}_3$ , 2  $\text{CHCH}_3$ ), 2.39 (t,  $J$  = 6.3 Hz, 2H,  $\text{NH}(\text{C})\text{OCH}_2$ ), 2.52 (t,  $J$  = 6.6 Hz, 2H,  $\text{CH}_2\text{CO}_2\text{CH}_3$ ), 3.03 (m, 2H,  $\text{NHCH}_2(\text{CH}_2)_{10}\text{CH}_3$ ), 4.00 (d,  $J$  = 5.1 Hz, 2H,  $\text{CH}_2\text{NH}$ ), 4.05 (m, 1H,  $\text{CHCH}_3$ ), 4.21 (m, 1H,  $\text{CHCH}_3$ ), 4.74 (s, 2H,  $\text{NHCO}_2\text{CH}_2$ ), 7.61 (d,  $J$  = 7.2 Hz, 1H,  $\text{NH}$ ), 7.74 (m, 1H,  $\text{NH}$ ), 7.93 (d,  $J$  = 7.8 Hz, 1H,  $\text{NH}$ ), 8.43 (t,  $J$  = 5.4 Hz, 1H,  $\text{NH}$ ). HRMS (MALDI): calcd for  $\text{C}_{30}\text{H}_{49}\text{N}_4\text{O}_7$ :  $([\text{M}+\text{H}]^+)$  577.3595; found: 577.3588.  $R_f$ : 0.3 ( $\text{CH}_2\text{Cl}_2/\text{MeOH}$  10:1).

***N*-{6-[*N'*(9-Fluorenylmethyloxycarbonyl)-L-alanyl]amido]hexa-2,4-diynyl-1-oxycarbonyl}-L-alanyl-L-alanine Dodecylamide **132**.** Following general procedure D, **129** (0.186 g, 0.73 mmol) and **79** (0.37 g, 0.72 mmol) were dissolved in a mixture of dry  $\text{CH}_2\text{Cl}_2$  (30 mL) and dry DMF (5 mL). DIEA (0.37 g, 2.86 mmol) and PyBOP (0.39 g, 0.76 mmol) were added, and the

solution was stirred at room temperature over night. The next day, the solvents were removed *in vacuo*. The crude material was dissolved in a 1:1 mixture of THF (10 mL) and MeOH (10 mL), and purified by precipitation in water (120 mL). The precipitate was filtered off and dried in HV. **132** (0.43 g, 78%) was obtained as a slightly brown solid material.

$^1\text{H}$  NMR (300.23 MHz, DMSO- $\text{D}_6$ ):  $\delta$  = 0.82 (t,  $J$  = 6.9 Hz, 3H,  $(\text{CH}_2)_{11}\text{CH}_3$ ), 1.1-1.5 (m, 29H,  $(\text{CH}_2)_{10}\text{CH}_3$ , 3  $\text{CHCH}_3$ ), 3.15 (m, 2H,  $\text{NHCH}_2(\text{CH}_2)_{10}\text{CH}_3$ ), 4.03 (s, 2H,  $\text{CH}_2\text{NH}$ ), 4.1-4.2 (m, 3H, 2  $\text{CHCH}_3$ , fluorenyl  $\text{CH}$ ), 4.2-4.4 (m, 3H,  $\text{CHCH}_3$ , Fmoc- $\text{CO}_2\text{CH}_2$ ), 4.65 (s, 2H,  $\text{CO}_2\text{CH}_2\text{C}\equiv\text{C}$ ), 7.26 (t,  $J$  = 7.2 Hz, 2H, aromatic  $\text{H}$ ), 7.35 (t,  $J$  = 7.2 Hz, 2H, aromatic  $\text{H}$ ), 7.5-7.8 (m, 3H, 3  $\text{NH}$ ), 7.74 (m, 2H, aromatic  $\text{H}$ ), 7.85-7.95 (m, 3H, 2 aromatic  $\text{H}$ ,  $\text{NH}$ ), 8.42 (m, 1H,  $\text{NH}$ ). HRMS (MALDI): calcd for  $\text{C}_{43}\text{H}_{57}\text{N}_5\text{O}_7\text{Na}$ : ( $[\text{M}+\text{Na}]^+$ ) 778.4156; found: 778.4150.  $R_f$ : 0.4 ( $\text{CH}_2\text{Cl}_2/\text{MeOH}$  10:1).

**Hexa-2,4-diynylene-1,6-bis(oxycarbonyl-L-alanyl-L-alanine Dodecylamide) 133.** Following general procedure D, **129** (0.513 g, 2 mmol) and **66** (0.34 g, 1 mmol) were dissolved in a mixture of dry  $\text{CH}_2\text{Cl}_2$  (50 mL) and dry DMF (5 mL). DIEA (0.65 g, 5 mmol) and PyBOP (1.06 g, 2.04 mmol) were added, and the solution was stirred at room temperature over night. The next day, the solvents were removed *in vacuo*. The crude material was dissolved in a 1:1 mixture of THF (10 mL) and MeOH (10 mL), and purified by precipitation in water (200 mL). The precipitate was filtered off and dried in HV. **133** (0.67 g, 82%) was obtained as a colorless solid material.

$^1\text{H}$  NMR (300.23 MHz, DMSO- $\text{D}_6$ ):  $\delta$  = 0.83 (t,  $J$  = 6.9 Hz, 6H, 2  $(\text{CH}_2)_{11}\text{CH}_3$ ), 1.1-1.5 (m, 52H, 2  $(\text{CH}_2)_{10}\text{CH}_3$ , 4  $\text{CHCH}_3$ ), 3.00 (m, 4H, 2  $\text{NHCH}_2(\text{CH}_2)_{10}\text{CH}_3$ ), 4.02 (m, 2H, 2  $\text{CHCH}_3$ ), 4.18 (m, 2H, 2  $\text{CHCH}_3$ ), 4.74 (s, 4H, 2  $\text{NHCO}_2\text{CH}_2$ ), 7.60 (d,  $J$  = 7.5 Hz, 2H, 2  $\text{NH}$ ), 7.71 (m, 2H, 2  $\text{NH}$ ), 7.90 (d,  $J$  = 7.5 Hz, 2H, 2  $\text{NH}$ ). HRMS (MALDI): calcd for  $\text{C}_{44}\text{H}_{76}\text{N}_6\text{O}_8\text{Na}$ : ( $[\text{M}+\text{Na}]^+$ ) 839.5617; found: 839.5618.  $R_f$ : 0.4 ( $\text{CH}_2\text{Cl}_2/\text{MeOH}$  10:1).

**N-(Penta-2,4-diynyl-1-oxycarbonyl)-L-alanyl-L-alanine Dodecylamide 134.** The TMS protected derivative **130** (0.10 g, 0.22 mmol) was dissolved in a mixture of MeOH (10 mL), EtOH (20 mL) and  $\text{H}_2\text{O}$  (2 mL).  $\text{AgNO}_3$  (0.044 g, 0.26 mmol) was added, and the reaction was monitored by thin layer chromatography. After 90 min, all starting material ( $R_f$ : 0.6 in  $\text{CH}_2\text{Cl}_2/\text{MeOH}$  10:1) was transformed into the silver acetylide ( $R_f$ : 0 in  $\text{CH}_2\text{Cl}_2/\text{MeOH}$  10:1), and KI (0.050 g, 0.30 mmol) was added to the solution. The reaction mixture was stirred over night, and a fine yellow precipitate of AgI formed. The solvents were removed *in vacuo*, the crude material was taken up in  $\text{CHCl}_3$ , and the AgI was filtered off. The material was dried and purified by column chromatography (silica gel,  $\text{CHCl}_3/\text{MeOH}$  24:1). **134** (0.077 g, 91%) was obtained as a slightly yellow, light-sensitive solid material.

$^1\text{H}$  NMR (300.23 MHz, DMSO- $\text{D}_6$ ):  $\delta$  = 0.91 (t,  $J$  = 6.9 Hz, 3H,  $(\text{CH}_2)_{11}\text{CH}_3$ ), 1.2-1.6 (m, 26H,  $(\text{CH}_2)_{10}\text{CH}_3$ ,  $\text{CHCH}_3$ ), 3.26 (m, 2H,  $\text{NHCH}_2(\text{CH}_2)_{10}\text{CH}_3$ ), 4.26 (m, 1H,  $\text{CHCH}_3$ ), 4.45 (m, 1H,  $\text{CHCH}_3$ ), 4.77 (s, 2H,  $\text{NHCO}_2\text{CH}_2$ ), 5.50 (bs, 1H,  $\text{NH}$ ), 6.17 (bs, 1H,  $\text{NH}$ ), 6.68 (bs, 1H,  $\text{NH}$ ). HRMS (MALDI): calcd for  $\text{C}_{24}\text{H}_{39}\text{N}_3\text{O}_4\text{Na}$  ( $[\text{M}+\text{Na}]^+$ ) 456.2838; found: 456.2833.  $R_f$ : 0.6 ( $\text{CH}_2\text{Cl}_2/\text{MeOH}$  10:1).

***N*-Propargyloxycarbonyl-[1- $^{13}\text{C}$ ]-alanine 135.** The  $^{13}\text{C}$ -labeled propargyl carbamate functionalized L-alanine derivative **135** was synthesized according to the protocol used for the unlabeled derivative **47**. Thus,  $^{13}\text{C}$ -labeled L-alanine was treated with propargyl chloroformate in 1N NaOH solution. After workup, the product (0.42 g, 44%) was obtained as a slightly yellow oil.

The analytics are equivalent to the non-labeled compound **47**. HRMS (MALDI): calcd for  $^{13}\text{C}_1\text{C}_6\text{H}_9\text{NO}_4$ : ( $[\text{M}]^+$ ) 172.0560; found 172.0559.

**hPI<sub>10</sub>-NH-Ala<sub>3</sub>-[1- $^{13}\text{C}$ ]-Ala-C(O)O-CH<sub>2</sub>-C $\equiv$ C-C-H 136.** Following general procedure E, **135** (0.034 g, 0.20 mmol) was dissolved in a mixture of dry DMF (2 mL) and dry  $\text{CH}_2\text{Cl}_2$  (10 mL). HOBT (0.036 g, 0.27 mmol) and EDCI (0.047 g, 0.25 mmol) were added to form the active ester intermediate. A second solution containing **45** (0.11 g, 0.107 mmol) and TEA (0.53 g, 5.2 mmol) in dry  $\text{CH}_2\text{Cl}_2$  (50 mL) was prepared, and both solutions were combined. The next day, the solution was washed twice with sat.  $\text{NaHCO}_3$  solution and once with sat. NaCl solution. The combined organic phases were dried over  $\text{MgSO}_4$ , filtered, and concentrated *in vacuo*. The crude product was purified by column chromatography (silica gel,  $\text{CH}_2\text{Cl}_2/\text{MeOH}$  10:1). **136** (0.085 g, 67%) was obtained as a colorless amorphous solid.

The analytics are equivalent to the non-labeled compound **91** except for: HRMS (MALDI): calcd for  $^{13}\text{C}_1\text{C}_{67}\text{H}_{129}\text{N}_5\text{O}_6\text{Na}$ : ( $[\text{M}+\text{Na}]^+$ ) 1135.987; found 1136.002.

**hPI<sub>10</sub>-NH-Ala<sub>3</sub>-[1- $^{13}\text{C}$ ]-Ala-C(O)O-CH<sub>2</sub>-C $\equiv$ C-C $\equiv$ C-CH<sub>2</sub>NHAc 137.** Following general procedure A, **136** (0.072 g, 0.06 mmol), **50** (0.136 g, 0.61 mmol) and the catalysts were dissolved in a mixture of dry  $\text{CH}_2\text{Cl}_2$  (20 mL) and dry THF (20 mL). Some drops of MeOH were added in order to obtain a clear solution. The solution was stirred over night and diluted with  $\text{CHCl}_3$  (100 mL). The solution was washed with sat.  $\text{NaHCO}_3$  solution and sat. NaCl solution. The combined organic phases were dried over  $\text{MgSO}_4$ , filtered, and concentrated *in vacuo*. The crude product was purified by repeated column chromatography (silica gel,  $\text{CH}_2\text{Cl}_2/\text{MeOH}$  20:1). **137** (0.039 g, 50%) was obtained as a brownish solid.

The analytics are equivalent to the non-labeled compound **92** except for: HRMS (MALDI): calcd for  $^{13}\text{C}_1\text{C}_{72}\text{H}_{134}\text{N}_6\text{O}_7\text{Na}$ : ( $[\text{M}+\text{Na}]^+$ ) 1231.025; found 1230.925.

**[<sup>15</sup>N]-(9-Fluorenylmethyloxycarbonyl)-L-alanyl-L-alanine *tert*-Butyl Ester 138.** Following general procedure D, <sup>15</sup>N-(9-fluorenylmethyloxycarbonyl)-L-alanine (0.50 g, 1.6 mmol) and L-alanine *tert*-butyl ester hydrochloride (0.29 g, 1.6 mmol) were dissolved in a mixture of dry CH<sub>2</sub>Cl<sub>2</sub> (150 mL) and dry DMF (50 mL). DIEA (0.63 g, 4.8 mmol) and PyBOP (0.89 g, 1.68 mmol) were added, and the reaction was stirred at room temperature over night. The solution was washed twice with 1M HCl and once with sat. NaCl solution. The combined organic phases were dried over MgSO<sub>4</sub>, filtered, and concentrated *in vacuo*. The crude material was purified by column chromatography (silica gel, CH<sub>2</sub>Cl<sub>2</sub>/MeOH 25:1). **138** (0.58 g, 83%) was obtained as a colorless solid.

The analytics are equivalent to the non-labeled compound **35** except for: HRMS (MALDI): calcd for C<sub>25</sub>H<sub>30</sub><sup>15</sup>N<sub>1</sub>NO<sub>5</sub>Na: ([M+Na]<sup>+</sup>) 462.2017; found 462.2017.

**[<sup>15</sup>N]-(9-Fluorenylmethyloxycarbonyl)-L-alanyl-L-alanine 139.** Following general procedure B, **138** (0.5 g, 0.44 mmol) was dissolved in dry CH<sub>2</sub>Cl<sub>2</sub> (10 mL), a large excess of TFA was added, and the solution was stirred for 5 h. **139** (0.43 g, 99%) was obtained as a slightly brown solid material.

The analytics are equivalent to the non-labeled compound **36** except for: HRMS (MALDI): calcd for C<sub>21</sub>H<sub>22</sub><sup>15</sup>N<sub>1</sub>NO<sub>5</sub>Na: ([M+Na]<sup>+</sup>) 406.1391; found 406.1383.

**hPI<sub>10</sub>-NH-Ala<sub>2</sub>-[<sup>15</sup>N]-Ala-Fmoc 140.** Following general procedure E, **139** (0.43 g, 1.13 mmol) was dissolved in a mixture of dry DMF (10 mL) and dry CH<sub>2</sub>Cl<sub>2</sub> (10 mL). HOBt (0.18 g, 1.39 mmol) and EDCI (0.41 g, 2.14 mmol) were added to form the active ester intermediate. A second solution containing **43** (0.80 g, 0.9 mmol) and TEA (0.6 g, 5.9 mmol) in dry CH<sub>2</sub>Cl<sub>2</sub> (100 mL) was prepared, and both solutions were combined. The next day, the solution was washed twice with sat. NaHCO<sub>3</sub> solution and once with sat. NaCl solution. The combined organic phases were dried over MgSO<sub>4</sub>, filtered, and concentrated *in vacuo*. TLC indicated that the product was pure and only a small amount was purified by column chromatography (silica gel, CH<sub>2</sub>Cl<sub>2</sub>/MeOH 25:1) for analytical purposes.

The analytics are equivalent to the non-labeled compound **44** except for: HRMS (MALDI): calcd for C<sub>81</sub>H<sub>142</sub><sup>15</sup>N<sub>1</sub>N<sub>3</sub>O<sub>5</sub>Na: ([M+Na]<sup>+</sup>) 1275.0848; found 000.0000.

**hPI<sub>10</sub>-NH-Ala<sub>2</sub>-[<sup>15</sup>N]-Ala-H 141.** Following general procedure C, **140** (1.29 g, 1.02 mmol) was dissolved in CHCl<sub>3</sub> (25 mL) and a large excess of piperidine was added. The solution was washed with sat. NaHCO<sub>3</sub> solution and sat. NaCl solution. The combined organic phases were dried over MgSO<sub>4</sub>, filtered, and concentrated *in vacuo*. The crude material was purified by column chromatography (silica gel, CH<sub>2</sub>Cl<sub>2</sub>/MeOH 10:1). **141** (0.57 g, 57%) was obtained as a colorless amorphous solid.

The analytics are equivalent to the non-labeled compound **45** except for: HRMS (MALDI): calcd for C<sub>61</sub>H<sub>122</sub><sup>15</sup>N<sub>1</sub>N<sub>3</sub>O<sub>3</sub>Na: ([M+Na]<sup>+</sup>) 982.939; found 982.907.

**hPI<sub>10</sub>-NH-Ala<sub>2</sub>-[<sup>15</sup>N]-Ala-Ala-C(O)O-CH<sub>2</sub>-C≡C-C≡C-CH<sub>2</sub>NHAc 142.** Following general procedure E, **68** (0.064 g, 0.24 mmol) was dissolved in a mixture of dry DMF (10 mL) and dry CH<sub>2</sub>Cl<sub>2</sub> (18 mL). HOBt (0.041 g, 0.30 mmol) and EDCI (0.055 g, 0.29 mmol) were added to form the active ester intermediate. A second solution containing **141** (0.118 g, 0.115 mmol) and TEA (0.75 g, 7.4 mmol) in dry CH<sub>2</sub>Cl<sub>2</sub> (50 mL) was prepared, and both solutions were combined. The solution was diluted with CHCl<sub>3</sub> (100 mL) and washed twice with sat. NaHCO<sub>3</sub> solution and once with sat. NaCl solution. The combined organic phases were dried over MgSO<sub>4</sub>, filtered, and concentrated *in vacuo*. The crude product was purified by column chromatography (silica gel, CH<sub>2</sub>Cl<sub>2</sub>/MeOH 24:1). **142** (0.080 g, 56%) was obtained as light-sensitive, colorless amorphous solid.

The analytics are equivalent to the non-labeled compound **92** except for HRMS (MALDI): calcd for C<sub>73</sub>H<sub>134</sub><sup>15</sup>N<sub>1</sub>N<sub>5</sub>O<sub>7</sub>Na: ([M+Na]<sup>+</sup>) 1231.018; found 1231.029.

**hPI<sub>10</sub>-NH-Ala-[1-<sup>13</sup>C]-Ala-Fmoc 143.** Following general procedure E, [1-<sup>13</sup>C]-labeled Fmoc-L-alanine (0.16 g, 0.51 mmol) was dissolved in a mixture of dry DMF (2 mL) and dry CH<sub>2</sub>Cl<sub>2</sub> (10 mL). HOBt (0.1 g, 0.74 mmol) and EDCI (0.16 g, 0.83 mmol) were added to form the active ester intermediate. A second solution containing **43** (0.45 g, 0.51 mmol) and TEA (0.26 g, 2.6 mmol) in dry CH<sub>2</sub>Cl<sub>2</sub> (100 mL) was prepared, and both solutions were combined. The solution was washed twice with 1M HCl and once with sat. NaCl solution. The combined organic phases were dried over MgSO<sub>4</sub>, filtered, and concentrated *in vacuo*. The crude material was purified by column chromatography (silica gel, CH<sub>2</sub>Cl<sub>2</sub>/MeOH 49:1). **143** (0.381 g, 66%) was obtained as an amorphous solid.

<sup>1</sup>H NMR (300.23 MHz, CDCl<sub>3</sub>): δ = 0.6-1.8 (m, 128H, aliphatic H, 2 CHCH<sub>3</sub>), 3.1-3.3 (m, 2H, CH<sub>2</sub>NHR), 4.1-4.3 (m, 2H, fluorenyl CH, CHCH<sub>3</sub>), 4.4-4.5 (m, 3H, Fmoc-NHCO<sub>2</sub>CH<sub>2</sub>, CHCH<sub>3</sub>), 5.4 (m, 1H, carbamate NH), 6.25 (m, 1H, amide NH), 6.72 (m, 1H, amide NH), 7.28 (t, J = 7.5 Hz, 2H, aromatic H), 7.40 (t, J = 7.5 Hz, 2H, aromatic H), 7.58 (d, J = 7.5 Hz, 2H, aromatic H), 7.76 (d, J = 7.5 Hz, 2H, aromatic H). HRMS (MALDI): calcd for <sup>13</sup>C<sub>1</sub>C<sub>77</sub>H<sub>137</sub>N<sub>3</sub>O<sub>4</sub>Na: ([M+Na]<sup>+</sup>) 1204.0540; found 1202.08. R<sub>f</sub>: 0.8 (CH<sub>2</sub>Cl<sub>2</sub>/MeOH 10:1).

**hPI<sub>10</sub>-NH-Ala-[1-<sup>13</sup>C]-Ala-H 144.** Following general procedure C, **143** (0.37 g, 0.31 mmol) was dissolved in CHCl<sub>3</sub> (15 mL) and a large excess of piperidine was added. The solvents were removed *in vacuo*, and the crude product was purified by column chromatography (silica gel, CH<sub>2</sub>Cl<sub>2</sub>/MeOH 15:1). **144** (0.25 g, 83%) was obtained as a colorless amorphous solid.

<sup>1</sup>H NMR (300.23 MHz, CDCl<sub>3</sub>): δ = 0.6-1.8 (m, 138H, aliphatic H, 2 CHCH<sub>3</sub>), 3.1-3.4 (m, 3H, CH<sub>2</sub>NHR, CHCH<sub>3</sub>), 4.33 (m, 1H, CHCH<sub>3</sub>), 5.8 (br s, 1H, amide NH), 6.5 (br s, 1H, amide NH). HRMS (MALDI): calcd for <sup>13</sup>C<sub>1</sub>C<sub>62</sub>H<sub>127</sub>N<sub>3</sub>O<sub>2</sub>Na: ([M+Na]<sup>+</sup>) 981.97; found 981.90. R<sub>f</sub>: 0.2 (CH<sub>2</sub>Cl<sub>2</sub>/MeOH 10:1).



**hPI<sub>10</sub>-NH-Ala-[1-<sup>13</sup>C]-Ala-[<sup>15</sup>N]-Ala-Fmoc 145.** Following general procedure E, [<sup>15</sup>N]-labeled *N*-(9-fluorenylmethyloxycarbonyl)-*L*-alanine (0.090 g, 0.29 mmol) was dissolved in a mixture of dry DMF (1 mL) and dry CH<sub>2</sub>Cl<sub>2</sub> (10 mL). HOBt (0.051 g, 0.38 mmol) and EDCI (0.094 g, 0.49 mmol) were added to form the active ester intermediate. A second solution containing **144** (0.247 g, 0.26 mmol) and TEA (0.15 g, 1.5 mmol) in dry CH<sub>2</sub>Cl<sub>2</sub> (50 mL) was prepared, and both solutions were combined. The solution was washed twice with sat. NaHCO<sub>3</sub> solution and once with sat. NaCl solution. The combined organic phases were dried over MgSO<sub>4</sub>, filtered, and concentrated *in vacuo*. The crude material was purified twice by column chromatography (silica gel, CH<sub>2</sub>Cl<sub>2</sub>/MeOH 24:1). **145** (0.190 g, 59%) was obtained as a colorless amorphous solid.

The analytics are equivalent to the non-labeled compound **44** except for: HRMS (MALDI): calcd for <sup>13</sup>C<sub>1</sub>C<sub>80</sub>H<sub>142</sub> <sup>15</sup>N<sub>1</sub>N<sub>3</sub>O<sub>5</sub>Na: ([M+Na]<sup>+</sup>) 1276.09; found 1275.95.

**hPI<sub>10</sub>-NH-Ala-[1-<sup>13</sup>C]-Ala-[<sup>15</sup>N]-Ala-H 146.** Following general procedure C, **145** (0.17 g, 0.136 mmol) was dissolved in CHCl<sub>3</sub> (15 mL) and a large excess of piperidine was added. The reaction was stirred over night, the solvents were removed *in vacuo*, and the crude product was purified by column chromatography (silica gel, CH<sub>2</sub>Cl<sub>2</sub>/MeOH 15:1). **146** (0.14 g, 94%) was obtained as a colorless amorphous solid.

The analytics are equivalent to the non-labeled compound **44** except for: HRMS (MALDI): calcd for <sup>13</sup>C<sub>1</sub>C<sub>65</sub>H<sub>132</sub> <sup>15</sup>N<sub>1</sub>N<sub>3</sub>O<sub>3</sub>Na: ([M+Na]<sup>+</sup>) 1054.02; found 1053.92.

**hPI<sub>10</sub>-NH-Ala-[1-<sup>13</sup>C]-Ala-[<sup>15</sup>N]-Ala-Ala-C(O)O-CH<sub>2</sub>-C≡C-C≡C-CH<sub>2</sub>NHAc 147.** Following general procedure E, **68** (0.053 g, 0.20 mmol) was dissolved in a mixture of dry DMF (3 mL) and dry CH<sub>2</sub>Cl<sub>2</sub> (7 mL). HOBt (0.054 g, 0.40 mmol) and EDCI (0.068 g, 0.35 mmol) were added to form the active ester intermediate. A second solution containing **146** (0.104 g, 0.10 mmol) and TEA (0.7 g, 6.9 mmol) in dry CH<sub>2</sub>Cl<sub>2</sub> (40 mL) was prepared, and both solutions were combined. The solution was washed twice with sat. NaHCO<sub>3</sub> solution and once with sat. NaCl solution. The combined organic phases were dried over MgSO<sub>4</sub>, filtered, and concentrated *in vacuo*. The crude material was purified by column chromatography (silica gel, CHCl<sub>3</sub>/MeOH 24:1). **147** (0.077 g, 60%) was obtained as a light-sensitive, colorless amorphous solid.

The analytics are equivalent to the non-labeled compound **92** except for: HRMS (MALDI): calcd for <sup>13</sup>C<sub>1</sub>C<sub>67</sub>H<sub>124</sub> <sup>15</sup>N<sub>1</sub>N<sub>5</sub>O<sub>7</sub>Na: ([M+Na]<sup>+</sup>) 1161.94; found 1161.93.

**hPI<sub>10</sub>-NH-Ala-[1-<sup>13</sup>C]-Ala-[<sup>15</sup>N]-Ala-Ala-C(O)O-CH<sub>2</sub>-C≡C-C≡C-TMS 148.** Following general procedure E, **87** (0.060 g, 0.22 mmol) was dissolved in a mixture of dry DMF (3 mL) and dry CH<sub>2</sub>Cl<sub>2</sub>

(12 mL). HOBt (0.033 g, 0.24 mmol) and EDCI (0.060 g, 0.31 mmol) were added to form the active ester intermediate. A second solution containing **146** (0.138 g, 0.134 mmol) and TEA (0.1 g, 1.0 mmol) in dry CH<sub>2</sub>Cl<sub>2</sub> (100 mL) was prepared, and both solutions were combined. The solution was washed twice with sat. NaHCO<sub>3</sub> solution and once with sat. NaCl solution. The combined organic phases were dried over MgSO<sub>4</sub>, filtered, and concentrated *in vacuo*. The crude material was purified by column chromatography (silica gel, CHCl<sub>3</sub>/MeOH 24:1). **148** (0.162 g, 95%) was obtained as an amorphous solid.

The analytics are equivalent to the non-labeled compound **102** except for HRMS (MALDI): calcd for <sup>13</sup>C<sub>1</sub>C<sub>62</sub>H<sub>117</sub><sup>15</sup>N<sub>1</sub>N<sub>4</sub>O<sub>6</sub>SiNa: ([M+Na]<sup>+</sup>) 1092.87; found 1092.75.

**hPI<sub>10</sub>-NH-Ala-[1-<sup>13</sup>C]-Ala-[<sup>15</sup>N]-Ala-Ala-C(O)O-CH<sub>2</sub>-C≡C-C≡C-H 149.** The labeled starting material **148** (0.080 g, 0.063 mmol) was dissolved in a mixture of CH<sub>2</sub>Cl<sub>2</sub> (70 mL) and THF (20 mL). The solution was cooled to 0 °C, and tetrabutylammonium fluoride trihydrate (0.023 g, 0.07 mmol) was added. The reaction mixture was stirred for 30 min, and the reaction was then quenched by an aqueous workup. After drying of the organic phase over MgSO<sub>4</sub> and removal of the solvent, an amorphous solid was obtained. The crude product was purified by column chromatography (silica gel, CHCl<sub>3</sub>/MeOH 24:1). **149** (0.071 g, 94%) was obtained as a colorless and amorphous solid.

The analytics are equivalent to the non-labeled compound **103** except for: HRMS (MALDI): calcd for <sup>13</sup>C<sub>1</sub>C<sub>64</sub>H<sub>119</sub><sup>15</sup>N<sub>1</sub>N<sub>4</sub>O<sub>6</sub>Na: ([M+Na]<sup>+</sup>) 1090.90; found 1090.83.

**<sup>13</sup>C-labeled derivatives 150, 151, 152, 153, and 154.** These compounds were obtained from the Meier group and had been prepared on the solid phase using a peptide synthesizer and standard Fmoc-protected amino acid building blocks. After purification by HPLC and lyophilization, the compounds were used in the following synthetic steps without further purification or analysis.

**hPI<sub>10</sub>-NH-[1-<sup>13</sup>C]-Ala-Ala<sub>2</sub>-Fmoc 155.** Following general procedure D, **150** (0.096 g, 0.211 mmol) was dissolved in a mixture of dry DMF (4 mL) and dry CH<sub>2</sub>Cl<sub>2</sub> (18 mL). PyBOP (0.21 g, 0.40 mmol), **41** (0.22 g, 0.27 mmol), and DIEA (0.12 g, 0.93 mmol) were added, and the reaction mixture stirred over night. The next day, the solvents were removed *in vacuo*, and the crude product was purified by column chromatography (silica gel, CH<sub>2</sub>Cl<sub>2</sub>/MeOH 24:1). **155** (0.208 g, 79%) was obtained as a colorless amorphous solid.

The analytics are equivalent to the non-labeled compound **44** except for: HRMS (MALDI): calcd for <sup>13</sup>C<sub>1</sub>C<sub>75</sub>H<sub>132</sub>N<sub>4</sub>O<sub>5</sub>Na: ([M+Na]<sup>+</sup>) 1205.01; found 1204.28.

**hPI<sub>10</sub>-NH-Ala-[1-<sup>13</sup>C]-Ala-Ala-Fmoc 156.** Following general procedure D, *N*-(9-fluorenylmethoxycarbonyl)-L-alanyl-[1-<sup>13</sup>C]-alanyl-L-alanine **151** (0.071 g, 0.156 mmol) was dissolved in a mixture of dry DMF (4 mL) and dry CH<sub>2</sub>Cl<sub>2</sub> (18 mL). PyBOP (0.133 g, 0.256 mmol), **41** (0.15 g, 0.184 mmol), and DIEA (0.12 g, 0.93 mmol) were added, and the reaction mixture stirred over night. The next day, the solvents were removed *in vacuo*, and the crude product was purified by column chromatography (silica gel, CH<sub>2</sub>Cl<sub>2</sub>/MeOH 24:1). **156** (0.182 g, 93%) was obtained as a colorless amorphous solid.

The analytics are equivalent to the non-labeled compound **44** except for: HRMS (MALDI): calcd for <sup>13</sup>C<sub>1</sub>C<sub>75</sub>H<sub>132</sub>N<sub>4</sub>O<sub>5</sub>Na: ([M+Na]<sup>+</sup>) 1205.01; found 1204.29.

**hPI<sub>10</sub>-NH-Ala<sub>2</sub>-[1-<sup>13</sup>C]-Ala-Fmoc 157.** Following general procedure D, *N*-(9-fluorenylmethoxycarbonyl)-[1-<sup>13</sup>C]-alanyl-L-alanyl-L-alanine **152** (0.063 g, 0.139 mmol) was dissolved in a mixture of dry DMF (4 mL) and dry CH<sub>2</sub>Cl<sub>2</sub> (18 mL). PyBOP (0.104 g, 0.20 mmol), **41** (0.15 g, 0.184 mmol) and DIEA (0.08 g, 0.62 mmol) were added, and the reaction mixture stirred over night. The next day, the solvents were removed *in vacuo*, and the crude product was purified by column chromatography (silica gel, CH<sub>2</sub>Cl<sub>2</sub>/MeOH 24:1). **157** (0.124 g, 71%) was obtained as a colorless amorphous solid.

The analytics are equivalent to the non-labeled compound **44** except for: HRMS (MALDI): calcd for <sup>13</sup>C<sub>1</sub>C<sub>80</sub>H<sub>142</sub>N<sub>4</sub>O<sub>5</sub>Na: ([M+Na]<sup>+</sup>) 1275.01; found 1274.37.

**hPI<sub>10</sub>-NH-[1-<sup>13</sup>C]-Ala-[1-<sup>13</sup>C]-Ala-Ala-Fmoc 158.** Following general procedure D, a mixture of *N*-(9-fluorenylmethoxycarbonyl)-L-alanyl-L-alanyl-L-alanine **39** (60.9 mg, 0.134 mmol, 0.66 eq) and *N*-(9-fluorenylmethoxycarbonyl)-L-alanyl-[1-<sup>13</sup>C]-alanyl-[1-<sup>13</sup>C]-alanine **153** (31.0 mg, 0.068 mmol, 0.34 eq) was dissolved in a mixture of dry DMF (4 mL) and dry CH<sub>2</sub>Cl<sub>2</sub> (18 mL). PyBOP (0.130 g, 2.50 mmol), **41** (0.20 g, 0.245 mmol, 1.22 eq) and DIEA (0.15 g, 1.16 mmol) were added, and the reaction mixture stirred over night. The solution was washed twice with sat. NaHCO<sub>3</sub> solution and once with sat. NaCl solution. The combined organic phases were dried over MgSO<sub>4</sub>, filtered, and concentrated *in vacuo*. The crude product was purified by column chromatography (silica gel, CH<sub>2</sub>Cl<sub>2</sub>/MeOH 24:1). **158** (0.21 g, 85%) was obtained as a colorless amorphous solid.

The analytics are equivalent to the non-labeled compound **44** except for: HRMS (MALDI): calcd for <sup>13</sup>C<sub>2</sub>C<sub>79</sub>H<sub>142</sub>N<sub>4</sub>O<sub>5</sub>Na: ([M+Na]<sup>+</sup>) 1276.09; found 1273.48.

**hPI<sub>10</sub>-NH-Ala-[1-<sup>13</sup>C]-Ala-[1-<sup>13</sup>C]-Ala-Fmoc 159.** Following general procedure D, a mixture of *N*-(9-fluorenylmethoxycarbonyl)-L-alanyl-L-alanyl-L-alanine **39** (50.0 mg, 0.11 mmol, 0.67 eq) and

*N*-(9-fluorenylmethoxycarbonyl)-[1-<sup>13</sup>C]-alanyl-[1-<sup>13</sup>C]-alanyl-L-alanine **154** (25.0 mg, 0.055 mmol, 0.33 eq) was dissolved in a mixture of dry DMF (8 mL) and dry CH<sub>2</sub>Cl<sub>2</sub> (25 mL). PyBOP (0.13 g, 0.25 mmol), **41** (0.20 g, 0.245 mmol, 1.22 eq), and DIEA (0.85 g, 66 mmol) were added, and the reaction mixture stirred over night. The next day, the solvents were removed *in vacuo*, and the crude product was purified by column chromatography (silica gel, CHCl<sub>3</sub>/MeOH 49:1). **159** (0.250 g, 100%) was obtained as a colorless amorphous solid.

The analytics are equivalent to the non-labeled compound **44** except for: HRMS (MALDI): calcd for <sup>13</sup>C<sub>2</sub>C<sub>79</sub>H<sub>142</sub>N<sub>4</sub>O<sub>5</sub>Na: ([M+Na]<sup>+</sup>) 1276.09; found 1273.34.

**hPI<sub>10</sub>-NH-[1-<sup>13</sup>C]-Ala-Ala<sub>2</sub>-H 160.** Following general procedure C, **158** (0.20 g, 0.16 mmol) was dissolved in CHCl<sub>3</sub> (25 mL) and a large excess of piperidine was added. The solvent was removed *in vacuo*, and the crude product was purified by column chromatography (silica gel, CH<sub>2</sub>Cl<sub>2</sub>/MeOH 24:1). The deprotected product **160** (0.116 g, 70%) was obtained as a colorless amorphous solid.

The analytics are equivalent to the non-labeled compound **45** except for: HRMS (MALDI): calcd for <sup>13</sup>C<sub>1</sub>C<sub>65</sub>H<sub>132</sub>N<sub>4</sub>O<sub>3</sub>Na: ([M+Na]<sup>+</sup>) 1053.02; found 1052.39.

**hPI<sub>10</sub>-NH-Ala-[1-<sup>13</sup>C]-Ala-Ala-H 161.** Following general procedure C, **156** (0.17 g, 0.136 mmol) was dissolved in CHCl<sub>3</sub> (25 mL) and a large excess of piperidine was added. The solvent was removed *in vacuo*, and the crude product was purified by column chromatography (silica gel, CH<sub>2</sub>Cl<sub>2</sub>/MeOH 24:1). **161** (0.114 g, 81%) was obtained as a colorless amorphous solid.

The analytics are equivalent to the non-labeled compound **45** except for: HRMS (MALDI): calcd for <sup>13</sup>C<sub>1</sub>C<sub>65</sub>H<sub>132</sub>N<sub>4</sub>O<sub>3</sub>Na: ([M+Na]<sup>+</sup>) 1053.0230; found 1052.33.

**hPI<sub>10</sub>-NH-Ala<sub>2</sub>-[1-<sup>13</sup>C]-Ala-H 162.** Following general procedure C, **157** (0.115 g, 0.092 mmol) was dissolved in CHCl<sub>3</sub> (25 mL) and a large excess of piperidine was added. The solvent was removed *in vacuo*, and the crude product was purified by column chromatography (silica gel, CH<sub>2</sub>Cl<sub>2</sub>/MeOH 24:1). **162** (0.074 g, 78%) was obtained as a colorless amorphous solid.

The analytics are equivalent to the non-labeled compound **45** except for: HRMS (MALDI): calcd for <sup>13</sup>C<sub>1</sub>C<sub>65</sub>H<sub>132</sub>N<sub>4</sub>O<sub>3</sub>Na: ([M+Na]<sup>+</sup>) 1053.0230; found 1052.34.

**hPI<sub>10</sub>-NH-[1-<sup>13</sup>C]-Ala-[1-<sup>13</sup>C]-Ala-Ala-H 163.** Following general procedure C, **158** (0.188 g, 0.15 mmol) was dissolved in CHCl<sub>3</sub> (25 mL) and a large excess of piperidine was added. The solvent was removed *in vacuo*, and the crude product was purified by column chromatography (silica gel, CH<sub>2</sub>Cl<sub>2</sub>/MeOH 24:1). **163** (0.14 g, 90%) was obtained as a colorless amorphous solid.

The analytics are equivalent to the non-labeled compound **45** except for: HRMS (MALDI): calcd for  $^{13}\text{C}_2\text{C}_{59}\text{H}_{122}\text{N}_4\text{O}_3\text{Na}$ :  $([\text{M}+\text{Na}]^+)$  983.95; found 981.33.

**hPI<sub>10</sub>-NH-Ala-[1- $^{13}\text{C}$ ]-Ala-[1- $^{13}\text{C}$ ]-Ala-H 164.** Following general procedure C, **159** (0.24 g, 0.19 mmol) was dissolved in  $\text{CHCl}_3$  (25 mL) and a large excess of piperidine was added. The solvent was removed *in vacuo*, and the crude product was purified by column chromatography (silica gel,  $\text{CH}_2\text{Cl}_2/\text{MeOH}$  24:1). **164** (0.198 g, 79%) was obtained as a colorless amorphous solid.

The analytics are equivalent to the non-labeled compound **45** except for: HRMS (MALDI): calcd for  $^{13}\text{C}_2\text{C}_{59}\text{H}_{122}\text{N}_4\text{O}_3\text{Na}$ :  $([\text{M}+\text{Na}]^+)$  983.95; found 981.53.

**hPI<sub>10</sub>-NH-[1- $^{13}\text{C}$ ]-Ala-Ala<sub>3</sub>-C(O)O-CH<sub>2</sub>-C $\equiv$ C-C $\equiv$ C-CH<sub>2</sub>NH-C(O)(CH<sub>2</sub>)<sub>2</sub>C(O)OMe 165.** Following general procedure E, **71** (0.078 g, 0.23 mmol) was dissolved in a mixture of dry DMF (4 mL) and dry  $\text{CH}_2\text{Cl}_2$  (8 mL). HOBt (0.05 g, 0.37 mmol) and EDCI (0.060 g, 0.31 mmol) were added to form the active ester intermediate. A second solution containing **160** (0.116 g, 0.112 mmol) and TEA (0.090 g, 0.90 mmol) in dry  $\text{CH}_2\text{Cl}_2$  (50 mL) was prepared, and both solutions were combined. The next day, the solvents were removed *in vacuo*, and the crude material was purified twice by column chromatography (silica gel,  $\text{CHCl}_3/\text{MeOH}$  24:1) and **165** (0.119 g, 78%) was obtained as a light-sensitive, colorless amorphous solid.

The analytics are equivalent to the non-labeled compound **93** except for: HRMS (MALDI): calcd for  $^{13}\text{C}_1\text{C}_{80}\text{H}_{148}\text{N}_6\text{O}_9\text{Na}$ :  $([\text{M}+\text{Na}]^+)$  1373.12; found 1372.37.

**hPI<sub>10</sub>-NH-Ala-[1- $^{13}\text{C}$ ]-Ala-Ala<sub>2</sub>-C(O)O-CH<sub>2</sub>-C $\equiv$ C-C $\equiv$ C-CH<sub>2</sub>NH-C(O)(CH<sub>2</sub>)<sub>2</sub>C(O)OMe 166.** Following general procedure E, **71** (0.072 g, 0.21 mmol) was dissolved in a mixture of dry DMF (4 mL) and dry  $\text{CH}_2\text{Cl}_2$  (8 mL). HOBt (0.044 g, 0.33 mmol) and EDCI (0.065 g, 0.34 mmol) were added to form the active ester intermediate. A second solution containing **161** (0.108 g, 0.105 mmol) and TEA (0.090 g, 0.90 mmol) in dry  $\text{CH}_2\text{Cl}_2$  (50 mL) was prepared, and both solutions were combined. The next day, the solvents were removed *in vacuo*, and the crude material was purified twice by column chromatography (silica gel,  $\text{CHCl}_3/\text{MeOH}$  24:1) and **166** (0.098 g, 70%) was obtained as a light-sensitive, colorless amorphous solid.

The analytics are equivalent to the non-labeled compound **93** except for: HRMS (MALDI): calcd for  $^{13}\text{C}_1\text{C}_{75}\text{H}_{138}\text{N}_6\text{O}_9\text{Na}$ :  $([\text{M}+\text{Na}]^+)$  1303.05; found 1302.27.

**hPI<sub>10</sub>-NH-Ala<sub>2</sub>-[1- $^{13}\text{C}$ ]-Ala-Ala-C(O)O-CH<sub>2</sub>-C $\equiv$ C-C $\equiv$ C-CH<sub>2</sub>NH-C(O)(CH<sub>2</sub>)<sub>2</sub>C(O)OMe 167.** Following general procedure E, **71** (0.042 g, 0.12 mmol) was dissolved in a mixture of dry DMF (4 mL)

and dry CH<sub>2</sub>Cl<sub>2</sub> (8 mL). HOBt (0.036 g, 0.27 mmol) and EDCI (0.042 g, 0.22 mmol) were added to form the active ester intermediate. A second solution containing **162** (0.064 g, 0.062 mmol) and TEA (0.060 g, 0.60 mmol) in dry CH<sub>2</sub>Cl<sub>2</sub> (50 mL) was prepared, and both solutions were combined. The next day, the solvents were removed *in vacuo*, and the crude material was purified twice by column chromatography (silica gel, CHCl<sub>3</sub>/MeOH 24:1) and **167** (0.065 g, 76%) was obtained as a light-sensitive, colorless amorphous solid.

The analytics are equivalent to the non-labeled compound **93** except for: HRMS (MALDI): calcd for <sup>13</sup>C<sub>1</sub>C<sub>80</sub>H<sub>148</sub>N<sub>6</sub>O<sub>9</sub>Na: ([M+Na]<sup>+</sup>) 1373.12; found 1372.37.

**hPI<sub>10</sub>-NH-[1-<sup>13</sup>C]-Ala-[1-<sup>13</sup>C]-Ala-Ala<sub>2</sub>-C(O)O-CH<sub>2</sub>-C≡C-C≡C-CH<sub>2</sub>NH-C(O)(CH<sub>2</sub>)<sub>2</sub>C(O)OMe 168.** Following general procedure E, **71** (0.105 g, 0.31 mmol) was dissolved in a mixture of dry DMF (5 mL) and dry CH<sub>2</sub>Cl<sub>2</sub> (10 mL). HOBt (0.048 g, 0.36 mmol) and EDCI (0.150 g, 0.78 mmol) were added to form the active ester intermediate. A second solution containing **163** (0.12 g, 0.116 mmol) and TEA (0.13 g, 1.3 mmol) in dry CH<sub>2</sub>Cl<sub>2</sub> (50 mL) was prepared, and both solutions were combined. The next day, the solvents were removed *in vacuo*, and the crude material was purified twice by column chromatography (silica gel, CHCl<sub>3</sub>/MeOH 24:1) and **168** (0.116 g, 74%) was obtained as a light-sensitive, colorless amorphous solid.

The analytics are equivalent to the non-labeled compound **93** except for: HRMS (MALDI): calcd for <sup>13</sup>C<sub>2</sub>C<sub>79</sub>H<sub>148</sub>N<sub>6</sub>O<sub>9</sub>Na: ([M+Na]<sup>+</sup>) 1374.13; found 1371.41.

**hPI<sub>10</sub>-NH-Ala-[1-<sup>13</sup>C]-Ala-[1-<sup>13</sup>C]-Ala-Ala-C(O)O-CH<sub>2</sub>-C≡C-C≡C-CH<sub>2</sub>NH-C(O)(CH<sub>2</sub>)<sub>2</sub>C(O)OMe 169.** Following general procedure E, **71** (0.059 g, 0.17 mmol) was dissolved in a mixture of dry DMF (4 mL) and dry CH<sub>2</sub>Cl<sub>2</sub> (8 mL). HOBt (0.03 g, 0.22 mmol) and EDCI (0.042 g, 0.22 mmol) were added to form the active ester intermediate. A second solution containing **164** (0.090 g, 0.087 mmol) and TEA (0.056 g, 0.56 mmol) in dry CH<sub>2</sub>Cl<sub>2</sub> (40 mL) was prepared, and both solutions were combined. The next day, the solvents were removed *in vacuo*, and the crude material was purified twice by column chromatography (silica gel, CHCl<sub>3</sub>/MeOH 24:1) and **169** (0.086 g, 73%) was obtained as a light-sensitive, colorless amorphous solid.

The analytics are equivalent to the non-labeled compound **93** except for: HRMS (MALDI): calcd for <sup>13</sup>C<sub>2</sub>C<sub>79</sub>H<sub>148</sub>N<sub>6</sub>O<sub>9</sub>Na: ([M+Na]<sup>+</sup>) 1374.13; found 1371.46.

**1,4-Bis(trimethylsilyl)butadiyne 170.** Hexachlorobutadiene (52.15 g, 200 mmol) was added dropwise to a solution of *n*-butyl lithium (800 mmol, 2.5M in hexanes) in dry THF (500 mL) at -78 °C. The reaction mixture was allowed to reach room temperature and stirred for another 2 h.

It was cooled to 0 °C, and trimethylsilyl chloride (43.45 g, 400 mmol) was added slowly. The reaction was complete after 20 min at room temperature. Most of the solvent was removed *in vacuo*. The black-brown residue was taken up in a large amount of CH<sub>2</sub>Cl<sub>2</sub>. The solution was washed twice with water and once with sat. NaCl solution. The organic phase was dried over Na<sub>2</sub>SO<sub>4</sub> filtered, and concentrated *in vacuo*. The crude product was purified by recrystallization from MeOH. 1,4-Bis(trimethylsilyl)butadiyne **170** (34.1 g, 89%) was obtained as brownish crystals.

<sup>1</sup>H NMR (300.23 MHz, CDCl<sub>3</sub>): δ = 0.17 (s, 18H, Si(CH<sub>3</sub>)<sub>3</sub>). <sup>13</sup>C NMR (75.49 MHz, CDCl<sub>3</sub>): δ = 0.3 (Si(CH<sub>3</sub>)<sub>3</sub>), 86.0 (C≡CSi), 88.3 (C≡CSi). Anal. calcd for C<sub>10</sub>H<sub>18</sub>Si<sub>2</sub>: C, 61.78%; H, 9.33%; Si, 28.89%; found: C, 61.78%; H, 9.54%. HRMS (EI): calcd for C<sub>10</sub>H<sub>18</sub>Si<sub>2</sub>: ([M]<sup>+</sup>) 194.0942; found: 194.0942. R<sub>f</sub>: 0.8 (CH<sub>2</sub>Cl<sub>2</sub>). m. p.: 111-111.5 °C.

**1-Iodo-4-(trimethylsilyl)butadiyne 171.** 1,4-Bis(trimethylsilyl)butadiyne **170** (4.0 g, 20.57 mmol) was dissolved in dry Et<sub>2</sub>O (200 mL). MeLi·LiI complex (22.67 mmol, 1 M solution in hexanes) was added via a syringe. The reaction mixture was stirred over night, cooled to -78 °C, and I<sub>2</sub> (5.22 g, 20.57 mmol) was added in one portion. The cooling bath was removed, the flask covered with aluminum foil, and the reaction mixture was stirred for 23 h at room temperature. The solution was washed with sat. Na<sub>2</sub>S<sub>2</sub>O<sub>3</sub> solution and with sat. NaCl solution. The organic phase was dried over MgSO<sub>4</sub>, filtered, and concentrated *in vacuo*. The dark brown crude material was purified by sublimation (1·10<sup>-2</sup> mbar, 30 °C). **171** (3.43 g, 67%) was obtained as a colorless crystalline material.

<sup>1</sup>H NMR (300.23 MHz, CDCl<sub>3</sub>): δ = 0.19 (s, 9H, Si(CH<sub>3</sub>)<sub>3</sub>). <sup>13</sup>C NMR (75.49 MHz, CDCl<sub>3</sub>): δ = -1.1 (C≡CI), -0.4 (Si(CH<sub>3</sub>)<sub>3</sub>), 78.9, 83.2, 88.8 (diacetylene C). Anal. calcd for C<sub>7</sub>H<sub>9</sub>ISi: C, 33.88%; H, 3.66%; I, 51.14%; Si, 11.32%; found: C, 33.91%; H, 3.71%; I, 51.05%. HRMS (EI): calcd for C<sub>6</sub>H<sub>6</sub>ISi: ([M-CH<sub>3</sub>]<sup>+</sup>) 232.9279; found: 232.9279. R<sub>f</sub>: 0.7 (hexanes). m. p.: 37-38 °C.

**1-Bromo-4-(trimethylsilyl)butadiyne 172.** 1,4-Bis(trimethylsilyl)butadiyne **170** (2.0 g, 10.29 mmol) was dissolved in dry Et<sub>2</sub>O (80 mL). MeLi·LiBr (12.36 mmol, 1 M solution in hexanes) was added via a syringe. The reaction mixture was stirred over night, cooled to -78 °C, and Br<sub>2</sub> (1.80 g, 11.20 mmol) was added in one portion. The cooling bath was removed, the flask covered with aluminum foil, and the reaction mixture was stirred over 23 h at room temperature. The solution was washed with sat. Na<sub>2</sub>S<sub>2</sub>O<sub>3</sub> solution and with sat. NaCl solution. The organic phase was dried over MgSO<sub>4</sub>, filtered, and concentrated *in vacuo*. The dark brown crude material was purified by column chromatography (silica gel, hexanes). **172** (1.73 g, 83%) was obtained as brownish oily material that was not perfectly pure.

<sup>1</sup>H NMR (300.23 MHz, CDCl<sub>3</sub>): δ = 0.19 (s, 9H, Si(CH<sub>3</sub>)<sub>3</sub>). <sup>13</sup>C NMR (75.49 MHz, CDCl<sub>3</sub>): δ = -0.3 (Si(CH<sub>3</sub>)<sub>3</sub>), 40.46 (C≡CBr), 66.1, 83.6, 88.3 (diacetylene C). R<sub>f</sub>: 0.65 (hexanes).

**7-(Trimethylsilyl)hepta-2,4,6-triynyl oxycarbonyl-L-alanine *tert*-Butyl Ester 173.** Following general procedure A, **46** (0.51 g, 2.2 mmol), **172** (0.53 g, 2.6 mmol) and the catalysts were dissolved in dry THF (30 mL). The solution was stirred for 2.5 h and then washed with 1M HCl, sat. NH<sub>4</sub>Cl solution and sat. NaCl solution. The combined organic phases were dried over MgSO<sub>4</sub>, filtered, and concentrated *in vacuo*. Column chromatography (silica gel, CH<sub>2</sub>Cl<sub>2</sub>/MeOH 24:1) afforded **70** (0.39 g, 51%) as an orange oil.

<sup>1</sup>H NMR (300.23 MHz, CDCl<sub>3</sub>): δ = 0.22 (s, 9H, Si(CH<sub>3</sub>)<sub>3</sub>), 1.37 (d, *J* = 6.9 Hz, 3H, CHCH<sub>3</sub>), 1.46 (s, 9H, C(CH<sub>3</sub>)<sub>3</sub>), 4.23 (m, 1H, CHCH<sub>3</sub>), 4.74 (m, 2H, NHCO<sub>2</sub>CH<sub>2</sub>), 5.32 (d, *J* = 7.2 Hz, 1H, NH). HRMS (EI): calcd for C<sub>16</sub>H<sub>25</sub>N<sub>2</sub>O<sub>4</sub>Si: ([M]<sup>+</sup>) 323.1547; found: 323.1546. R<sub>f</sub>: 0.3 (CH<sub>2</sub>Cl<sub>2</sub>).

**Hepta-2,4,6-triynyl-1-oxycarbonyl-L-alanine 175.** Following general procedure B, **173** (0.10 g, 0.29 mmol) was dissolved in dry CH<sub>2</sub>Cl<sub>2</sub> (10 mL), a large excess of TFA was added, and the solution was stirred over night. **175** (0.078 g, 93%) was obtained as a brownish oil.

<sup>1</sup>H NMR (300.23 MHz, CDCl<sub>3</sub>): δ = 0.21 (s, 9H, Si(CH<sub>3</sub>)<sub>3</sub>), 1.49 (d, *J* = 7.2 Hz, 3H, CHCH<sub>3</sub>), 4.43 (m, 1H, CHCH<sub>3</sub>), 4.77 (s, 2H, NHCO<sub>2</sub>CH<sub>2</sub>), 5.31 (m, 1H, NH). HRMS (EI): calcd for C<sub>12</sub>H<sub>17</sub>NO<sub>4</sub>Si: ([M]<sup>+</sup>) 267.0921; found: 267.0923. R<sub>f</sub>: 0.15 (CH<sub>2</sub>Cl<sub>2</sub>/MeOH 10:1).

**hPI<sub>10</sub>-NH-Ala<sub>2</sub>-Fmoc 176.** Following general procedure D, Fmoc-L-alanine (0.76 g, 2.45 mmol) and **43** (2.0 g, 2.45 mmol) were dissolved in a mixture of dry DMF (3 mL) and dry CH<sub>2</sub>Cl<sub>2</sub> (20 mL). DIEA (1.27 g, 9.8 mmol) and PyBOP (1.38 g, 2.57 mmol) were added, and the reaction mixture was stirred for 3 h at room temperature. The solution was washed twice with sat. NaHCO<sub>3</sub> solution and sat. NaCl solution. The organic phase was dried over MgSO<sub>4</sub>, filtered, and concentrated *in vacuo*. The crude product was purified by repeated column chromatography (silica gel, 49:1). **176** (2.13 g, 78%) was obtained as an amorphous solid.

<sup>1</sup>H NMR (300.23 MHz, CDCl<sub>3</sub>): δ = 0.6-1.8 (m, 126H, aliphatic *H*, 2 CHCH<sub>3</sub>), 3.1-3.3 (m, 2H, CH<sub>2</sub>NHR), 4.1-4.3 (m, 2H, fluorenyl *CH*, CHCH<sub>3</sub>), 4.4-4.5 (m, 3H, Fmoc-NHCO<sub>2</sub>CH<sub>2</sub>, CHCH<sub>3</sub>), 5.3 (m, 1H, carbamate *NH*), 6.1 (m, 1H, amide *NH*), 6.52 (m, 1H, amide *NH*), 7.31 (t, *J* = 7.5 Hz, 2H, aromatic *H*), 7.41 (t, *J* = 7.2 Hz, 2H, aromatic *H*), 7.58 (d, *J* = 7.5 Hz, 2H, aromatic *H*), 7.78 (d, *J* = 7.5 Hz, 2H, aromatic *H*). HRMS (MALDI): calcd for <sup>13</sup>C<sub>1</sub>C<sub>77</sub>H<sub>137</sub>N<sub>3</sub>O<sub>4</sub>Na: ([M+Na]<sup>+</sup>) 1204.0540; found 1202.08. R<sub>f</sub>: 0.8 (CH<sub>2</sub>Cl<sub>2</sub>/MeOH 10:1).

**hPI<sub>10</sub>-NH-Ala<sub>2</sub>-H 177.** Following general procedure C, **176** (2.11 g, 1.9 mmol) was dissolved in CHCl<sub>3</sub> (30 mL) and a large excess of piperidine was added. The solvents were removed *in vacuo*, and the crude product was purified by column chromatography (silica gel, CH<sub>2</sub>Cl<sub>2</sub>/MeOH 24:1). **177** (1.32 g, 78%) was obtained as a colorless amorphous solid.



$^1\text{H}$  NMR (300.23 MHz,  $\text{CDCl}_3$ ):  $\delta$  = 0.5-2.0 (m, 200H, aliphatic  $H$ , 2  $\text{CHCH}_3$ ), 3.1-3.4 (m, 3H,  $\text{CH}_2\text{NHR}$ ,  $\text{CHCH}_3$ ), 4.5 (m, 1H,  $\text{CHCH}_3$ ), 8.2 (br s, 1H, amide  $\text{NH}$ ). HRMS (MALDI): calcd for  $^{13}\text{C}_1\text{C}_{62}\text{H}_{127}\text{N}_3\text{O}_2\text{Na}$ : ( $[\text{M}+\text{Na}]^+$ ) 981.97; found 981.90.  $R_f$ : 0.2 ( $\text{CH}_2\text{Cl}_2/\text{MeOH}$  10:1).

**hPI<sub>10</sub>-NH-Ala<sub>3</sub>-C(O)O-CH<sub>2</sub>-C $\equiv$ C-C $\equiv$ C-TMS 178.** Following general procedure E, **87** (0.10 g, 0.37 mmol) was dissolved in a mixture of dry DMF (2 mL) and dry  $\text{CH}_2\text{Cl}_2$  (8 mL). HOBt (0.067 g, 0.5 mmol) and EDCI (0.12 g, 0.63 mmol) were added to form the active ester intermediate. A second solution containing **43** (0.33 g, 0.37 mmol) and TEA (0.15 g, 1.5 mmol) in dry  $\text{CH}_2\text{Cl}_2$  (100 mL) was prepared, and both solutions were combined. The solution was washed twice with 1M HCl and once with sat. NaCl solution. The combined organic phases were dried over  $\text{MgSO}_4$ , filtered, and concentrated *in vacuo*. The crude material was purified by column chromatography (silica gel,  $\text{CHCl}_3/\text{MeOH}$  24:1). **178** (0.30 g, 70%) was obtained as an amorphous solid.

$^1\text{H}$  NMR (300.23 MHz,  $\text{CDCl}_3$  / TFA 50:1):  $\delta$  = 0.19 (s, 9H,  $\text{Si}(\text{CH}_3)_3$ ), 0.6-1.9 (m, 124H, aliphatic  $H$ , 3  $\text{CHCH}_3$ ), 3.2-3.4 (m, 2H,  $\text{CH}_2\text{NHR}$ ), 4.36 (m, 1H,  $\text{CHCH}_3$ ), 4.54 (m, 2H, 2  $\text{CHCH}_3$ ), 4.75 (m, 2H,  $\text{NHCO}_2\text{CH}_2$ ), 6.0/6.7 (2 m, 1H, carbamate  $\text{NH}$ ), 6.8-6.9 (m, 1H, amide  $\text{NH}$ ), 7.4-7.5 (m, 1H,  $\text{NH}$ ), 7.7-7.8 (m, 1H,  $\text{NH}$ ). HRMS (MALDI): calcd for  $\text{C}_{65}\text{H}_{122}\text{N}_4\text{O}_5\text{SiNa}$ : ( $[\text{M}+\text{Na}]^+$ ) 1089.91; found: 1089.80.  $R_f$ : 0.5 ( $\text{CH}_2\text{Cl}_2/\text{MeOH}$  10:1).

**hPI<sub>10</sub>-NH-Ala<sub>3</sub>-C(O)O-CH<sub>2</sub>-C $\equiv$ C-C $\equiv$ C-C $\equiv$ C-TMS 179.** Following general procedure E, **175** (0.06 g, 0.2 mmol) was dissolved in a mixture of dry DMF (1.5 mL) and dry  $\text{CH}_2\text{Cl}_2$  (7 mL). HOBt (0.048 g, 0.35 mmol) and EDCI (0.06 g, 0.31 mmol) were added to form the active ester intermediate. A second solution containing **177** (0.18 g, 0.2 mmol) and TEA (0.12 g, 0.12 mmol) in dry  $\text{CH}_2\text{Cl}_2$  (100 mL) was prepared, and both solutions were combined. The solution was washed twice with 1M HCl and once with sat. NaCl solution. The combined organic phases were dried over  $\text{MgSO}_4$ , filtered, and concentrated *in vacuo*. The crude material was purified by column chromatography (silica gel,  $\text{CHCl}_3/\text{MeOH}$  24:1). **179** (0.16 g, 66%) was obtained as an amorphous solid.

$^1\text{H}$  NMR (300.23 MHz,  $\text{CDCl}_3$  / TFA 50:1):  $\delta$  = 0.20 (s, 1.3H,  $\text{Si}(\text{CH}_3)_3$ ), 0.6-1.9 (m, 128H, aliphatic  $H$ , 3  $\text{CHCH}_3$ ), 2.17 (s, 0.5H, triacetylene  $H$ ), 3.2-3.4 (m, 2H,  $\text{CH}_2\text{NHR}$ ), 4.3-4.4 (m, 1H,  $\text{CHCH}_3$ ), 4.54 (m, 2H, 2  $\text{CHCH}_3$ ), 4.75 (m, 2H,  $\text{NHCO}_2\text{CH}_2$ ), 6.0/6.7 (2 m, 1H, carbamate  $\text{NH}$ ), 6.8-6.9 (m, 1H, amide  $\text{NH}$ ), 7.4-7.5 (m, 1H,  $\text{NH}$ ), 7.7-7.8 (m, 1H,  $\text{NH}$ ). HRMS (MALDI): calcd for  $\text{C}_{62}\text{H}_{112}\text{N}_4\text{O}_5\text{SiNa}$ : ( $[\text{M}+\text{Na}]^+$ ) 1043.83; found: 1041.83.  $R_f$ : 0.5 ( $\text{CH}_2\text{Cl}_2/\text{MeOH}$  10:1).

**hPI<sub>10</sub>-NH-Ala<sub>3</sub>-C(O)O-CH<sub>2</sub>-C $\equiv$ C-C $\equiv$ C-H 180.** The starting material **178** (0.25 g, 0.22 mmol) was dissolved in a mixture of  $\text{CHCl}_3$  (20 mL), MeOH (20 mL), EtOH (3 mL) and water (3 drops). AgOTf

(0.068 g, 0.26 mmol) was added, and the increasingly turbid solution was stirred for 30 min. TLC indicated a complete formation of the silver acetylide ( $R_f$ :0), and KI (0.15 g, 0.9 mmol) was added. The solution was stirred for 4 h, all solvents were removed, and the crude material was purified by column chromatography ( $\text{CHCl}_3/\text{MeOH}$  24:1). **180** (0.146 g, 62%) was obtained as a slightly yellow, amorphous material.

$^1\text{H}$  NMR (300.23 MHz,  $\text{CDCl}_3$  / TFA 50:1):  $\delta$  = 0.6-1.9 (m, 113H, aliphatic  $H$ , 3  $\text{CHCH}_3$ ), 2.22 (s, 0.54H, diacetylene  $H$ ), 3.2-3.4 (m, 2H,  $\text{CH}_2\text{NHR}$ ), 4.3-4.4 (m, 1H,  $\text{CHCH}_3$ ), 4.54 (m, 2H, 2  $\text{CHCH}_3$ ), 4.75 (m, 2H,  $\text{NHCO}_2\text{CH}_2$ ), 6.0/6.7 (2 m, 1H, carbamate  $\text{NH}$ ), 6.8-6.9 (m, 1H, amide  $\text{NH}$ ), 7.4-7.5 (m, 1H,  $\text{NH}$ ), 7.7-7.8 (m, 1H,  $\text{NH}$ ). HRMS (MALDI): calcd for  $\text{C}_{62}\text{H}_{114}\text{N}_4\text{O}_5\text{Na}$ : ( $[\text{M}+\text{Na}]^+$ ) 1017.87; found: 1017.76.  $R_f$ : 0.5 ( $\text{CH}_2\text{Cl}_2/\text{MeOH}$  10:1).

**hPI<sub>10</sub>-NH-Ala<sub>3</sub>-C(O)O-CH<sub>2</sub>-C $\equiv$ C-C $\equiv$ C-C $\equiv$ C-H 181.** The starting material **179** (0.15 g, 0.14 mmol) was dissolved in a mixture of  $\text{CHCl}_3$  (20 mL), MeOH (20 mL), EtOH (3 mL) and water (3 drops). AgOTf (0.05 g, 0.19 mmol) was added, and the increasingly turbid solution was stirred for 30 min. TLC indicated a complete formation of the silver acetylide ( $R_f$ :0), and KI (0.04 g, 0.24 mmol) was added. The solution was stirred for 4 h, all solvents were removed, and the crude material was purified by column chromatography ( $\text{CHCl}_3/\text{MeOH}$  24:1). **181** (0.12 g, 88%) was obtained as a brownish, amorphous material.

$^1\text{H}$  NMR (300.23 MHz,  $\text{CDCl}_3$  / TFA 50:1):  $\delta$  = 0.6-1.9 (m, 130H, aliphatic  $H$ , 3  $\text{CHCH}_3$ ), 2.17 (s, 0.3H, triacetylene  $H$ ), 3.2-3.4 (m, 2H,  $\text{CH}_2\text{NHR}$ ), 4.3-4.4 (m, 1H,  $\text{CHCH}_3$ ), 4.54 (m, 2H, 2  $\text{CHCH}_3$ ), 4.75 (m, 2H,  $\text{NHCO}_2\text{CH}_2$ ), 6.0/6.7 (2 m, 1H, carbamate  $\text{NH}$ ), 6.8-6.9 (m, 1H, amide  $\text{NH}$ ), 7.4-7.5 (m, 1H,  $\text{NH}$ ), 7.7-7.8 (m, 1H,  $\text{NH}$ ).  $R_f$ : 0.5 ( $\text{CH}_2\text{Cl}_2/\text{MeOH}$  10:1).

**(hPI<sub>10</sub>-NH-Ala<sub>3</sub>-C(O)O-CH<sub>2</sub>-C $\equiv$ C-C $\equiv$ C-)<sub>2</sub> 182.** The terminal diacetylene **180** (0.13 g, 0.11 mmol) was dissolved in  $\text{CH}_2\text{Cl}_2$  (30 mL). The Hay catalyst was prepared in a second flask containing  $\text{CH}_2\text{Cl}_2$  (20 mL), CuCl (11.3 mg, 0.11 mmol), and TMEDA (0.03 g, 0.22 mmol). The supernatant of the catalyst solution was added to the reaction mixture and the green solution was stirred for 4 d. The solution was filtered through a silica-gel plug, the obtained crude material was purified by column chromatography ( $\text{CHCl}_3/\text{MeOH}$  24:1) twice, and the still greenish solution in  $\text{CHCl}_3$  was washed with sat.  $\text{NH}_4\text{Cl}$  solution as well as cyanide solutions to remove residual copper. **182** (0.095 g, 73%) was obtained as a slightly greenish amorphous material.

$^1\text{H}$  NMR (300.23 MHz,  $\text{CDCl}_3$  / TFA 50:1):  $\delta$  = 0.6-1.9 (m, 276H, aliphatic  $H$ , 6  $\text{CHCH}_3$ ), 3.2-3.4 (m, 4H, 2  $\text{CH}_2\text{NHR}$ ), 4.3-4.4 (m, 1H,  $\text{CHCH}_3$ ), 4.5-4.7 (m, 4H, 4  $\text{CHCH}_3$ ), 4.7-4.9 (m, 3H,  $\text{NHCO}_2\text{CH}_2$ ), 6.0/6.7 (2 m, 2H, 2 carbamate  $\text{NH}$ ), 6.8-6.9 (m, 1H, amide  $\text{NH}$ ), 7.4-7.5 (m, 1H,  $\text{NH}$ ), 7.6 (m, 1H,  $\text{NH}$ ),

7.7-7.8 (m, 2H, NH). HRMS (MALDI): calcd for  $C_{124}H_{226}N_8O_{10}Na$ :  $([M+Na]^+)$  2010.73; found: 2010.72.  
R<sub>f</sub>: 0.4 (CH<sub>2</sub>Cl<sub>2</sub>/MeOH 10:1).

**(hPI<sub>10</sub>-NH-Ala<sub>3</sub>-C(O)O-CH<sub>2</sub>-C≡C-C≡C-C≡C)<sub>2</sub> 183.** The terminal triacetylene **181** (0.067 g, 0.05 mmol) was dissolved in CH<sub>2</sub>Cl<sub>2</sub> (15 mL). The Hay catalyst was prepared in a second flask containing CH<sub>2</sub>Cl<sub>2</sub> (10 mL), CuCl (6 mg, 0.05 mmol), and TMEDA (0.02 g, 0.14 mmol). The supernatant of the catalyst solution was added to the reaction mixture and the green/brown solution was stirred for 4 d. The solution was filtered through a silica-gel plug, the obtained crude material was purified by column chromatography (CHCl<sub>3</sub>/MeOH 24:1) twice to obtain **183** (0.055 g, 82%) as a brown amorphous material.

<sup>1</sup>H NMR (300.23 MHz, CDCl<sub>3</sub> / TFA 50:1):  $\delta$  = 0.6-1.9 (m, 259H, aliphatic H, 6 CHCH<sub>3</sub>), 3.2-3.4 (m, 4H, 2 CH<sub>2</sub>NHR), 4.3-4.4 (m, 1H, CHCH<sub>3</sub>), 4.5-4.7 (m, 4H, 4 CHCH<sub>3</sub>), 4.7-4.9 (m, 2H, NHCO<sub>2</sub>CH<sub>2</sub>), 6.0/6.7 (2 m, 2H, 2 carbamate NH), 6.8-6.9 (m, 1H, amide NH), 7.4-7.5 (m, 1H, NH), 7.6 (m, 1H, NH), 7.7-7.8 (m, 2H, NH). HRMS (MALDI): calcd for  $C_{128}H_{226}N_8O_{10}Na$ :  $([M+Na]^+)$  2058.73; found: 2058.75.  
R<sub>f</sub>: 0.4 (CH<sub>2</sub>Cl<sub>2</sub>/MeOH 10:1).





## References



## 6 References

- [1] R. Lakes, *Nature* **1993**, *361*, 511.
- [2] D. Tirrell, *Hierarchical Structures in Biology as a Guide for New Materials Technology*, National Academies Press, Washington, **1994**.
- [3] M. Muthukumar, C. K. Ober, E. L. Thomas, *Science* **1997**, *277*, 1225.
- [4] S. Hecht, *Materials Today* **2005**, *8*, 48-55.
- [5] C. J. Hawker, K. L. Wooley, *Science* **2005**, *309*, 1200.
- [6] E. W. Meijer, P. H. J. Schenning Albert, *Nature* **2002**, *419*, 353.
- [7] F. J. M. Hoeben, P. Jonkheijm, E. W. Meijer, A. P. H. J. Schenning, *Chem. Rev.* **2005**, *105*, 1491.
- [8] S. H. Gellman, *Acc. Chem. Res.* **1998**, *31*, 173.
- [9] D. J. Hill, M. J. Mio, R. B. Prince, T. S. Hughes, J. S. Moore, *Chem. Rev.* **2001**, *101*, 3893.
- [10] S. Hecht, I. Huc, editors, *Foldamers: Structure, Properties and Applications*, Wiley-VCH, Weinheim (Germany), **2007**.
- [11] J.-M. Lehn, *Angew. Chem.* **1988**, *100*, 91-116.
- [12] J.-M. Lehn, *Science* **2002**, *295*, 2400.
- [13] R. E. Martin, F. Diederich, *Angew. Chem. Int. Ed.* **1999**, *38*, 1351.
- [14] G. H. Gelinck, H. E. A. Huitema, E. van Veenendaal, E. Cantatore, L. Schrijnemakers, J. B. P. H. van der Putten, T. C. T. Geuns, M. Beenhakkers, J. B. Giesbers, B.-H. Huisman, E. J. Meijer, E. M. Benito, F. J. Touwslager, A. W. Marsman, B. J. E. van Rens, D. M. de Leeuw, *Nature Mater.* **2004**, *3*, 106.
- [15] R. Iwaura, F. J. M. Hoeben, M. Masuda, A. P. H. J. Schenning, E. W. Meijer, T. Shimizu, *J. Am. Chem. Soc.* **2006**, *128*, 13298.
- [16] R. W. Sinkeldam, F. J. M. Hoeben, M. J. Pouderoijen, I. De Cat, J. Zhang, S. Furukawa, S. De Feyter, J. A. J. M. Vekemans, E. W. Meijer, *J. Am. Chem. Soc.* **2006**, *128*, 16113.
- [17] A. P. H. J. Schenning, P. Jonkheijm, E. Peeters, E. W. Meijer, *J. Am. Chem. Soc.* **2001**, *123*, 409.
- [18] P. Jonkheijm, F. J. M. Hoeben, R. Kleppinger, J. Van Herrikhuyzen, A. P. H. J. Schenning, E. W. Meijer, *J. Am. Chem. Soc.* **2003**, *125*, 15941.
- [19] F. Würthner, Z. Chen, F. J. M. Hoeben, P. Osswald, C.-C. You, P. Jonkheijm, J. von Herrikhuyzen,

- A. P. H. J. Schenning, P. P. A. M. van der Schoot, E. W. Meijer, E. H. A. Beckers, S. C. J. Meskers, R. A. J. Janssen, *J. Am. Chem. Soc.* **2004**, *126*, 10611.
- [20] A. P. H. J. Schenning, J. van Herrikhuyzen, P. Jonkheijm, Z. Chen, F. Wuerthner, E. W. Meijer, *J. Am. Chem. Soc.* **2002**, *124*, 10252.
- [21] H. Sirringhaus, N. Tessler, R. H. Friend, *Science* **1998**, *280*, 1741.
- [22] A. F. M. Kilbinger, A. P. H. J. Schenning, F. Goldoni, W. J. Feast, E. W. Meijer, *J. Am. Chem. Soc.* **2000**, *122*, 1820.
- [23] A. P. H. J. Schenning, A. F. M. Kilbinger, F. Biscarini, M. Cavallini, H. J. Cooper, P. J. Derrick, W. J. Feast, R. Lazzaroni, P. Leclere, L. A. McDonell, E. W. Meijer, S. C. J. Meskers, *J. Am. Chem. Soc.* **2002**, *124*, 1269.
- [24] P. Leclere, M. Surin, P. Viville, R. Lazzaroni, A. F. M. Kilbinger, O. Henze, W. J. Feast, M. Cavallini, F. Biscarini, A. P. H. J. Schenning, E. W. Meijer, *Chem. Mater.* **2004**, *16*, 4452.
- [25] M. Surin, R. Lazzaroni, W. J. Feast, A. P. H. J. Schenning, E. W. Meijer, P. Leclere, *Synth. Met.* **2004**, *147*, 67.
- [26] S. Westenhoff, A. Abrusci, W. J. Feast, O. Henze, A. F. M. Kilbinger, A. P. H. J. Schenning, C. Silva, *Adv. Mater.* **2006**, *18*, 1281.
- [27] S.-I. Kawano, N. Fujita, S. Shinkai, *Chem. Eur. J.* **2005**, *11*, 4735.
- [28] A. F. M. Kilbinger, W. J. Feast, *J. Mater. Chem.* **2000**, *10*, 1777.
- [29] O. Henze, M. Fransen, P. Jonkheijm, E. W. Meijer, W. J. Feast, A. P. H. J. Schenning, *J. Polym. Sci., Part A: Polym. Chem.* **2003**, *41*, 1737.
- [30] O. Henze, D. Parker, W. J. Feast, *J. Mater. Chem.* **2003**, *13*, 1269.
- [31] O. Henze, W. J. Feast, *J. Mater. Chem.* **2003**, *13*, 1274.
- [32] G. Cik, Z. Vegh, F. Sersen, J. Kristin, B. Lakatos, P. Fejdi, *Synth. Met.* **2005**, *149*, 31.
- [33] W. Li, T. Maddux, L. Yu, *Macromolecules* **1996**, *29*, 7329.
- [34] M. A. Hempenius, B. M. W. Langeveld-Voss, J. A. E. H. van Haare, R. A. J. Janssen, S. S. Sheiko, J. P. Spatz, M. Möller, E. W. Meijer, *J. Am. Chem. Soc.* **1998**, *120*, 2798.
- [35] J. Liu, E. Sheina, T. Kowalewski, R. D. McCullough, *Angew. Chem. Int. Ed.* **2002**, *41*, 329.
- [36] S. Holdcroft, *Adv. Mater.* **2001**, *13*, 1753.
- [37] C. D. Dimitrakopoulos, P. R. L. Malenfant, *Adv. Mater.* **2002**, *14*, 99.
- [38] T. Nakano, Y. Okamoto, *Chem. Rev.* **2001**, *101*, 4013.
- [39] J. J. L. M. Cornelissen, J. J. J. M. Donners, R. de Gelder, W. S. Graswinckel, G. A. Metselaar, A. E. Rowan, N. A. J. M. Sommerdijk, R. J. M. Nolte, *Science* **2001**, *293*, 676.
- [40] J. J. L. M. Cornelissen, W. S. Graswinckel, P. J. H. M. Adams, G. H. Nachttegaal, A. P. M. Kentgens, N. A. J. M. Sommerdijk, R. J. M. Nolte, *J. Polym. Sci., Part A: Polym. Chem.* **2001**, *39*, 4255.



- [41] J. J. L. M. Cornelissen, W. S. Graswinckel, A. E. Rowan, N. A. J. M. Sommerdijk, R. J. M. Nolte, *J. Polym. Sci., Part A: Polym. Chem.* **2003**, *41*, 1725.
- [42] G. A. Metselaar, J. J. L. M. Cornelissen, A. E. Rowan, R. J. M. Nolte, *Angew. Chem. Int. Ed.* **2005**, *44*, 1990.
- [43] J. J. L. M. Cornelissen, M. Fischer, N. A. J. M. Sommerdijk, R. J. M. Nolte, *Science* **1998**, *280*, 1427.
- [44] A. Kros, W. Jesse, G. A. Metselaar, J. J. L. M. Cornelissen, *Angew. Chem. Int. Ed.* **2005**, *44*, 4349.
- [45] L. Pu, *Macromol. Rapid Commun.* **2000**, *21*, 795.
- [46] S. R. Wyatt, Q.-S. Hu, X.-L. Yan, W. D. Bare, L. Pu, *Macromolecules* **2001**, *34*, 7983–7988.
- [47] H.-C. Zhang, L. Pu, *Tetrahedron* **2003**, *59*, 1703.
- [48] L. Zheng, R. C. Urian, Y. Liu, A. K. Y. Jen, L. Pu, *Chem. Mater.* **2000**, *12*, 13.
- [49] L. Pu, *Chem. Eur. J.* **1999**, *5*, 2227.
- [50] L. Pu, *Chem. Rev.* **1998**, *98*, 2405.
- [51] H. Cheng, L. Pu, *Macromol. Chem. Phys.* **1999**, *200*, 1274–1283.
- [52] B. M. W. Langeveld-Voss, R. A. J. Janssen, M. P. T. Christiaans, S. C. J. Meskers, H. P. J. M. Dekkers, E. W. Meijer, *J. Am. Chem. Soc.* **1996**, *118*, 4908.
- [53] B. M. W. Langeveld-Voss, M. P. T. Christiaans, R. A. J. Janssen, E. W. Meijer, *Macromolecules* **1998**, *31*, 6702.
- [54] B. M. W. Langeveld-Voss, R. J. M. Waterval, R. A. J. Janssen, E. W. Meijer, *Macromolecules* **1999**, *32*, 227.
- [55] E. R. Lermo, B. M. W. Langeveld-Voss, R. A. J. Janssen, E. W. Meijer, *Chem. Commun.* **1999**, 791.
- [56] J. R. Matthews, F. Goldoni, A. P. H. J. Schenning, E. W. Meijer, *Chem. Commun.* **2005**, 5503.
- [57] E. Yashima, T. Matsushima, Y. Okamoto, *J. Am. Chem. Soc.* **1997**, *119*, 6345.
- [58] E. Yashima, K. Maeda, Y. Okamoto, *Nature* **1999**, *399*, 449.
- [59] R. Nomura, J. Tabei, T. Masuda, *J. Am. Chem. Soc.* **2001**, *123*, 8430.
- [60] G. Gao, F. Sanda, T. Masuda, *Macromolecules* **2003**, *36*, 3932.
- [61] G. Gao, F. Sanda, T. Masuda, *Macromolecules* **2003**, *36*, 3938.
- [62] H. Zhao, F. Sanda, T. Masuda, *Macromolecules* **2004**, *37*, 8888.
- [63] J. Tabei, M. Shiotsuki, F. Sanda, T. Masuda, *Macromolecules* **2005**, *38*, 9448.
- [64] F. Sanda, H. Araki, T. Masuda, *Macromolecules* **2004**, *37*, 8510.
- [65] F. Sanda, H. Araki, T. Masuda, *Macromolecules* **2005**, *38*, 10605.
- [66] F. Sanda, S. Nishiura, M. Shiotsuki, T. Masuda, *Macromolecules* **2005**, *38*, 3075.
- [67] H. Zhao, F. Sanda, T. Masuda, *Macromol. Chem. Phys.* **2006**, *207*, 1921.
- [68] D. Yue, T. Fujii, K. Terada, J. Tabei, M. Shiotsuki, F. Sanda, T. Masuda, *Macromol. Rapid Commun.* **2006**, *27*, 1460.

- [69] D. Yue, M. Shiotsuki, F. Sanda, T. Masuda, *Polymer* **2007**, *48*, 68.
- [70] F. Sanda, T. Teraura, T. Masuda, *J. Polym. Sci., Part A: Polym. Chem.* **2004**, *42*, 4641.
- [71] H. Zhao, F. Sanda, T. Masuda, *Polymer* **2006**, *47*, 2596.
- [72] B. S. Li, K. K. L. Cheuk, L. Ling, J. Chen, X. Xiao, C. Bai, B. Z. Tang, *Macromolecules* **2003**, *36*, 77.
- [73] K. K. L. Cheuk, J. W. Y. Lam, L. M. Lai, Y. Dong, B. Z. Tang, *Macromolecules* **2003**, *36*, 9752.
- [74] S. Li Bing, Z. Kang Shi, K. L. Cheuk Kevin, L. Wan, L. Ling, C. Bai, Z. Tang Ben, *Langmuir* **2004**, *20*, 7598.
- [75] V. Percec, E. Aqad, M. Peterca, J. G. Rudick, L. Lemon, J. C. Ronda, B. B. De, P. A. Heiney, E. W. Meijer, *J. Am. Chem. Soc.* **2006**, *128*, 16365.
- [76] L. Brunsveld, B. J. B. Folmer, E. W. Meijer, R. P. Sijbesma, *Chem. Rev.* **2001**, *101*, 4071.
- [77] H. Frauenrath, *Prog. Polym. Sci.* **2005**, *30*, 325.
- [78] A. Mueller, D. F. O'Brien, *Chem. Rev.* **2002**, *102*, 727.
- [79] G. R. Desiraju, *Angew. Chem. Int. Ed.* **1995**, *34*, 2311-27.
- [80] G. Wegner, *Z. Naturforsch., B* **1969**, *24*, 824.
- [81] V. Enkelmann, *Adv. Polym. Sci.* **1984**, *63*, 91.
- [82] A. Aggeli, I. A. Nyrkova, M. Bell, R. Harding, L. Carrick, T. C. B. McLeish, A. N. Semenov, N. Boden, *Proc. Natl. Acad. Sci. U. S. A.* **2001**, *98*, 11857.
- [83] C. W. G. Fishwick, A. J. Beevers, L. M. Carrick, C. D. Whitehouse, A. Aggeli, N. Boden, *Nano Lett.* **2003**, *3*, 1475.
- [84] A. Aggeli, M. Bell, N. Boden, J. N. Keen, T. C. B. McLeish, I. Nyrkova, S. E. Radford, A. Semenov, *J. Mater. Chem.* **1997**, *7*, 1135.
- [85] D. J. Selkoe, *Nature* **2003**, *426*, 900.
- [86] R. Tycko, *Curr. Opin. Struct. Biol.* **2004**, *14*, 96-103.
- [87] O. S. Makin, L. C. Serpell, *FEBS Journal* **2005**, *272*, 5950-5961.
- [88] R. Nelson, D. Eisenberg, *Adv. Protein Chem.* **2006**, *73*, 235.
- [89] M. Sunde, L. C. Serpell, M. Bartlam, P. E. Fraser, M. B. Pepys, C. C. F. Blake, *J. Mol. Biol.* **1997**, *273*, 729.
- [90] O. Sumner Makin, L. C. Serpell, *J. Mol. Biol.* **2004**, *335*, 1279-1288.
- [91] O. N. Antzutkin, J. J. Balbach, R. D. Leapman, N. W. Rizzo, J. Reed, R. Tycko, *Proc. Natl. Acad. Sci. U. S. A.* **2000**, *97*, 13045-13050.
- [92] A. T. Petkova, Y. Ishii, J. J. Balbach, O. N. Antzutkin, R. D. Leapman, F. Delaglio, R. Tycko, *Proc. Natl. Acad. Sci. U. S. A.* **2002**, *99*, 16742-16747.
- [93] T. Luhrs, C. Ritter, M. Adrian, D. Riek-Loher, B. Bohrmann, H. Dobeli, D. Schubert, R. Riek, *Proc. Natl. Acad. Sci. U. S. A.* **2005**, *102*, 17342-17347.

- [94] F. Shewmaker, R. B. Wickner, R. Tycko, *Proc. Natl. Acad. Sci. U. S. A.* **2006**, *103*, 19754-19759.
- [95] J. C. C. Chan, N. A. Oyler, W.-M. Yau, R. Tycko, *Biochemistry* **2005**, *44*, 10669-10680.
- [96] A. V. Kajava, U. Baxa, R. B. Wickner, A. C. Steven, *Proc. Natl. Acad. Sci. U. S. A.* **2004**, *101*, 7885-7890.
- [97] A. V. Kajava, U. Aebi, A. C. Steven, *J. Mol. Biol.* **2005**, *348*, 247-252.
- [98] J. L. Jimenez, E. J. Nettleton, M. Bouchard, C. V. Robinson, C. M. Dobson, H. R. Saibil, *Proc. Natl. Acad. Sci. U. S. A.* **2002**, *99*, 9196-9201.
- [99] J. Jenkins, R. Pickersgill, *Prog. Biophys. Mol. Biol.* **2001**, *77*, 111-175.
- [100] M. F. Perutz, J. T. Finch, J. Berriman, A. Lesk, *Proc. Natl. Acad. Sci. U. S. A.* **2002**, *99*, 5591-5595.
- [101] H. Wille, D. Michelitsch Melissa, V. Guenebaut, S. Supattapone, A. Serban, E. Cohen Fred, A. Agard David, B. Prusiner Stanley, *Proc. Natl. Acad. Sci. U. S. A.* **2002**, *99*, 3563-8.
- [102] R. Nelson, M. R. Sawaya, M. Balbirnie, A. O. Madsen, C. Riek, R. Grothe, D. Eisenberg, *Nature* **2005**, *435*, 773.
- [103] M. R. Sawaya, S. Sambashivan, R. Nelson, M. I. Ivanova, S. A. Sievers, M. I. Apostol, M. J. Thompson, M. Balbirnie, J. J. W. Wiltzius, H. T. McFarlane, A. O. Madsen, C. Riek, D. Eisenberg, *Nature* **2007**, *447*, 453.
- [104] H. A. Lashuel, S. R. LaBrenz, L. Woo, L. C. Serpell, J. W. Kelly, *J. Am. Chem. Soc.* **2000**, *122*, 5262.
- [105] T. Scheibel, R. Parthasarathy, G. Sawicki, X.-M. Lin, H. Jaeger, S. L. Lindquist, *Proc. Natl. Acad. Sci. U. S. A.* **2003**, *100*, 4527.
- [106] A. Aggeli, M. Bell, N. Boden, J. N. Keen, P. F. Knowles, T. C. McLeish, M. Pitkeathly, S. E. Radford, *Nature* **1997**, *386*, 259.
- [107] C. Whitehouse, J. Fang, A. Aggeli, M. Bell, R. Brydson, W. G. Fishwick Colin, R. Henderson Jim, M. Knobler Charles, W. Owens Robert, H. Thomson Neil, D. A. Smith, N. Boden, *Angew. Chem. Int. Ed.* **2005**, *44*, 1965.
- [108] W. G. J. Hol, L. M. Halie, C. Sander, *Nature* **1981**, *294*, 532-6.
- [109] S. Krauthaeuser, L. A. Christianson, D. R. Powell, S. H. Gellman, *J. Am. Chem. Soc.* **1997**, *119*, 11719-11720.
- [110] H.-A. Klok, S. Lecommandoux, *Adv. Mater.* **2001**, *13*, 1217.
- [111] J. H. Collier, P. B. Messersmith, *Adv. Mater.* **2004**, *16*, 907.
- [112] H. M. Koenig, A. F. M. Kilbinger, *Angew. Chem. Int. Ed.* **2007**, *46*, 8334-8340.
- [113] M. Mutter, H. Mutter, R. Uhmman, E. Bayer, *Biopolymers* **1976**, *15*, 917-27.
- [114] G. M. Bonora, C. Toniolo, M. Mutter, *Polymer* **1978**, *19*, 1382-6.
- [115] C. Toniolo, G. M. Bonora, M. Mutter, *J. Am. Chem. Soc.* **1979**, *101*, 450.
- [116] G. M. Bonora, M. Palumbo, C. Toniolo, M. Mutter, *Makromol. Chem.* **1979**, *180*, 1293.

- [117] C. Toniolo, G. M. Bonora, V. N. R. Pillai, M. Mutter, *Macromolecules* **1980**, *13*, 772.
- [118] T. S. Burkoth, T. L. S. Benzinger, D. N. M. Jones, K. Hallenga, S. C. Meredith, D. G. Lynn, *J. Am. Chem. Soc.* **1998**, *120*, 7655.
- [119] P. Thiyagarajan, T. S. Burkoth, V. Urban, S. Seifert, T. L. S. Benzinger, D. M. Morgan, D. Gordon, S. C. Meredith, D. G. Lynn, *J. Appl. Crystallogr.* **2000**, *33*, 535.
- [120] T. S. Burkoth, T. L. S. Benzinger, V. Urban, D. G. Lynn, S. C. Meredith, P. Thiyagarajan, *J. Am. Chem. Soc.* **1999**, *121*, 7429.
- [121] T. S. Burkoth, T. L. S. Benzinger, V. Urban, D. M. Morgan, D. M. Gregory, P. Thiyagarajan, R. E. Botto, S. C. Meredith, D. G. Lynn, *J. Am. Chem. Soc.* **2000**, *122*, 7883.
- [122] I. W. Hamley, I. A. Ansari, V. Castelletto, H. Nuhn, A. Roesler, H. A. Klok, *Biomacromolecules* **2005**, *6*, 1310-1315.
- [123] J. C. M. van Hest, D. A. Tirrell, *Chem. Commun.* **2001**, 1897-1904.
- [124] O. Rathore, D. Y. Sogah, *Macromolecules* **2001**, *34*, 1477.
- [125] O. Rathore, D. Y. Sogah, *J. Am. Chem. Soc.* **2001**, *123*, 5231.
- [126] J. H. Collier, P. B. Messersmith, *Bioconjugate Chem.* **2003**, *14*, 748.
- [127] J. Hentschel, E. Krause, H. G. Börner, *J. Am. Chem. Soc.* **2006**, *128*, 7722.
- [128] D. Eckhardt, M. Groenewolt, E. Krause, H. G. Börner, *Chem. Commun.* **2005**, 2814.
- [129] J. Hentschel, H. G. Börner, *J. Am. Chem. Soc.* **2006**, *128*, 14142-14149.
- [130] H. Rettig, E. Krause, H. G. Börner, *Macromol. Rapid Commun.* **2004**, *25*, 1251-1256.
- [131] J. M. Smeenk, M. B. J. Otten, J. Thies, D. A. Tirrell, H. G. Stunnenberg, J. C. M. van Hest, *Angew. Chem. Int. Edit.* **2005**, *44*, 1968-71.
- [132] T. Mori, K. Shimoyama, Y. Fukawa, K. Minagawa, M. Tanaka, *Chem. Lett.* **2005**, *34*, 116.
- [133] T. Mori, Y. Fukawa, K. Shimoyama, K. Minagawa, M. Tanaka, *Int. J. Mod. Phys. B* **2006**, *20*, 3872-3877.
- [134] G. Wegner, *Makromol. Chem.* **1970**, *134*, 219.
- [135] G. Wegner, *Makromol. Chem.* **1971**, *145*, 85.
- [136] G. Wegner, *Makromol. Chem.* **1972**, *154*, 35.
- [137] E. Haedicke, E. C. Mez, C. H. Krauch, G. Wegner, J. Kaiser, *Angew. Chem., Int. Ed. Engl.* **1971**, *10*, 266.
- [138] R. H. Baughman, *J. Polym. Sci., Polym. Phys. Ed.* **1974**, *12*, 1511.
- [139] R. H. Baughman, K. C. Yee, *J. Polym. Sci., Part D: Macromol. Rev.* **1978**, *13*, 219.
- [140] V. Enkelmann, G. Wegner, *Angew. Chem. Int. Ed.* **1977**, *89*, 416.
- [141] B. Tieke, G. Wegner, D. Naegele, H. Ringsdorf, *Angew. Chem. Int. Ed.* **1976**, *15*, 764.
- [142] D. Day, H. Ringsdorf, *J. Polym. Sci., Polym. Lett. Ed.* **1978**, *16*, 205.

- [143] K. E. Huggins, S. Son, S. I. Stupp, *Macromolecules* **1997**, *30*, 5305.
- [144] D. H. Charych, J. O. Nagy, W. Spevak, M. D. Bednarski, *Science* **1993**, *261*, 585.
- [145] L. Hsu, G. L. Cvetanovich, S. I. Stupp, *J. Am. Chem. Soc.* **2008**, *130*, 3892–3899.
- [146] K. H. Park, J.-S. Lee, H. Park, E.-H. Oh, J.-M. Kim, *Chem. Commun.* **2007**, 410-412.
- [147] M. George, R. G. Weiss, *Chem. Mater.* **2003**, *15*, 2879.
- [148] Q. Cheng, M. Yamamoto, R. C. Stevens, *Langmuir* **2000**, *16*, 5333.
- [149] S. B. Lee, R. Koepsel, D. B. Stolz, H. E. Warriner, A. J. Russell, *J. Am. Chem. Soc.* **2004**, *126*, 13400.
- [150] M. Masuda, T. Hanada, Y. Okada, K. Yase, T. Shimizu, *Macromolecules* **2000**, *33*, 9233.
- [151] X. Nie, G. Wang, *J. Org. Chem.* **2006**, *71*, 4734-4741.
- [152] J. H. Fuhrhop, P. Blumtritt, C. Lehmann, P. Luger, *J. Am. Chem. Soc.* **1991**, *113*, 7437.
- [153] D. A. Frankel, D. F. O'Brien, *J. Am. Chem. Soc.* **1991**, *113*, 7436.
- [154] G. N. Patel, R. R. Chance, J. D. Witt, *J. Polym. Sci., Pol. Lett.* **1978**, *16*, 607-14.
- [155] G. N. Patel, E. K. Walsh, *J. Polym. Sci., Pol. Lett.* **1979**, *17*, 203-208.
- [156] G. N. Patel, R. R. Chance, J. D. Witt, *J. Chem. Phys.* **1979**, *70*, 4387-4392.
- [157] R. R. Chance, G. N. Patel, J. D. Witt, *J. Chem. Phys.* **1979**, *71*, 206-211.
- [158] R. H. Baughman, R. R. Chance, *J. Polym. Sci., Pol. Phys.* **1976**, *14*, 2037-2045.
- [159] R. R. Chance, *Macromolecules* **1980**, *13*, 396-398.
- [160] M. L. Shand, R. R. Chance, *Phys. Rev. B* **1982**, *25*, 4431-4436.
- [161] K. C. Lim, J. Fincher, C. R., A. J. Heeger, *Phys. Rev. Lett.* **1983**, *50*, 1934.
- [162] K. C. Lim, A. J. Heeger, *J. Chem. Phys.* **1985**, *82*, 522.
- [163] A. J. Berlinsky, F. Wudl, K. C. Lim, C. R. Fincher, A. J. Heeger, *J. Polym. Sci., Polym. Phys. Ed.* **1984**, *22*, 847.
- [164] G. Wenz, M. A. Mueller, M. Schmidt, G. Wegner, *Macromolecules* **1984**, *17*, 837.
- [165] A. F. Drake, P. Udvarhelyi, D. J. Ando, D. Bloor, J. S. Obhi, S. Mann, *Polymer* **1989**, *30*, 1063-1067.
- [166] C. Bustamante, I. Tinoco, M. Maestre, *Proc. Natl. Acad. Sci. USA* **1983**, *80*, 3568-3572.
- [167] P. Deb, Z. Yuan, L. Ramsey, T. W. Hanks, *Macromolecules* **2007**, *40*, 3533-3537.
- [168] O. J. Dautel, M. Robitzer, J. P. Lere-Porte, F. Serein-Spirau, J. J. E. Moreau, *J. Am. Chem. Soc.* **2006**, *128*, 16213.
- [169] N. Fujita, Y. Sakamoto, M. Shirakawa, M. Ojima, A. Fujii, M. Ozaki, S. Shinkai, *J. Am. Chem. Soc.* **2007**, *129*, 4134-4135.
- [170] R. Giesa, R. C. Schulz, *Polym. Int.* **1994**, *33*, 43-60.
- [171] G. M. Bonora, M. Palumbo, C. Toniolo, M. Mutter, *Makromol. Chem.* **1979**, *180*, 1293–304.
- [172] A. Mehta, R. Jaouhari, T. J. Benson, K. T. Douglas, *Tetrahedron Lett.* **1992**, *33*, 5441–4.
- [173] L. A. Carpino, B. J. Cohen, J. Stephens, Kenton E., S. Y. Sadat-Aalae, J. H. Tien, D. C. Langridge,

- J. Org. Chem.* **1986**, *51*, 3732.
- [174] E. Jahnke, *Synthesis of Building Blocks for New Carbon-Rich Materials*, Diploma Thesis, Freie Universität Berlin (Germany), **2005**.
- [175] S. Müller, *Surface-Functionalized Dendrimers with Potential Application for Anticancer-Therapy: Synthesis and in vitro Cytotoxicity*, Ph. D. Thesis, Freie Universität Berlin (Germany), **2004**.
- [176] K. Sonogashira, Y. Tohda, N. Hagihara, *Tetrahedron Lett.* **1975**, 4467–70.
- [177] A. S. Hay, *J. Org. Chem.* **1962**, *27*, 3320.
- [178] B. R. G, S. Surajit, C. Srinivasan, *Chem. Commun.* 812–3.
- [179] C. Cai, A. Vasella, *Helv. Chim. Acta* **1995**, *78*, 2053.
- [180] L. Capella, A. Degl’Innocenti, G. Reginato, A. Ricci, M. Taddei, G. Seconi, *J. Org. Chem.* **1989**, *54*, 1473–6.
- [181] R. Xu, V. Gramlich, H. Frauenrath, *J. Am. Chem. Soc.* **2006**, *128*, 5541.
- [182] H. Yun, S. J. Danishefsky, *J. Org. Chem.* **2003**, *68*, 4519.
- [183] F. Straus, L. Kollex, W. Heyn, R. Kuhnel, *Chem. Ber.* **1930**, *63B*, 1868–85.
- [184] W. J. Balfour, C. C. Greig, S. Visaisouk, *J. Org. Chem.* **1974**, *39*, 725–6.
- [185] E. R. Zubarev, M. U. Pralle, E. D. Sone, S. I. Stupp, *J. Am. Chem. Soc.* **2001**, *123*, 4105.
- [186] D. L. Hughes, *Org. Reactions* **1992**, *42*, 335–656.
- [187] R. Xu, *The Phenyl-Perfluorophenyl Interaction as a Supramolecular Synthone for Topochemical Polymerizations*, Ph. D. Thesis, ETH Zürich (Switzerland), **2008**.
- [188] B. R. Singh, “Basic Aspects of the Technique and Applications of Infrared Spectroscopy of Peptides and Proteins”, in *Infrared Analysis of Peptides and Proteins (ACS Symposium Series Vol. 750)*, B. R. Singh (ed.), American Chemical Society, Washington DC (USA), 2000.
- [189] S. Krimm, “Interpreting Infrared Spectra of Peptides and Proteins”, in *Infrared Analysis of Peptides and Proteins (ACS Symposium Series Vol. 750)*, B. R. Singh (ed.), American Chemical Society, Washington DC (USA), 2000.
- [190] P. I. Haris, “Fourier Transform Infrared Spectroscopic Studies of Peptides: Potentials and Pitfalls”, in *Infrared Analysis of Peptides and Proteins (ACS Symposium Series Vol. 750)*, B. R. Singh (ed.), American Chemical Society, Washington DC (USA), 2000.
- [191] Y. N. Chirgadze, N. A. Nevskaya, *Biopolymers* **1976**, *15*, 627.
- [192] J. Bandekar, S. Krimm, *Biopolymers* **1988**, *27*, 909.
- [193] W. Qian, J. Bandekar, S. Krimm, *Biopolymers* **1991**, *31*, 193.
- [194] Y. N. Chirgadze, N. A. Nevskaya, *Biopolymers* **1976**, *15*, 607.
- [195] W. H. Moore, S. Krimm, *Biopolymers* **1976**, *15*, 2465–83.

- [196] A. M. Dwivedi, S. Krimm, *Macromolecules* **1982**, *15*, 186.
- [197] R. A. Kammerer, D. Kostrewa, J. Zurdo, A. Detken, C. Garcia-Echeverria, J. D. Green, S. A. Müller, B. H. Meier, F. K. Winkler, C. M. Dobson, M. O. Steinmetz, *Proc. Natl. Acad. Sci. U S A* **2004**, *101*, 4435–4440.
- [198] D. Seebach, T. Sifferlen, D. J. Bierbaum, M. Rueping, B. Jaun, B. Schweizer, J. Schaefer, A. K. Mehta, R. D. O'Connor, B. H. Meier, M. Ernst, A. Glattli, *Helv. Chim. Acta* **2002**, *85*, 2877–2917.
- [199] K. Schmidt-Rohr, *Macromolecules* **1996**, *29*, 3975–81.
- [200] J. D. van Beek, L. Beaulieu, H. Schäfer, M. Demura, T. Asakura, B. H. Meier, *Nature* **405**, 1077–9.
- [201] J. D. van Beek, S. Hess, F. Vollrath, B. H. Meier, *Proc. Natl. Acad. Sci. U S A* **2002**, *99*, 10266–10271.
- [202] J. D. van Beek, B. H. Meier, *J. Magn. Res.* **2006**, *178*, 106–120.
- [203] J. Yao, D. Xiao, X. Chen, P. Zhou, T. Yu, Z. Shao, *Macromolecules* **2003**, *36*, 7508.
- [204] G. Wenz, G. Wegner, *Makromol. Chem., Rapid Commun.* **1982**, *3*, 231.
- [205] A.-S. Millerioux, *Synthesis of Diacetylene Macromonomers Synthesis of Diacetylene Macromonomers and their Polymerization in Solution*, Master Thesis, ETH Zürich (Switzerland), **2006**.
- [206] J. P. Fouassier, B. Tieke, G. Wegner, *Isr. J. Chem.* **1980**, *18*, 227.
- [207] A. J. Melveger, R. H. Baughman, *J. Polym. Sci., Pol. Phys.* **1973**, *11*, 603–19.
- [208] R. H. Baughman, J. D. Witt, K. C. Yee, *J. Chem. Phys.* **1974**, *60*, 4755–9.
- [209] D. Keller, C. Bustamante, *J. Chem. Phys.* **1986**, *84*, 2972–2980.
- [210] J. Weiss, *Hierarchical Self-Organization of Diacetylene-Functionalized Oligopeptide Polymers*, Master Thesis, Freie Universität Berlin (Germany), **2007**.
- [211] S. Okada, K. Hayamizu, H. Matsuda, A. Masaki, N. Minami, H. Nakanishi, *Macromolecules* **1994**, *27*, 6259.
- [212] A. Sarkar, S. Okada, K. Komatsu, H. Nakanishi, H. Matsuda, *Macromolecules* **1998**, *31*, 5624.
- [213] H. Matsuzawa, S. Okada, A. Sarkar, H. Nakanishi, H. Matsuda, *J. Polym. Sci., Part A: Polym. Chem.* **1999**, *37*, 3537.
- [214] A. Sarkar, S. Okada, H. Matsuzawa, H. Matsuda, H. Nakanishi, *J. Mater. Chem.* **2000**, *10*, 819.
- [215] N. Severin, I. M. Okhupkin, A. R. Khokhlov, J. P. Rabe, *Nano Lett.* **2006**, *6*, 1018–1022.
- [216] N. Severin, J. Barner, A. A. Kalachev, J. P. Rabe, *Nano Lett.* **2004**, *4*, 577–579.

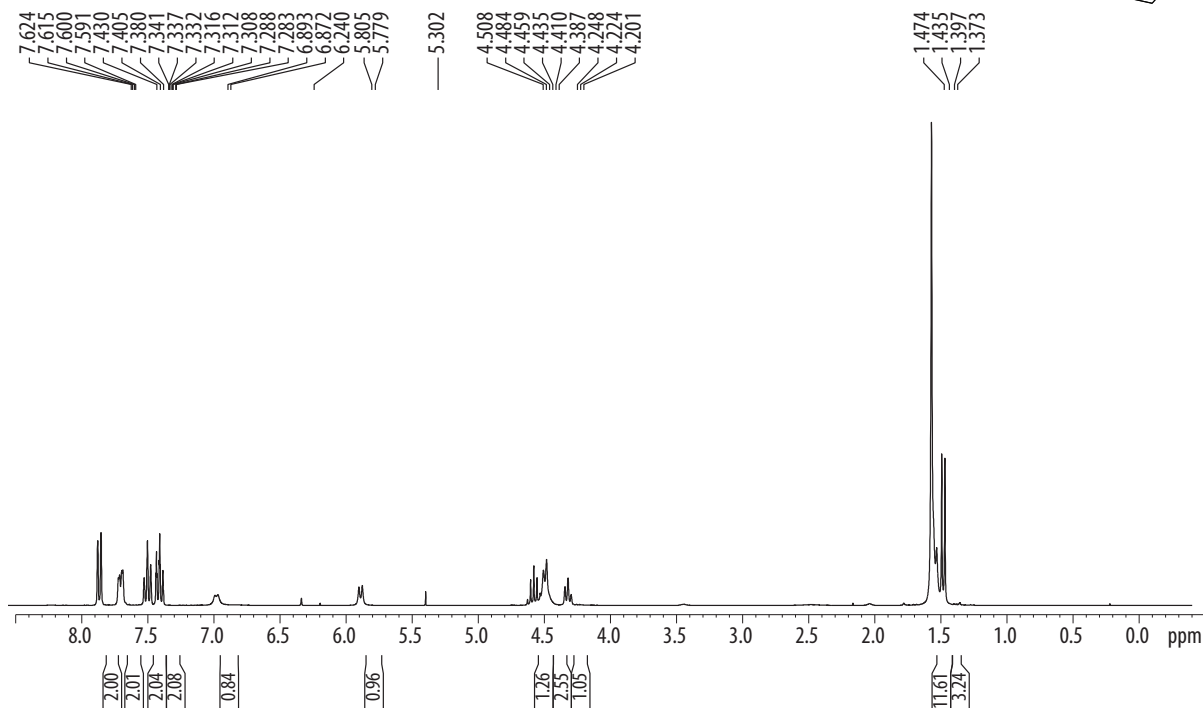
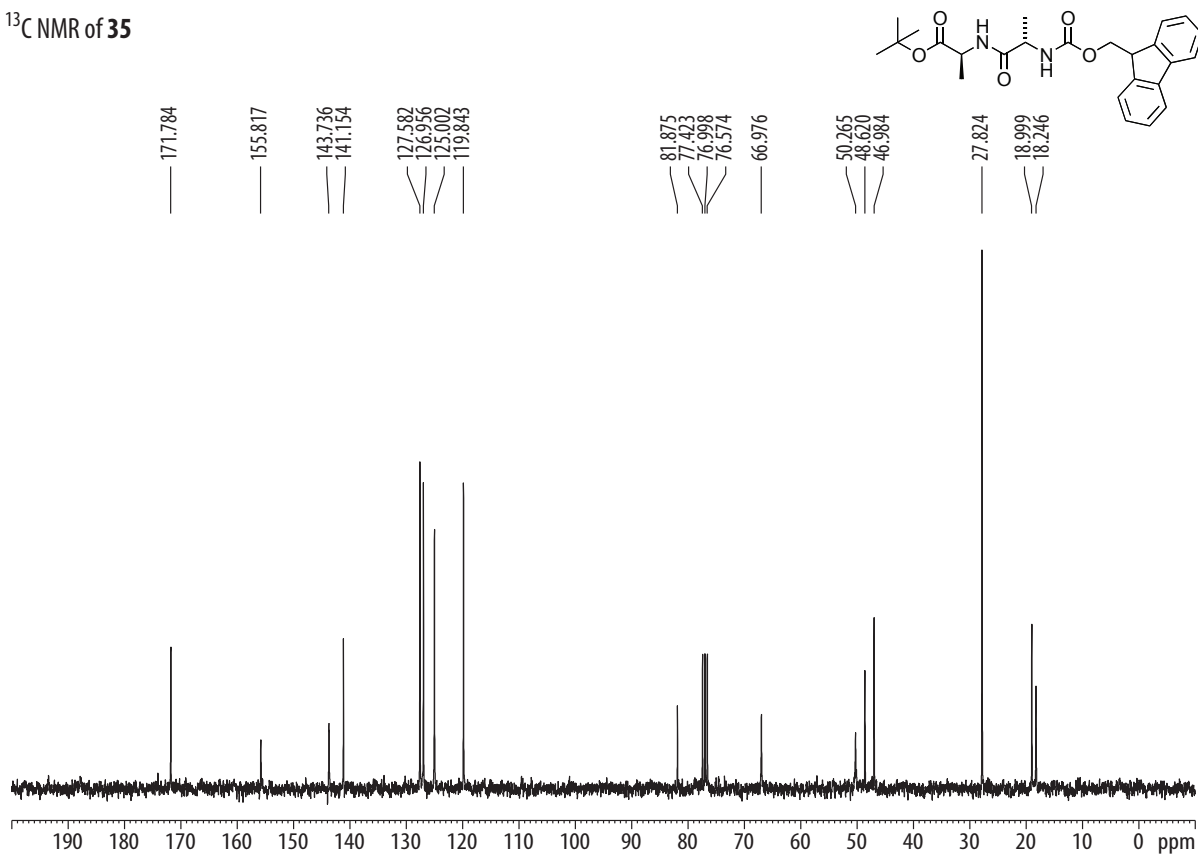


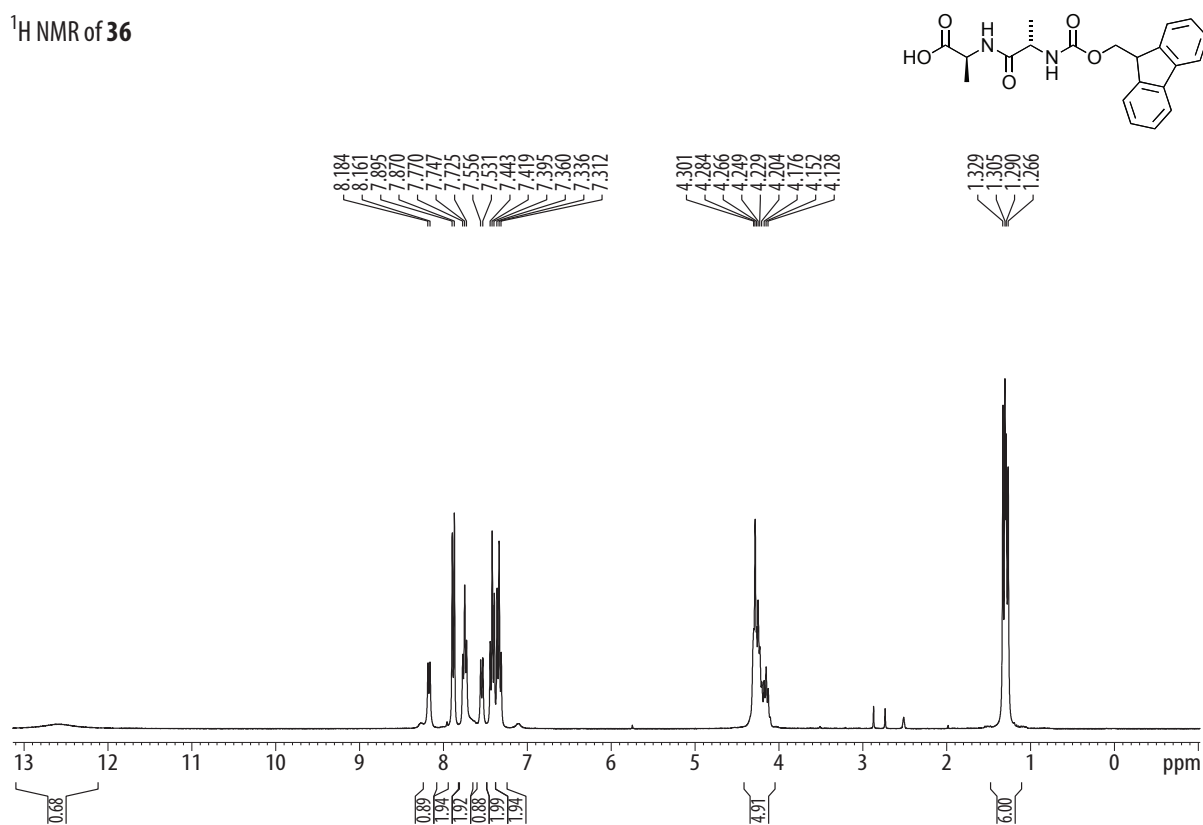
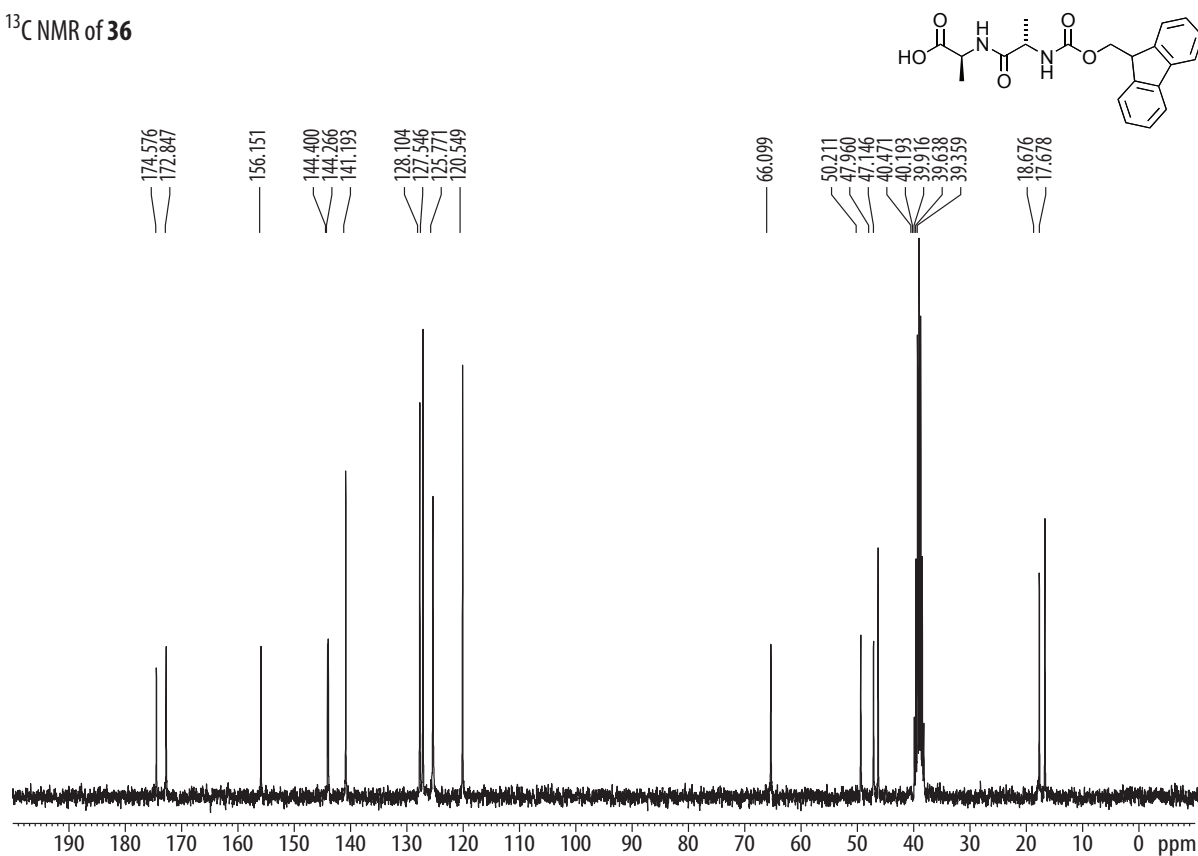


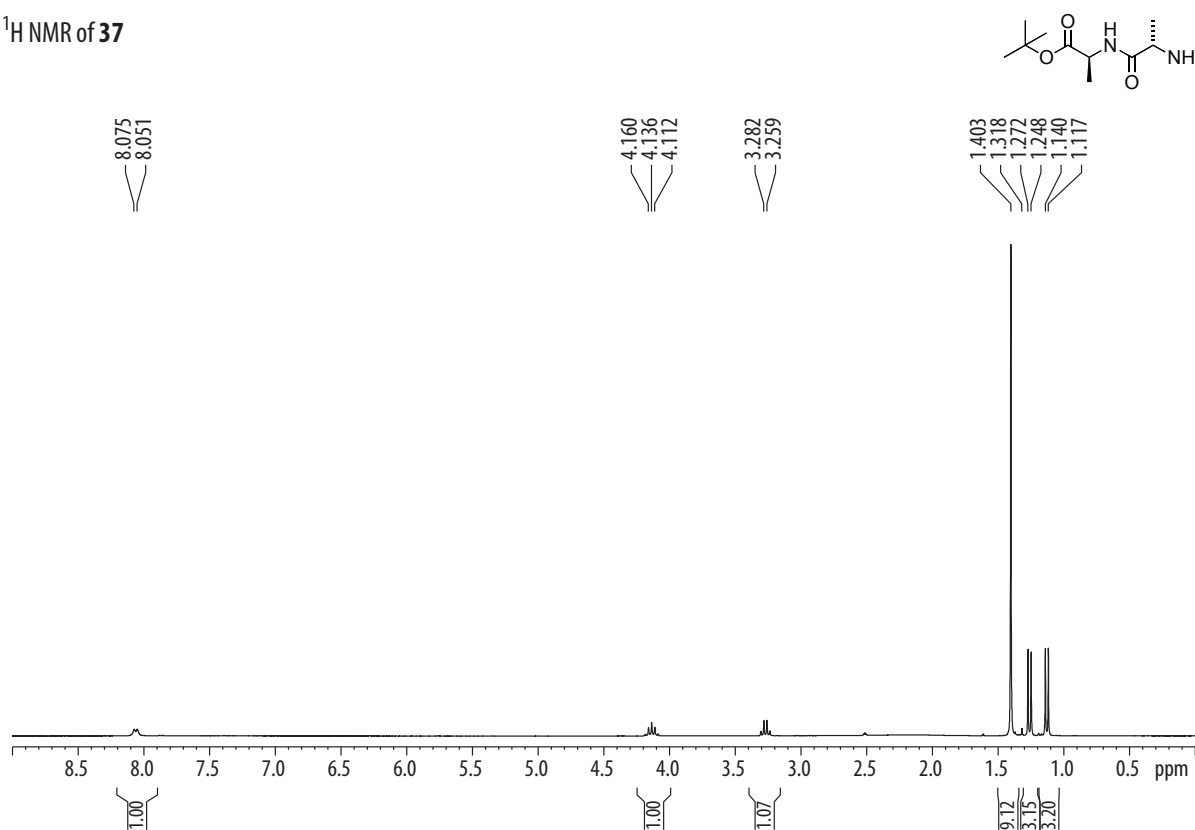
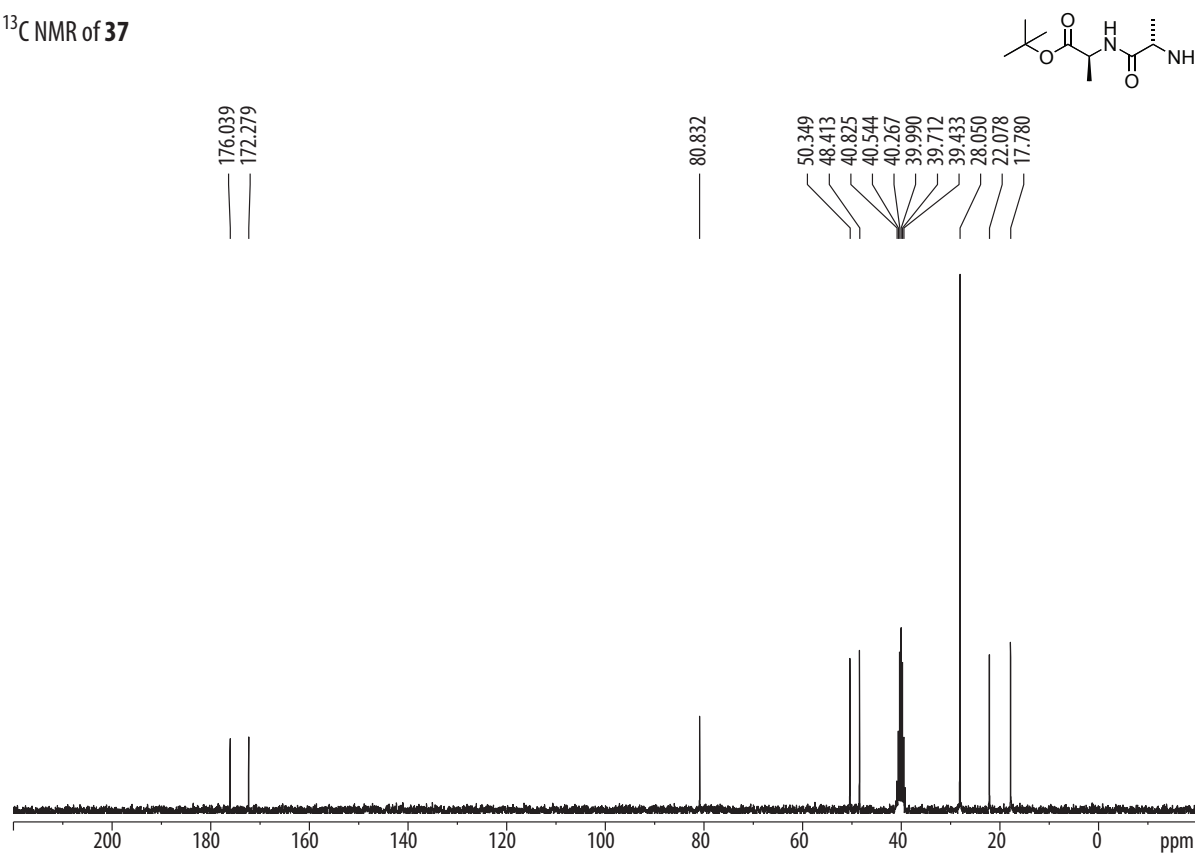
## 7 Spectra Appendix

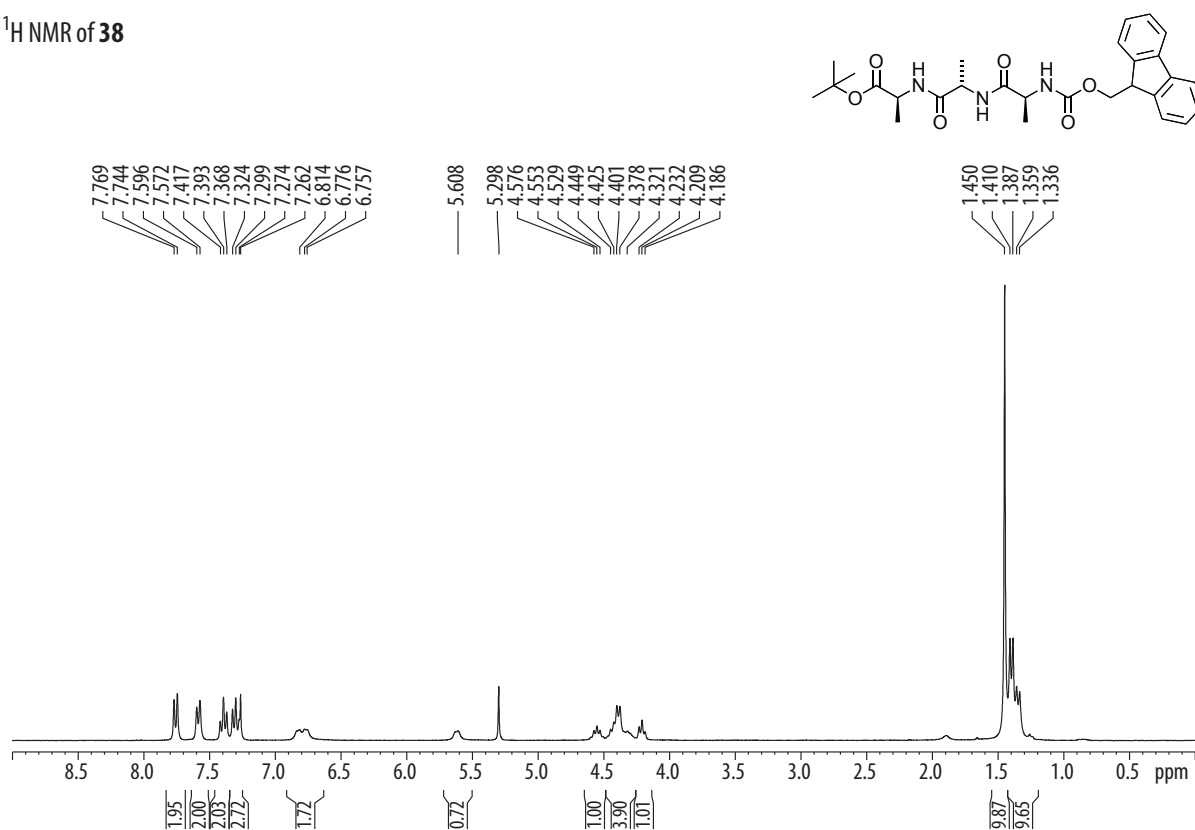
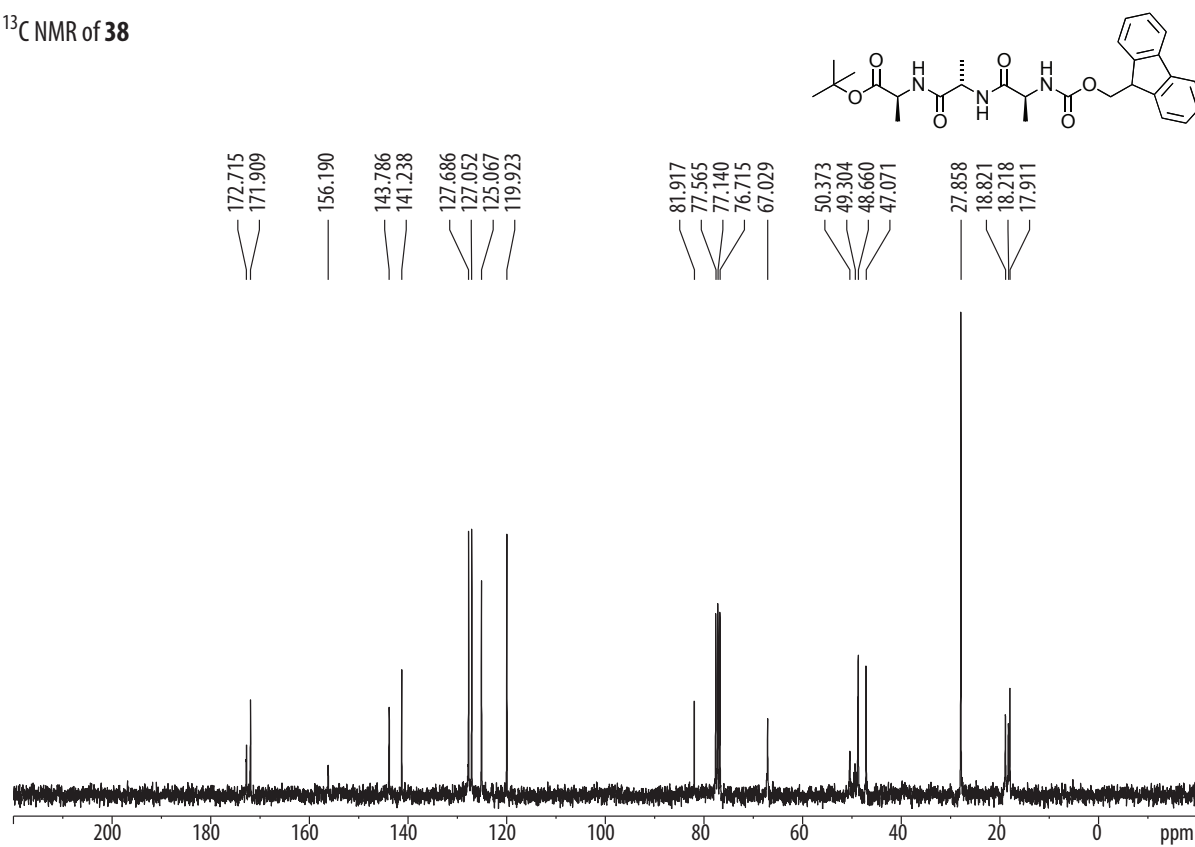


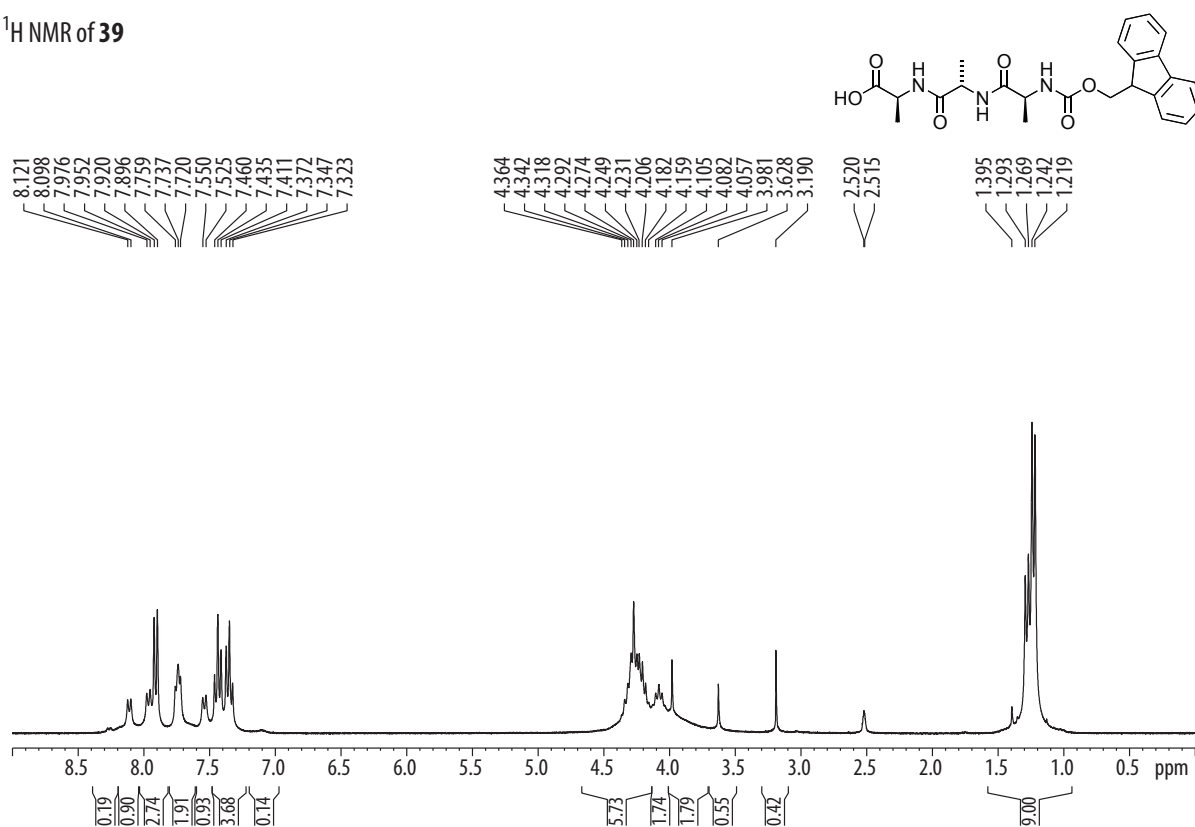
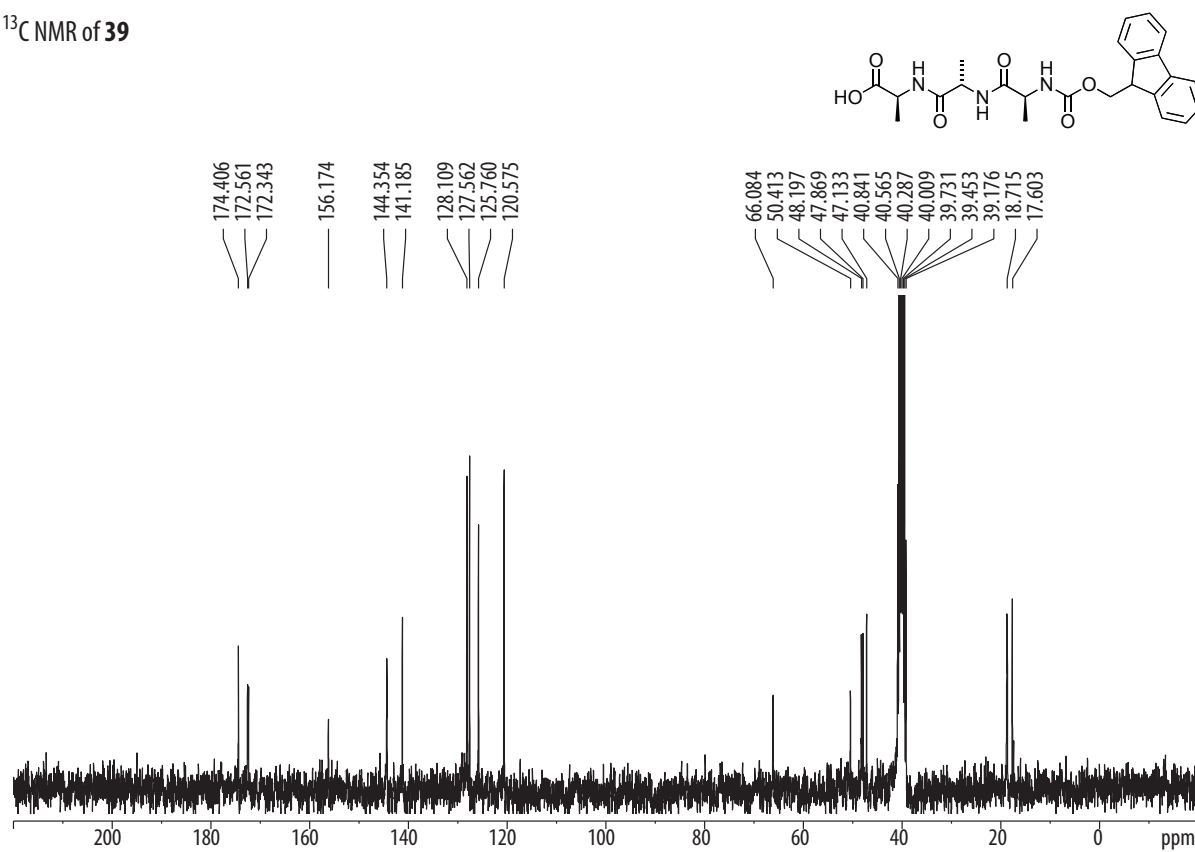


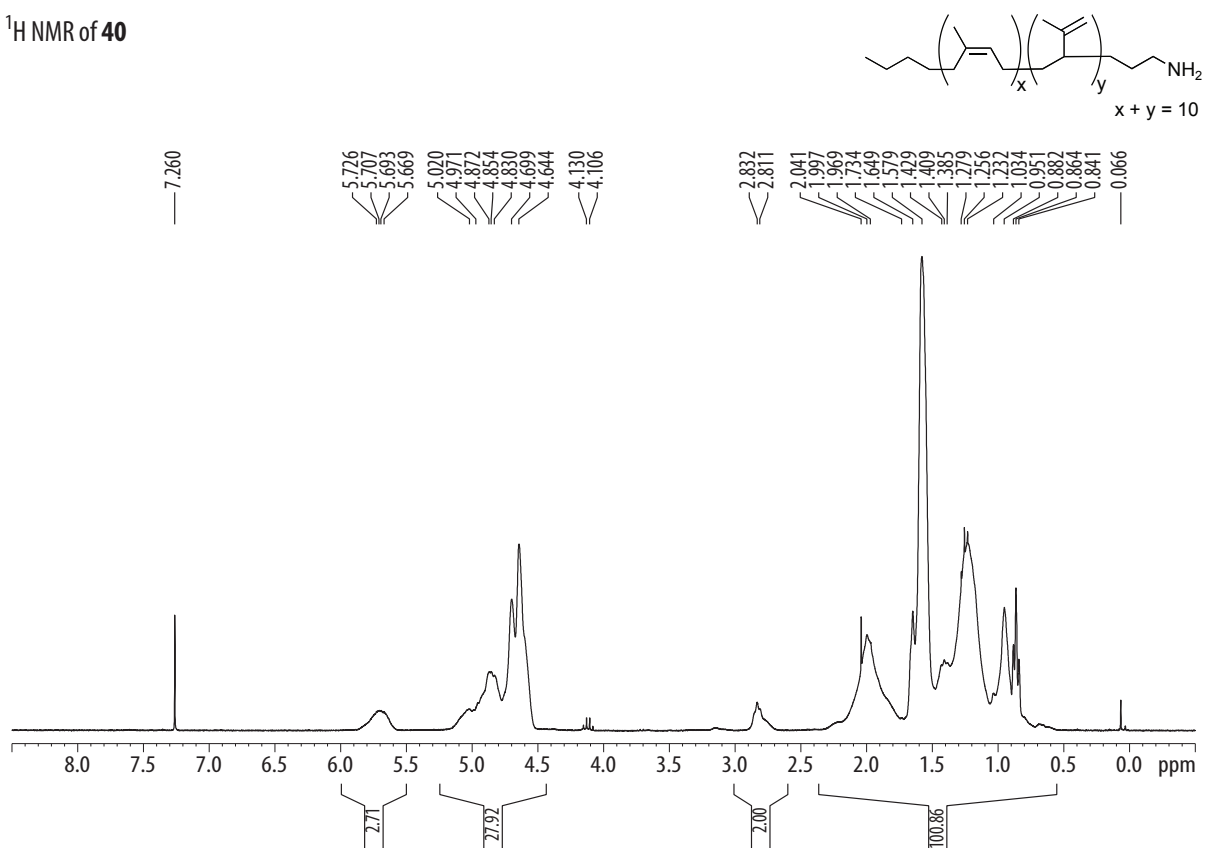
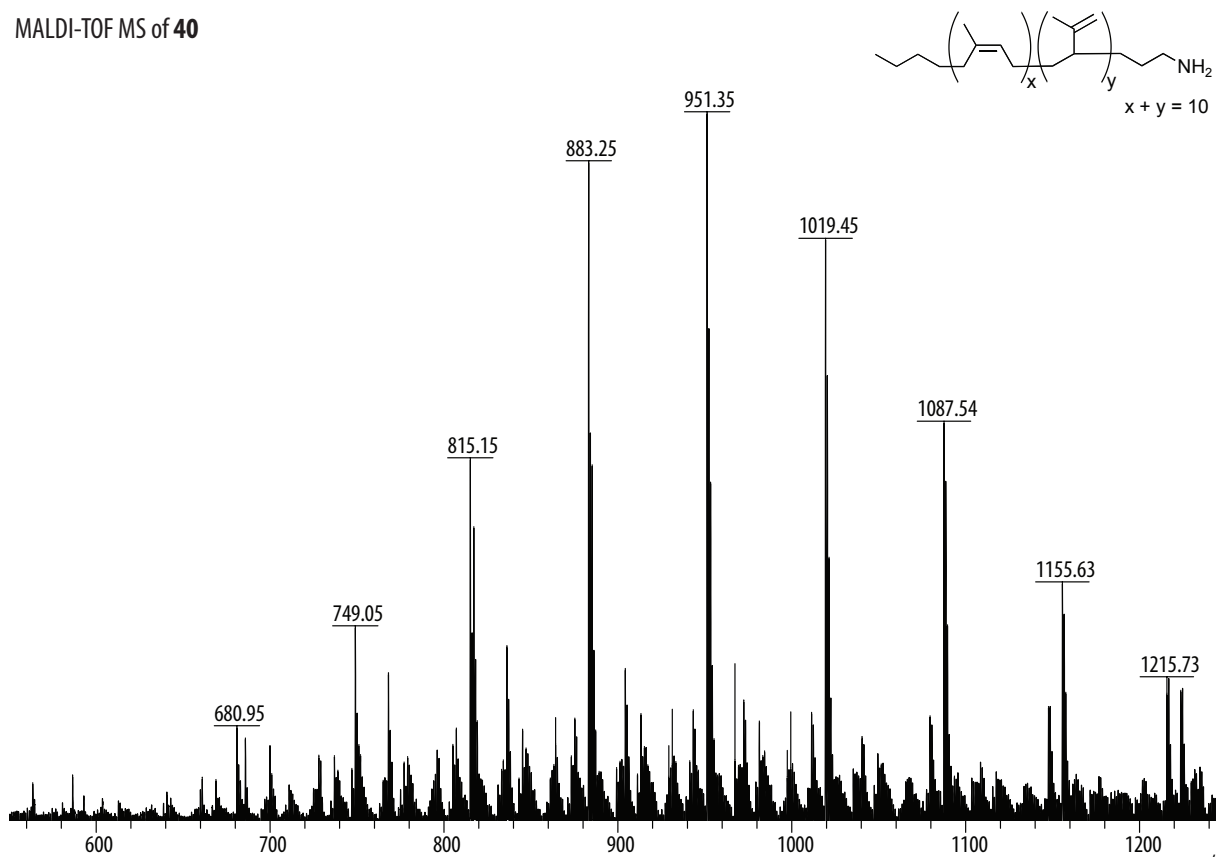
<sup>1</sup>H NMR of 35<sup>13</sup>C NMR of 35

<sup>1</sup>H NMR of **36**<sup>13</sup>C NMR of **36**

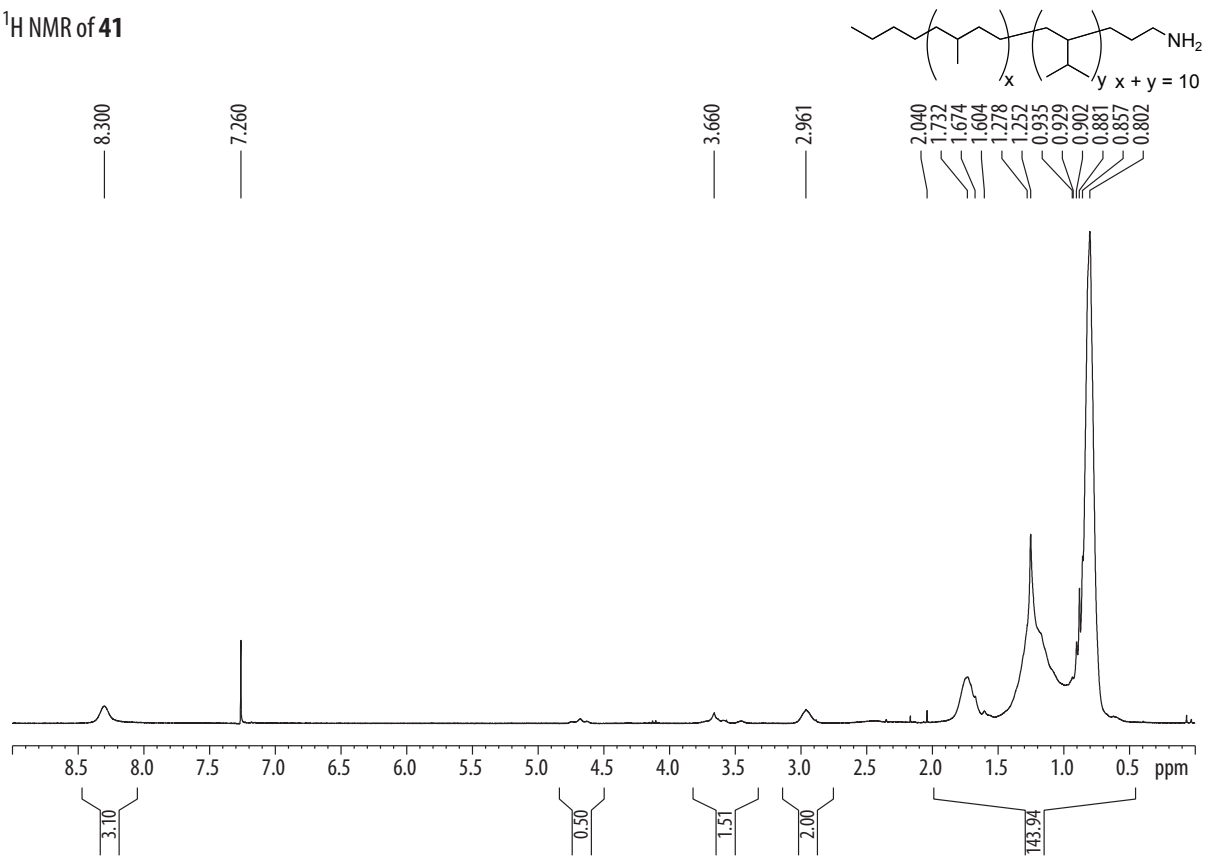
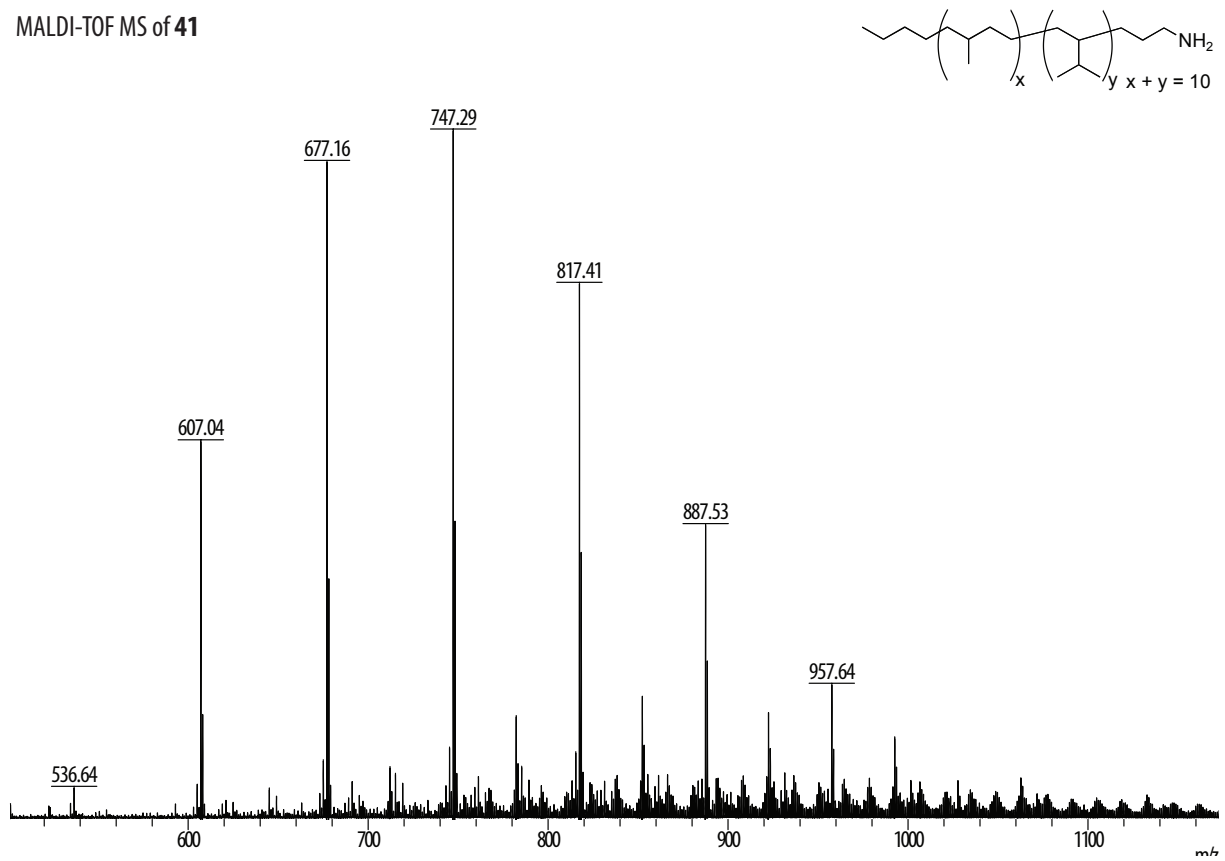
<sup>1</sup>H NMR of **37**<sup>13</sup>C NMR of **37**

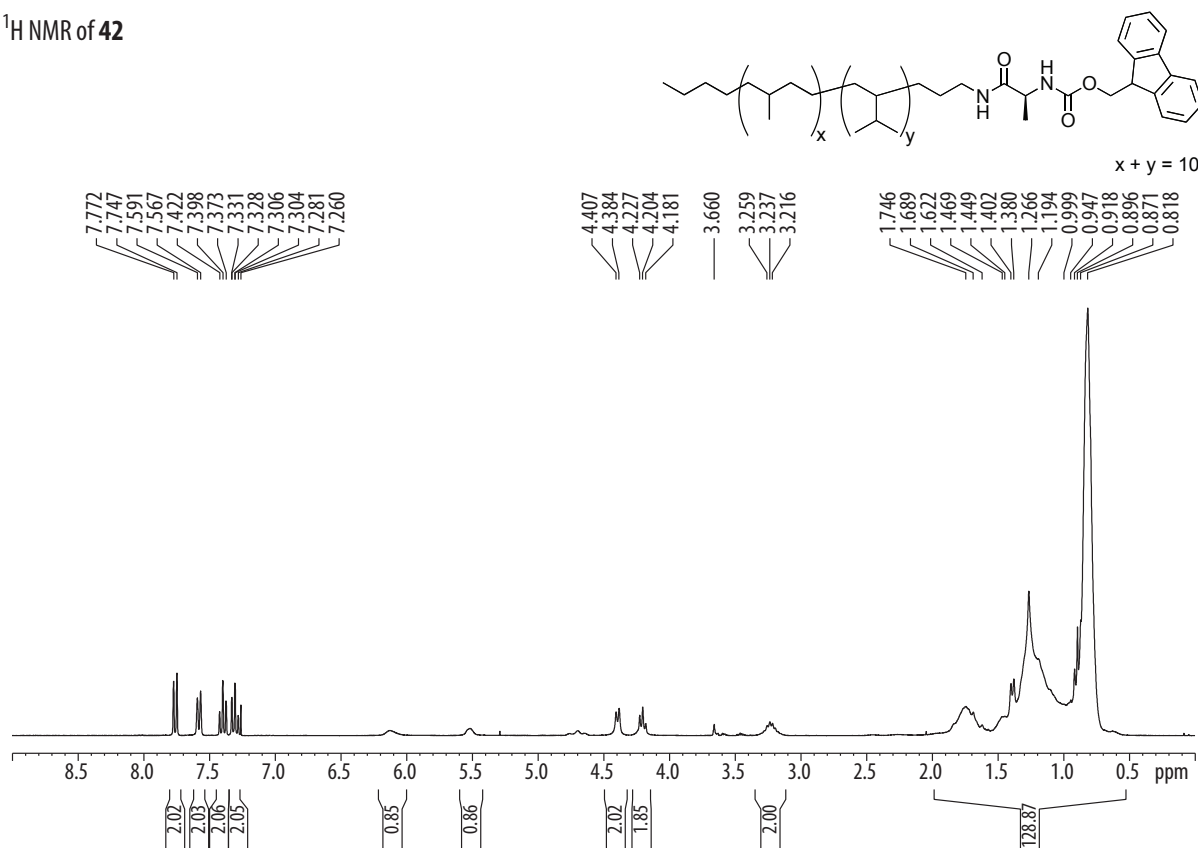
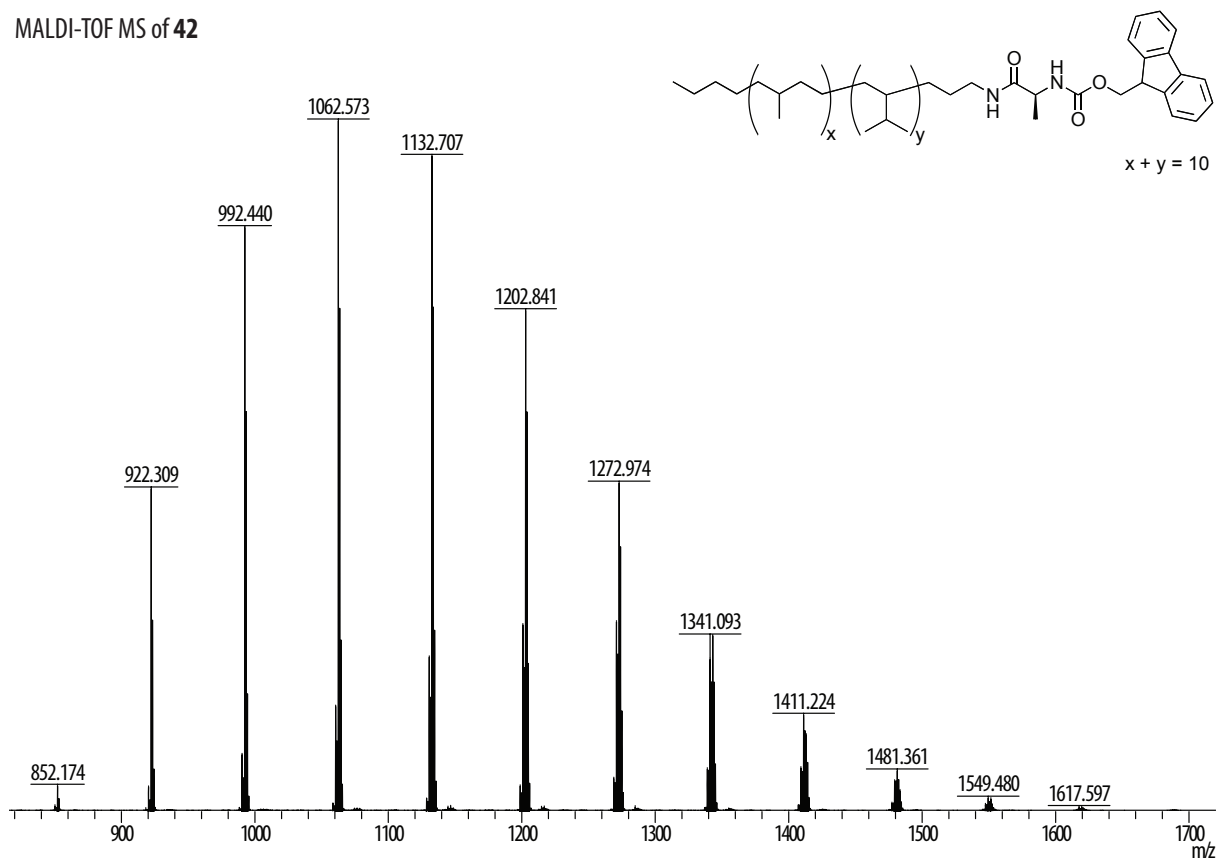
<sup>1</sup>H NMR of 38<sup>13</sup>C NMR of 38

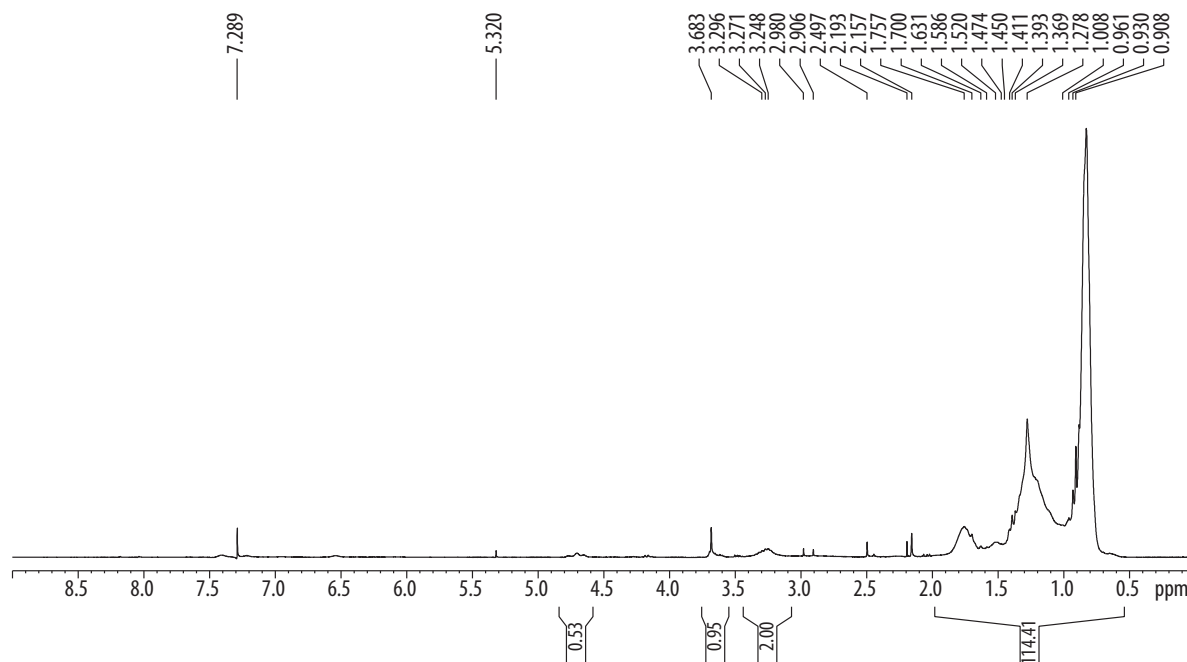
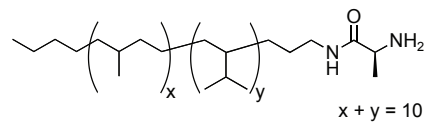
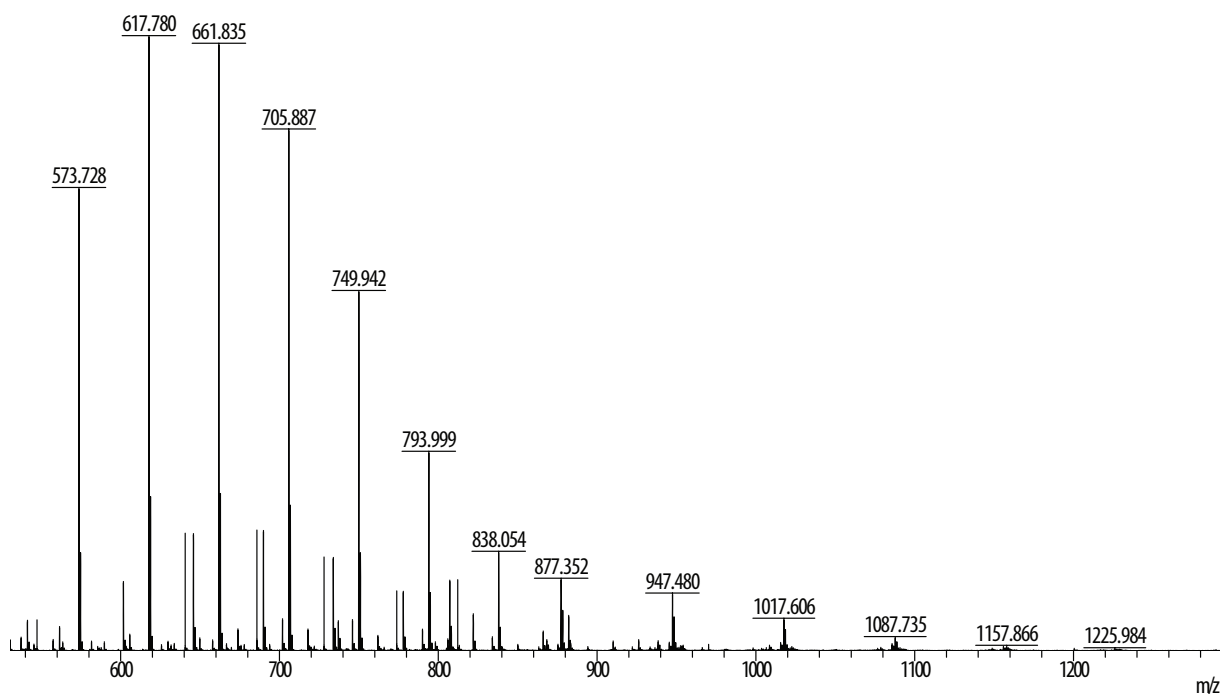
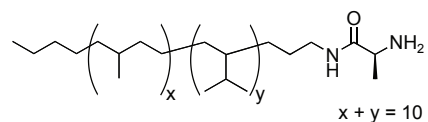
<sup>1</sup>H NMR of 39<sup>13</sup>C NMR of 39

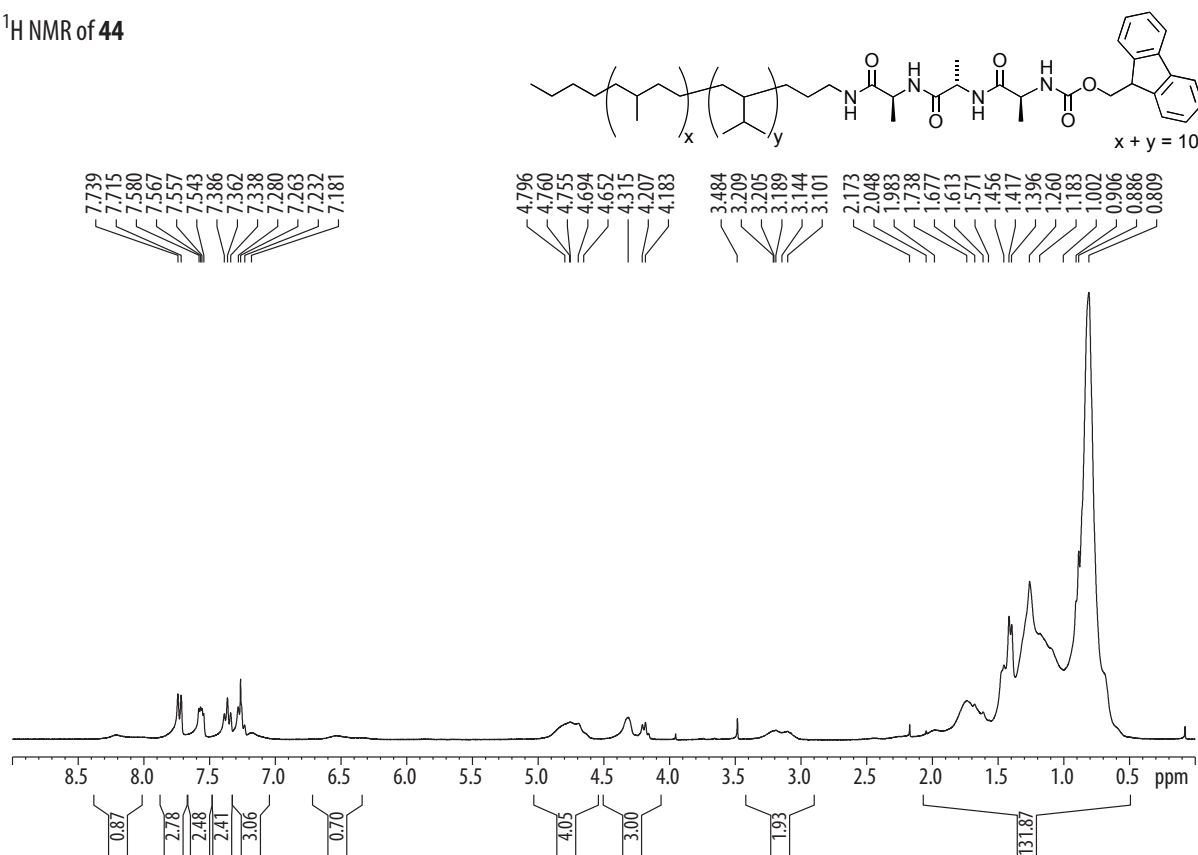
$^1\text{H}$  NMR of **40**MALDI-TOF MS of **40**



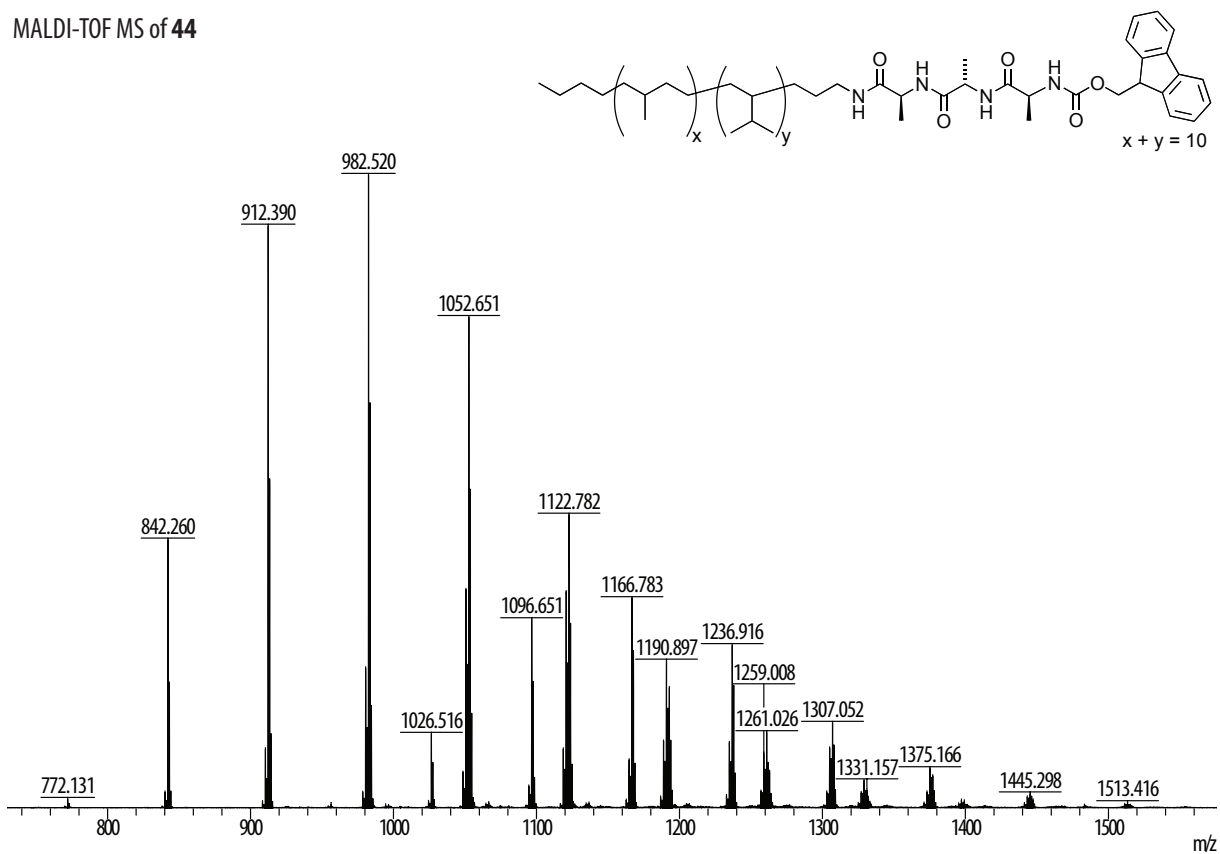
$^1\text{H}$  NMR of **41**MALDI-TOF MS of **41**

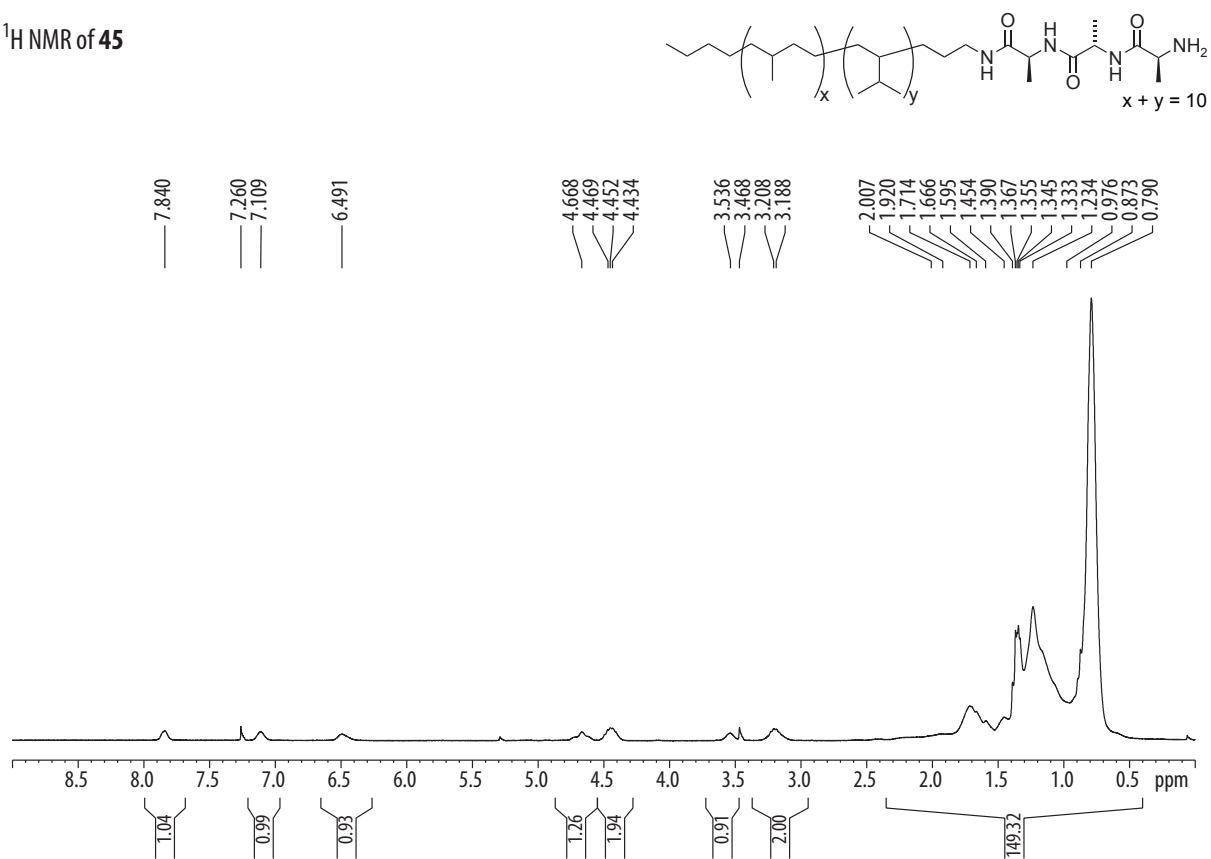
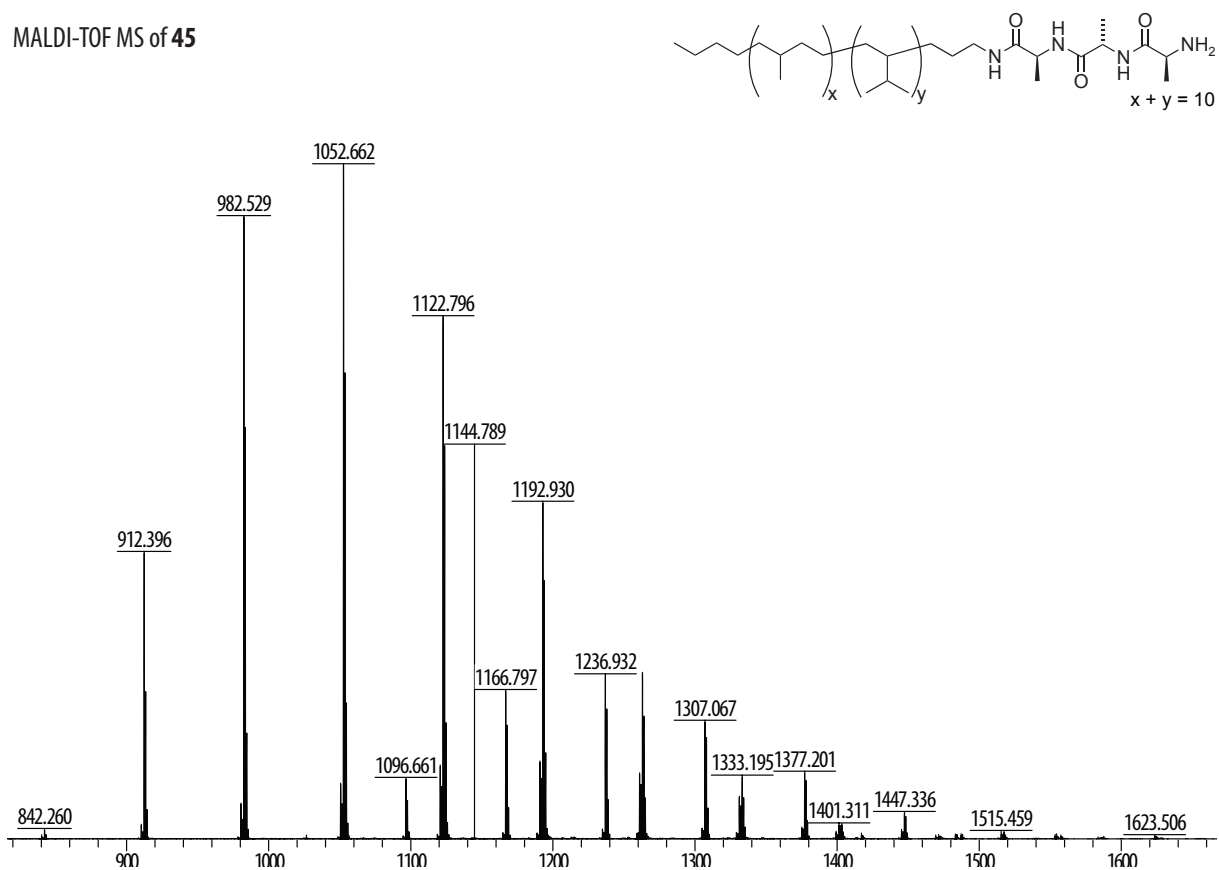
$^1\text{H}$  NMR of **42**MALDI-TOF MS of **42**

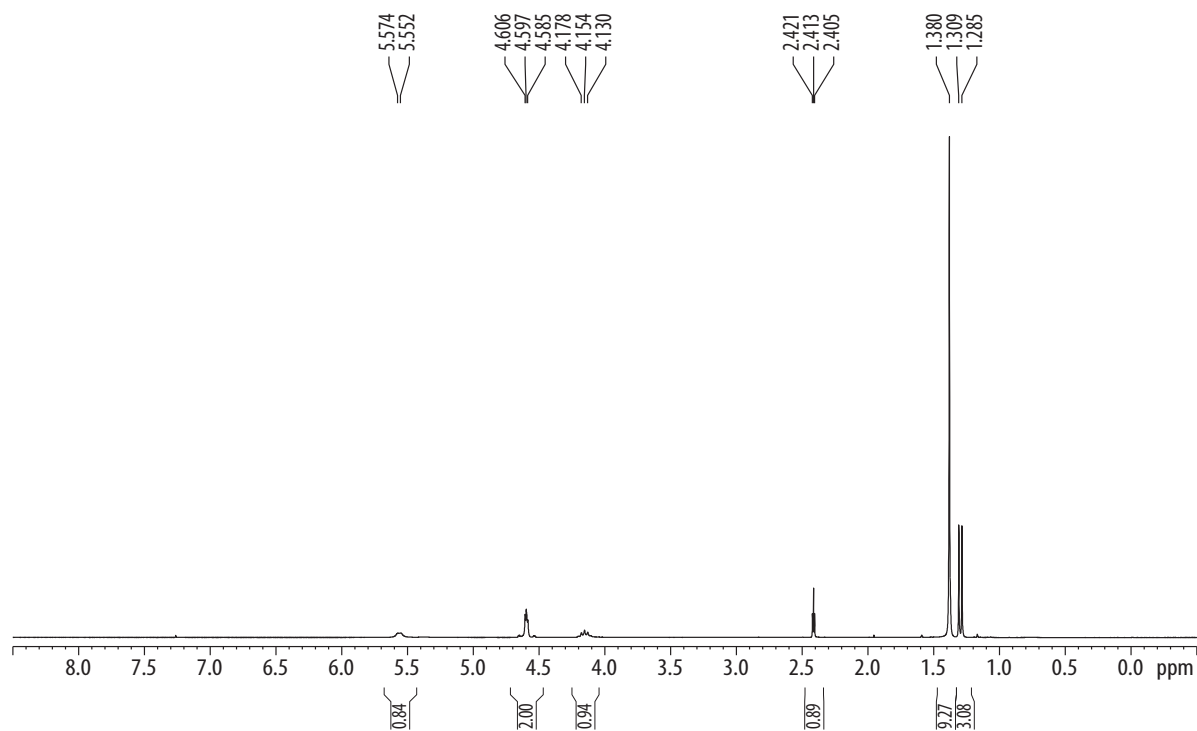
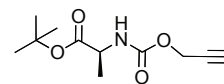
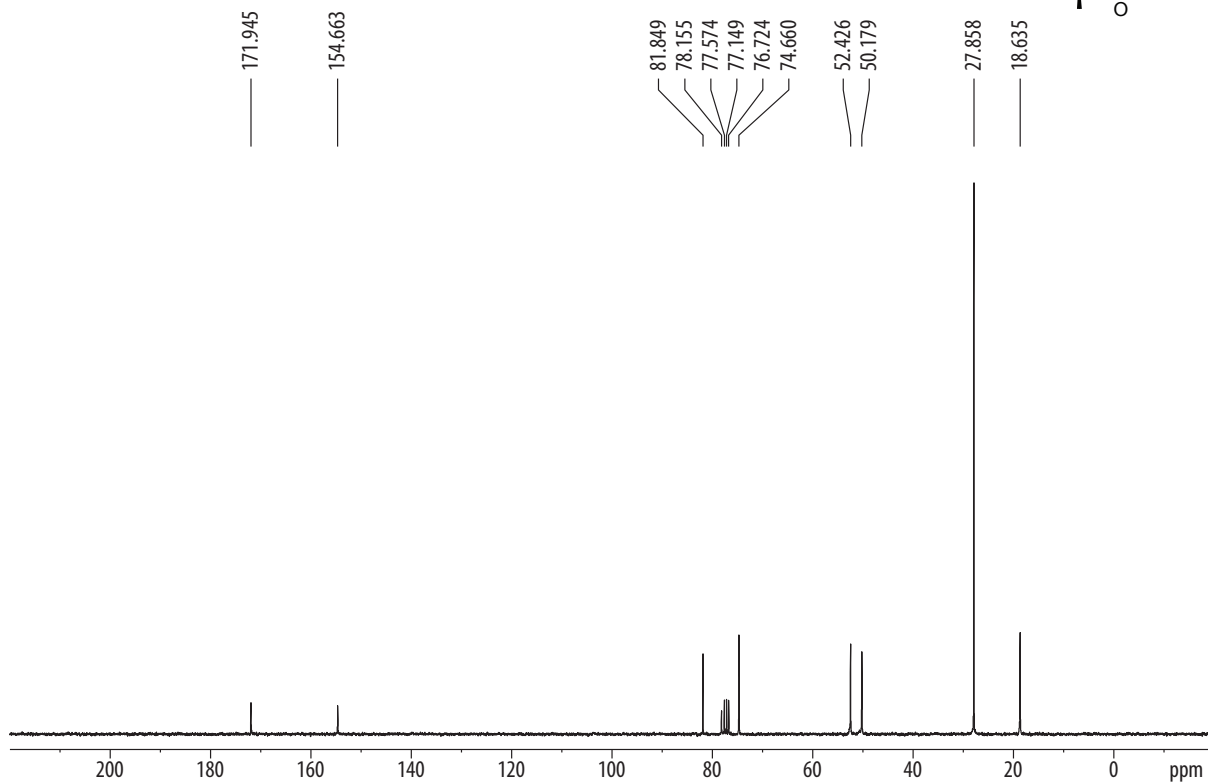
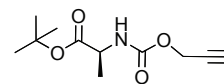
$^1\text{H}$  NMR of **43**MALDI-TOF MS of **43**

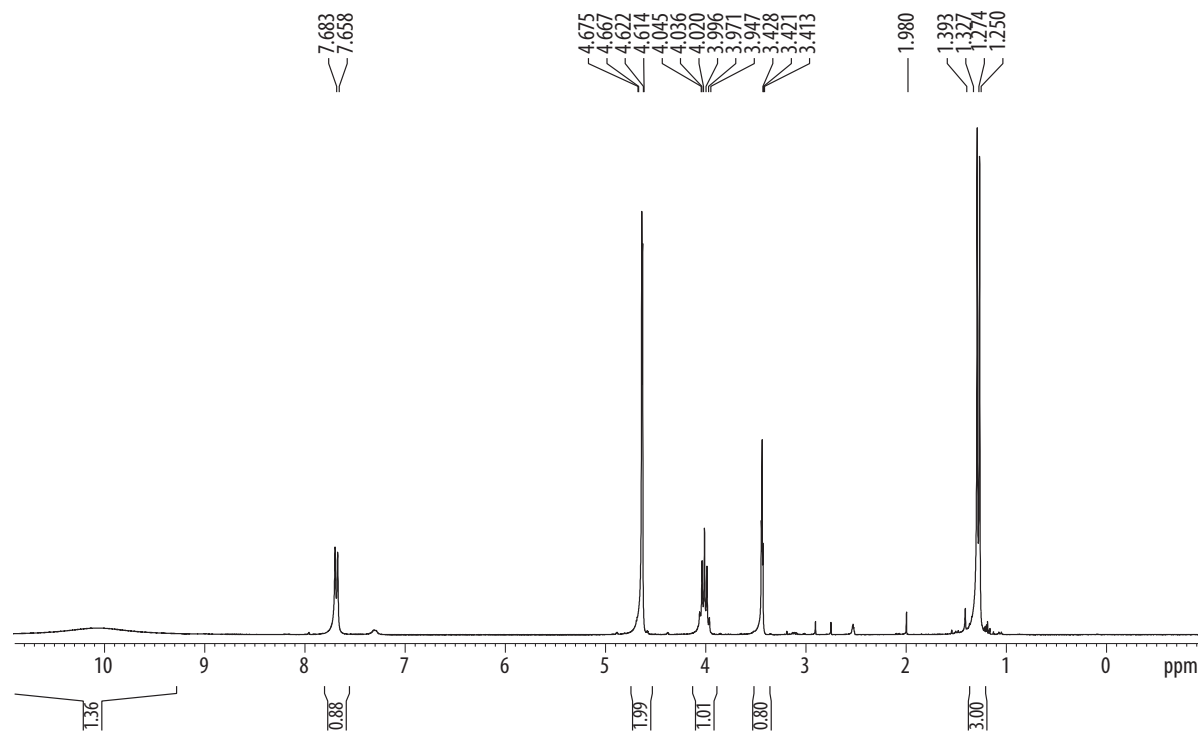
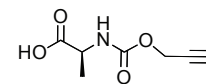
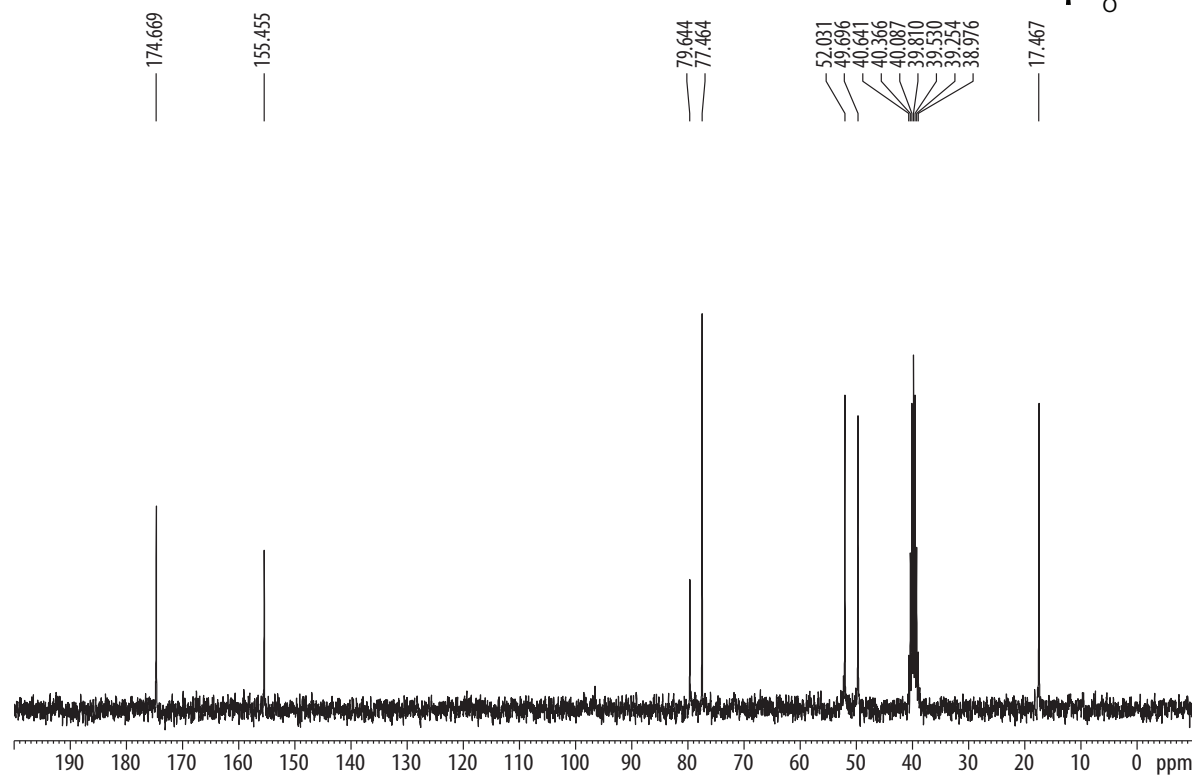
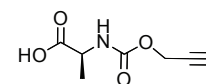
<sup>1</sup>H NMR of 44

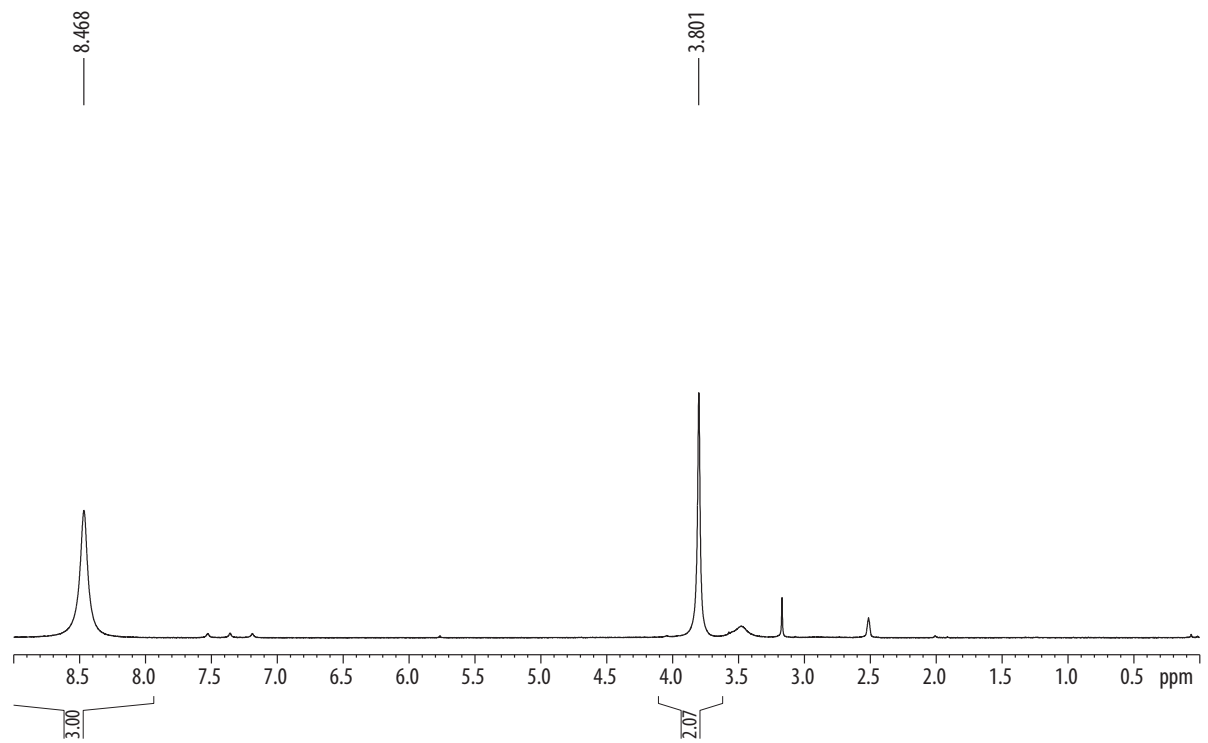
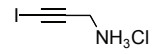
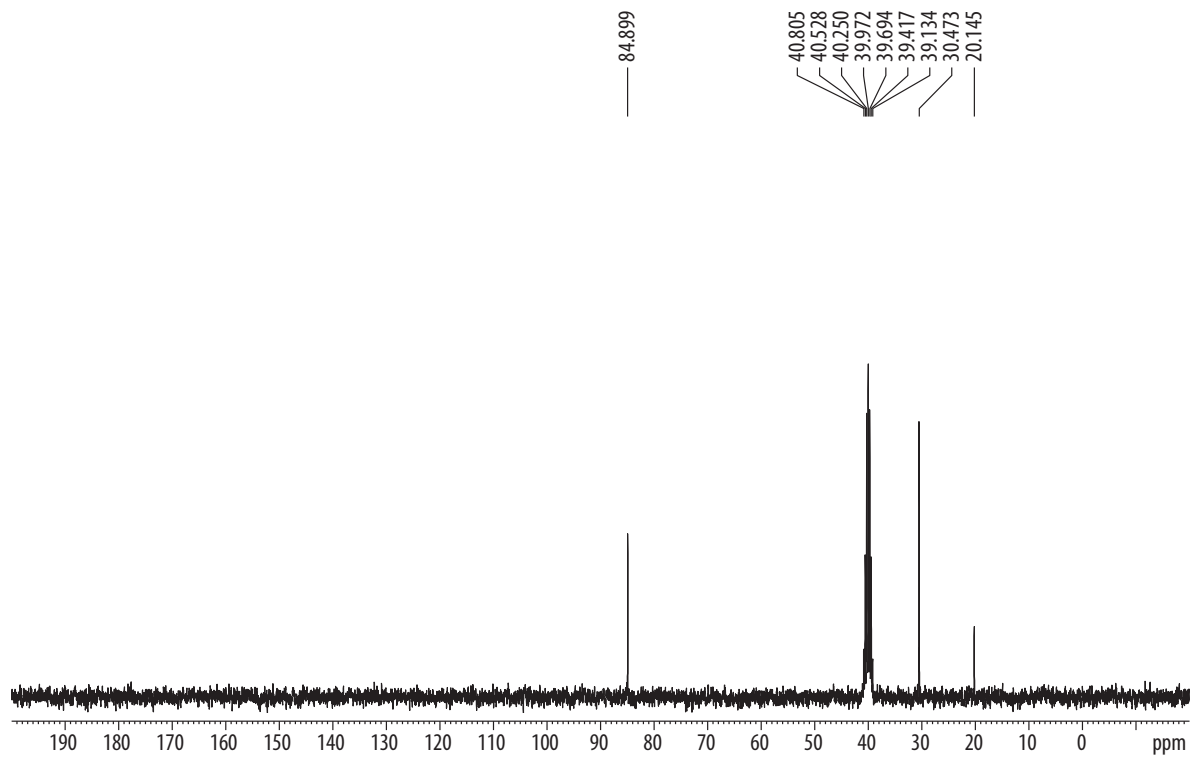
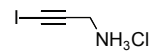
## MALDI-TOF MS of 44



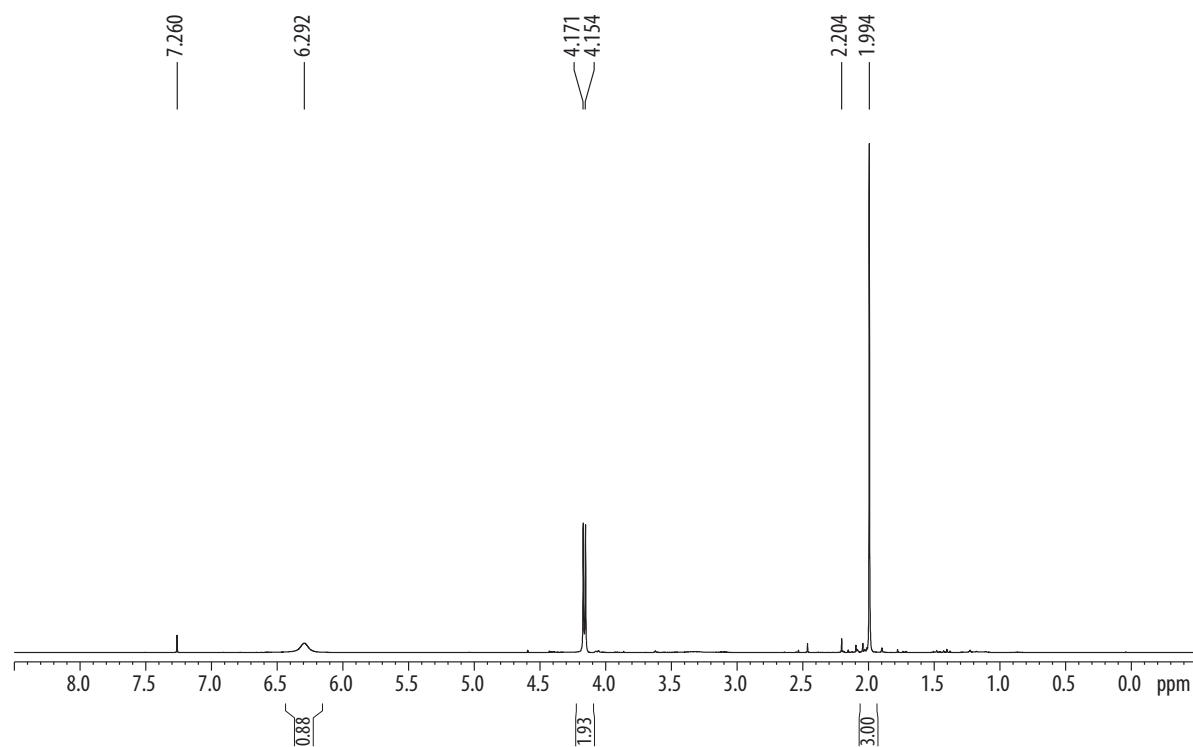
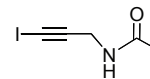
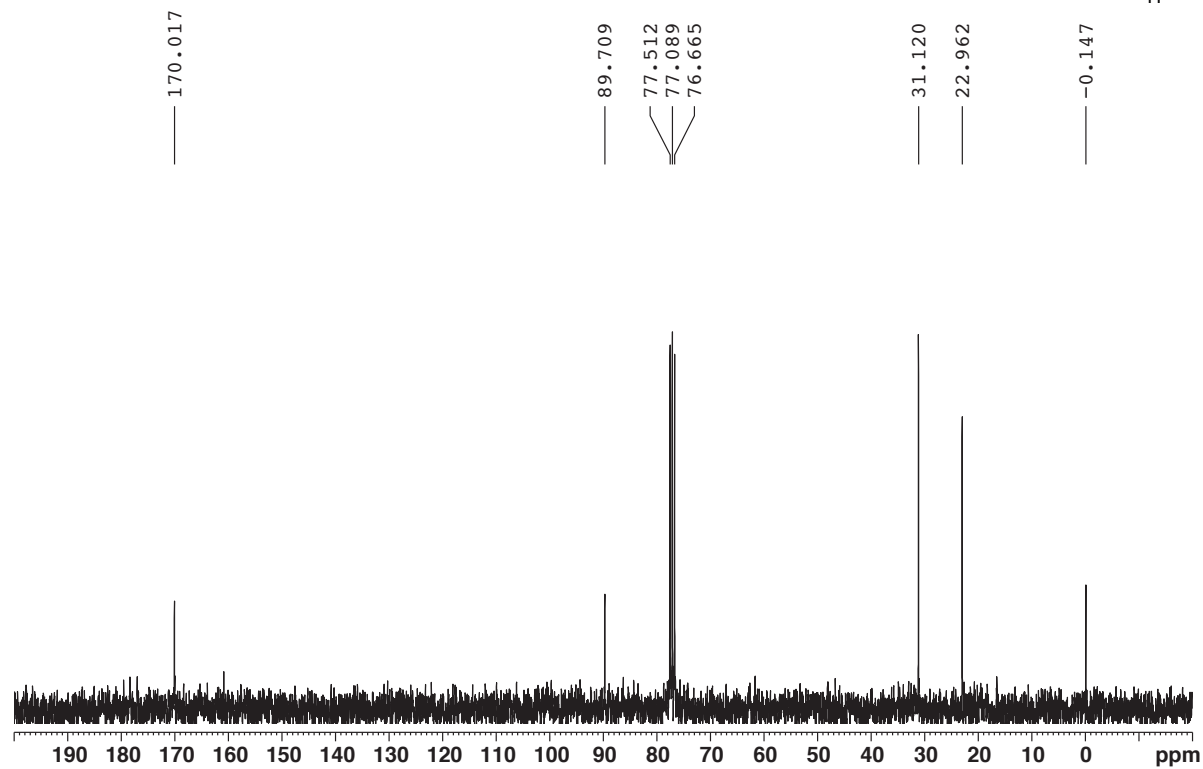
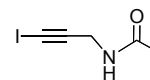
$^1\text{H}$  NMR of **45**MALDI-TOF MS of **45**

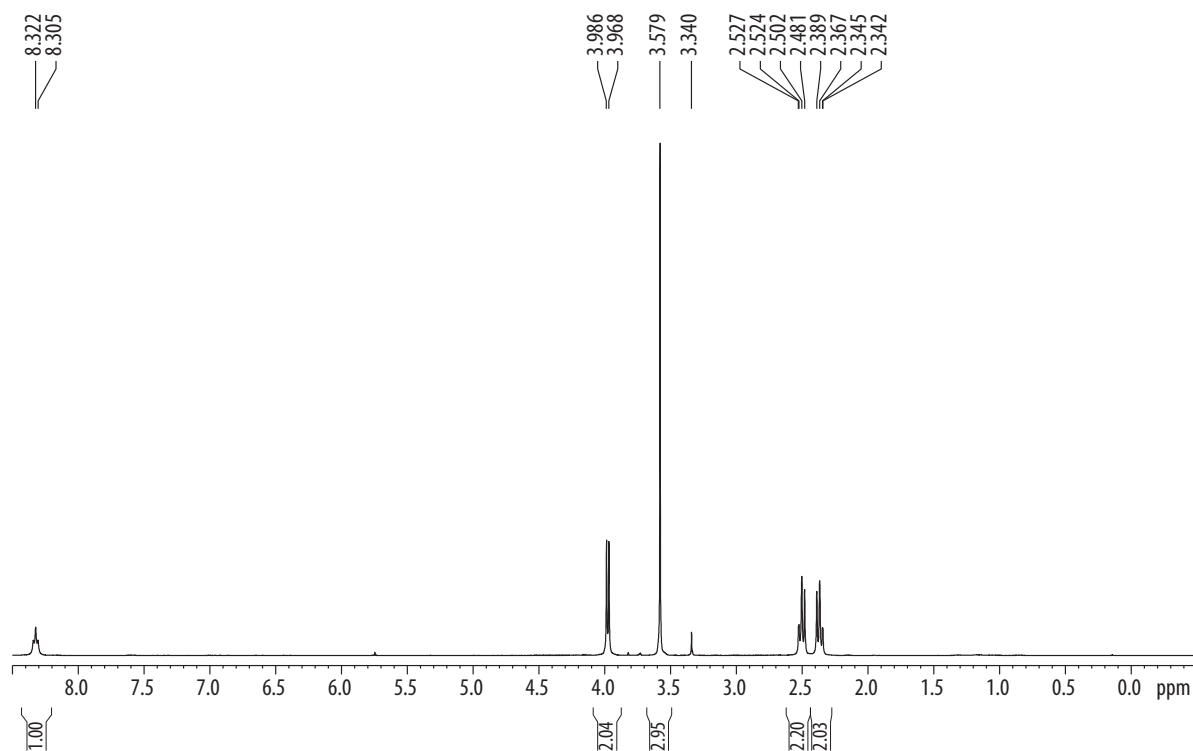
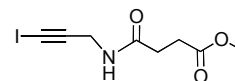
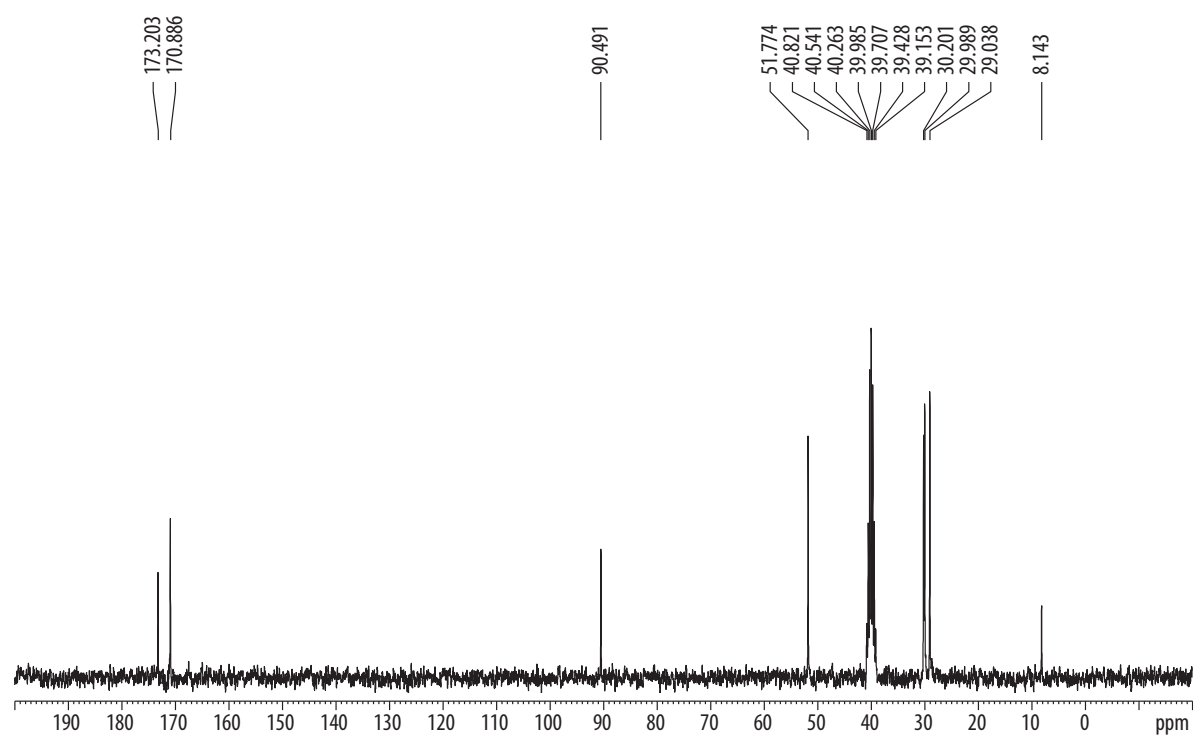
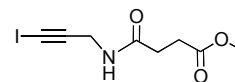
<sup>1</sup>H NMR of **46**<sup>13</sup>C NMR of **46**

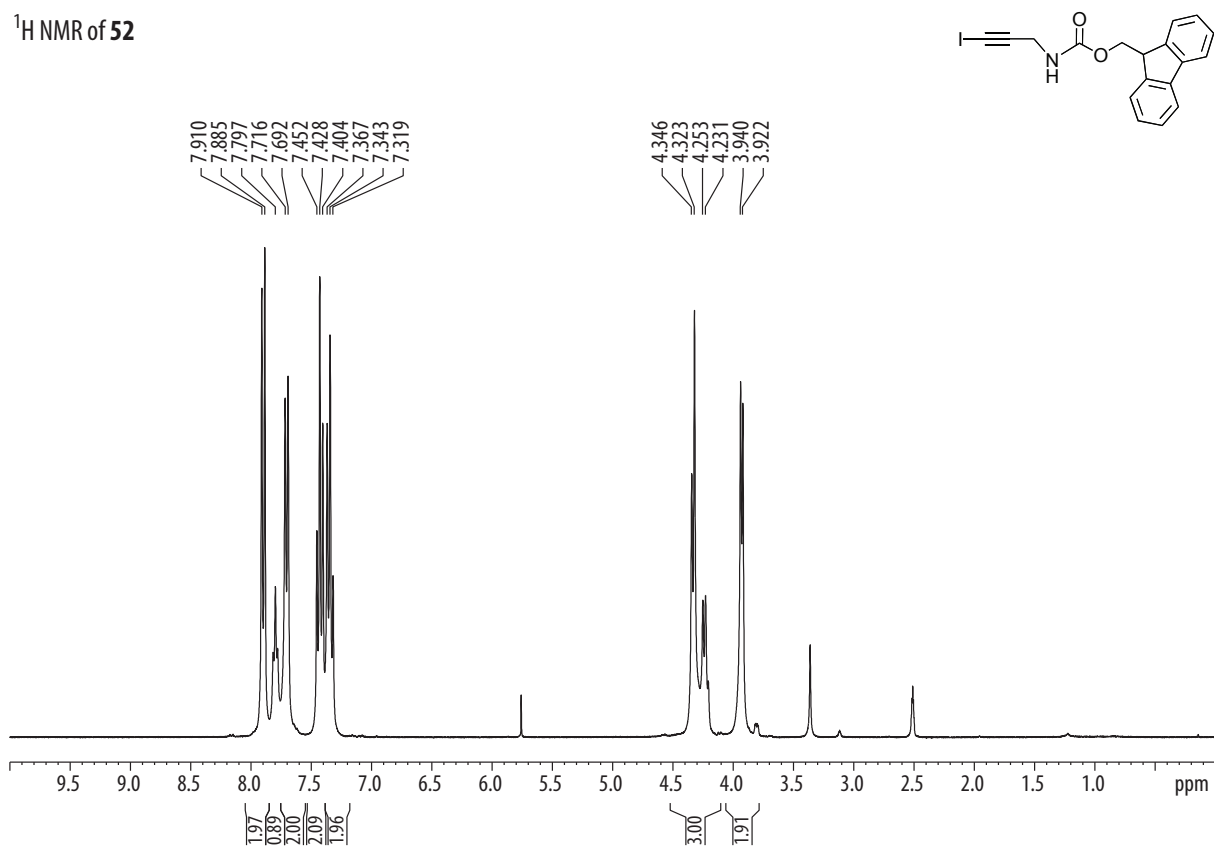
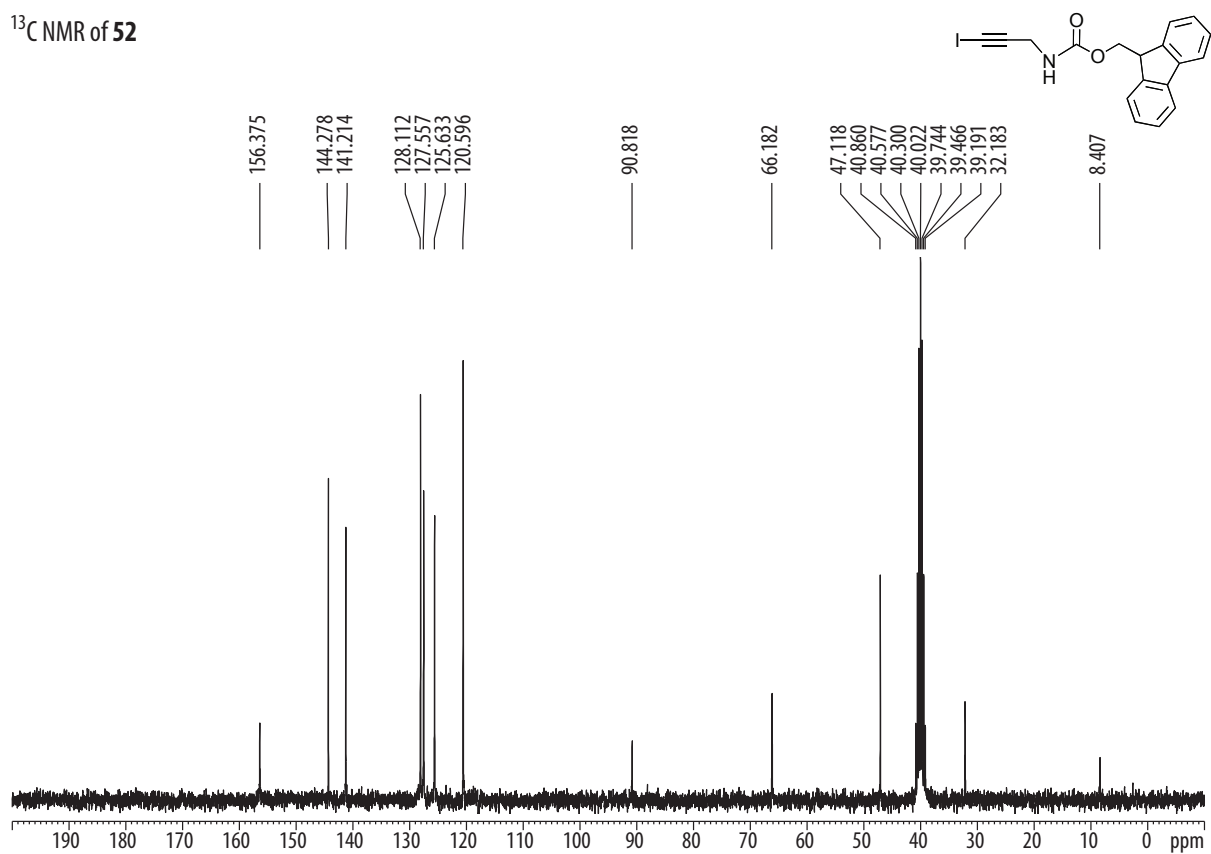
<sup>1</sup>H NMR of **47**<sup>13</sup>C NMR of **47**

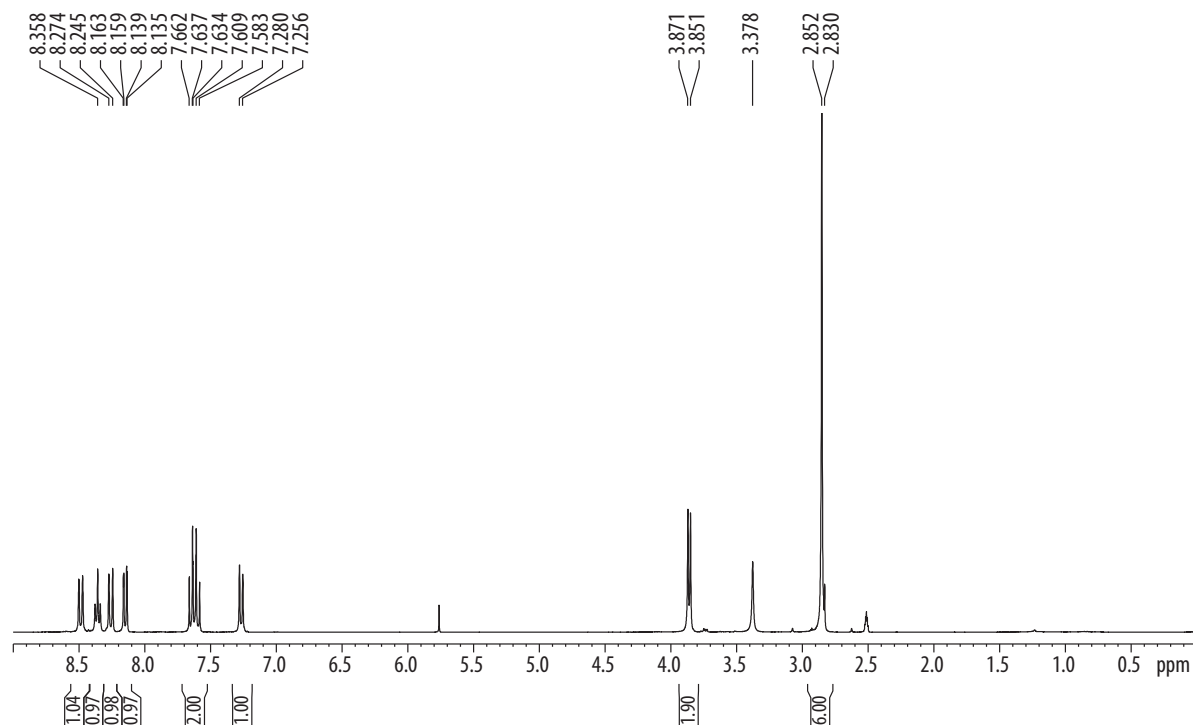
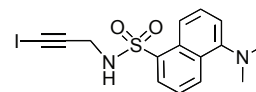
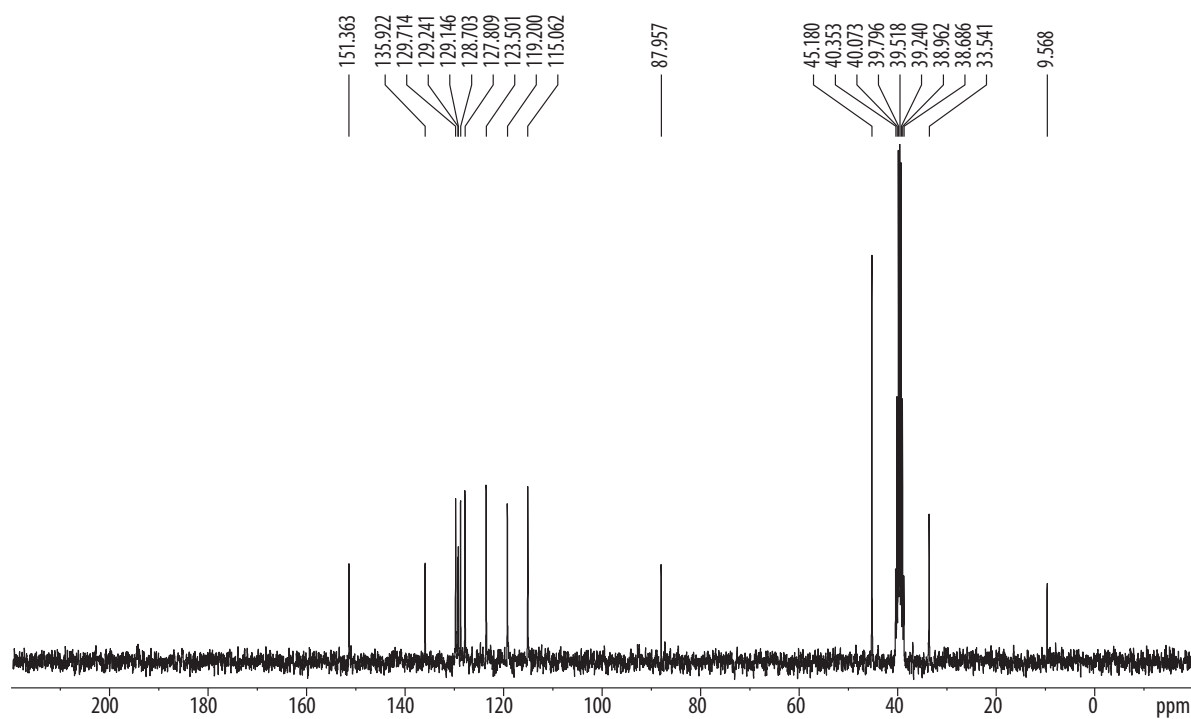
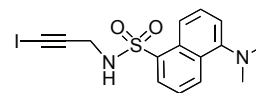
<sup>1</sup>H NMR of **49**<sup>13</sup>C NMR of **49**

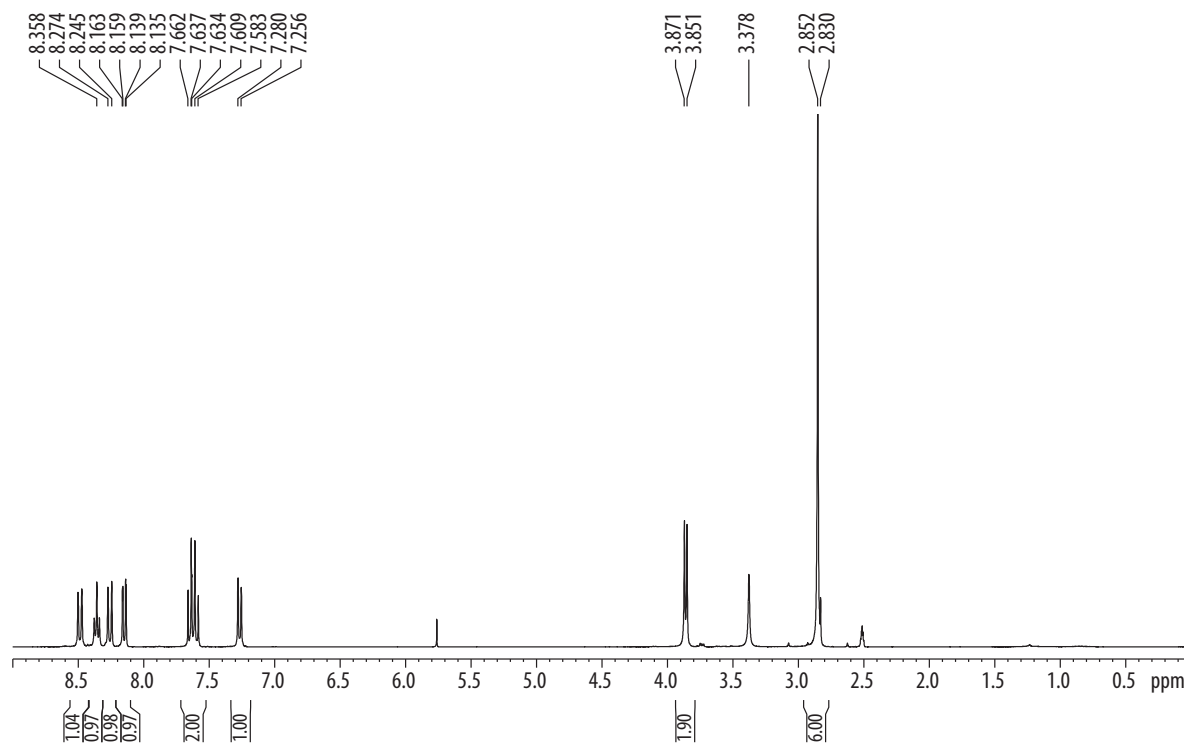
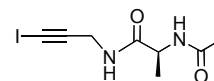
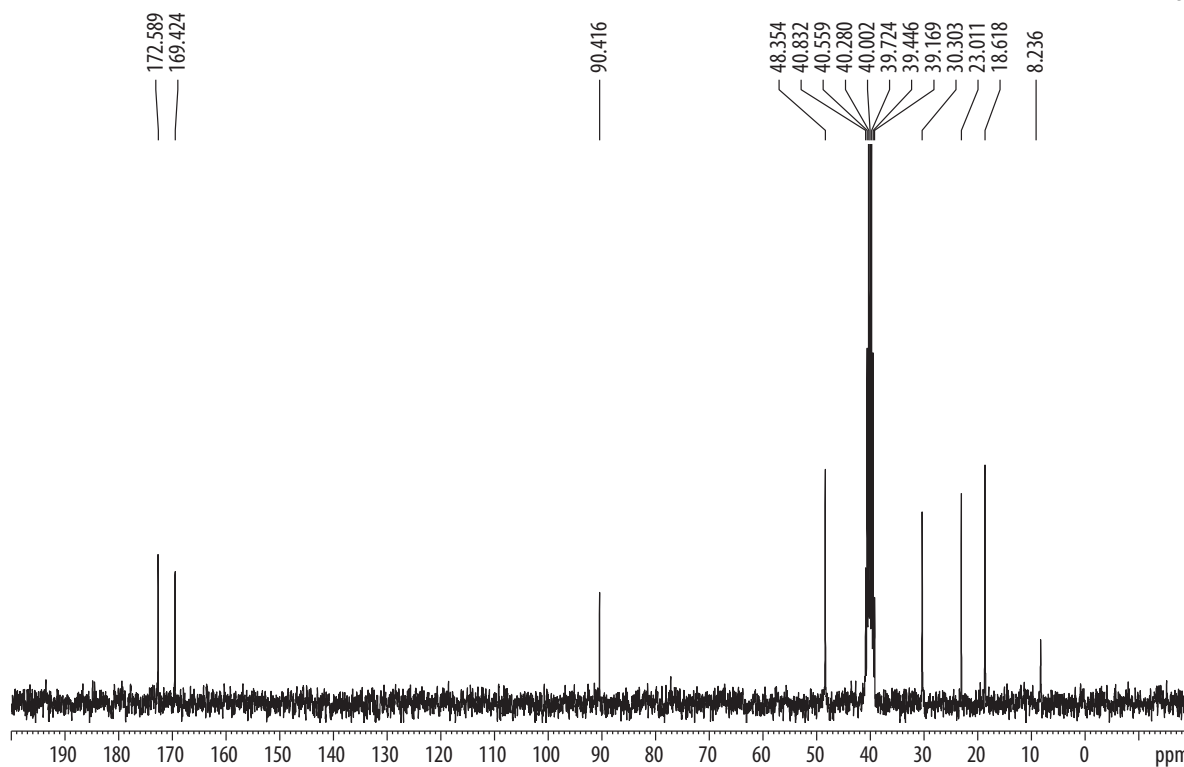
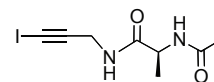


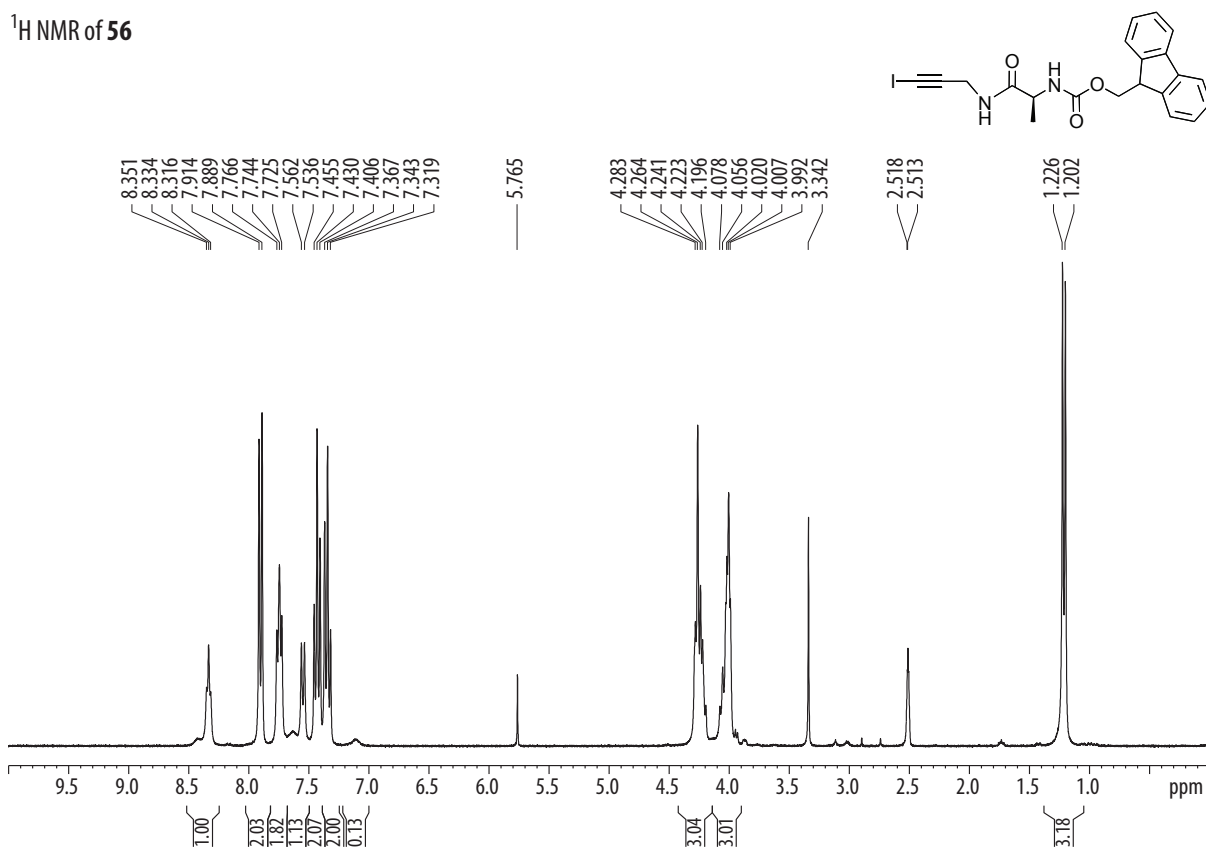
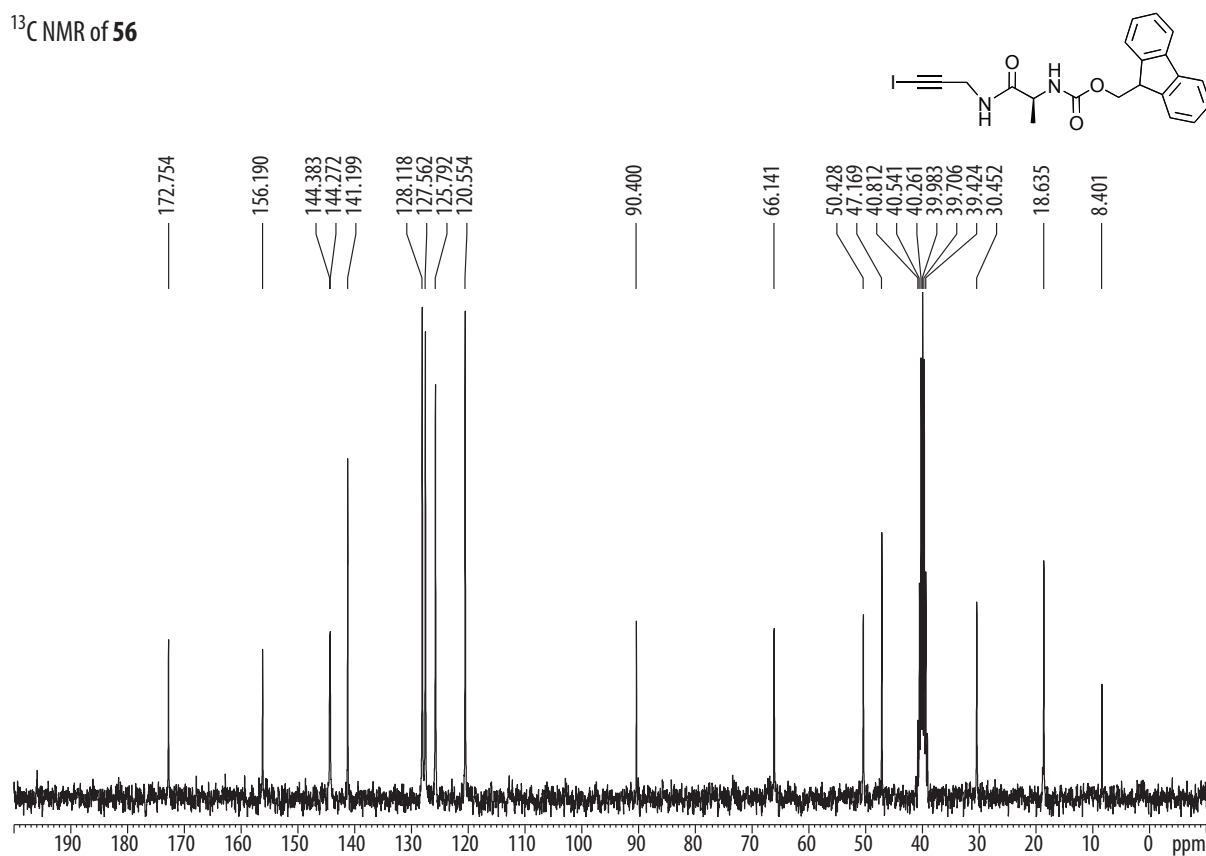
<sup>1</sup>H NMR of **50**<sup>13</sup>C NMR of **50**

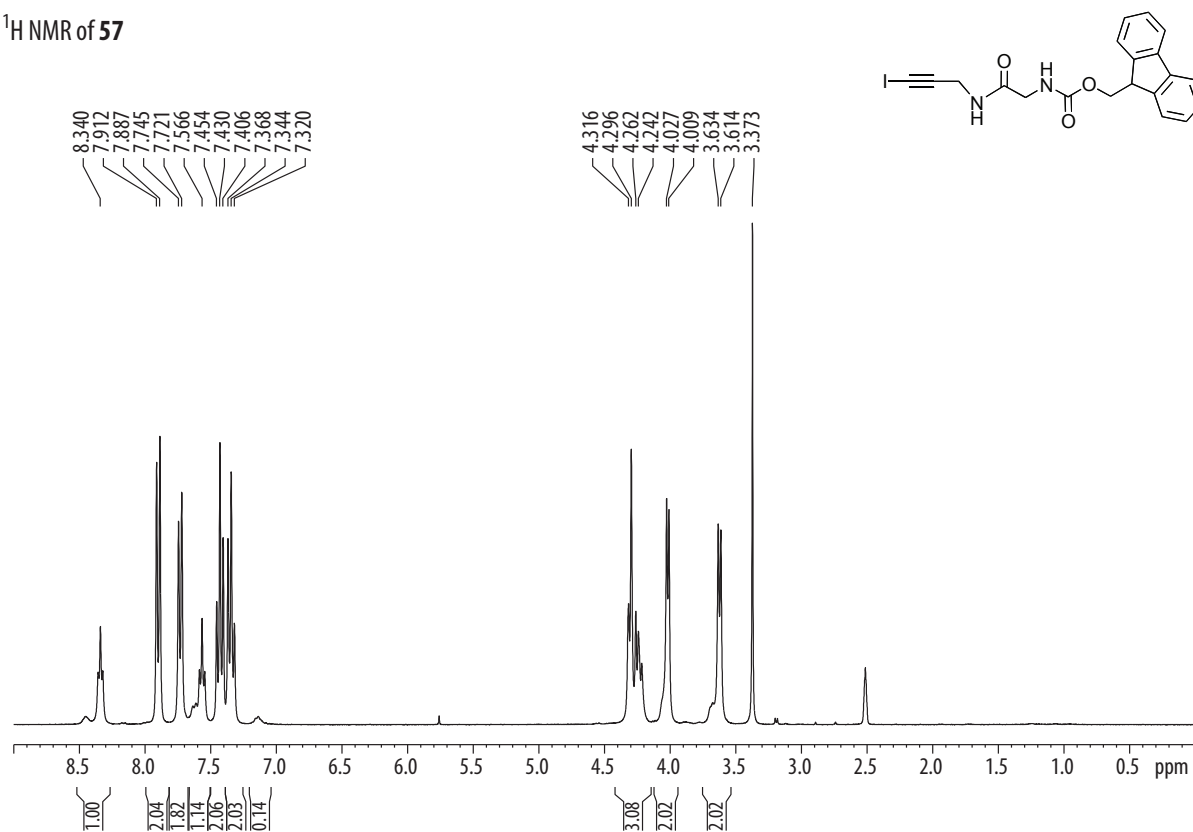
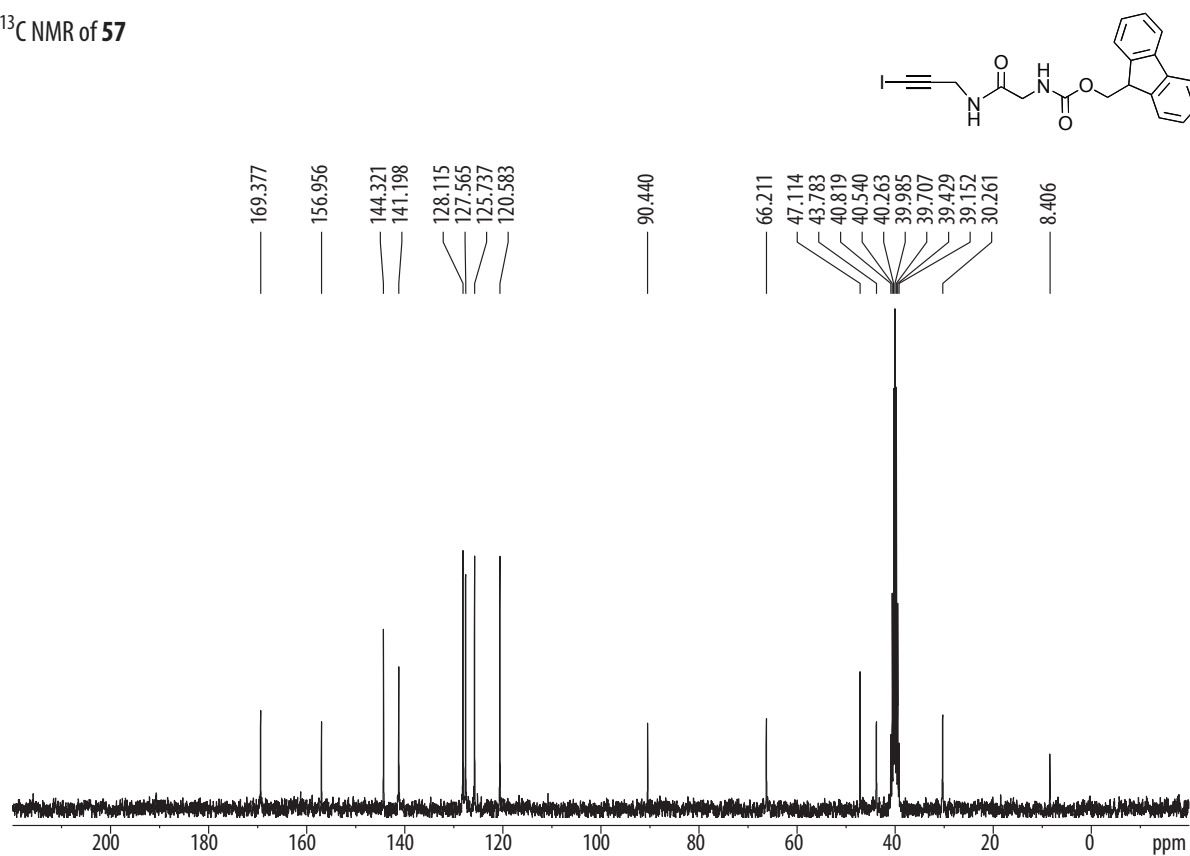
<sup>1</sup>H NMR of 51<sup>13</sup>C NMR of 51

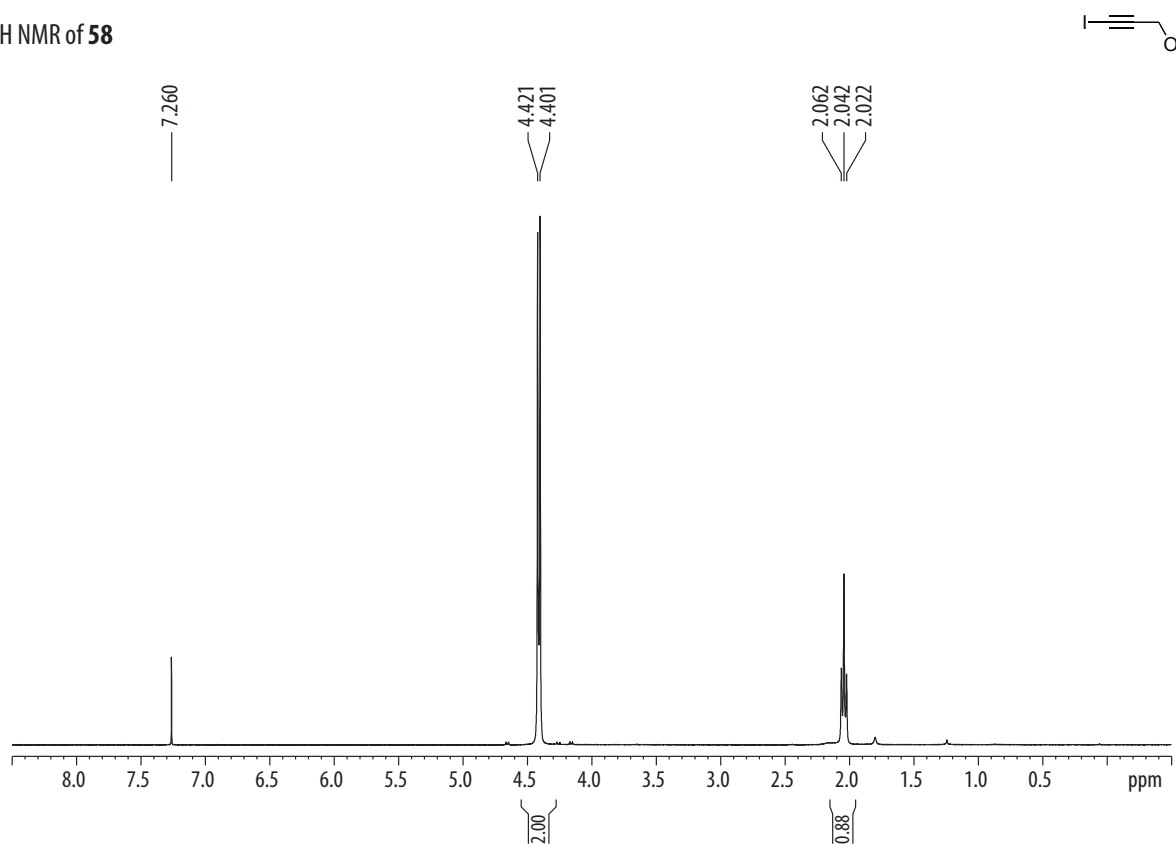
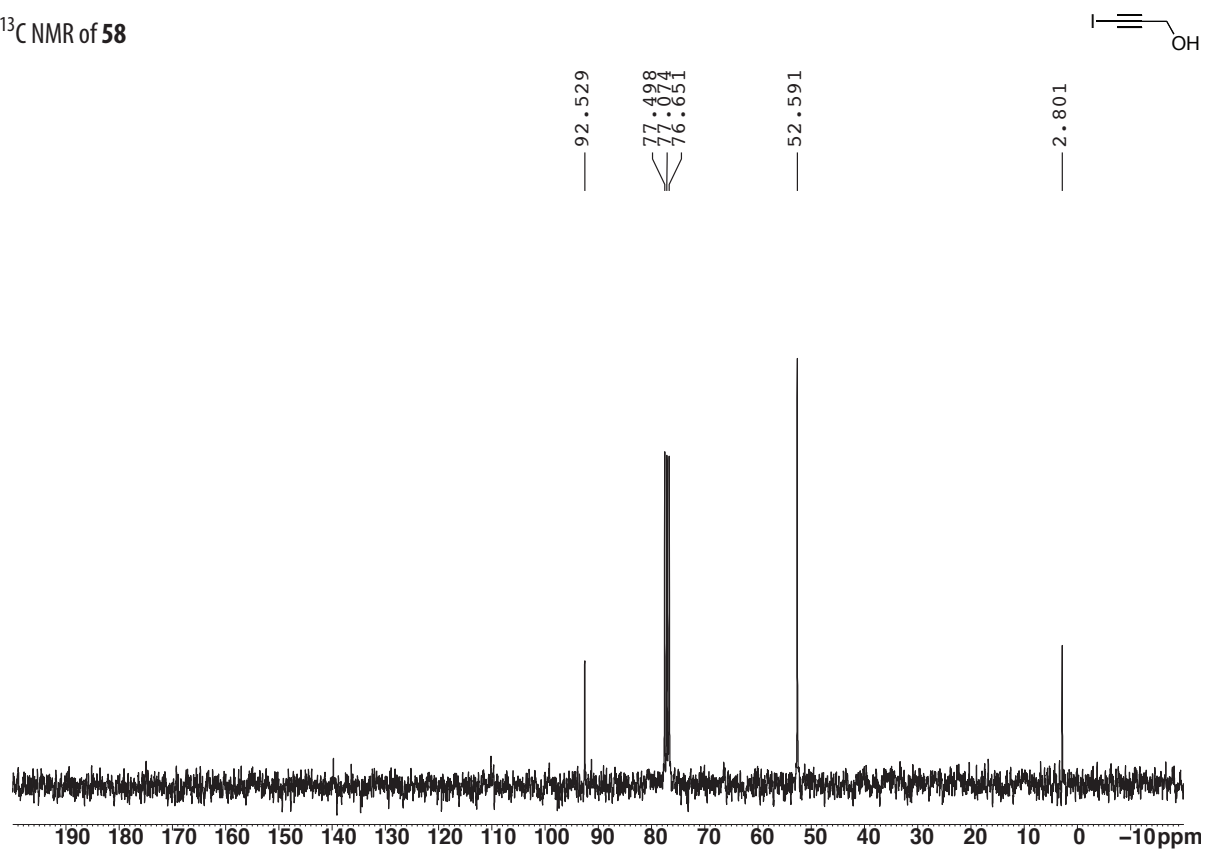
<sup>1</sup>H NMR of 52<sup>13</sup>C NMR of 52

<sup>1</sup>H NMR of 53<sup>13</sup>C NMR of 53

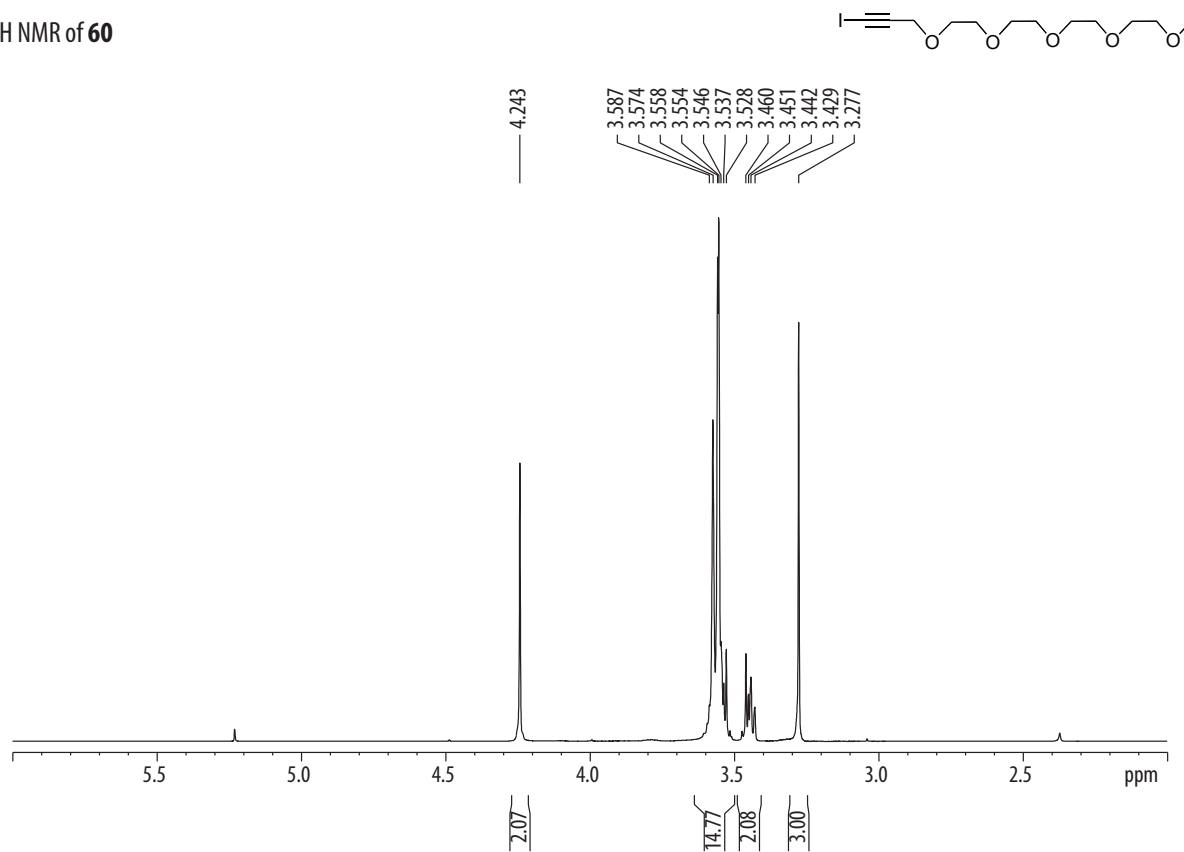
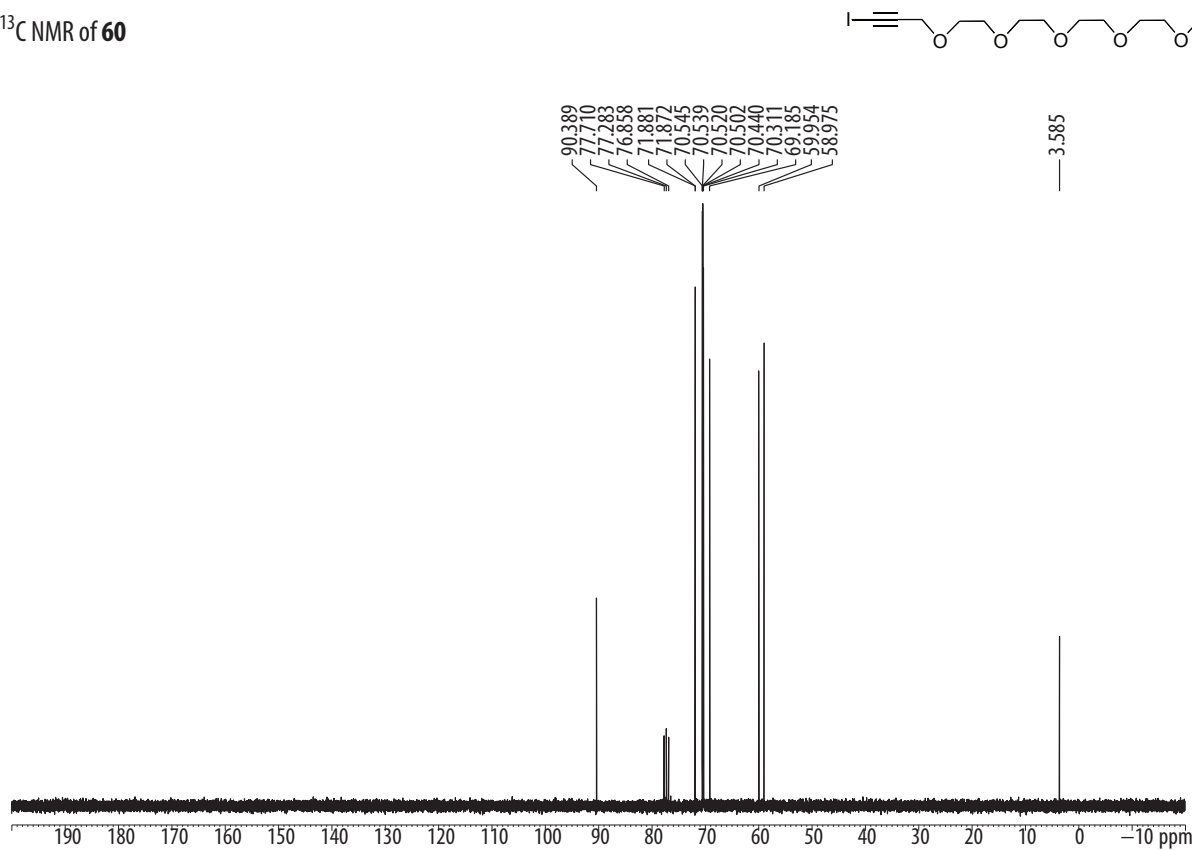
<sup>1</sup>H NMR of 55<sup>13</sup>C NMR of 55

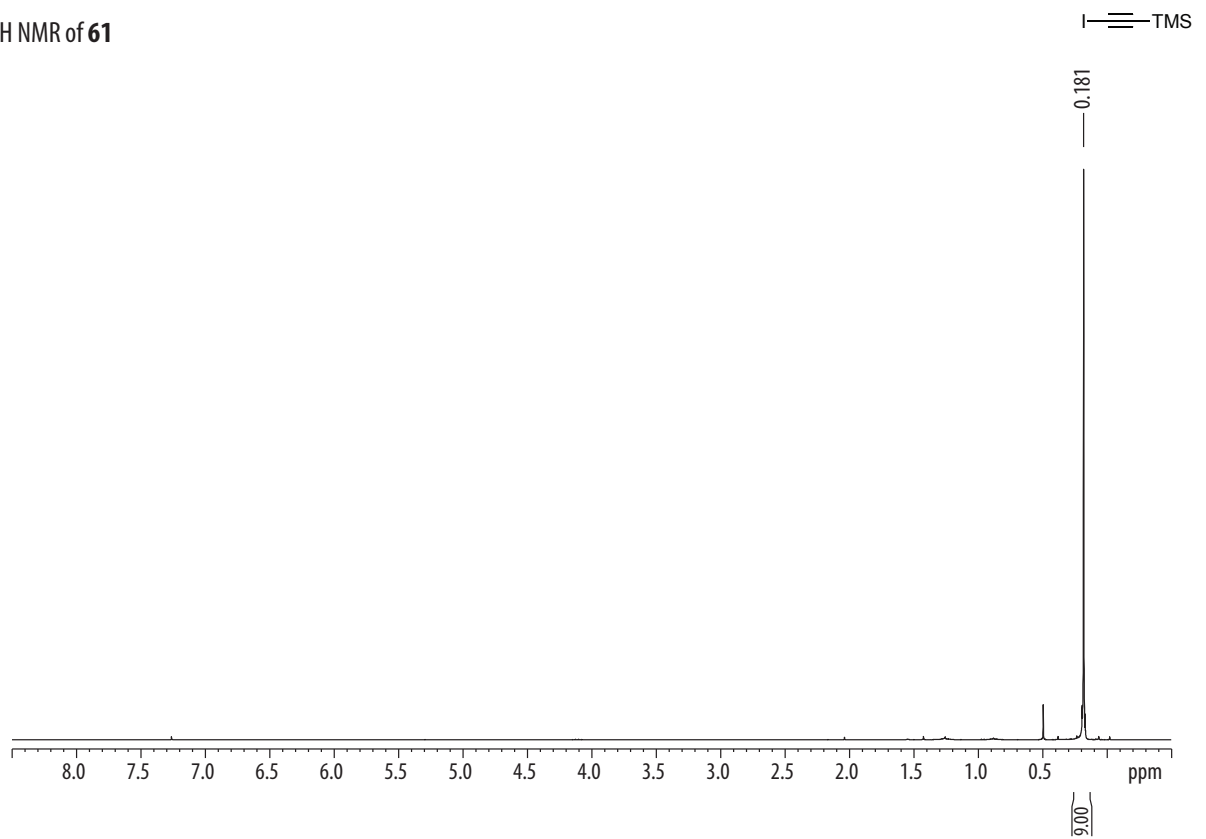
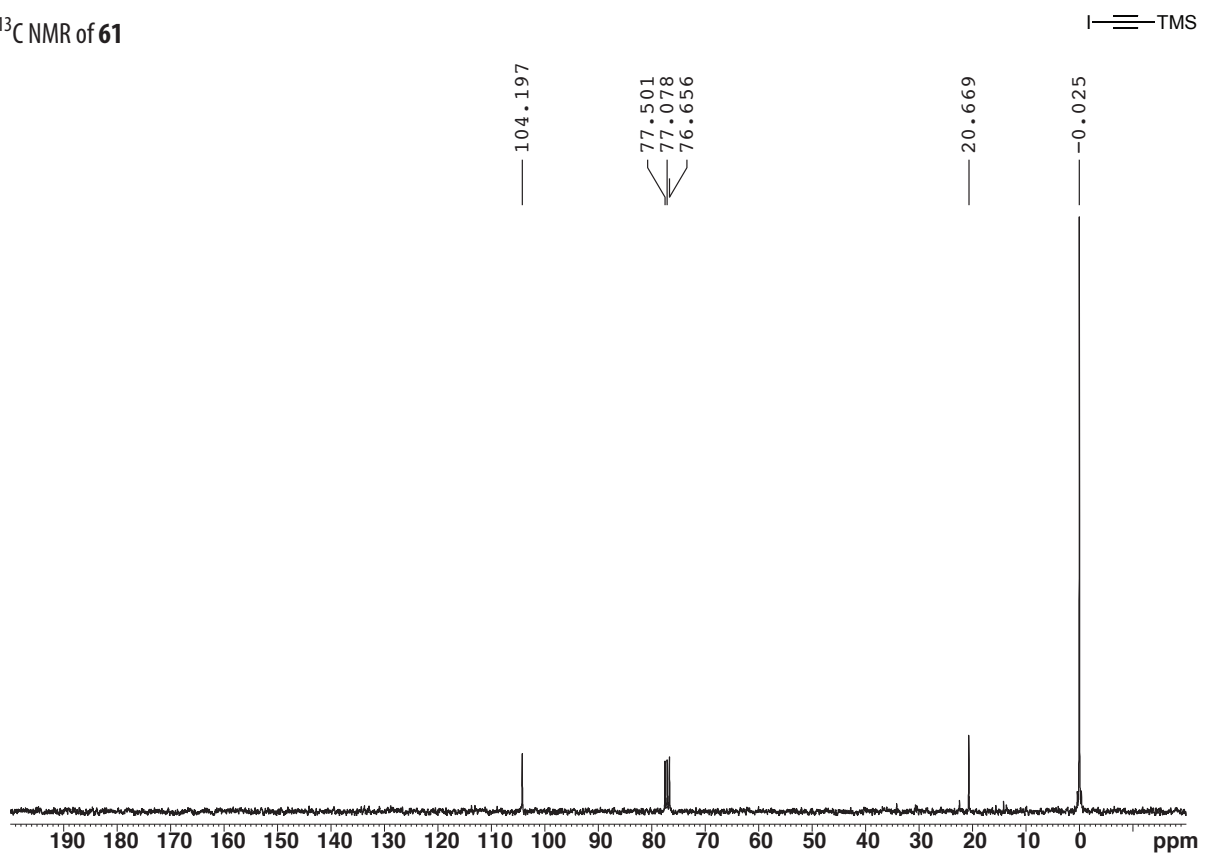
<sup>1</sup>H NMR of 56<sup>13</sup>C NMR of 56

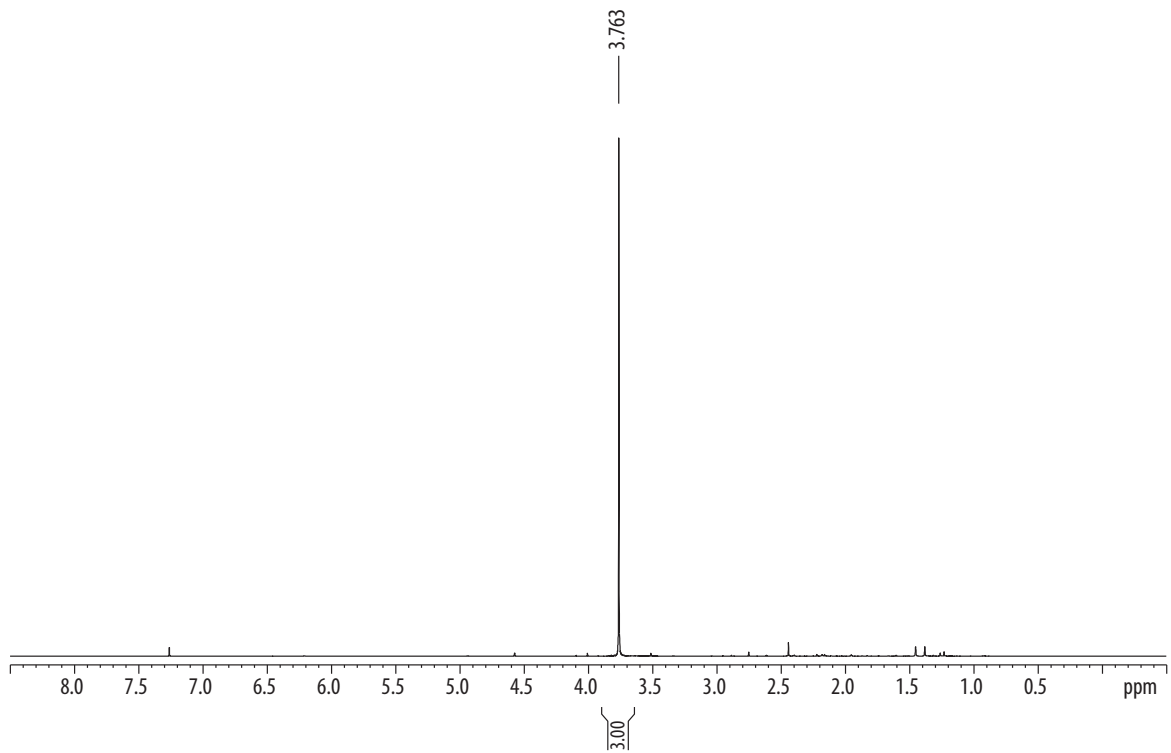
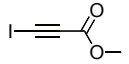
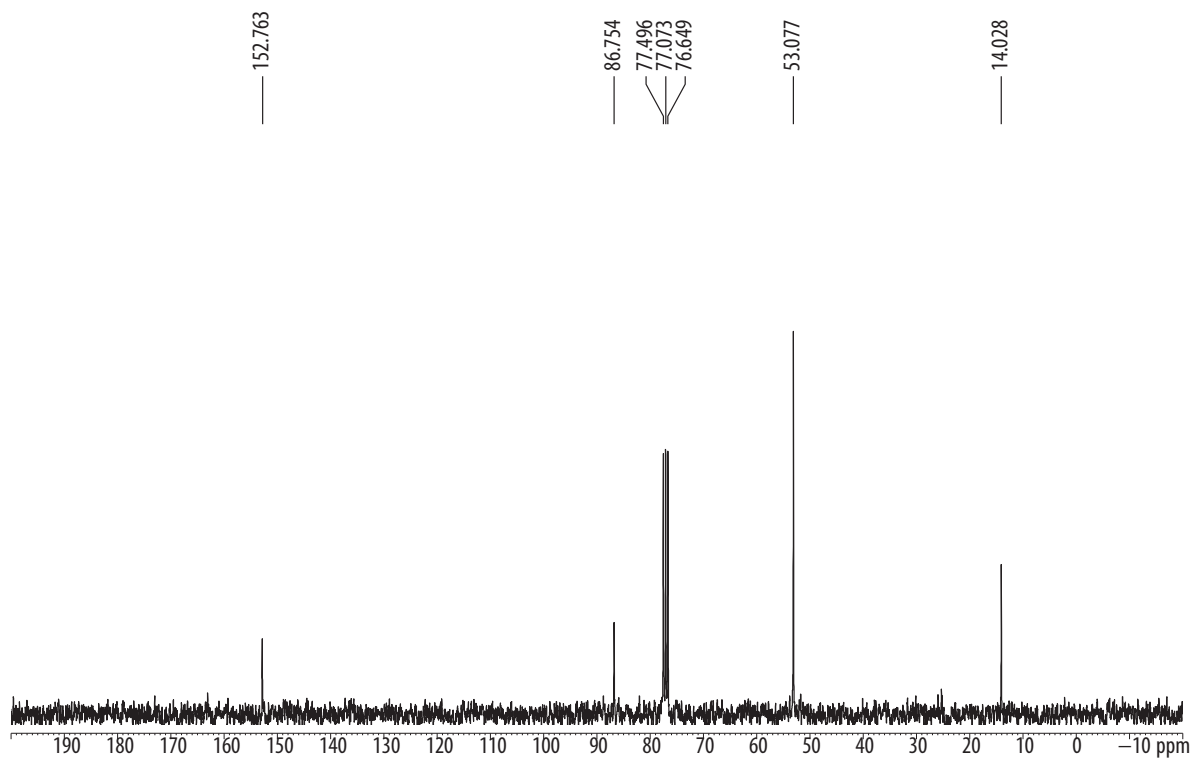
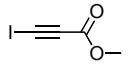
<sup>1</sup>H NMR of 57<sup>13</sup>C NMR of 57

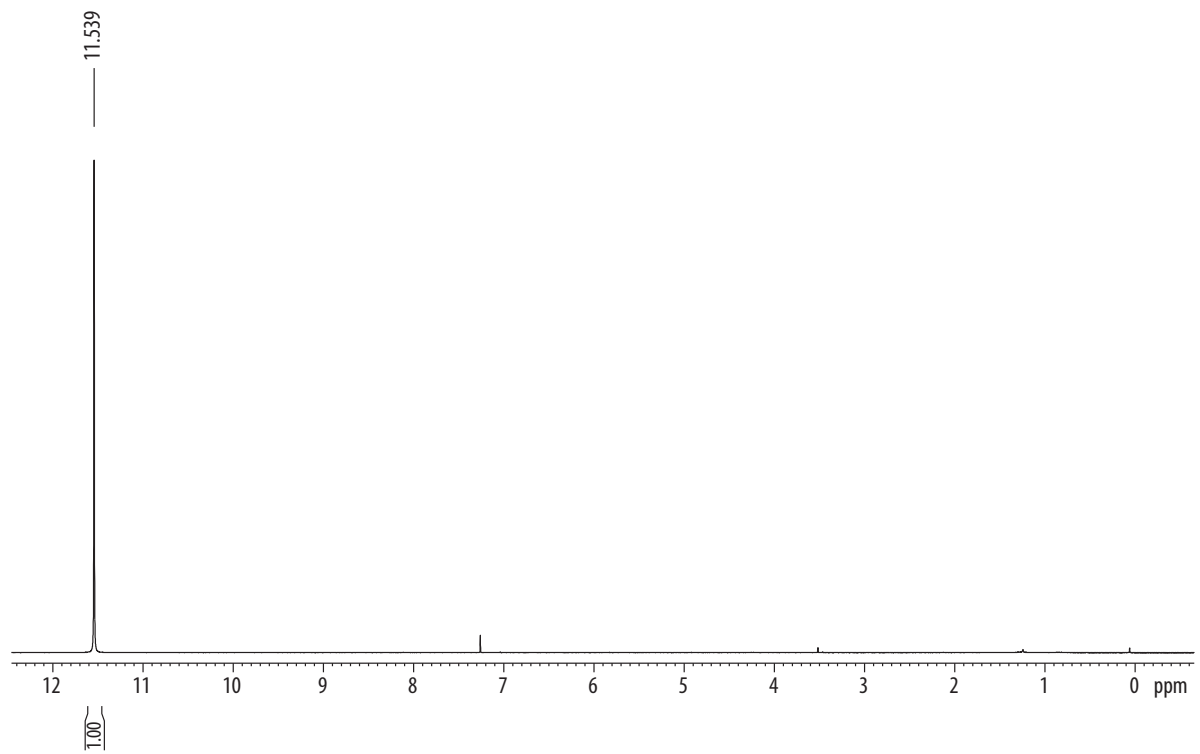
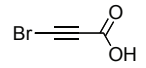
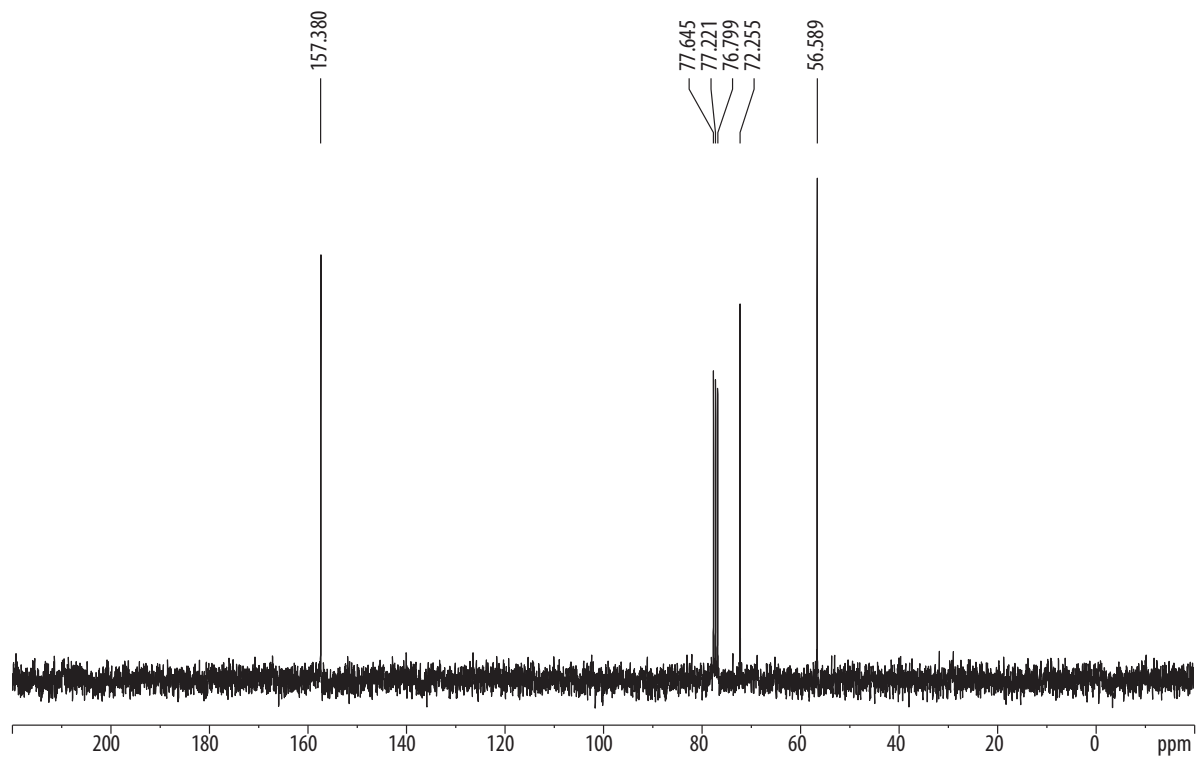
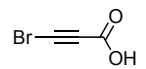
$^1\text{H}$  NMR of **58** $^{13}\text{C}$  NMR of **58**

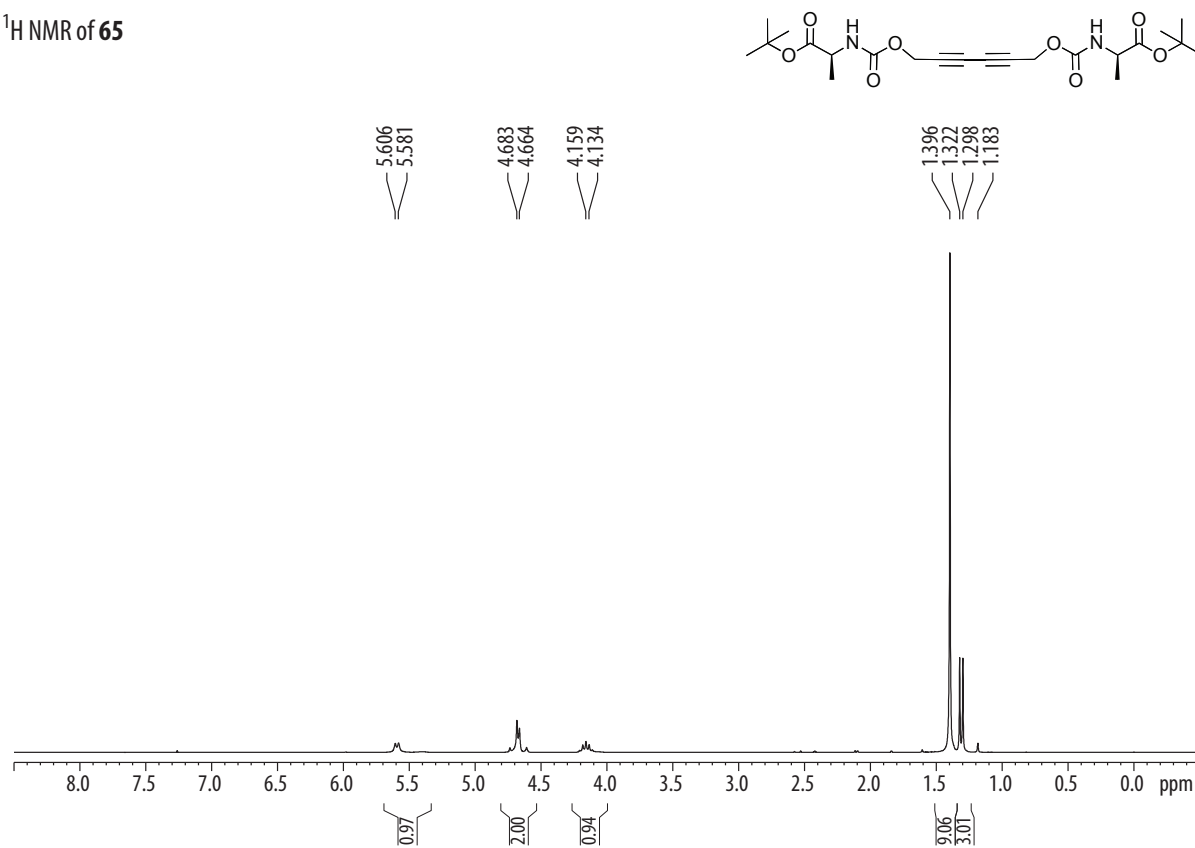
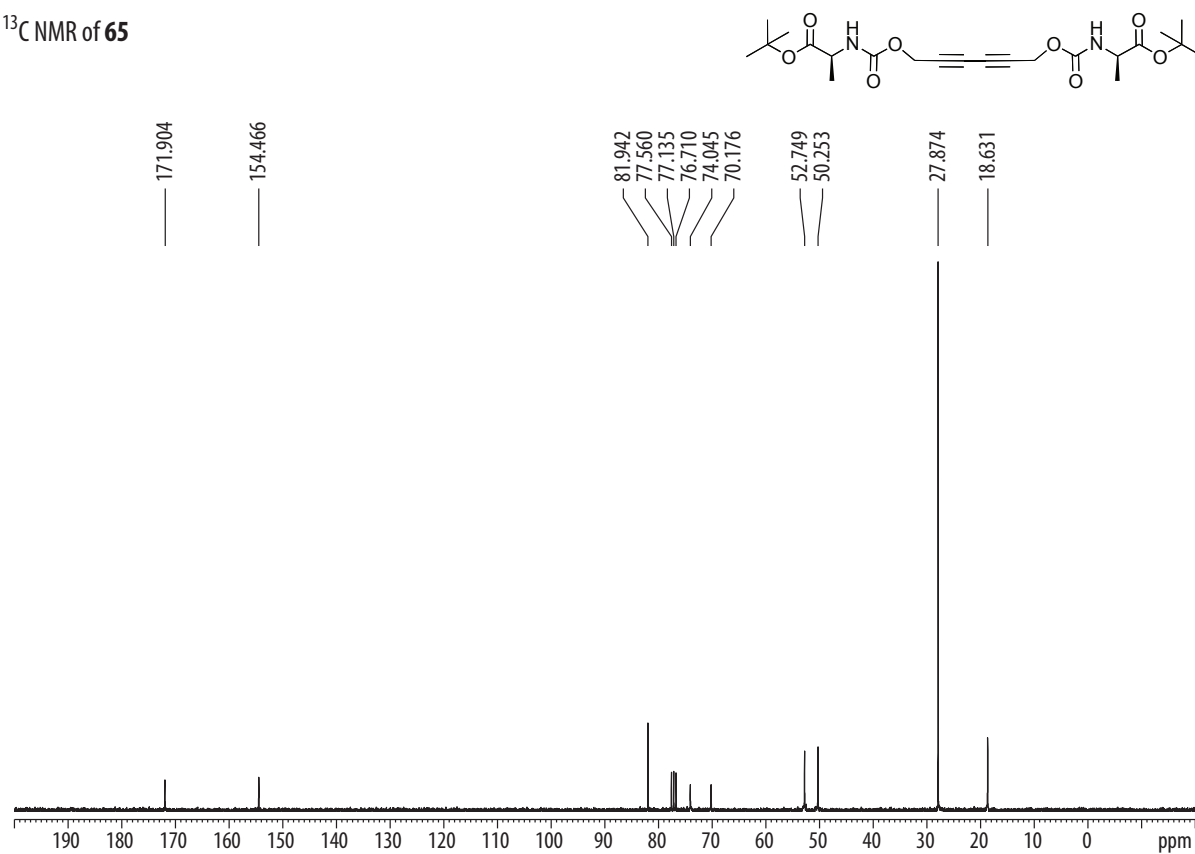


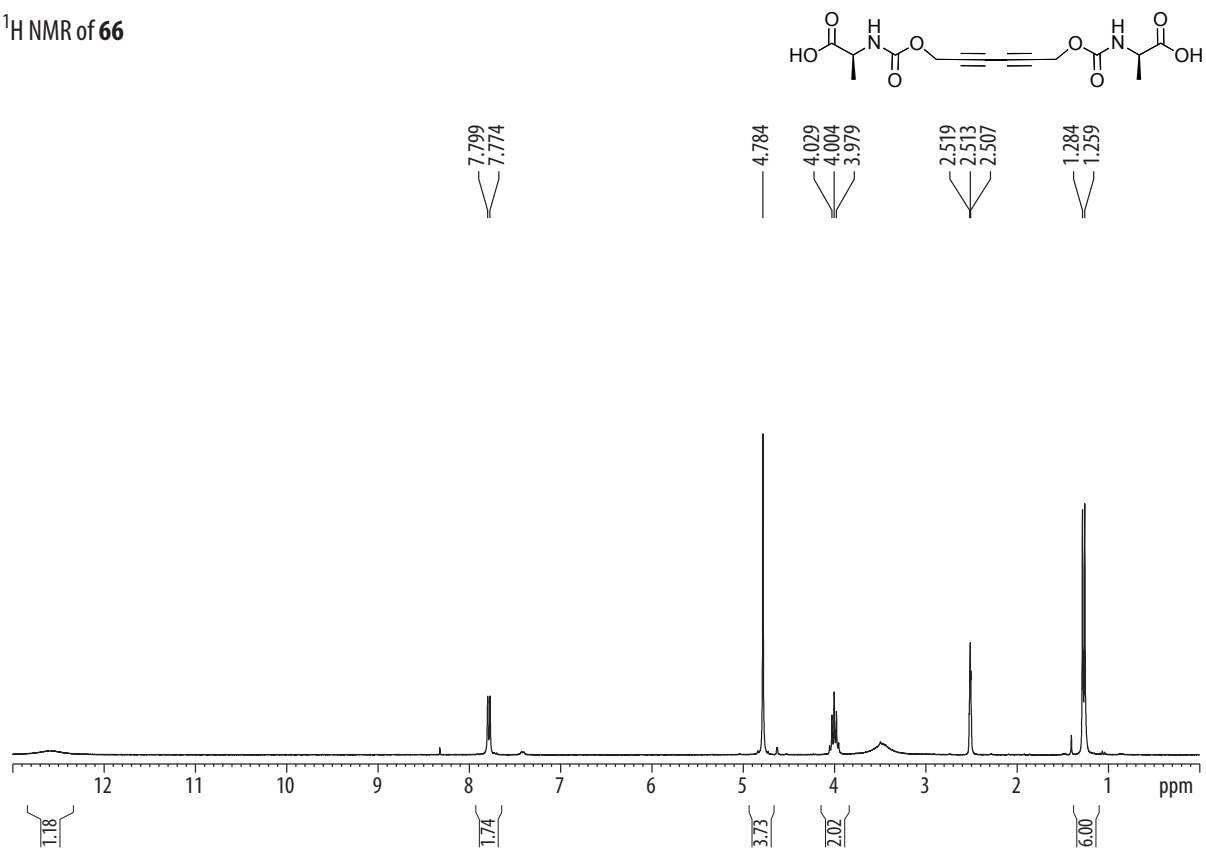
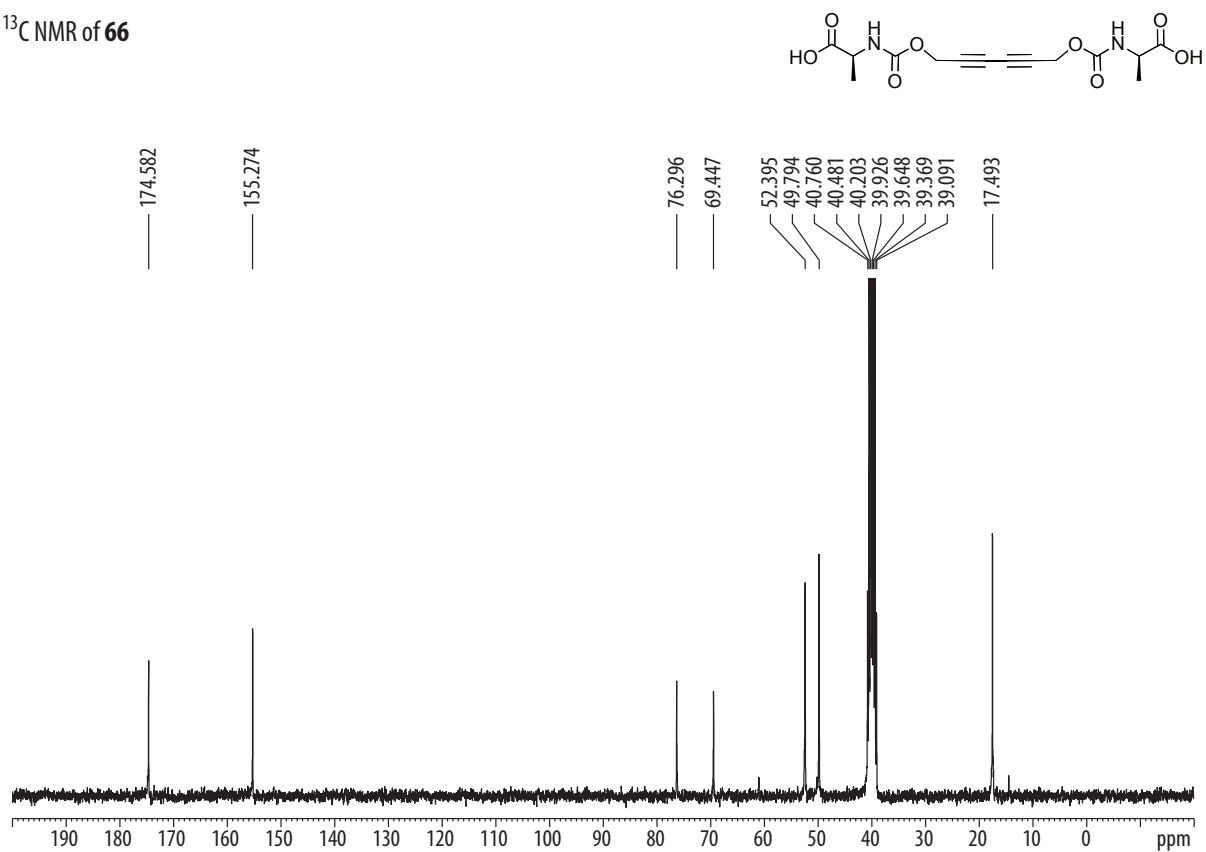
$^1\text{H}$  NMR of **60** $^{13}\text{C}$  NMR of **60**

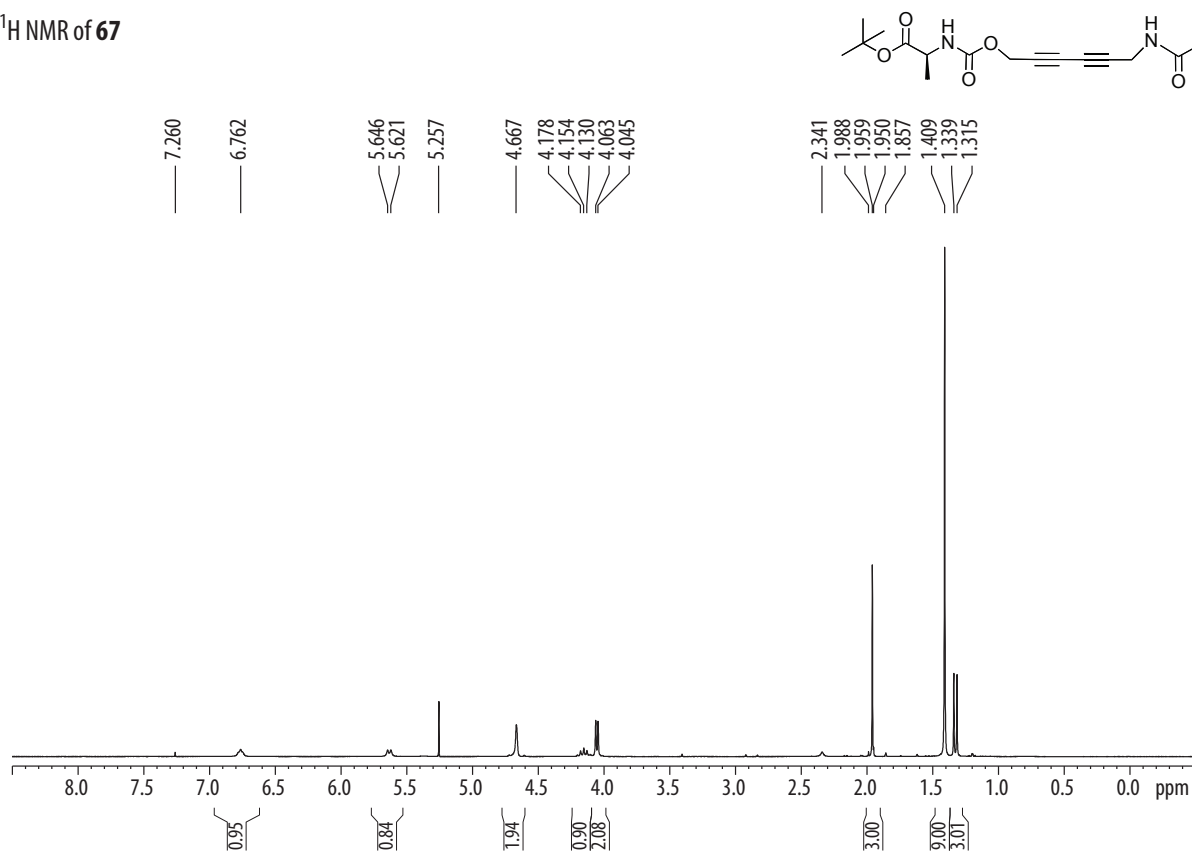
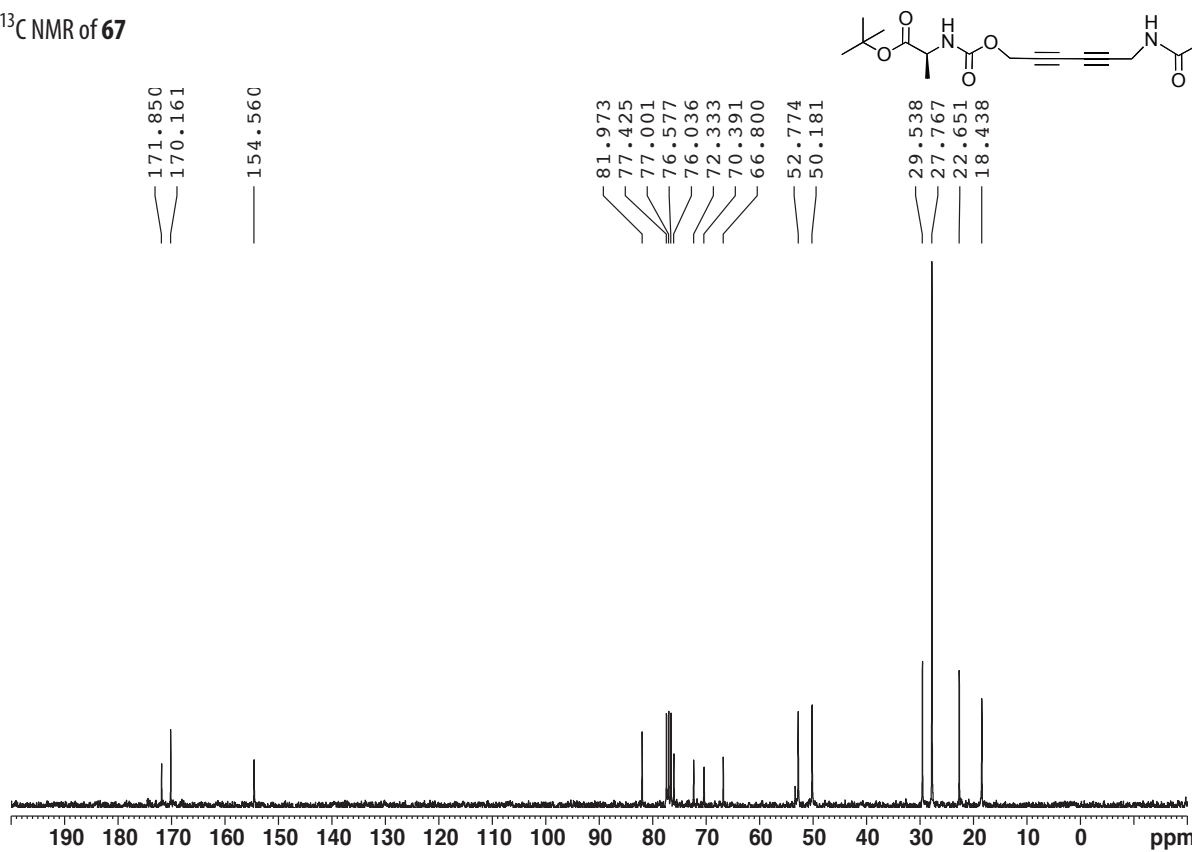
<sup>1</sup>H NMR of **61**<sup>13</sup>C NMR of **61**

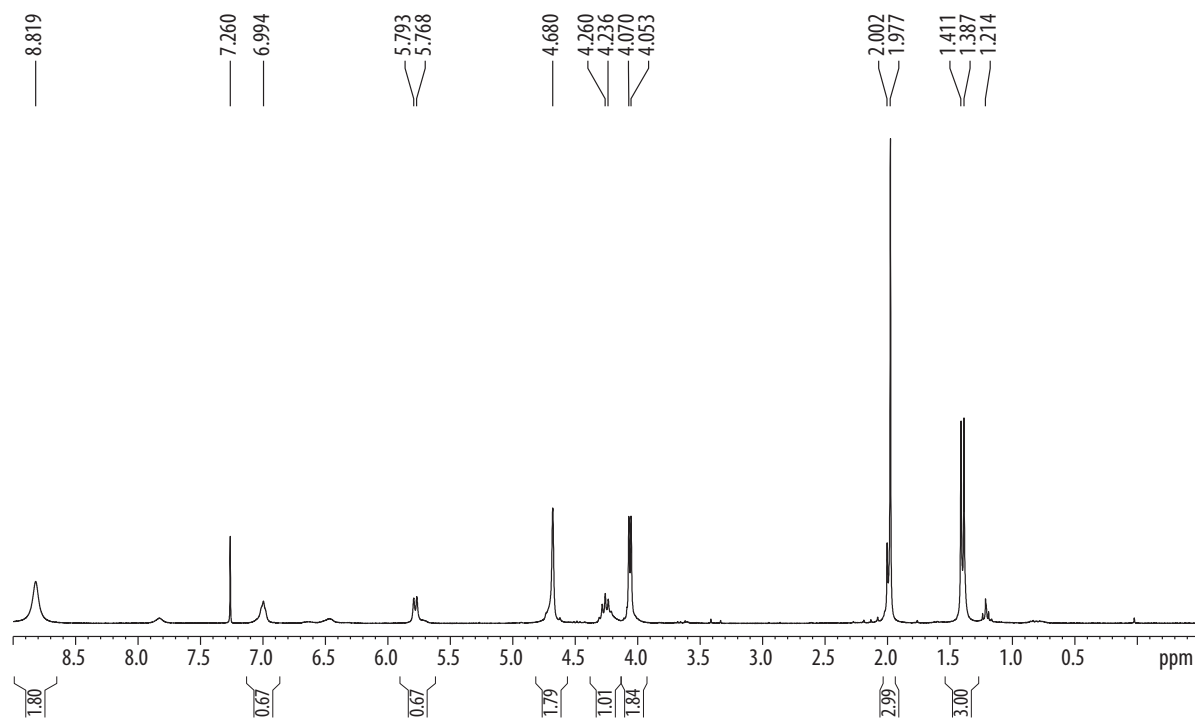
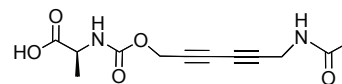
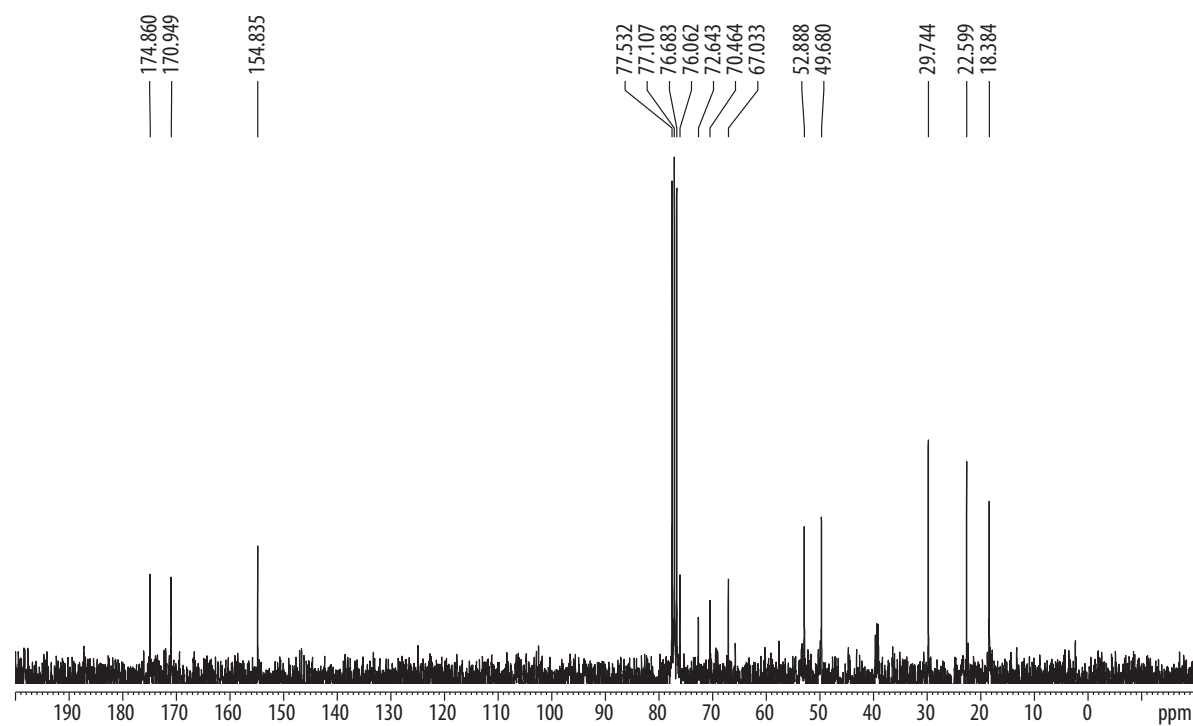
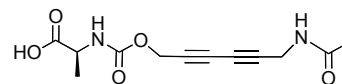
<sup>1</sup>H NMR of **62**<sup>13</sup>C NMR of **62**

$^1\text{H}$  NMR of **64** $^{13}\text{C}$  NMR of **64**

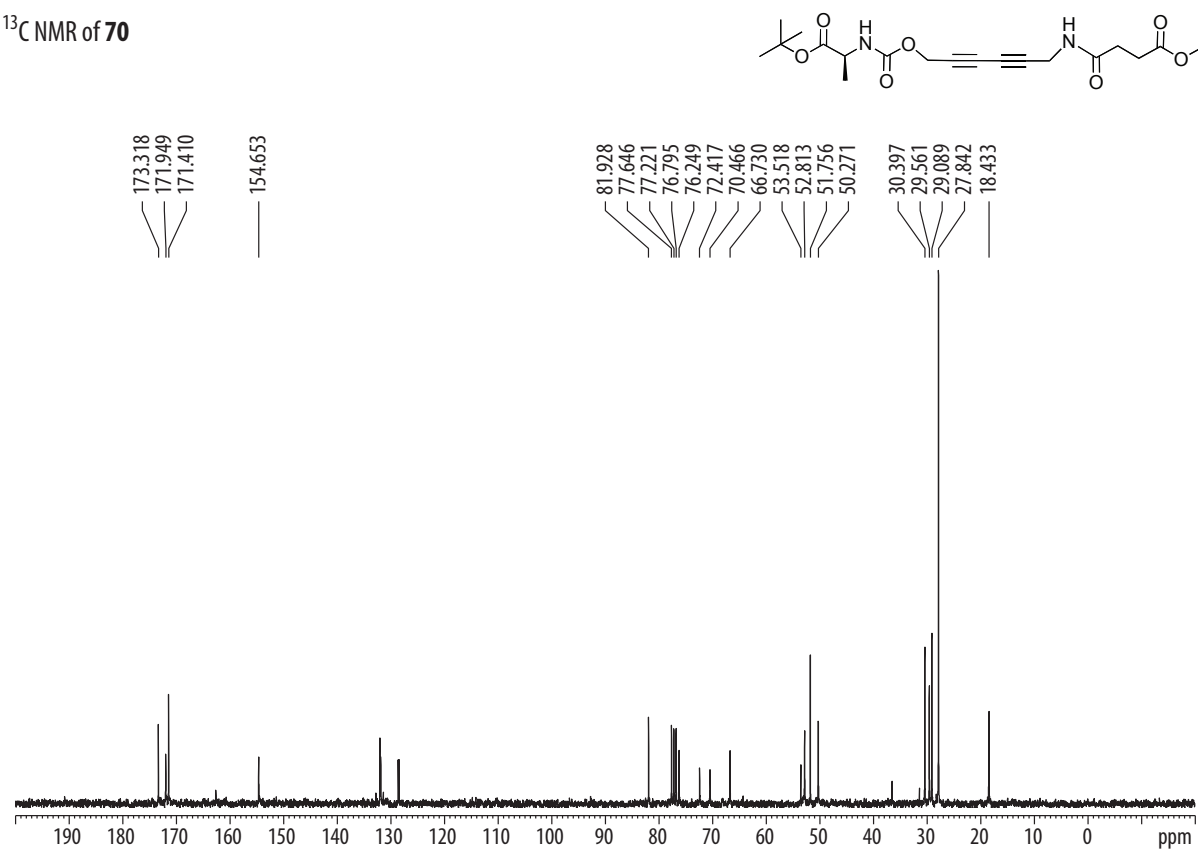
<sup>1</sup>H NMR of **65**<sup>13</sup>C NMR of **65**

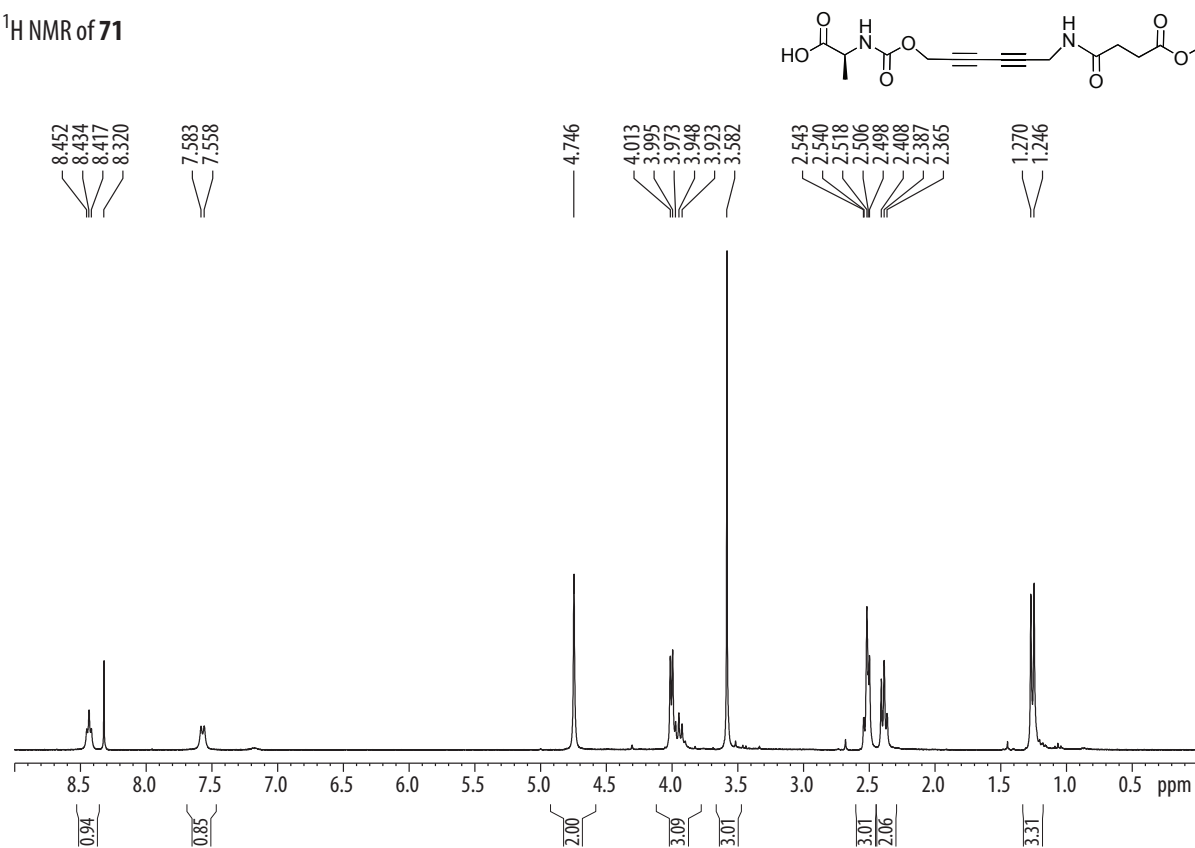
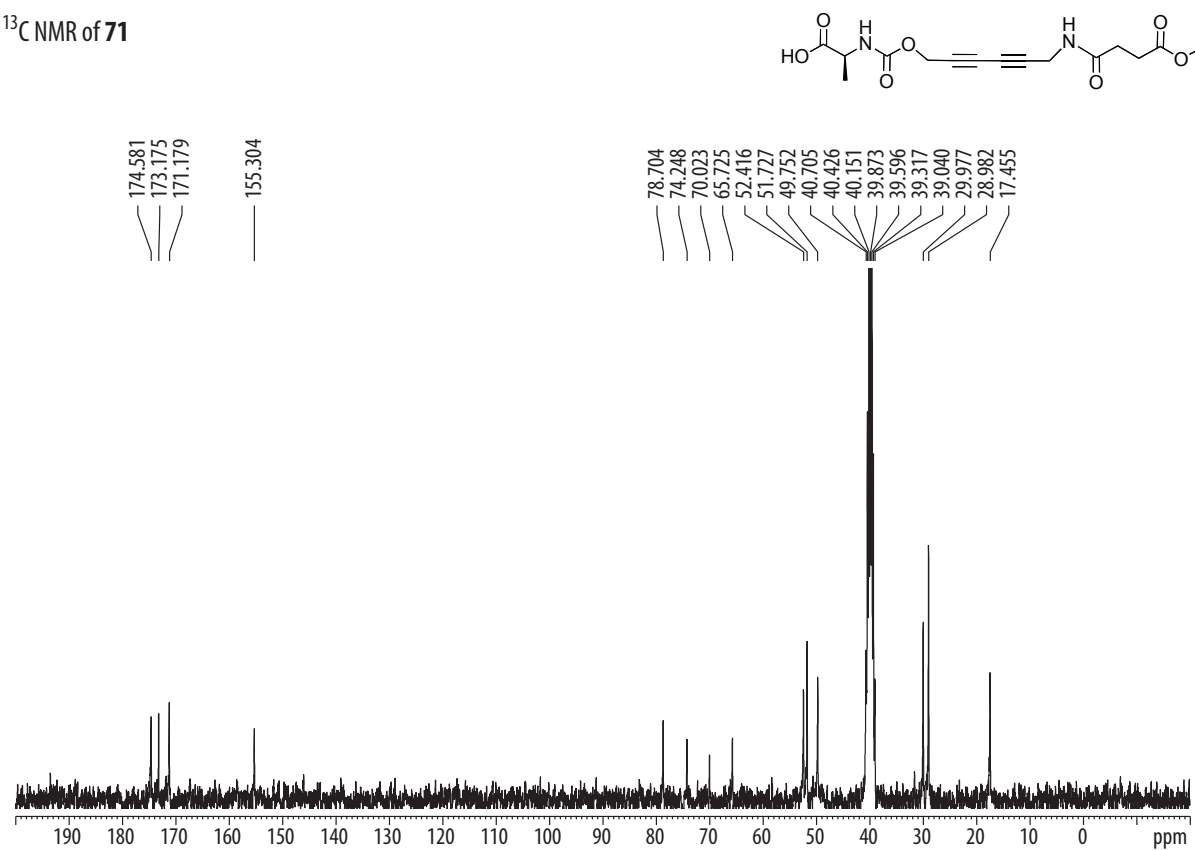
<sup>1</sup>H NMR of **66**<sup>13</sup>C NMR of **66**

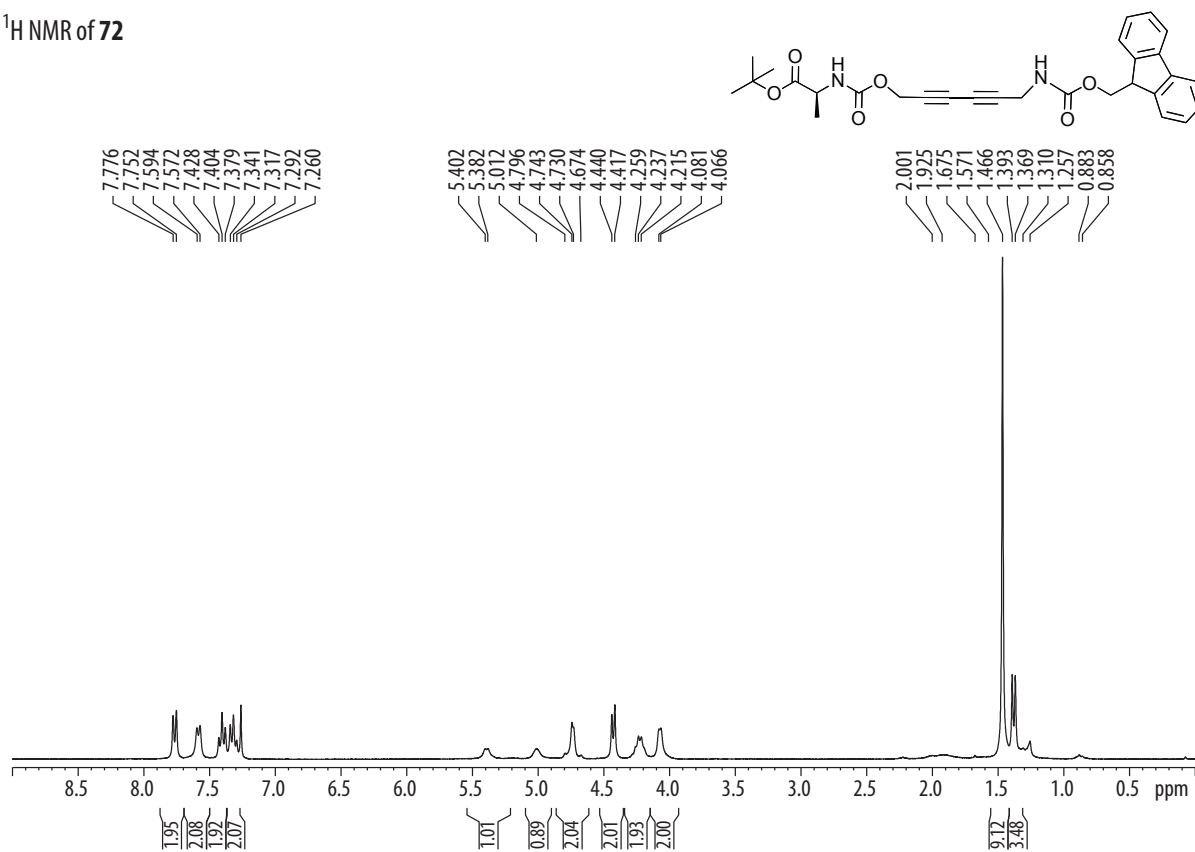
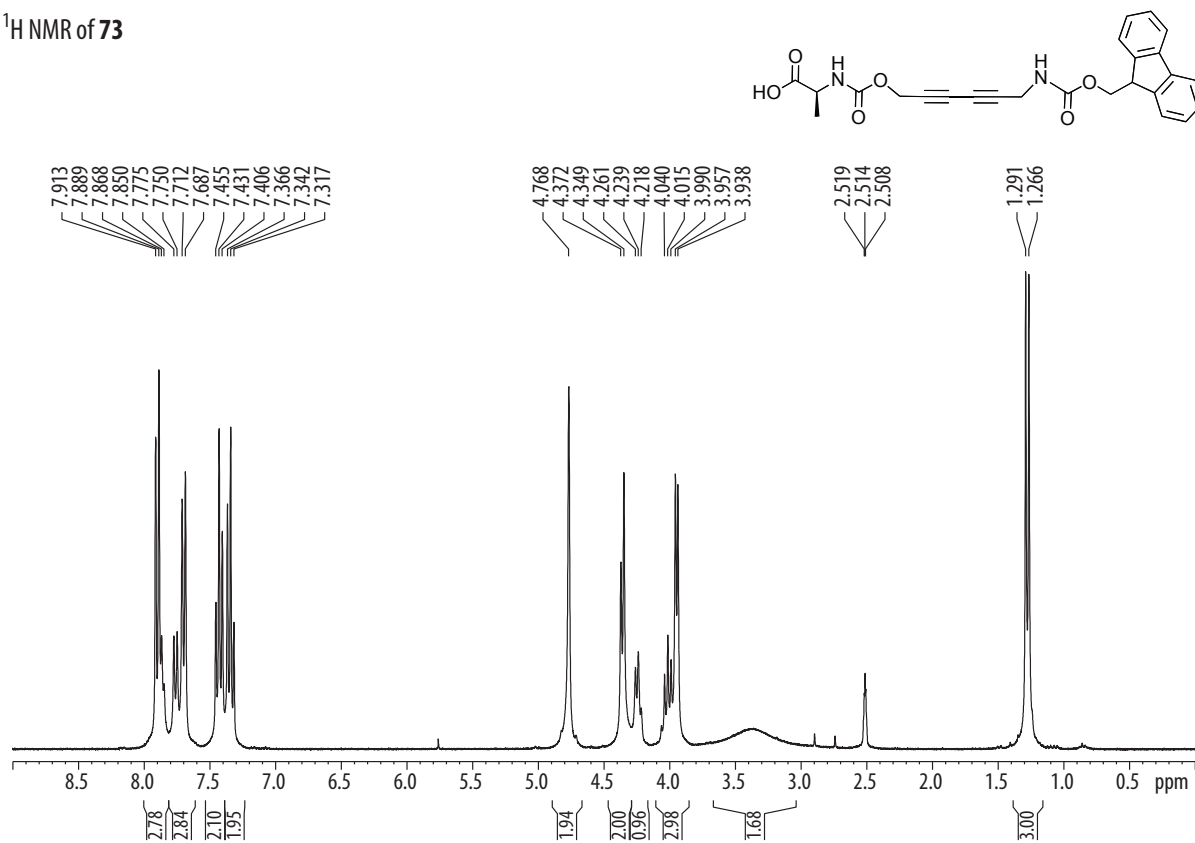
<sup>1</sup>H NMR of **67**<sup>13</sup>C NMR of **67**

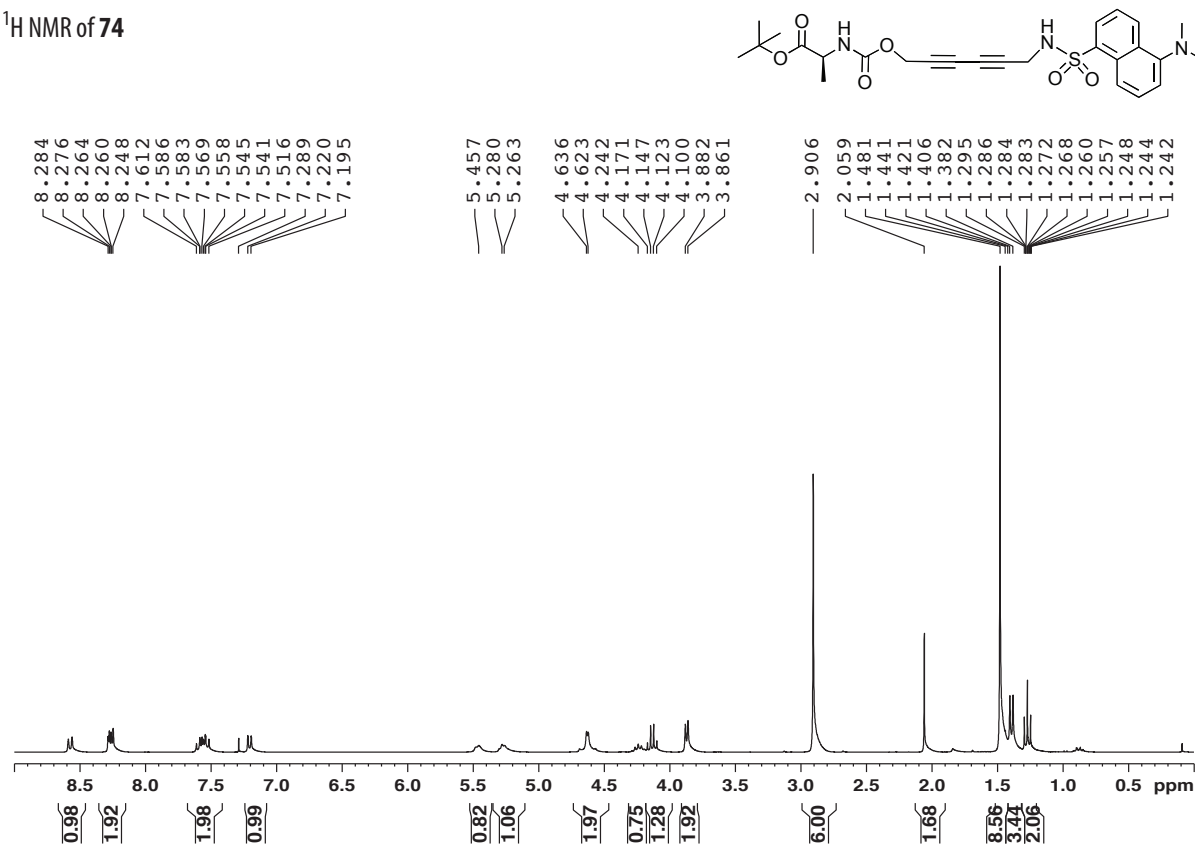
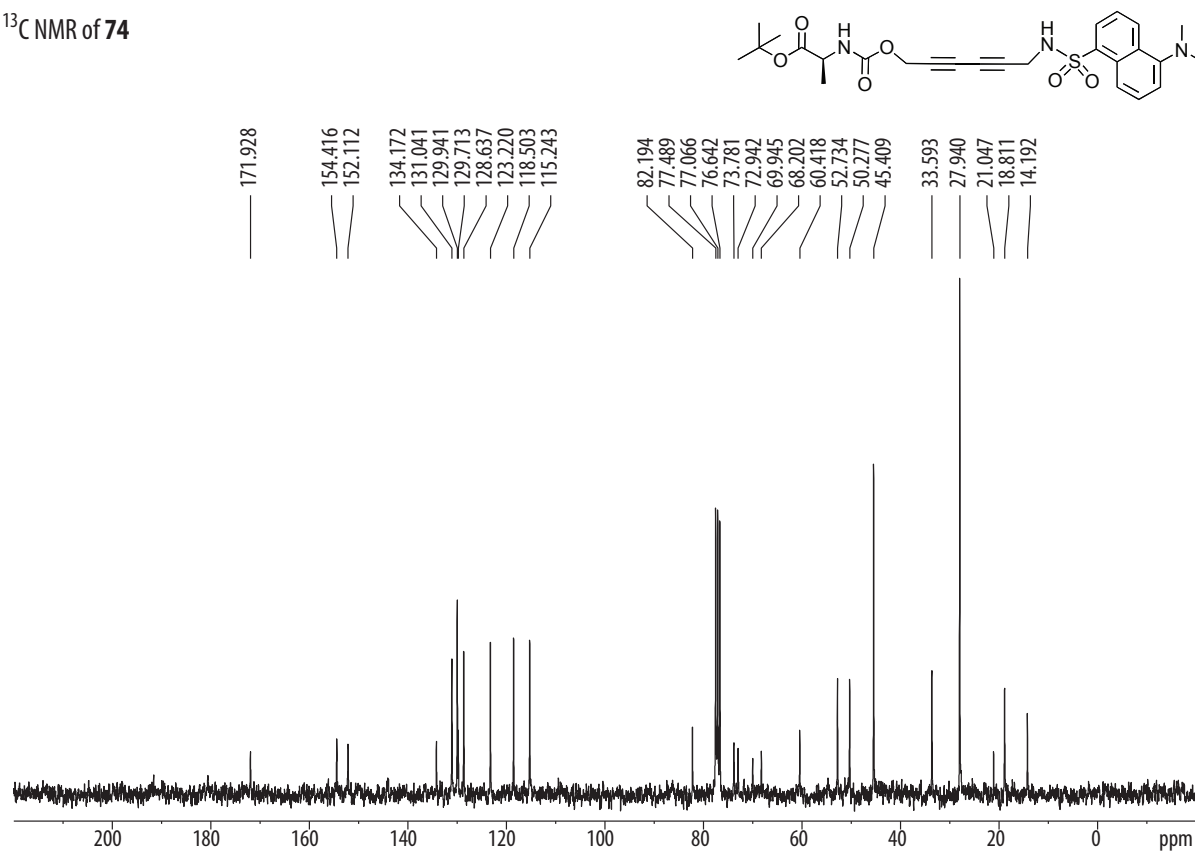
<sup>1</sup>H NMR of **68**<sup>13</sup>C NMR of **68**

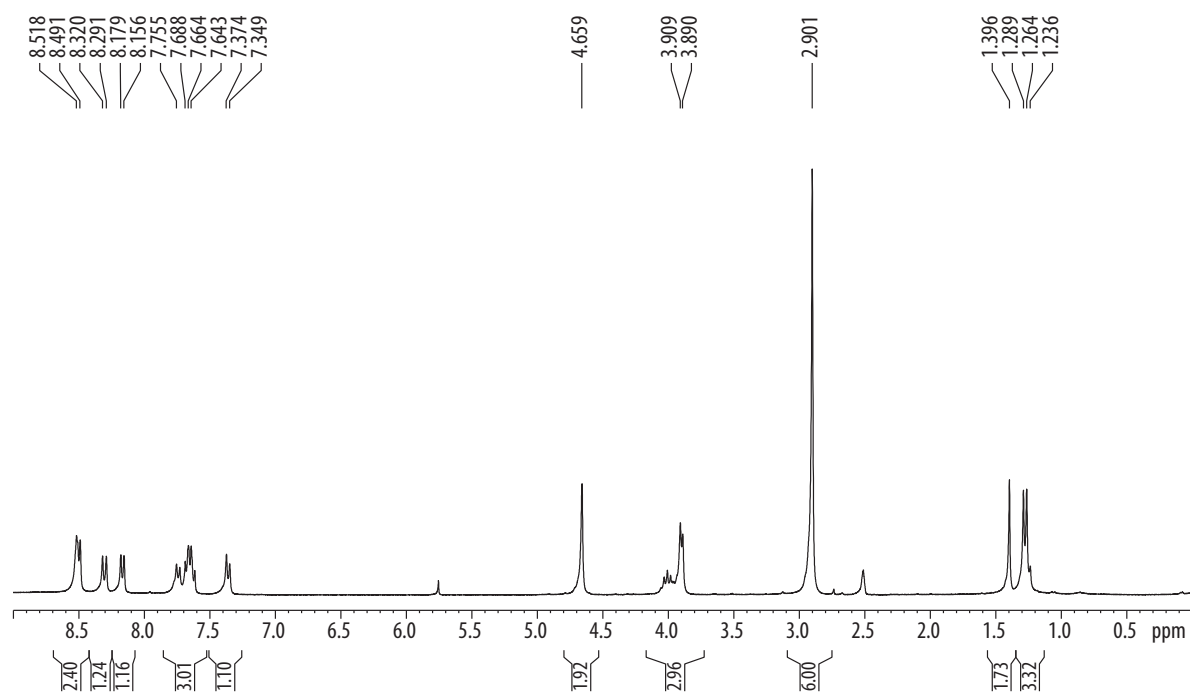
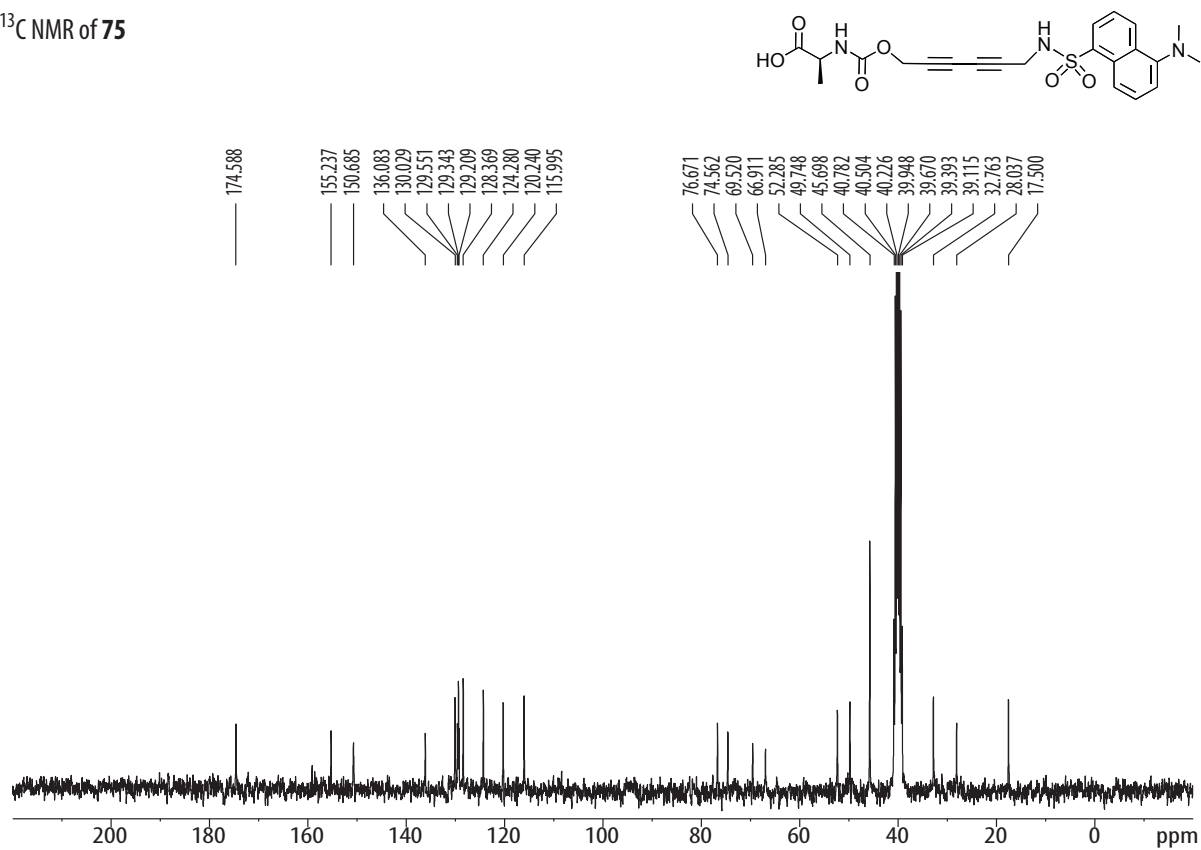


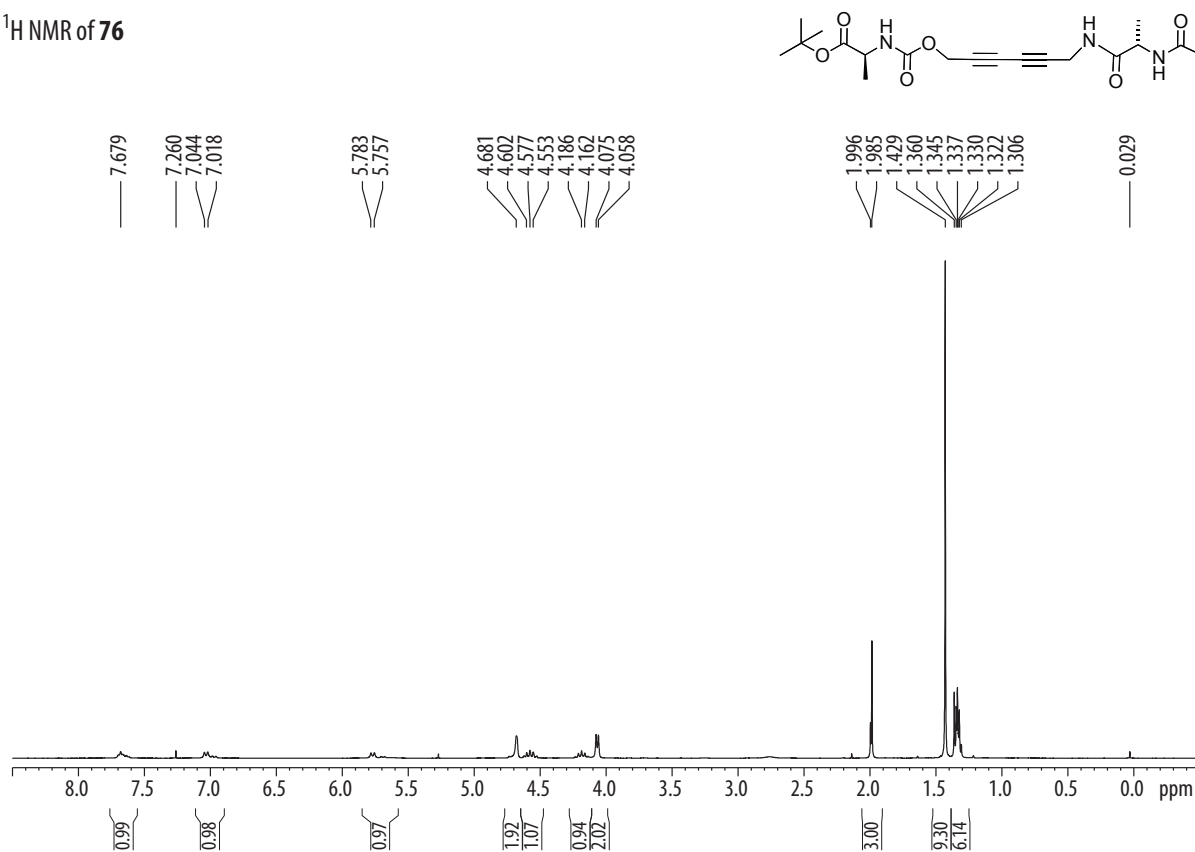
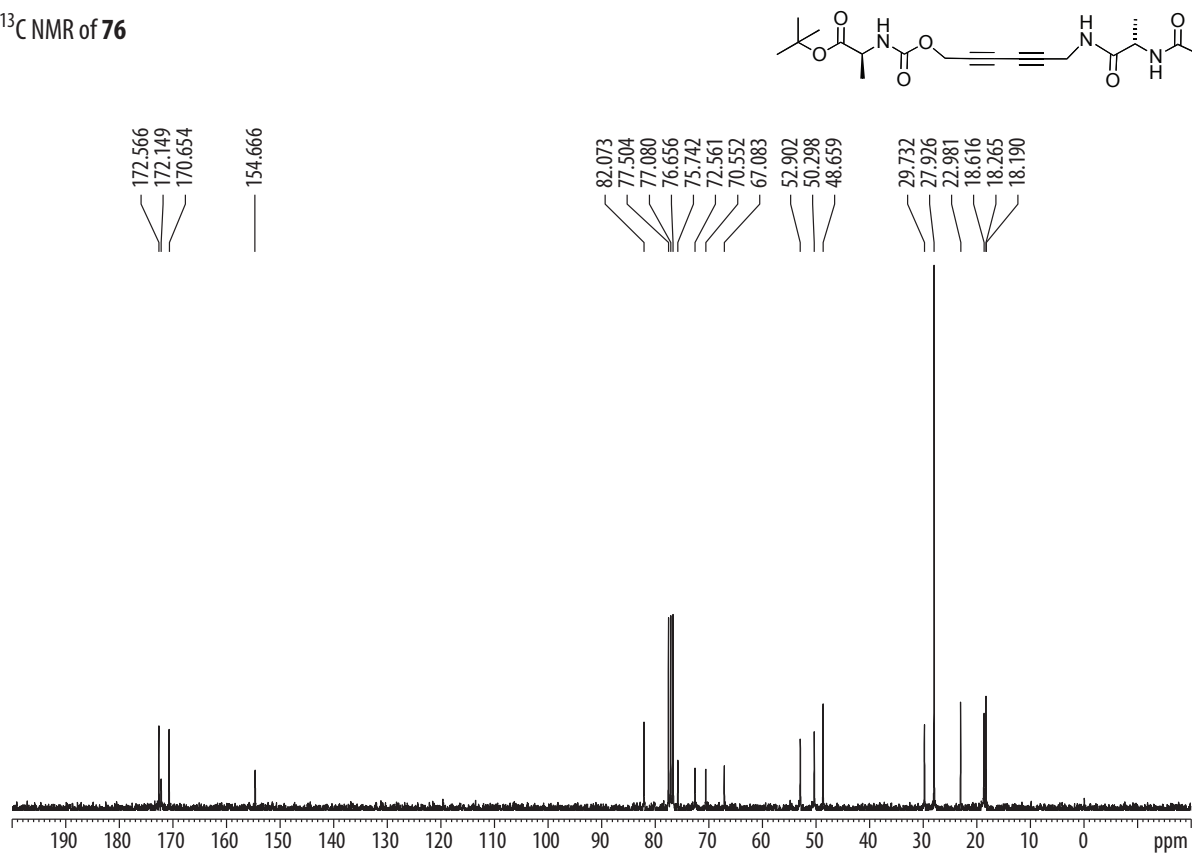
<sup>1</sup>H NMR of **70**<sup>13</sup>C NMR of **70**

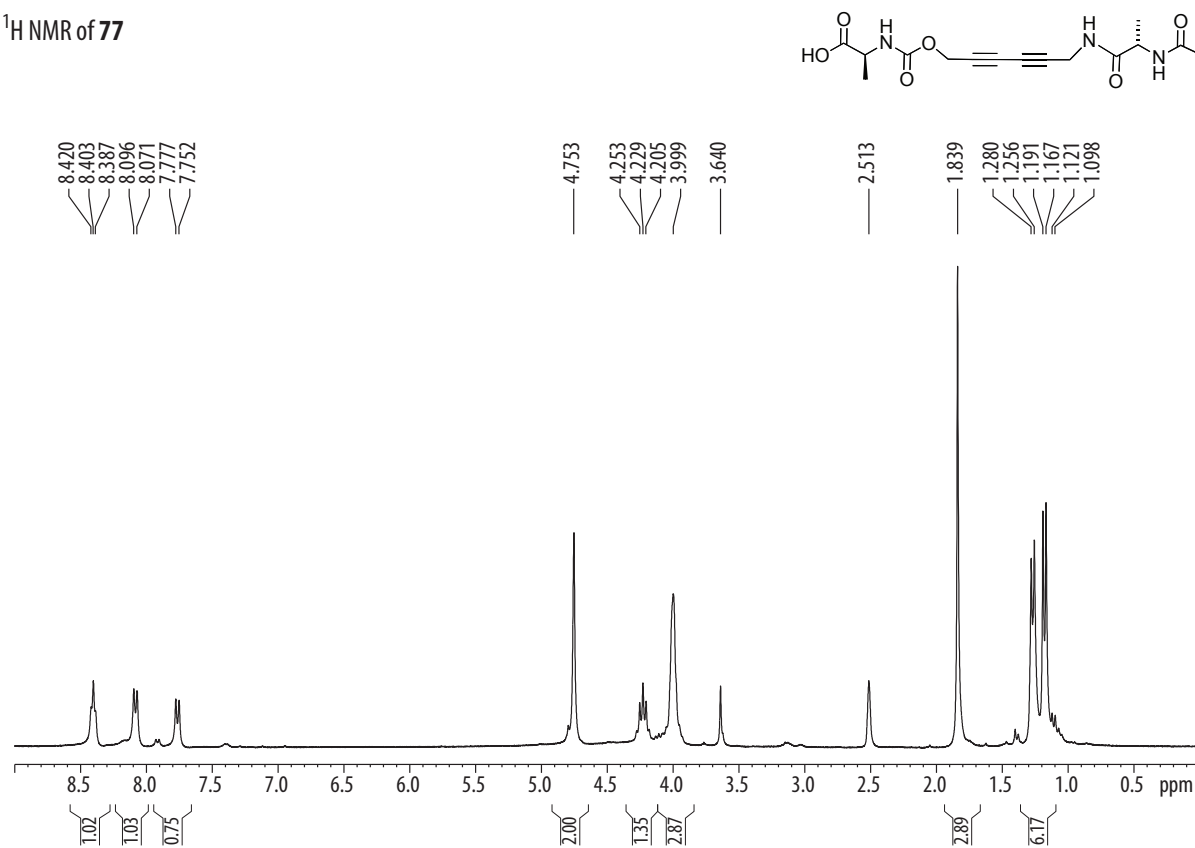
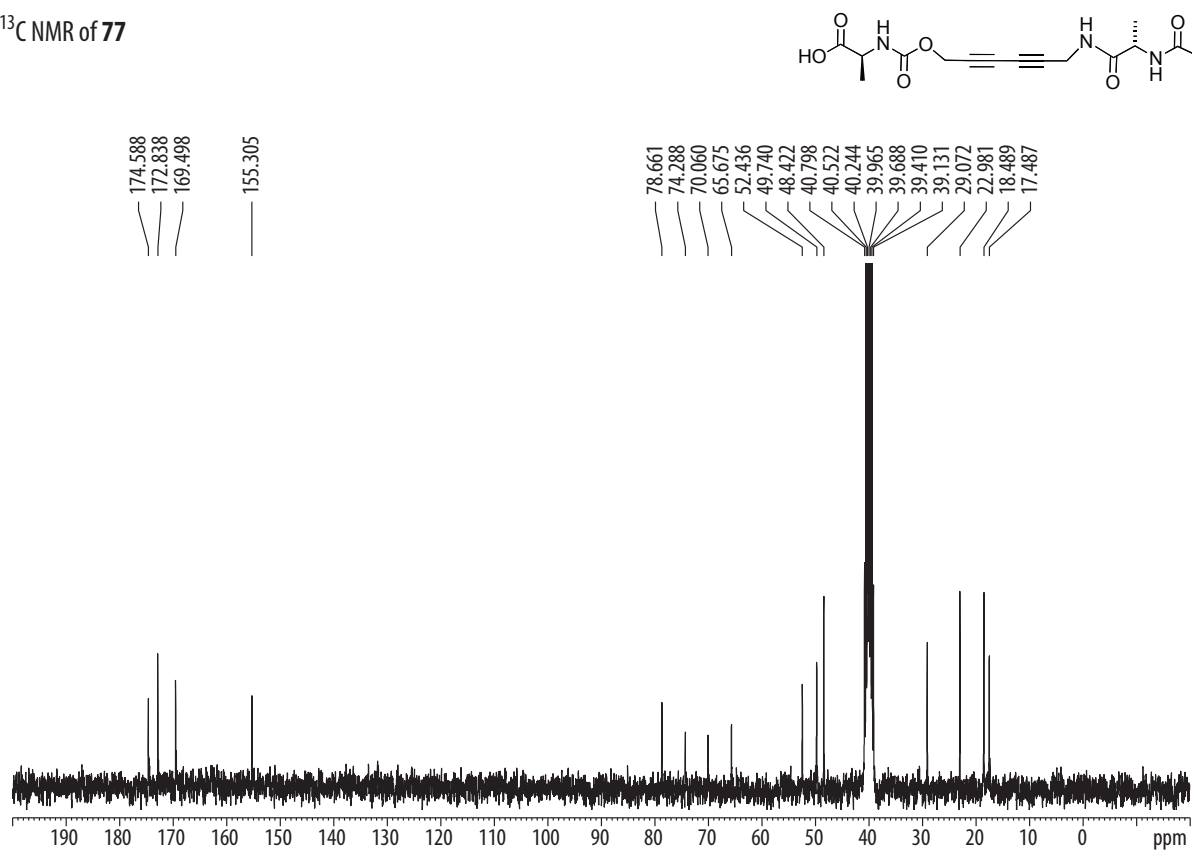
<sup>1</sup>H NMR of 71<sup>13</sup>C NMR of 71

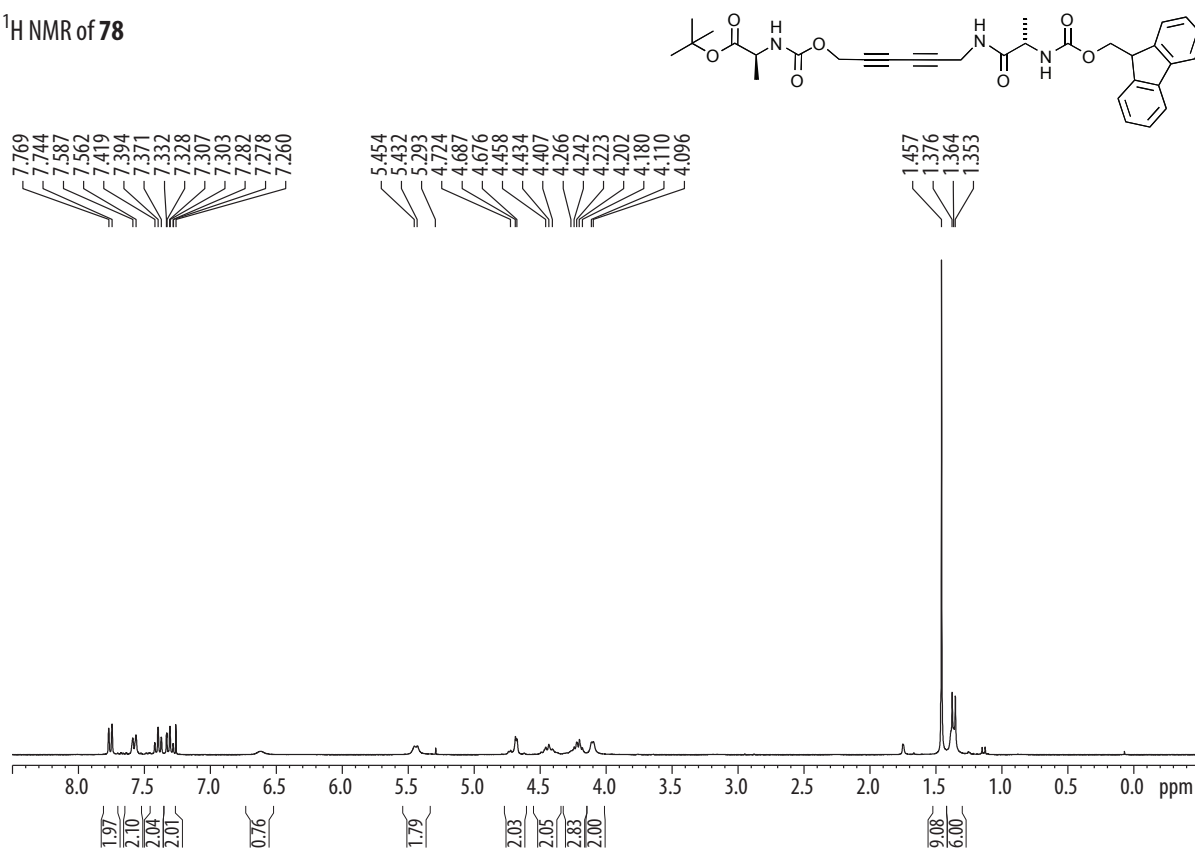
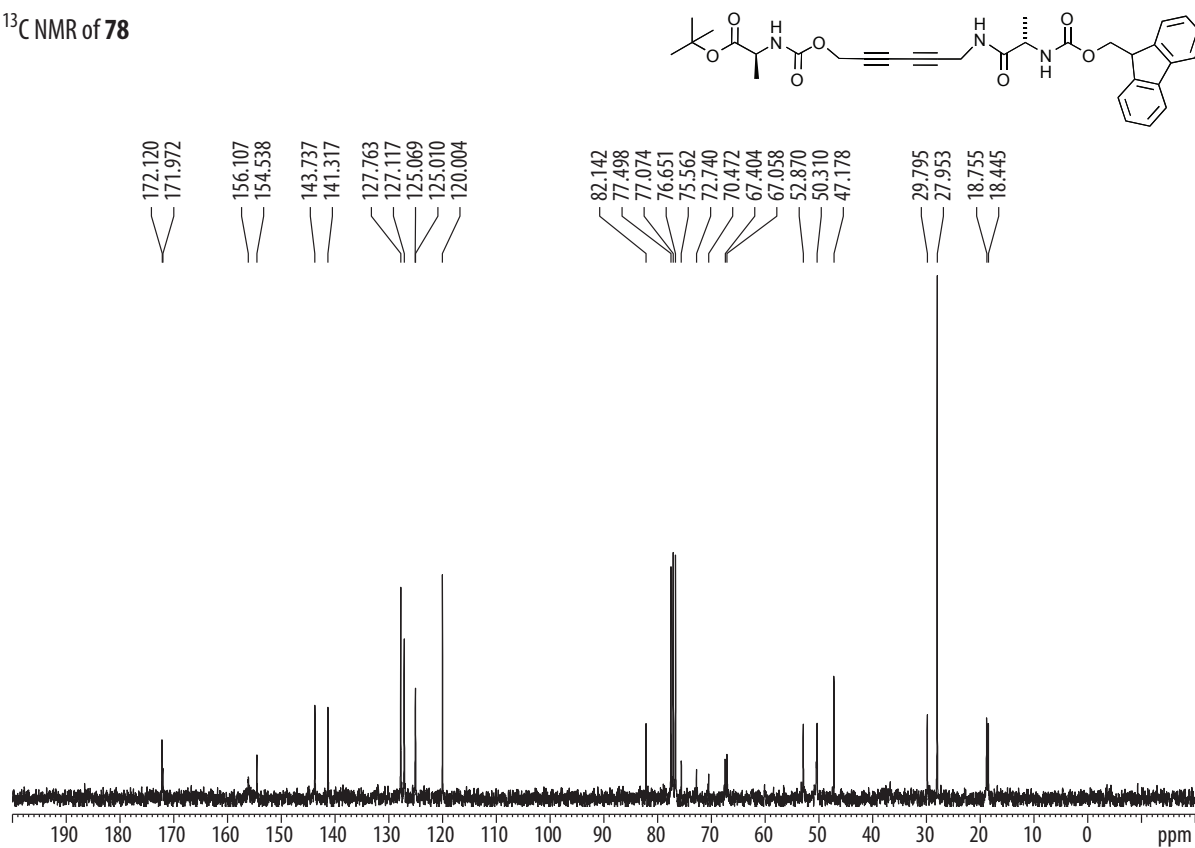
<sup>1</sup>H NMR of 72<sup>1</sup>H NMR of 73

<sup>1</sup>H NMR of 74<sup>13</sup>C NMR of 74

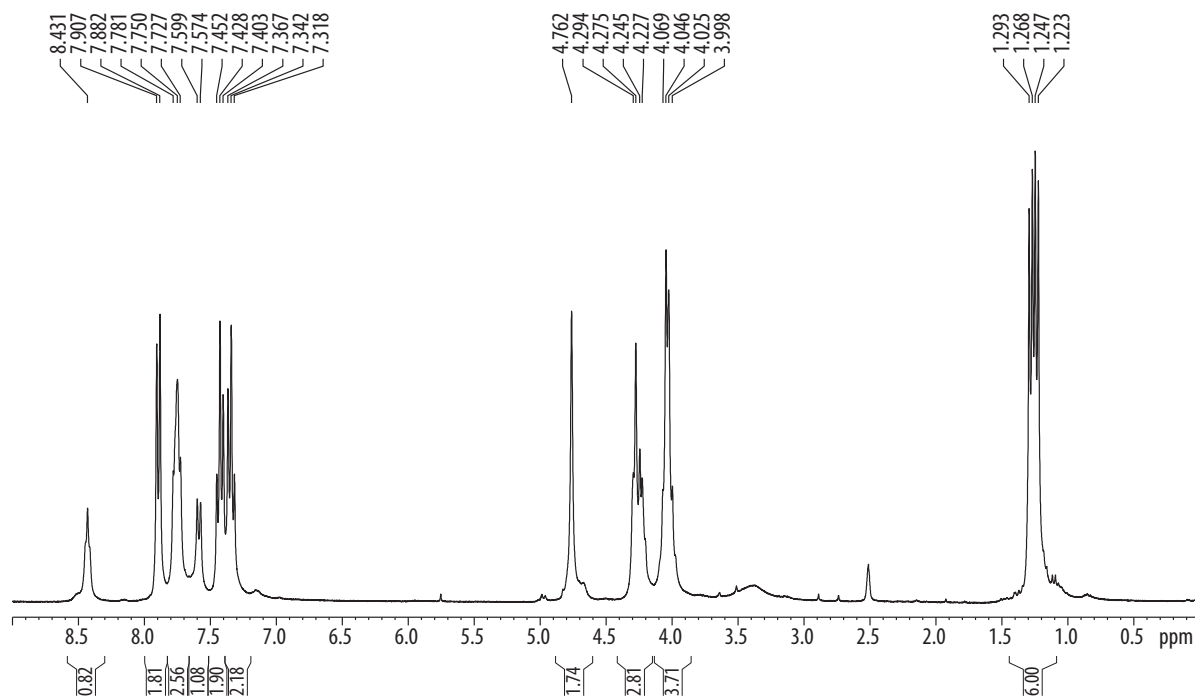
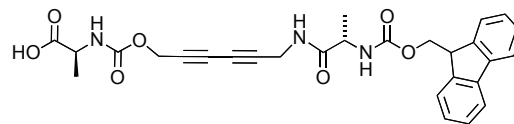
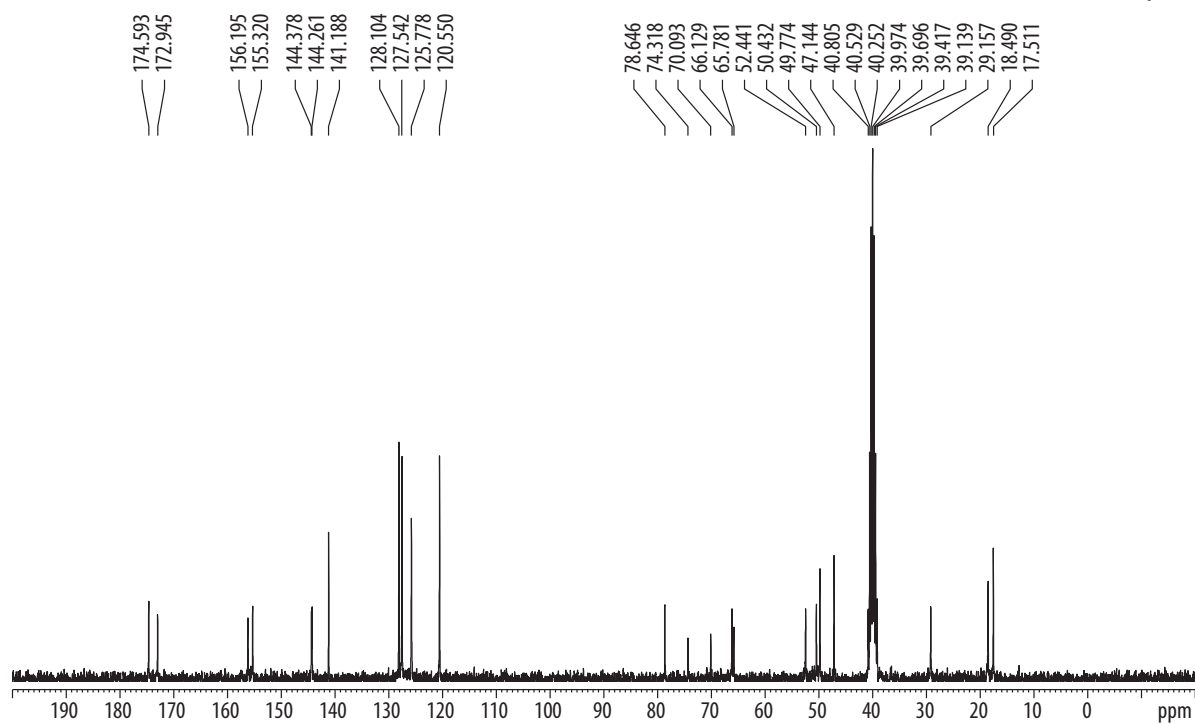
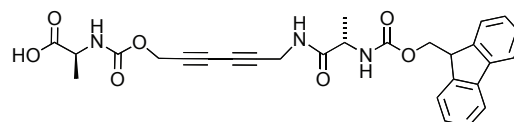
<sup>1</sup>H NMR of 75<sup>13</sup>C NMR of 75

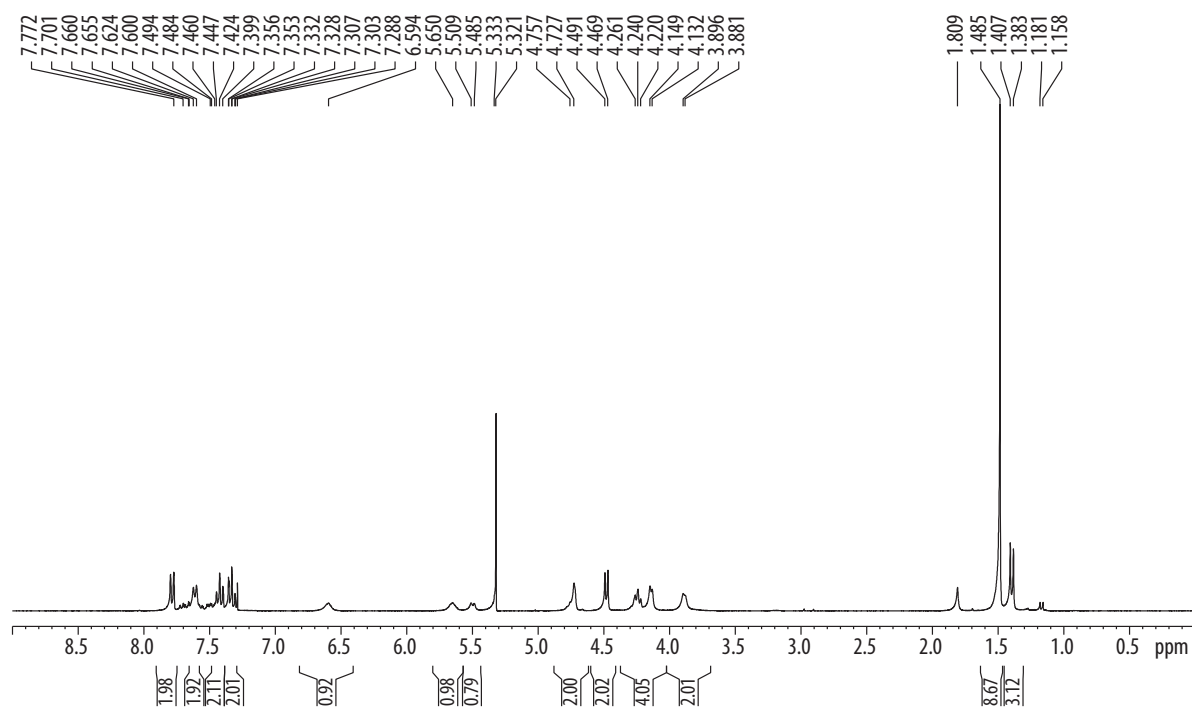
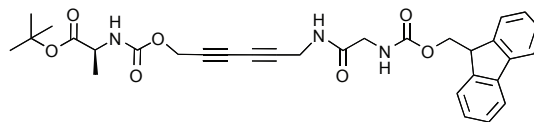
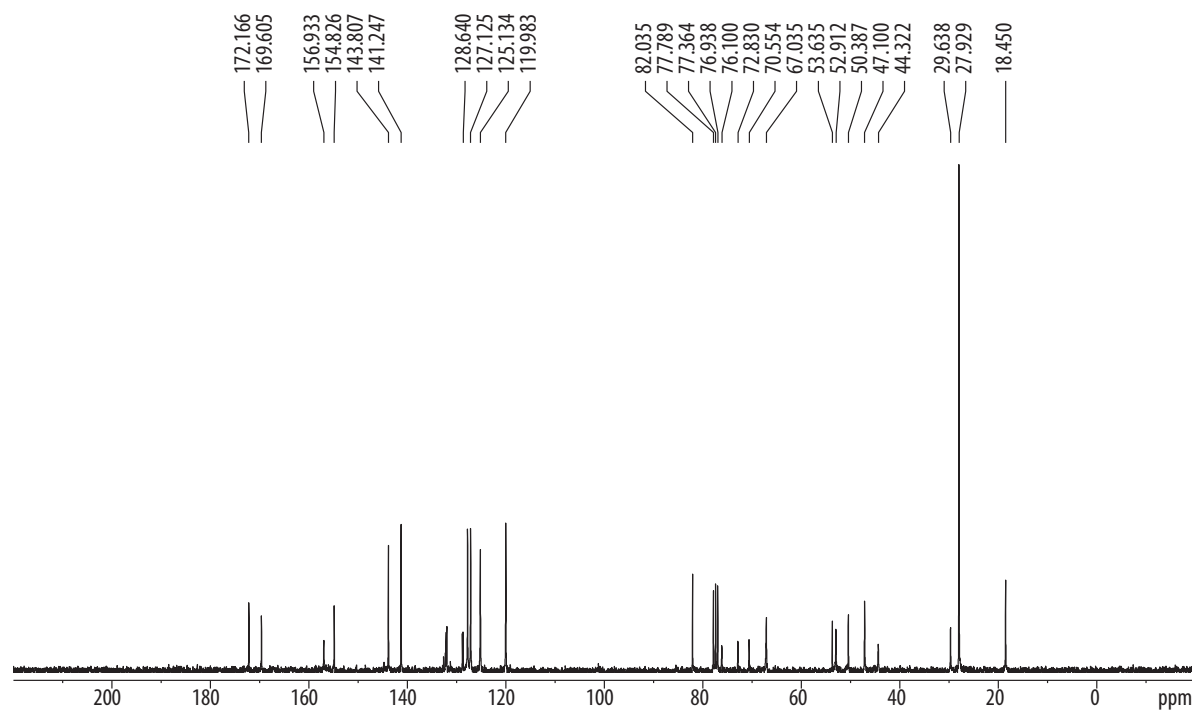
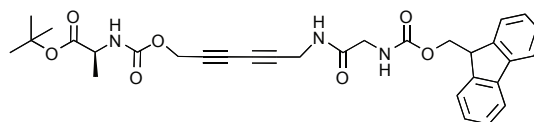
<sup>1</sup>H NMR of 76<sup>13</sup>C NMR of 76

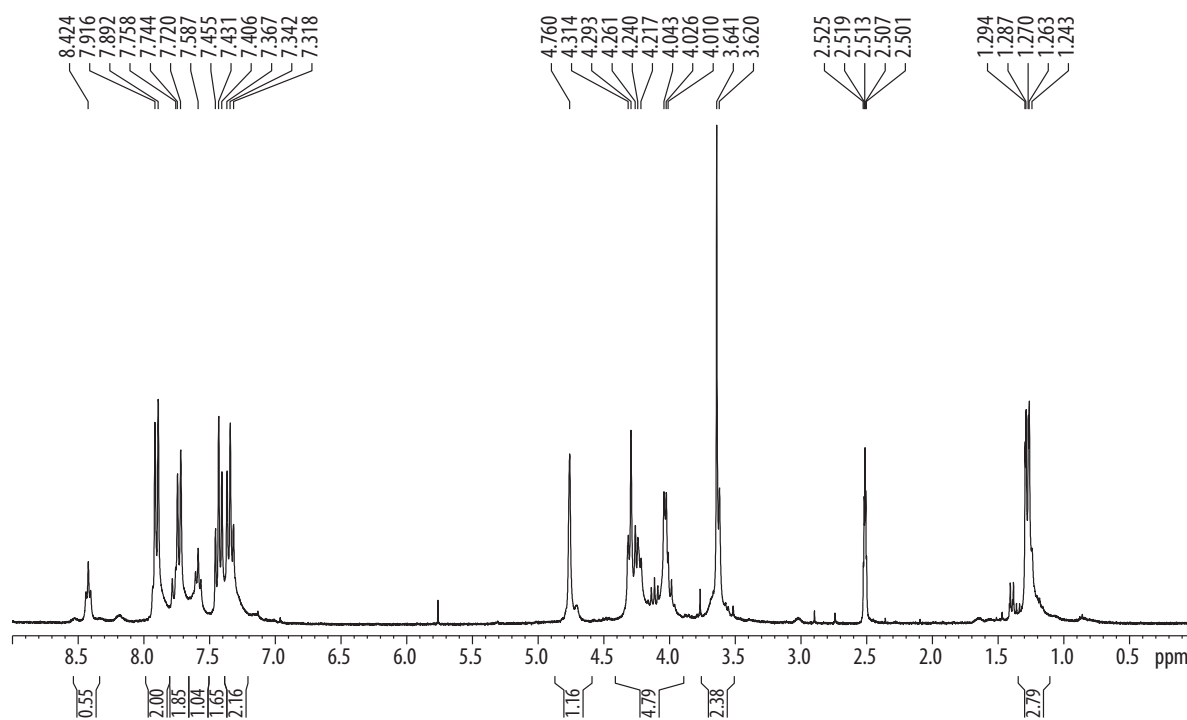
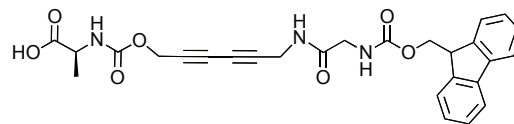
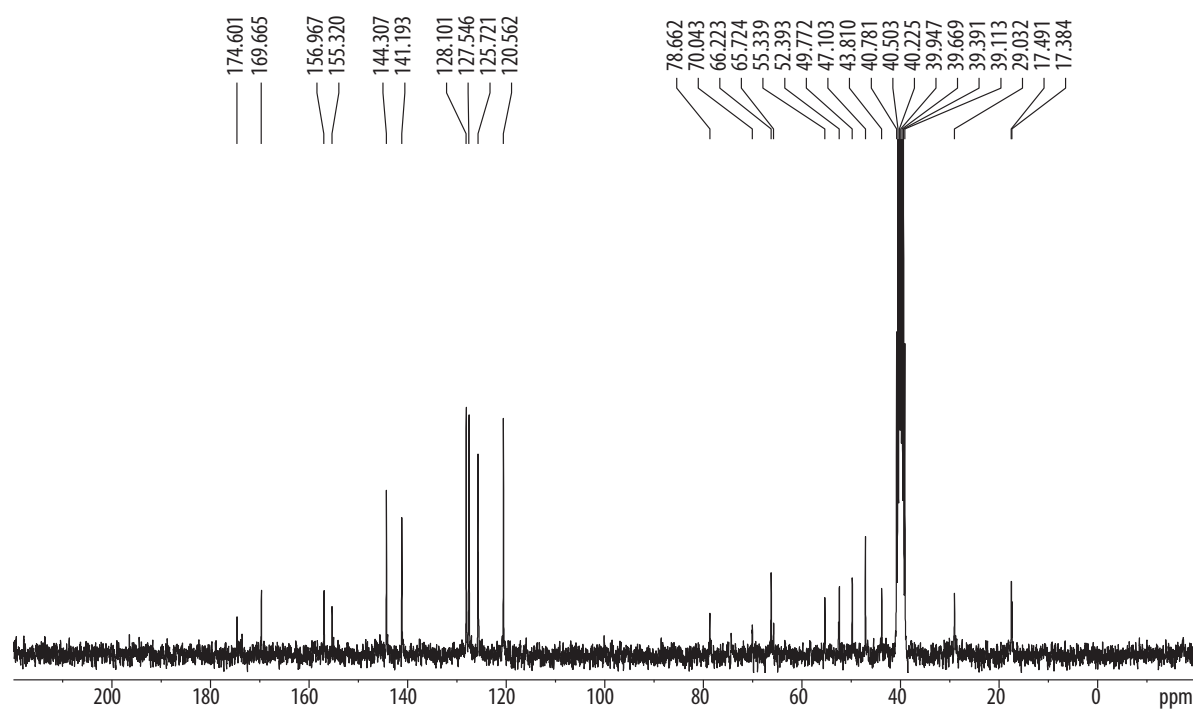
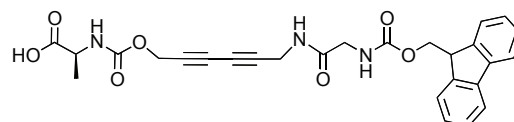
<sup>1</sup>H NMR of 77<sup>13</sup>C NMR of 77

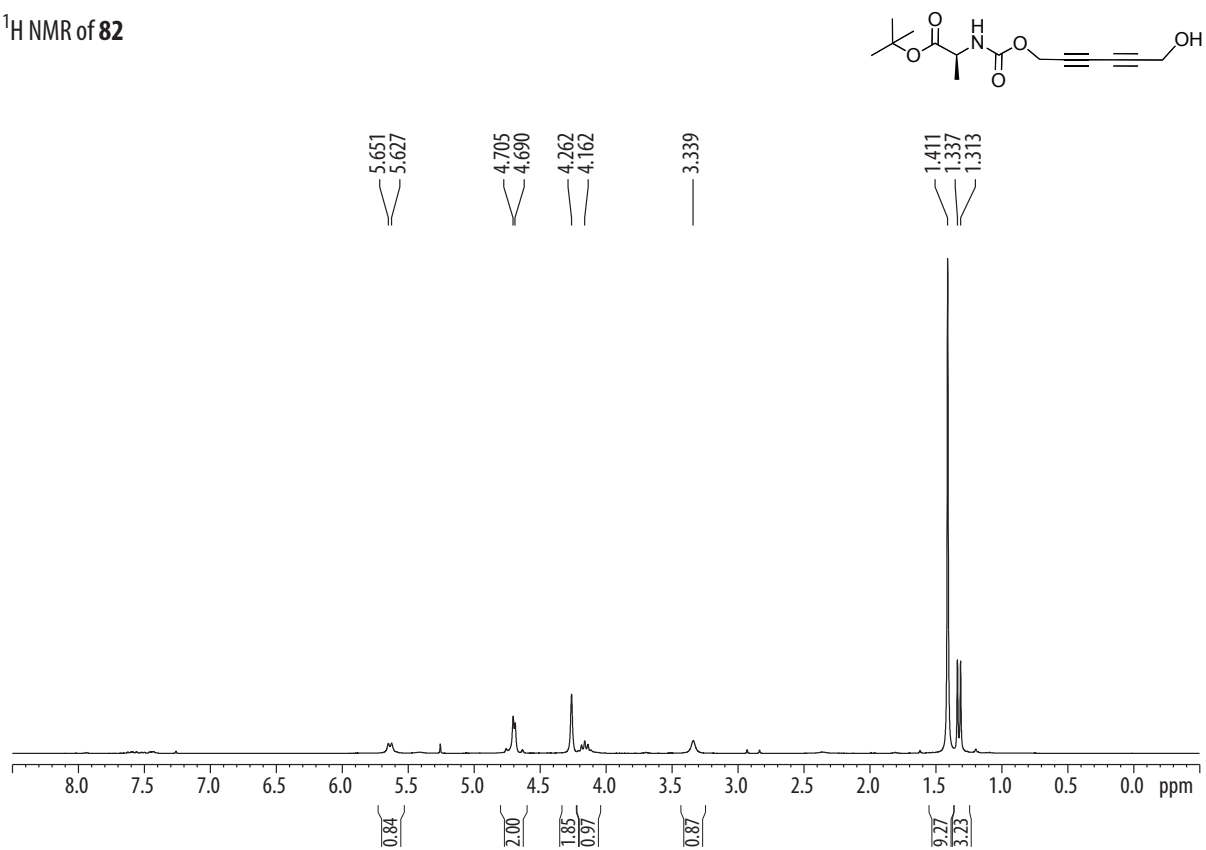
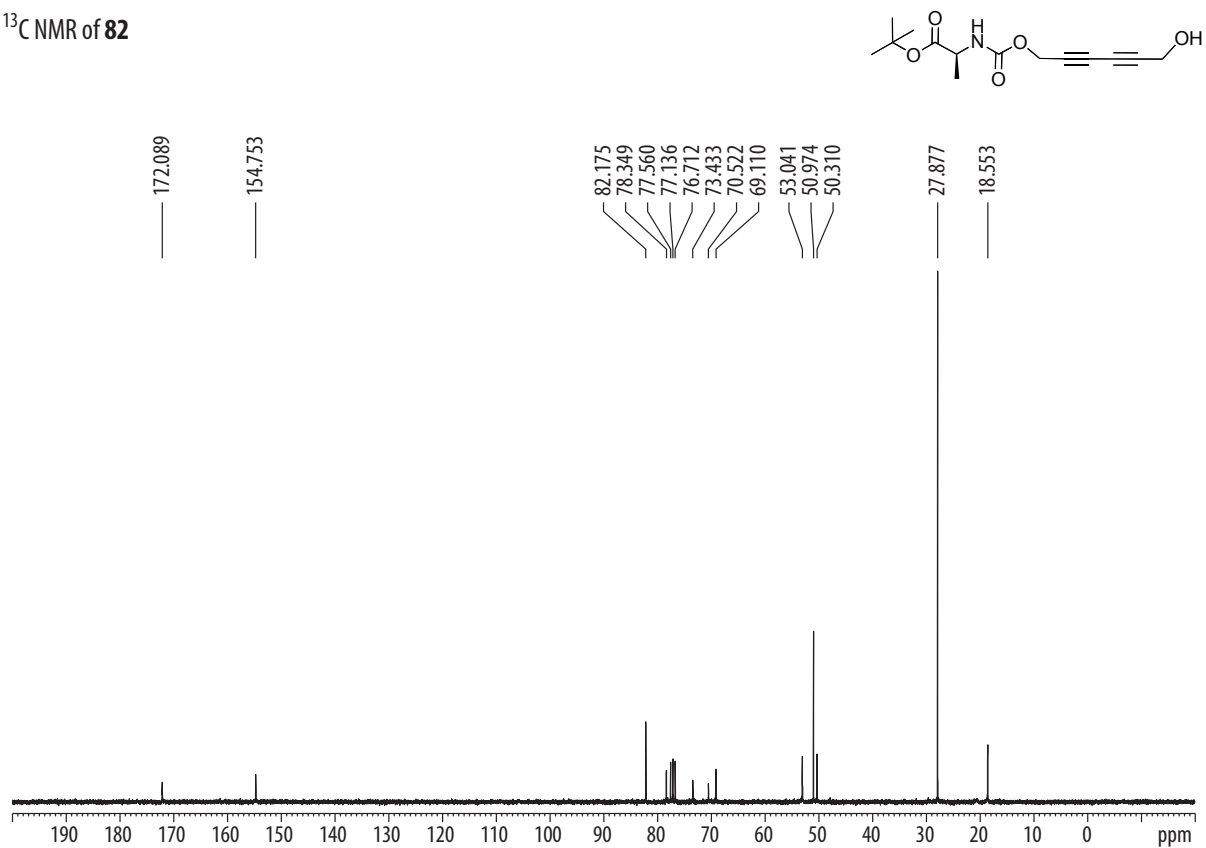
<sup>1</sup>H NMR of 78<sup>13</sup>C NMR of 78

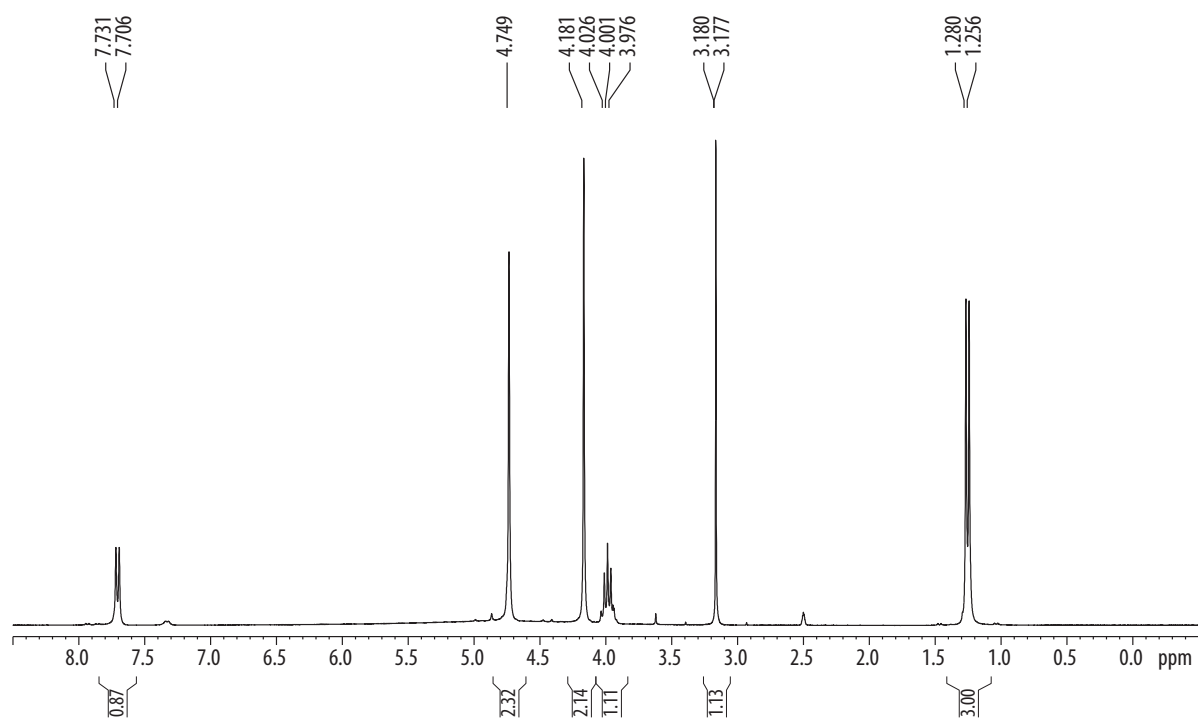
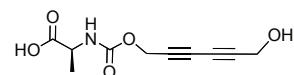
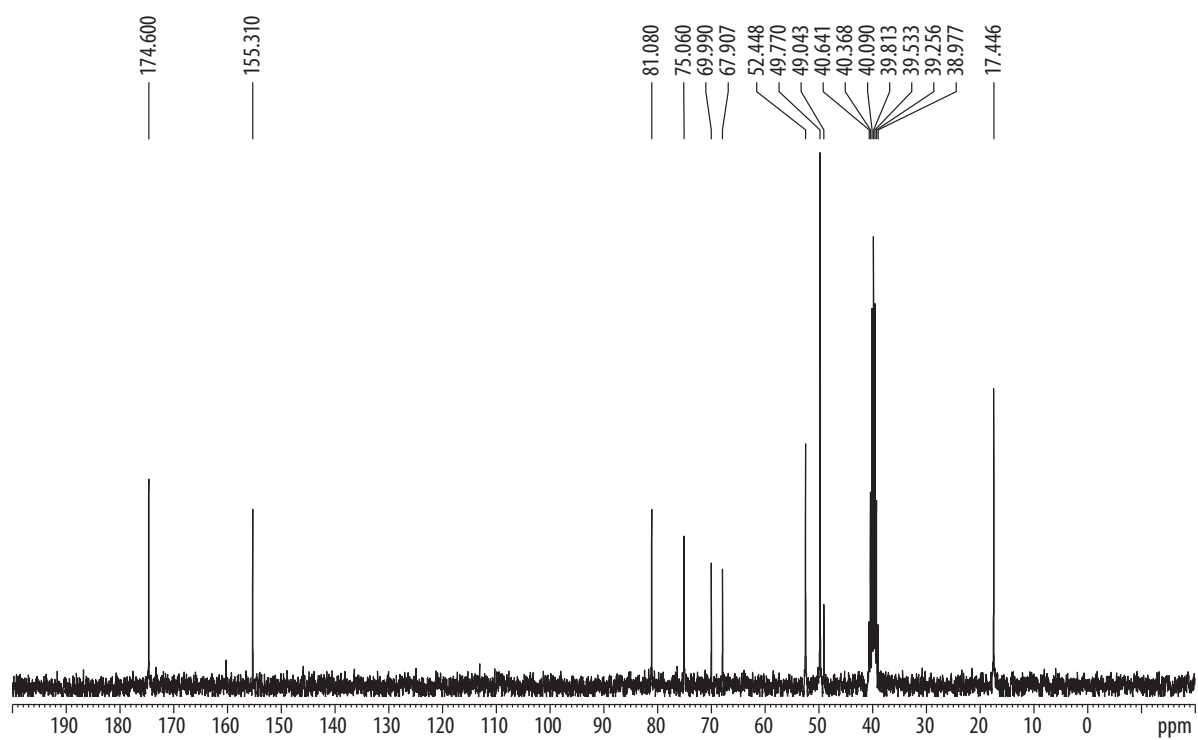
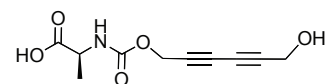


<sup>1</sup>H NMR of 79<sup>13</sup>C NMR of 79

<sup>1</sup>H NMR of **80**<sup>13</sup>C NMR of **80**

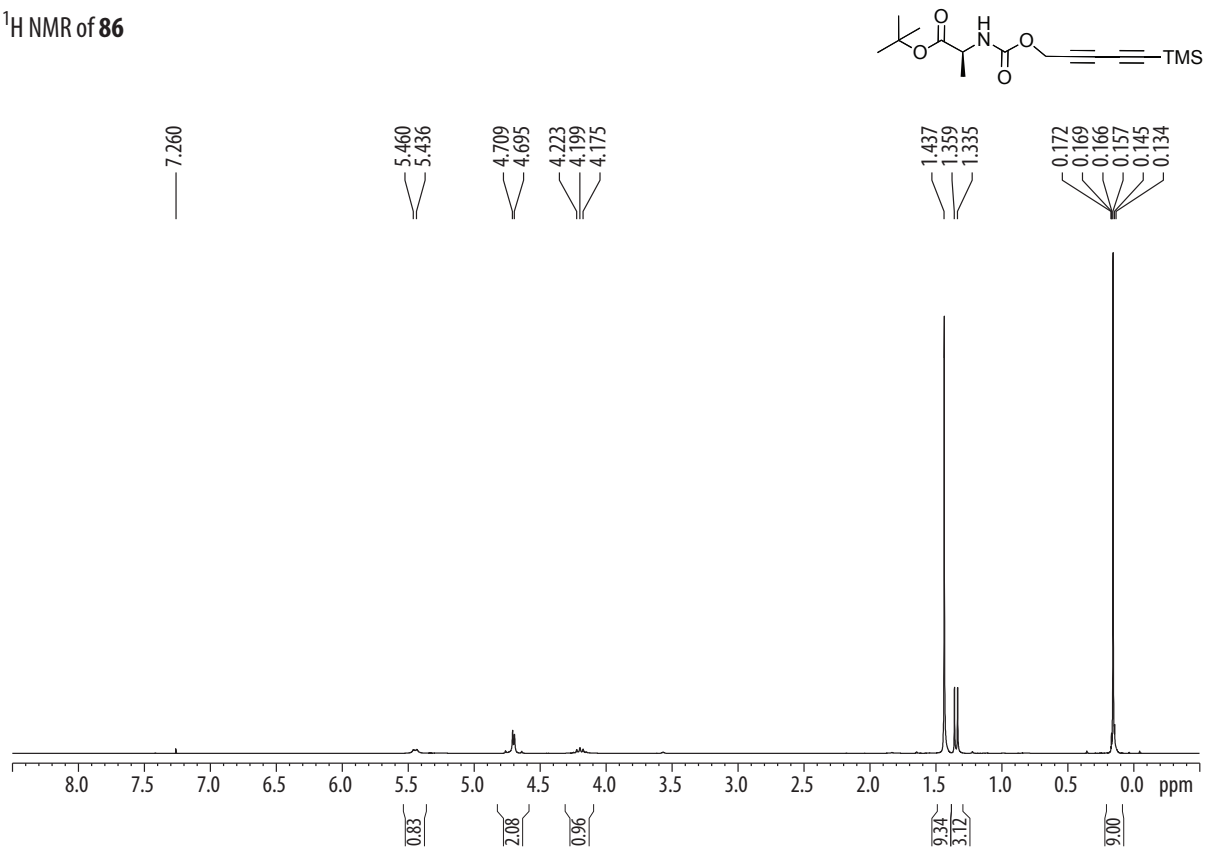
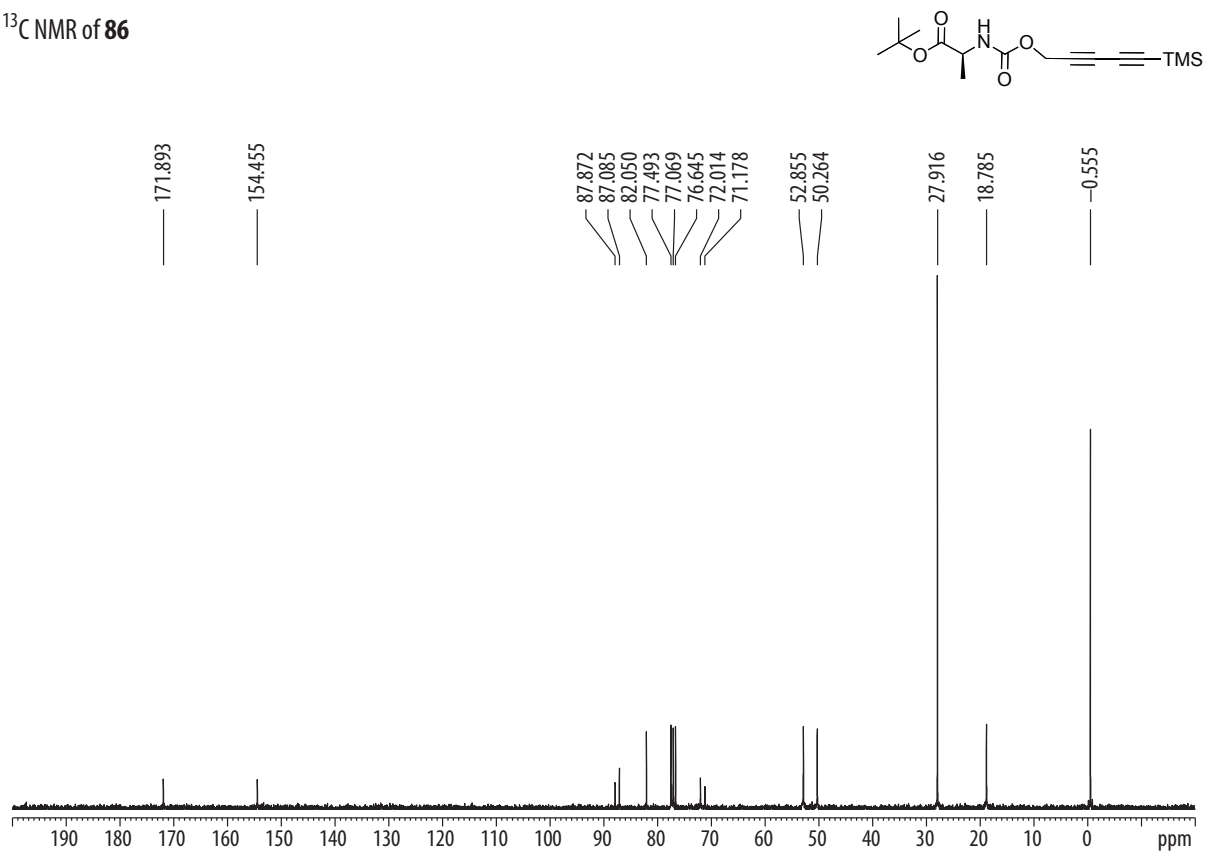
<sup>1</sup>H NMR of **81**<sup>13</sup>C NMR of **81**

<sup>1</sup>H NMR of **82**<sup>13</sup>C NMR of **82**

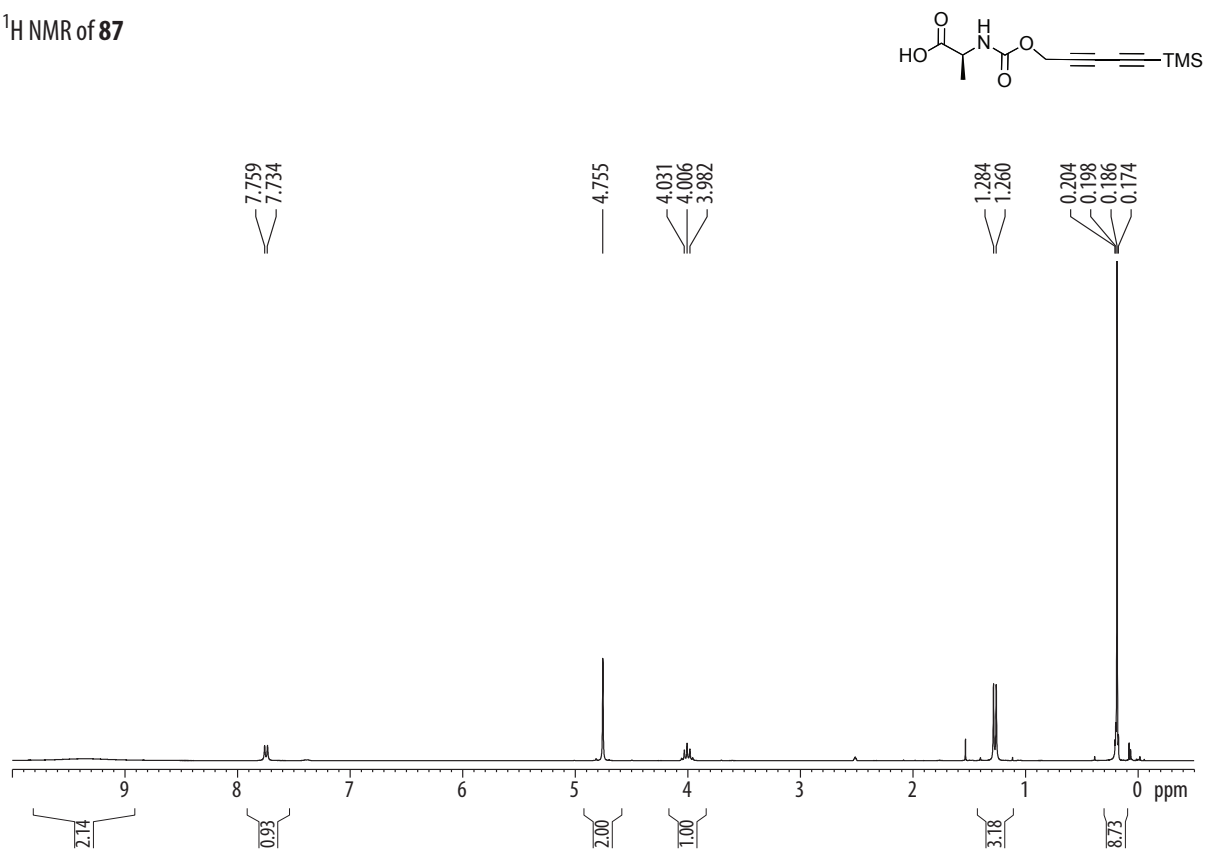
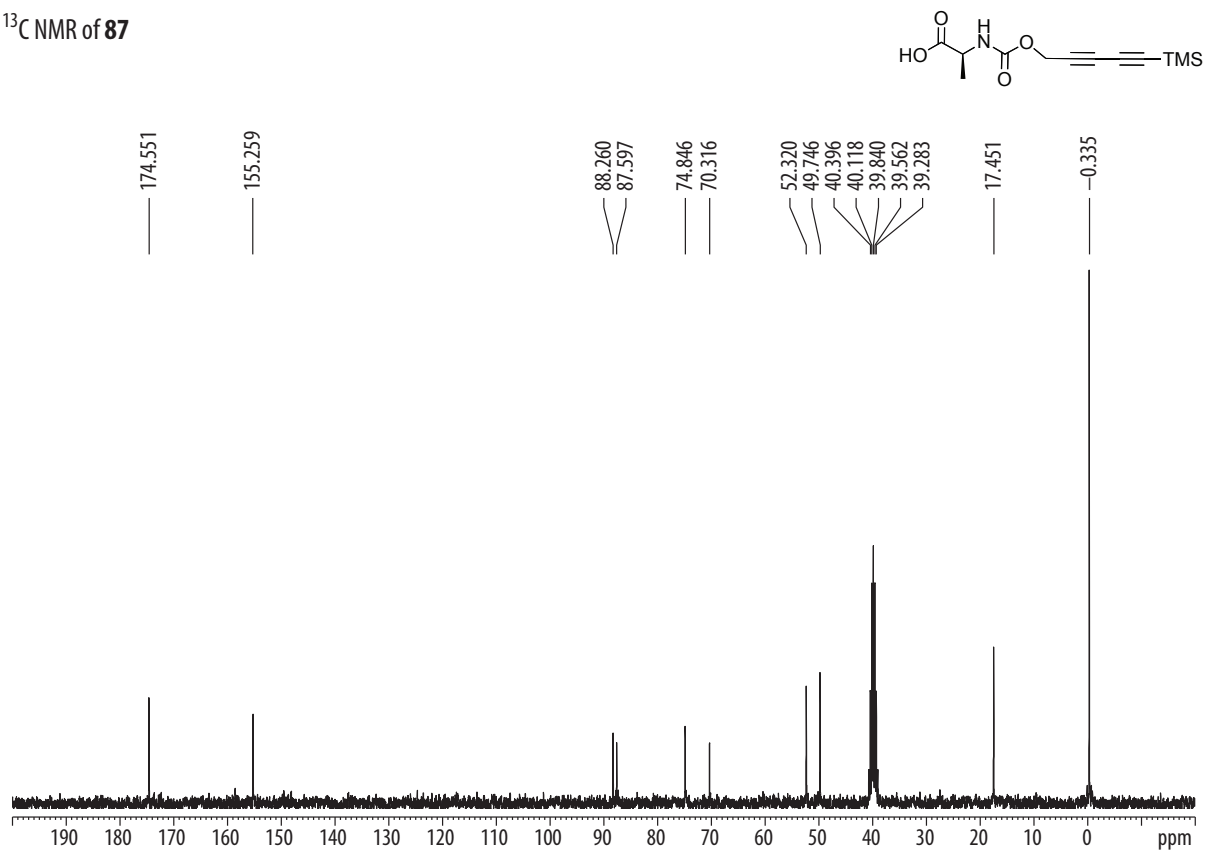
<sup>1</sup>H NMR of **83**<sup>13</sup>C NMR of **83**

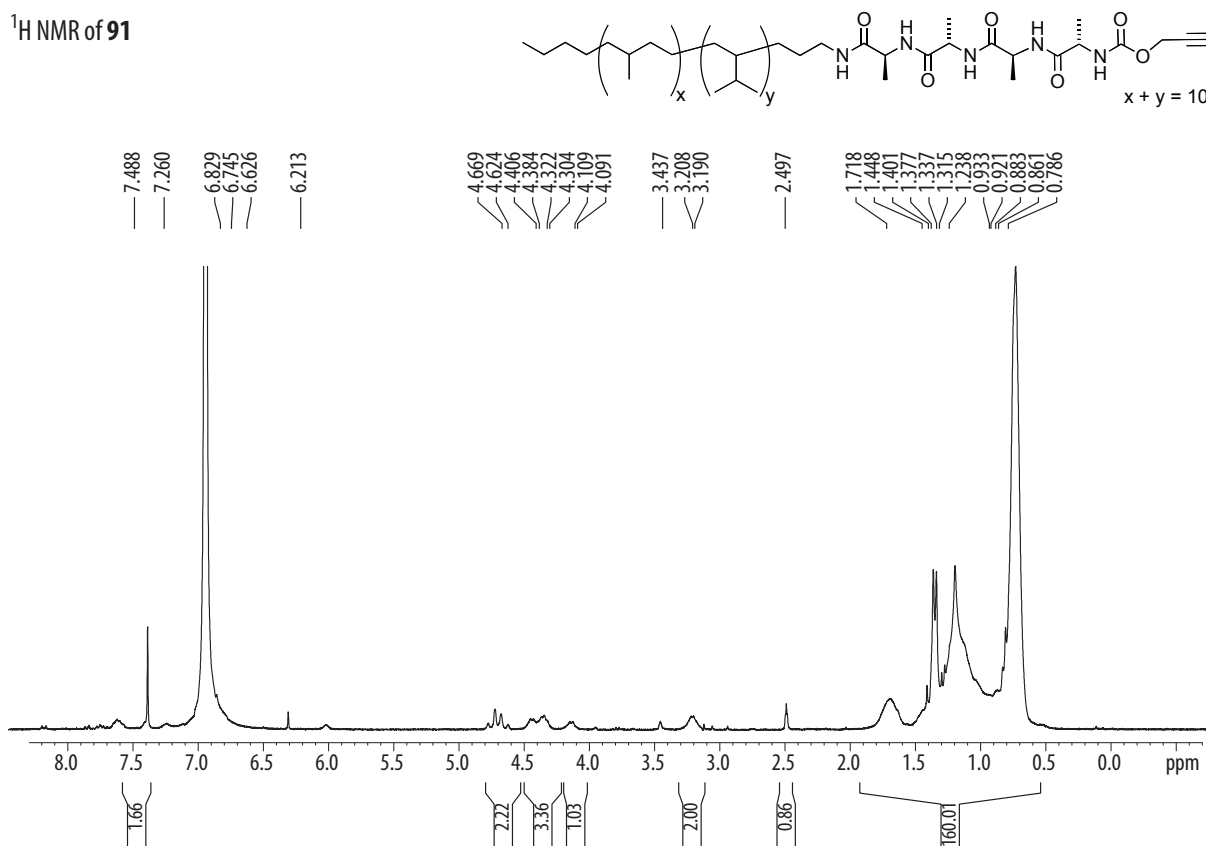
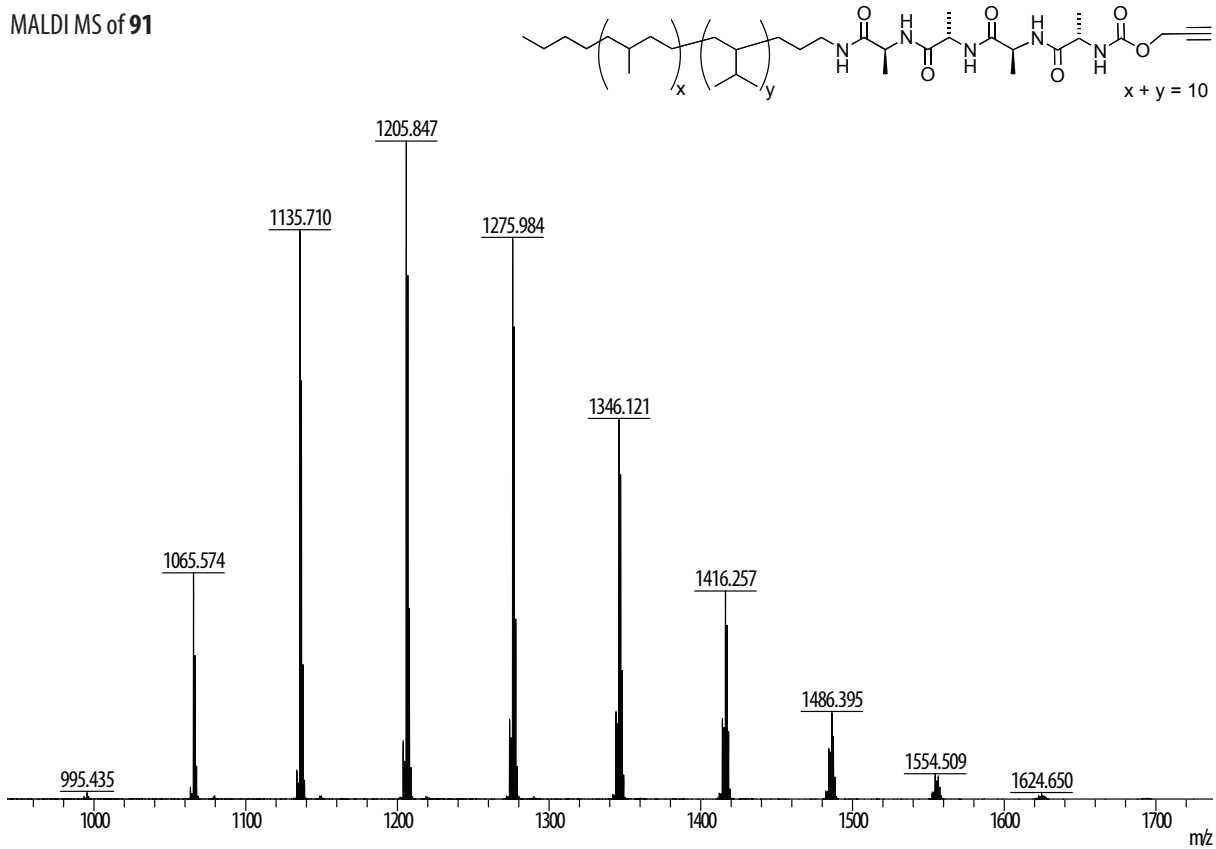


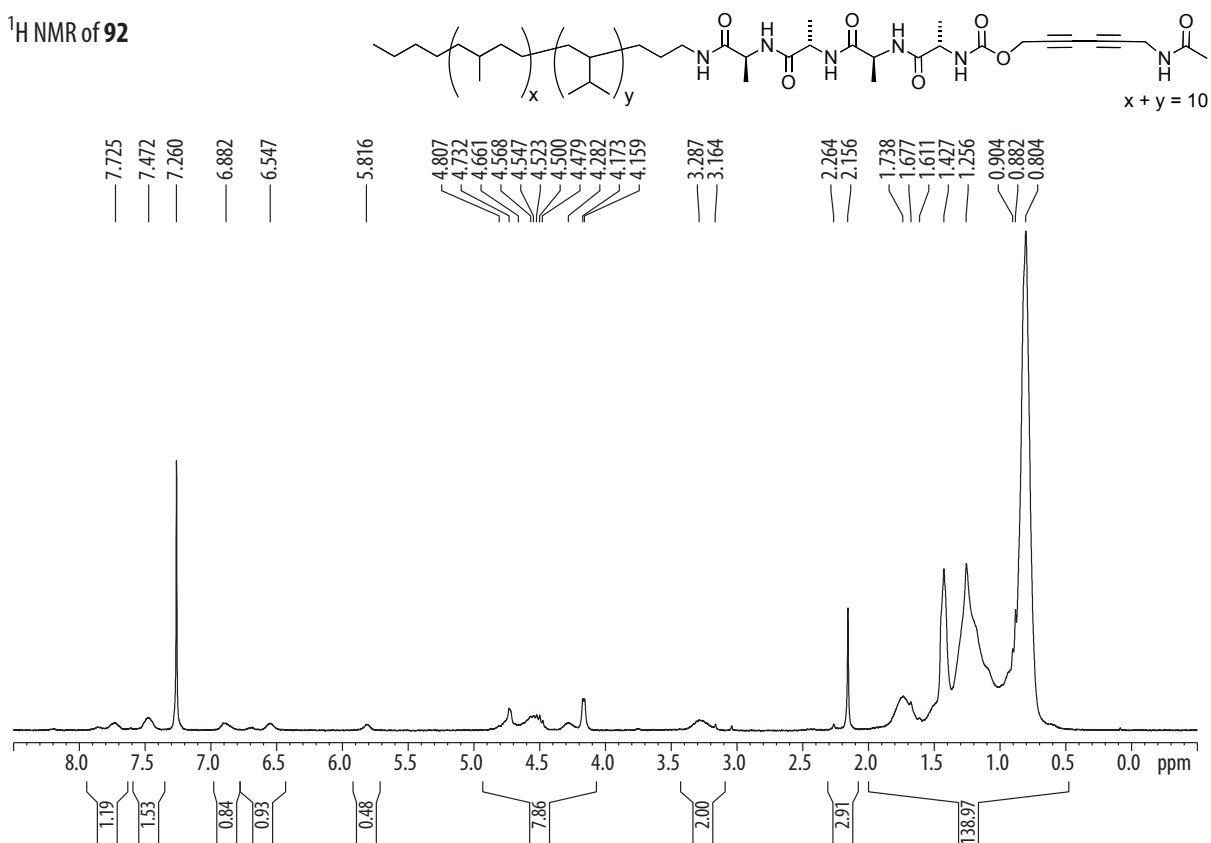
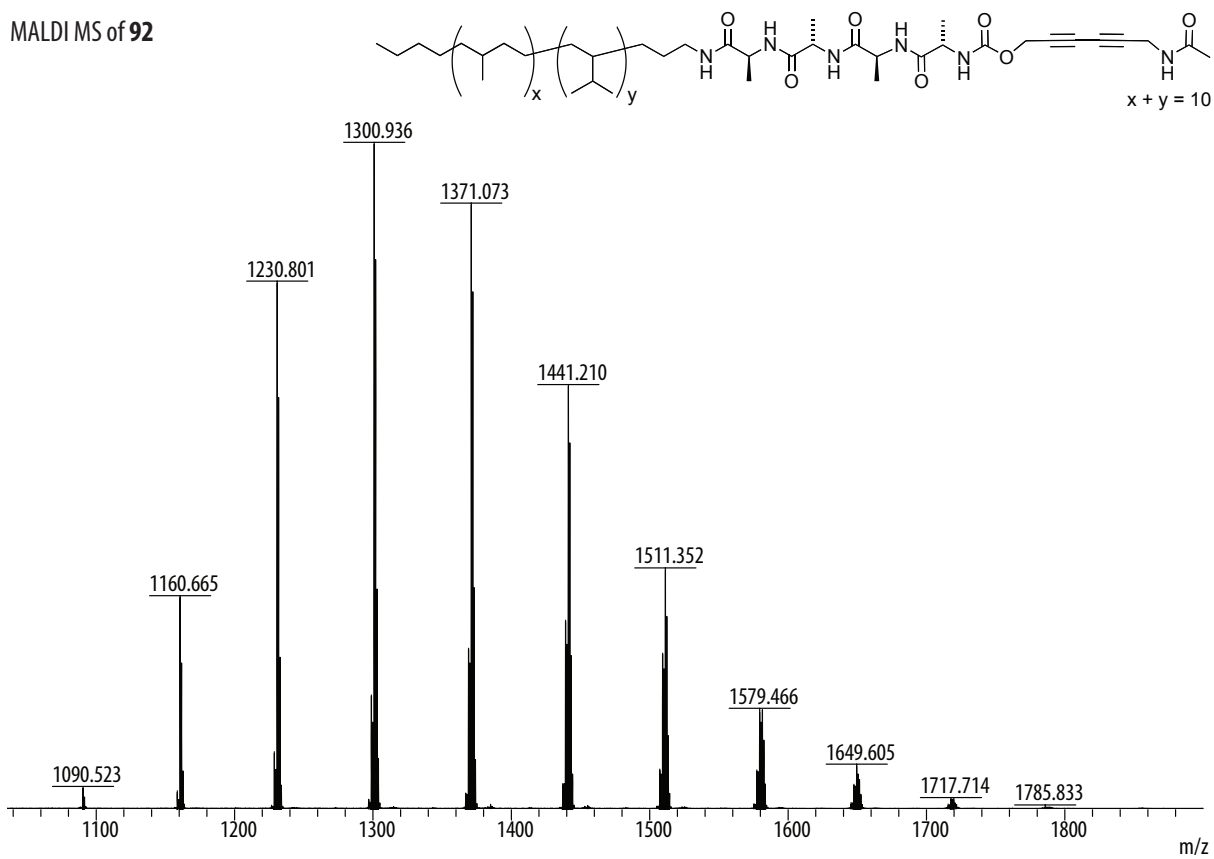


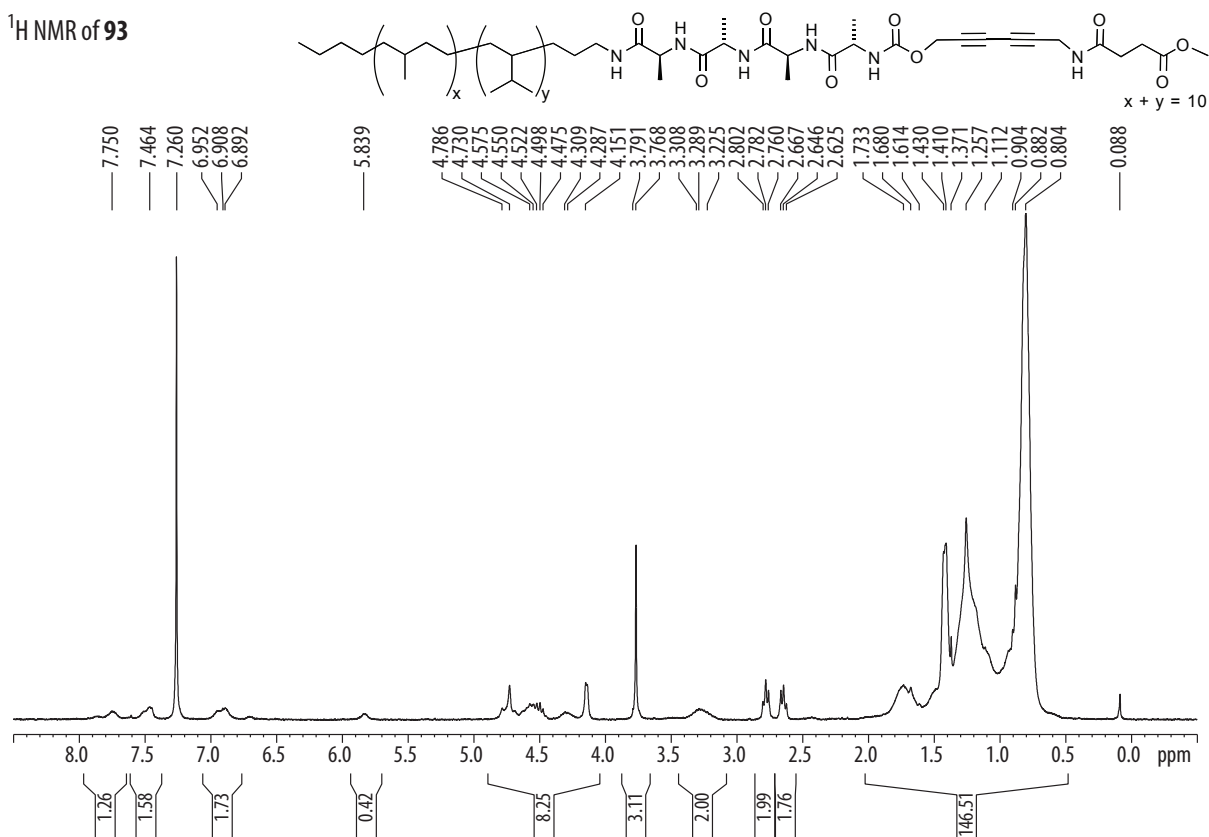
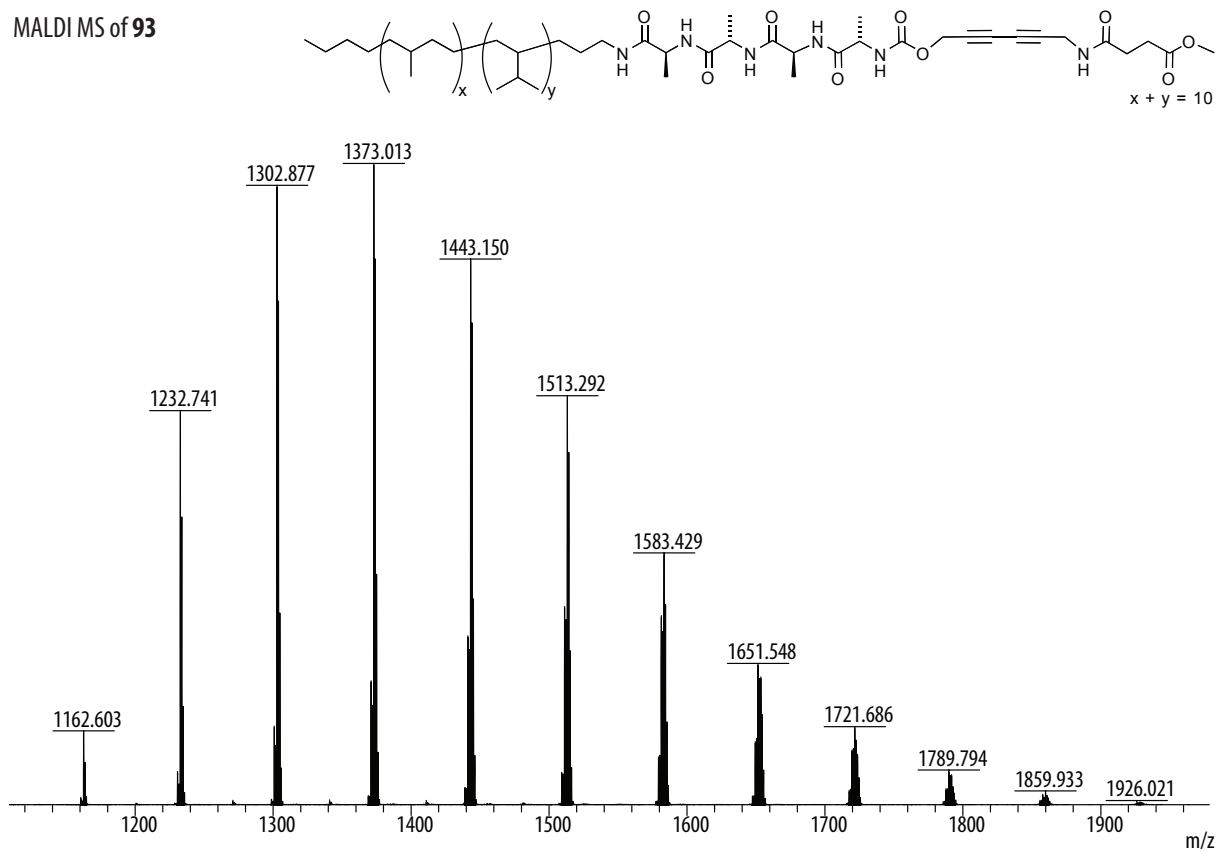
<sup>1</sup>H NMR of **86**<sup>13</sup>C NMR of **86**



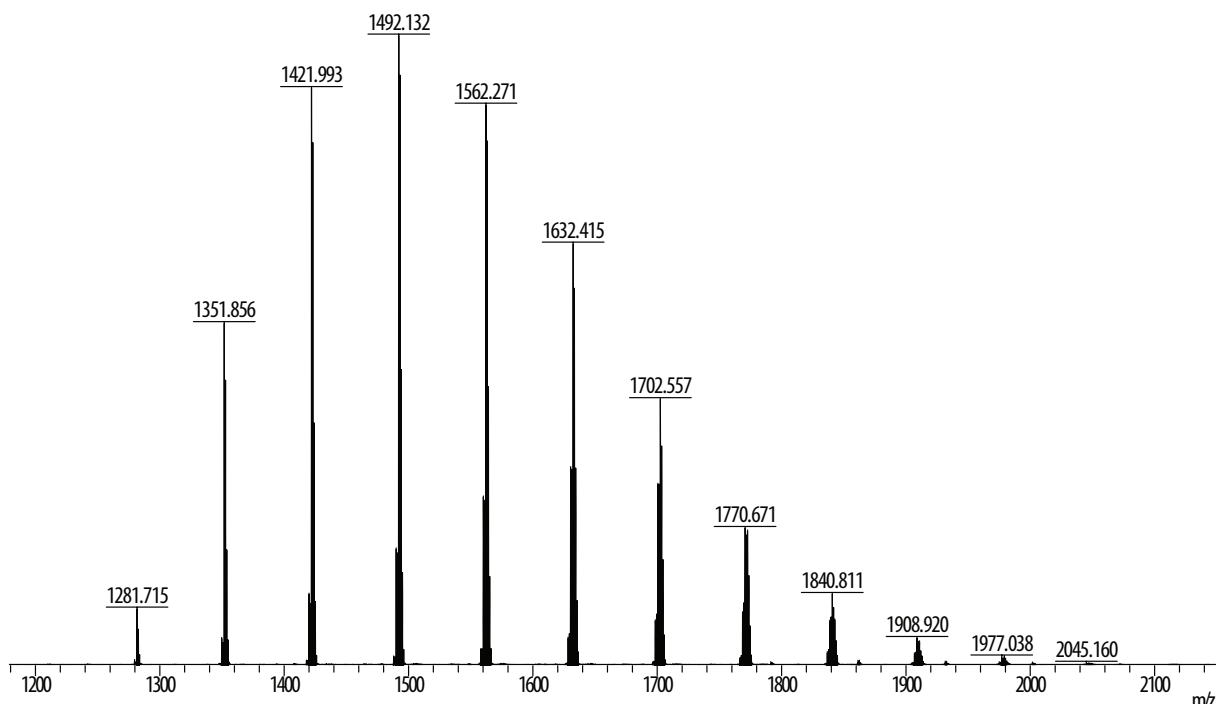
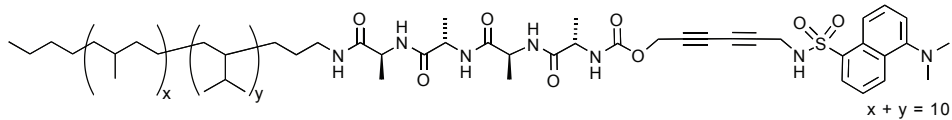
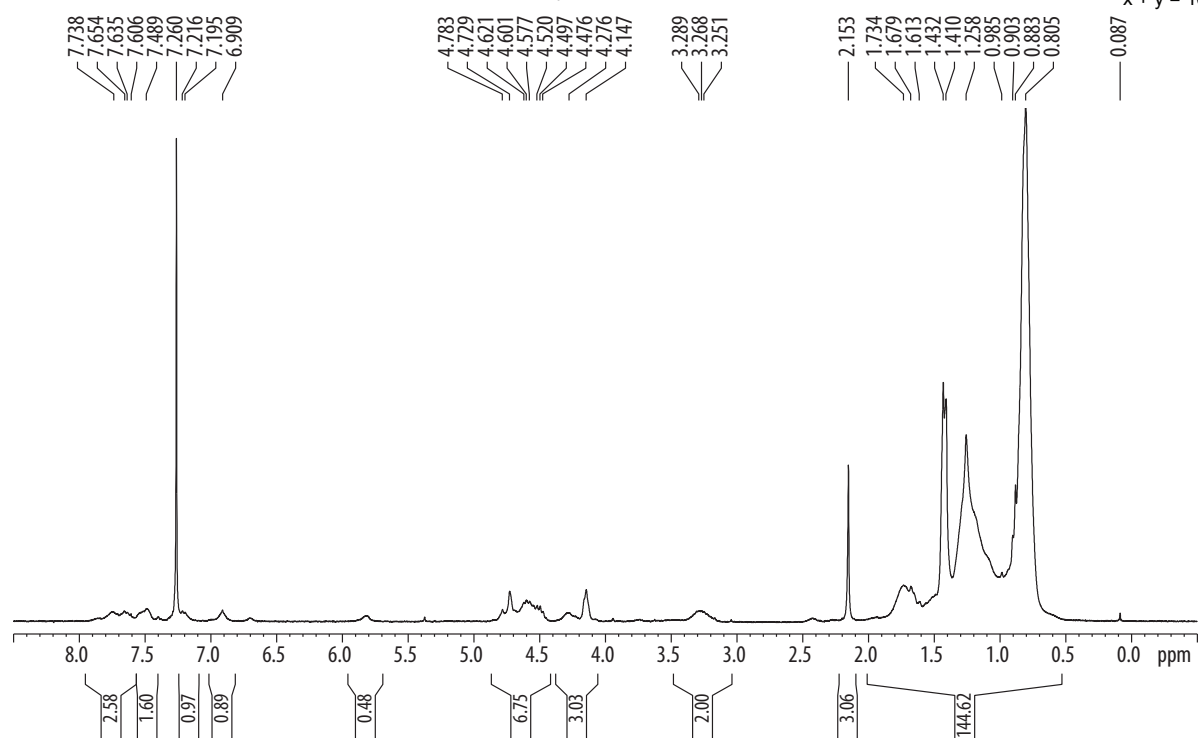
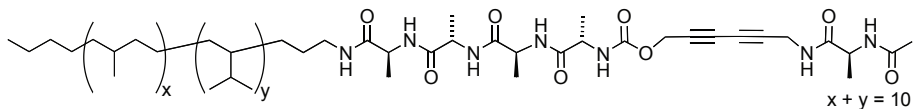
<sup>1</sup>H NMR of **87**<sup>13</sup>C NMR of **87**

$^1\text{H}$  NMR of **91**MALDI MS of **91**

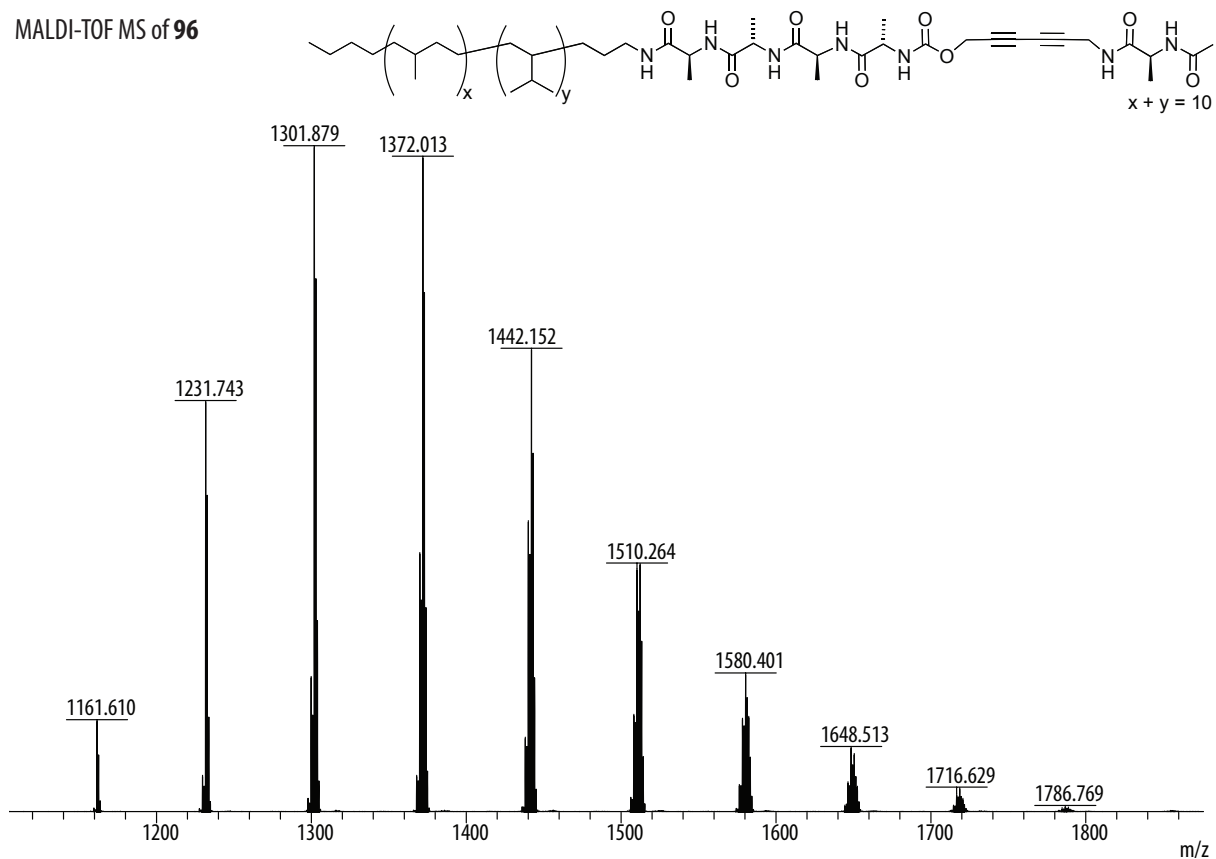
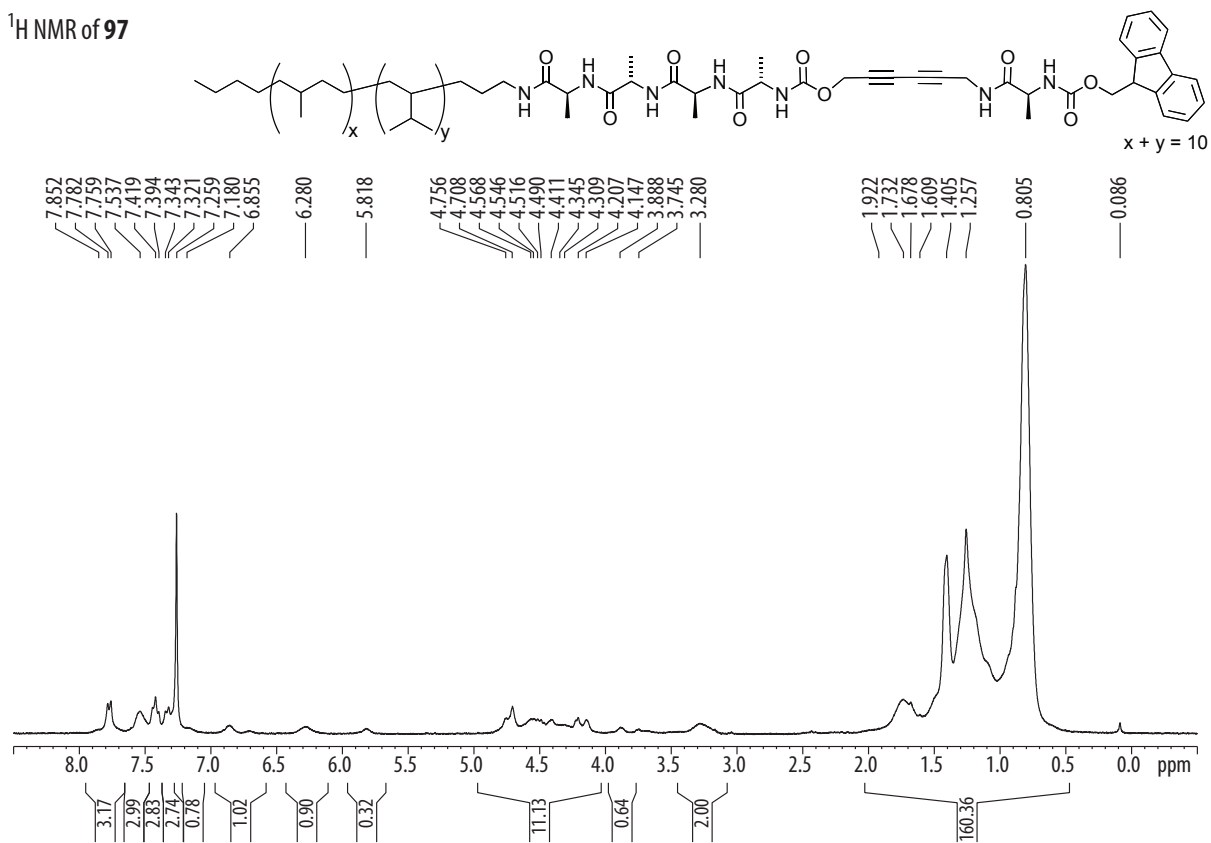
$^1\text{H}$  NMR of **92**MALDI MS of **92**

$^1\text{H}$  NMR of **93**MALDI MS of **93**

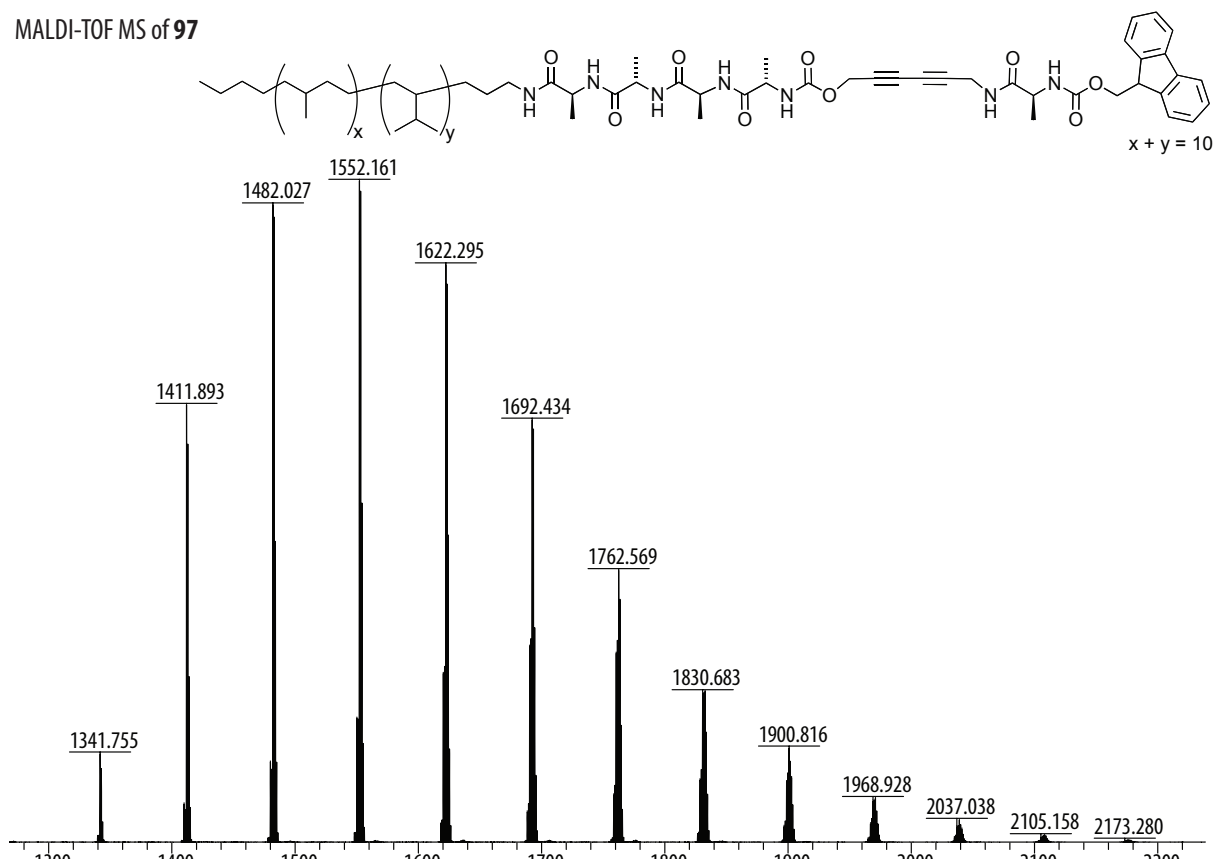
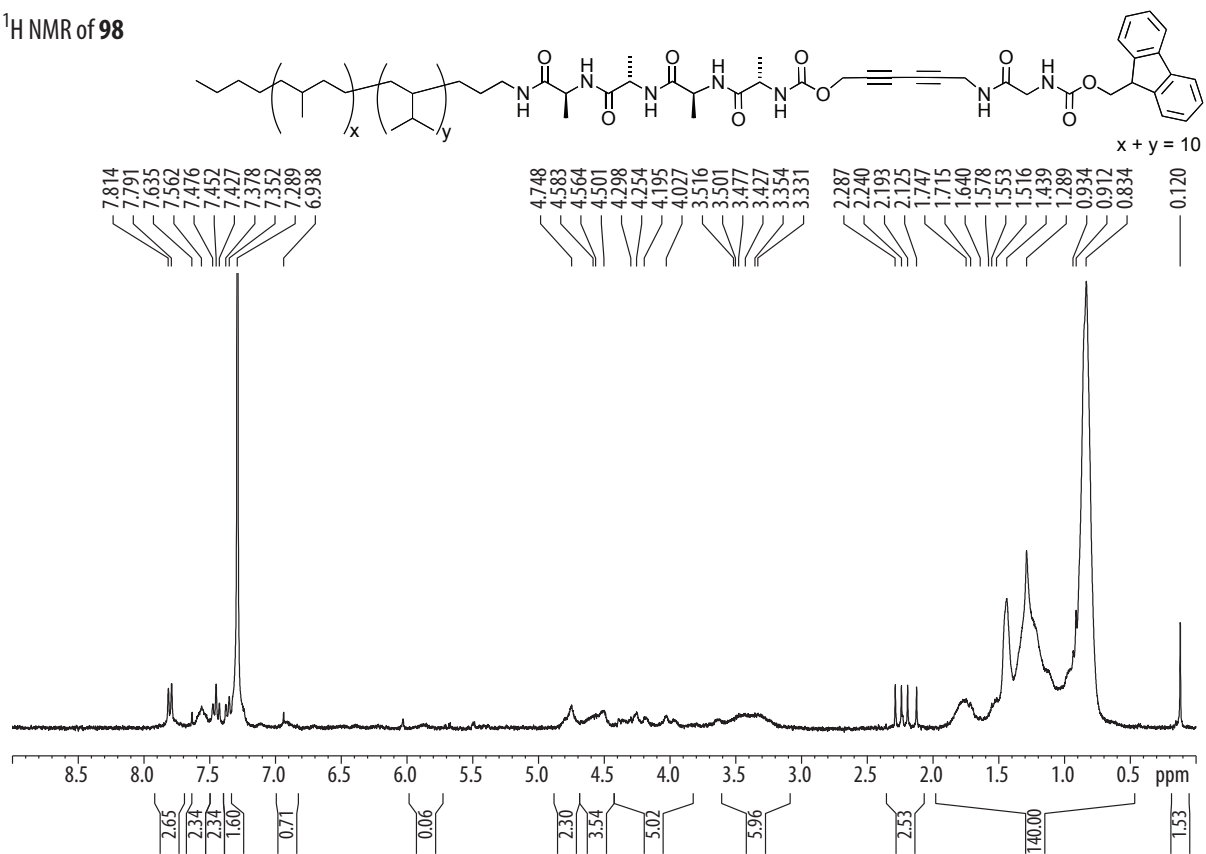


MALDI-TOF MS of **95** $^1\text{H}$  NMR of **96**

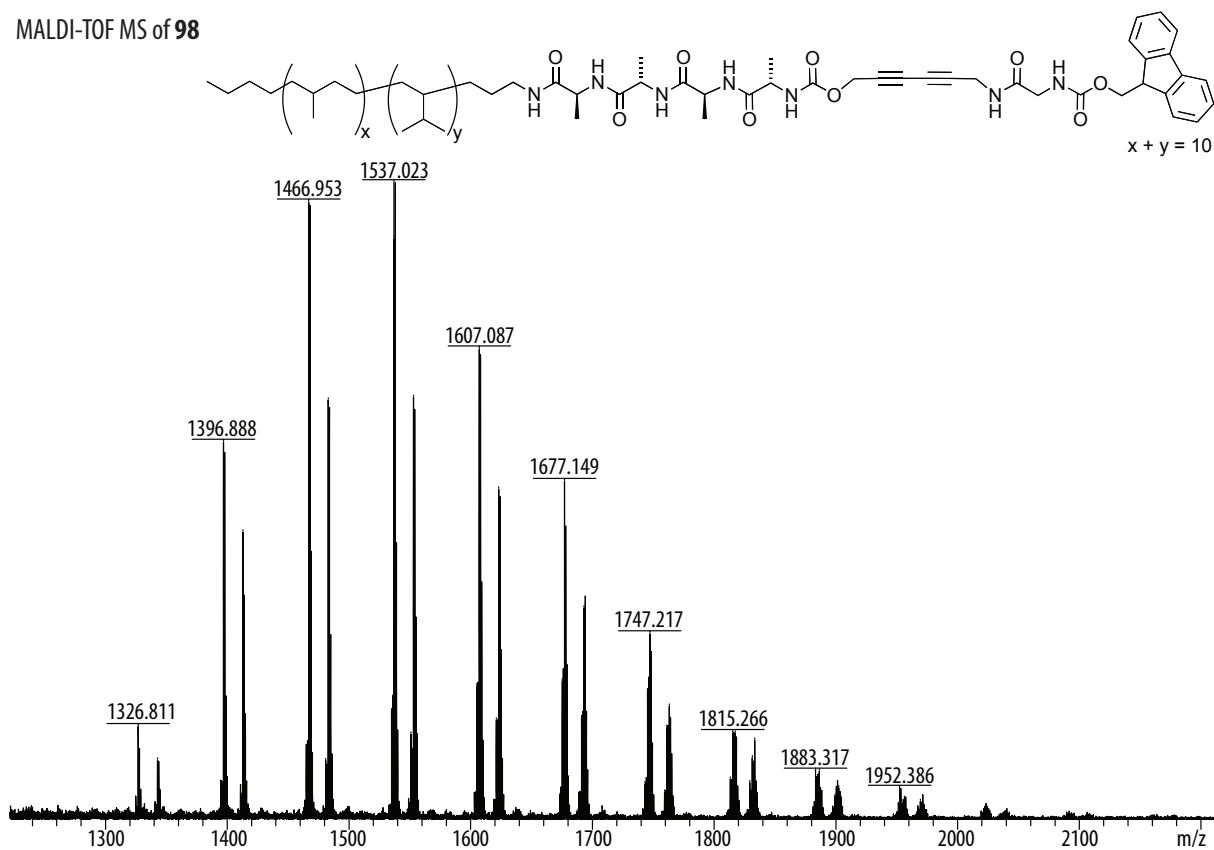
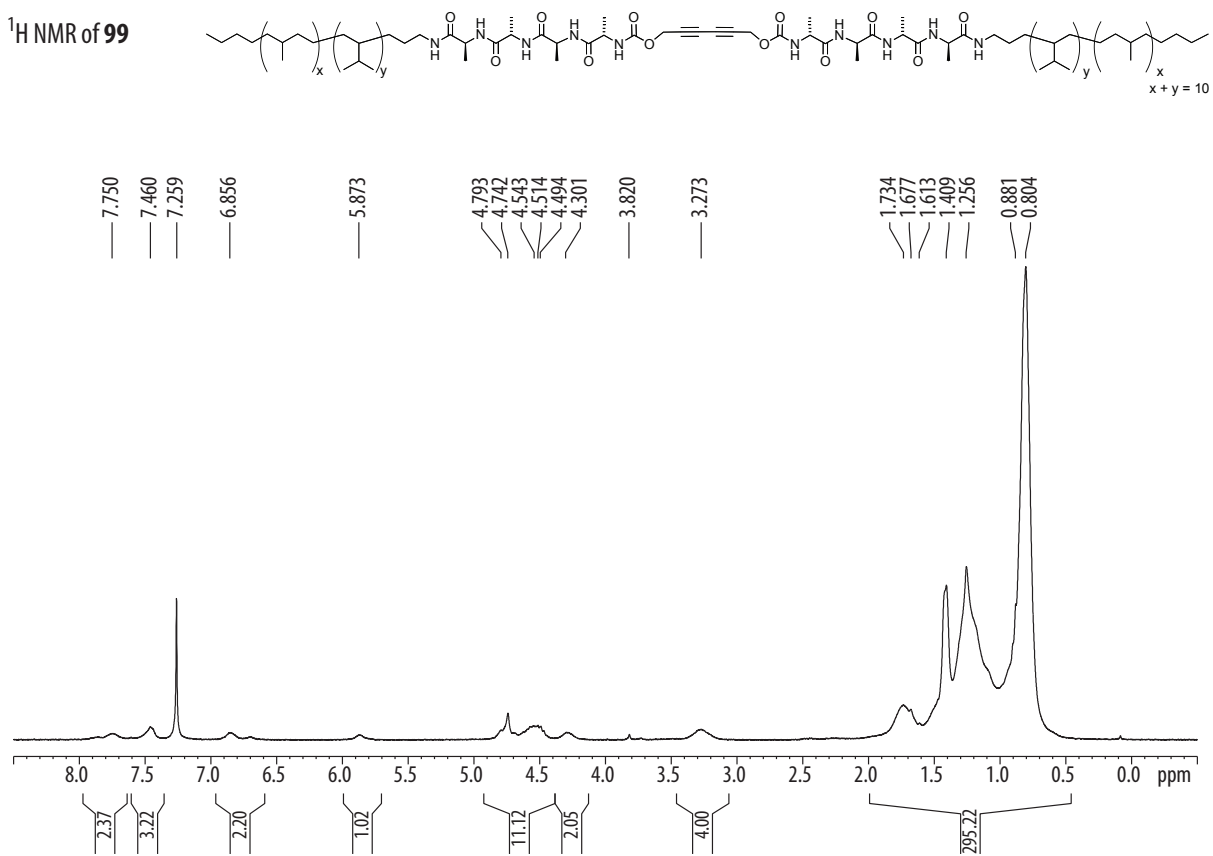
## MALDI-TOF MS of 96

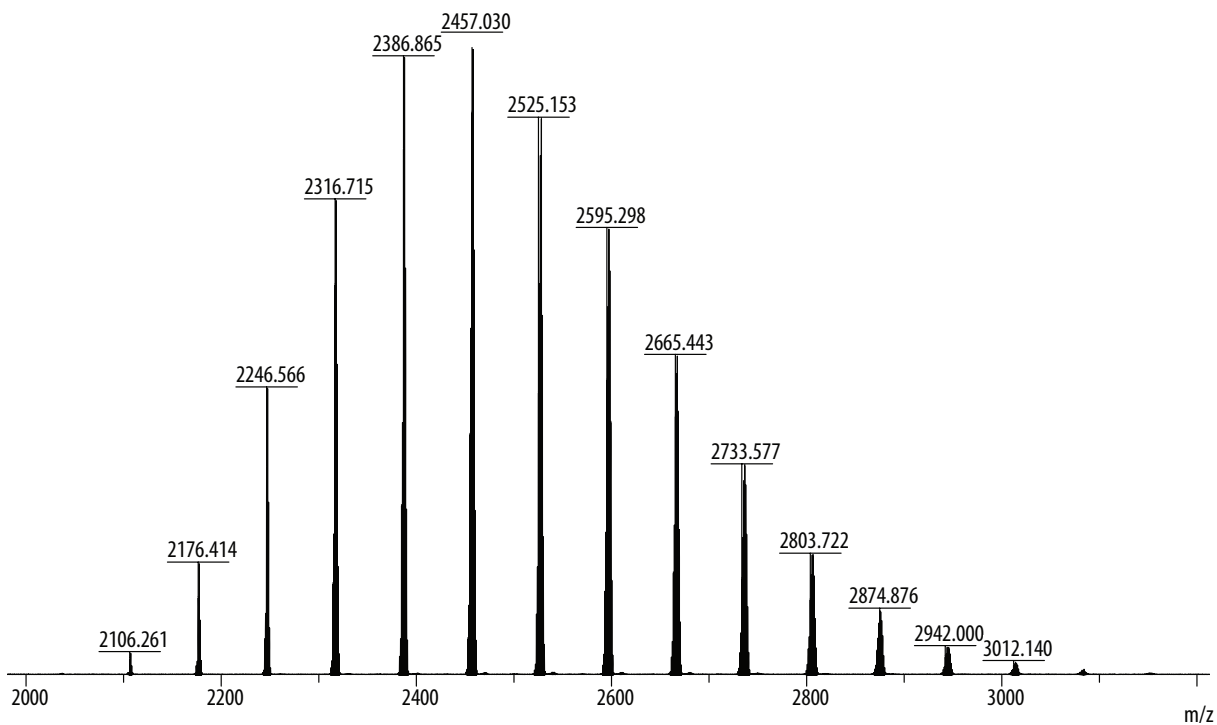
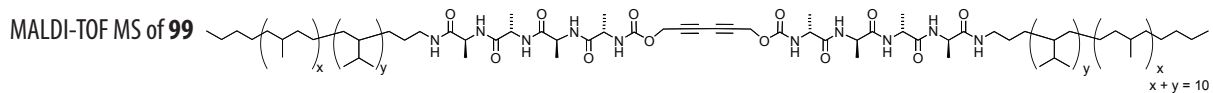
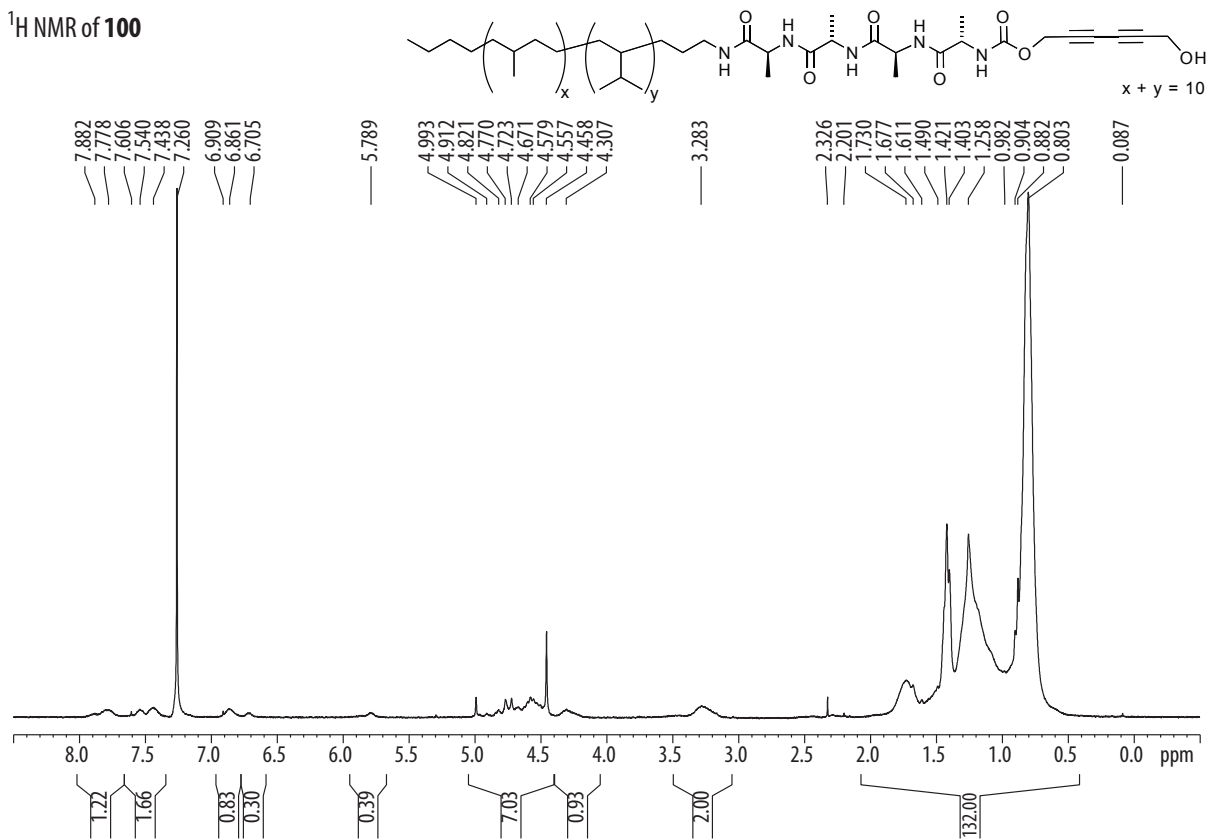
 $^1\text{H}$  NMR of 97

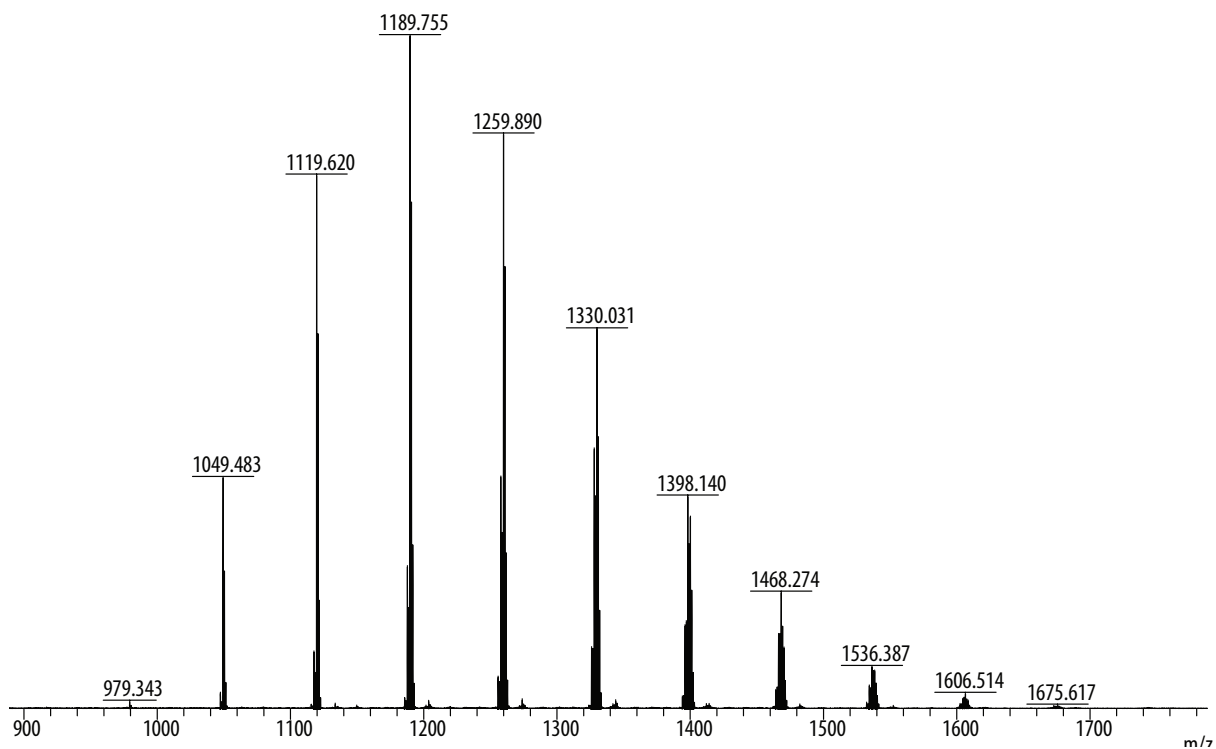
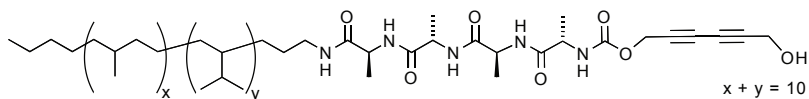
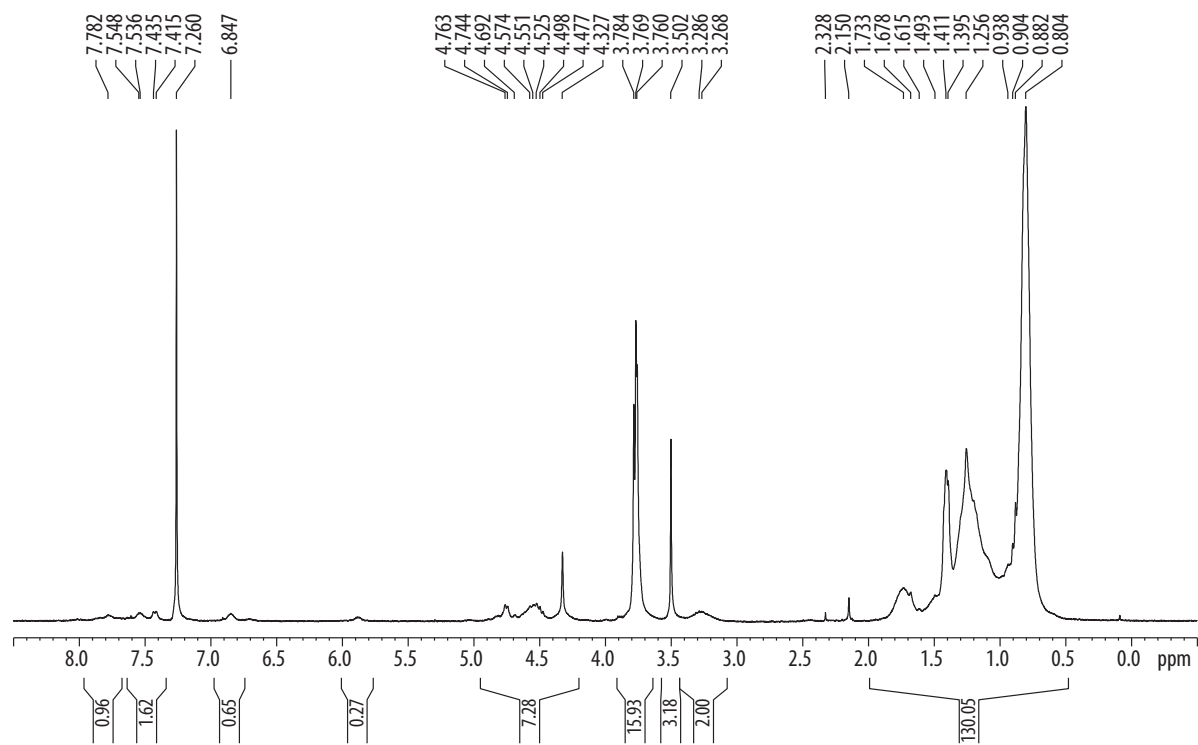
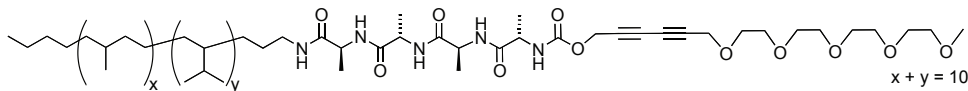
## MALDI-TOF MS of 97

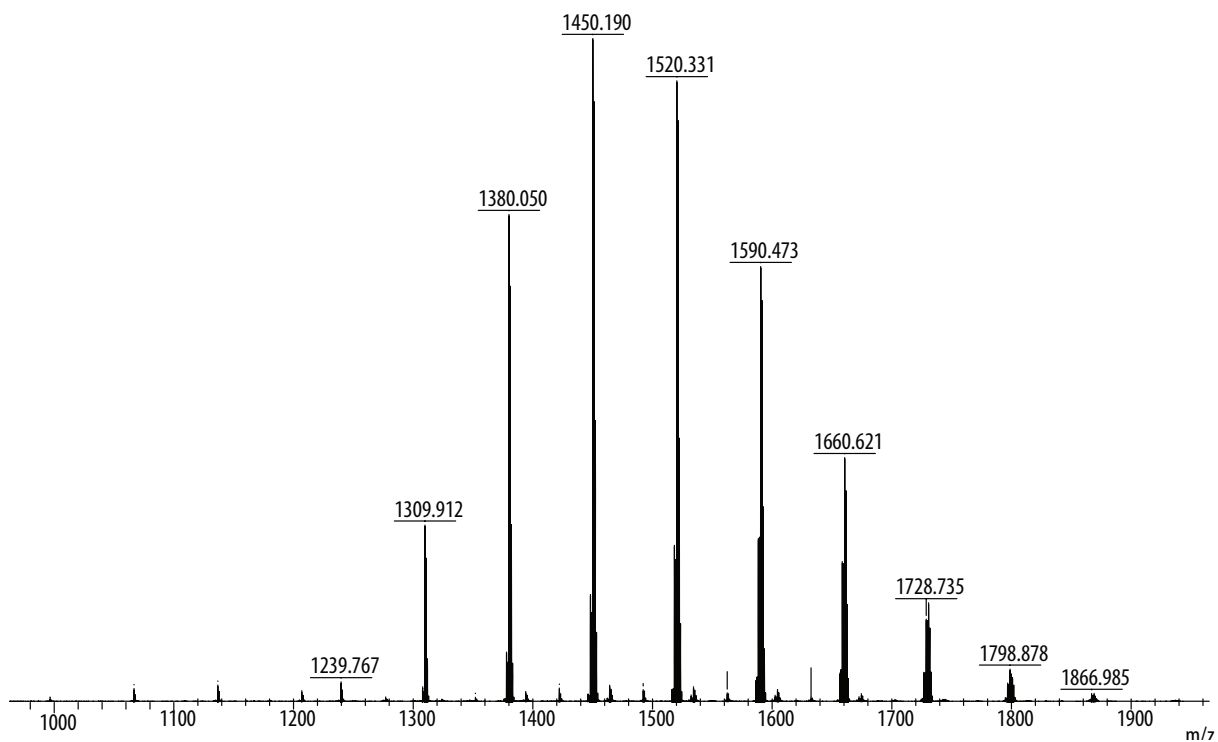
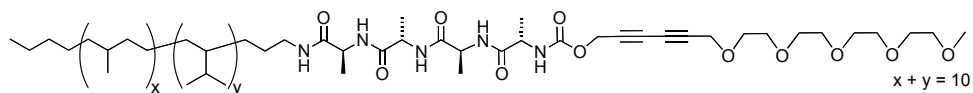
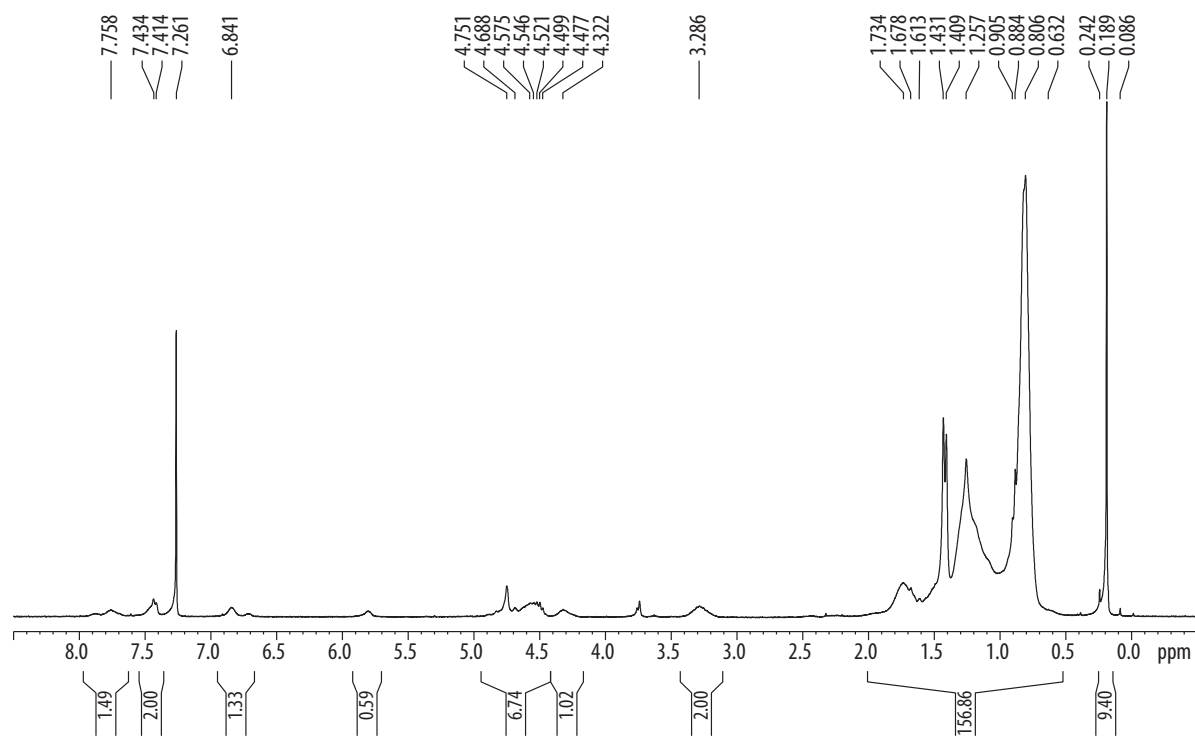
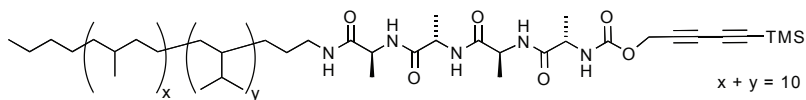
 $^1\text{H}$  NMR of 98

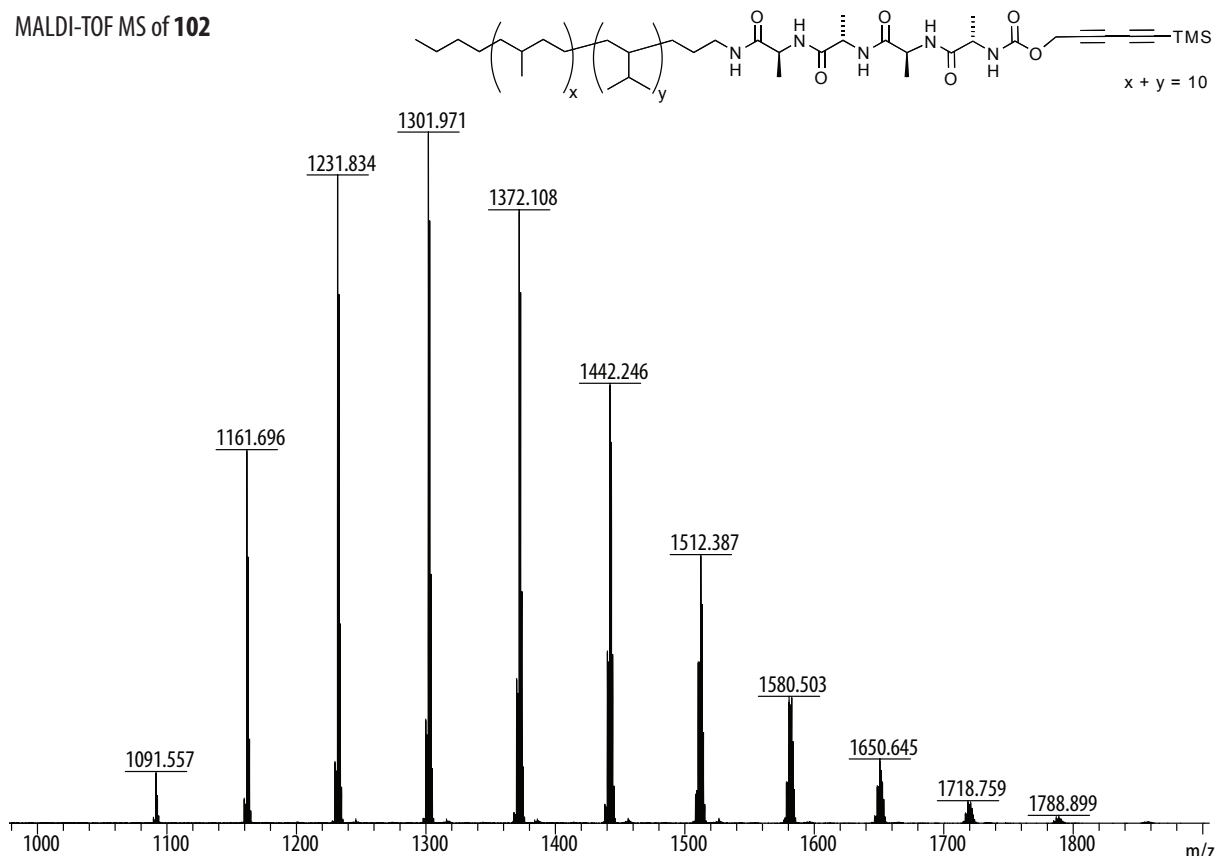
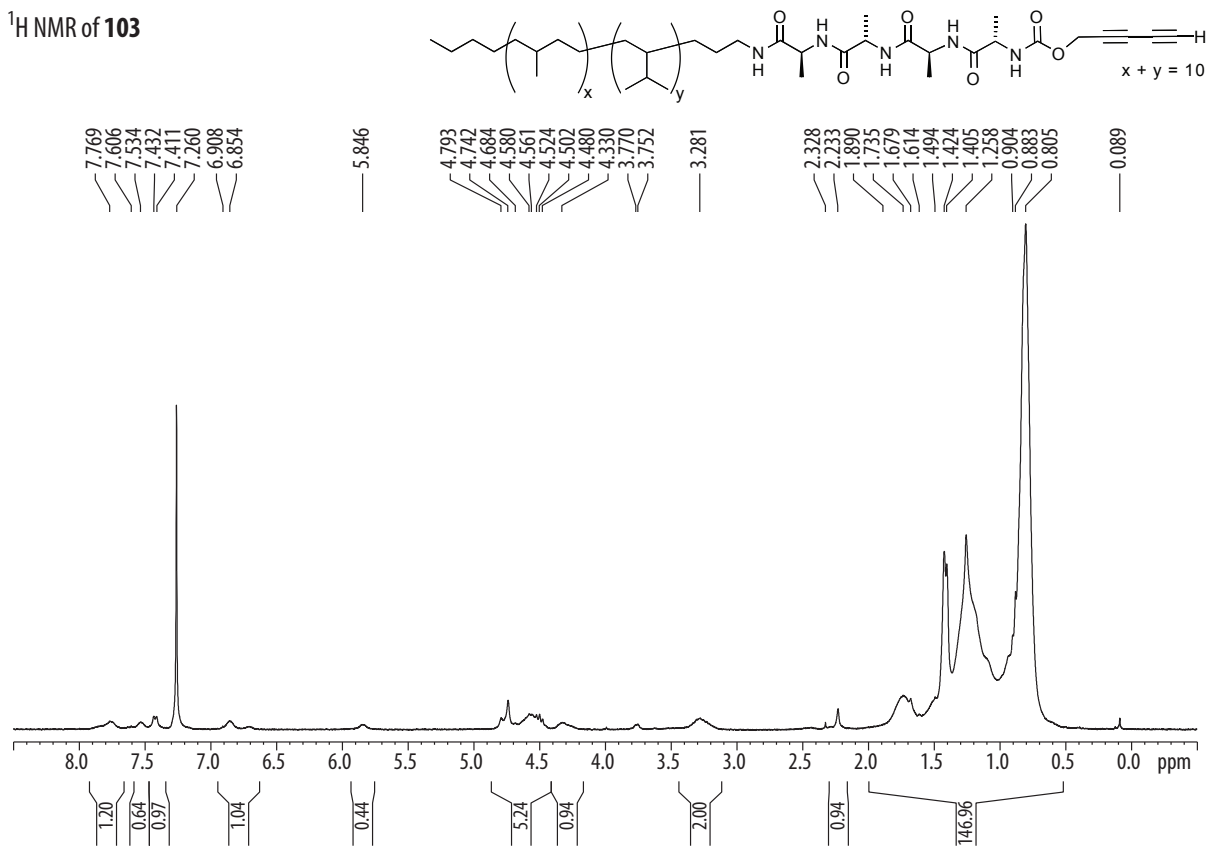


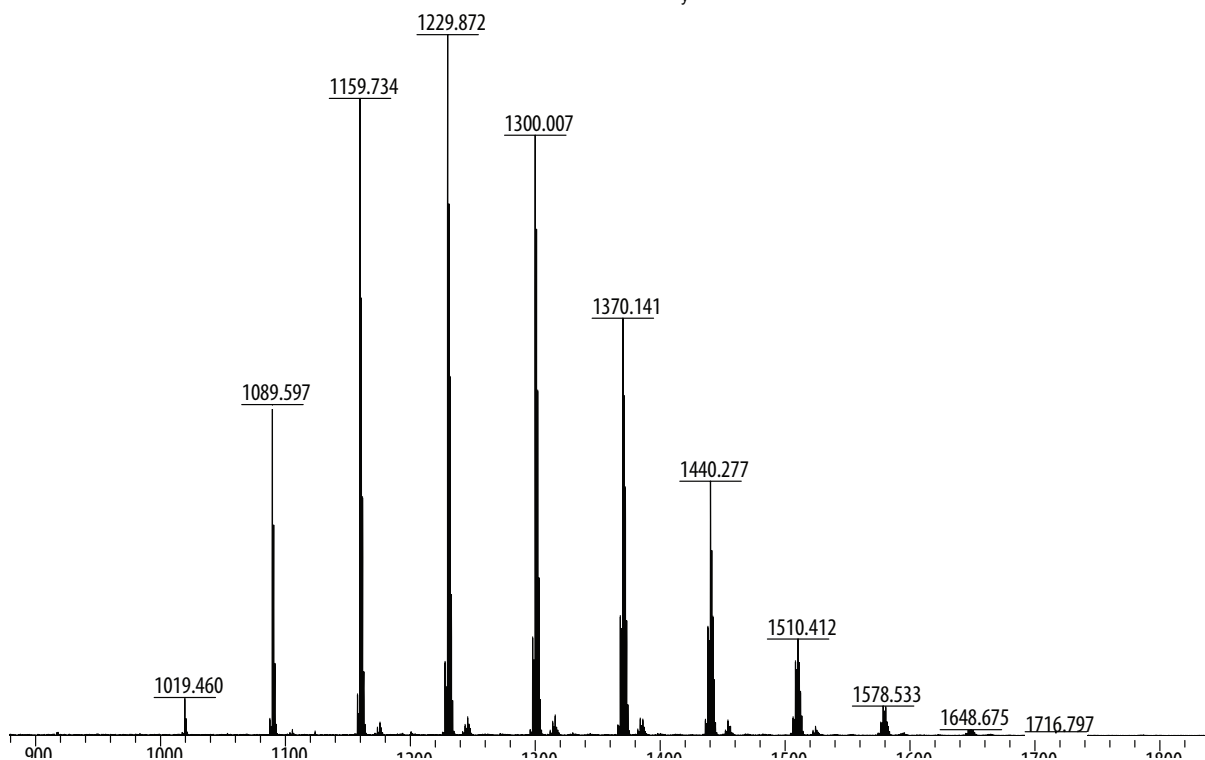
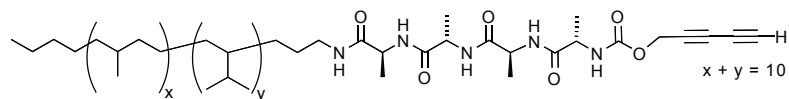
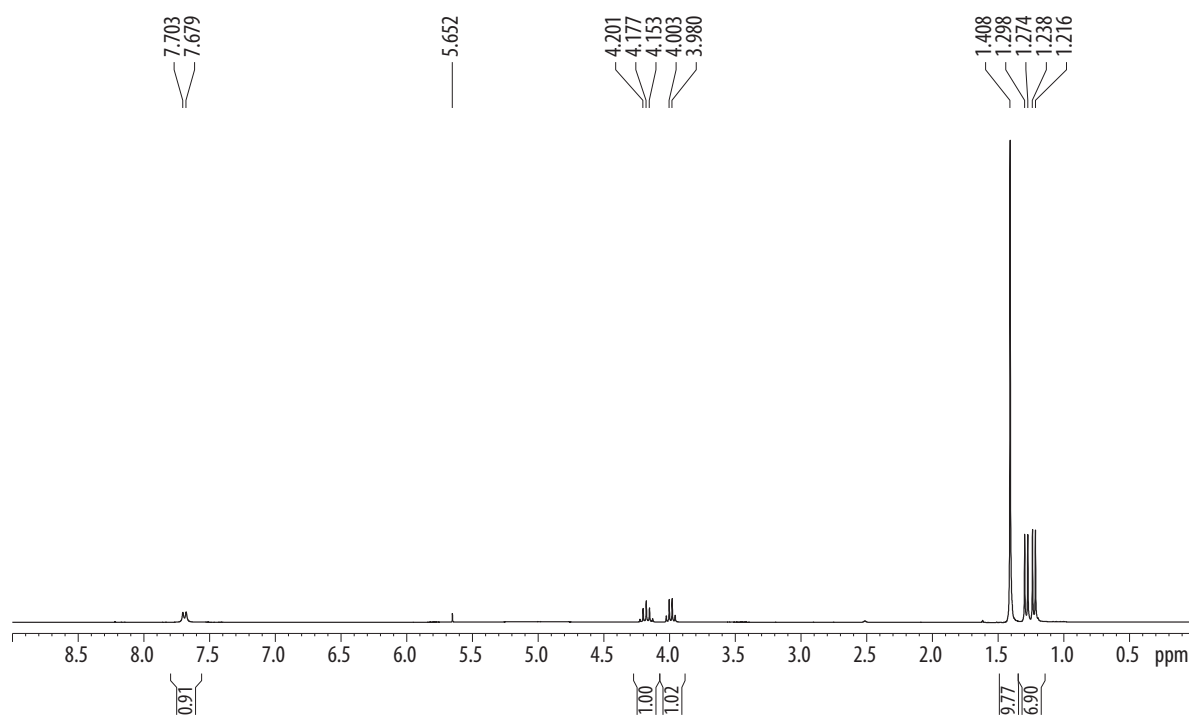
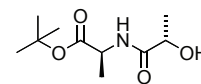
MALDI-TOF MS of **98** $^1H$  NMR of **99**

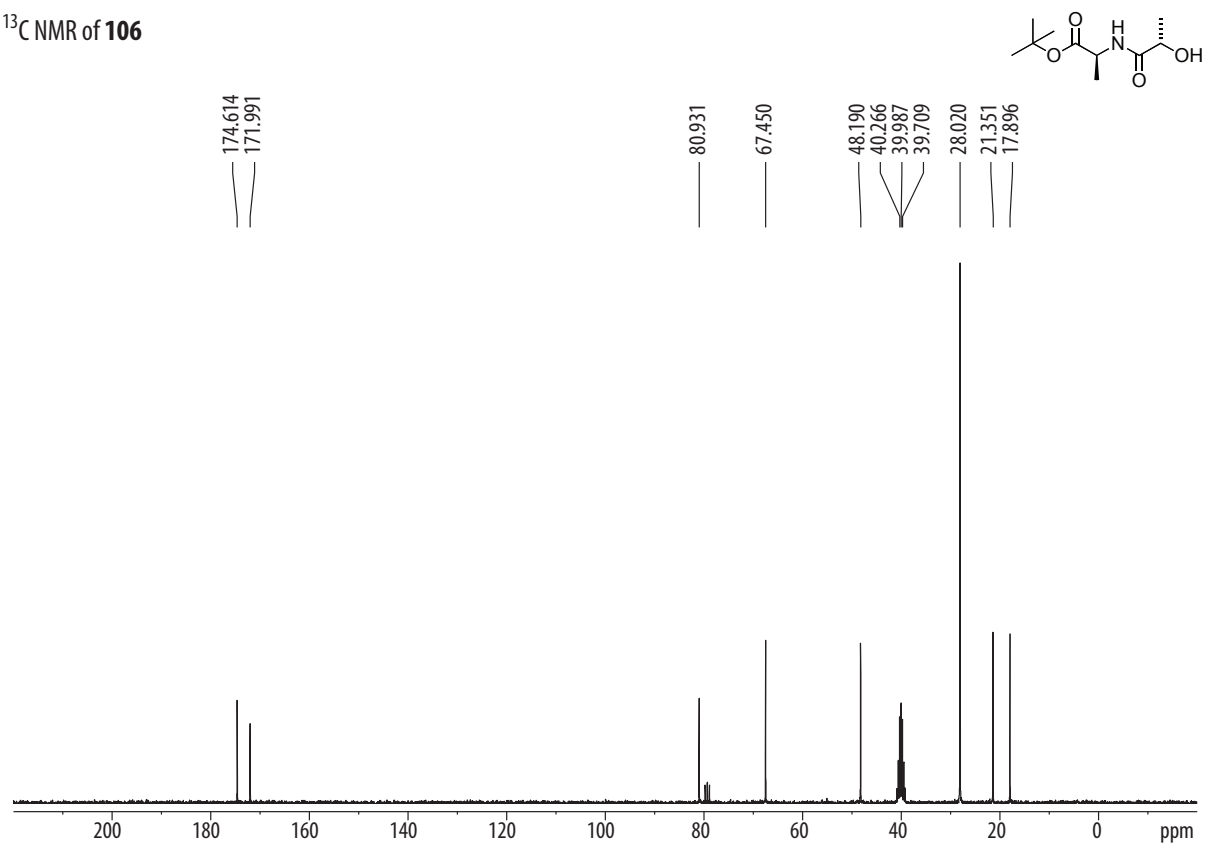
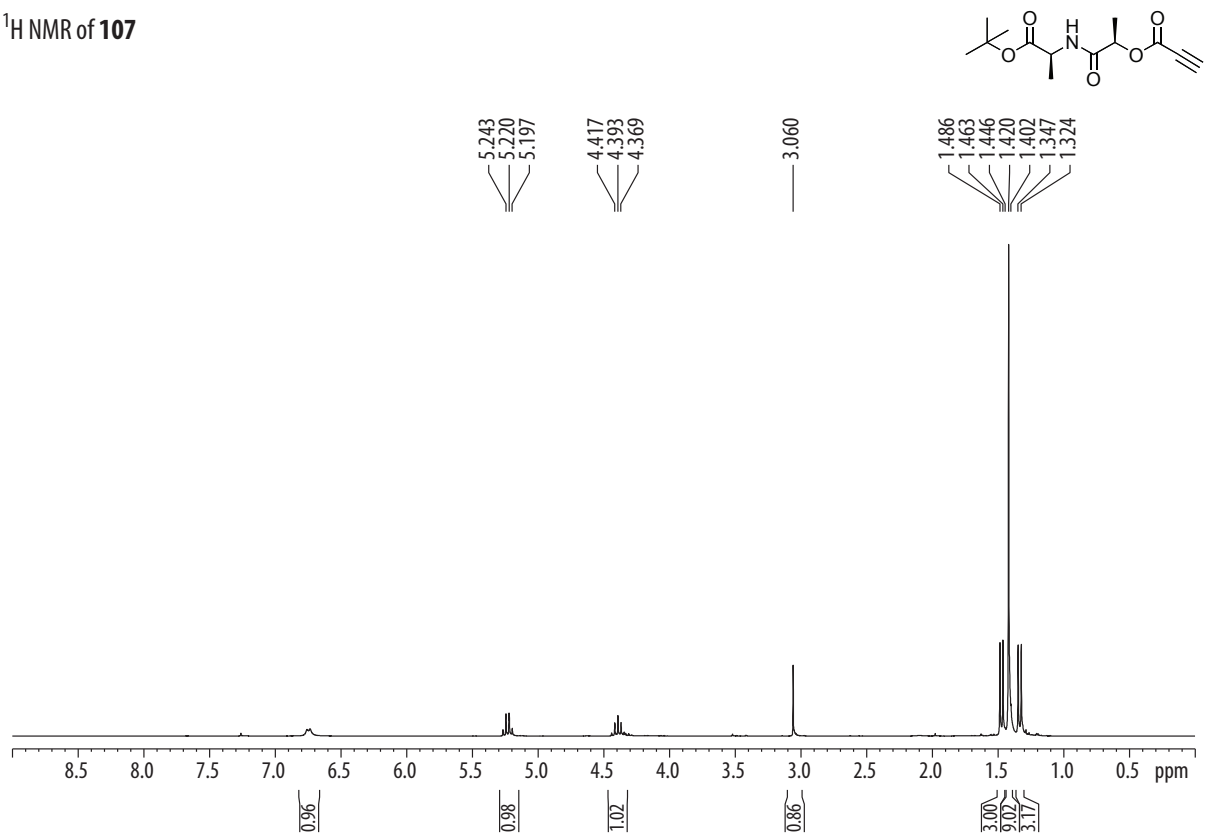
<sup>1</sup>H NMR of **100**

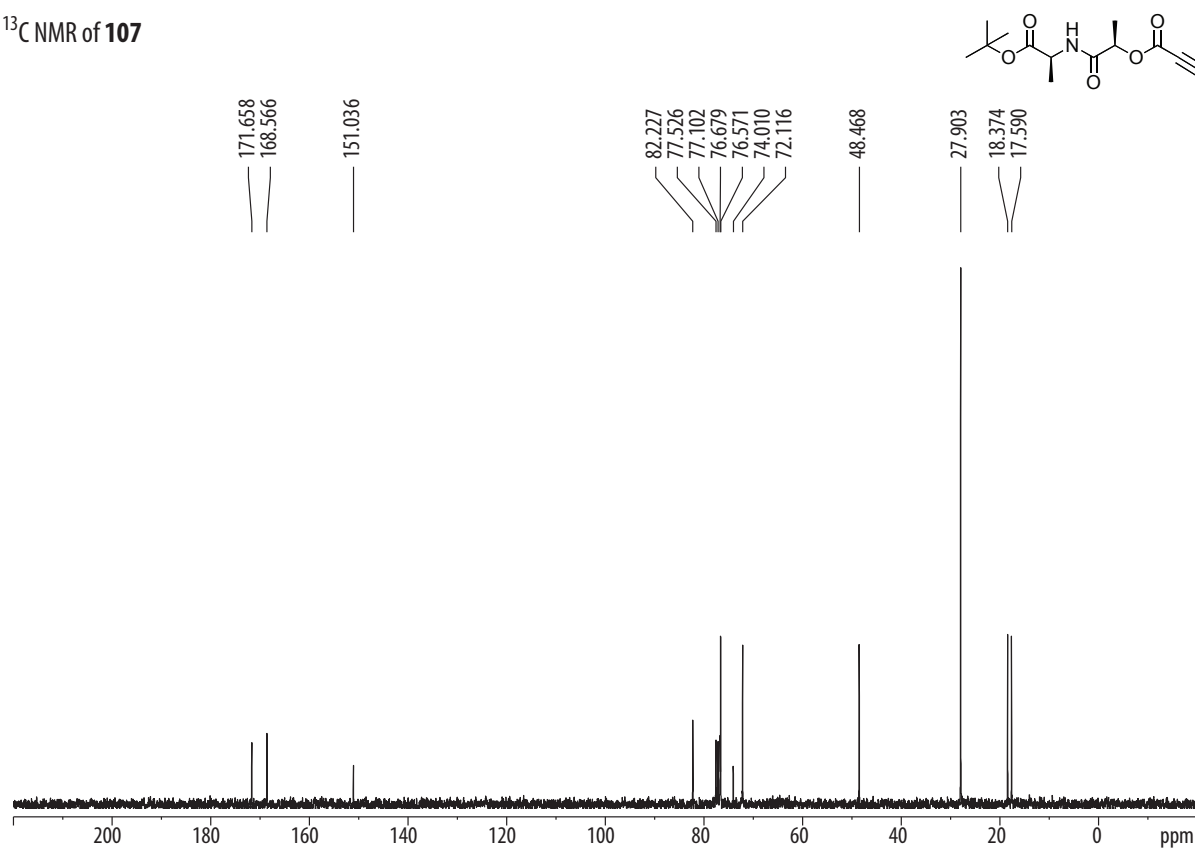
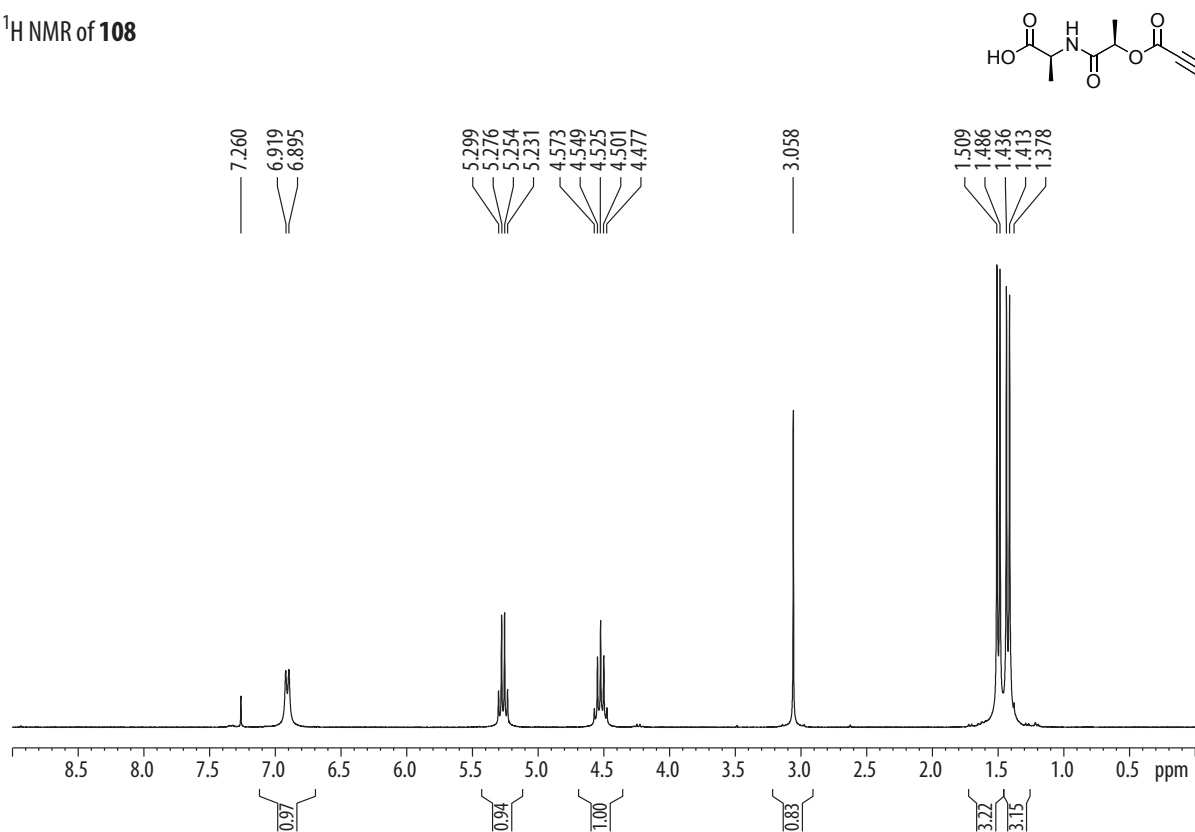
MALDI-TOF MS of **100** $^1\text{H}$  NMR of **101**

MALDI-TOF MS of **101** $^1\text{H}$  NMR of **102**

MALDI-TOF MS of **102** $^1\text{H}$  NMR of **103**

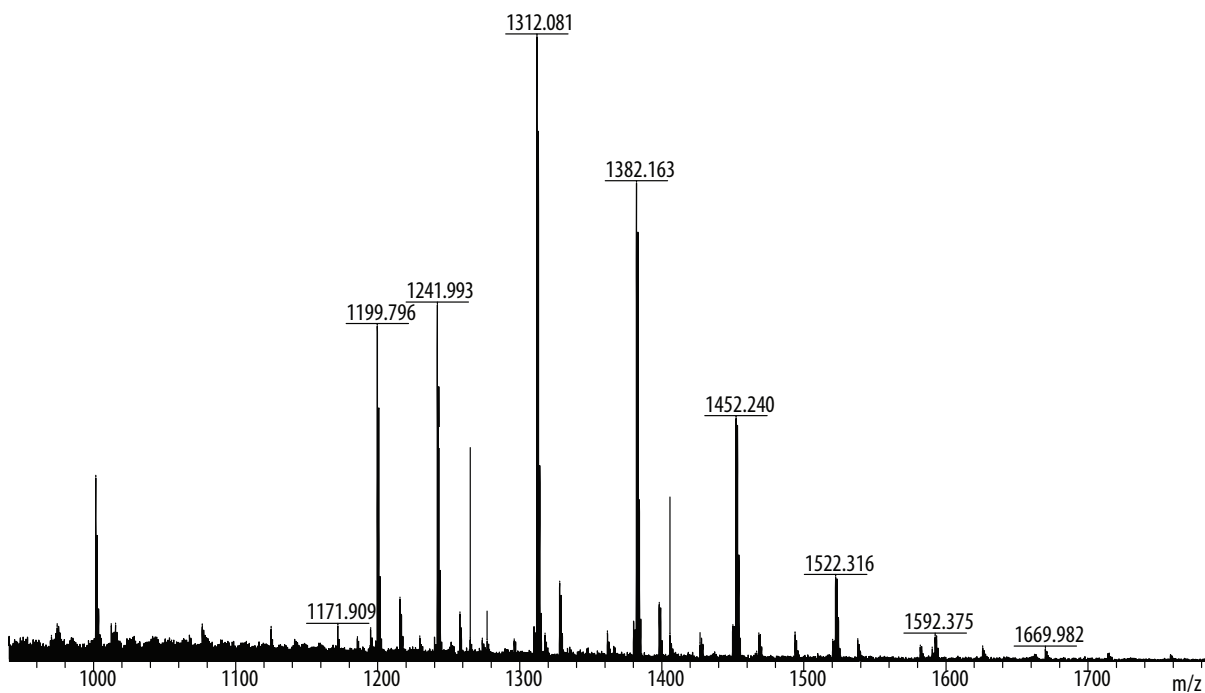
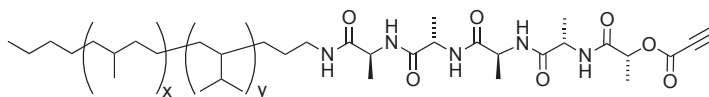
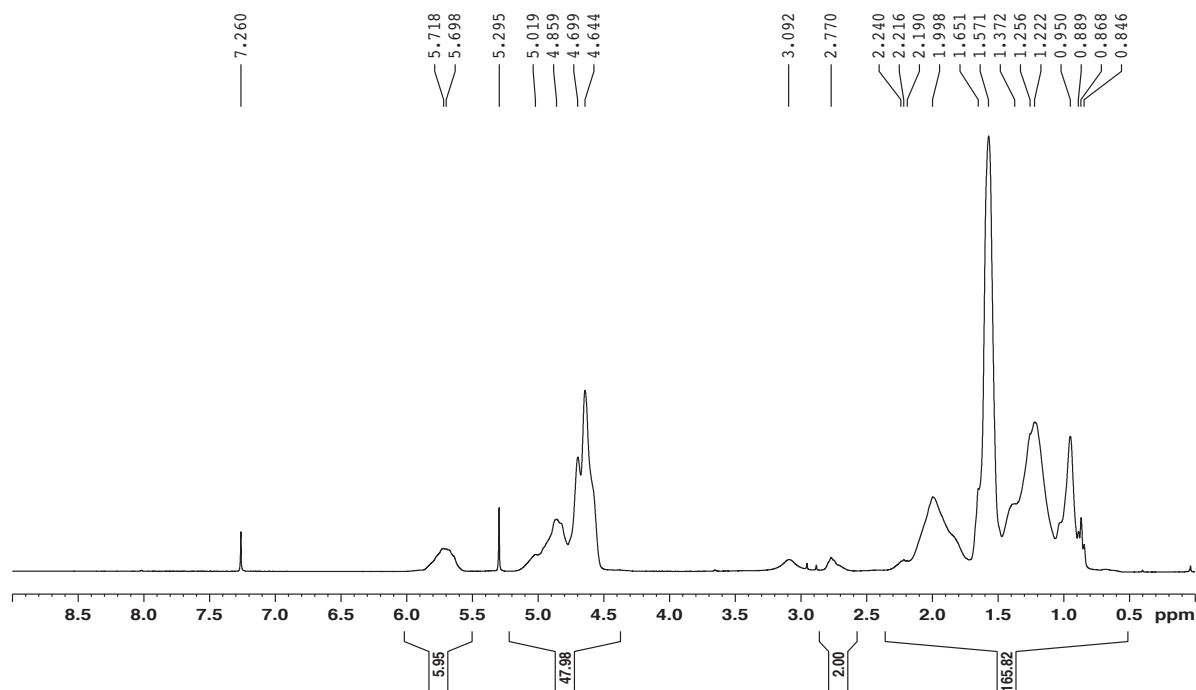
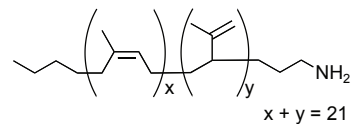
MALDI-TOF MS of **103** $^1\text{H}$  NMR of **106**

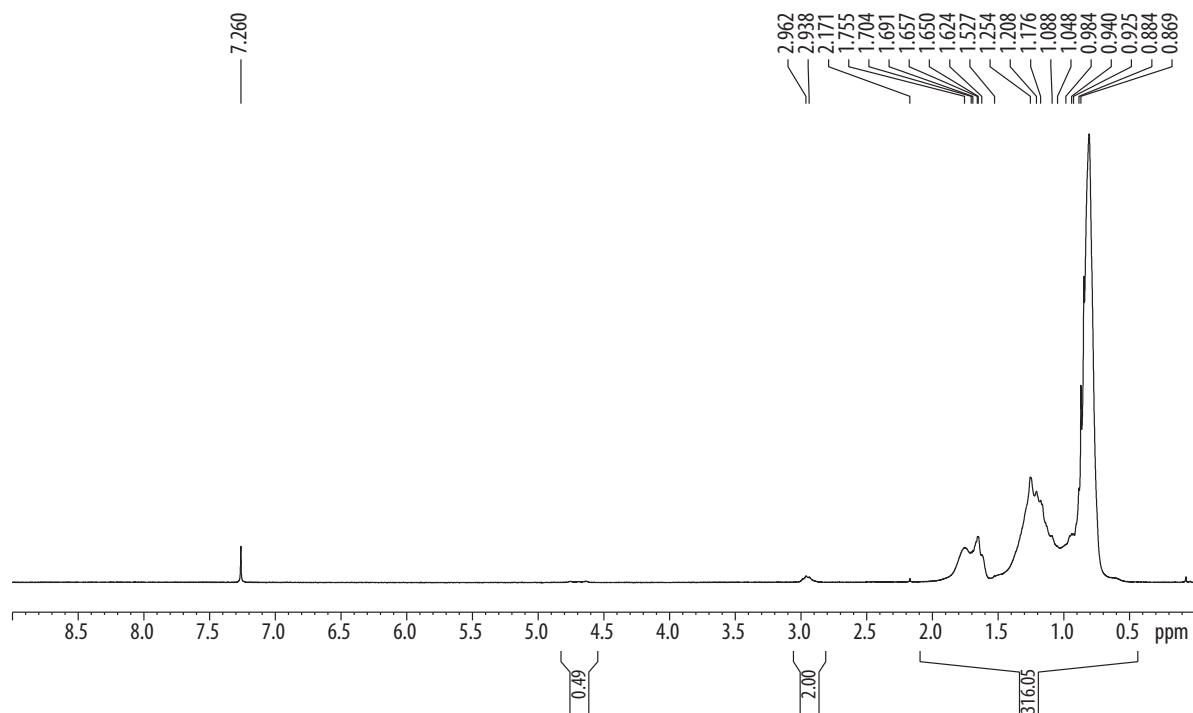
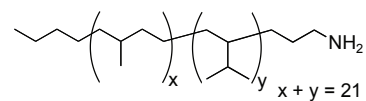
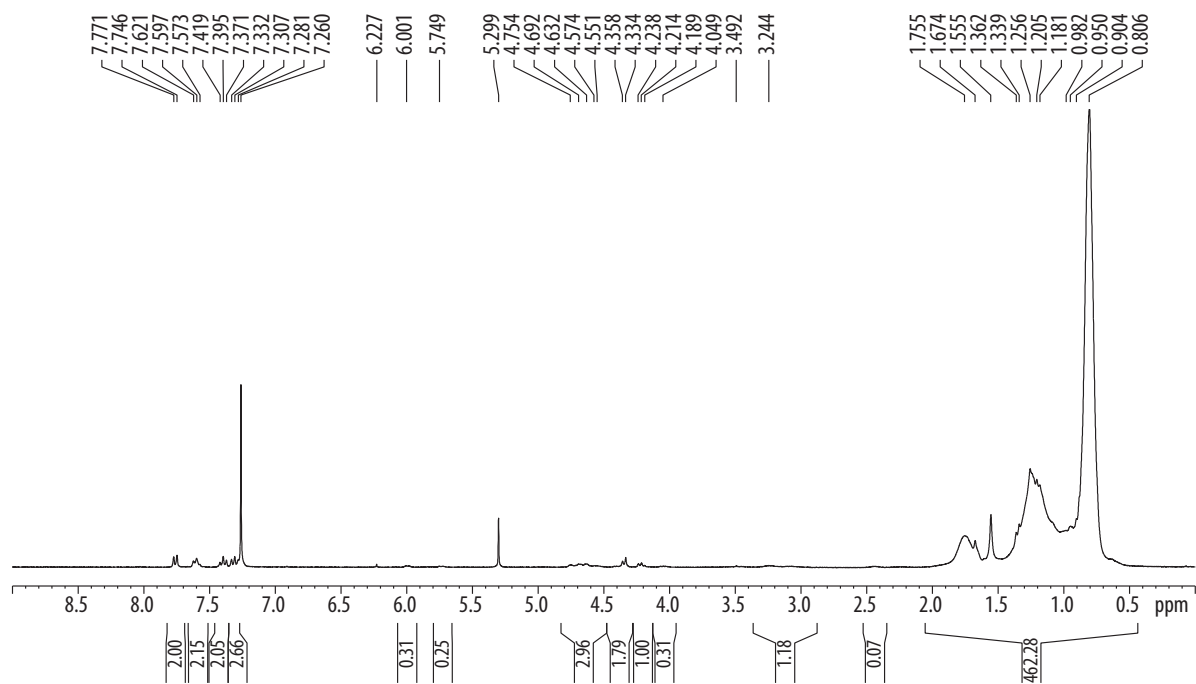
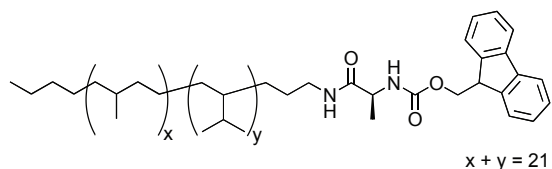
$^{13}\text{C}$  NMR of **106** $^1\text{H}$  NMR of **107**

$^{13}\text{C}$  NMR of **107** $^1\text{H}$  NMR of **108**

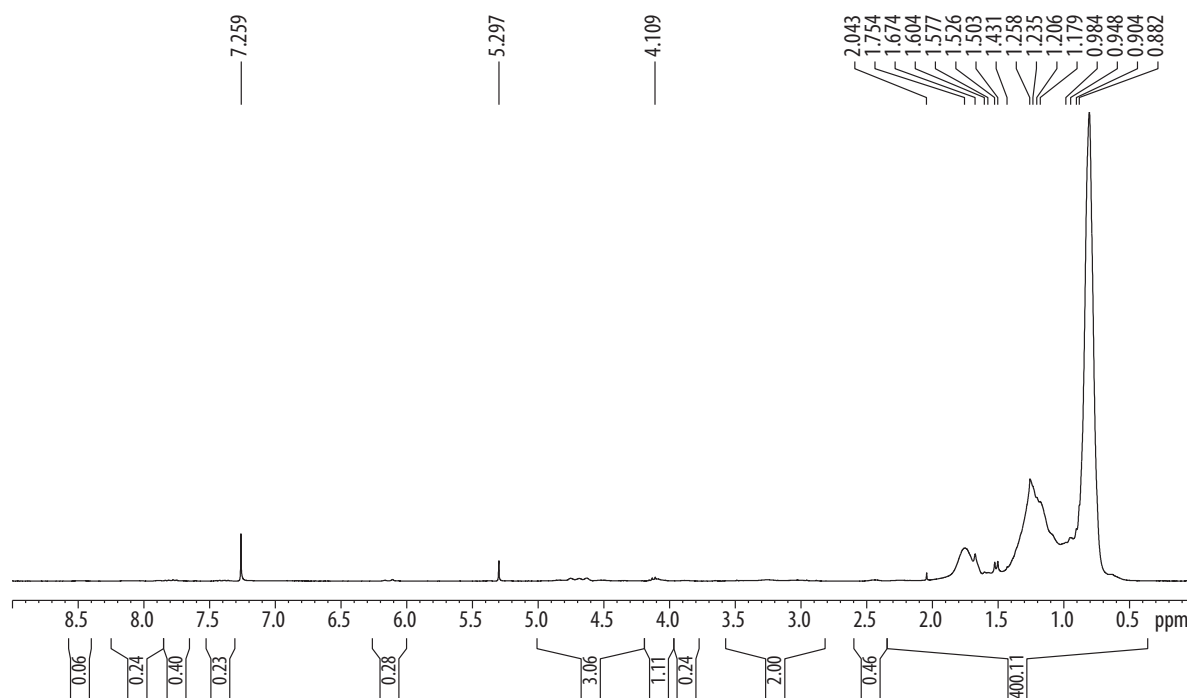
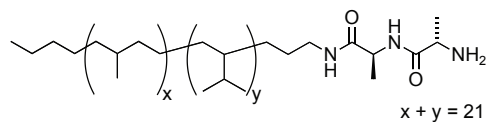
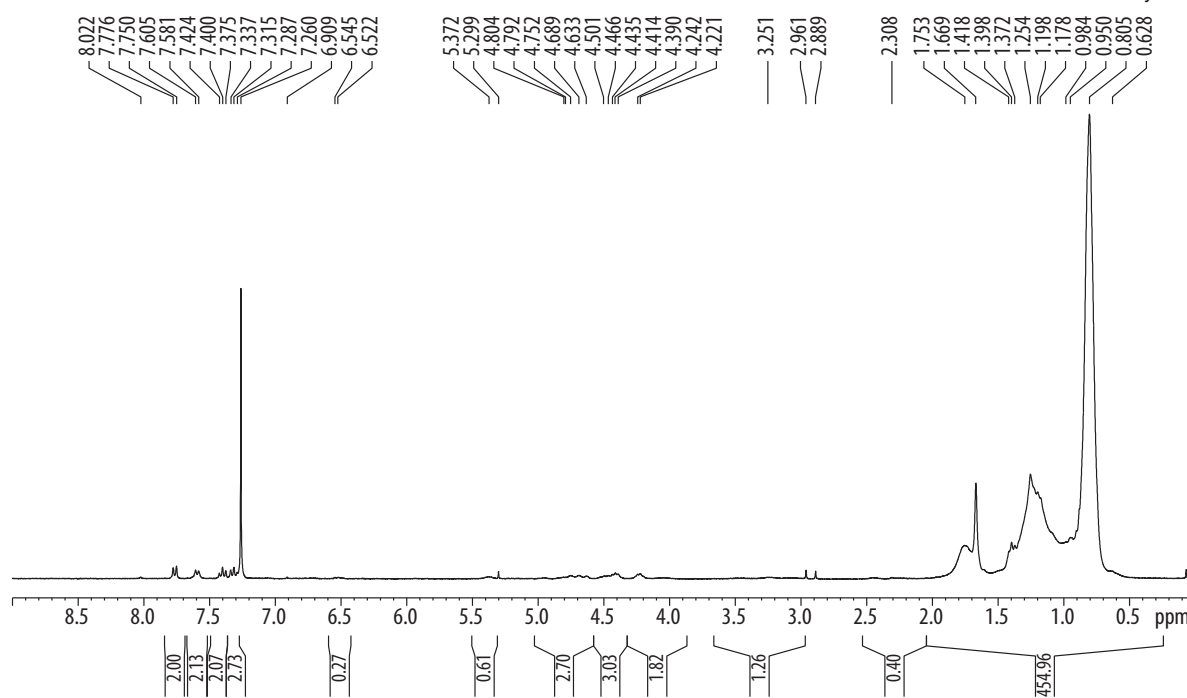
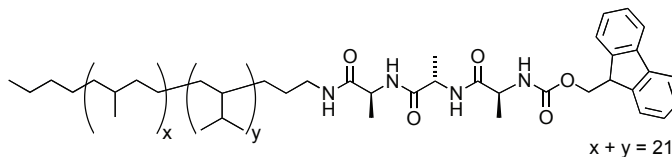


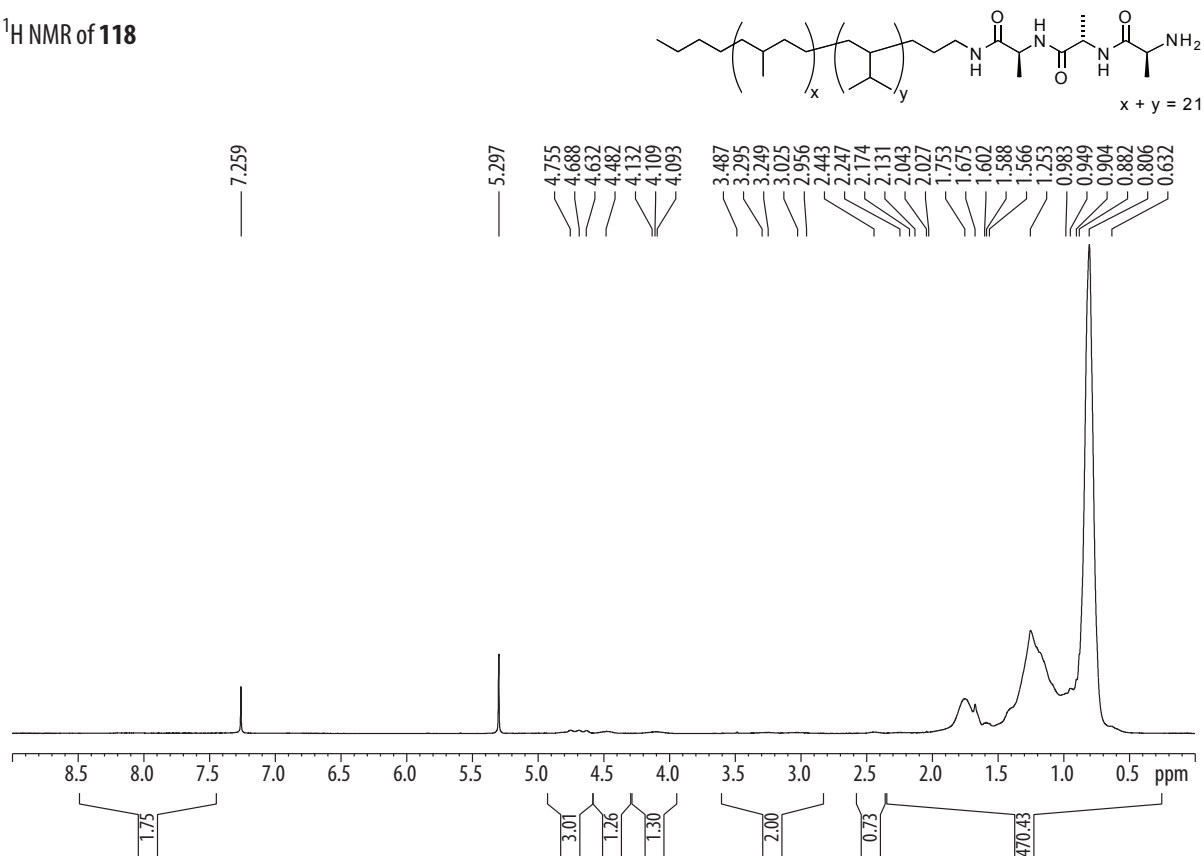
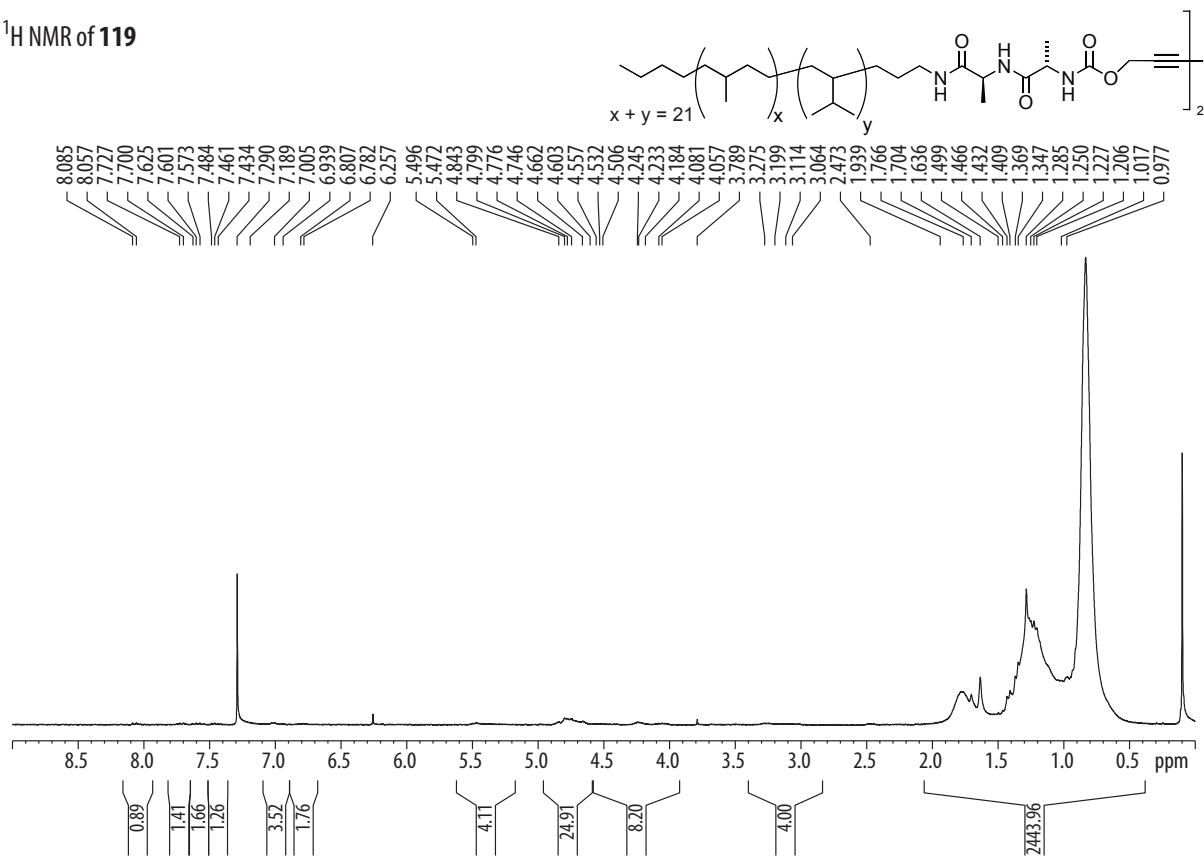


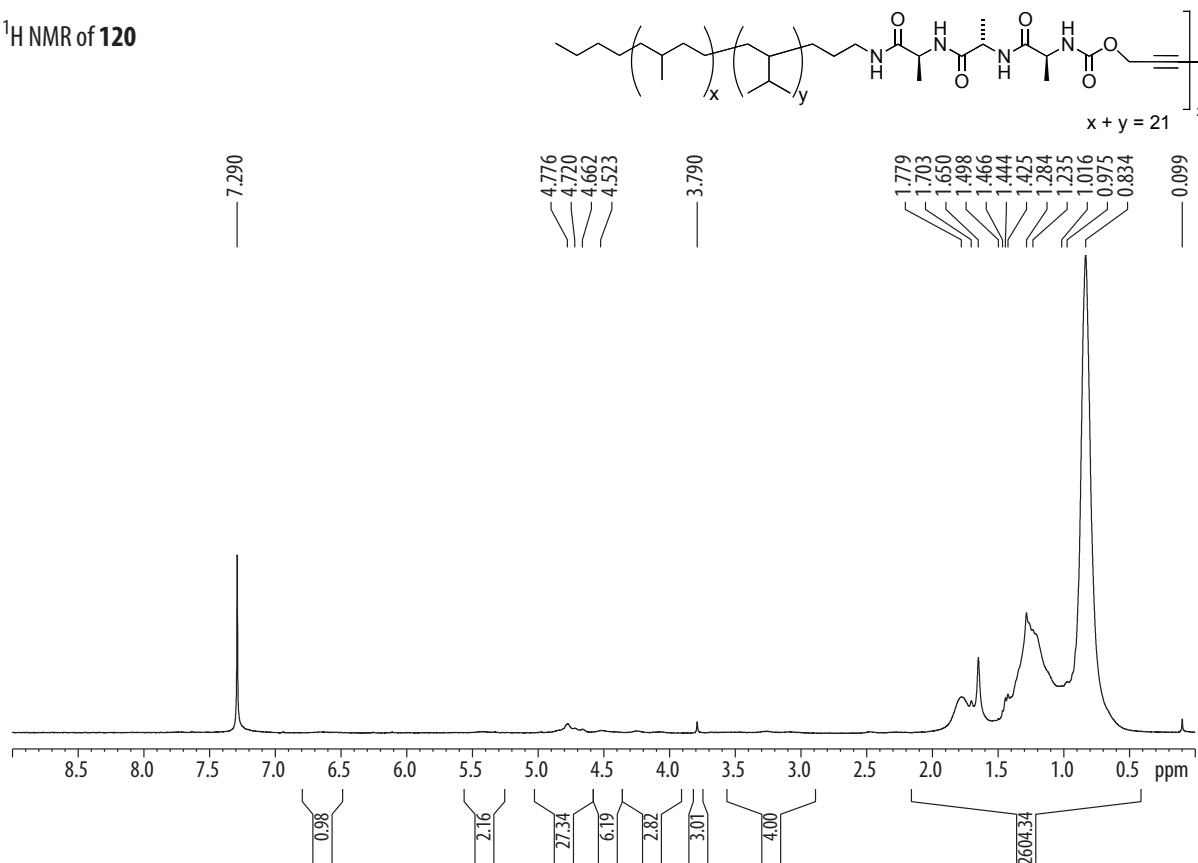
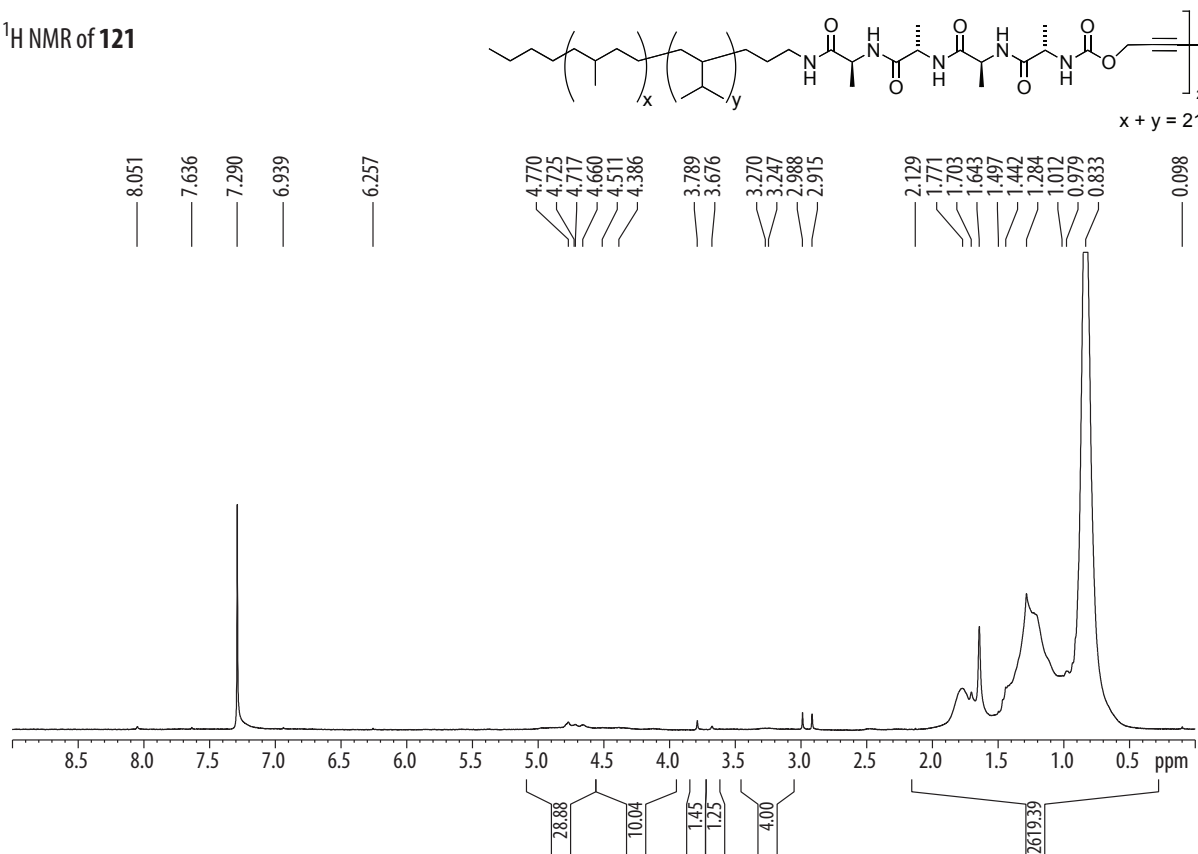
MALDI-TOF MS of **109** $^1\text{H}$  NMR of **111**

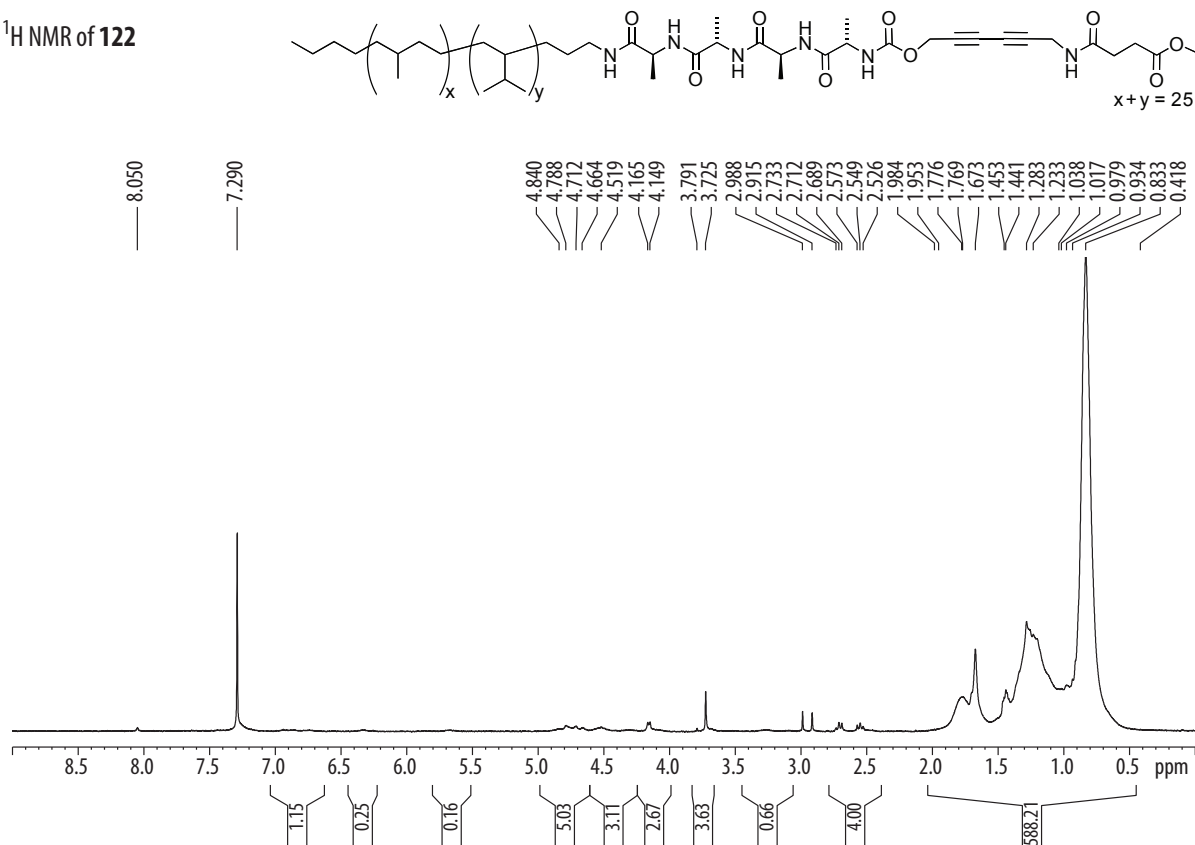
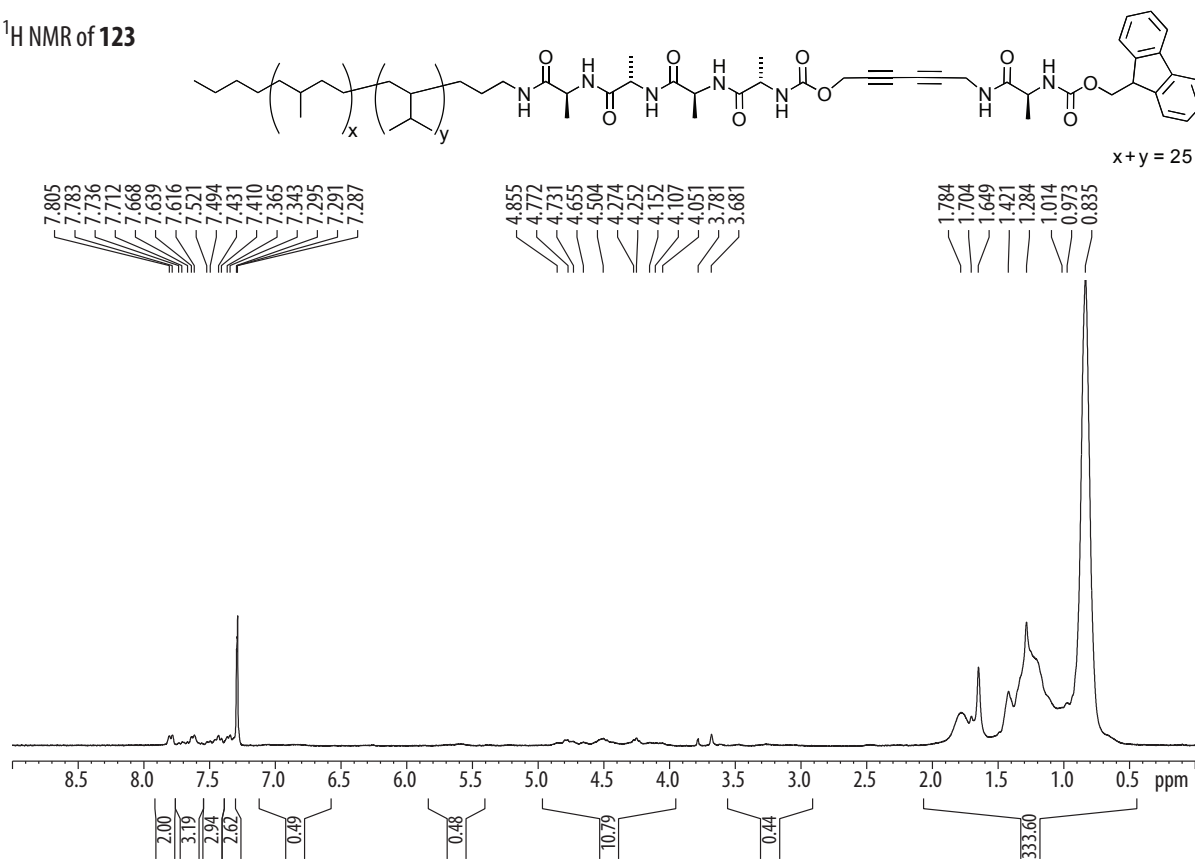
$^1\text{H}$  NMR of **112** $^1\text{H}$  NMR of **113**



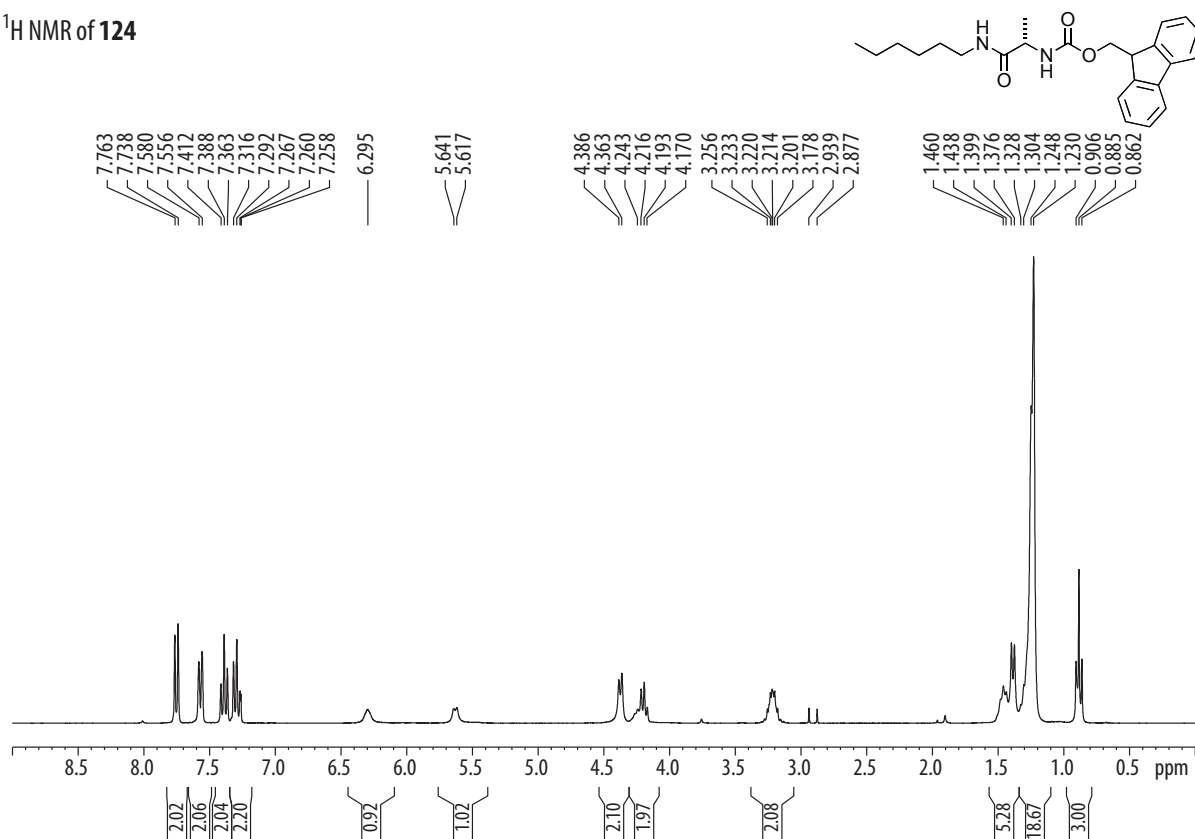
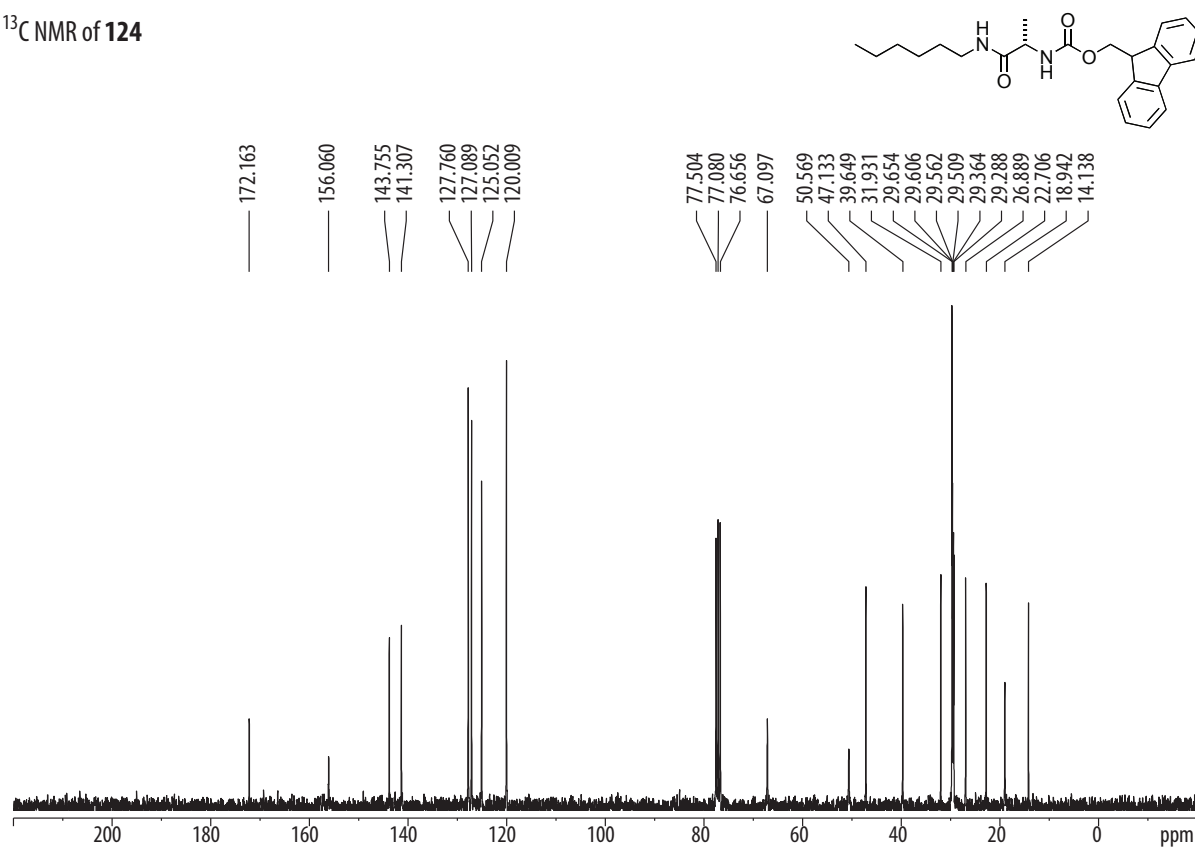
$^1\text{H}$  NMR of **116** $^1\text{H}$  NMR of **117**

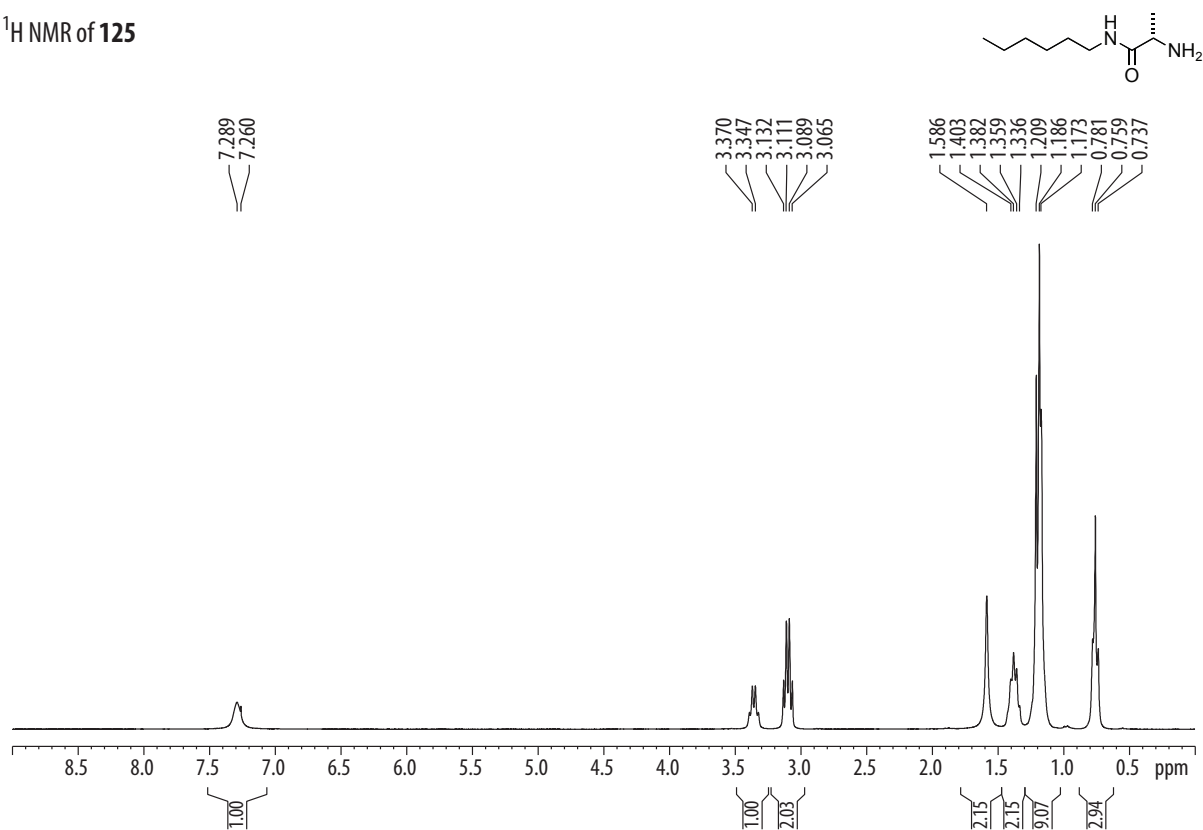
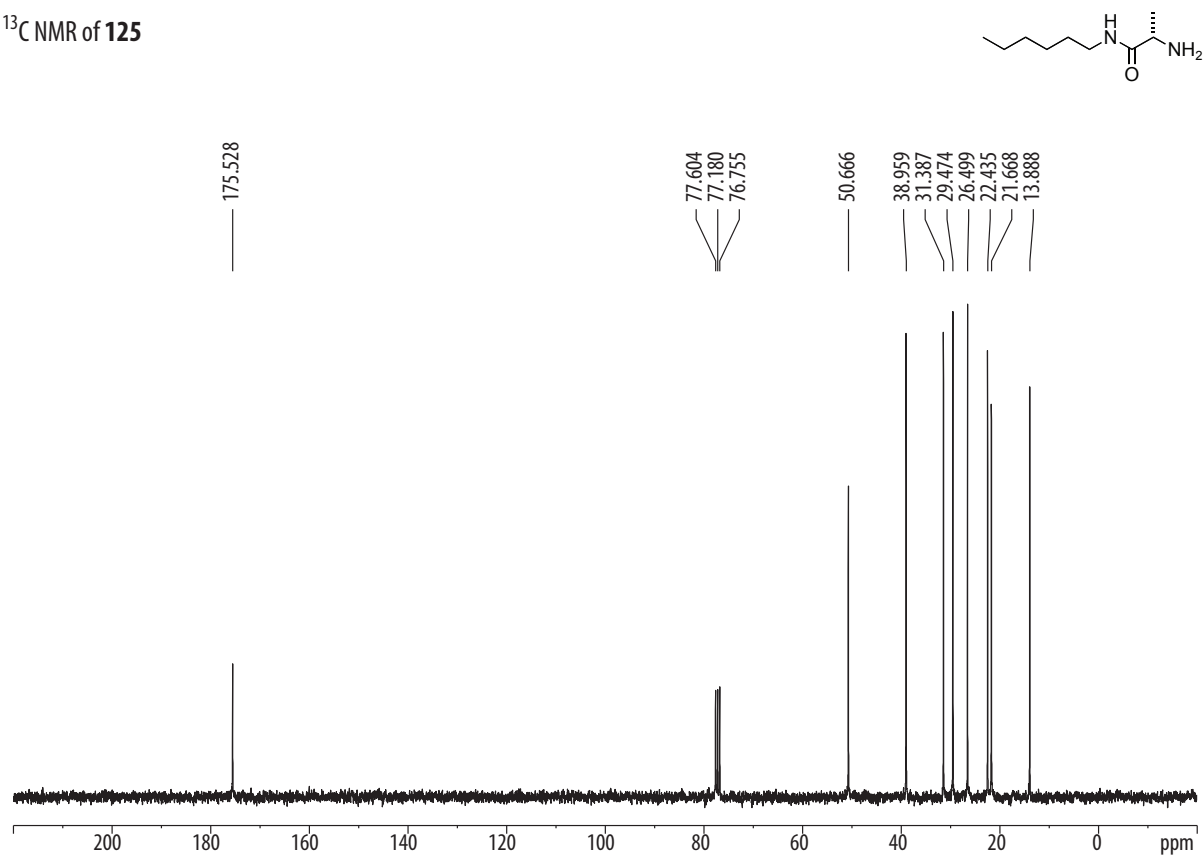
$^1\text{H}$  NMR of 118 $^1\text{H}$  NMR of 119

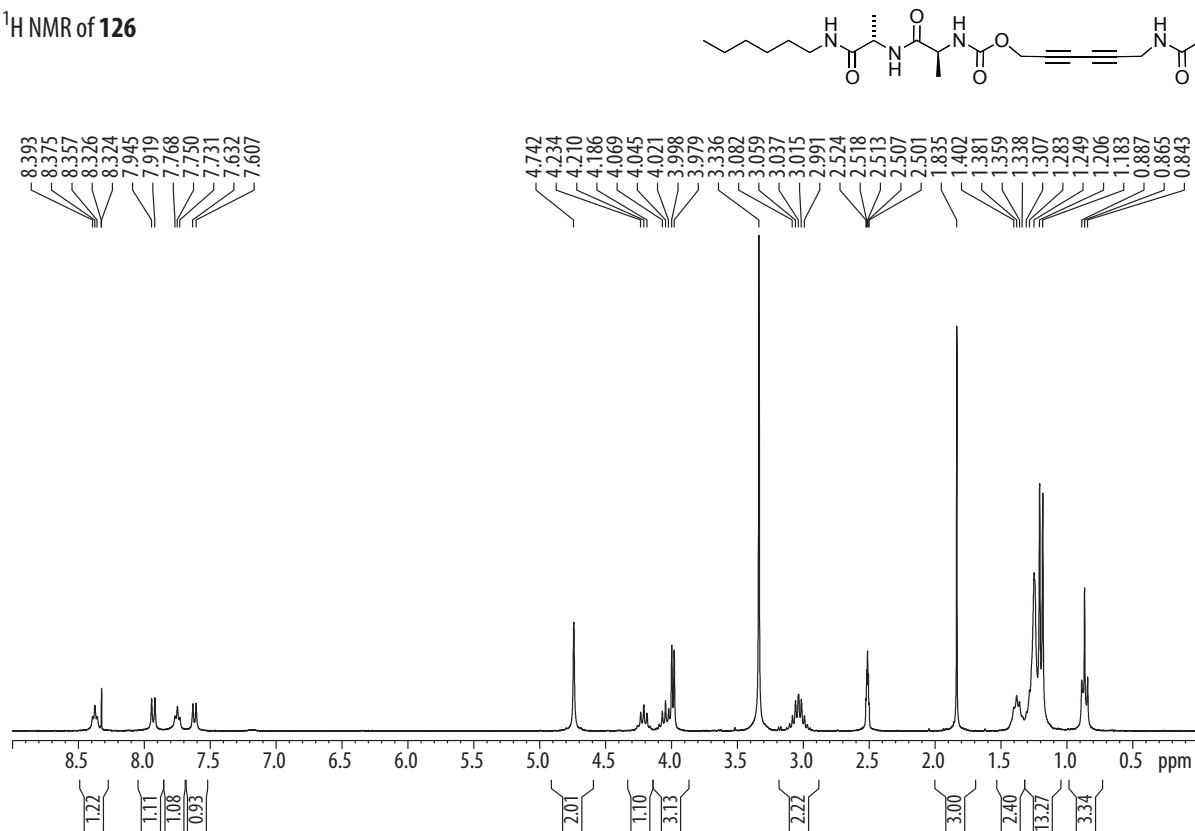
$^1\text{H}$  NMR of 120 $^1\text{H}$  NMR of 121

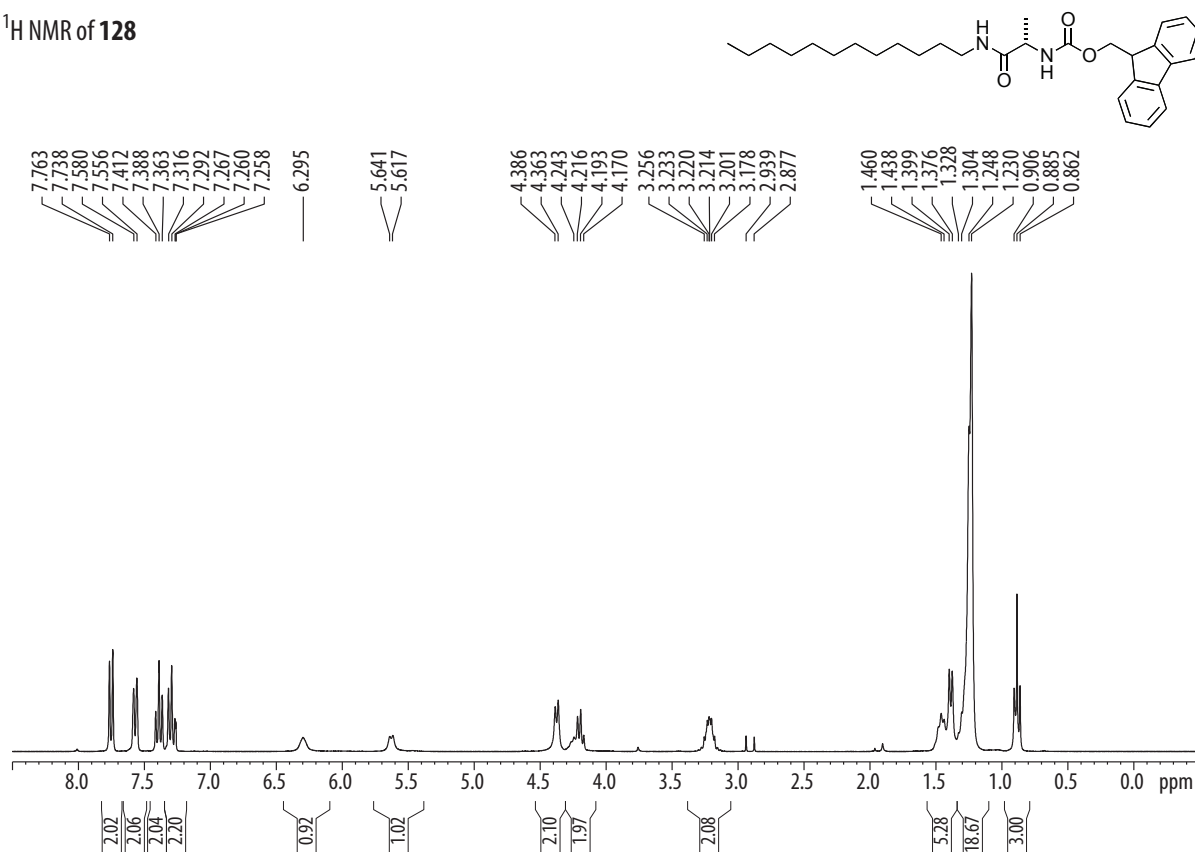
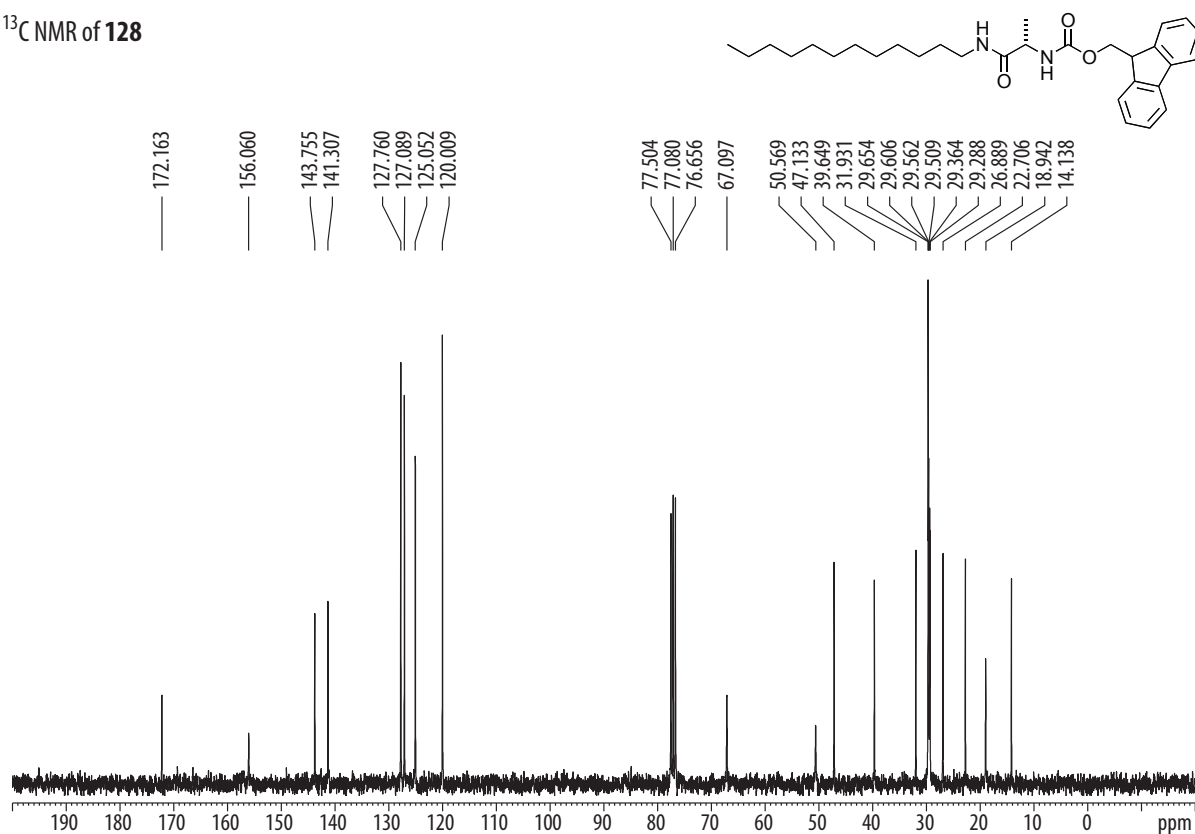
$^1\text{H}$  NMR of **122** $^1\text{H}$  NMR of **123**

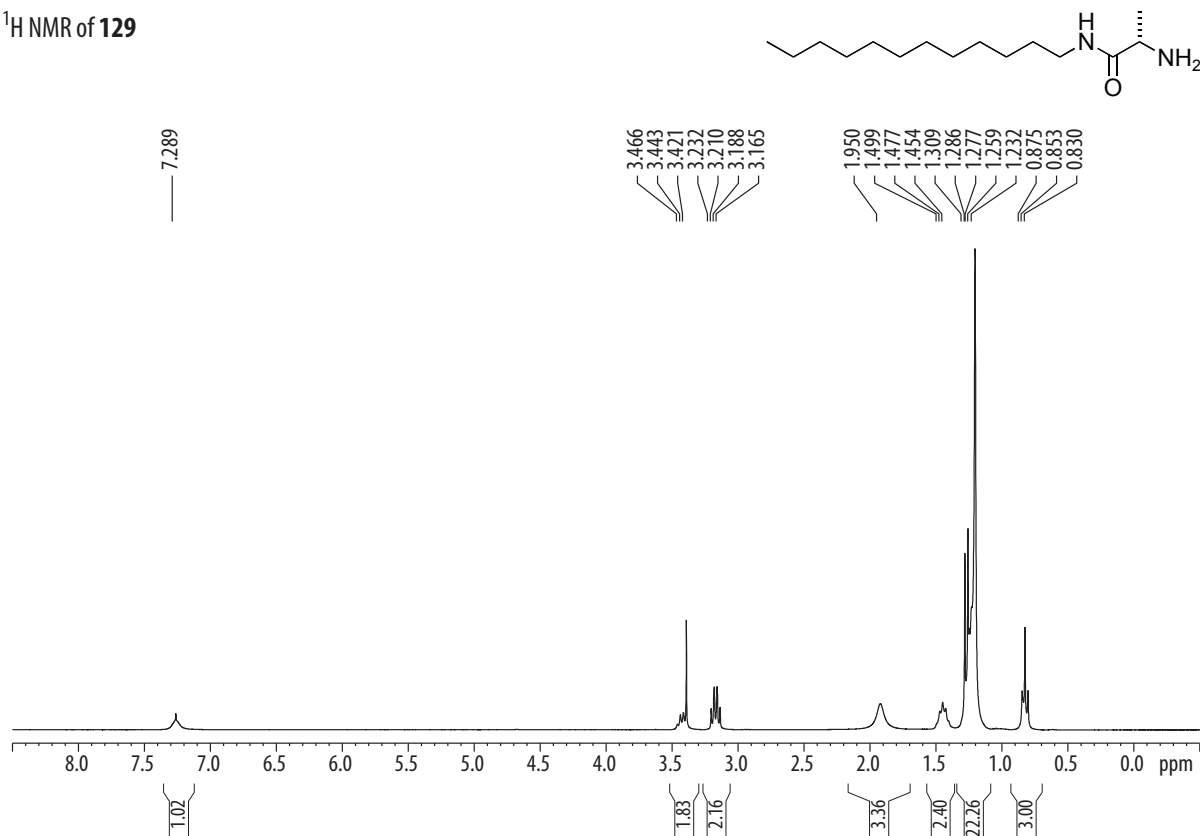
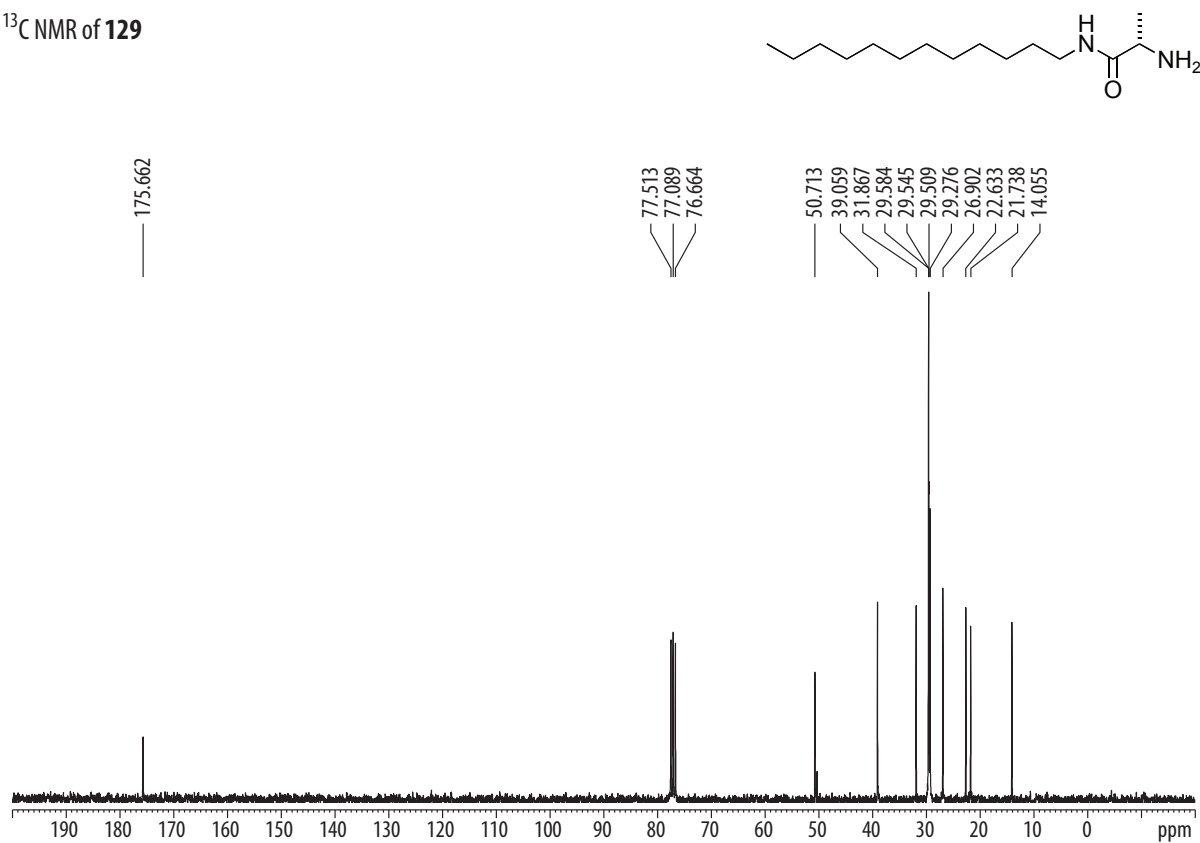


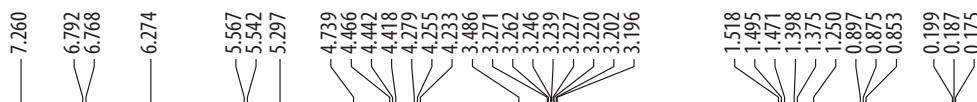
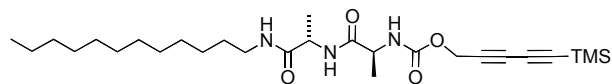
<sup>1</sup>H NMR of **124**<sup>13</sup>C NMR of **124**

$^1\text{H}$  NMR of **125** $^{13}\text{C}$  NMR of **125**

<sup>1</sup>H NMR of 126<sup>1</sup>H NMR of 127

<sup>1</sup>H NMR of 128<sup>13</sup>C NMR of 128

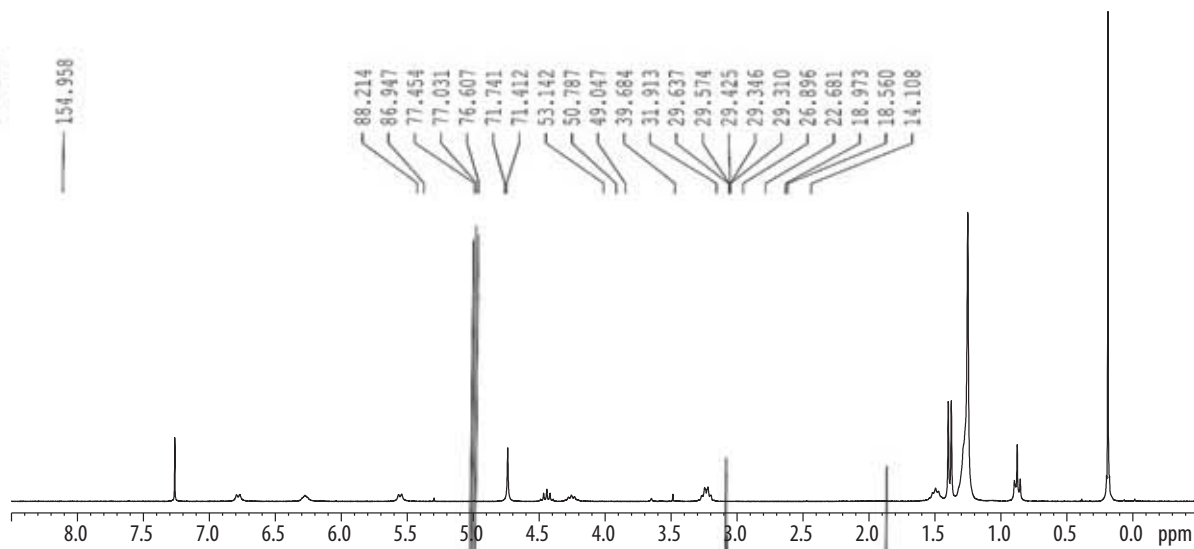
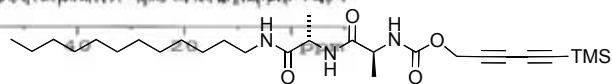
<sup>1</sup>H NMR of **129**<sup>13</sup>C NMR of **129**

$^1\text{H}$  NMR of **130**

171.974  
171.824

154.958

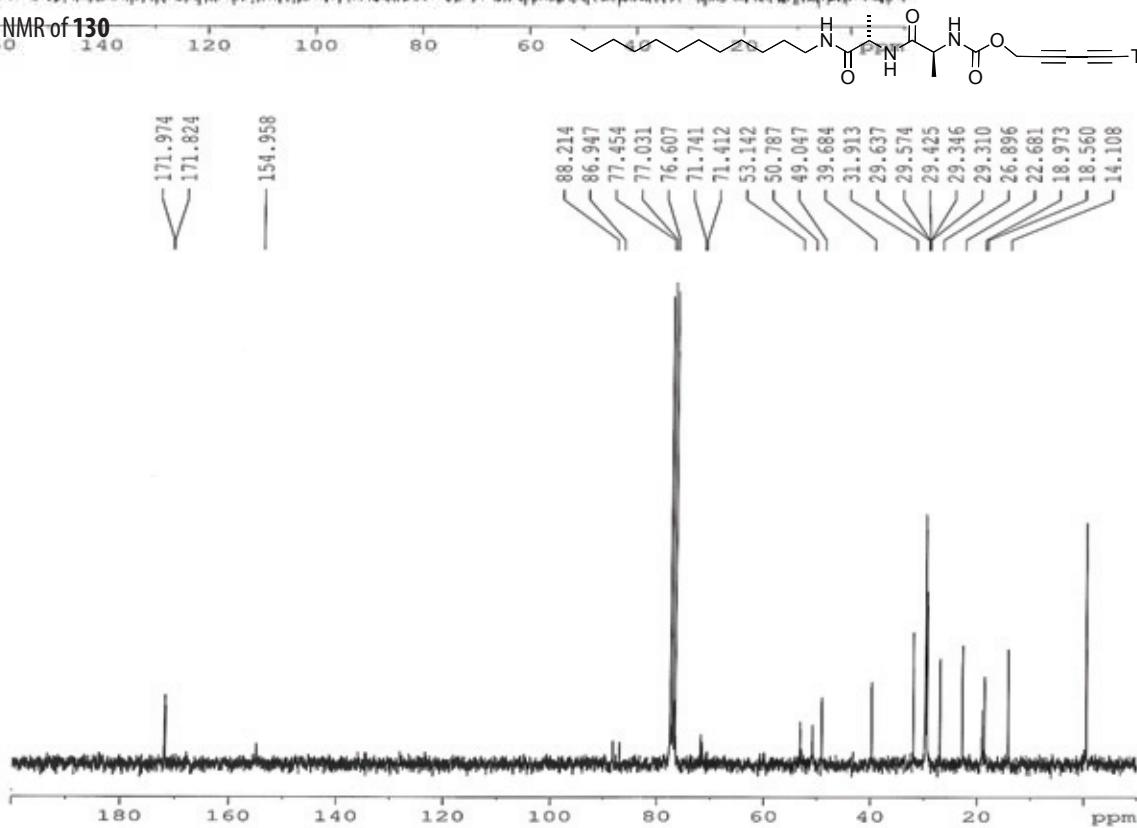
88.214  
86.947  
77.454  
77.031  
76.607  
71.741  
71.412  
53.142  
50.787  
49.047  
39.684  
31.913  
29.637  
29.574  
29.425  
29.346  
29.310  
26.896  
22.681  
18.973  
18.560  
14.108

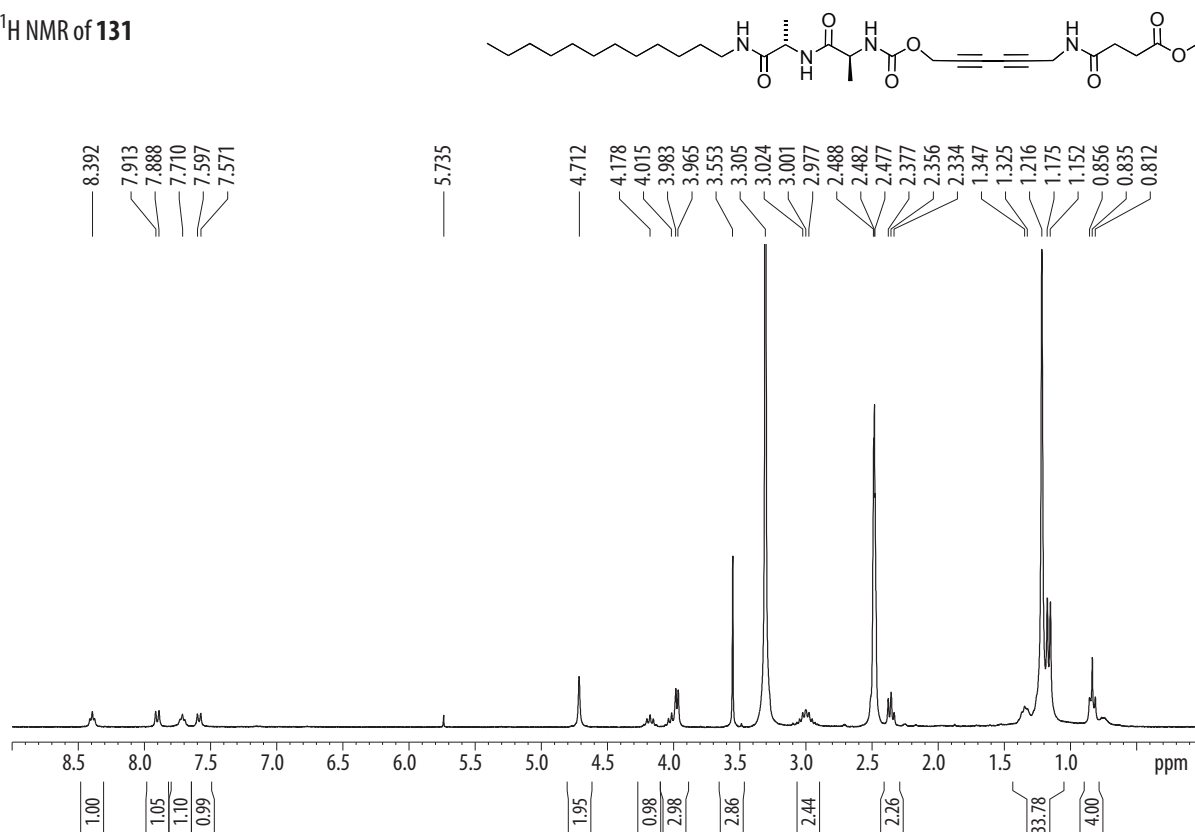
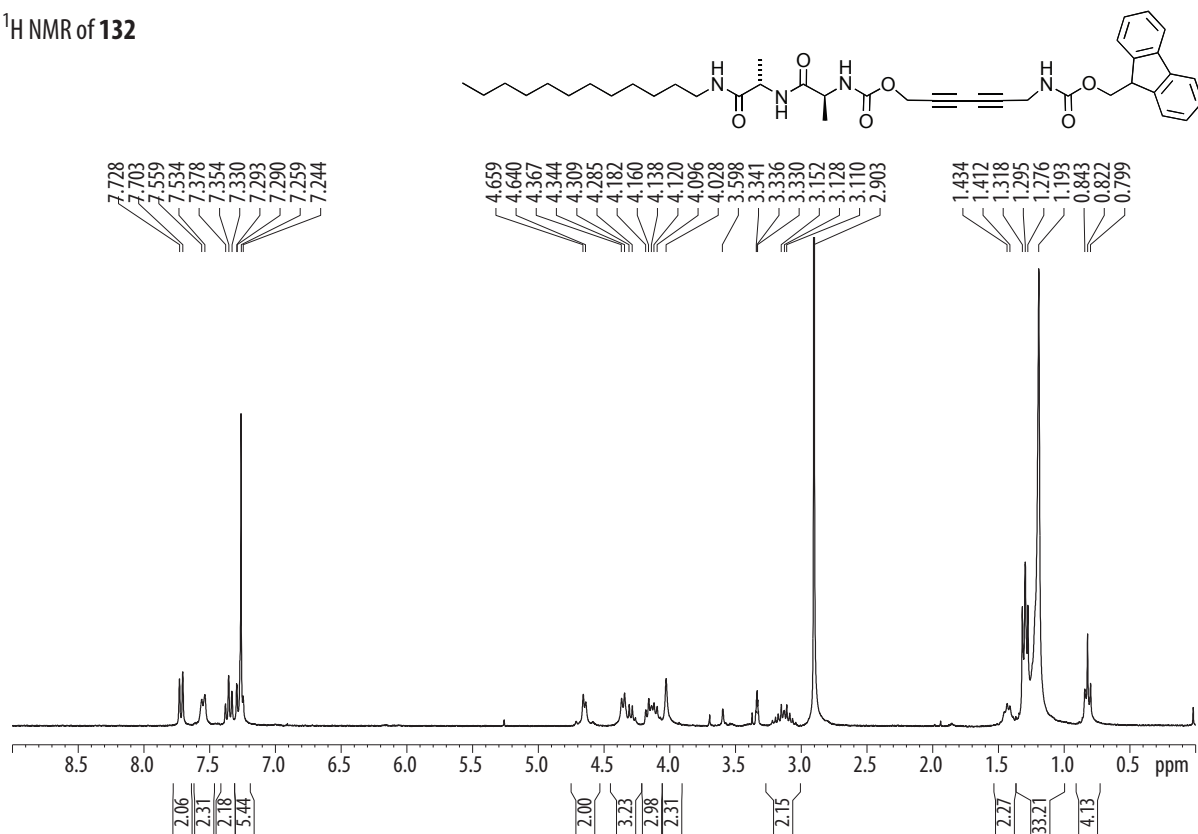
 $^{13}\text{C}$  NMR of **130**

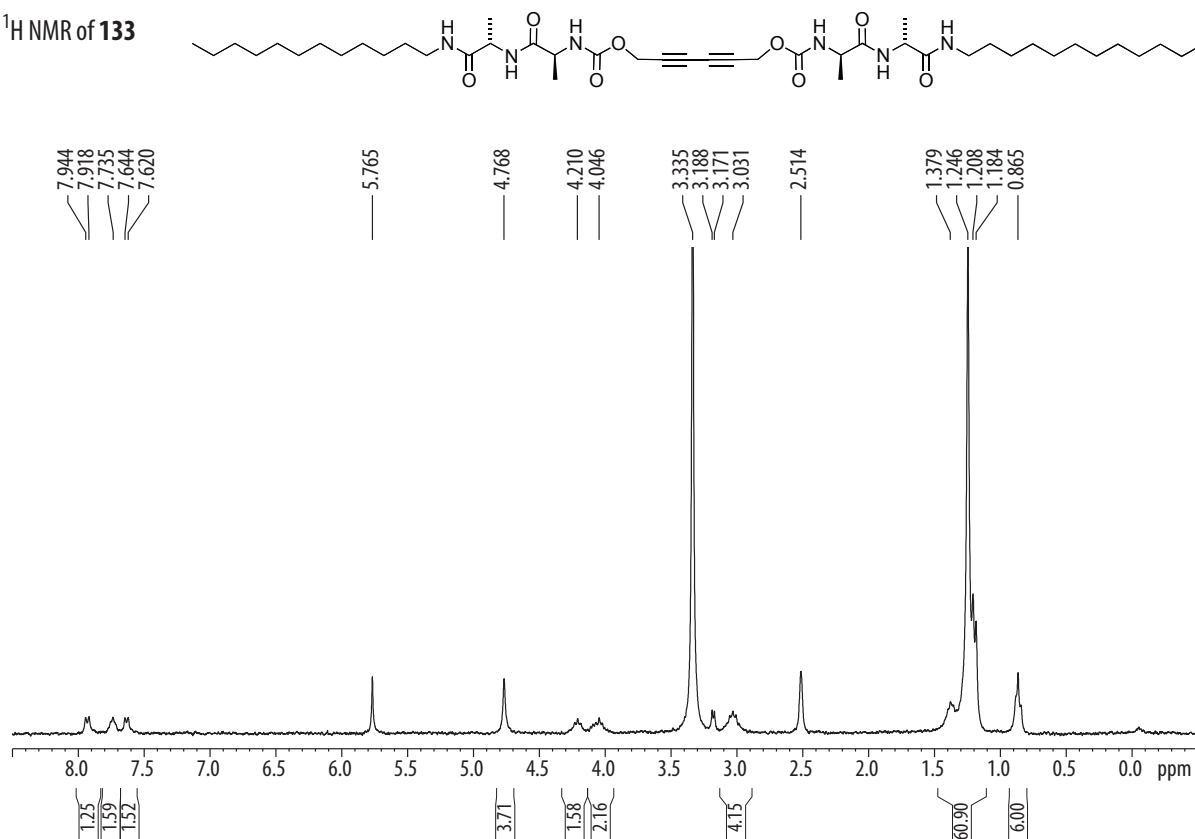
171.974  
171.824

154.958

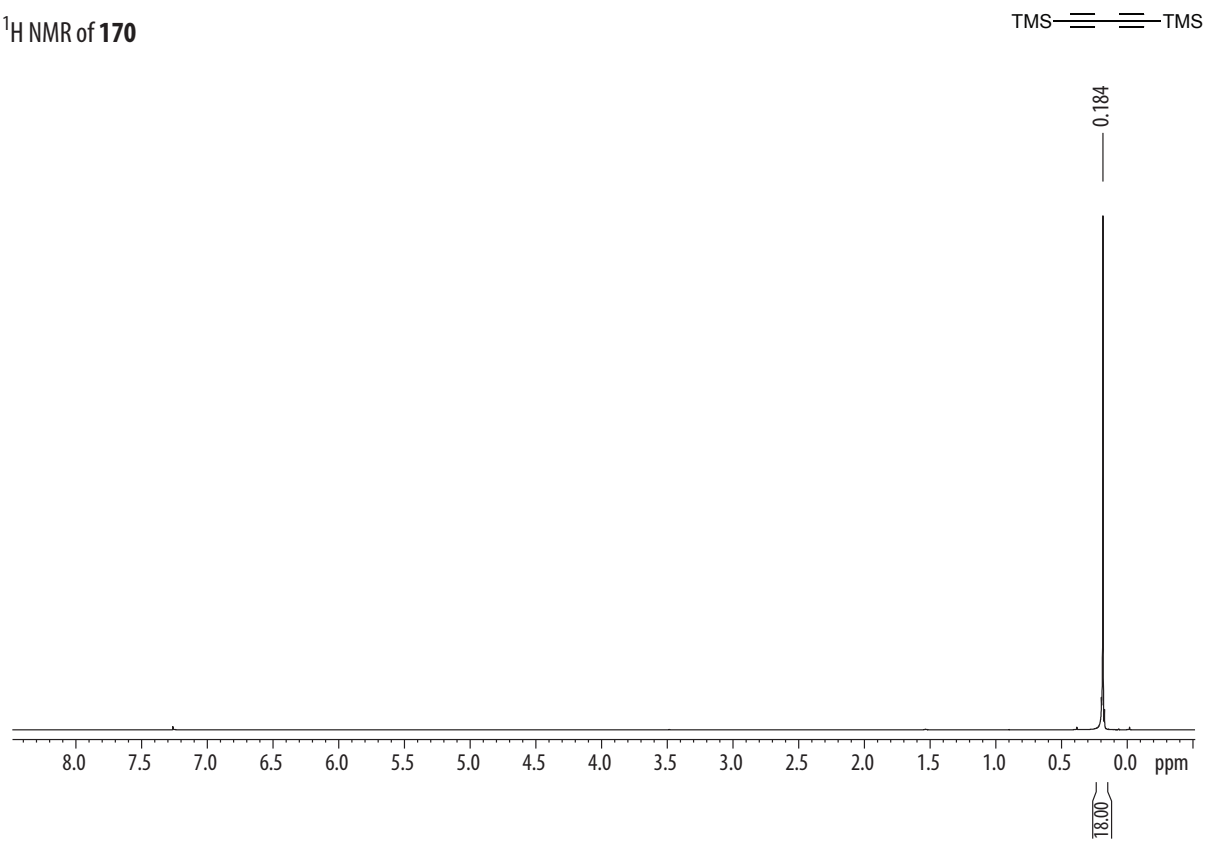
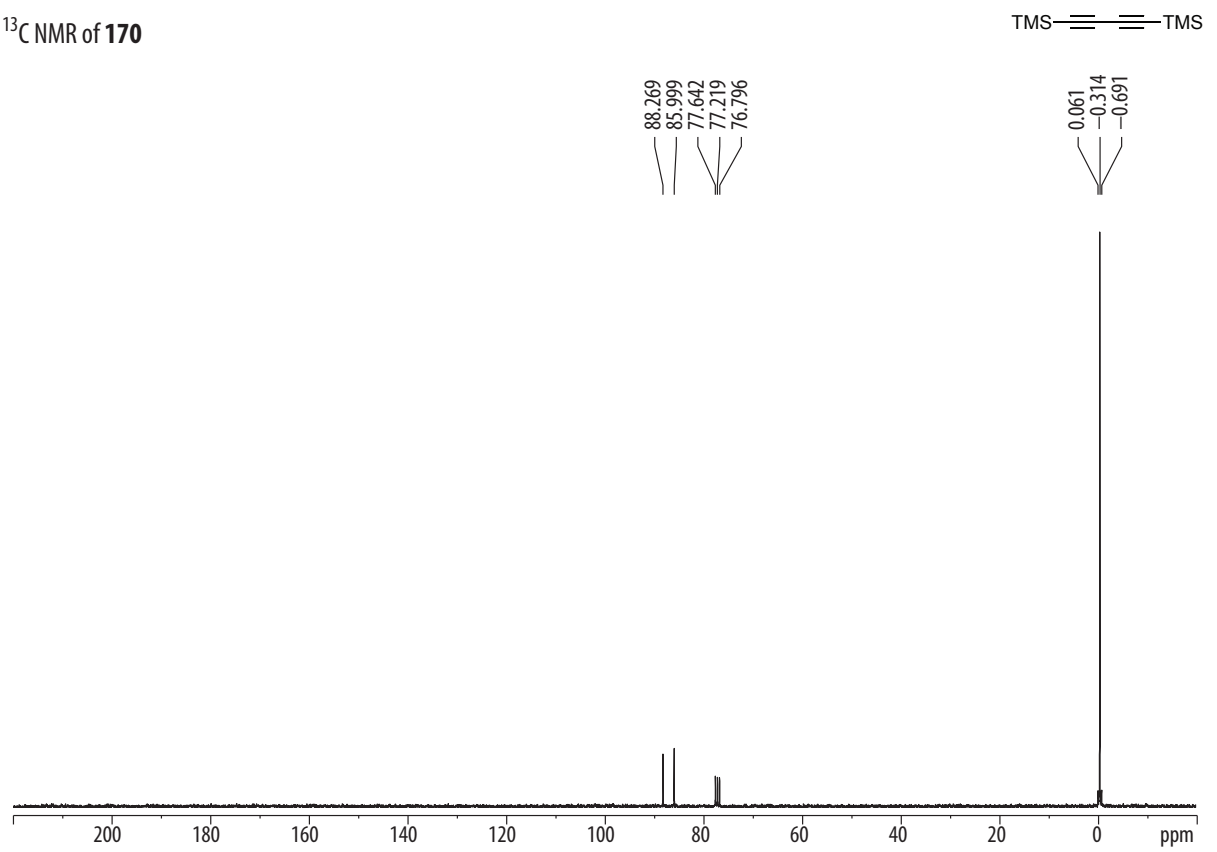
88.214  
86.947  
77.454  
77.031  
76.607  
71.741  
71.412  
53.142  
50.787  
49.047  
39.684  
31.913  
29.637  
29.574  
29.425  
29.346  
29.310  
26.896  
22.681  
18.973  
18.560  
14.108

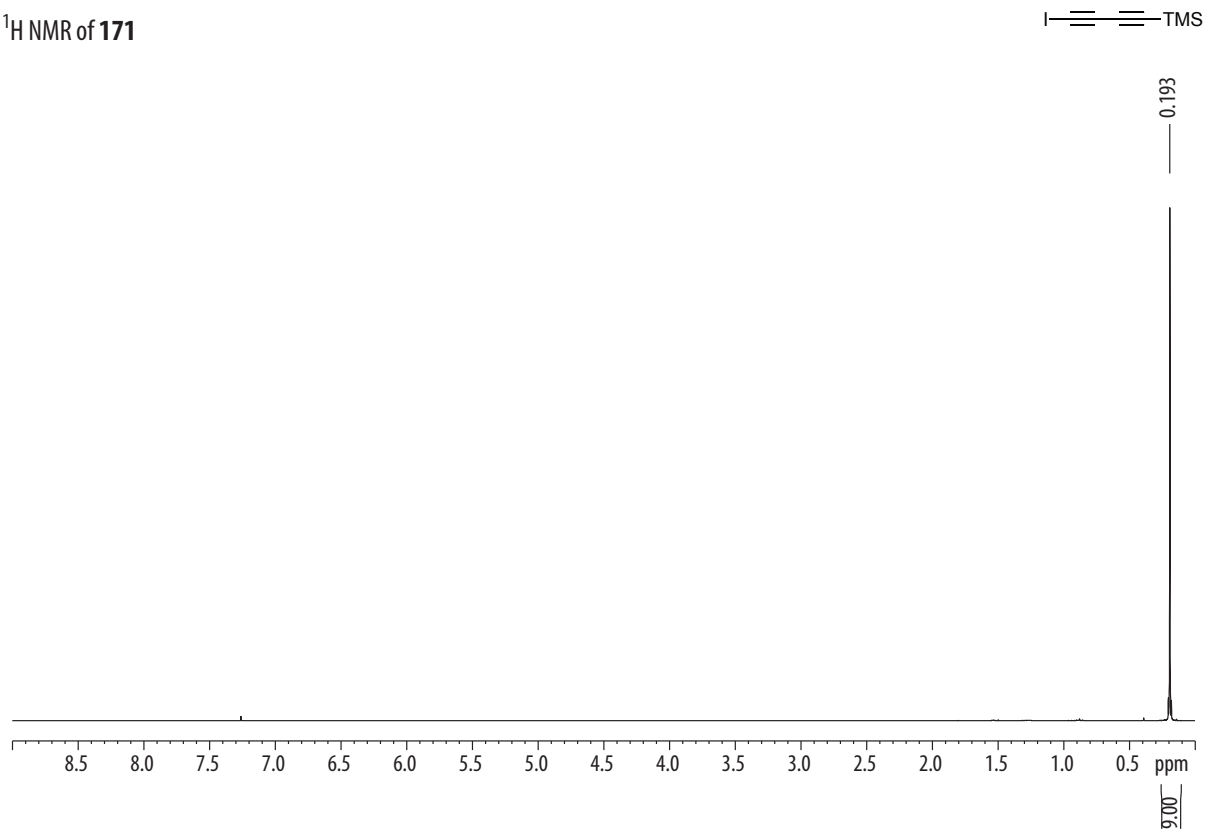
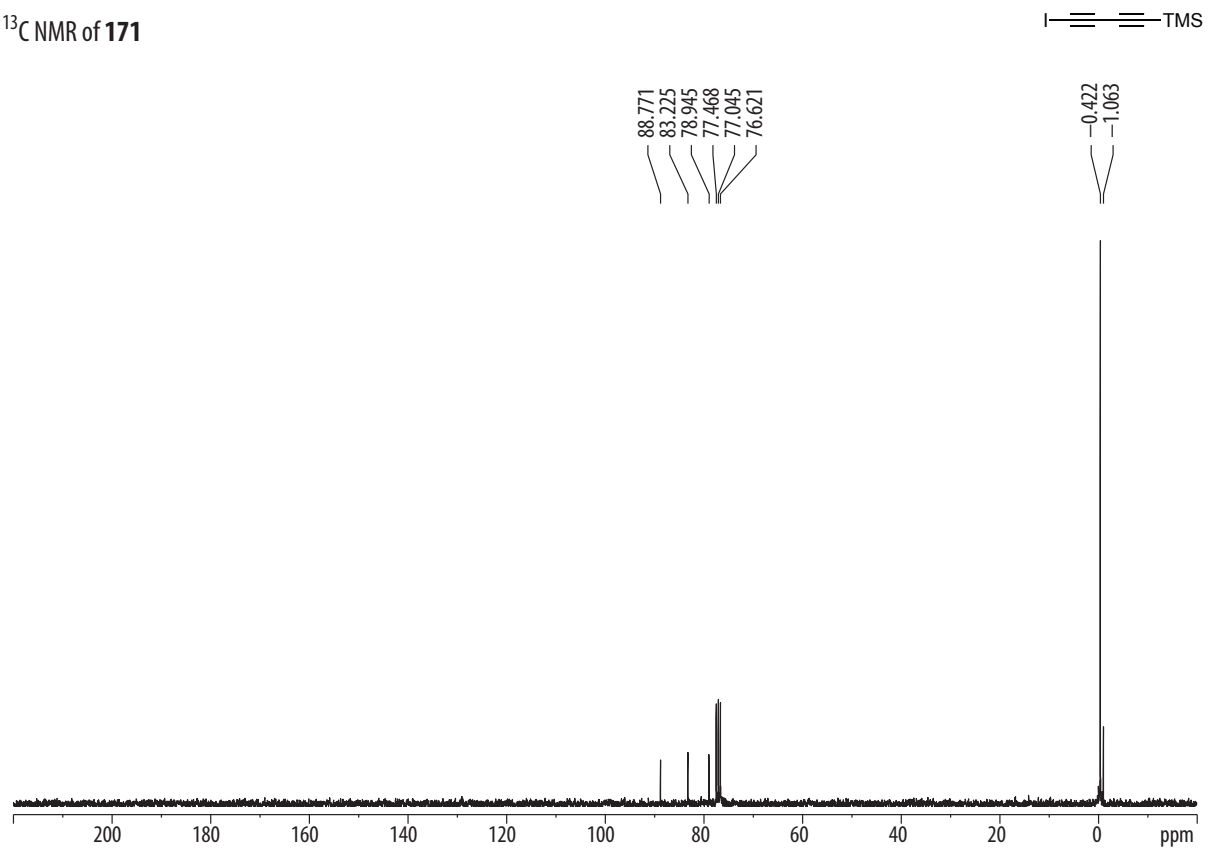


<sup>1</sup>H NMR of 131<sup>1</sup>H NMR of 132

$^1\text{H}$  NMR of **133** $^1\text{H}$  NMR of **134**

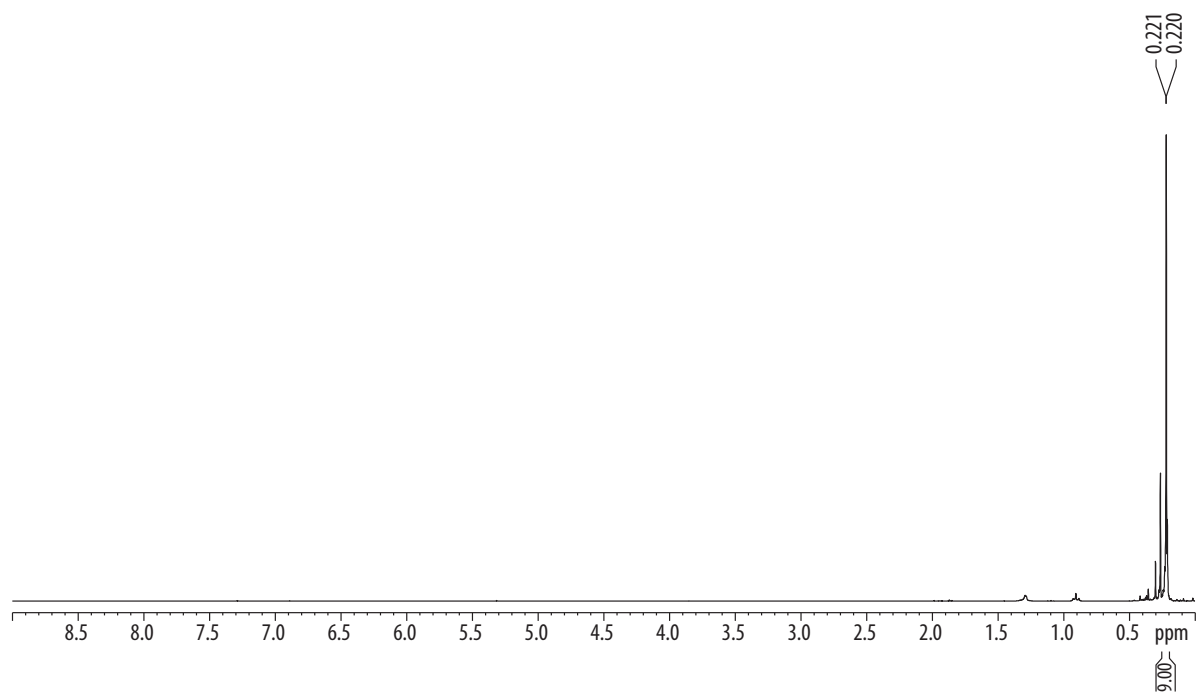


<sup>1</sup>H NMR of **170**<sup>13</sup>C NMR of **170**

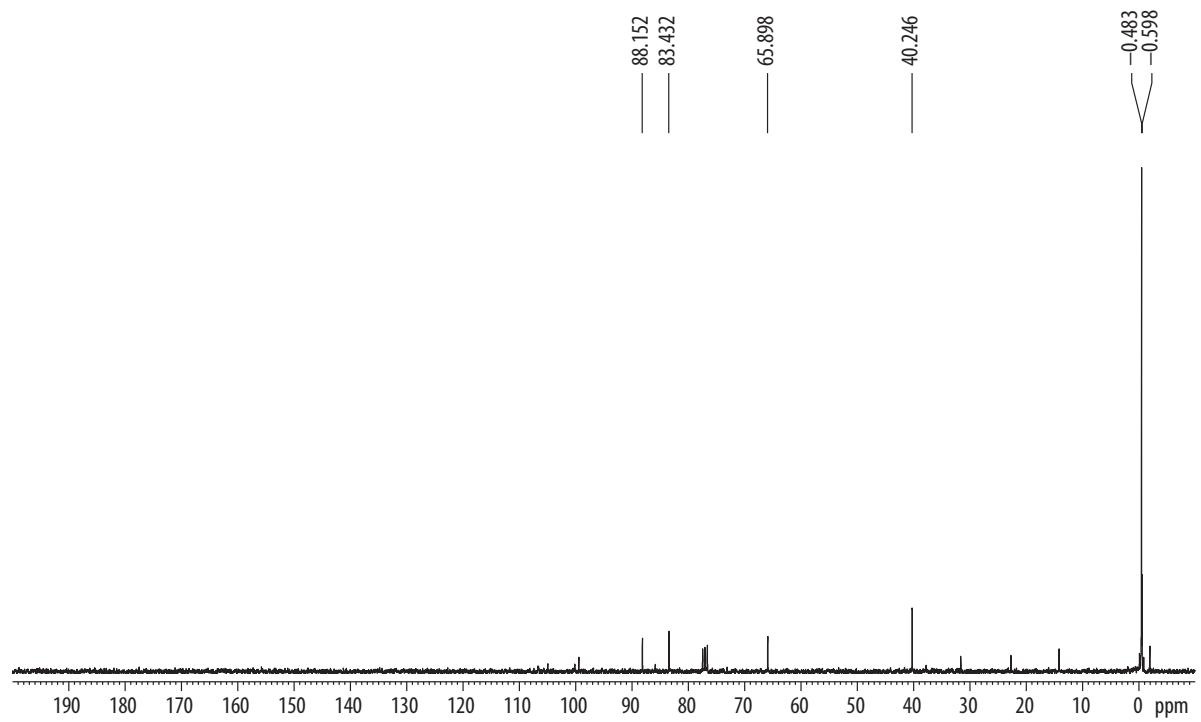
<sup>1</sup>H NMR of **171**<sup>13</sup>C NMR of **171**

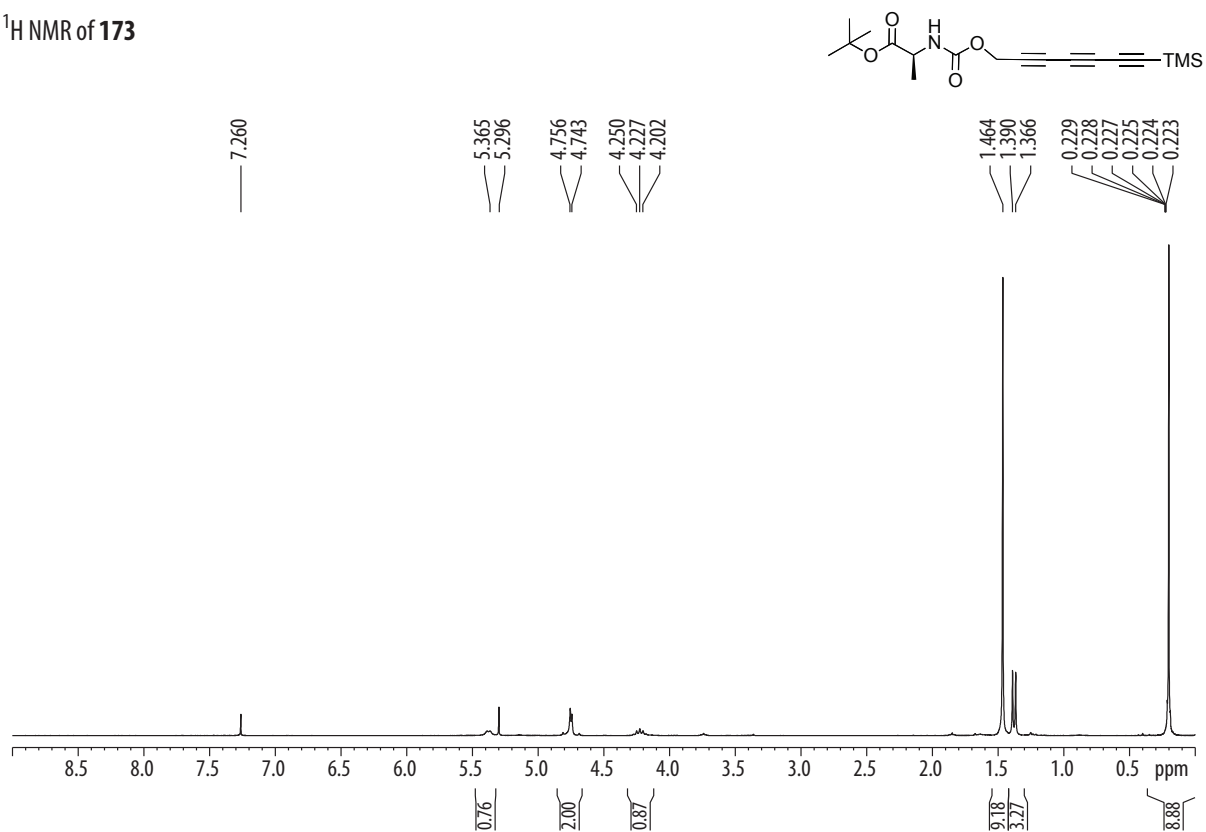
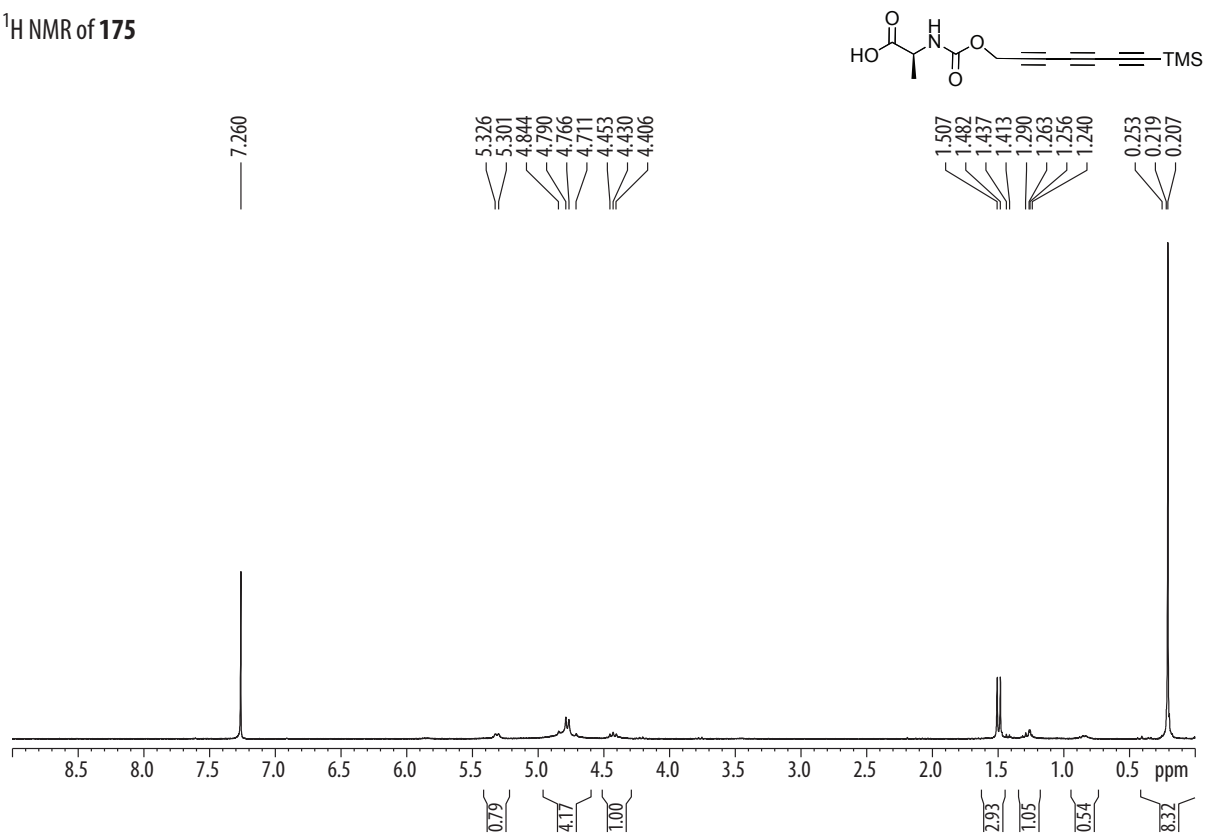
<sup>1</sup>H NMR of **172**

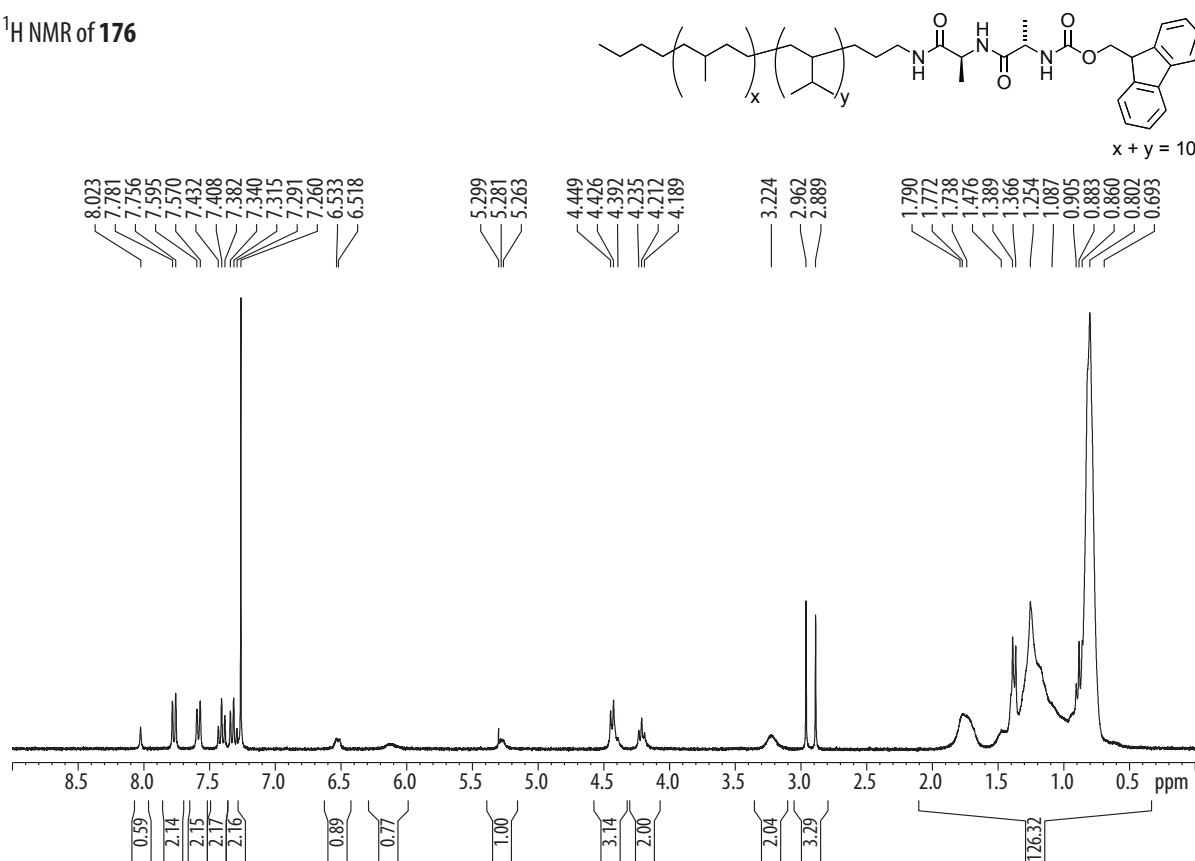
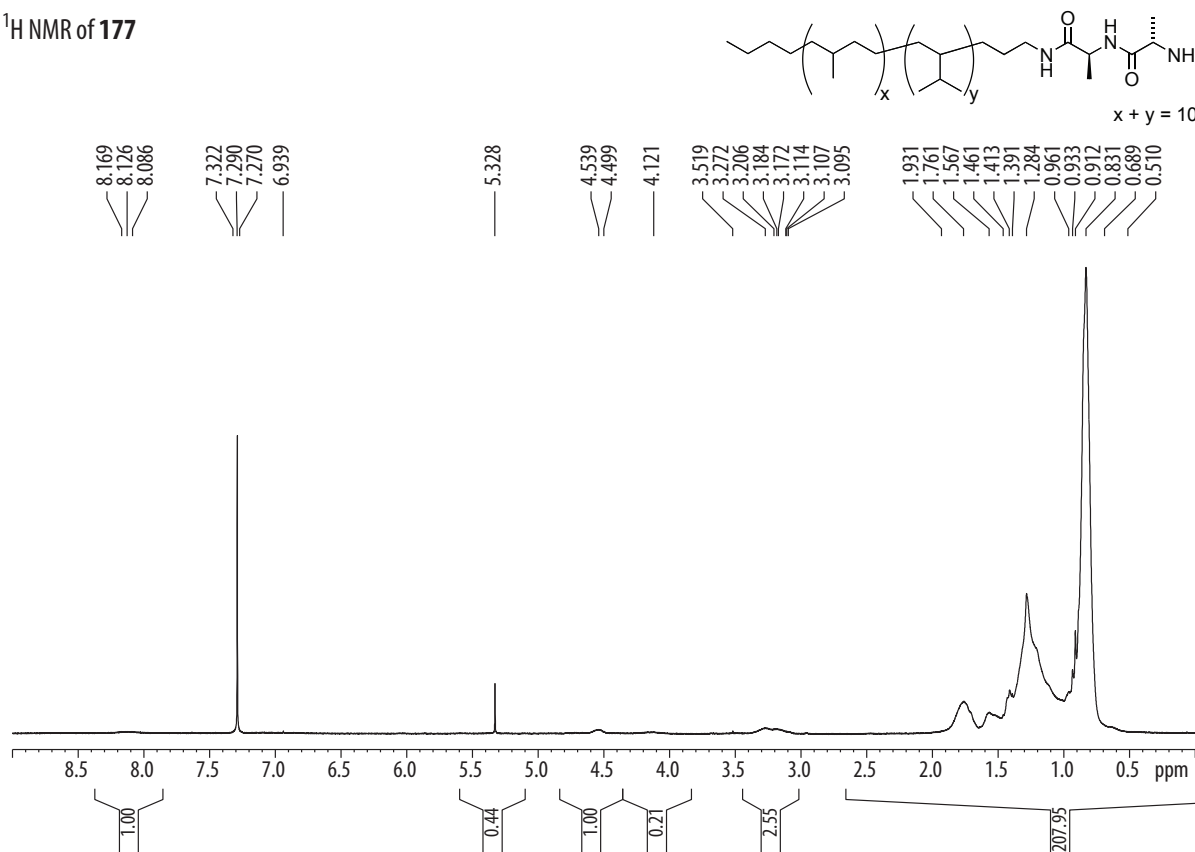
Br—C≡C—C≡C—TMS

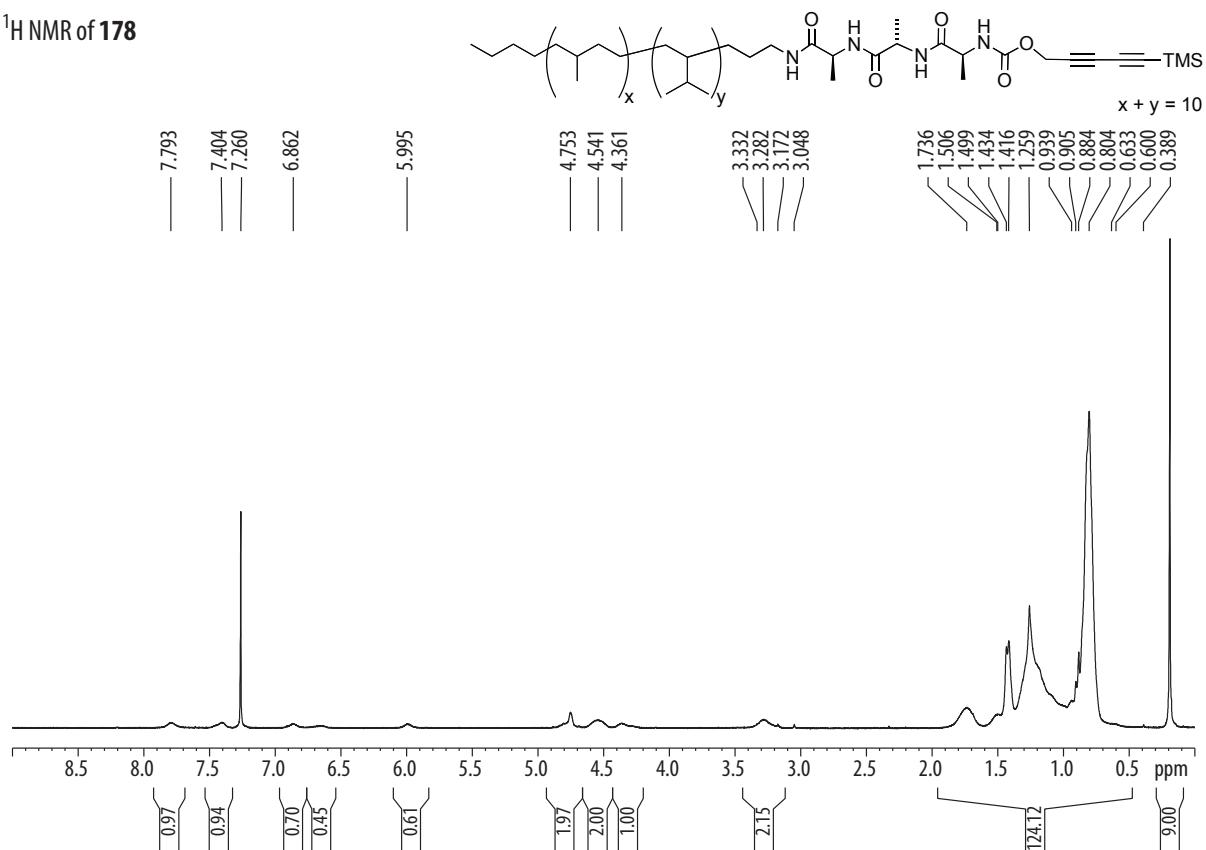
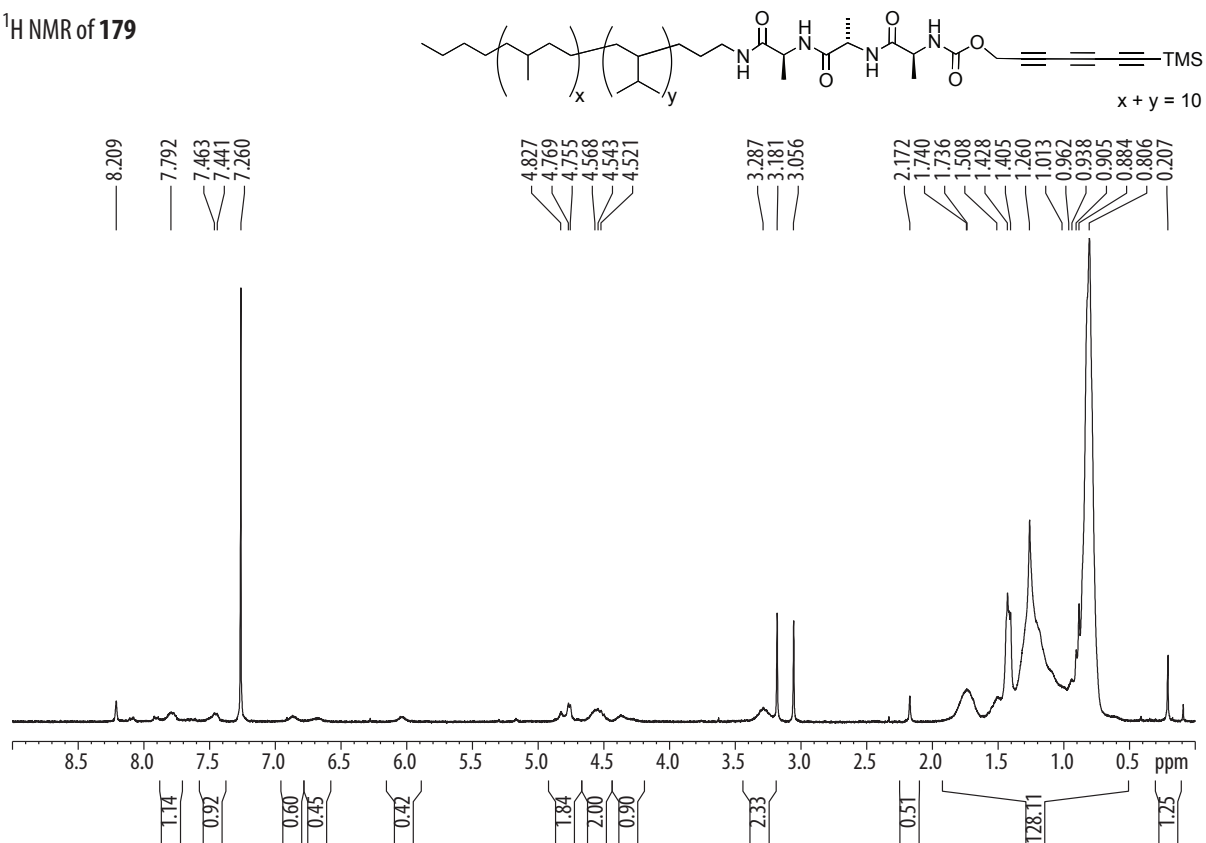
<sup>13</sup>C NMR of **172**

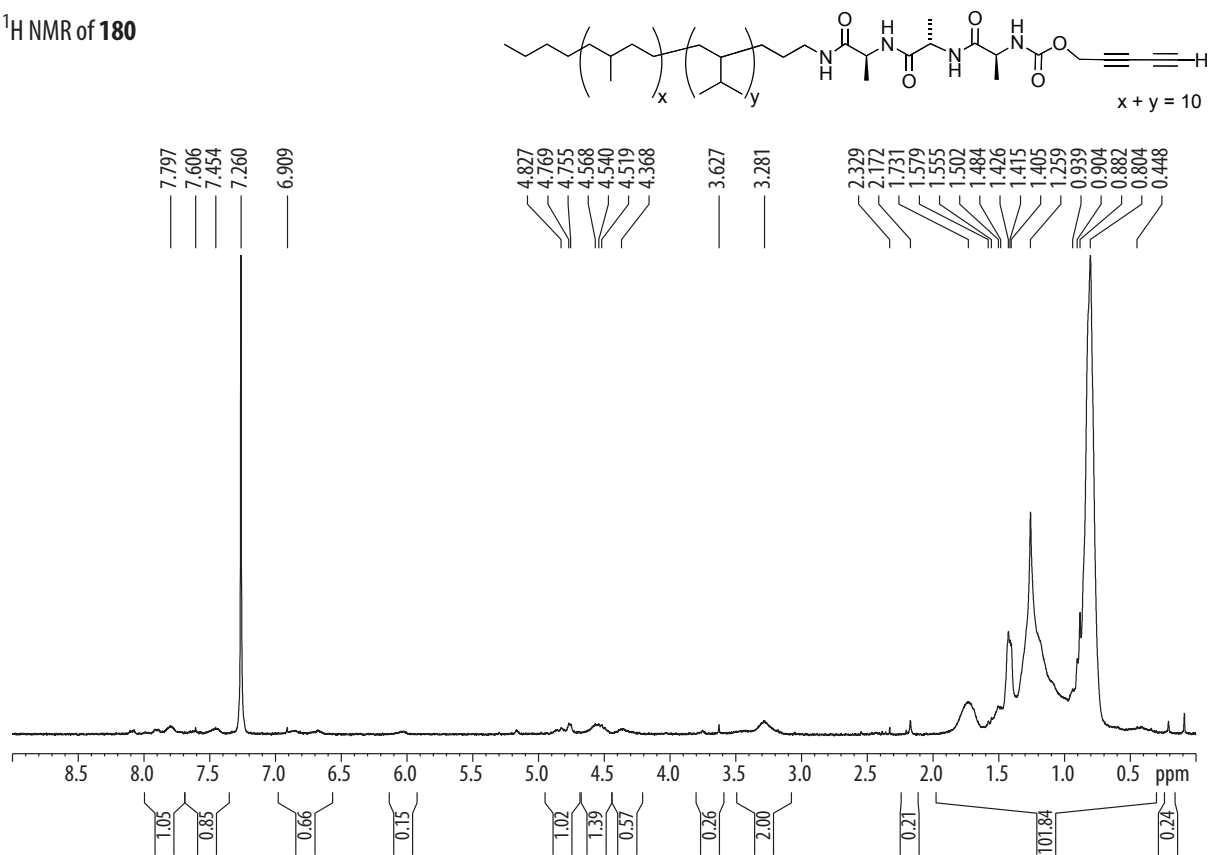
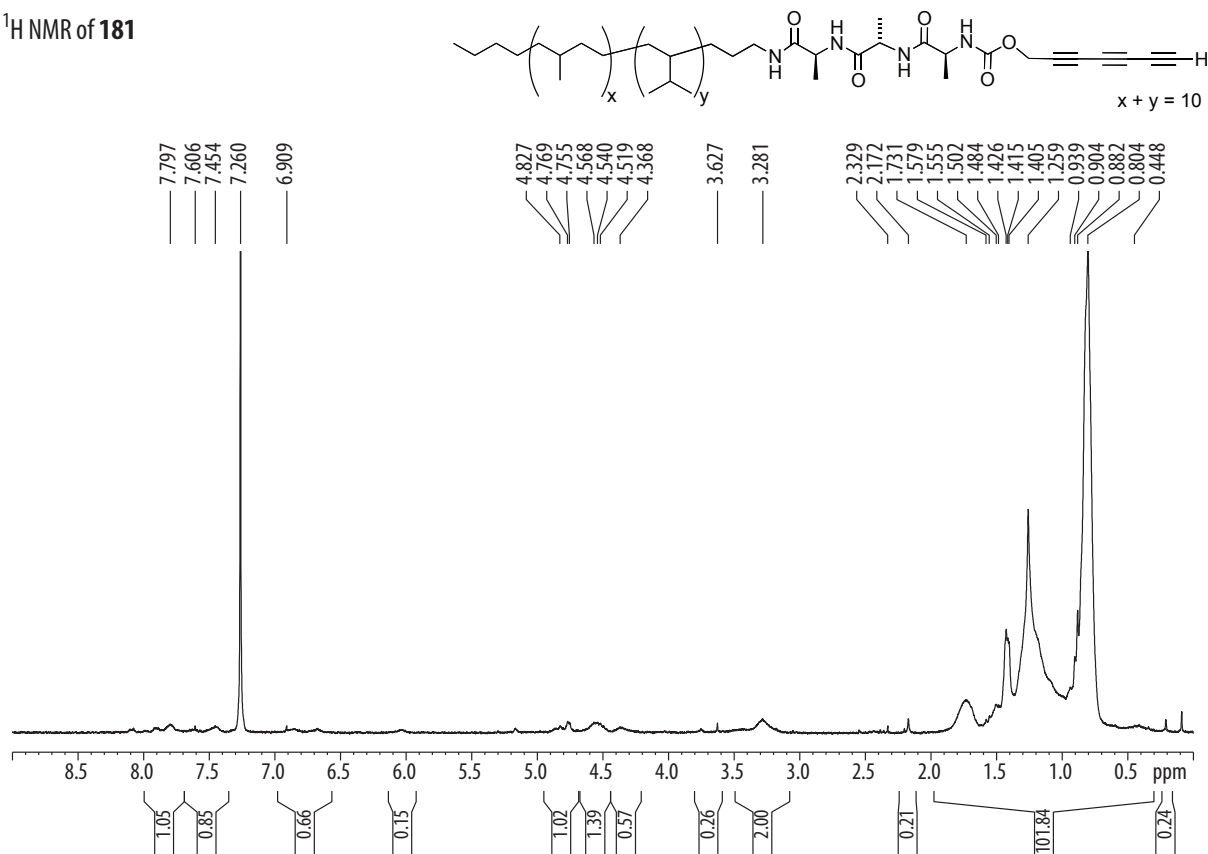
Br—C≡C—C≡C—TMS

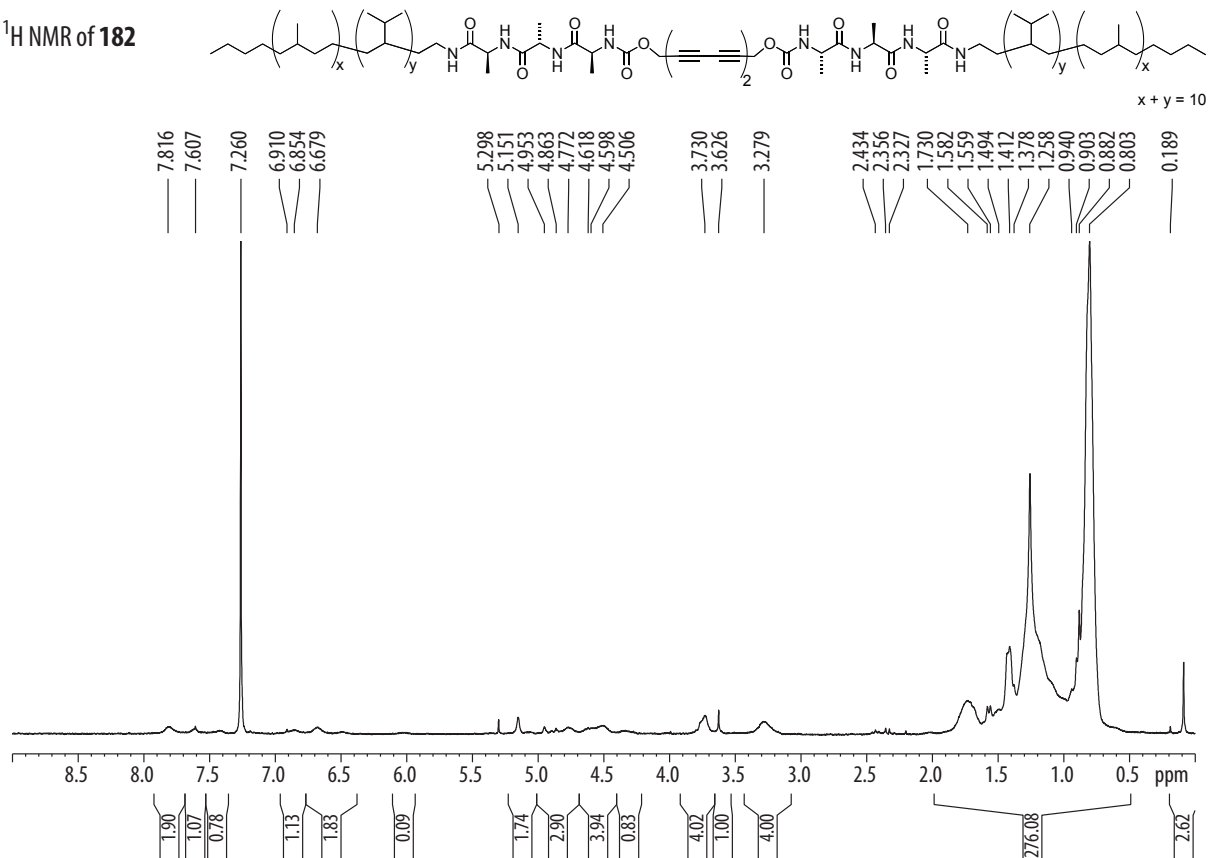
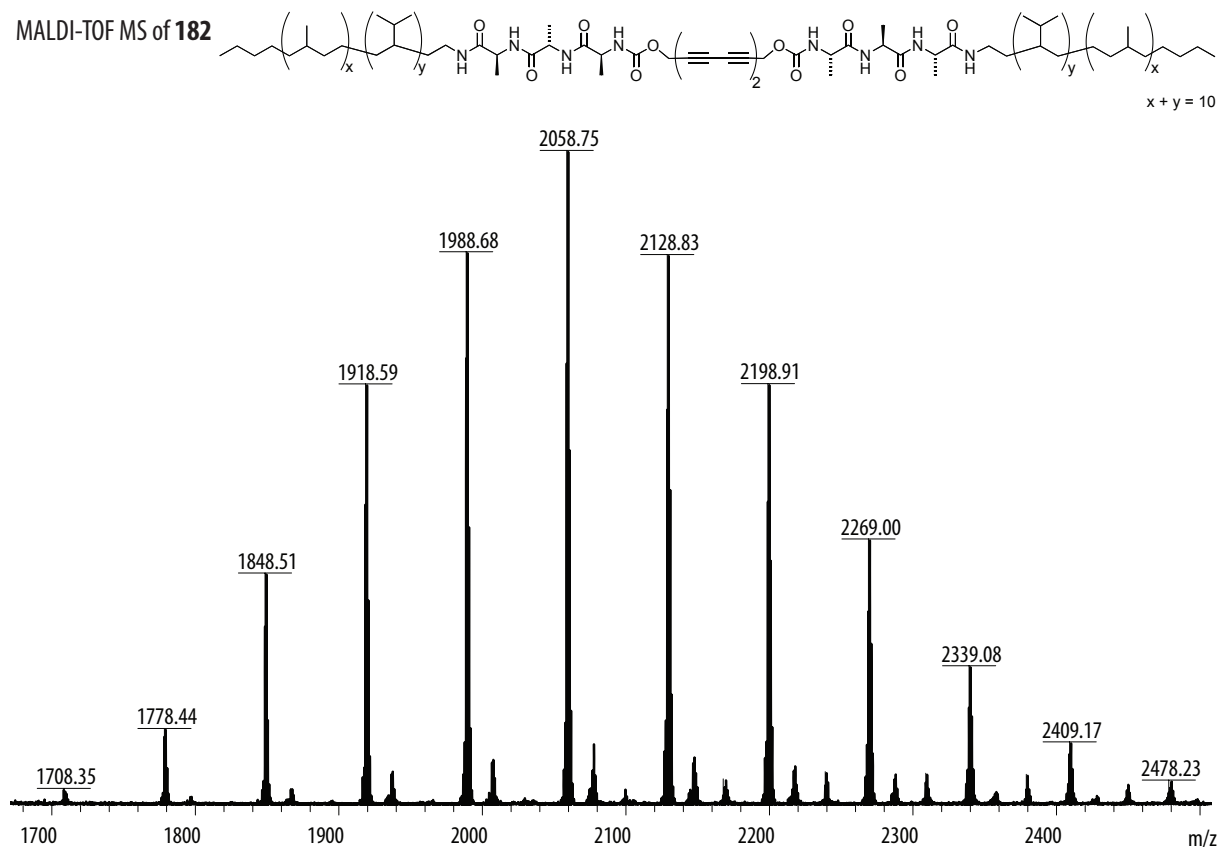


$^1\text{H}$  NMR of **173** $^1\text{H}$  NMR of **175**

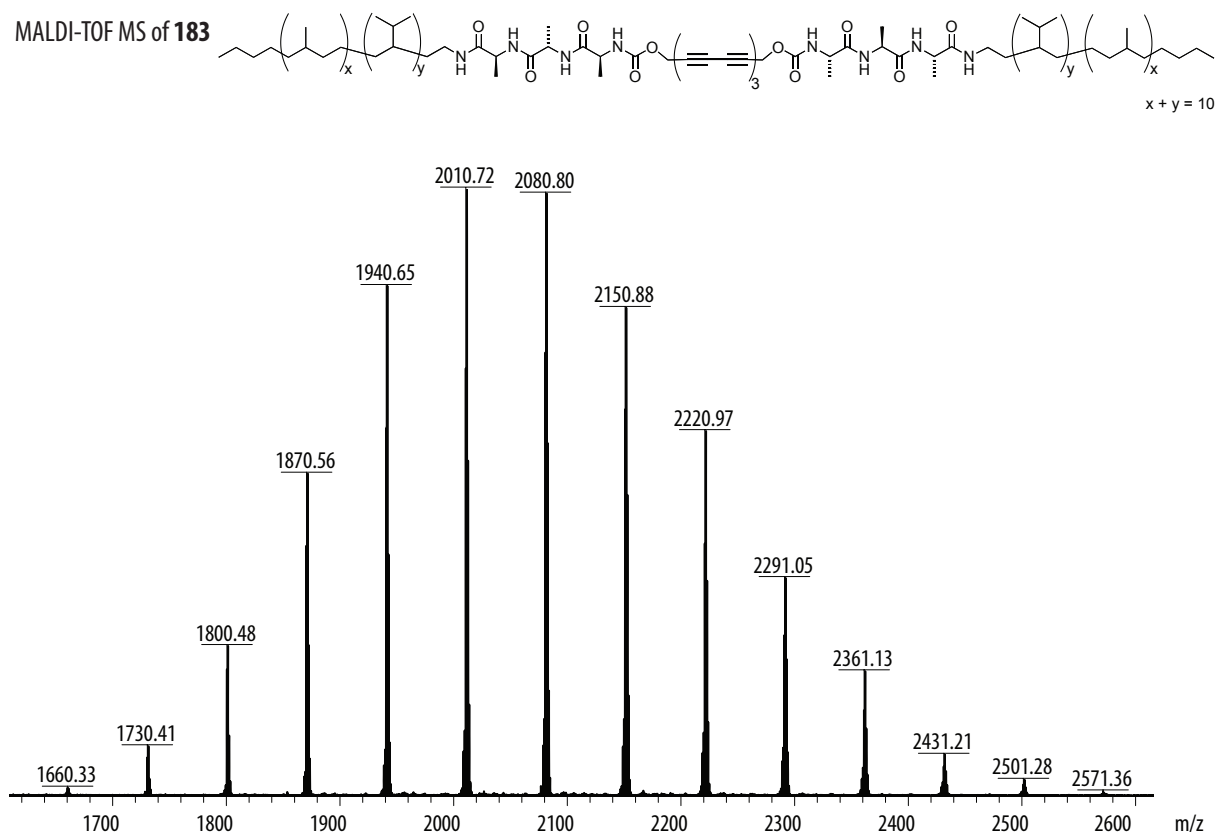
$^1\text{H}$  NMR of **176** $^1\text{H}$  NMR of **177**

$^1\text{H}$  NMR of 178 $^1\text{H}$  NMR of 179

$^1\text{H}$  NMR of **180** $^1\text{H}$  NMR of **181**

$^1\text{H NMR}$  of **182**MALDI-TOF MS of **182**



$^1\text{H}$  NMR of **183**MALDI-TOF MS of **183**





# Curriculum Vitae



# 8 Curriculum Vitae

## Personal Information

Name	Eike Jahnke
Address	Mutschellenstrasse 17 CH-8002 Zurich Switzerland
Date and Place of Birth	July 09, 1979, Zossen, Germany
Marital Status	married
Children	one daughter, born September 10, 2007
Citizenship	German

## School Education

1986 – 1992	Primary school: Karl-Liebknecht Schule in Blankenfelde, Germany
1992 – 1999	High school: Ulrich-von-Hutten Gymnasium Berlin-Tempelhof, Germany

## University Education

10/2000 – 10/2004	Studies of Chemistry at the Free University Berlin, Germany
10/2004 – 03/2005	Diploma thesis at the Department of Materials at ETH Zurich, Switzerland; Supervisors: Prof. C. Stark (FU Berlin) and Dr. H. Frauenrath (ETH Zurich)
since 04/2005	Ph.D. thesis in the group of Prof. A. D. Schlüter and Dr. Holger Frauenrath at the Department of Materials at ETH Zurich, Switzerland

---

## Awards and Fellowships

7/1999	Award for the best high school student in the natural sciences
11/2005 – 10/2007	Ph.D. fellowship from the “Stiftung Stipendien-Fonds des Verbands der Chemischen Industrie in Deutschland”
07/2008 – 06/2009	Postdoctoral Fellowship from the “Deutscher Akademischer Austausch Dienst” (DAAD)

## Further Experience

since 2005	Supervision of two Master students and five undergraduate students during advanced research laboratory courses
	Teaching assistant in two polymer chemistry lab courses with the supervision of thirty students each
	Participation in lectures and projects “Innovation and Technology Management” as well as “Business Process Management” within the framework of the “Materials and Economics” program at ETH Zurich

## Language Skills

German	native language
English	fluent in reading/writing as well as listening/speaking
French	basic knowledge

## Miscellaneous

07/1999 – 04/2000	Obligatory Military Service in the German army (Bundeswehr)
-------------------	---

